frontiers | Research Topics

Complexity of tumor microenvironment: A major culprit in cancer development

Edited by
Ihtisham Bukhari, Yang Mi, Rick Francis Thorne and Yuanwei Zhang

Published in
Frontiers in Endocrinology

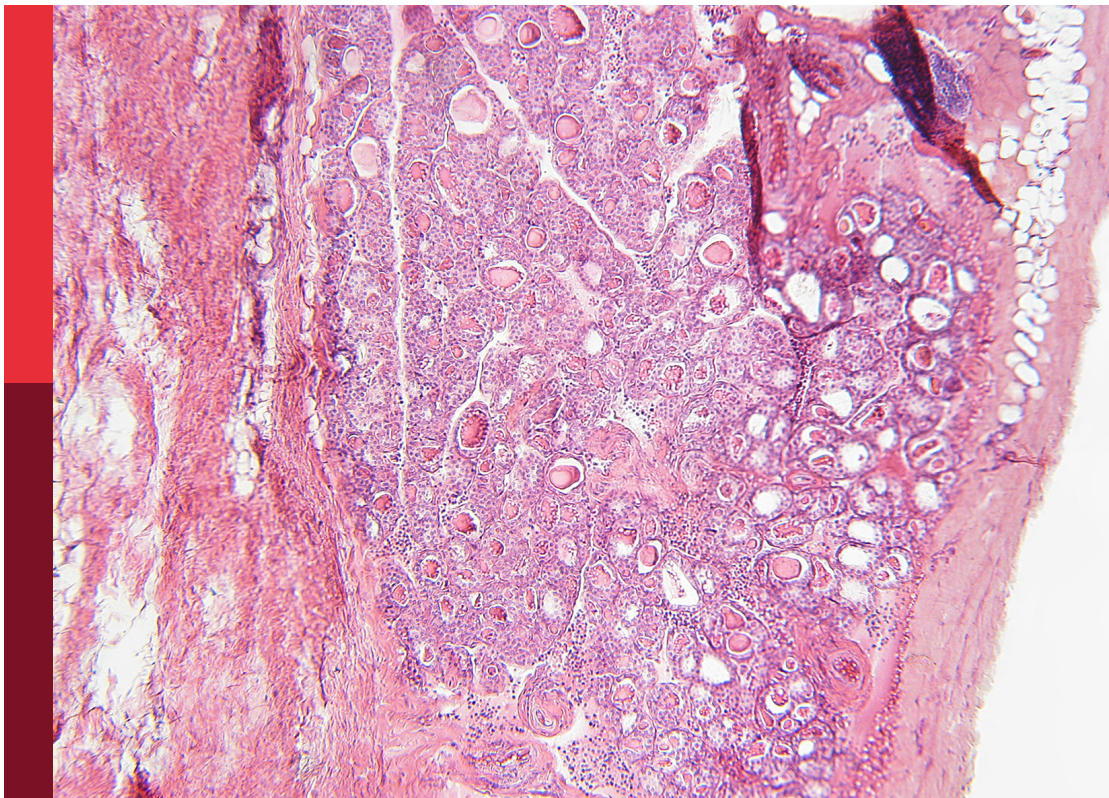

ISSN 1664-8714
ISBN 978-2-83250-696-7
DOI 10.3389/978-2-83250-696-7

About Frontiers

Frontiers is more than just an open access publisher of scholarly articles: it is a pioneering approach to the world of academia, radically improving the way scholarly research is managed. The grand vision of Frontiers is a world where all people have an equal opportunity to seek, share and generate knowledge. Frontiers provides immediate and permanent online open access to all its publications, but this alone is not enough to realize our grand goals.

Frontiers journal series

The Frontiers journal series is a multi-tier and interdisciplinary set of open-access, online journals, promising a paradigm shift from the current review, selection and dissemination processes in academic publishing. All Frontiers journals are driven by researchers for researchers; therefore, they constitute a service to the scholarly community. At the same time, the *Frontiers journal series* operates on a revolutionary invention, the tiered publishing system, initially addressing specific communities of scholars, and gradually climbing up to broader public understanding, thus serving the interests of the lay society, too.

Dedication to quality

Each Frontiers article is a landmark of the highest quality, thanks to genuinely collaborative interactions between authors and review editors, who include some of the world's best academicians. Research must be certified by peers before entering a stream of knowledge that may eventually reach the public - and shape society; therefore, Frontiers only applies the most rigorous and unbiased reviews. Frontiers revolutionizes research publishing by freely delivering the most outstanding research, evaluated with no bias from both the academic and social point of view. By applying the most advanced information technologies, Frontiers is catapulting scholarly publishing into a new generation.

What are Frontiers Research Topics?

Frontiers Research Topics are very popular trademarks of the *Frontiers journals series*: they are collections of at least ten articles, all centered on a particular subject. With their unique mix of varied contributions from Original Research to Review Articles, Frontiers Research Topics unify the most influential researchers, the latest key findings and historical advances in a hot research area.

Find out more on how to host your own Frontiers Research Topic or contribute to one as an author by contacting the Frontiers editorial office: frontiersin.org/about/contact

Complexity of tumor microenvironment: A major culprit in cancer development

Topic editors

Ihtisham Bukhari — Fifth Affiliated Hospital of Zhengzhou University, China
Yang Mi — Henan Key Laboratory for Helicobacter pylori & Microbiota and Gastrointestinal Cancer, China
Rick Francis Thorne — The University of Newcastle, Australia
Yuanwei Zhang — University of Science and Technology of China, China

Citation

Bukhari, I., Mi, Y., Thorne, R. F., Zhang, Y., eds. (2023). *Complexity of tumor microenvironment: A major culprit in cancer development*.
Lausanne: Frontiers Media SA. doi: 10.3389/978-2-83250-696-7

Table of contents

frontiers | Frontiers in Endocrinology

TYPE Editorial
PUBLISHED 20 October 2022
DOI 10.3389/fendo.2022.1059885

OPEN ACCESS

EDITED AND REVIEWED BY
Antonino Belfiore,
University of Catania, Italy

*CORRESPONDENCE
Rick Francis Thorne
rickfthorne@gmail.com
Yang Mi
miyang198@126.com

SPECIALTY SECTION
This article was submitted to Cancer Endocrinology, a section of the journal Frontiers in Endocrinology

RECEIVED 02 October 2022
ACCEPTED 10 October 2022
PUBLISHED 20 October 2022

CITATION
Bukhari I, Zhang Y, Thorne RF and Mi Y (2022) Editorial: Complexity of tumor microenvironment: A major culprit in cancer development.
Front. Endocrinol. 13:1059885.
doi: 10.3389/fendo.2022.1059885

Editorial: Complexity of tumor microenvironment: A major culprit in cancer development

Ihtisham Bukhari[1,2], Yuanwei Zhang[3], Rick Francis Thorne[2,4]* and Yang Mi[1]*

[1]Henan Key Laboratory of Helicobacter pylori, Microbiota and Gastrointestinal Cancers, Marshall Medical Research Center, Fifth Affiliated Hospital of Zhengzhou University, Zhengzhou, China, [2]Henan Provincial and Zhengzhou City Key Laboratory of Noncoding RNA and Cancer Metabolism, Henan International Join Laboratory of Non-coding RNA and Metabolism in Cancer, Translational Research Institute, Henan Provincial People's Hospital, Academy of Medical Sciences, Zhengzhou University, Zhengzhou, Henan, China, [3]School of Life Sciences, University of Science and Technology of China, Hefei, Anhui, China, [4]School of Environmental and Life Sciences, University of Newcastle, Callaghan, NSW, Australia

KEYWORDS

tumor microenvironment, cancer development, immune cell infiltration, prognosis, immune function

Editorial on the Research Topic
Complexity of tumor microenvironment: A major culprit in cancer development

The tumor microenvironment (TME) is a complex landscape composed of intrinsic and extrinsic elements besides tumor cells including various immune cells, tumor-related stromal cells, and endothelial cells along with extracellular matrix components (1–3). Notably, the ability of tumor cells to invade surrounding tissues or metastasize through blood and lymphatic vessels implicitly involves cooperation with elements of the TME (4–6). In this regard, infiltrating immune cells such as T cells, B cells, macrophages, dendritic cells, monocytes, neutrophils, and mast cells have been associated with cancer development and progression (6–8). Additionally, these cells stimulate the host immune response by releasing cytokines, cytokine receptors, and other factors, which directly or indirectly promote or alternatively inhibit tumor cell proliferation (9, 10). Collectively these processes direct key events such as tumor recurrence, metastasis, and response to the immunotherapy (11, 12), thereby influencing clinical outcomes (13–15). However, the detailed profiles of immune cell infiltration and differentially expressed genes (metabolic, immune-related, or others) in many cancers continue to be elucidated (7, 16, 17). Several metabolic factors have shown an association with pathogenesis and progression of various cancers (18, 19) such as *de novo* lipid biosynthesis is a crucial regulator in the prostate cancer (20–22). An anecdotal observation metabolic health of the individuals may influence the prognosis and treatment of the cancers.

Indeed, support for this intriguing hypothesis is gaining momentum, for example, androgen deprivation therapy (ADT) reduces testosterone in the body which inhibits the prostate cancer (23–25). However, studying constituents of the TME can help understand

the underlying mechanisms of cancer development and progression (26–29). It has been well established that metabolic factors and infiltrating cells in TME potentially serve as prognostic markers in various cancers (30, 31). Recent advances and improvements in cancer therapy have shifted the treatment focus toward hormonal therapy and immunotherapy such as immune checkpoint inhibitors (ICIs) and chimeric antigen receptor (CAR) T-cell adoptive immunotherapy. The latter involves manipulating T cells in the laboratory to add artificial receptors that can invoke attacks against cancer cells (32–34). However, CAR-T therapy remains limited by the lack of appropriate targets in solid tumors (33, 35–37). However, advanced-stage patients or those presenting with unfavorable tumors inevitably face disease progression with dire outcomes (38–40). Thus, more comprehensive studies related to the genetic regulation of tumors through metabolic and endocrine factors, immune cell infiltration, and immune functions are urgently required to identify the underlying mechanisms of cancer development and progression towards improved biomarkers and/or applications of targeted therapy.

The current Research Topic aimed to collect studies reporting advancements in clinical and basic research related to the tumor microenvironment and regulation of cancers through metabolic, endocrine factors, and immune cells. After a rigorous review process, the current volume presents an authoritative collection of twelve articles exploring new dimensions in this research field.

First, the review by Aguilar-Cazares et al. provides a systematic account of the current literature describing the roles of inflammatory mediators within the tumor microenvironment, particularly their dynamics in growing tumors. Here inflammatory factors including IL-6, IL-1, TNF-α, G-CSF, and GM-CSF produced by cancer cells and stromal cells make essential contributions to cancer-associated inflammation. Ye et al. further describe the activation of inflammation in diabetic pancreatic cancer patients *via* the infiltration of CD8+T cells into the TME, which intriguingly acts to reduce tumor growth and metastasis. Similarly, Huang et al. using single-cell analysis of pancreatic cancer developed a four-gene predictive model which also indicated the differential infiltration of memory B-cell subtypes into the TME.

Treating solid tumors is always challenging with surgical resection, chemotherapy and radiotherapy being the longstanding options. However, the resurgence of immunotherapy over recent years, for example, involving CAR-T cells has shown promising results in hematological malignancies. Gastrointestinal cancers such as hepatocellular carcinoma (HCC) are some of the most lethal cancers and generally, patients with such solid tumors have not presently benefited from CAR-T approaches. The review by Guizhen et al. investigates the factors preventing CAR-T success in HCC, dissecting the evidence for why the TME represents a significant barrier to the infiltration, survival and activity of CAR-T cells. Taking cues from other cancer types, they conclude that modifying CAR-T cells may help their persistence in the TME or otherwise combinatorial approaches such as combining CAR-T with immune checkpoint inhibitors. Moreover, Dong et al. showed that cancer-associated fibroblast (CAF) related genes are significantly associated with immune regulation in HCC. Patients with tumors showing higher CAF gene expression were resistant to chemotherapy (cisplatin and doxorubicin) and tyrosine kinase inhibitors (TKI) (sorafenib) with worse overall survival.

Similarly, Zhang et al. used the TKI Aumolertinib to treat a lung cancer case with brain metastasis coupled with Osimertinib-induced cardiotoxicity. The patient showed significant recovery after Aumolertinib treatment with negligible adverse effects recorded, suggesting clinical outcomes could be improved by supplementing TKIs with CAR-T or other immunotherapies. A further enlightening report linking the TME with cancer prognosis by Li et al. presented evidence for the differential expression of immune-related genes in lung cancer. They found that Ribonucleotide Reductase Regulatory Subunit M2 (RRM2) represented a potential new metabolic checkpoint and therapeutic target. Ge et al. also reported the prognostic significance of pyroptosis-derived lncRNAs from lung adenocarcinoma tissues, which could be used as alternative therapeutic targets.

Yan et al. constructed an eight-gene model for low and high-risk prognostication in diffuse large B cell lymphoma (DLBCL) patients, interestingly showing that low-risk cases exhibited a proinflammatory immune cell-enrichment profile. An alternative DNA damage repair gene signature predicting survival in cutaneous melanoma patients revealed by Liang et al. showed that positive benefits were associated with immune cell enrichment in the TME together with the expression of immune checkpoint-related genes. Additionally, Jiang et al. considered PET/CT a promising method for early diagnosing lesions in patients with biochemical recurrence of prostate cancer. Finally, Wang et al. showed how hypoxic conditions enhance the stemness and proliferative capacity of rat peripheral blood-derived mesenchymal stromal cells (PBMSCs), a finding of interest to tissue engineering but also in cancer models.

Conclusion and prospects

The tumor microenvironment is a unique tissue landscape that must be understood if therapeutic strategies against cancer are to be successful. Twelve contributions to this topic highlight different aspects of how TME affects cancer outcomes. Most

studies report the identification of molecular markers that may be potentially used as diagnostic, therapeutic, and prognostic targets. Altogether, these studies increase our biological understanding of cancer and tumor microenvironment aspects but especially highlight the cruciality of PDL1, CAR-T, and TKIs in cancer treatment. It can be anticipated that these contributions will find broad applications, ranging from purely scientific endeavors to clinical guidelines for cancer treatment.

Author contributions

All authors listed have made a substantial, direct, and intellectual contribution to the work and approved it for publication.

Conflict of interest

The authors declare that the research was conducted in the absence of any commercial or financial relationships that could be construed as a potential conflict of interest.

Publisher's note

References

1. Talaat IM, Kim B. A brief glimpse of a tangled web in a small world: Tumor microenvironment. *Front Med (Lausanne)* (2022) 9:1002715. doi: 10.3389/fmed.2022.1002715

2. Galmiche A, Rak J, Roumenina LT, Saidak Z. Coagulome and the tumor microenvironment: an actionable interplay. *Trends Cancer* (2022) 8:369–83. doi: 10.1016/j.trecan.2021.12.008

3. Mao X, Xu J, Wang W, Liang C, Hua J, Liu J, et al. Crosstalk between cancer-associated fibroblasts and immune cells in the tumor microenvironment: new findings and future perspectives. *Mol Cancer* (2021) 20:131. doi: 10.1186/s12943-021-01428-1

4. Chen J, Zhu H, Yin Y, Jia S, Luo X. Colorectal cancer: Metabolic interactions reshape the tumor microenvironment. *Biochim Biophys Acta Rev Cancer* (2022), 1877(5):188797. doi: 10.1016/j.bbcan.2022.188797

5. Kuznetsova A, Popova O, Panchenkov D, Dyuzheva T, Ivanov A. Pancreatic ductal adenocarcinoma: tumor microenvironment and problems in the development of novel therapeutic strategies. *Clin Exp Med* (2022). doi: 10.1007/s10238-022-00886-1

6. Okita R, Mimura-Kimura Y, Kawamoto N, Yamamoto N, Umeda M, Okada M, et al. Effects of tumor-infiltrating CD8+ T cells, PD1/PD-L1 axis, and expression patterns of HLA class I on the prognosis of patients with malignant pleural mesothelioma who underwent extra-pleural pneumonectomy. *Cancer Immunol Immunother* (2022). doi: 10.1007/s00262-022-03292-4

7. Shi X, Yang J, Deng S, Xu H, Wu D, Zeng Q, et al. TGF-beta signaling in the tumor metabolic microenvironment and targeted therapies. *J Hematol Oncol* (2022) 15:135. doi: 10.1186/s13045-022-01349-6

8. Zhu X, Liang R, Lan T, Ding D, Huang S, Shao J, et al. Tumor-associated macrophage-specific CD155 contributes to M2-phenotype transition, immunosuppression, and tumor progression in colorectal cancer. *J Immunother Cancer* (2022) 10(9):e004219. doi: 10.1136/jitc-2021-004219

9. Fenner A. Immune infiltration associated with outcomes. *Nat Rev Urol* (2022) 19:256. doi: 10.1038/s41585-022-00594-1

10. Laumont CM, Banville AC, Gilardi M, Hollern DP, Nelson BH. Tumour-infiltrating b cells: immunological mechanisms, clinical impact and therapeutic opportunities. *Nat Rev Cancer* (2022) 22:414–30. doi: 10.1038/s41568-022-00466-1

11. Joshi VB, Spiess PE, Necchi A, Pettaway CA, Chahoud J. Immune-based therapies in penile cancer. *Nat Rev Urol* (2022) 19:457–74. doi: 10.1038/s41585-022-00617-x

12. Shimu AS, Wei HX, Li Q, Zheng X, Li B. The new progress in cancer immunotherapy. *Clin Exp Med* (2022). doi: 10.1007/s10238-022-00887-0

13. Shi Q, Shen Q, Liu Y, Shi Y, Huang W, Wang X, et al. Increased glucose metabolism in TAMs fuels O-GlcNAcylation of lysosomal cathepsin b to promote cancer metastasis and chemoresistance. *Cancer Cell* (2022). doi: 10.1016/j.ccell.2022.08.012

14. Wen H, Li F, Bukhari I, Mi Y, Guo C, Liu B, et al. Comprehensive analysis of colorectal cancer immunity and identification of immune-related prognostic targets. *Dis Markers* (2022) 30(2022):7932655. doi: 10.1155/2022/7932655

15. Ren F, Zhao Q, Zhao M, Zhu S, Liu B, Bukhari I, et al. Immune infiltration profiling in gastric cancer and their clinical implications. *Cancer Sci* (2021) 112:3569–84. doi: 10.1111/cas.15057

16. Mossa F, Robesti D, Sumankalai R, Corey E, Titus M, Kang Y, et al. Subtype and site specific-induced metabolic vulnerabilities in prostate cancer. *Mol Cancer Res* (2022). doi: 10.1158/1541-7786.MCR-22-0250

17. Yang Y, Li S, Wang Y, Zhao Y, Li Q. Protein tyrosine kinase inhibitor resistance in malignant tumors: molecular mechanisms and future perspective. *Signal Transduct Target Ther* (2022) 7:329. doi: 10.1038/s41392-022-01168-8

18. Kamal MA, Mandour YM, Abd EL-Aziz MK, Stein U, El Tayebi HM. Small molecule inhibitors for hepatocellular carcinoma: Advances and challenges. *Molecules* (2022) 27(17):5537. doi: 10.3390/molecules27175537

19. Yin X, Chen Y, Ruze R, Xu R, Song J, Wang C, et al. The evolving view of thermogenic fat and its implications in cancer and metabolic diseases. *Signal Transduct Target Ther* (2022) 7:324. doi: 10.1038/s41392-022-01178-6

20. Stopsack KH, Gerke TA, Andren O, Andersson SO, Giovannucci EL, Mucci LA, et al. Cholesterol uptake and regulation in high-grade and lethal prostate cancers. *Carcinogenesis* (2017) 38:806–11. doi: 10.1093/carcin/bgx058

21. Zadra G, Photopoulos C, Loda M. The fat side of prostate cancer. *Biochim Biophys Acta* (2013) 1831:1518–32. doi: 10.1016/j.bbalip.2013.03.010

22. Cui MY, Yi X, Cao ZZ, Zhu DX, Wu J. Targeting strategies for aberrant lipid metabolism reprogramming and the immune microenvironment in esophageal cancer: A review. *J Oncol* (2022) 2022:4257359. doi: 10.1155/2022/4257359

23. Rouleau M, Neveu B, Caron P, Morin F, Toren P, Lacombe L, et al. Extensive alteration of androgen precursor levels after castration in prostate cancer patients and their association with active androgen level. *J Urol* (2022). doi: 10.1097/JU.0000000000002923

24. Balagobi B, Gobishangar S, Sarma ST, Brammah RT, Jenil A. A young patient with prostatic carcinoma with testicular metastasis. *Int J Surg Case Rep* (2022) 99:107653. doi: 10.1016/j.ijscr.2022.107653

25. Xu Z, Wei F, Wang J, Ma S, Kan Y, Li B, et al. Neoadjuvant androgen deprivation therapy combined with abiraterone acetate in patients with locally advanced or metastatic prostate cancer: When to perform radical prostatectomy? *Cancer Med* (2022). doi: 10.1002/cam4.5255

26. Xiao J, Liu Z, Wang J, Zhang S, Zhang Y. Identification of cuprotosis-mediated subtypes, the development of a prognosis model, and influence immune microenvironment in hepatocellular carcinoma. *Front Oncol* (2022) 12:941211. doi: 10.3389/fonc.2022.941211

27. Zhuang Z, Gao C. Development of a clinical prognostic model for metabolism-related genes in squamous lung cancer and correlation analysis of immune microenvironment. *BioMed Res Int* (2022), 2022:6962056. doi: 10.1155/2022/6962056

28. Zhang Y, Kong X, Xin S, Bi L, Sun X. Discovery of lipid metabolism-related genes for predicting tumor immune microenvironment status and prognosis in prostate cancer. *J Oncol* (2022), 2022:8227806. doi: 10.1155/2022/8227806

29. Mucileanu A, Chira R, Mircea PA. PD-1/PD-L1 expression in pancreatic cancer and its implication in novel therapies. *Med Pharm Rep* (2021) 94:402–10. doi: 10.15386/mpr-2116

30. Huang, Alexander PB, Li QJ, Wang XF. GABAergic signaling beyond synapses: an emerging target for cancer therapy. *Trends Cell Biol* (2022) S0962–8924(22)00195–7. doi: 10.1016/j.tcb.2022.08.004

31. Kocher F, Puccini A, Untergasser G, Martowicz A, Zimmer K, Pircher A, et al. Multi-omic characterization of pancreatic ductal adenocarcinoma relates CXCR4 mRNA expression levels to potential clinical targets. *Clin Cancer Res* (2022) 16:CCR-22-0275. doi: 10.1158/1078-0432.CCR-22-0275

32. Masone MC. Genetically engineered CAR T cells to hack prostate cancer TME. *Nat Rev Urol* (2022) 19:255. doi: 10.1038/s41585-022-00599-w

33. Kim TJ, Lee YH, Koo KC. Current and future perspectives on CAR-T cell therapy for renal cell carcinoma: A comprehensive review. *Investig Clin Urol* (2022) 63:486–98. doi: 10.4111/icu.20220103

34. Yang M, Olaoba OT, Zhang C, Kimchi ET, Staveley-O'carroll KF, Li G. Cancer immunotherapy and delivery system: An update. *Pharmaceutics* (2022) 14 (8):1630. doi: 10.3390/pharmaceutics14081630

35. Guizhen Z, Guanchang J, Liwen L, Huifen W, Zhigang R, Ranran S, et al. The tumor microenvironment of hepatocellular carcinoma and its targeting strategy by CAR-T cell immunotherapy. *Front Endocrinol (Lausanne)* (2022) 13:918869. doi: 10.3389/fendo.2022.918869

36. Fuchsl F, Krackhardt AM. Paving the way to solid tumors: Challenges and strategies for adoptively transferred transgenic T cells in the tumor microenvironment. *Cancers (Basel)* (2022) 14(17):4192. doi: 10.3390/cancers 14174192

37. Adachi K, Tamada K. Paving the road to make chimeric antigen receptor-T cell therapy effective against solid tumors. *Cancer Sci* (2022). doi: 10.1111/ cas.15552

38. Zhang T, Liu Q, Zhu Y, Huang Y, Qin J, Wu X, et al. Lymphocyte and macrophage infiltration in omental metastases indicates poor prognosis in advance stage epithelial ovarian cancer. *J Int Med Res* (2021) 49:3000605211066245. doi: 10.1177/03000605211066245

39. Li F, Wen H, Bukhari I, Liu B, Guo C, Ren F, et al. Relationship between CNVs and immune cells infiltration in gastric tumor microenvironment. *Front Genet* (2022) 13:869967. doi: 10.3389/fgene.2022.869967

40. Xu ZW. Gene mining of immune microenvironment in hepatocellular carcinoma. *Med (Baltimore)* (2022) 101:e30453. doi: 10.1097/MD.00000 00000030453

frontiers in Endocrinology

ORIGINAL RESEARCH
published: 25 January 2022
doi: 10.3389/fendo.2021.826667

Immune Infiltration of CD8+ T Cells in Patients With Diabetic Pancreatic Cancer Reduces the Malignancy of Cancer Tissues: An *In Silico* Study

*Zheng Ye[1,2], Delin Liu[1], Dechen Liu[1,3,4], Yinqi Lv[1], Yidi Zhang[1], Jun Zhang[1], Jiantong Bao[1], Xuelu Yuan[5], Jiaying Hou[6] and Ling Li[1,3,4]**

[1] Department of Endocrinology, Zhongda Hospital, School of Medicine, Southeast University, Nanjing, China, [2] State Key Laboratory of Bioelectronics, School of Biological Science and Medical Engineering, Southeast University, Nanjing, China, [3] Institute of Glucose and Lipid Metabolism, Southeast University, Nanjing, China, [4] Department of Clinical Science and Research, Zhongda Hospital, School of Medicine, Southeast University, Nanjing, China, [5] Department of Endocrinology, Yixing Second People's Hospital, Wuxi, China, [6] Department of Endocrinology, Changji Branch, First Affiliated Hospital of Xinjiang Medical University, Xinjiang, China

OPEN ACCESS

Edited by:
Ihtisham Bukhari,
Fifth Affiliated Hospital of Zhengzhou University, China

Reviewed by:
Umar Raza,
National University of Medical Sciences (NUMS), Pakistan
Yi Jin,
Central South University, China
Wenbo Zou,
Chinese PLA General Hospital, China

***Correspondence:**
Ling Li
dr_liling@126.com

Specialty section:
This article was submitted to Cancer Endocrinology, a section of the journal Frontiers in Endocrinology

Received: 01 December 2021
Accepted: 28 December 2021
Published: 25 January 2022

Citation:
Ye Z, Liu D, Liu D, Lv Y, Zhang Y, Zhang J, Bao J, Yuan X, Hou J and Li L (2022) Immune Infiltration of CD8+ T Cells in Patients With Diabetic Pancreatic Cancer Reduces the Malignancy of Cancer Tissues: An In Silico Study. Front. Endocrinol. 12:826667. doi: 10.3389/fendo.2021.826667

Background: Although the functional damage of the diabetic pancreas can affect the postoperative recovery of pancreatic cancer patients, there is no significant difference in the prognosis of pancreatic cancer patients with a history of diabetes and ordinary pancreatic cancer patients. There is still no practical theory to explain this phenomenon.

Materials and Method: The mRNA expression profile data of 141 cases and 51 cases with clinical data of diabetes status were obtained from the TCGA database and the GEO database, respectively. The CRA001160 data set was obtained in the TISCH database. The Seurat was used to process single-cell expression profile sequencing data. The Cibersortx was used to construct a feature matrix of single-cell sequencing data and to deconvolve Bulk-RNAseq data to obtain each pancreatic cancer patients' tumour invasion score. TIDE was used to assess the immune escape potential of the tumour. MiRNet was used to construct the miRNA-mRNA regulatory network.

Result: Compared with regular pancreatic cancer patients, the immune-related signal transduction pathways in diabetic pancreatic cancer patients are in an activated state. In patients with diabetic pancreatic cancer, the infiltration score of CD8+ T cells is high, and the infiltration score of corresponding malignant tumour cells is low. The Bayesian classifier can distinguish diabetic pancreatic cancer patients from non-diabetic pancreatic cancer patients based on 10 signature genes. The miRNA-mRNA regulatory network suggests that regulation by miRNA can influence mRNA expression and thus prognostic survival of pancreatic cancer patients.

Conclusion: The activation of inflammatory-related signalling pathways in diabetic pancreatic cancer patients increases the immune infiltration of CD8+ T cells in cancer patients and reduces the development of malignant tumour tissues. The expression of 10 signature genes allowed the diagnosis of diabetic and non-diabetic pancreatic cancer

patients. The miRNA-mRNA regulatory network may be the main cause of the differences in the tumour inflammatory microenvironment between the two groups of patients. These findings help us further understand the immune microenvironment of patients with diabetic pancreatic cancer.

Keywords: pancreatic cancer, diabetes, tumor microenvironment, miRNA-mRNA regulation network, immune therapy

INTRODUCTION

Pancreatic cancer has one of the highest mortality rates of any cancer type, with an overall five-year survival (OS) rate of less than 5%. Despite the tremendous breakthroughs in cancer treatments with advances in medical technology and complementary therapies, the prognosis for pancreatic cancer patients remains poor (1, 2). Understanding the pathogenesis of pancreatic cancer and the factors that drive its rapid growth is of great importance to the treatment and control of pancreatic cancer. Numerous studies have shown that diabetes is a major risk factor for the development of pancreatic cancer. Diabetes mellitus is a metabolic disease characterised by high blood sugar. Prolonged hyperglycemia causes chronic damage and dysfunction in various tissues, especially the eyes, kidneys, heart, blood vessels and nervous system. A large number of studies have reported an epidemiological association between diabetes and pancreatic cancer. Data have shown that approximately 50% of newly diagnosed patients with pancreatic cancer are diabetic (3, 4). The incidence of pancreatic cancer among new diabetics may reach 0.85%, which is eight times higher than expected. Despite the fact that diabetes affects the recovery of patients after radiotherapy, chemotherapy and surgical resection of pancreatic cancer, there is no significant difference in the overall survival of pancreatic cancer patients with diabetes (5, 6). Although this conclusion is still controversial, no well-established theory is still available to explain the phenomenon.

The tumour microenvironment of pancreatic cancer is of great importance to the progression and metastasis of the pancreas. The pancreatic cancer microenvironment is mainly composed of cancer cells, stromal cells and extracellular components. The main cells that promote the progression of pancreatic cancer are pancreatic stellate cells (PSC), regulatory T cells (Treg), myeloid suppressor cells (MDSC) and tumour-associated macrophages (TAM). These cells can co-maintain the microenvironment through the exocrine secretion of a number of cellular matrices and inflammatory factors (7). The main features of the pancreatic cancer microenvironment are hyperdense cell proliferation and extensive immunosuppression (8). The pancreatic cancer microenvironment promotes the proliferation of pancreatic cancer and escapes immune surveillance by directly suppressing tumour immunity and inducing the proliferation and metastasis of immunosuppressed cells. No research team has focused on the characteristics of the tumour microenvironment in diabetic pancreatic cancer patients. Widespread elevated levels of inflammatory factors are present in diabetic patients (9). The increased levels of these inflammatory factors may affect the tumour microenvironment in diabetic patients with pancreatic cancer, thereby triggering crosstalk of the cellular components of the pancreatic cancer microenvironment. A recent study has shown that a high-glucose environment in tumors can promote the proliferation of immune-related cells in tumors, without significantly affecting tumour cells. The main reason for the high rate of glucose consumption by tumors is not the cancer cells, but the immune cells in the tumour tissue. All these studies suggest a complex state of the tumour microenvironment in diabetic pancreatic cancer patients (10).

In this study we compared the differences in expression profiles between diabetic and non-diabetic pancreatic cancer patients by two separate data sets (TCGA PAAD, GSE79668). The composition of the 13 types of cells in the tumour microenvironment from these bulk-RNAseq data was assessed by a matrix of features of the 13 types of cells in the pancreatic cancer microenvironment obtained from single-cell sequencing data (CRA001160), revealing differences in the tumour microenvironment of diabetic versus non-diabetic pancreatic cancer. Differential miRNAs from diabetic and non-diabetic pancreatic cancer patients were compared by TCGA PAAD miRNA sequencing data, and miRNA-mRNA regulatory networks were constructed from differentially expressed genes. These results have important implications for our further understanding of the unique characteristics of the tumour microenvironment and the progression of pancreatic cancer in diabetic pancreatic cancer patients. On the other hand, it also reveals that CD8+ T cell-based immunotherapy may be effective in pancreatic cancer; interfering with the immune microenvironment of the tumour through miRNA may be an effective means to improve the prognosis of pancreatic cancer.

METHODS

Patients and Datasets

The mRNA expression profile and microRNA expression profile data for 141 PAAD cancer samples were downloaded from the TCGA database (11) (HTTPS://portal.gdc.cancer.gov/projects/TCGA-HNSC) and included information on their clinicopathology. Among them were 35 patients with diabetic pancreatic cancer and 106 patients with non-diabetic pancreatic cancer. Fifty-one pancreatic cancer samples from GSE79668 (12) were downloaded from the GEO database (13), along with

Abbreviations: TCGA, The Cancer Genome Atlas; GEO, Gene Expression Omnibus; TIDE, Tumor Immune Dysfunction and Exclusion; GSEA, Gene Set Enrichment Analysis; PAAD, Pancreatic adenocarcinoma; TISCH, Tumor Immune Single-cell Hub.

clinicopathological information on these samples. The numbers of patients with diabetic pancreatic cancer and non-diabetic pancreatic cancer were 22, 29 respectively. The single cell expression profile matrix for CRA001160 (14) was downloaded from TISCH (15) and contains expression profile data for 57,443 single cells. Cell annotation information from the data source paper was used in this study for a total of 13 major cell types including Acinar, B, CD8Tex, Ductal, Endocrine, Endothelial, Fibroblasts, M1, Malignant, Monocyte, pDC, Plasma, Stellate.

Overexpression Analysis and GSEA

Differential analysis of mRNA expression profiles between diabetic pancreatic cancer and non-diabetic pancreatic cancer patients in PAAD samples was performed by the DESeq2 (16) package of R software (FDR<0.05, |log2foldchange|>1). Gene Ontology (GO) (17) and Kyoto Encyclopedia of Genes and Genomes (KEGG) (18) functional annotations were done for up- and down-regulated genes in diabetic pancreatic cancer by the ClusterprofileR (19) package of R software, respectively. The differentially expressed genes were ranked according to their log2foldchange and functional enrichment analysis was performed on the differentially expressed genes using GSEA (20).

Assessment of Tumour Microenvironmental Status in Pancreatic Cancer

The pancreatic cancer tumour tissue single cell sequencing dataset (CRA001160) was non-linearly dimensionalised, clustered, visualized and annotated with 13 major cell types by the Seurat package of R software (21). One hundred cells from each major cell type were randomly selected to reconstitute a pancreatic cancer tumour microenvironment expression profile of 1300 cells. The CIBERSORTx (22) was used to process the new single cell expression profiles to construct a signature matrix of these 13 major cell types. Using these 13 cell type feature matrices, the 141 pancreatic cancer patients from TCGA PAAD and 51 pancreatic cancer patients from GSE79668 were deconvoluted respectively, resulting in an ABSOLUTE score matrix of the 13 major cell types in the tumour tissues of these pancreatic cancer patients. The higher the Absolute score for a cell type, the higher the absolute percentage of this cell type in the tumour tissue. The TIDE (http://tide.dfci.harvard.edu/faq/) (23) computational framework was used to assess the functional status of T lymphocytes in the tumour microenvironment. Using the TIDE computational framework, scores for tumour immune dysfunction and immune rejection status can be obtained. These scores could be applied to assess the potential for tumour immune escape.

Construction of a Classifier for Distinguishing Pancreatic Diabetes Mellitus From Non-Pancreatic Diabetes Mellitus

In order to diagnose pancreatic cancer diabetes versus non-pancreatic cancer diabetes at the expression profile level, machine learning models were used to construct diagnostic models. Firstly, the voom function of the limma (24) package of the R software was used to transform the count matrix of the expression profile into a normalized expression profile matrix. The removebatcheffect function was then used to remove the batch effect from the TCGA PAAD dataset and the GSE79668 dataset. the TCGA PAAD dataset was used for feature extraction and machine learning model construction and the GSE79668 dataset was used to assess the generalization capability of the model. Four machine learning models (SVM, Random Forest, Naïve Bayes, Logistic Regression) were used to construct classifiers for diabetes and non-diabetes. Two metrics, ROC curve and Calibration curve, were used to evaluate the performance of the models.

Construction of miRNA-mRNA Regulatory Network and Survival Analysis

Differential expression analysis of the count matrix of miRNA expression profiles of TCGA PAAD patients (diabetic pancreatic cancer vs. non-diabetic pancreatic cancer) was done by DESeq2 of R software. The miRNAs with significant differences were obtained according to the filtering conditions of pvalue<0.001,|log2foldchange|>0.5. Venn diagrams were used to visualize the relationship between differential genes in diabetic pancreatic cancer and non-diabetic pancreatic cancer in TCGA PAAD and GSE79668. Genes that were significantly upregulated in both datasets were used to construct miRNA-mRNA regulatory networks. The miRNet (25) (https://www.mirnet.ca/) was used to construct the miRNA-mRNAt regulatory network. miRNA target genes were predicted using the miRTarBase V8.0 database (26). The network nodes were pruned according to their degree, and nodes with degree > 1 were retained. The networks were then functionally annotated by GO, KEGG and REACTOME (27) databases. Finally Kaplan-Meier Plotter (28) (https://kmplot.com/analysis/) was used to do survival analysis on the screened differential miRNAs.

Statistical Analysis

Absolute scores of cell types were compared between groups using the Wilcox test. Univariate survival analysis was performed by Kaplan-Meier survival analysis with the log-rank test. Orange3 (version:3.28) (29) was used to build machine learning models.

RESULT

Differential Expression Profiles of Tumor Tissues From Diabetic and Non-Diabetic Pancreatic Cancer Patients

In order to find differences between diabetic and non-diabetic pancreatic cancer patients, DESeq2 was used to investigate the differences in expression profiles between the two groups. In the TCGA PAAD dataset, 215 genes were upregulated and 190 genes were downregulated in cancer tissues from patients with diabetic pancreatic cancer (**Figure 1A**). 338 genes were upregulated and 79 genes were downregulated in tumour tissues from patients with diabetic pancreatic cancer (**Figure 1B**) in the GSE79668

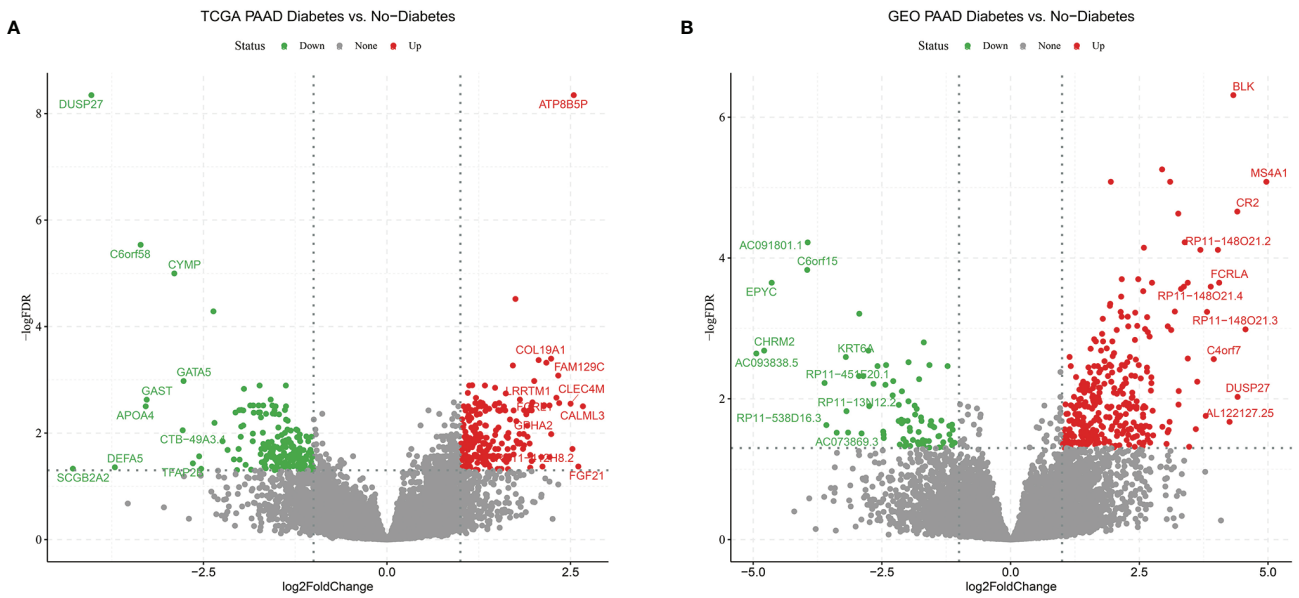

FIGURE 1 | Volcano plot **(A)** Differentially expressed genes in the TCGA PAAD dataset for diabetic vs. non-diabetic. **(B)** Differentially expressed genes between diabetic and non-diabetic in the GSE79668 dataset. FDR<0.05,abs(log2FoldChange)>1 used as cutoff value for the volcano plot.

dataset (FDR<0.05, |log2Foldchange|>1). GO and KEGG databases performed functional enrichment analysis and GSEA for upregulated and downregulated genes in these two datasets, respectively. The functional enrichment results of the TCGA PAAD dataset showed that among the up-regulated genes, the overexpressed genes analysed by GO enrichment were mainly enriched in immune response-activating cell surface receptor signaling pathway, immune response -activating signal transduction, antigen receptor-mediated signaling pathway and other signaling pathways (**Figure 2A**). The GSEA results showed that the higher ranked genes in the GO database were mainly enriched in signalling pathways such as lymphocyte migration, plasma membrane signaling receptor complex, positive regulation of leucocyte cell-cell adhesion, positive regulation of T cell activation, T cell receptor complex (**Figures 2B, C**). In the KEGG database, these upregulated genes are mainly enriched in signalling pathways such as Cytokine-cytokine receptor interaction, Primary immunodeficiency, Chemokine signaling pathway (**Figure 2D**). The GSEA results showed that the higher ranked genes in the KEGG database were mainly enriched in signalling pathways such as Chemokine signaling pathway, Cytokine-cytokine receptor interaction, Natural killer cell mediated cytotoxicity, Osteoclast differentiation, Yersinia infection (**Figures 2E, F**). The functional enrichment of the GSE79668 dataset showed that the upregulated genes in the GO database were mainly enriched in signalling pathways such as T cell activation, lymphocyte differentiation, lymphocyte proliferation (**Figure 2G**). The results of GSEA enrichment showed that Antigen binding, B cell receptor signaling pathway, immunoglobulin complex, plasma membrance signaling receptor complex, T cell receptor complex were activated in the tumor tissues of pancreatic cancer and diabetes (**Figures 2H, I**). In the KEGG database, overexpressed genes were mainly enriched in signal pathways such as Hematopoietic cell lineage, Cytokine-cytokine receptor interaction, and T cell receptor signaling pathway (**Figure 2J**). The results of GSEA enrichment showed that Chemokien signaling pathway, Cytokine-cytokine receptor interaction, JAK-STAT signaling pathway, Measles, Natural killer cell mediated cytotoxicity and other signaling pathways were in an activated state (**Figures 2K, L**). In contrast, the two datasets showed relatively large differences in the results of signalling pathway enrichment in the genes that were down-regulated (**Supplementary Figure S1**). These results suggest that inflammatory and immune-related signalling pathways are extensively activated in the tumour tissue of diabetic pancreatic cancer patients. This "hot" immune state reflects the specific tumour microenvironment of tumour tissue in diabetic pancreatic cancer patients.

Differences in the Tumour Microenvironment of Tumour Tissue in Diabetic and Non-Diabetic Pancreatic Cancer Patients

To further investigate the tumour microenvironment in diabetic patients with pancreatic cancer, the CRA001160 dataset was used to construct a signature matrix of the 13 major cell types in pancreatic cancer. We constructed a new expression profile matrix consisting of 1300 cells from 13 major cell types, 100 cells of each type were randomly selected (**Figure 3A**). The Cibersortx was used to construct a signature matrix of the pancreatic cancer tumour microenvironment. Ultimately, a feature matrix of 13 cell types, consisting of 3706 genes, was constructed (**Figure 3B**). Each cell type has its own unique

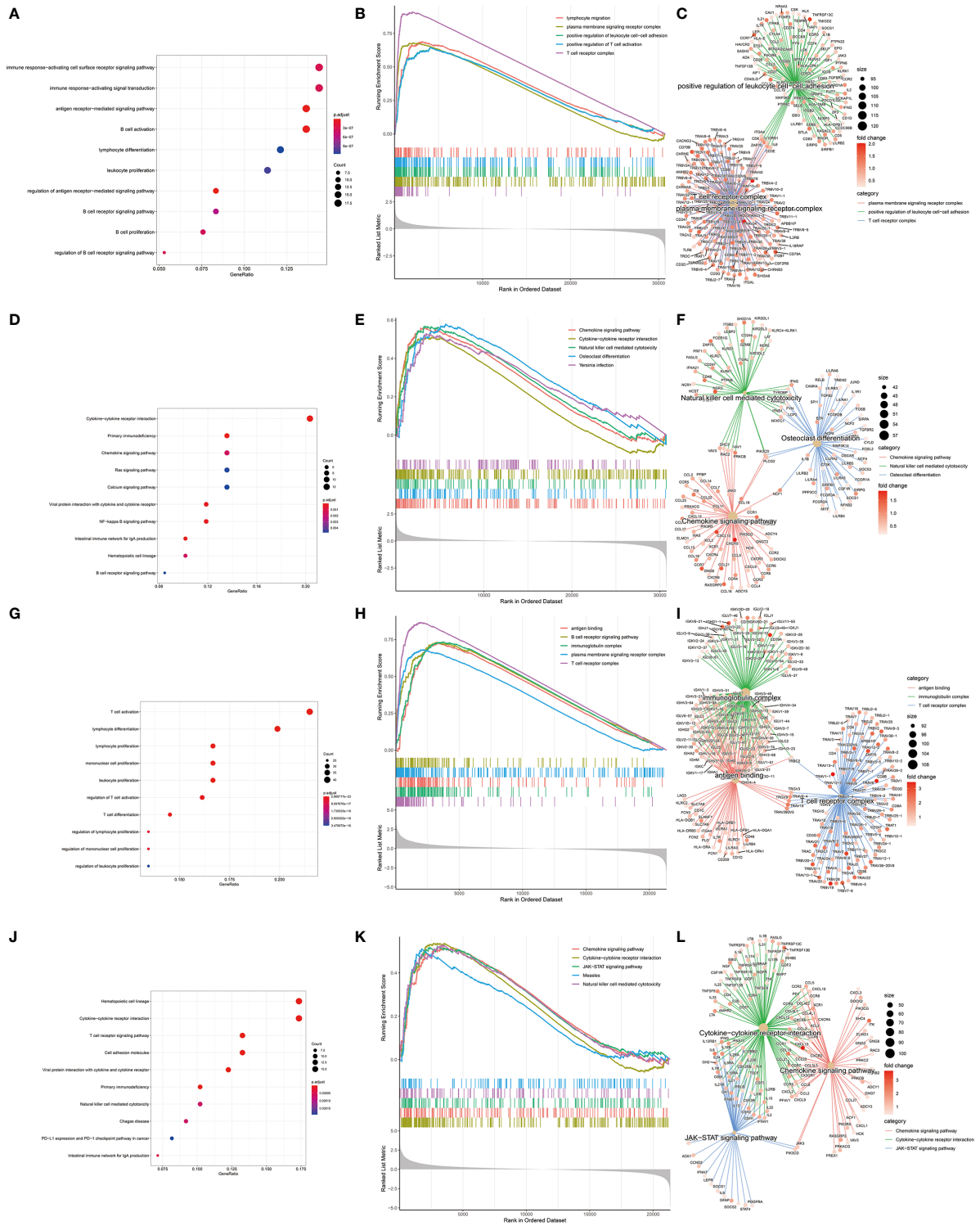

FIGURE 2 | KEGG, GEO enrichment analysis of upregulated genes in diabetic pancreatic cancer patients and GSEA results. **(A–C)** Functional enrichment of GO overexpressed genes, GSEA and gene regulatory networks in the TCGA PAAD dataset, respectively. **(D–F)** Functional enrichment of KEGG overexpressed genes, GSEA and gene expression regulatory network in TCGA PAAD dataset, respectively. **(G–I)** Functional enrichment of GO overexpressed genes, GSEA and gene expression regulatory network in the GSE79668 dataset, respectively. **(J–L)** is the functional enrichment of KEGG overexpressed genes, GSEA and gene expression regulatory network in the GSE79668 dataset, respectively.

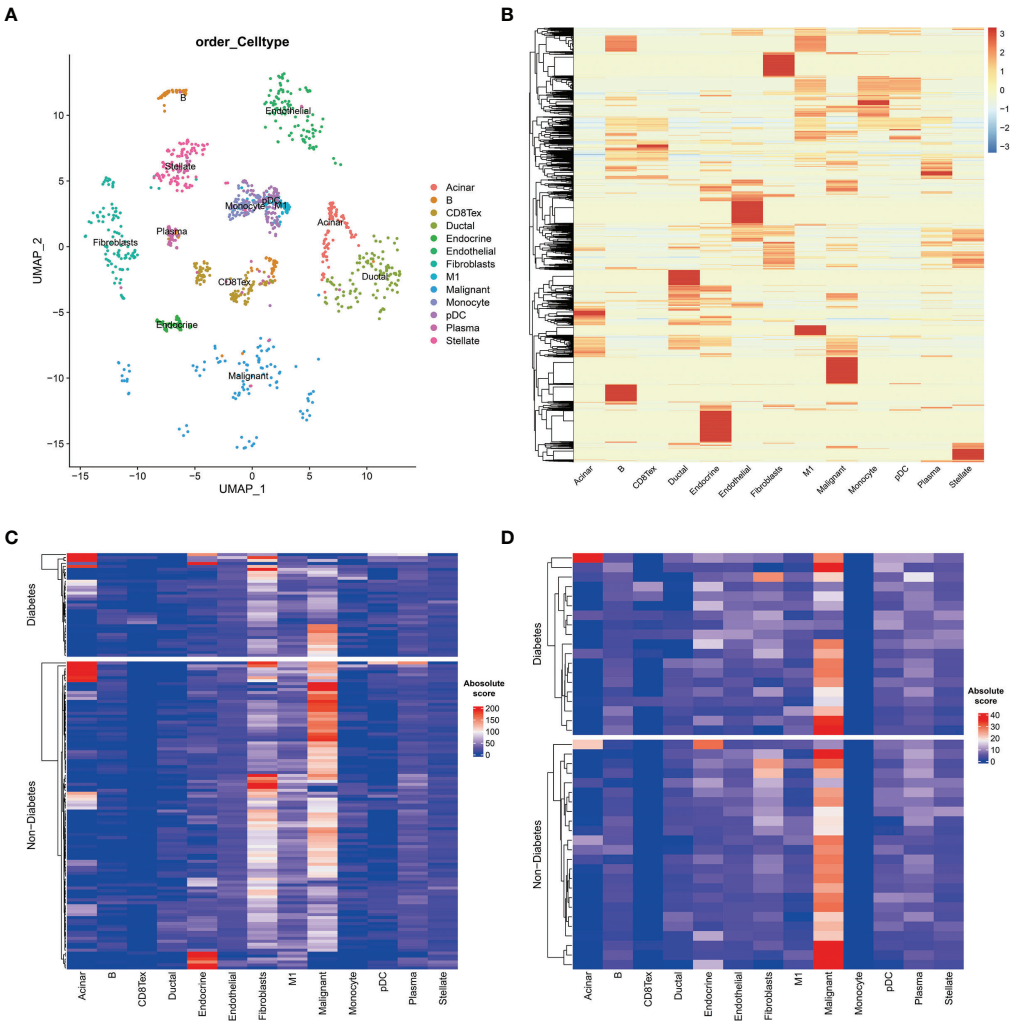

FIGURE 3 | Cell type expression profile signature matrix. From the 13 clustered cell populations of the PAAD scRNAseq dataset, 100 cells of each cell type were randomly screened and the expression profile feature matrix of these cell types was obtained by the CIBERSORTX algorithm. **(A)** Two-dimensional scatter clustering plot of umap for the 13 cell types obtained by PAAD scRNAseq. **(B)** Feature matrices obtained by the CIBERSORTX algorithm. **(C)** Absolute score clustering heat map of the 13 cells from the TCGA PAAD dataset. **(D)** Absolute score clustering heat map of 13 cells from the GSE79668 dataset.

expression pattern. The signature matrix was used to deconvolve the bulk-RNAseq matrix. We eventually obtained heat maps of the tumour microenvironment distribution for the TCGA PAAD dataset (**Figure 3C**) and the GSE79668 dataset (**Figure 3D**). As can be observed from the figure, the tumour immune microenvironment showed significant differences in both Diabetes and Non-Diabetes in the two independent datasets. In the TCGA PAAD dataset, CD8Tex was significantly higher in the Diabetic pancreatic cancer than in the Diabetic group ($p<0.01$), while the opposite was true for Malignant ($p<0.01$). Fibroblast and Malignant are the most predominant components of pancreatic cancer tissue (**Figure 4A**). In the GSE79668 dataset, we similarly found that CD8Tex immune infiltration was significantly higher in diabetic pancreatic cancer patients than in the non-diabetic group ($p<0.01$), while Malignant composition was significantly lower than in the non-diabetic group ($p<0.05$) (**Figure 4B**). It further suggests that the tumour microenvironment in pancreatic cancer diabetes is in a "hot" immune state and that malignant cell infiltration is significantly lower in this state. To further elucidate the characteristics of the immune microenvironment in pancreatic cancer tumour tissue, the Absolute Score of 13 cells was used to calculate the correlation of these cells. The results suggest that Malignant showed a significant negative correlation with Endocrine, Endothelial, Fibroblast, pDC, Plasma, and Stellate in the TCGA PAAD dataset ($p<0.05$). CD8Tex, on the other hand, showed a significant positive correlation ($p<0.05$) with B cells, pDC, and Stellate cells, and a negative correlation with M1 (**Figure 4C**), where CD8Tex and Malignant's Absolute Score showed a significant negative correlation ($R=-0.32$, $p<0.001$) (**Figure 4D**). Malignant showed a negative correlation with Endocrine, Fibroblasts, Stellate in the GSE79668 dataset ($p<0.05$). CD8Tex showed a positive correlation ($p<0.05$) with Monocle (**Figure 4E**).

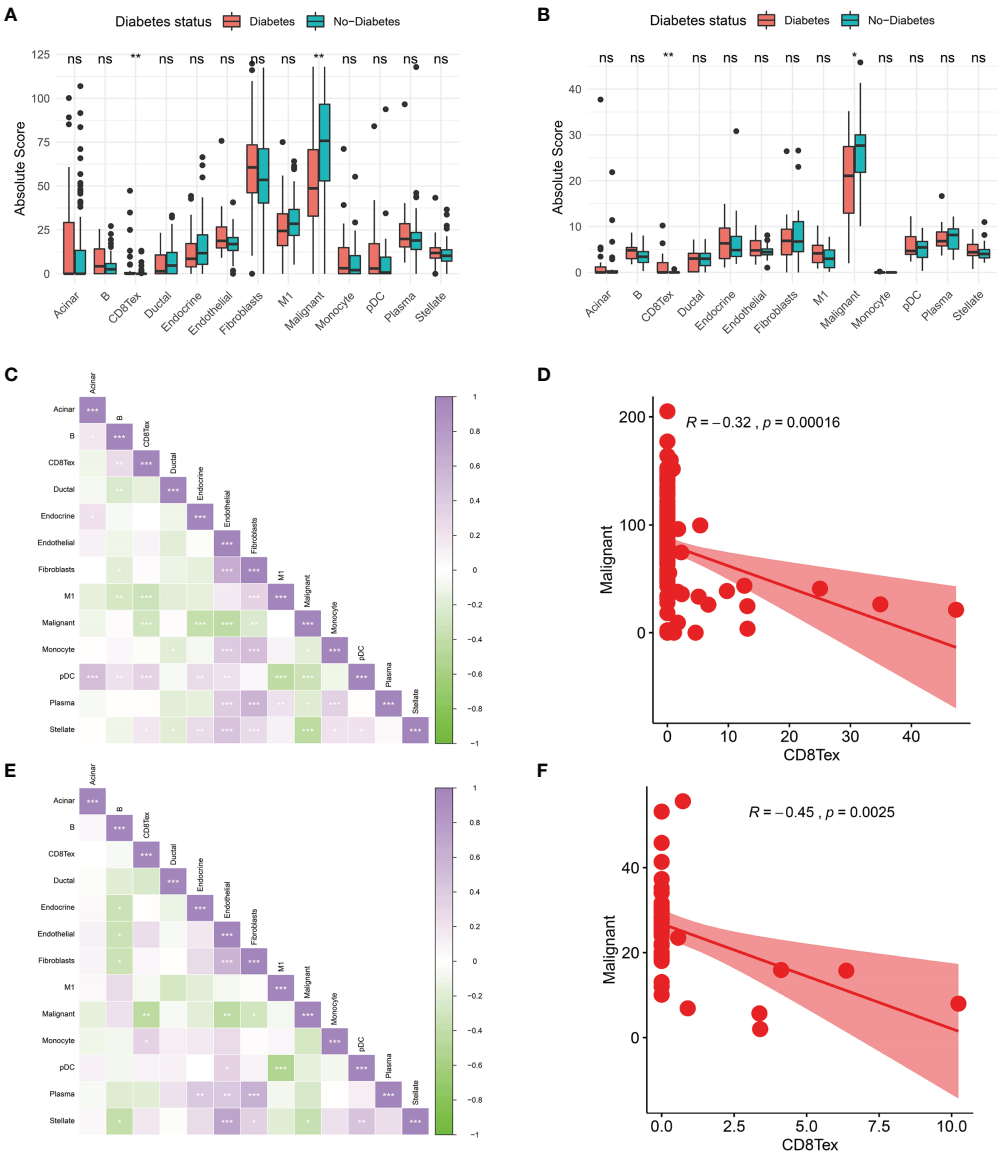

FIGURE 4 | Comparison of the tumor immune microenvironment in patients with diabetic pancreatic cancer versus non-diabetic pancreatic cancer. **(A)** Mean value test of Absolute Score of tumor tissues of 13 cells in the TCGA PAAD dataset. **(B)** Mean value test (wilcox-test) of Absolute Score of tumour tissue from 13 cells in the GSE79668 dataset. **(C)** Correlation of Absolute scores of 13 cell types in the TCGA PAAD dataset. **(D)** Correlation of Malignant and CD8Tex in the TCGA PAAD dataset. **(E)** Correlation of Absolute scores of 13 cell species in the GSE79668 dataset. **(F)** Correlation between Malignant and CD8Tex in the GSE79668 dataset. (Spearman correlation test). ns, Not Significant, *p < 0.05, **p < 0.01, ***p < 0.001.

In the GSE79668 dataset, CD8Tex and Malignant also showed a significant negative correlation (R=-0.45, p<0.01) (**Figure 4F**). These results suggest a relationship between cells in the unique tumour microenvironment of diabetic pancreatic cancer.

Relationship Between Tumour Microenvironment and Prognosis of Pancreatic Cancer Patients

Based on the Absolute Score obtained by CibersortX, it is possible to assess the relationship between the cells that make up the tumour microenvironment of pancreatic cancer and the prognostic survival of the cancer. Immune infiltration of M1 in the TCGA PAAD dataset was then a high risk factor for pancreatic cancer (**Figure 5A**, HR=1.03, p<0.01), in both diabetic and non-diabetic groups (**Figure 5B**). Malignant was also a high risk factor for pancreatic cancer (**Figure 5C**, HR=1.01, p<0.05), however it showed no significance in the diabetic group. A higher Endocrine score was a beneficial factor for pancreatic cancer (**Figure 5A**, HR=0.98, p<0.05), a result that was the same in the non-diabetic group, yet showed greater individual variability in the diabetic group (**Figure 5D**). The results of the Kaplan-Miere survival analysis showed that

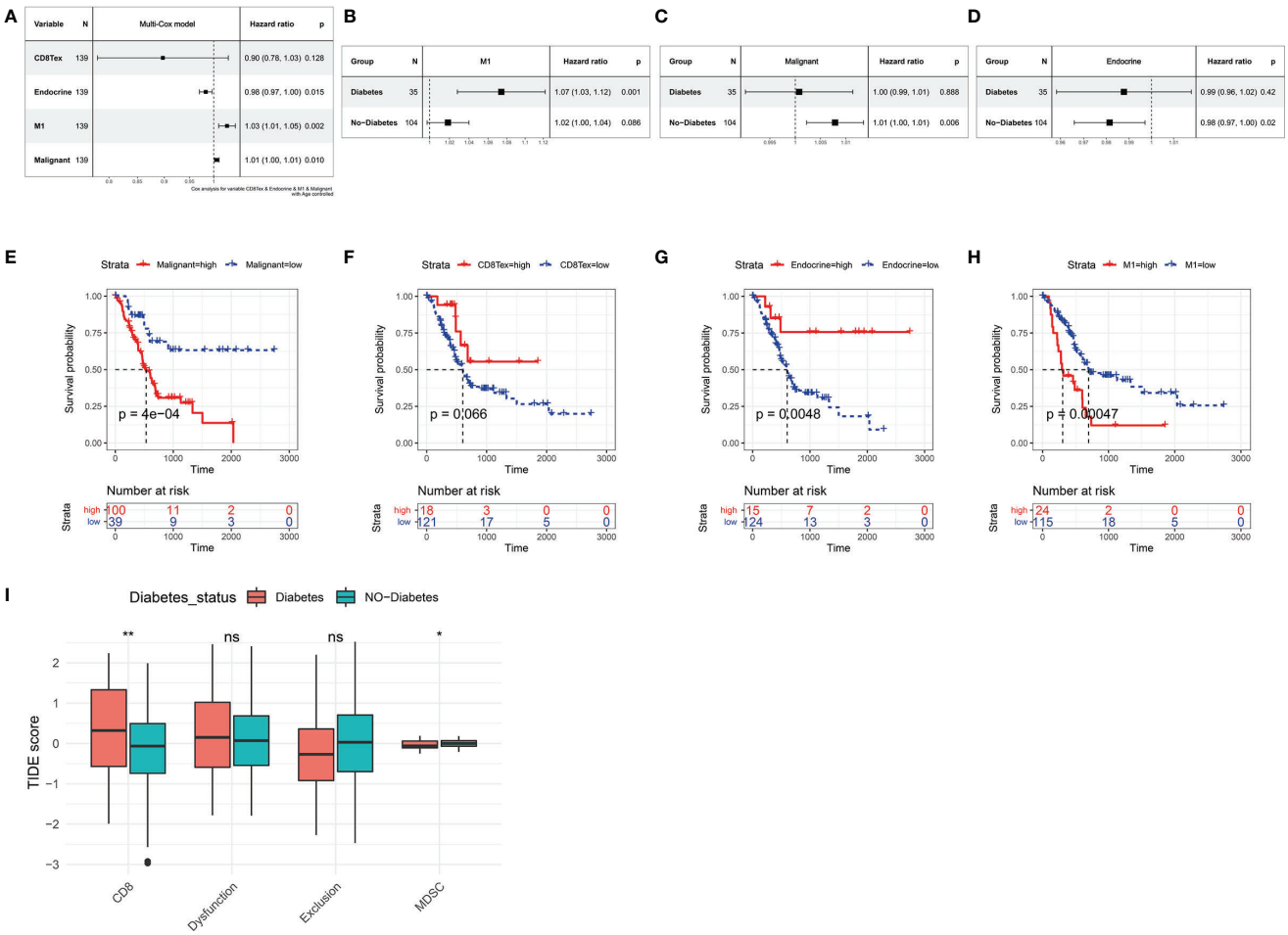

FIGURE 5 | Relationship between tumor microenvironment components and prognostic survival of cancer patients in the TCGA PAAD dataset. **(A)** Relationship between the proportion of CD8Tex, Endocrine, M1, Malignant in the tumor microenvironment and the prognosis of PAAD patients. **(B)** Relationship between immune infiltration of M1 cells and prognostic survival in diabetic and non-diabetic pancreatic cancer patients. immune infiltration of M1 cells is a high risk factor in diabetic pancreatic cancer patients. **(C)** Relationship between infiltration of Malignant cells and prognostic survival in diabetic and non-diabetic pancreatic cancer patients. In non-diabetic pancreatic cancer, infiltration of Malignant is a high risk factor. **(D)** Association of Endocrine cell scoring in the tumour microenvironment with prognostic survival in patients with diabetic and non-diabetic pancreatic cancer. In patients with non-diabetic pancreatic cancer, the proportion of Endocrine was a beneficial factor. **(E–H)** The Absolute scores of Malignant, CD8Tex, Endocrine, and M1 were used to group PAAD patients and compare the differences in prognostic survival between patients in higher and lower groups, respectively. **(A–D)** All used one-way cox proportional regression models to assess HR for risk factors, logrank was used to test the statistical significance of the results, and all used the patient's age as a correction factor. **(I)**TIDE computational framework to assess the immune functional status of the tumour microenvironment. ns, Not Significant, *p < 0.05, **p < 0.01, ***p < 0.001.

patients with high CD8Tex and Endocrine scores showed better prognostic survival, while patients with high Malignant and M1 scores showed poorer prognostic survival (**Figures 5E–H**). However, in the GSE79668 dataset, the results of the survival analysis were not statistically significant due to the small number of samples (**Supplementary Figure S2**).

Comparison of Immune Cell Function in the Immune Microenvironment of Diabetic Pancreatic Cancer and Non-Diabetic Pancreatic Cancer

In our previous study, we found a higher degree of immune infiltration of CD8Tex in the tumour microenvironment of diabetic pancreatic cancer patients compared to normal pancreatic cancer. To further investigate the functional status of these CD8Tex in pancreatic cancer diabetes, the TIDE calculation framework was used to assess the immune dysfunction and exclusion status of pancreatic cancer tumour tissue. We combined TCGA PAAD and GSE79668 to assess the tumour immune status of each sample using the TIDE calculation framework (**Figure 5I**). The results showed that the score of CD8 was higher in diabetic pancreatic cancer compared to non-diabetic pancreatic cancer (wilcox.test,p<0.001), while the score of Myeloid-derived suppressor cells was lower (wilcox.test, p<0.05). This result is consistent with the previous findings, suggesting that the tumour microenvironment in diabetic

pancreatic cancer is in a "hot" immune state. DysFunction scores did not differ significantly between the two groups, indicating that the immune function of T lymphocytes in the tumour microenvironment of pancreatic cancer did not significantly diverge between the two subgroups. In addition, although Exclusion scores did not show a significant difference between the two subgroups, immune infiltration scores were lower in the diabetic pancreatic cancer group ($p<0.1$). The above findings suggest that diabetic pancreatic cancer patients have a higher degree of immune infiltration of T lymphocytes than non-diabetic patients, and that the immune function status of T lymphocytes may be even better.

Construction of a Classifier for Diabetic and Non-Diabetic Pancreatic Cancer Patients

141 cases from the TCGA PAAD dataset were used to train a machine learning classifier for differentiating pancreatic cancer diabetes from non-pancreatic cancer diabetes. Using Gini ratio, we obtained 10 signature genes from the TCGA PAAD dataset for differentiating pancreatic cancer diabetes from non-pancreatic cancer diabetes (**Table 1**). The 10 genes are RASIP1, CCDC30, TTC30B, PSENEN, IKZF3, SETDB2, HCN3, TMEM190, EEF1A1P5, C6orf62. Leave one out was used to assess the stability of four machine learning models. The AUC, CA, F1, Precision, Recall were used to assess the predictive power of the models. The results show that the Naïve Bayes classifier performs best in this binary classification task (**Table 2**, **Figures 6A, B**). In the validation set, the Naïve Bayes classifier also obtained the best performance (**Table 3** and **Figures 6C, D**). We constructed a Nomogram of the Naïve Bayes classifier based on these 10 features (**Figure 6E**). The main role of this model is to be used to classify the large number of samples with unlabelled diabetes status in the GEO database, thus helping the researcher to obtain a larger number of usable samples.

Immune-Related miRNA-mRNA Regulatory Network in Diabetic Pancreatic Cancer Tumor Tissue

MiRNAs can influence the regulation of gene expression by interfering with the expression of mRNAs. Given that diabetic pancreatic cancer has a specific "hot" immune state in the tumour microenvironment, the miRNA-mRNA regulatory network may be important for the maintenance of this immune state. TCGA PAAD miRNA expression profile data were used for differential expression analysis of diabetic pancreatic cancer versus non-diabetic pancreatic cancer (**Figure 7A**). Based on the filtering criteria of pvalue<0.001, |log2Foldchange|>0.5, we obtained four miRNAs upregulated in diabetic pancreatic cancer (hsa-mir-301a, hsa-mir-3065, hsa-mir-205, hsa-mir-592) and one downregulated miRNA (hsa-mir-150). By combining the results of TCGA PAAD and GSE79668, we found 36 genes upregulated in diabetic pancreatic cancer (**Figure 7B**). Using the miRNet, we constructed a miRNA-mRNA regulatory network (**Figure 7C**). TLR10, MS4A1, BTLA were the main nodes linking the miRNA regulatory module to the mRNA regulatory module. kEGG, Reactome, GO : BP databases were used for functional enrichment analysis of genes in the regulatory network, respectively. The results of the KEGG functional enrichment showed that this regulatory network is mainly associated with Prostate cancer, Rheumatoid arthritis, Fatty acid metabolism, etc (**Figure 7D**). The results of the functional enrichment of the Reactome database indicate that this regulatory network is mainly associated with TCR signaling, PIP3 activates AKT signaling, PI3K events in ERBB4 signaling, etc (**Figure 7E**). The results of the functional enrichment of the GO : BP database indicate that

TABLE 1 | Feature gene extraction.

Gene	Info. gain	Gain ratio	Gini	ANOVA	χ^2	ReliefF	FCBF
RASIP1	0.135	0.067	0.049	4.037	3.577	0.042	0.106
CCDC30	0.127	0.064	0.059	3.837	1.761	0.028	0.100
TTC30B	0.114	0.057	0.056	4.196	5.255	0.013	0.000
PSENEN	0.107	0.054	0.047	3.150	1.360	0.035	0.000
IKZF3	0.106	0.053	0.047	6.338	4.898	0.025	0.082
SETDB2	0.104	0.052	0.046	4.631	1.181	0.051	0.000
HCN3	0.104	0.052	0.045	4.594	7.702	0.041	0.000
TMEM190	0.103	0.051	0.056	8.716	10.614	0.025	0.079
EEF1A1P5	0.099	0.049	0.043	8.858	7.268	0.000	0.076
C6orf62	0.097	0.049	0.047	11.060	8.161	0.026	0.000

TABLE 2 | Evaluate the model with leave one out.

Model	AUC	CA	F1	Precision	Recall
SVM	0.447	0.710	0.626	0.560	0.710
Random Forest	0.784	0.761	0.687	0.726	0.761
Naive Bayes	0.914	0.870	0.873	0.880	0.870
Logistic Regression	0.660	0.732	0.677	0.665	0.732

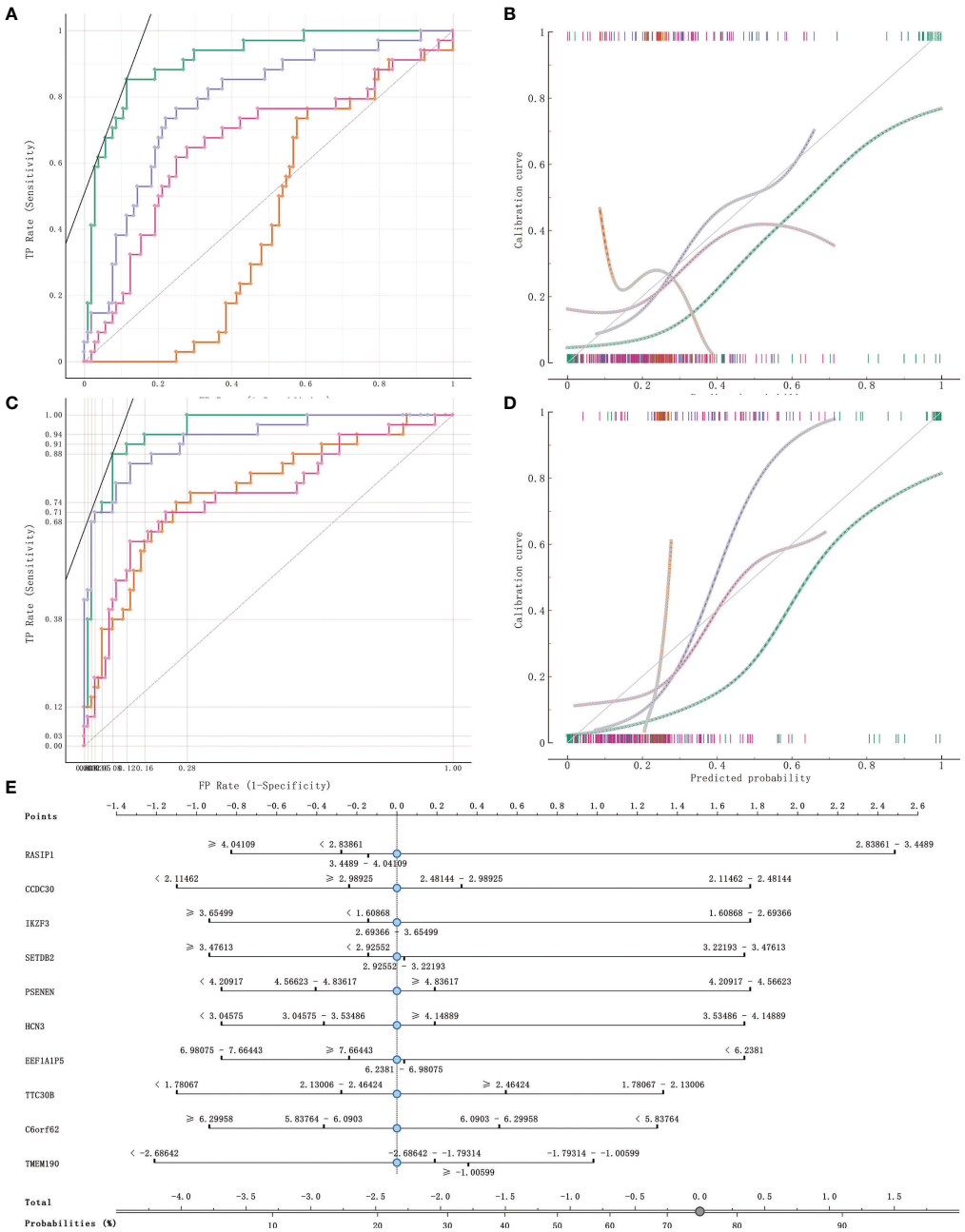

FIGURE 6 | Model evaluation and model validation of classification models. **(A, B)** training dataset (TCGA PAAD sample set) used to evaluate AUC and model correction curves for 4 classifiers. **(C, D)** testing dataset (GSE79668) used to evaluate AUC and model correction curves for 4 classifiers. **(E)** The nomogram plot of the naïve Bayesian model. Green refers to Naïve Bayes, orange to SVM, cyan blue to RandomForest and rose to logistic regression.

TABLE 3 | Classifier model testing.

Model	AUC	CA	F1	Precision	Recall
SVM	0.771	0.783	0.710	0.831	0.783
Random Forest	0.928	0.841	0.810	0.868	0.841
Naive Bayes	0.954	0.891	0.894	0.903	0.891
Logistic Regression	0.758	0.775	0.722	0.754	0.775

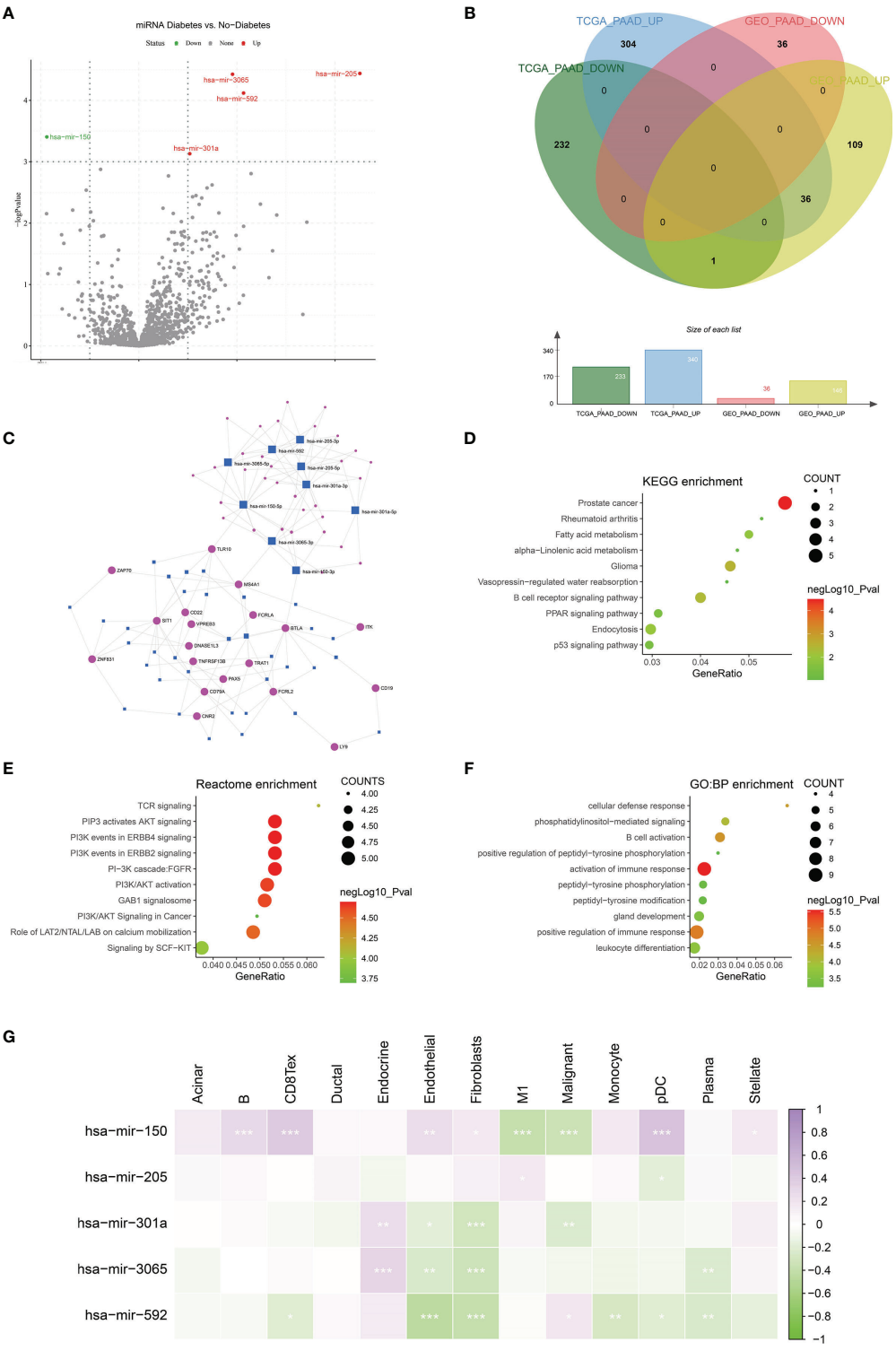

FIGURE 7 | Construction of miRNA-mRNA regulatory network. **(A)** Differential expression analysis was performed on the Diabetes and no-diabetes subgroups of the TCGA PAAD miRNA dataset to find miRNAs that were significantly different between the two groups.**(B)** Screening of the intersection of differentially expressed genes from the TCGA PAAD dataset and the GSE79668 dataset. 36 genes that were highly expressed in pancreatic cancer diabetic patients were screened. genes were screened out. **(C)** Construction of miRNA-mRNA network interactions maps based on differentially expressed miRNAs and mRNAs. **(D–F)** Functional enrichment analysis of miRNA-mRNA regulatory networks. miRNA-mRNA networks are functionally enriched, mainly in immune and cancer-related signalling pathways. **(G)** The relationship between miRNAs and cellular infiltration in tumor microenvironment cells (Spearman correlation test, *p < 0.05, **p < 0.01, ***p < 0.001).

this regulatory network is mainly associated with cellular defense response, The results of functional enrichment in the GO : BP database suggest that this regulatory network is mainly associated with cellular defense response, phosphatidylinositol-mediated signaling, B cell activation and other signaling pathways (**Figure 7F**). To reveal the relationship between miRNAs and the tumour microenvironment, we calculated the spearman correlations of hsa-mir-150, hsa-mir205, hsa-mir-301a, hsa-mir-3065, hsa-mir-592 with 13 cell types (**Figure 7G**). The results showed that hsa-mir-150 positively correlated with B, CD8Tex, Endothelial, Fibroblasts, pDC, and Stellate cells ($p<0.05$), while negatively correlated with M1 and Malignant ($p<0.05$). This result suggests that hsa-mir-150 can promote the proliferation of cancer inflammation-related cells and inhibit cancer progression. Hsa-mir-301a was negatively correlated with Endothelial ($p<0.05$), Fibroblasts, and Malignant, and positively correlated with Endocrine ($p<0.05$). It suggests that hsa-mir-301a may promote the maintenance of Endocrine and inhibit cancer progression. Hsa-mir-3065 was positively correlated with Endocrine ($p<0.05$) and negatively correlated with Endothelial, Fibroblasts, and Plasma ($p<0.05$), this result suggests that hsa-mir-3065 may be important for maintaining Endocrine and inhibiting vascularization and fibrosis in tumor tissues.Hsa-mir-592 was negatively correlated with CD8Tex, Endothelial, Fibroblasts, Monocyte, pDC, and Plasma ($p<0.05$) and negatively correlated with Malignant ($p>0.05$), suggesting that its role in the tumour microenvironment may primarily be to inhibit tumour vascularisation and fibrosis and promote cancer progression. To demonstrate the important role of these miRNAs, the Kaplan-Meier Plotter was used to assess the relationship between these five miRNAs and prognostic survival of cancer patients. The results showed that high expression of hsa-mir-3065 (**Figure 8A**, HR=0.5, $p<0.01$),hsa-mir-592 (**Figure 8B**, HR=0.64, $p<0.05$), hsa-mir-301a (**Figure 8C**, HR=0.55, $p<0.05$),hsa-mir-150 (**Figure 8D**, HR=0.71, $p=0.095$) was a pancreatic cancer beneficial factor, while high expression of hsa-mir-205 was a risk factor for pancreatic cancer (**Figure 8E**, HR=1.99, $p<0.01$). These results demonstrate that we can modulate the miRNA-mRNA regulatory network through miRNAs, thereby altering the state of the tumour immune microenvironment in pancreatic cancer tissues and thereby improving the prognostic survival of pancreatic cancer patients.

DISCUSSION

Diabetes mellitus and pancreatic cancer are two interrelated diseases. The results of some studies suggest that diabetes has no significant effect on the duration of OS (5, 30). However, other studies have shown that diabetes significantly reduces OS (31, 32). A recent meta-analysis has shown that diabetes is associated with increased overall mortality in patients with pancreatic cancer and that patient survival also depends on the stage of the tumour and the duration of diabetes (33). These results suggest a complex mechanism for the presence of diabetes in patients with pancreatic cancer.

In this study, we explored differences in the tumour microenvironment between diabetic and non-diabetic pancreatic cancers. We studied two separate datasets with diabetic status in pancreatic cancer patients, from the TCGA-PAAD dataset and the GSE79668 dataset, respectively. After differential analysis, overexpression analysis and GSEA analysis, we found that immune and inflammation-related signalling pathways were activated in the tumour tissues of diabetic pancreatic cancer patients relative to the normal pancreatic cancer patients. The "hot" immune status of pancreatic cancer tumor tissue means higher immune cell infiltration and better prognosis for survival (34). The "hot" immune state in the tumor tissue of diabetic pancreatic cancer patients is most probably due to their diabetes-induced chronic inflammatory response (35). To further explore the composition of the pancreatic cancer tumour microenvironment at the cellular level, we constructed a matrix of immune cell infiltration characteristics of 13 pancreatic cancer microenvironments using single cell sequencing data to analyse the differences in the cellular composition of the tumour microenvironment in diabetic pancreatic cancer patients compared to non-diabetic pancreatic cancer patients. The results showed that CD8Tex scores were higher and Malignant cell scores were lower in diabetic pancreatic cancer compared to normal pancreatic cancer patients. Significant differences were found between the two subgroups. A significant negative correlation was shown between CD8Tex and Malignant. This suggests that immune infiltration of CD8Tex can significantly reduce the malignant progression of pancreatic cancer. It is in general accordance with the pathological section data from the TCGA-PAAD dataset (**Supplementary Figure S3**). We also found that the mean scores of Acinar cell, B cell and stellate cell were higher in diabetic pancreatic cancer, although less significant. The findings of the tumour microenvironment scores were consistent for both datasets. This non-significance may be caused by the small number of diabetic pancreatic cancer samples. CD8+ cytotoxic T cells are the main functional cells of cellular immunity, which can directly recognize tumour cells and secrete cytotoxic factors such as perforin and granzyme to kill tumour cells (36). A recent systematic appraisal and meta-analysis has shown that high tumour infiltration of T cells in pancreatic cancer promises better survival, and in particular that high infiltration of CD8+ T cells leads to better prognostic outcomes. T-cell infiltration located at the centre of the tumour has the greatest impact on cancer survival (37). Evidence from another study suggests that the spatial distribution of CD8+ T cells in the tumour microenvironment of pancreatic ductal carcinoma has an important impact on prognosis (38). From our results, patients with high CD8+ T cell immune infiltration had better prognostic survival. CD8+ T cells improve prognostic survival by killing malignant tumour cells and thus inhibiting their progression. Although the prognostic survival of diabetic pancreatic cancer patients with high infiltration of CD8+ T cells was not significantly improved in our study, it suggests that the two diseases, diabetes and pancreatic cancer, show a complex pattern of relationship in the tumour tissue of patients with diabetes combined with pancreatic cancer. Furthermore, we

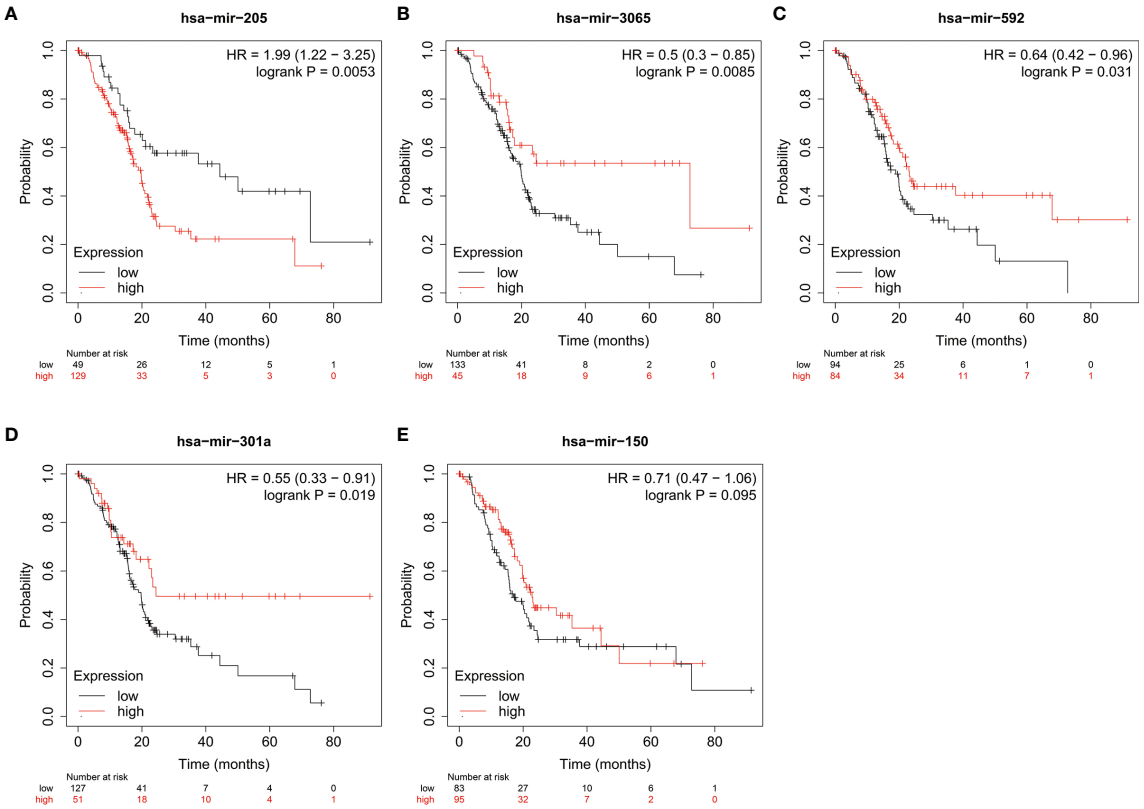

FIGURE 8 | The relationship between miRNA and prognostic survival of PAAD patients. **(A–C)** High expression of hsa-mir-3065 (HR=0.50, $p < 0.01$), hsa-mir-592 (HR=0.64, $p<0.05$) and hsa-mir-301a (HR=0.55, $p < 0.05$) is a beneficial factor for PAAD. **(D)** High expression of hsa-mir-150 was a beneficial factor for PAAD, although not significant (HR=0.71, $0.05<p<0.1$). **(E)** High expression of hsa-mir-205 is a high risk factor for PAAD (HR=1.99, $p < 0.01$).

found that high infiltration of Malignant and M1 cells correlated highly with prognostic survival in pancreatic cancer. In the TCGA PAAD dataset, immune infiltration of M1 was a high risk factor for pancreatic cancer prognosis in both the diabetic and non-diabetic groups.

We estimated the functional status of T lymphocytes in pancreatic cancer diabetes versus non-pancreatic cancer diabetes using the TIDE computational framework. The results showed that there was no significant difference in the dysfunctional scores of T lymphocytes between the two subgroups, while the immune escape scores of T lymphocytes may have been lower in the diabetic pancreatic cancer group. These findings suggest that T lymphocytes in the tumour microenvironment of diabetic pancreatic cancer patients are not only more infiltrated than in non-diabetic patients, but may also be more functional.

In addition, we constructed a Naïve Bayes classifier using a machine learning approach. This classifier has excellent classification ability to distinguish patients with diabetic pancreatic cancer from those with non-diabetic pancreatic cancer. This classifier could be used to automatically classify pancreatic cancer RNA sequencing data in databases without diabetes status annotation, thereby expanding the sample size for pancreatic cancer diabetes studies. No research team has done anything related to this so far.

Diabetic pancreatic cancer is in a “hot” immune state, and miRNAs may be critical in maintaining such an immune state. Through differential expression analysis, we identified five significantly differentially expressed miRNAs from the TCGA PAAD miRNA expression profile dataset, including hsa-mir-301a, hsa-mir-3065, hsa-mir-205, hsa-mir-592 and hsa-mir-150. The results of the Kaplan-Miere survival analysis show that these genes are prognostically essential in pancreatic cancer.Hsa-mir-301a can promote pancreatic cancer progression by down-regulating the SMAD4 gene (39). Hsa-mir-3065 can affect the growth of melanoma cells through multiple antitumor effects. However, its relevance to pancreatic cancer has been relatively little studied (40). Hsa-mir-205 is a highly conserved miRNA whose regulated genes are mainly involved in tumourigenesis, progression, cellular value-added and epithelial-to-mesenchymal transition processes. miRNA-205 is a potential biologic drug for cancer therapy (41). Gemcitabine combined with miRNA-205 regimen shows promising results in patients with advanced pancreatic cancer (42). High expression of Hsa-mir-592 can promote the value-added migration of colon cancer (43), and mir-592 in serum can be used as an early diagnostic marker for colon cancer (44). Hsa-mir-150 can promote the progression of non-small cell lung cancer by targeting FOXO4 (45). hsa-mir-

150 can act as a plasma marker (46) of pancreatic cancer progression and a prognostic marker (47). All these studies have demonstrated the importance of these five miRNAs in the diagnosis and treatment of cancer. *via* miRNet, we construct miRNA-mRNA regulatory networks for differentially expressed miRNAs and mRNAs. Functional enrichment analysis of the KEGG, Reactome, and GO : BP databases revealed that these genes are closely related to the inflammatory response. Three genes, TLR10, MS4A1, and BTLA, are the hub genes linking the miRNA regulatory module and the mRNA regulatory module. TLR10 is a member of a family encoding toll-like receptors (TLRs) that perform important roles in pathogen recognition and activation of the innate immune system (48). MS4A1, also known as CD20, encodes a B-lymphocyte surface molecule that plays a role in the development and differentiation of B cells into plasma cells. CD20-positive pancreatic cancers with a high degree of B-cell infiltration have a better prognostic survival rate (49). The protein encoded by BTLA (CD272) contains an immunoglobulin (Ig) structural domain and is a receptor that transmits inhibitory signals as well as suppressing immune responses. It has been shown that BTLA can be considered as a prognostic marker for pancreatic cancer (50). In the miRNA regulatory module, we found that the direct targets of action of these miRNAs include a large number of oncogene (e.g. TP53, PTEN, ERBB3, etc.). It illustrates the potential of these miRNAs as gene therapy agents. These results suggest that miRNAs can influence the state of the pancreatic cancer tumour microenvironment through the regulation of their target genes, thereby improving prognostic survival in pancreatic cancer.

In summary, we have discovered differences in the tumour microenvironment between diabetic and non-diabetic pancreatic cancers for the first time and compared the differences between the two at the genetic and cellular levels. The "hot" immune state of diabetic pancreatic cancer may contribute to the reduction of malignant cells in the pancreatic cancer tumour microenvironment, thus affecting the progression and prognosis of diabetic pancreatic cancer.

DATA AVAILABILITY STATEMENT

The datasets presented in this study can be found in online repositories. The names of the repository/repositories and accession number(s) can be found in the article/**Supplementary Material**.

AUTHOR CONTRIBUTIONS

ZY: Methodology, Software, Validation, Formal analysis, Investigation, Writing-Original Draft, Data Curation, Supervision. DLL: Writing- Review & Editing, Formal analysis, Investigation, Data Curation. DCL: Formal analysis, Investigation YZ: Software, Validation. YL: Visualization, Supervision. JZ: Visualization, Supervision, Methodology. JB: Writing- Review & Editing. XY: Data Curation, Supervision. JH: Methodology. LL: Conceptualization, Project administration, Visualization, Supervision, Methodology, Investigation Supervision. All authors contributed to the article and approved the submitted version.

FUNDING

This work was supported by National Natural Science Foundation of China (81970717, 82000740 and 82170845), grants from the Key Research & Development Program of Jiangsu Province (BE2018742).

SUPPLEMENTARY MATERIAL

The Supplementary Material for this article can be found online at: https://www.frontiersin.org/articles/10.3389/fendo.2021.826667/full#supplementary-material

Supplementary Figure S1 | KEGG, GEO analysis of upregulated genes in non-diabetic pancreatic cancer patients and GSEA enrichment analysis of patients. **(A–C)** GO functional enrichment, GSEA and gene regulatory network maps in the TCGA PAAD dataset, respectively. **(D–F)** KEGG functional enrichment, GSEA and gene expression regulatory network from TCGA PAAD dataset, respectively. **(G–I)** GO functional enrichment, GSEA and gene expression regulatory network from GSE79668 dataset, respectively.

Supplementary Figure S2 | Relationship between tumor microenvironment components and prognostic survival of cancer patients in the GSE79668 dataset. **(A)** Relationship between scores of CD8Tex, Endocrine, M1, and Malignant and prognostic survival of patients. **(B)** Comparison of prognostic survival of patients grouped with high and low tumour immune scores of Malignant. The results showed some difference but not significant ($0.05<p<0.1$).

Supplementary Figure S3 | Comparison of H&E staining of diabetic pancreatic cancer vs. non-diabetic pancreatic cancer tissues. Diabetic pancreatic cancer tissue sections(A: TCGA-IB-AAUR-01A-02-TSB,C:TCGA-IB-AAUP-01A-01-TSA, E:TCGA-Q3-A5QY-01A-01-TSA) and non-diabetic pancreatic cancer tissue sections (B:TCGA-HV-A7OP-01A-TS1,D: TCGA-2L-AAQJ-01A-TS1, F:TCGA-FB-AAPP-01A-01-TSA) obtained from the TCGA-PAAD dataset. The diabetic pancreatic cancer tissue section has a more pronounced lymphocytic infiltration, while the non-diabetic pancreatic cancer tissue has a more apparent deterioration of the cancerous tissue.

REFERENCES

1. Jemal A, Siegel R, Ward E, Murray T, Xu J, Smigal C, et al. Cancer Statistics, 2006. *CA Cancer J Clin* (2006) 56:106–30. doi: 10.3322/canjclin.56.2.106
2. Jennifer R. Cancer Statistics. *JAMA* (2013) 310:982. doi: 10.1001/jama.2013.5289
3. Pannala R, Leirness JB, Bamlet WR, Basu A, Petersen GM, Chari STJG. Prevalence and Clinical Profile of Pancreatic Cancer–Associated Diabetes Mellitus. *Gastroenterology* (2008) 134:981–7. doi: 10.1053/j.gastro.2008.01.039
4. Aggarwal G, Rabe KG, Petersen GM, Chari STJP. New-Onset Diabetes in Pancreatic Cancer: A Study in the Primary Care Setting. *Pancreatology* (2012) 12:156–61. doi: 10.1016/j.pan.2012.02.003

5. Nakai Y, Isayama H, Sasaki T, Mizuno S, Sasahira N, Kogure H, et al. Clinical Outcomes of Chemotherapy for Diabetic and Nondiabetic Patients With Pancreatic Cancer: Better Prognosis With Statin Use in Diabetic Patients. *Pancreas* (2013) 42:202–8. doi: 10.1097/MPA.0b013e31825de678
6. Vickers M, Powell E, Asmis T, Jonker D, Hilton J, O'Callaghan C, et al. Comorbidity, Age and Overall Survival in Patients With Advanced Pancreatic Cancer–Results From NCIC CTG PA. 3: A Phase III Trial of Gemcitabine Plus Erlotinib or Placebo. *Eur J Cancer* (2012) 48:1434–42. doi: 10.1016/j.ejca.2011.10.035
7. Chronopoulos A, Robinson B, Sarper M, Cortes E, Auernheimer V, Lachowski D, et al. ATRA Mechanically Reprograms Pancreatic Stellate Cells to Suppress Matrix Remodelling and Inhibit Cancer Cell Invasion. *Nature Comm* (2016) 7:1–12. doi: 10.1038/ncomms12630
8. Neesse A, Algul H, Tuveson DA, Gress TM. Stromal Biology and Therapy in Pancreatic Cancer: A Changing Paradigm. *Gut* (2015) 64:1476–84. doi: 10.1136/gutjnl-2015-309304
9. Garcia C, Feve B, Ferre P, Halimi S, Baizri H, Bordier L, et al. Diabetes and Inflammation: Fundamental Aspects and Clinical Implications. *Diabetes Metab* (2010) 36:327–38. doi: 10.1016/j.diabet.2010.07.001
10. Reinfeld BI, Madden MZ, Wolf MM, Chytil A, Bader JE, Patterson AR, et al. Cell-Programmed Nutrient Partitioning in the Tumour Microenvironment. *Nature* (2021) 593:282–8. doi: 10.1038/s41586-021-03442-1
11. Tomczak K, Czerwinska P, Wiznerowicz M. The Cancer Genome Atlas (TCGA): An Immeasurable Source of Knowledge. *Contemp Oncol (Pozn)* (2015) 19:A68–77. doi: 10.5114/wo.2014.47136
12. Kirby MK, Ramaker RC, Gertz J, Davis NS, Johnston BE, Oliver PG, et al. RNA Sequencing of Pancreatic Adenocarcinoma Tumors Yields Novel Expression Patterns Associated With Long-Term Survival and Reveals a Role for ANGPTL4. *Mol Oncol* (2016) 10:1169–82. doi: 10.1016/j.molonc.2016.05.004
13. Barrett T, Wilhite SE, Ledoux P, Evangelista C, Kim IF, Tomashevsky M, et al. NCBI GEO: Archive for Functional Genomics Data Sets—Update. *Nucleic Acids Res* (2012) 41:D991–5. doi: 10.1093/nar/gks1193
14. Peng J, Sun B-F, Chen C-Y, Zhou J-Y, Chen Y-S, Chen H, et al. Single-Cell RNA-Seq Highlights Intra-Tumoral Heterogeneity and Malignant Progression in Pancreatic Ductal Adenocarcinoma. *Cell Res* (2019) 29:725–38. doi: 10.1038/s41422-019-0195-y
15. Sun D, Wang J, Han Y, Dong X, Ge J, Zheng R, et al. TISCH: A Comprehensive Web Resource Enabling Interactive Single-Cell Transcriptome Visualization of Tumor Microenvironment. *Nucleic Acids Res* (2021) 49:D1420–30. doi: 10.1093/nar/gkaa1020
16. Love MI, Huber W, Anders S. Moderated Estimation of Fold Change and Dispersion for RNA-Seq Data With Deseq2. *Genome Biol* (2014) 15:550. doi: 10.1186/s13059-014-0550-8
17. Harris MA, Clark J, Ireland A, Lomax J, Ashburner M, Foulger R, et al. The Gene Ontology (GO) Database and Informatics Resource. *Nucleic Acids Res* (2004) 32:D258–61. doi: 10.1093/nar/gkh036
18. Kanehisa M, Goto S. KEGG: Kyoto Encyclopedia of Genes and Genomes. *Nucleic Acids Res* (2000) 28:27–30. doi: 10.1093/nar/28.1.27
19. Yu G, Wang L-G, Han Y, He Q-Y. Clusterprofiler: An R Package for Comparing Biological Themes Among Gene Clusters. *J Omics: J Integr Biol* (2012) 16:284–7. doi: 10.1089/omi.2011.0118
20. Subramanian A, Kuehn H, Gould J, Tamayo P, Mesirov JP. GSEA-P: A Desktop Application for Gene Set Enrichment Analysis. *Bioinformatics* (2007) 23:3251–3. doi: 10.1093/bioinformatics/btm369
21. Hao Y, Hao S, Andersen-Nissen E, Mauck WM, Zheng S, Butler A, et al. Integrated Analysis of Multimodal Single-Cell Data. *Cell* (2021) 13:3573–87.e29. doi: 10.1016/j.cell.2021.04.048
22. Newman AM, Liu CL, Green MR, Gentles AJ, Feng W, Xu Y, et al. Robust Enumeration of Cell Subsets From Tissue Expression Profiles. *Nat Methods* (2015) 12:453–7. doi: 10.1038/nmeth.3337
23. Jiang P, Gu S, Pan D, Fu J, Sahu A, Hu X, et al. Signatures of T Cell Dysfunction and Exclusion Predict Cancer Immunotherapy Response. *Nature Med* (2018) 24:1550–8. doi: 10.1038/s41591-018-0136-1
24. Ritchie ME, Phipson B, Wu D, Hu Y, Law CW, Shi W, et al. Limma Powers Differential Expression Analyses for RNA-Sequencing and Microarray Studies. *Nucleic Acids Res* (2015) 43:e47. doi: 10.1093/nar/gkv007
25. Chang L, Zhou G, Soufan O, Xia J. Mirnet 2.0: Network-Based Visual Analytics for miRNA Functional Analysis and Systems Biology. *Nucleic Acids Res* (2020) 48:W244–51. doi: 10.1093/nar/gkaa467
26. Huang H-Y, Lin Y.-C.-D., Li J, Huang K-Y, Shrestha S, Hong H-C, et al. Mirtarbase 2020: Updates to the Experimentally Validated microRNA–Target Interaction Database. *Nucleic Acids Res* (2020) 48:D148–D154S. doi: 10.1093/nar/gkz896
27. Fabregat A, Jupe S, Matthews L, Sidiropoulos K, Gillespie M, Garapati P, et al. The Reactome Pathway Knowledgebase. *Nucleic Acids Res* (2018) 46:D649–55. doi: 10.1093/nar/gkx1132
28. Nagy Á., Munkácsy G, Győrffy B. Pancancer Survival Analysis of Cancer Hallmark Genes. *Sci Rep* (2021) 11:1–10. doi: 10.1038/s41598-021-84787-5
29. Demšar J, Curk T, Erjavec A, Gorup Č., Hočevar T, Milutinovič M, et al. Orange: Data Mining Toolbox in Python. *J Mach Learn Res* (2013) 14:2349–53. doi: 10.5555/2567709.2567736
30. Dandona M, Linehan D, Hawkins W, Strasberg S, Gao F, Wang-Gillam A. Influence of Obesity and Other Risk Factors on Survival Outcomes in Patients Undergoing Pancreaticoduodenectomy for Pancreatic Cancer. *Pancreas* (2011) 40:931–7. doi: 10.1097/MPA.0b013e318215a9b1
31. Cannon RM, LeGrand R, Chagpar RB, Ahmad SA, McClaine R, Kim HJ, et al. Multi-Institutional Analysis of Pancreatic Adenocarcinoma Demonstrating the Effect of Diabetes Status on Survival After Resection. *HPB (Oxf)* (2012) 14:228–35. doi: 10.1111/j.1477-2574.2011.00432.x
32. van de Poll-Franse LV, Houterman S, Janssen-Heijnen ML, Dercksen MW, Coebergh JWW, Haak HR. Less Aggressive Treatment and Worse Overall Survival in Cancer Patients With Diabetes: A Large Population Based Analysis. *Int J Cancer* (2007) 120:1986–92. doi: 10.1002/ijc.22532
33. Mao Y, Tao M, Jia X, Xu H, Chen K, Tang H, et al. Effect of Diabetes Mellitus on Survival in Patients With Pancreatic Cancer: A Systematic Review and Meta-Analysis. *Sci Rep* (2015) 5:17102. doi: 10.1038/srep17102
34. Huang X, Zhang G, Tang T, Liang T. Identification of Tumor Antigens and Immune Subtypes of Pancreatic Adenocarcinoma for mRNA Vaccine Development. *Mol Cancer* (2021) 20:44. doi: 10.1186/s12943-021-01310-0
35. Lontchi-Yimagou E, Sobngwi E, Matsha TE, Kengne AP. Diabetes Mellitus and Inflammation. *Curr Diabetes Rep* (2013) 13:435–44. doi: 10.1007/s11892-013-0375-y
36. Farhood B, Najafi M, Mortezaee K. CD8(+) Cytotoxic T Lymphocytes in Cancer Immunotherapy: A Review. *J Cell Physiol* (2019) 234:8509–21. doi: 10.1002/jcp.27782
37. Orhan A, Vogelsang RP, Andersen MB, Madsen MT, Holmich ER, Raskov H, et al. The Prognostic Value of Tumour-Infiltrating Lymphocytes in Pancreatic Cancer: A Systematic Review and Meta-Analysis. *Eur J Cancer* (2020) 132:71–84. doi: 10.1016/j.ejca.2020.03.013
38. Carstens JL, De Sampaio PC, Yang D, Barua S, Wang H, Rao A, et al. Spatial Computation of Intratumoral T Cells Correlates With Survival of Patients With Pancreatic Cancer. *Nature Comm* (2017) 8:1–13. doi: 10.1038/ncomms15095
39. Xia X, Zhang K, Cen G, Jiang T, Cao J, Huang K, et al. MicroRNA-301a-3p Promotes Pancreatic Cancer Progression *via* Negative Regulation of SMAD4. *Oncotarget* (2015) 6:21046–63. doi: 10.18632/oncotarget.4124
40. Palkina N, Komina A, Aksenenko M, Moshev A, Savchenko A, Ruksha T. miR-204-5p and miR-3065-5p Exert Antitumor Effects on Melanoma Cells. *Oncol Lett* (2018) 15:8269–80. doi: 10.3892/ol.2018.8443
41. Chauhan N, Dhasmana A, Jaggi M, Chauhan SC, Yallapu MM. miR-205: A Potential Biomedicine for Cancer Therapy. *Cells* (2020) 9:1957. doi: 10.3390/cells9091957
42. Mittal A, Chitkara D, Behrman SW, Mahato RI. Efficacy of Gemcitabine Conjugated and miRNA-205 Complexed Micelles for Treatment of Advanced Pancreatic Cancer. *Biomaterials* (2014) 35:7077–87. doi: 10.1016/j.biomaterials.2014.04.053
43. Pan Z, Xie R, Song W, Gao C. MicroRNA−592 Promotes Cell Proliferation, Migration and Invasion in Colorectal Cancer by Directly Targeting SPARC. *Mol Med Rep* (2021) 23:1–1. doi: 10.3892/mmr.2021.11900
44. Pan Z, Miao LJOL. Serum microRNA−592 Serves as a Novel Potential Biomarker for Early Diagnosis of Colorectal Cancer. *Oncol Lett* (2020) 20:1119–26. doi: 10.3892/ol.2020.11682

45. Li H, Ouyang R, Wang Z, Zhou W, Chen H, Jiang Y, et al. MiR-150 Promotes Cellular Metastasis in non-Small Cell Lung Cancer by Targeting FOXO4. *Sci Rep* (2016) 6:39001. doi: 10.1038/srep39001
46. Ali S, Almhanna K, Chen W, Philip PA, Sarkar FH. Differentially Expressed miRNAs in the Plasma may Provide a Molecular Signature for Aggressive Pancreatic Cancer. *Am J Trans Res* (2011) 3:28. doi: 10.1016/B978-0-12-385524-4.00004-0
47. Lee KH, Lee JK, Choi DW, Do IG, Sohn I, Jang KT, et al. Postoperative Prognosis Prediction of Pancreatic Cancer With Seven microRNAs. *Pancreas* (2015) 44:764–8. doi: 10.1097/MPA.0000000000000346
48. Neuper T, Frauenlob T, Sarajlic M, Posselt G, Wessler S, Horejs-Hoeck J. TLR2, TLR4 and TLR10 Shape the Cytokine and Chemokine Release of H. Pylori-Infected Human DCs. *Int J Mol Sci* (2020) 21:3897. doi: 10.3390/ijms21113897
49. Brunner M, Maier K, Rümmele P, Jacobsen A, Merkel S, Benard A, et al. Upregulation of CD20 positive B-cells and B-cell aggregates in the tumor infiltration zone is associated with better survival of patients with pancreatic ductal adenocarcinoma. *Int J Mol Sci* (2020) 21:1779. doi: 10.3390/ijms21051779
50. Bian B, Fanale D, Dusetti N, Roque J, Pastor S, Chretien AS, et al. Prognostic Significance of Circulating PD-1, PD-L1, Pan-BTN3As, BTN3A1 and BTLA in Patients With Pancreatic Adenocarcinoma. *Oncoimmunology* (2019) 8: e1561120. doi: 10.1080/2162402X.2018.1561120

Conflict of Interest: The authors declare that the research was conducted in the absence of any commercial or financial relationships that could be construed as a potential conflict of interest.

Publisher's Note: All claims expressed in this article are solely those of the authors and do not necessarily represent those of their affiliated organizations, or those of the publisher, the editors and the reviewers. Any product that may be evaluated in this article, or claim that may be made by its manufacturer, is not guaranteed or endorsed by the publisher.

frontiers | Frontiers in Endocrinology

ORIGINAL RESEARCH
published: 14 April 2022
doi: 10.3389/fendo.2022.846357

Identification and Validation of a Prognostic Prediction Model in Diffuse Large B-Cell Lymphoma

*Jiaqin Yan[1], Wei Yuan[1,2,3], Junhui Zhang[4], Ling Li[1], Lei Zhang[1], Xudong Zhang[1] and Mingzhi Zhang[1]**

[1] Department of Oncology, The First Affiliated Hospital of Zhengzhou University, Zhengzhou, China, [2] The Academy of Medical Sciences, Zhengzhou University, Zhengzhou, China, [3] State Key Laboratory of Esophageal Cancer Prevention and Treatment, Zhengzhou University, Zhengzhou, China, [4] Otorhinolaryngology, The Third Affiliated Hospital of Zhengzhou University, Zhengzhou, China

Background: Diffuse large B-cell lymphoma (DLBCL) is a heterogeneous group with varied pathophysiological, genetic, and clinical features, accounting for approximately one-third of all lymphoma cases worldwide. Notwithstanding that unprecedented scientific progress has been achieved over the years, the survival of DLBCL patients remains low, emphasizing the need to develop novel prognostic biomarkers for early risk stratification and treatment optimization.

Method: In this study, we screened genes related to the overall survival (OS) of DLBCL patients in datasets GSE117556, GSE10846, and GSE31312 using univariate Cox analysis. Survival-related genes among the three datasets were screened according to the criteria: hazard ratio (HR) >1 or <1 and p-value <0.01. Least Absolute Shrinkage and Selection Operator (LASSO) and multivariate Cox regression analysis were used to optimize and establish the final gene risk prediction model. The TCGA-NCICCR datasets and our clinical cohort were used to validate the performance of the prediction model. CIBERSORT and ssGSEA algorithms were used to estimate immune scores in the high- and low-risk groups.

Results: We constructed an eight-gene prognostic signature that could reliably predict the clinical outcome in training, testing, and validation cohorts. Our prognostic signature also performed distinguished areas under the ROC curve in each dataset, respectively. After stratification based on clinical characteristics such as cell-of-origin (COO), age, eastern cooperative oncology group (ECOG) performance status, international prognostic index (IPI), stage, and MYC/BCL2 expression, the difference in OS between the high- and low-risk groups was statistically significant. Next, univariate and multivariate analyses revealed that the risk score model had a significant prediction value. Finally, a nomogram was established to visualize the prediction model. Of note, we found that the low-risk group was enriched with immune cells.

OPEN ACCESS

Edited by:
Rick Francis Thorne, The University of Newcastle, Australia

Reviewed by:
Niaz Muhammad, Minhaj University Lahore, Pakistan
Muhammad Riaz Khan, Université de Sherbrooke, Canada

***Correspondence:**
Mingzhi Zhang
mingzhi_zhang1@163.com

Specialty section:
This article was submitted to Cancer Endocrinology, a section of the journal Frontiers in Endocrinology

Received: *31 December 2021*
Accepted: *25 February 2022*
Published: *14 April 2022*

Citation:
Yan J, Yuan W, Zhang J, Li L, Zhang L, Zhang X and Zhang M (2022) Identification and Validation of a Prognostic Prediction Model in Diffuse Large B-Cell Lymphoma. Front. Endocrinol. 13:846357. doi: 10.3389/fendo.2022.846357

Conclusion: In summary, we identified an eight-gene prognostic prediction model that can effectively predict survival outcomes of patients with DLBCL and built a nomogram to visualize the perdition model. We also explored immune alterations between high- and low-risk groups.

Keywords: prediction model, immune cell infiltration, nomogram, stratification analyses, diffuse large B-cell lymphoma

INTRODUCTION

Lymphoma is the fourth most common cancer and the sixth leading cause of cancer death in the United States (1). Diffuse large B-cell lymphoma (DLBCL) accounts for approximately one-third of all lymphoma cases worldwide (2–4). In the current World Health Organization (WHO) lymphoma classification, about 80% of DLBCL cases are designated as not otherwise specified (NOS) (2). Three molecularly distinct forms of DLBCL have been identified by gene expression patterns, specifically an activated B cell-like (ABC) and germinal center B-cell-like (GCB) types and a small amount were unclassified DLBCL (UC) (5–7). Lymphomas with rearrangements of MYC with BCL2 and/or BCL6 are called "double-hit lymphomas"(DHL) or "triple-hit lymphomas"(THL) (8). There also exist one subtype called "double-expressor lymphomas" (DELs), defined as co-expression of MYC and BCL2 (9). DLBCL comprises a heterogeneous group with pathophysiological, genetic and clinical features (4). Albeit significant efforts have been made to better understand lymphomas, the overall survival (OS) of DLBCL patients remains dismal (5, 10). Accordingly, developing novel prognostic biomarkers for early risk stratification and treatment optimization is imperative.

It is well established that clinical prognosis systems for DLBCL, including the rituximab international prognostic index (IPI), age-adjusted IPI, and NCCN-IPI, use clinical factors for risk stratification of patients (4). Although IPI is easy to apply during clinical practice, it does not fully account for disease heterogeneity (11, 12). An increasing body of evidence suggests that patients with the ABC disease subtype have significantly poorer outcomes with standard up-front rituximab-containing chemoimmunotherapy than patients with GCB disease (13). A survival-related gene prognostic model, in combination with other prognostic indicators such as IPI and cell of origin (COO), might improve our assessment of patient prognosis for individualized treatment.

It is widely acknowledged that the tumor microenvironment (TME) of patients with lymphoma comprises endothelial cells, fibroblasts, adipocytes, and immune cells and is a key factor for tumor initiation and metastasis (14, 15). Several studies have focused on the potential role of the TME, especially the immune status in DLBCL pathogenesis (16, 17). Therefore, it is critical to better characterize the TME to develop the treatments for DLBCL patients (18).

Thanks to high-throughput genome sequencing technique, there had been several studies exploring potential prognostic biomarkers of DLBCL patients on genomic level. Xie et al. for example, investigated the prognostic value of m6A regulators and established an m6A-based prognostic gene signature for DLBCL (19). Feng et al. constructed a 14-gene prognostic signature deriving from immune-related genes for 216 DLBCL patients (20). Luo et al. identified the aging-related genes associated with prognostic value in DLBCL patients (21). In this study, we integrated the transcriptome data from the Gene Expression Omnibus (GEO), The Cancer Genome Atlas (TCGA), and our clinical cohort and constructed an eight-gene signature-based prediction model. Furthermore, we explored the immune alterations in high- and low-risk groups.

METHODS AND MATERIALS

Collection of Clinical DLBCL Specimens

DLBCL specimens were obtained through biopsy in the First Affiliated Hospital of Zhengzhou University and frozen at −80°C for storage. All participants provided written informed consent for the use of their specimens in this study. Clinicopathological features of 45 DLBCL patients from the First Affiliated Hospital of Zhengzhou University are performed in **Supplementary Table 1**. The study protocol was approved by the ethics committee of the First Affiliated Hospital of Zhengzhou University (ethics number 2021-KY-0835-001).

Selection of DLBCL Gene Expression Datasets

We systematically explored publicly available DLBCL gene expression datasets with corresponding clinical information of patients from the GEO (https://www.ncbi.nlm.nih.gov/geo/) and TCGA (https://portal.gdc.cancer.gov/) databases. For this study, we gathered a total of 2,335 patients with DLBCL from four cohorts, including GSE117556 (n = 928), GSE10846 (n = 420), GSE31312 (n = 498), and TCGA-NCICCR (n = 489) (**Table 1**) and our clinical cohort (n = 45). Patients with incomplete transcriptomic data and clinical data were excluded. Ultimately, we included 928 patients from GSE117556, 414 from GSE10846, 470 from GSE31312, and 234 from TCGA-NCICCR. The GSE10846 and GSE31312 datasets used the GPL570 platform, while the GSE117556 dataset used the GPL14951 platform.

Construction and Validation of Prediction Model

In this study, we used univariate Cox analysis to screen genes related to the OS of DLBCL patients in the GSE117556,

TABLE 1 | Characteristics of the included datasets.

Dataset ID	Country	Number of samples	GPL ID	Number of rows per platform
GSE117556	UK	928	GPL14951	29,377
GSE10846	USA	420	GPL570	54,675
GSE31312	USA	498	GPL570	54,675
TCGA-NCICCR	USA	489	NA	56,753
Clinical cohort	China	45	NA	NA

GSE, Gene Expression Omnibus Series; GPL, Gene Expression Omnibus Platform; UK, United Kingdom; USA, United States of America; NA, Not Available.

GSE10846, and GSE31312 datasets. Genes with hazard ratio (HR) >1 and HR <1 were defined as the risk and protective genes. A p-value <0.01 was the cutoff point. The risk genes and protective genes shared by the three datasets were intersected and combined with Least Absolute Shrinkage and Selection Operator (LASSO) regression and multivariate Cox regression to build the final gene risk prediction model (22). We conducted univariate and multivariate Cox regression analyses using the R package "survival." Another R package "glmnet" was used for the LASSO Cox regression analysis (23). The risk score (RS) of each sample was calculated by multivariate Cox regression analysis. The correlation analysis was based on the R package "corrplot," and the forest plots for univariate and multivariate analyses were constructed by R package "forestplot."

TME Characterization Analysis

We employed two algorithms to assess immune infiltration in DLBCL. CIBERSORT (http://cibersort.stanford.edu/) algorithm was used to obtain the proportion of 22 immune cell types with a threshold of $p < 0.05$ (24). We applied Single-Sample Gene Set Enrichment Analysis (ssGSEA) to assess the infiltration level of 28 different immune cells in DLBCL expression profile data by the "GSVA" package (25). The R package "ggpubr" was used to visualize differences in the distributions of immune-related cells in the low- and high-risk patient groups from the overall cohort. "***," "**," "*," and "ns" indicate $p < 0.001$, $p < 0.01$, $p < 0.05$, and not significant, respectively, for the Kruskal–Wallis test.

Quantitative Real-Time Polymerase Chain Reaction

Total RNA was isolated from the specimens harvested using TRIzol reagent (Invitrogen Corporation, Carlsbad, CA, # A33250). The Prime Script RT reagent kit with genomic DNA eraser (TaKaRa, Tokyo, Japan, #RR037A) was used to synthesize complementary DNA (cDNA). Quantitative real-time polymerase chain reaction (qRT-PCR) analyses were detected by SYBR Green Master Mix (TaKaRa), and the primers for qRT-PCR analyses are listed in **Supplementary Table 2**. The $2^{-\Delta CT}$ method was utilized to calculate the relative mRNA expression of each gene.

Statistical Analysis

Statistical analyses were performed with R (version 3.6.3). The Kaplan–Meier method was used to assess the differences in survival time, and the log-rank test was used to determine the statistical significance. Time-dependent receiver operating characteristic (ROC) curve analysis was used to measure the prognostic performance by comparing the areas under curves (AUC). The nomogram was plotted using the "rms" package (26). The difference in immune infiltration levels between high- and low-risk groups was calculated by Kruskal–Wallis test, and a p-value < 0.05 was statistically significant.

RESULTS

Identification and Validation of a Prognostic Signature

To identify the prognostic signature of DLBCL, we performed a multiple-step analysis (**Figure 1**). We first screened the GEO database and selected three datasets for univariate Cox proportional hazards regression to identify candidate genes significantly related to OS. We conducted univariate Cox analysis in the GSE117556, GSE10846, and GSE31312 datasets with $p < 0.01$ as the cutoff value. In total, 1,426, 1,904, and 1,788 candidate protective genes (with hazard ratios (HR) <1) and 890, 2,958, and 2,525 candidate risk genes (with HR >1) were identified in GSE117556, GSE10846, and GSE31312, respectively. A total of 11 genes were candidate protective genes after intersecting the candidate protective genes (**Figure 2A**). Similarly, after matching the candidate risk genes identified in the three datasets, 13 common genes are retained (**Figure 2B**).

The detailed information on these genes is listed in **Table 2**. Next, GSE117556 was assigned as the training dataset, and the LASSO was applied to screen the candidate genes, yielding eight genes (**Supplementary Figures 1A, B**). Ultimately, the HRs of the eight genes were acquired by conducting multivariate Cox regression analysis. The forest plot (**Supplementary Figure 1C**) showed that HK2, GAB1, GRPEL1, RCSD1, PLAC8L1, and RASAL1 were risk factors (HR >1), and CAPG and PDPN were protective factors (HR <1) for OS. Finally, the following risk score model was established: risk score = 0.271 × HK2 expression + 0.182 × GAB1 expression + 0.172 × RASAL1 expression − 0.254 × CAPG expression − 0.358 × PDPN expression + 0.362 × GRPEL1 expression + 0.370 × RCSD1 expression + 0.177 × PLAC8L1 expression. Each patient was assigned a risk score with the prognostic model. According to the median risk score, patients

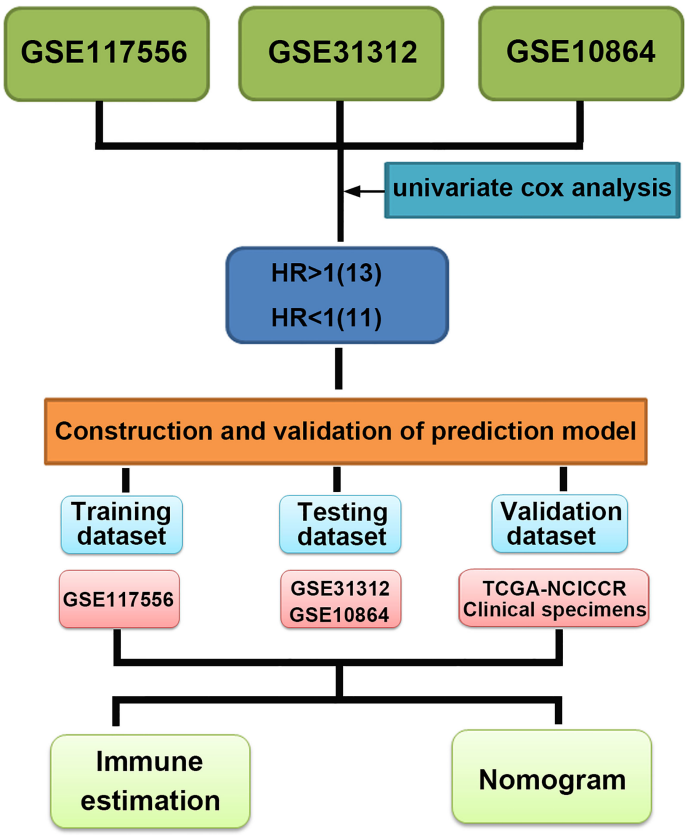

FIGURE 1 | Multistep analysis of the study.

in the GSE117556 dataset were stratified into high-and low-risk groups. Of the eight-gene prognostic signature, HK2 have the most significant correlation with worse survival. Through analyzing the RT-PCR results deriving from our clinical specimens, We found HK2 had high expressed in high stage DLBCL (**Supplementary Figure 2A**). To further explore the function of HK2, we first identified genes that correlated with HK2 in the GSE117556 dataset (**Supplementary Figure 2B**). We then utilized positive and negative correlated genes to perform GO and KEGG enrichment analyses. Results revealed that positive correlated genes were involved in cell cycle (**Supplementary Figure 2C**) and negative correlated genes were involved in immune response (**Supplementary Figure 2D**). These results partly reflect genomic differences between high- and low-risk groups.

To further verify the predicting model, we analyzed the survival of high- and low-risk groups. Patients in the low-risk group demonstrated a longer survival time than those in the high-risk group (**Supplementary Figure 3**). Consistently, the Kaplan–Meier curve indicated that patients in the high-risk group had significantly worse prognoses than low-risk patients (log-rank test $p < 0.001$) (**Figure 2C**). We further validated the risk score model in the testing dataset GSE 31312 (log-rank test $p < 0.001$) (**Supplementary Figure 4A**) and GSE 10864 (log-rank test $p < 0.001$) (**Supplementary Figure 4B**), TCGA-NCICCR dataset (log-rank test $p = 0.0052$) (**Figure 2D**), and our clinical specimens (log-rank test $p = 0.024$) (**Figure 2E**), the results were consistent with the training dataset findings. The predictive power of the risk score model was assessed by time-dependent ROC, which yielded good performance in the above datasets. In dataset GSE117556, the AUC values for 1-, 3-, and 5-year overall survival were 0.7, 0.74, and 0.89, respectively. In TCGA-NCICCR dataset, the AUC values for 1-, 3-, and 5-year overall survival predictions were 0.61, 0.60, and 0.62, respectively. Our clinical cohort yielded AUC values of 0.74, 0.79, and 0.78 for the 1-, 3-, and 5-year overall survival, respectively (**Figures 2F–H**). In dataset GSE31312, the AUC values for 1-, 3-, and 5-year overall survival were 0.64, 0.7, and 0.74, respectively. In dataset GSE10864, the AUC values for 1-year overall survival were 0.56 (**Supplementary Figures 4C, D**). The above AUC curves provided an objective validation of the clinical application value of our model.

Validation of the Accuracy of the Risk Score Model

We used GSE117556 as the training dataset to detect the correlation and interdependence between the eight risk genes,

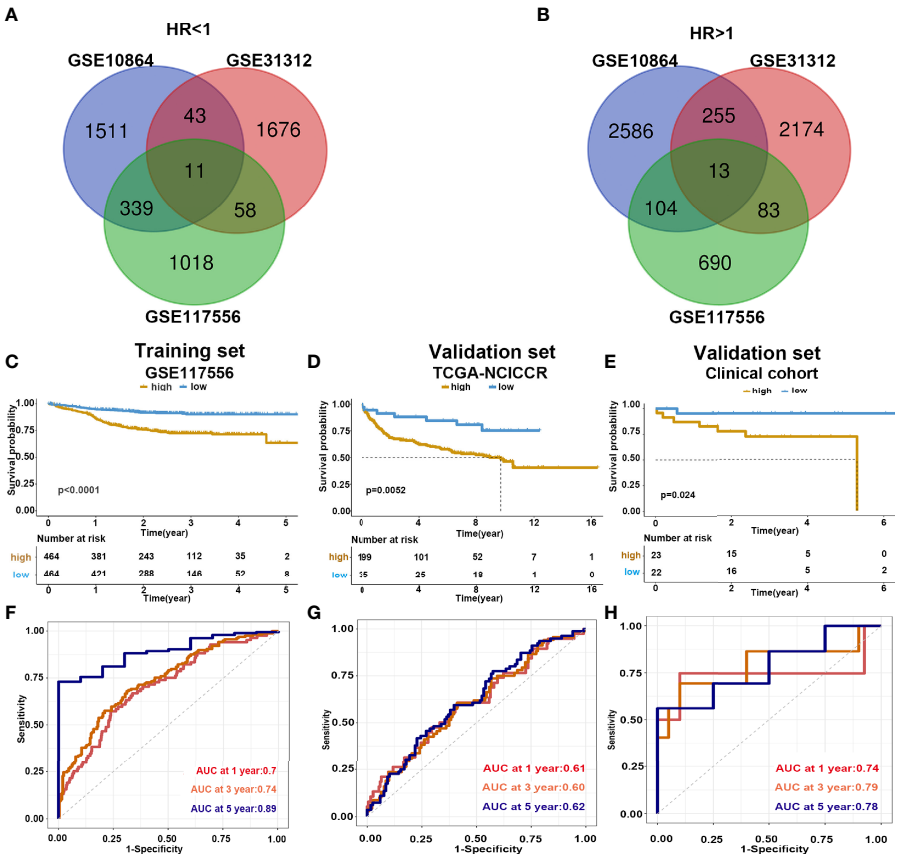

FIGURE 2 | Construction and validation of prediction model. **(A, B)** Venn diagram shows the common protective and risk genes identified by three datasets. **(C–E)** Kaplan–Meier analysis for the eight-gene signature in the GSE117556, TCGA-NCICCR, and our clinical cohort, respectively. **(F–H)** Time-dependent ROC curve analysis of 1, 3, and 5 years in GSE117556, TCGA-NCICCR, and our clinical cohort.

which proved that our prognostic signature could minimize data bias caused by gene collinearity (**Figure 3A**). Using the median risk score as the cutoff point, the training set was classified into low- and high-risk groups. Our results suggest that the risk score model has significant value for evaluating characteristic genes. The eight genes were differentially expressed between the two groups, indicating their role in contributing to the prognosis of DLBCL (**Figure 3B**). Analysis of validation dataset TCGA-NCICCR yielded consistent results (**Figures 3C, D**).

Validation of Risk Score Model Based on Different Clinical Parameters and Subgroups

It has been established that DLBCL exhibits a significant heterogeneity in cell origin, clinical manifestations, gene expression profiles, and so on. To verify the effectiveness of the risk signature in the existing clinical subgroups, we conducted a series of subgroup analyses on dataset GSE117556. Stratification based on clinical characteristics such as COO, ECOG, MYC/BCL2 double expression, lactate dehydrogenase (LDH) value, age, stage, and gender was conducted. Among those subtypes, patients in the high-risk groups had worse survival outcomes than patients in the low-risk group (log-rank test $p < 0.05$; **Figure 4** and **Supplementary Figure 5**). These findings validated that our risk model yielded good predictive performance after stratifying for different clinicopathological characteristics.

The Landscape of Immune Cell Infiltration in the TME of DLBCL

To further explore the potential survival mechanisms related to the risk score model, mRNA data from dataset GSE117556 were first used to detect the proportion of 22 immune cell types in each sample *via* the CIBERSORT algorithm. As shown in **Figure 5A**, the proportion of immune cells was significantly different between the high- and low-risk score groups. Compared with the low-risk group, the high-risk group exhibited increased B-cell infiltrations, with less-naive CD4 T cell, T follicular helper cell, M0 macrophages, M1 macrophages, and other proinflammatory cells. Consistent results were obtained when ssGSEA was applied (**Figure 5B**).

TABLE 2 | Detail information of selected common genes in three datasets.

Gene symbol	Gene name	Datasets (HR/*p*-value)		
		GSE117556	GSE31312	GSE10864
COL1A1	Collagen type I alpha 1 chain	0.763 ($p < 0.001$)	0.043 ($p = 0.009$)	0.829 ($p = 0.004$)
ST6GALNAC5	ST6N-Acetylgalactosaminide alpha-2,6-sialyltransferase 5	0.727 ($p < 0.001$)	0.184 ($p = 0.009$)	0.796 ($p < 0.001$)
CAPG	Capping actin protein, gelsolin like	0.728 ($p < 0.001$)	0.145 ($p < 0.001$)	0.793 ($p < 0.001$)
LRRC15	Leucine-rich repeat containing 15	0.656 ($p < 0.001$)	0.166 ($p = 0.001$)	0.790 ($p < 0.001$)
PDPN	Podoplanin	0.656 ($p < 0.001$)	0.214 ($p = 0.005$)	0.841 ($p < 0.001$)
NEK6	NIMA-related kinase 6	0.610 ($p < 0.001$)	0.205 ($p = 0.004$)	0.660 ($p < 0.001$)
PTPN14	Protein tyrosine phosphatase nonreceptor type 14	0.738 ($p = 0.002$)	0.183 ($p = 0.002$)	0.813 ($p < 0.001$)
LOX	Lysyl oxidase	0.656 ($p = 0.008$)	0.161 ($p = 0.001$)	0.862 ($p < 0.001$)
RBP5	Retinol-binding protein 5	0.754 ($p = 0.006$)	0.215 ($p = 0.001$)	0.870 ($p = 0.005$)
NRP2	Neuropilin 2	0.747 ($p = 0.002$)	0.237 ($p = 0.003$)	0.773 ($p = 0.003$)
DST	Dystonin	0.792 ($p = 0.005$)	0.042 ($p < 0.001$)	0.748 ($p = 0.001$)
MSL1	MSL complex subunit 1	1.592 ($p = 0.004$)	12.721 ($p < 0.001$)	1.459 ($p = 0.002$)
GRPEL1	GrpE-like 1, mitochondrial	1.797 ($p < 0.001$)	4.534 ($p = 0.008$)	1.877 ($p < 0.001$)
RCSD1	RCSD domain-containing 1	1.807 ($p < 0.001$)	8.005 ($p < 0.001$)	1.300 ($p < 0.001$)
PLAC8L1	PLAC8-like 1	1.277 ($p = 0.004$)	5.033 ($p = 0.001$)	1.449 ($p < 0.001$)
PRC1	Protein regulator of cytokinesis 1	1.745 ($p = 0.001$)	3.910 ($p = 0.005$)	1.330 ($p = 0.001$)
RASAL1	RAS protein activator-like 1	1.368 ($p < 0.001$)	3.056 ($p = 0.007$)	1.220 ($p = 0.001$)
LARS	Leucyl-TRNA synthetase 1	2.088 ($p = 0.001$)	5.419 ($p = 0.007$)	1.599 ($p < 0.001$)
SNHG7	Small nucleolar RNA host gene 7	1.238 ($p = 0.006$)	4.498 ($p = 0.002$)	1.439 ($p < 0.001$)
WDR12	WD repeat domain 12	1.812 ($p = 0.001$)	8.049 ($p = 0.001$)	1.526 ($p = 0.003$)
PI4K2B	Phosphatidylinositol 4-kinase type 2 beta	1.637 ($p = 0.004$)	3.868 ($p = 0.004$)	1.537 ($p = 0.006$)
MMACHC	Metabolism of cobalamin-associated C	1.430 ($p < 0.001$)	5.033 ($p = 0.009$)	1.770 ($p < 0.001$)
HK2	Hexokinase 2	1.320 ($p = 0.004$)	4.455 ($p < 0.001$)	1.438 ($p < 0.001$)
GAB1	GRB2-associated binding protein 1	1.277 ($p = 0.008$)	2.634 ($p = 0.007$)	1.235 ($p = 0.008$)

In contrast with the high-risk group, tumor-infiltrating lymphocytes (TIL), antigen-presenting cells were significantly enriched in the low-risk groups. We further applied the above two algorithms to the validation dataset TCGA-NCICCR. Similar results were obtained from GSE117556 analysis results. Immune signatures between the high- and low-risk groups were different, and the low-score group was significantly infiltrated with proinflammatory immune cells (**Figures 5C, D**). In addition, we analyzed immune-related genes between the two groups and further approved the above findings (**Supplementary Figure 6**).

Validation of the Performance of Our Prediction Model

To evaluate the performance of our risk score model on the prognosis of DLBCL patients, we integrated the clinicopathological characteristics with risk score signatures in different algorithms. As shown in **Figure 6A**, univariate Cox regression analysis demonstrated that the risk score model was a significant predictor of OS in patients with DLBCL ($p < 0.0001$, HR = 1.377), compared with other clinicopathological characteristics. Multivariate Cox regression analysis showed that the risk score model was an independent prognostic factor for poor prognosis ($p < 0.0001$, HR = 1.380) (**Figure 6B**). Compared with other indicators, the risk score was superior for predicting the patient prognosis (AUC = 0.820) (**Figure 6C**). Finally, we established a nomogram based on the above clinical parameters to predict patient prognosis quantitatively. Accordingly, our nomogram has huge prospects for clinical application for predicting the OS of individual DLBCL patients (**Figure 6D**).

DISCUSSION

Notwithstanding that unprecedented scientific progress has been achieved over the years, the survival of DLBCL patients remains relatively low. In this regard, the cure rate of DLBCL ranges from 40% to 60% following standard frontline immunochemotherapy (5). However, a poor prognosis has been reported for patients with refractory disease, those who relapse after salvage chemotherapy and autologous stem cell transplant or chimeric antigen receptor T-cell therapy, highlighting the need for novel therapeutic approaches (27, 28). Indeed, good prediction models, like good therapies, are best compared head-to-head in novel patient populations (29). Therefore, developing a novel prognostic model in combination with other prognostic indicators IPI and COO might be necessary to assess the patient prognosis for individualized treatment. In recent years, an increasing number of studies have been conducted to identify novel prognostic indicators. For instance, Schmitz et al. applied exome and transcriptome sequencing methods on 574 DLBCL biopsy samples to construct a new genetic subtype for DLBCL classification to guide therapy (30). Han et al. demonstrated that piRNA-30473, which promotes DLBCL progression by regulating m6A RNA methylation in DLBCL, can improve the prognostic stratification and therapeutic approach (31). With the development of next-generation sequencing, many prognostic

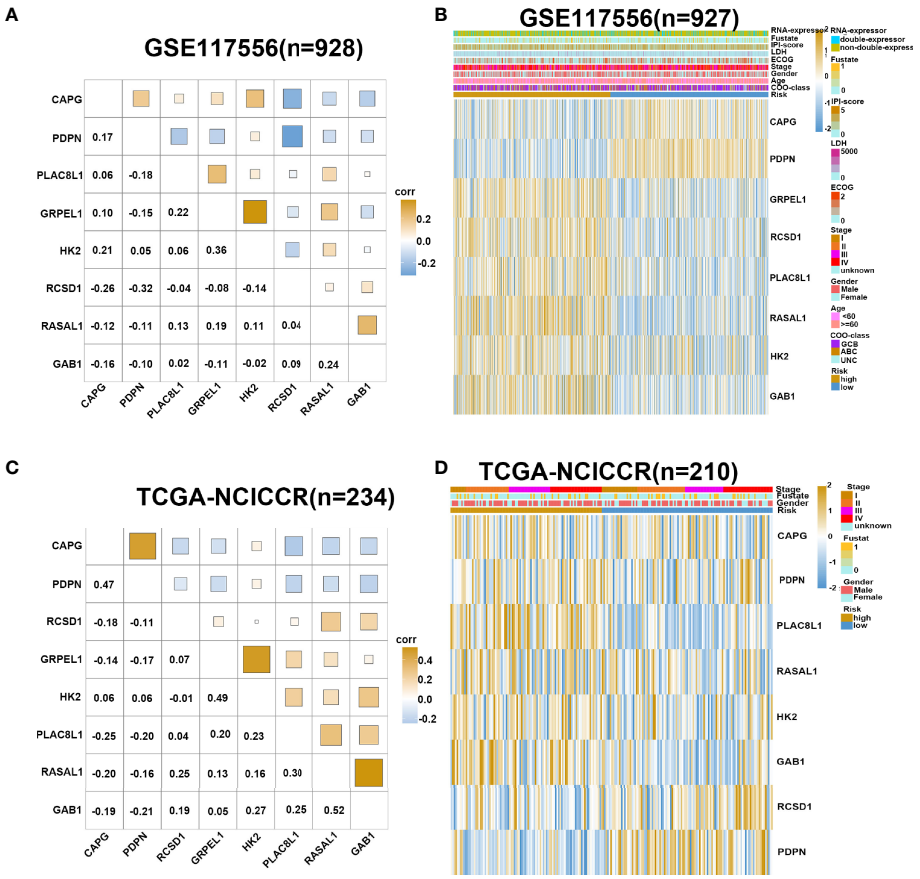

FIGURE 3 | Gene expression in high- and low-risk group. **(A)** Corrplot shows correlation of eight genes in GSE117556 dataset. **(B)** Heatmap shows gene expression of eight genes and clinical parameters in high- and low-risk group in GSE117556 dataset. **(C)** Corrplot shows correlation of eight genes in TCGA-NCICCR dataset. **(D)** Heatmap shows gene expression of eight genes and clinical parameters in high- and low-risk groups in TCGA-NCICCR dataset.

cancer models have been established in recent years (32–34) based on public transcriptomic databases such as the GEO and TCGA datasets.

The present study explored DLBCL gene expression datasets with corresponding clinical information of patients from the GEO to identify candidate genes that were significantly related to OS. After performing univariate Cox proportional hazards regression analysis, 11 protective and 13 risk genes were identified. Finally, we constructed an eight-gene prognostic signature through the LASSO method and multivariate Cox regression analysis. There had been several previous studies that were consistent and corroborated with the prognostic value of our risk score model. For example, HK2, GAB1, and RASAL1 were risk genes in our model. HK2 is known to be a key metabolic enzyme by promoting glucose uptake in cells and facilitating the Warburg effect. HK2 had been explored as a major player in helping maintain the highly malignant state in many types of cancer (35–37). Bhalla et al. also provided strong support for the direct contribution of HK2 in B-cell lymphoma development and suggested that HK2 is a key metabolic driver of the DLBCL phenotype (38). GAB1, which is widely distributed in various body tissues, is capable of promoting cell proliferation, and its expression may enhance the carcinogenesis and cancer progression (39, 40). Chang et al. clarified that RASAL1 was increased in ovarian adenocarcinoma tumorous tissues and HEY cells, which correlated with poor prognosis in ovarian adenocarcinoma patients (41). Kaplan–Meier analysis demonstrated that the risk model could predict the outcome for patients with DLBCL in training, testing, and validating datasets. Similar conclusions were reached when our clinical cohort data were applied. ROC curve analysis consistently indicated the good performance of our risk model. We then conducted correlation analysis to evaluate the collinearity among the eight prognostic genes. Importantly, we found that the correlation among these genes was low, suggesting that the regression coefficients of this model were reliable and stable (42).

At present, different approaches are adopted in clinical practice to evaluate the occurrence and development of DLBCL at different levels, including gene expression patterns (ABC, GCB, UC), ECOG, IPI, DELs, LDH, age-adjusted IPI, gender, stages, and so on. Patients with the GCB subtype, for

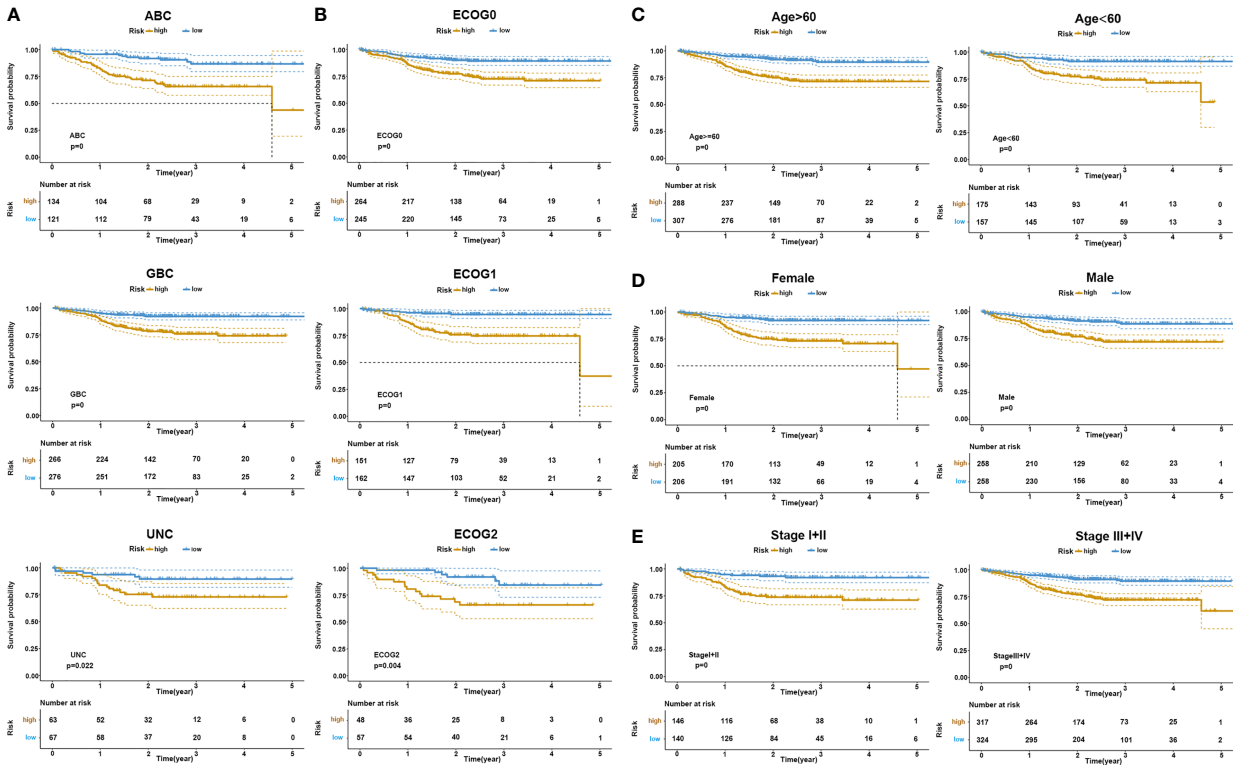

FIGURE 4 | KM survival stratification analyses in the GSE117556 dataset. **(A)** COO subgroup. **(B)** ECOG stage. **(C)** Age. **(D)** Gender. **(E)** Clinical stage.

example, usually have a better prognosis than the ABC subtype (6, 43). It has been established that DELs are generally aggressive and respond poorly to currently available therapies (9, 44, 45). Moreover, IPI and age-adjusted IPI have been developed as models for predicting outcomes based on clinical factors from more than 4,000 patients (46, 47). However, despite overall improvements in DLBCL patient outcomes, 30%–40% of patients develop relapsed or refractory disease (48). In the present study, after stratification based on clinical characteristics such as gene expression patterns (ABC, GCB, UC), ECOG, IPI, DELs, LDH, age-adjusted IPI, gender, and Ann Arbor stages, the difference in OS between the high- and low-risk groups was still statistically significant. This finding suggests that our model can be combined with existing clinical parameters to reduce false positives and negatives, improve diagnostic accuracy, and provide effective treatment.

An increasing body of evidence suggests that the TME affects the prognosis of DLBCL patients. Lenz et al. analyzed gene expression in 181 pretreatment biopsy specimens derived from DLBCL patients and found that the survival of patients with DLBCL was affected by immune cells, fibrosis, and angiogenesis in the tumor microenvironment (49). Mueller et al. also demonstrated that DLBCL recruited T cells and monocytes *via* CCL5 to support B-cell survival and proliferation (50). By immunohistochemical staining, Chang et al. showed the presence of CD1a+ dendritic cells (DCs) and increased granzyme B+ T cells within tumors was associated with a favorable prognosis (51). It has been established that M1 cells play a proinflammatory and anticancer role in the TME of DLBCL, while M2 type plays an immunosuppressive role to promote cancer progression (47, 52, 53). Herein, we used two algorithms to evaluate the TME of patients with DLBCL and found that patients in the high-risk score group exhibited significant B-cell infiltration with mild infiltration of M0, M1, CD8+ T cells, and DCs. Our results suggest the presence of an immunosuppressive TME in patients from the high-risk group leading to cancer progression. Finally, we evaluated the potential value of applying our risk score model to clinical practice. Based on the results of univariate regression analysis, multivariate regression analysis, and nomogram, our model has huge prospects for application in clinical practice.

However, our study was significantly limited by its retrospective nature as DLBCL samples were from different platforms, which may be a source of sampling bias. Well-designed prospective clinical trials should be conducted in the future to highlight the role of our prediction model in DLBCL progression and metastasis.

CONCLUSIONS

In summary, this study identified an eight-gene prognostic signature that can effectively predict DLBCL patient outcomes. The eight-gene prognostic model related to TME in combination

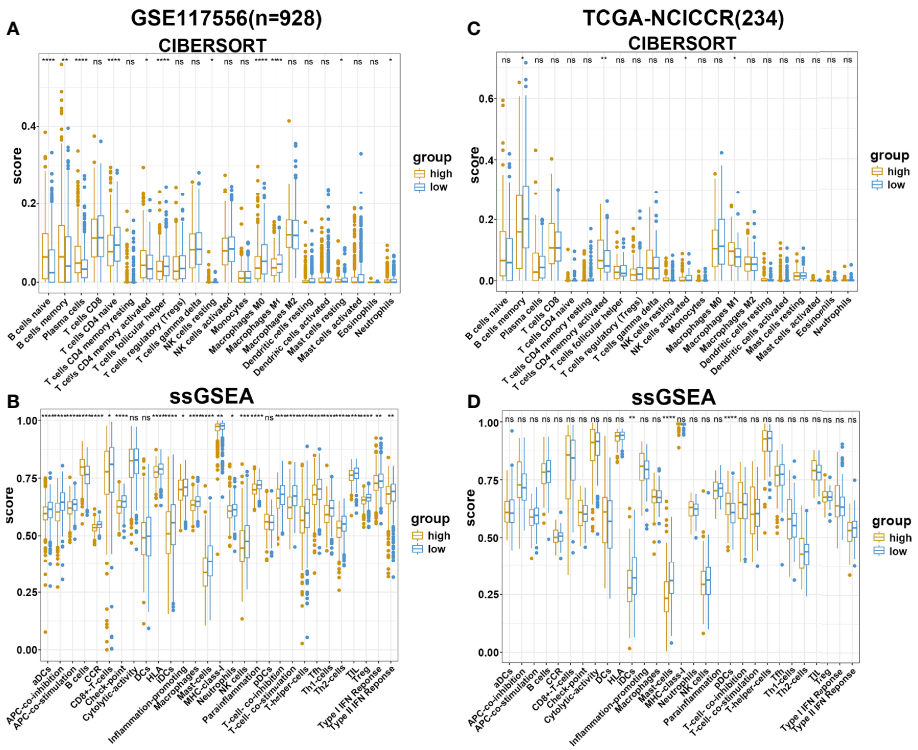

FIGURE 5 | Immune estimation in high- and low-risk groups. **(A, B)** The difference of immune infiltration in high- and low-risk groups estimated by CIBERSORT and ssGSEA in the GSE117556 datasets. **(C, D)** The difference of immune infiltration in high- and low-risk groups estimated by CIBERSORT and ssGSEA in TCGA-NCICCR datasets. ns, Not Significant; * P < 0.05; ** P < 0.01; *** P < 0.001; **** P < 0.0001.

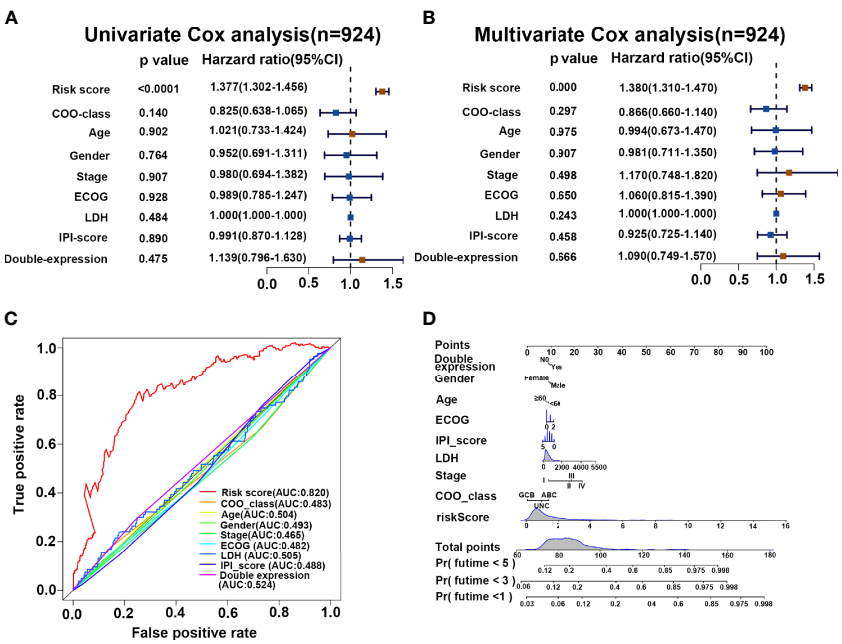

FIGURE 6 | Risk score is a superior biomarker for evaluating the prognosis of DLBCL. **(A, B)** Forest plot summary of the univariate and multivariable analyses of risk score and other clinical parameters. **(C)** ROC analysis of risk score and other clinical parameters. **(D)** Nomogram integrating the risk score and clinical parameters for predicting the probability of patient mortality at 1, 3, and 5 years of OS.

with other prognostic indicators IPI and COO might be useful to clinicians when evaluating the prognosis of patients for individualized treatment.

DATA AVAILABILITY STATEMENT

The datasets GSE117556, GSE10846 and GSE31312 for this study can be found in the GEO (https://www.ncbi.nlm.nih.gov/geo).The datasets NCICCR for this study can be found at TCGA (https://portal.gdc.cancer.gov/repository).

ETHICS STATEMENT

The studies involving human participants were reviewed and approved by the ethics committee of the First Affiliated Hospital of Zhengzhou University. The patients/participants provided their written informed consent to participate in this study.

AUTHOR CONTRIBUTIONS

MZ, JY, and LL contributed to the design and implementation of the research. WY and JZ contributed to the analysis of the results and to the writing of the manuscript. JY, LZ, and XZ designed the figures. All authors listed have made a substantial, direct, and intellectual contribution to the work and approved it for publication.

FUNDING

This work was supported by the National Natural Science Foundation of China (Grant no. 81500174).

SUPPLEMENTARY MATERIAL

The Supplementary Material for this article can be found online at: https://www.frontiersin.org/articles/10.3389/fendo.2022.846357/full#supplementary-material

Supplementary Figure 1 | Selection of genes for constructing predicting model. **(A)** LASSO coefficient profiles of 24 genes. **(B)** Partial likelihood deviance plot. **(C)** Forest plot shows the multivariable Cox regression analysis of eight genes.

Supplementary Figure 2 | Exploring function of HK2. **(A)** RT-PCR analysis showing HK2 expression stage I+II and III+IV. **(B)** Correlation analysis of HK2. **(C)** GO enrichment analysis of negative and positive correlated genes. **(D)** KEGG enrichment analysis of negative and positive correlated genes.

Supplementary Figure 3 | Survival information of the patients between high- and low-risk group. **(A)** The correlation of risk score and patient numbers. **(B)** The correlation of risk score and survival time.

Supplementary Figure 4 | Validation of prediction model in testing set. **(A, B)** Kaplan-Meier analysis between high and low risk group in GSE31312 and GSE10864 datasets. **(C, D)** ROC curve analysis of GSE31312 and GSE10864 datasets.

Supplementary Figure 5 | KM survival stratifcation analyses in GSE117556 dataset. **(A)** MYC/BCL2 expression. **(B)** LDH level.

Supplementary Figure 6 | Expression of immune-related genes in high and low risk group. **(A, B)** Boxplot showed difference of immune-related genes in high and low risk group in GSE117556 and TCGA-NCICCR dataset, respectively.

REFERENCES

1. Teras LR, DeSantis CE, Cerhan JR, Morton LM, Jemal A, Flowers CR. 2016 US Lymphoid Malignancy Statistics by World Health Organization Subtypes. *CA Cancer J Clin* (2016) 66:443–59. doi: 10.3322/caac.21357
2. Sukswai N, Lyapichev K, Khoury JD, Medeiros LJ. Diffuse Large B-Cell Lymphoma Variants: An Update. *Pathology* (2020) 52:53–67. doi: 10.1016/j.pathol.2019.08.013
3. Pasqualucci L, Dalla-Favera R. Genetics of Diffuse Large B-Cell Lymphoma. *Blood* (2018) 131:2307–19. doi: 10.1182/blood-2017-11-764332
4. Liu Y, Barta SK. Diffuse Large B-Cell Lymphoma: 2019 Update on Diagnosis, Risk Stratification, and Treatment. *Am J Hematol* (2019) 94:604–16. doi: 10.1002/ajh.25460
5. Alizadeh AA, Eisen MB, Davis RE, Ma C, Lossos IS, Rosenwald A, et al. Distinct Types of Diffuse Large B-Cell Lymphoma Identified by Gene Expression Profiling. *Nature* (2000) 403:503–11. doi: 10.1038/35000501
6. Hans C, Weisenburger D, Greiner T, Gascoyne R, Delabie J, Ott G, et al. Confirmation of the Molecular Classification of Diffuse Large B-Cell Lymphoma by Immunohistochemistry Using a Tissue Microarray. *Blood* (2004) 103:275–82. doi: 10.1182/blood-2003-05-1545
7. Reddy A, Zhang J, Davis N, Moffitt A, Love C, Waldrop A, et al. Genetic and Functional Drivers of Diffuse Large B Cell Lymphoma. *Cell* (2017) 171:481–94.e15. doi: 10.1016/j.cell.2017.09.027
8. Aukema SM, Siebert R, Schuuring E, van Imhoff GW, Kluin-Nelemans HC, Boerma EJ, et al. Double-Hit B-Cell Lymphomas. *Blood* (2011) 117:2319–31. doi: 10.1182/blood-2010-09-297879
9. Riedell P, Smith S. Double Hit and Double Expressors in Lymphoma: Definition and Treatment. *Cancer* (2018) 124:4622–32. doi: 10.1002/cncr.31646
10. Miyazaki K. Treatment of Diffuse Large B-Cell Lymphoma. *J Clin Exp Hematop* (2016) 56:79–88. doi: 10.3960/jslrt.56.79
11. Alizadeh AA, Gentles AJ, Alencar AJ, Liu CL, Kohrt HE, Houot R, et al. Prediction of Survival in Diffuse Large B-Cell Lymphoma Based on the Expression of 2 Genes Reflecting Tumor and Microenvironment. *Blood* (2011) 118:1350–8. doi: 10.1182/blood-2011-03-345272
12. Zelenetz AD, Abramson JS, Advani RH, Andreadis CB, Byrd JC, Czuczman MS, et al. NCCN Clinical Practice Guidelines in Oncology: Non-Hodgkin's Lymphomas. *J Natl Compr Canc Netw* (2010) 8:288–334. doi: 10.6004/jnccn.2010.0021
13. Gutiérrez-García G, Cardesa-Salzmann T, Climent F, González-Barca E, Mercadal S, Mate JL, et al. Gene-Expression Profiling and Not Immunophenotypic Algorithms Predicts Prognosis in Patients With Diffuse Large B-Cell Lymphoma Treated With Immunochemotherapy. *Blood* (2011) 117:4836–43. doi: 10.1182/blood-2010-12-322362
14. Yin Z, Dong C, Jiang K, Xu Z, Li R, Guo K, et al. Heterogeneity of Cancer-Associated Fibroblasts and Roles in the Progression, Prognosis, and Therapy of Hepatocellular Carcinoma. *J Hematol Oncol* (2019) 12:101. doi: 10.1186/s13045-019-0782-x
15. Zhang D, He W, Wu C, Tan Y, He Y, Xu B, et al. Scoring System for Tumor-Infiltrating Lymphocytes and Its Prognostic Value for Gastric Cancer. *Front Immunol* (2019) 10:71. doi: 10.3389/fimmu.2019.00071
16. Autio M, Leivonen SK, Brück O, Mustjoki S, Jørgensen JM, Karjalainen-Lindsberg ML, et al. Immune Cell Constitution in the Tumor Microenvironment Predicts the Outcome in Diffuse Large B-Cell

Lymphoma. *Haematologica* (2020) 106(3):718–29. doi: 10.3324/haematol.2019.243626
17. Cioroianu AI, Stinga PI, Sticlaru L, Cioplea MD, Nichita L, Popp C, et al. Tumor Microenvironment in Diffuse Large B-Cell Lymphoma: Role and Prognosis. *Anal Cell Pathol (Amst)* (2019) 2019:8586354. doi: 10.1155/2019/8586354
18. Opinto G, Vegliante MC, Negri A, Skrypets T, Loseto G, Pileri SA, et al. The Tumor Microenvironment of DLBCL in the Computational Era. *Front Oncol* (2020) 10:351. doi: 10.3389/fonc.2020.00351
19. Xie Z, Li M, Hong H, Xu Q, He Z, Peng Z. Expression of N(6)-Methyladenosine (M(6)A) Regulators Correlates With Immune Microenvironment Characteristics and Predicts Prognosis in Diffuse Large Cell Lymphoma (DLBCL). *Bioengineered* (2021) 12:6115–33. doi: 10.1080/21655979.2021.1972644
20. Feng P, Li H, Pei J, Huang Y, Li G. Identification of a 14-Gene Prognostic Signature for Diffuse Large B Cell Lymphoma (DLBCL). *Front Genet* (2021) 12:625414. doi: 10.3389/fgene.2021.625414
21. Luo C, Nie H, Yu L. Identification of Aging-Related Genes Associated With Prognostic Value and Immune Microenvironment Characteristics in Diffuse Large B-Cell Lymphoma. *Oxid Med Cell Longev* (2022) 2022:3334522. doi: 10.1155/2022/3334522
22. He R, Zuo S. A Robust 8-Gene Prognostic Signature for Early-Stage Non-Small Cell Lung Cancer. *Front Oncol* (2019) 9:693. doi: 10.3389/fonc.2019.00693
23. Friedman J, Hastie T, Tibshirani R. Regularization Paths for Generalized Linear Models *via* Coordinate Descent. *J Stat Softw* (2010) 33:1–22. doi: 10.18637/jss.v033.i01
24. Newman A, Liu C, Green M, Gentles A, Feng W, Xu Y, et al. Robust Enumeration of Cell Subsets From Tissue Expression Profiles. *Nat Methods* (2015) 12:453–7. doi: 10.1038/nmeth.3337
25. Bindea G, Mlecnik B, Tosolini M, Kirilovsky A, Waldner M, Obenauf A, et al. Spatiotemporal Dynamics of Intratumoral Immune Cells Reveal the Immune Landscape in Human Cancer. *Immunity* (2013) 39:782–95. doi: 10.1016/j.immuni.2013.10.003
26. Iasonos A, Schrag D, Raj GV, Panageas KS. How to Build and Interpret a Nomogram for Cancer Prognosis. *J Clin Oncol* (2008) 26:1364–70. doi: 10.1200/JCO.2007.12.9791
27. Chapuy B, Stewart C, Dunford AJ, Kim J, Kamburov A, Redd RA, et al. Molecular Subtypes of Diffuse Large B Cell Lymphoma Are Associated With Distinct Pathogenic Mechanisms and Outcomes. *Nat Med* (2018) 24:679–90. doi: 10.1038/s41591-018-0016-8
28. Crombie J. Classifying DLBCL Subtypes for Optimal Treatment. *Oncol (Williston Park)* (2019) 33(10):686504.
29. Link B. Foreseeing What Is to Happen in DLBCL. *Blood* (2020) 135:2014–5. doi: 10.1182/blood.2020005678
30. Schmitz R, Wright G, Huang D, Johnson C, Phelan J, Wang J, et al. Genetics and Pathogenesis of Diffuse Large B-Cell Lymphoma. *N Engl J Med* (2018) 378:1396–407. doi: 10.1056/NEJMoa1801445
31. Han H, Fan G, Song S, Jiang Y, Qian C, Zhang W, et al. piRNA-30473 Contributes to Tumorigenesis and Poor Prognosis by Regulating M6a RNA Methylation in DLBCL. *Blood* (2021) 137:1603–14. doi: 10.1182/blood.2019003764
32. Ye Z, Zou S, Niu Z, Xu Z, Hu Y. A Novel Risk Model Based on Lipid Metabolism-Associated Genes Predicts Prognosis and Indicates Immune Microenvironment in Breast Cancer. *Front Cell Dev Biol* (2021) 9:691676. doi: 10.3389/fcell.2021.691676
33. Cao R, Yuan L, Ma B, Wang G, Tian Y. Immune-Related Long Non-Coding RNA Signature Identified Prognosis and Immunotherapeutic Efficiency in Bladder Cancer (BLCA). *Cancer Cell Int* (2020) 20:276. doi: 10.1186/s12935-020-01362-0
34. Zhu G, Xia H, Tang Q, Bi F. An Epithelial-Mesenchymal Transition-Related 5-Gene Signature Predicting the Prognosis of Hepatocellular Carcinoma Patients. *Cancer Cell Int* (2021) 21:166. doi: 10.1186/s12935-021-01864-5
35. Chen J, Yu Y, Li H, Hu Q, Chen X, He Y, et al. Long Non-Coding RNA PVT1 Promotes Tumor Progression by Regulating the miR-143/HK2 Axis in Gallbladder Cancer. *Mol Cancer* (2019) 18:33. doi: 10.1186/s12943-019-0947-9
36. Mathupala SP, Ko YH, Pedersen PL. Hexokinase II: Cancer's Double-Edged Sword Acting as Both Facilitator and Gatekeeper of Malignancy When Bound to Mitochondria. *Oncogene* (2006) 25:4777–86. doi: 10.1038/sj.onc.1209603
37. Fan K, Fan Z, Cheng H, Huang Q, Yang C, Jin K, et al. Hexokinase 2 Dimerization and Interaction With Voltage-Dependent Anion Channel Promoted Resistance to Cell Apoptosis Induced by Gemcitabine in Pancreatic Cancer. *Cancer Med* (2019) 8:5903–15. doi: 10.1002/cam4.2463
38. Bhalla K, Jaber S, Nahid MN, Underwood K, Beheshti A, Landon A, et al. Role of Hypoxia in Diffuse Large B-Cell Lymphoma: Metabolic Repression and Selective Translation of HK2 Facilitates Development of DLBCL. *Sci Rep* (2018) 8:744–. doi: 10.1038/s41598-018-19182-8
39. Sang H, Li T, Li H, Liu J. Down-Regulation of Gab1 Inhibits Cell Proliferation and Migration in Hilar Cholangiocarcinoma. *PloS One* (2013) 8:e81347–e. doi: 10.1371/journal.pone.0081347
40. Liu H, Li G, Zeng W, Zhang P, Fan F, Tu Y, et al. Combined Detection of Gab1 and Gab2 Expression Predicts Clinical Outcome of Patients With Glioma. *Med Oncol* (2014) 31:77. doi: 10.1007/s12032-014-0077-6
41. Chang RX, Cui AL, Dong L, Guan SP, Jiang LY, Miao CX. Overexpression of RASAL1 Indicates Poor Prognosis and Promotes Invasion of Ovarian Cancer. *Open Life Sci* (2019) 14:133–40. doi: 10.1515/biol-2019-0015
42. Basagaña X, Barrera-Gómez J. Reflection on Modern Methods: Visualizing the Effects of Collinearity in Distributed Lag Models. *Int J Epidemiol* (2021) 51(1):334–44. doi: 10.1093/ije/dyab179
43. Sarkozy C, Sehn L. Management of Relapsed/Refractory DLBCL. *Best Pract Res Clin Haematol* (2018) 31:209–16. doi: 10.1016/j.beha.2018.07.014
44. Aggarwal A, Rafei H, Alakeel F, Finianos AN, Liu M-L, El-Bahesh E, et al. Outcome of Patients With Double-Expressor Lymphomas (DELs) Treated With R-CHOP or R-EPOCH. *Blood* (2016) 128:5396. doi: 10.1182/blood.V128.22.5396.5396
45. Hu S, Xu-Monette Z, Tzankov A, Green T, Wu L, Balasubramanyam A, et al. MYC/BCL2 Protein Coexpression Contributes to the Inferior Survival of Activated B-Cell Subtype of Diffuse Large B-Cell Lymphoma and Demonstrates High-Risk Gene Expression Signatures: A Report From The International DLBCL Rituximab-CHOP Consortium Program. *Blood* (2013) 121:4021–31; quiz 250. doi: 10.1182/blood-2012-10-460063
46. Martelli M, Ferreri AJM, Agostinelli C, Di Rocco A, Pfreundschuh M, Pileri SA. Diffuse Large B-Cell Lymphoma. *Crit Rev Oncol/Hematol* (2013) 87:146–71. doi: 10.1016/j.critrevonc.2012.12.009
47. Papageorgiou S, Thomopoulos T, Katagas I, Bouchla A, Pappa V. Prognostic Molecular Biomarkers in Diffuse Large B-Cell Lymphoma in the Rituximab Era and Their Therapeutic Implications. *Ther Adv Hematol* (2021) 12:20406207211013987. doi: 10.1177/20406207211013987
48. Klyuchnikov E, Bacher U, Kroll T, Shea T, Lazarus H, Bredeson C, et al. Allogeneic Hematopoietic Cell Transplantation for Diffuse Large B Cell Lymphoma: Who, When and How? *Bone Marrow Transplant* (2014) 49:1–7. doi: 10.1038/bmt.2013.72
49. Lenz G, Wright G, Dave S, Xiao W, Powell J, Zhao H, et al. Stromal Gene Signatures in Large-B-Cell Lymphomas. *N Engl J Med* (2008) 359:2313–23. doi: 10.1056/NEJMoa0802885
50. Mueller C, Boix C, Kwan W, Daussy C, Fournier E, Fridman W, et al. Critical Role of Monocytes to Support Normal B Cell and Diffuse Large B Cell Lymphoma Survival and Proliferation. *J Leukocyte Biol* (2007) 82:567–75. doi: 10.1189/jlb.0706481
51. Chang K, Huang G, Jones D, Lin Y. Distribution Patterns of Dendritic Cells and T Cells in Diffuse Large B-Cell Lymphomas Correlate With Prognoses. *Clin Cancer Res* (2007) 13:6666–72. doi: 10.1158/1078-0432.CCR-07-0504
52. Staiger A, Altenbuchinger M, Ziepert M, Kohler C, Horn H, Huttner M, et al. A Novel Lymphoma-Associated Macrophage Interaction Signature (LAMIS) Provides Robust Risk Prognostication in Diffuse Large B-Cell Lymphoma Clinical Trial Cohorts of the DSHNHL. *Leukemia* (2020) 34:543–52. doi: 10.1038/s41375-019-0573-y
53. Kridel R, Steidl C, Gascoyne R. Tumor-Associated Macrophages in Diffuse Large B-Cell Lymphoma. *Haematologica* (2015) 100:143–5. doi: 10.3324/haematol.2015.124008

Conflict of Interest: The authors declare that the research was conducted in the absence of any commercial or financial relationships that could be construed as a potential conflict of interest.

this article, or claim that may be made by its manufacturer, is not guaranteed or endorsed by the publisher.

frontiers | Frontiers in Endocrinology

ORIGINAL RESEARCH
published: 12 May 2022
doi: 10.3389/fendo.2022.873662

The Proliferation and Stemness of Peripheral Blood-Derived Mesenchymal Stromal Cells Were Enhanced by Hypoxia

Pengzhen Wang[1*], *Pingping Zhu*[2], *Chaosheng Yu*[3] *and Jian Wu*[3]

[1] Guangzhou Institute of Traumatic Surgery, Guangzhou Red Cross Hospital, Jinan University, Guangzhou, China, [2] Department of Neurology, Guangzhou Red Cross Hospital, Jinan University, Guangzhou, China, [3] Department of Otorhinolaryngology, Guangzhou Red Cross Medicine, Jinan University, Guangzhou, China

OPEN ACCESS

Edited by:
Ihtisham Bukhari,
Fifth Affiliated Hospital of Zhengzhou University, China

Reviewed by:
Fu Wang,
Xi'an Jiaotong University, China
Zoey Xia,
Second Hospital of Tianjin Medical University, China

***Correspondence:**
Pengzhen Wang
wang521jnu@163.com

Specialty section:
This article was submitted to Cancer Endocrinology, a section of the journal Frontiers in Endocrinology

Received: *11 February 2022*
Accepted: *05 April 2022*
Published: *12 May 2022*

Citation:
Wang P, Zhu P, Yu C and Wu J (2022) The Proliferation and Stemness of Peripheral Blood-Derived Mesenchymal Stromal Cells Were Enhanced by Hypoxia. Front. Endocrinol. 13:873662. doi: 10.3389/fendo.2022.873662

This study aimed to address the dilemma of low peripheral blood-derived mesenchymal stromal cell (PBMSC) activity and reduced phenotype in bone or cartilage tissue engineering. Rat PBMSCs (rPBMSCs) were obtained by density gradient centrifugation, and stromal cell characteristics were confirmed by flow cytometry (FCM) and multi-differentiation potential induction experiments. Cell growth curve, viability experiments, and clone formation experiments were performed by [3-(4,5-dimethylthiazol-2-yl)-5-(3-carboxymethoxyphenyl)-2-(4-sulfophenyl)-2H-tetrazolium] (MTS) and cell counting, and the cell cycle was confirmed by cell FCM. The proliferation signal pathway and stemness-related proteins were detected by molecular methods including Western blot and real-time polymerase chain reaction. *CD73, CD90*, and *CD105* were highly expressed, and *CD14, CD19, CD34, CD45*, and *HLA-DR* were barely expressed in rPBMSCs. rPBMSCs possessed the potential to differentiate into chondrocytes, adipocytes, and osteoblasts under their respective induction conditions. Cell growth curve and viability experiments were performed under hypoxic conditions: 19% O_2, 5% O_2, and 1% O_2. Specifically, 5% O_2 accelerated the proliferation and expression of the stemness of PBMSCs. Cycle experiments proved that hypoxia promoted the cell transition from the G1 phase to the S phase. Molecular experiments confirmed that 5% O_2 hypoxia significantly elevated the expressions of hypoxia-inducible factor 1α and β-catenin and simultaneously the expressions of cycle-related genes including *CyclinE/CDK2* and stemness-related genes including *Nanog* and *SOX2*. The appropriate concentration of hypoxia (i.e., 5% O_2) enhanced the proliferation and stemness of rPBMSCs and increased the multidirectional differentiation potential of stromal cells. The proposed culture method could improve the viability and maintain the phenotype of rPBMSCs in cartilage or bone tissue engineering.

Keywords: peripheral blood-derived mesenchymal stromal cells (PBMSCs), hypoxia, HIF-1α, proliferation, stemness

INTRODUCTION

In recent years, mesenchymal stromal cells (MSCs) derived from adults have been widely used not only for bioregenerative tissue engineering but also for pathophysiological research and cell and gene therapy of bone diseases (1–4). Many studies have confirmed that bone marrow-derived MSCs are a relatively stable source, but the low yield and traumatic source of stromal cells had limited preclinical and clinical applications (5, 6). In recent literature, the applications of peripheral blood-derived MSCs (PBMSCs) in tissue engineering have attracted increasing attention because of their relatively easy collection, abundant sources, and multilineage differentiation potential (7, 8).

The committee of the International Society for Cellular Therapy standardized the criteria for defining human MSCs for basic and preclinical research. That is, cells can adhere and the MSC population must positively express *CD105*, *CD73*, and *CD90* and negatively express *CD45*, *CD34*, *CD14* or *CD11b*, *CD79a* or *CD19*, and *HLA-DR*. MSCs also have the potential to differentiate into chondrocytes, osteoblasts, and adipocytes (9). When many cells are needed for research or clinical applications, PBMSCs can take on this important task (10, 11). However, the reduced activity of PBMSCs cultured *in vitro* and phenotype loss easily limit this demand (11). Therefore, the key to cartilage tissue engineering is to provide phenotype-maintaining MSCs expanded *in vitro*. Some growth factors or physical factors, such as basic fibroblast growth factor (bFGF) (12), transforming growth factor-β (TGF-β) (13), and oxygen level (14), play a decisive role in stromal cell survival or proliferation. Thus, TGF-β, bFGF, and oxygen levels have affected stromal cell survival or proliferation (12–14). Hypoxia is a simple and easy-to-operate strategy with few side effects. The exposure of MSCs to a hypoxic environment for a moderate time could enhance cell survival characteristics and tissue repair capabilities, and this conclusion was confirmed by recent studies (15). To enhance the therapeutic effect, several studies have conducted hypoxic pretreatments in many disease-related organs and tissues, such as cardiomyocytes (16). In the literature, compared with normoxic conditions, a hypoxic condition significantly promotes MSCs to further express *Oct4*, *cMyc*, *Nanog*, and *SOX2*. Simultaneously, hypoxia-cultured MSCs exhibited a better growth trend and a higher proportion of S phase cells than normoxia-cultured MSCs (14–16).

Oxygen gradients derived from the bone marrow niche create hypoxic conditions for stromal and stem cells (17). Hypoxia strongly affects several aspects of cell biology, such as angiogenesis, innate immunity, cell proliferation, and stemness (18). The effects of hypoxia on stem cells are usually mediated by HIF-1α and HIF2α (19). The literature reported that incubation of umbilical cord derived mesenchymal stem cells (UC-derived MSCs) with different concentrations of oxygen resulted in increased cell proliferation under hypoxia. In this case, significant levels of HIF-1α could be observed in hypoxic MSCs cultured in 2.5% or 5% O_2 (20). Hypoxia-inducible factor 1α (HIF-1α), as a pivotal transcription factor regulating stress and adaptive responses to oxygen concentration (21), usually interacts directly with numerous proteins to regulate its function (22–24). Most classically, differentiation, proliferation, angiogenesis, and migration are directly correlated with HIF-1α and β-catenin (25–27). However, how HIF-1α is expressed in PBMSCs and how it regulates the maintenance of stemness and cell proliferation remain unclear.

This study hypothesized that hypoxia could promote the proliferation and differentiation of rPBMSCs by activating the expressions of HIF-1α, β-catenin, proliferative-related genes, and stemness-related genes. Thus, this study examined the ability of rPBMSCs to proliferate and maintain MSC phenotypes under different concentrations of oxygen *in vitro* culture to explore the effects and mechanisms of hypoxia on the maintenance of rPBMSC proliferation and stemness.

MATERIALS AND METHODS

Isolation and Culture of rPBMSCs

The animal ethics committee of Guangzhou Red Cross Hospital approved the research. Following previously published methods (28), a 3 cm × 3 cm wound was made on the back skin of the rats. The wound was disinfected every day, and the rats were provided with enough food and water to ensure their normal activities and survival. After 1 week, 0.8% pentobarbital was injected into the abdominal cavity of these animals for anesthesia. After anesthetization, approximately 5 mL of abdominal aortic blood was collected using a fine-needle approach, and the blood sample was diluted to 1:1 by PBS. Mononuclear cells (MNCs) were separated and collected with Ficoll separation solution (GBCBIO Technologies, Guangzhou, China) and centrifuged at 2000 rpm for 35 min. The middle layer was pipetted with a thin tube and washed twice with phosphate-buffered saline (PBS). MNCs (2×10^6/mL) were seeded onto the T-25 flask with 10 mL of complete Dulbecco's Modified Eagle Medium (Gibco, MA). The complete medium contained 1% penicillin/streptomycin (Gibco), 20 ng/mL bFGF (R&D Systems, MN), and 20% fetal bovine serum (Gibco). With 21 days of culture, the cell convergence was 80%, and the third-generation cells digested by 0.25% trypsin were used for subsequent experiments. Representative bright-field images were captured by an inverted phase-contrast microscope (Nikon ECLIPSE Ts2, Nikon).

Immunophenotype Analysis of rPBMSCs

The cell immune phenotypes of third-generation PBMSCs (P3 PBMSCs) were identified by flow cytometry (FCM). *CD73*, *CD105*, and *CD90* (R&D Systems, US) were selected as positive markers of rPBMSCs, whereas *CD14*, *CD19*, *CD34*, *CD45*, and *HLA-DR* (BD biosciences, US) were chosen as negative markers of rPBMSCs. rPBMSCs (2×10^5 cells/mL) were resuspended in PBS and mixed in *CD14*, *CD19*, *CD34*, *CD45*, *CD73*, *CD90*, *CD105*, and *HLA-DR* antibody solutions for 30 min, and the cell samples were then loaded on the machine for analysis.

Cell Cycle Distribution Assay

rPBMSCs treated under normoxic and hypoxic (5% O_2) conditions for 24 h were collected, and rPBMSCs were then fixed with 70% (V/V) ethanol overnight. Moreover, 50 μg/mL propidium iodide (PI) (Beyotime Biotechnology, Shanghai, China) was diluted by PBS solution containing 1% Triton X-100. Cells were fully infiltrated in the freshly prepared PI solution for 30 min and were analyzed by a BD FACScan flow cytometer (BD Company, CA).

Multilineage Differentiation Potential Assay

P3 rPBMSCs were seeded into a 24-well plate at a density of 2 × 10^4/well and cultured at 37°C in an incubator with 5% CO_2. When the cells grow to 70% confluence, chondrogenesis induction, osteoinduction, and adipogenesis tests were performed. For chondrogenesis, cells were induced for 21 days in a chondrogenesis induction medium kit (RAXMX-90041, Cyagen Biosciences, US). The differentiation was evaluated by alcian blue staining. For osteogenesis, the cultures were induced with an osteogenesis induction medium kit (RAXMX-90021, Cyagen Biosciences, CA). After culture for 21 days, alizarin red staining was performed to evaluate the osteogenic products. For adipogenesis, cells were induced for 21 days in an adipogenesis induction medium kit (RAXMX-90031, Cyagen Biosciences). The formation of lipid vacuoles was assessed by Oil Red O staining. All images were captured under an inverted phase-contrast microscope (Nikon ECLIPSE Ts2, Nikon).

Multilineage Differentiation Potential of rPBMSCs Cultured Under Normoxic (21% O_2 and 5% CO_2) or Hypoxic (5% O_2 and 5% CO_2) Conditions

P3 rPBMSCs were seeded into a 24-well plate at a density of 2 × 10^4/well and cultured at 37°C in a 21% O_2 and 5% CO_2 incubator or a 5% O_2 and 5% CO_2 incubator. The induction medium and experimental procedures performed in the subsequent experiments were the same as the methods described in "Multilineage Differentiation Potential Assay."

Determination of the Growth Curve of rPBMSCs and the MTS Assay

P3, P5, and P6 rPBMSCs (2× 10^3/well) were inoculated in microplates (24-well) in 5% CO_2 incubators with a gradient concentration of oxygen at 37°C. The experiments were set up as the control group (21% O_2 and 5% CO_2), 19% O_2 and 5% CO_2 hypoxia group, 5% O_2 and 5% CO_2 hypoxia group, and 1% O_2 and 5% CO_2 hypoxia group, with three replicate wells in each group. Starting from the next day, each group of cells was digested and counted accurately with a cell counter at each time point (Days 1–8). The growth curves of each cell group were made according to the number of cells. For the MTS assay, the above-mentioned groups of cells were planted on the well plate after Day 8, and the absorbance was measured at 450 nm by a multifunctional microplate reader (BioTek, US).

Assessment of Population Doubling Levels

After the cells reached 80-90% confluency, cells were passaged and counted. Calculate the cumulative population doubling (CPD) value using the following formula (29):

$$\frac{\log10(\text{ cells harvested }) - \log10(\text{ cells reseeded })}{\log 10} \quad (2)$$

CPD was plotted against time in culture and performed in triplicate for each counting procedure.

Assay for Colony Formation

Moreover, 500 rPBMSCs were cultured in 6-well plates in an incubator capable of adjusting oxygen concentration for 14 days. After fixation with paraformaldehyde for 15 min, 1 mL of crystal violet staining solution was added to the culture plate for staining clones for 30 min. Under an inverted phase-contrast microscope (Nikon ECLIPSE Ts2, Nikon), the number of clones containing more than 50 cells was counted.

Western Blot

rPBMSCs were collected after normoxic and hypoxic (5% O_2) treatments for 5 days, and whole-cell lysates were prepared for Western blotting in radioimmunoprecipitation assay buffer. Then, 30 μg of protein was loaded into the sample well, dispersed in the gel according to the molecular weight, and directly transferred to the poly(vinylidene fluoride) membrane (Bio-Rad, CA) in a band-to-band manner through the semi-dry transfer method. The membranes were immersed in a square dish filled with primary antibody diluent. These antibodies (HIF-1α, 36169; β-catenin, 8400; *SOX2*, 3579; *CyclinE*, 4132; *Nanog*, 8822; *GAPDH* [glyceraldehyde 3-phosphate dehydrogenase], 5174) were purchased from Cell Signaling Technology (MA), and when used, the dilution ratio was 1:1000. On the next day, membranes were incubated with secondary anti-rabbit/mouse IgG, HRP-linked antibody (#7074/7076, 1:3000, Cell Signaling Technology). The electrochemiluminescence detection mixture was used to detect the protein on the membranes. ChemiDoc XRS imaging system with Image Lab software (Bio-Rad) was used to analyze the graphs.

Immunofluorescence Microscopy

Furthermore, 10^4/well rPBMSCs were seeded in glass slides placed in plates treated under normoxia and hypoxia (5% O_2) for 5 days. After sequential fixation, blocking, incubation of primary (β-catenin,1:200, 8242, Cell Signaling Technology; HIF-1α, 1:200, #36169, Cell Signaling Technology) and secondary (1:200, ZF0311, OriGene Technologies, MD) antibodies, a fluorescence microscope (Ti2-U, Nikon) was used to observe and capture pictures of interest.

Real-Time Polymerase Chain Reaction (PCR)

The culture method of rPBMSCs was the same as with Western blot. Total RNA obtained by the TRIzol method was reversed into cDNA in the PrimeScript RT Master mix reaction system

(Takara Bio, Japan). With reference to the instructions, SYBR-Green reagent (Takara Bio) was used to perform real-time PCR in triplicate in a fluorescence quantitative PCR instrument (Jena, Germany). GAPDH was used as a control to analyze relative gene expression in the $2^{-\Delta\Delta Ct}$ formula (30). Primer sequences are presented in **Table 1**.

Statistical Analysis

Data in three replicates are presented as mean ± standard deviation. Student's t-test or one-way analysis of variance was used to analyze differences between the two groups and among multiple groups; $P < 0.05$ was used to mark significant differences.

RESULTS

In this study, rPBMSCs were successfully isolated and cultured. Stromal cell characteristics were proved by FCM and multi-differentiation potential induction experiments. The cell growth curves of P3, P5, and P6 rPBMSCs cultured under different oxygen concentrations were drawn based on the number counted at each time point. Then, the 5% hypoxia condition that significantly promoted cell growth was used for subsequent experiments. Hypoxia (5%) significantly increased the number of stromal cell clones and the proportion of S phase cells. Real-time RCR and Western blot results revealed that hypoxia (5%) significantly promoted the expressions of HIF-1α, β-catenin, and proliferation-related and stemness-related genes.

Characterization and Identification of rPBMSCs

On the day after inoculation, round or polygonal adherent cells were observed in the primary culture. After 7 days, colonies gradually formed. After approximately 16 days, the cell coverage area was 70%–80% of the bottom of the culture flask. At approximately 21 days later, the cell growth reached 100% (**Figure 1A**). Flow cytometry experiments revealed that rPBMSCs had high expression of *CD73*, *CD90*, and *CD105*, extremely low expressions of *CD14*, *CD19*, *CD34*, *CD45*, and *HLA-DR* (**Figure 1B**). Oil Red O staining indicated that rPBMSCs can differentiate into adipocytes embellished by red-stained lipid droplets. Alician blue staining demonstrated that after 21 days of induction, rPBMSCs could differentiate into chondrocytes embellished by blue-stained proteoglycans. Alizarin red staining presented that rPBMSCs could differentiate into osteoblasts embellished by red-stained bone nodules under osteogenic conditions (**Figure 1C**).

Hypoxia Promoted rPBMSC Growth and Proliferation

The results of the experiments are displayed in **Figures 2A, B**. In the first 2 days of culture, different concentrations of O_2 had no noticeable effects on the proliferation of third-generation PBMSCs (P3 rPBMSCs), fifth-generation PBMSCs (P5 rPBMSCs), and sixth-generation PBMSCs (P6 rPBMSCs). After 3 days, hypoxia (5% O_2) significantly increased the number of cells and proliferation rate of P3, P5, and P6 rPBMSCs. After 8 days, the cells approached the plateau stage. At this time, the number of P3 rPBMSCs in the control group, 19% O_2 hypoxia, 5% O_2 hypoxia, and 1% O_2 hypoxia groups were 55×10^3, 70×10^3, 96×10^3, and 71×10^3, respectively. Statistical analysis showed that compared with the number of P3 rPBMSCs in the control group, those in the 19% O_2 hypoxia, 5% O_2 hypoxia, and 1% O_2 hypoxia groups were increased significantly ($P < 0.05$). Compared with 19% O_2 hypoxia and 5% O_2 hypoxia, 1% O_2 hypoxia further increased the number of P3 rPBMSCs ($P < 0.05$). Similar to the growth curve, 5% O_2 hypoxia significantly promoted the absorbance of P3 rPBMSCs seeded at Day 8. The CPD curve of P6 PBMSCs proved that the CPD value of PBMSCs in the 5% hypoxia group was significantly higher than that in the normoxia group. Compared with the normoxia group, the CPD values for P6 PBMSCs in the 19% O_2 hypoxia and 1% O_2 hypoxia groups did not change significantly on Day 7. The shape of the growth curve and viability of P5 and P6 rPBMSCs were similar with those of P3 rPBMSCs, but the amounts of rPBMSCs and optical density values of P5 and P6 on Day 8 were lower than those of P3 rPBMSCs. Based on the cell growth curve and MTT assay results, 5% O_2 hypoxia was selected for subsequent experiments. As presented in **Figures 2C, D**, 5% O_2 hypoxia significantly promoted the formation of rPBMSC colonies. The number of rPBMSC colonies in the 5% O_2 hypoxia group was increased by 53% compared with that in the control group ($P < 0.05$).

Hypoxia Promoted Cell Cycle Transition and Maintained the Trilineage Differentiation Capacity of rPBMSCs

FCM was used to investigate the cell cycle transition of rPBMSCs treated under normoxia and hypoxia (5% O_2). Hypoxia exerted a significant increase and decrease in the number of S phase and

TABLE 1 | Sequences of primers used for gene amplification.

Genes	Forward	Reverse
GAPDH	5′-CCTGGAGAAACCTGCCAAGTAT-3′	5′-TAGCCCAGGATGCCCTTTAGT-3
β-catenin	5′- TCTGCGAACTTGCTCAGGAC -3′	5′- GAACTGGTCAGCTCAACCGA -3′
CyclinE	5′- TCCGCTTACTAGAAGTGTTTGT -3′	5′- TGTGGAAGGATAGCGATTGGG-3′
CDK2	5′- AGCTCTGCTTGCGTTCCAT -3′	5′- ACGTGCCCTCTCCAATCTTC -3′
Nanog	5′- TTAAGCTGTCTGGTCCGAGG -3′	5′- CTGAGAGAACACAGTCCGCA -3′
SOX2	5′- AGTGGTACGTTAGGCGCTTC-3′	5′- ATCGCCCGGAGTCTAGTTCT-3′
HIF-1α	5′- GGGTACGTGAGGCATGTTGA-3	5′- CCGTCGGTCAGACCAGAAAA -3′

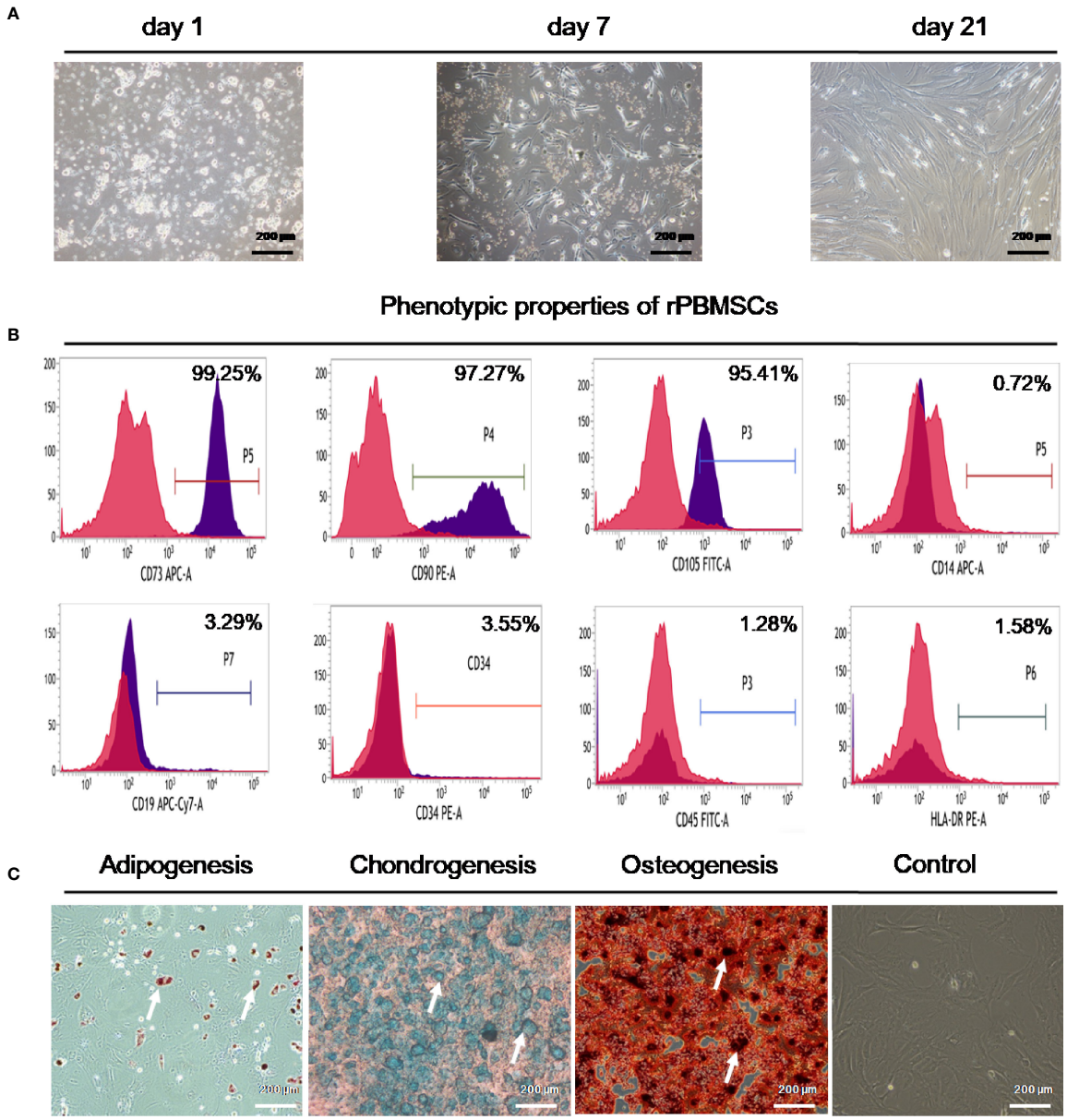

FIGURE 1 | Characteristics of rPBMSCs. **(A)** Morphology of rPBMSCs cultured for 1 day, 7 days, and 21 days. **(B)** Immunocytochemical staining demonstrated a positive expression of *CD73*, *CD90*, and *CD105* and negative expressions of *CD14, CD19, CD34, CD45 CD45*, and *HLA-DR*. **(C)** Multilineage differentiation capacities of rPBMSCs. Magnification, 200×. rPBMSCs, rat peripheral blood-derived mesenchymal stromal cells.

G1 phase cells, respectively (**Figures 3A, B**). Moreover, 5% O_2 hypoxia increased the percentage of rPBMSCs in the S phase from 27.26% to 46.32% ($P < 0.05$) and reduced the percentage of rPBMSCs in the G1 phase from 58.24% to 47.19% ($P < 0.05$). These data indicated that 5% O_2 hypoxia increased the DNA synthesis and cell cycle of rPBMSC progression at the S phase. After 21 days of culture with a differentiation agent under hypoxia or normoxia, the effect of hypoxia on the pluripotency of rPBMSCs was investigated. **Figure 3C** illustrates that hypoxia increased the ability of induced cells to differentiate into three lines, including osteoblasts, chondrocytes, and adipocytes.

Hypoxia Activated the Expression of β-Catenin and HIF-1α in rPBMSCs

As displayed in **Figure 4A**, 5% O_2 hypoxia significantly increased the HIF-1α (red) nuclei expression in rPBMSCs, compared with the control rPBMSCs. Simultaneously, the nuclei expression for

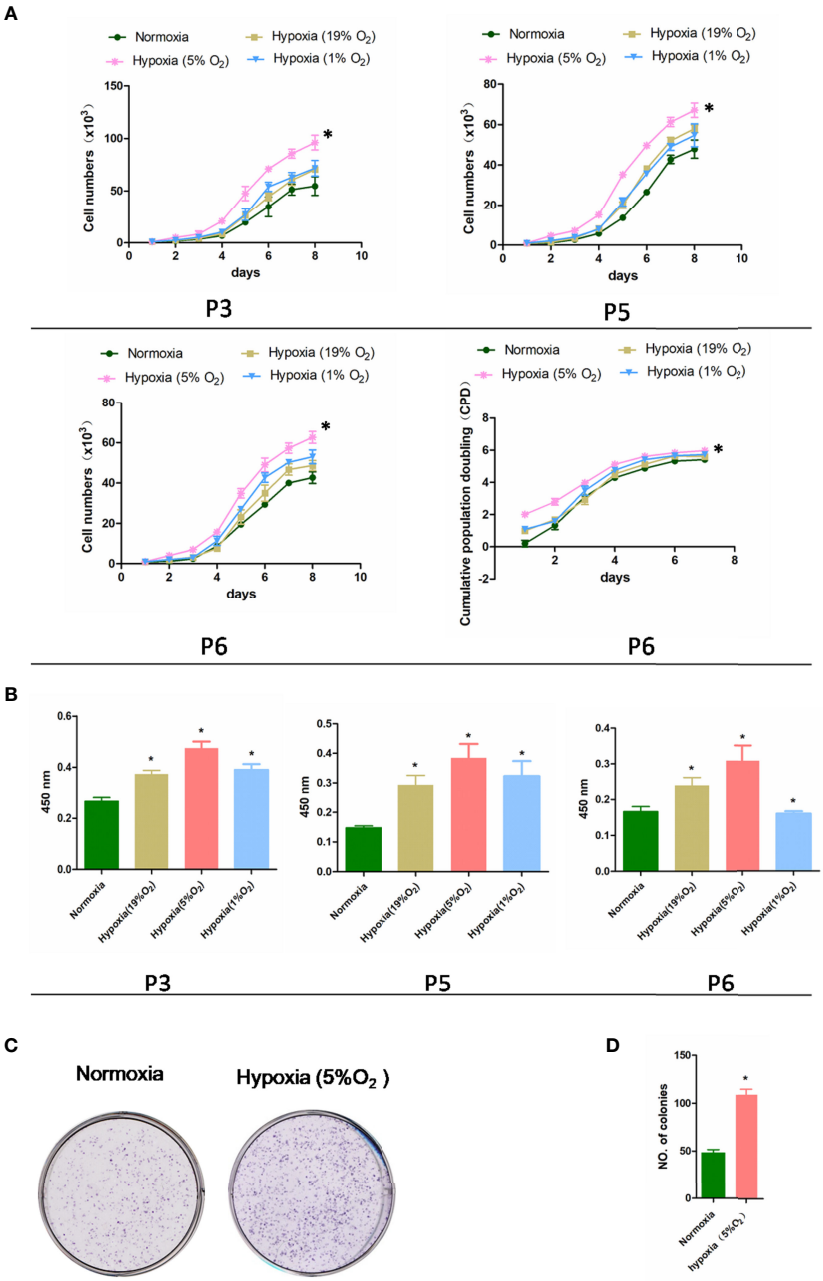

FIGURE 2 | Effect of hypoxia on rPBMSC proliferation. **(A)** The cell growth curves of third-generation PBMSCs (P3 PBMSCs), fifth-generation PBMSCs (P5 PBMSCs), and sixth-generation PBMSCs (P6 PBMSCs) were drawn based on the number of cells counted at each time point, the cumulative population doubling curve of sixth-generation PBMSCs (P6 PBMSCs) was determined based on cell culture time. **(B)** Absorbance of P3, P5, and P6 rPBMSCs treated under normoxia and hypoxia (5% O_2) at Day 8. **(C)** Hypoxia increased the number of rPBMSC colonies. **(D)** Measurement of the number of colonies in each group. All data are presented as means ± SEM. P < 0. 05; * vs control group. rPBMSCs, rat peripheral blood-derived mesenchymal stromal cells.

β-catenin (green) in rPBMSCs was also upregulated significantly with 5% O_2 hypoxia. Immunohistochemistry results (**Figure 4B**) that 5% O_2 hypoxia stimulated the upregulation of HIF-1α and β-catenin expressions are consistent with the promotion of HIF-1α and β-catenin stabilization and nuclear translocation in immunofluorescence experiments (**Figures 4C, D**).

Hypoxia Intensified the Expression of Cycle-Associated Genes and Stemness Genes in rPBMSCs

For the objective investigation that hypoxia regulated the self-renewal and stemness of rPBMSCs, pluripotency factors and *Cyclin E/CDK2* were primarily selected as indicators. Compared

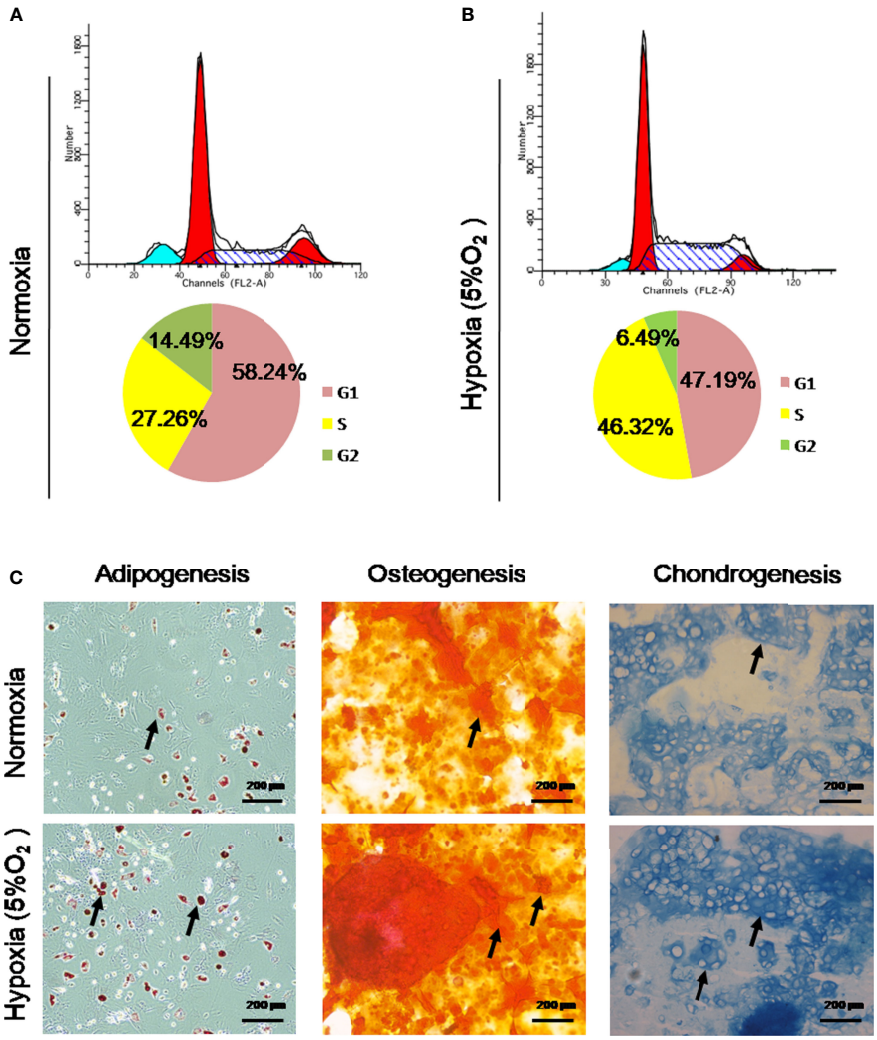

FIGURE 3 | Hypoxia promoted cell cycle transition and maintained the trilineage differentiation capacity of rPBMSCs. **(A, B)** Hypoxia promoted cell cycle transition, as determined by flow cytometry. **(C)** rPBMSCs were cultured under normoxia and hypoxia (5% O_2) for chondrogenic differentiation, osteogenic differentiation, and adipogenic differentiation for 21 days. Magnification, 200×. Arrows indicate lipid droplets, proteoglycans, and calcium nodules. rPBMSCs, rat peripheral blood-derived mesenchymal stromal cells.

with normoxia, hypoxia significantly triggered upregulation of mRNA and protein expression for β-catenin, CDK2, and Cyclin E in rPBMSCs (**Figures 5A–C**). Moreover, the mRNA and protein expressions of *HIF-1α*, *Nanog*, and *SOX2* were significantly increased by hypoxia (**Figures 5D–F**).

DISCUSSION

As a typical representative of adult pluripotent stromal cells, PBMSCs provide various possibilities for clinical application and transformation in the field of regenerative medicine (31). PBMSCs are abundant in the body and have strong proliferation and self-renewal ability, as well as the potential to differentiate into multiple cell types (32). However, some problems and obstacles are still encountered in the application and transformation of MSCs in cartilage tissue engineering, including the reduced activity and phenotype of seed cells *in vitro* (33). Thus, this study aimed to determine a hypoxic culture method that allows PBMSCs to maintain their ability to proliferate and self-renew during expansion *in vitro*. For this reason, this study mainly focused on three aspects, namely, (1) successful isolation, culture, and identification of rPBMSCs; (2) proliferation, phenotype maintenance, and differentiation potential of hypoxia-treated rPBMSCs; and (3) proliferation- and phenotype-related gene expressions of hypoxia-treated PBMSCs. This study proposes a culture method that is conducive to maintaining self-renewal and proliferation capabilities to ensure cell yield and long-term expansion.

In this study, rPBMSCs were successfully isolated and cultured, and third-generation rPBMSCs were selected for FCM for phenotypic identification. rPBMSCs did not express

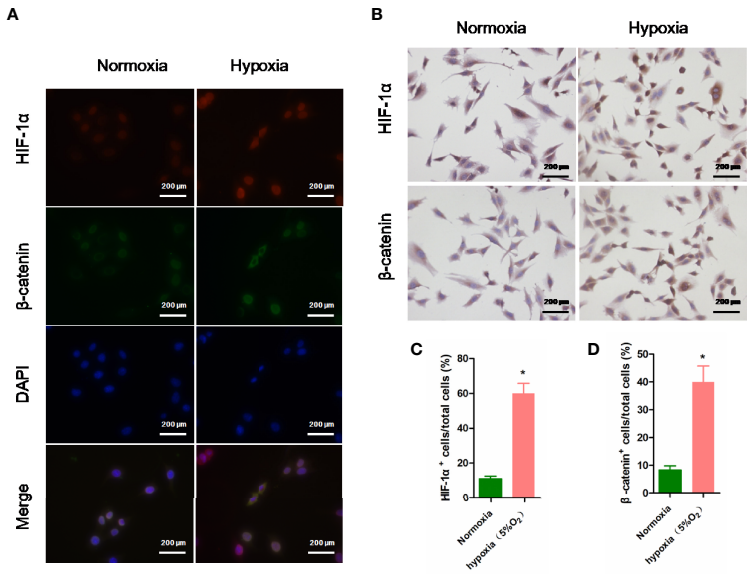

FIGURE 4 | Immunoassay of HIF-1α and β-catenin in rPBMSCs under normoxia and hypoxia (5% O_2). **(A)** Nuclear expression of HIF-1α (red) and β-catenin (green) in rPBMSCs treated under normoxia and hypoxia (5% O_2) for 5 days. **(B)** Nuclear expression of HIF-1α (brown) and β-catenin (brown) in rPBMSCs treated under normoxia and hypoxia (5% O_2) for 5 days. **(C, D)** Quantitative analysis of HIF-1α (brown) and β-catenin (brown) in rPBMSCs in panel **(B)**. Magnification, 200×. All data are presented as means ± SEM. P < 0. 05; * vs control group. rPBMSCs, rat peripheral blood-derived mesenchymal stromal cells; HIF-1α, hypoxia-inducible factor 1α.

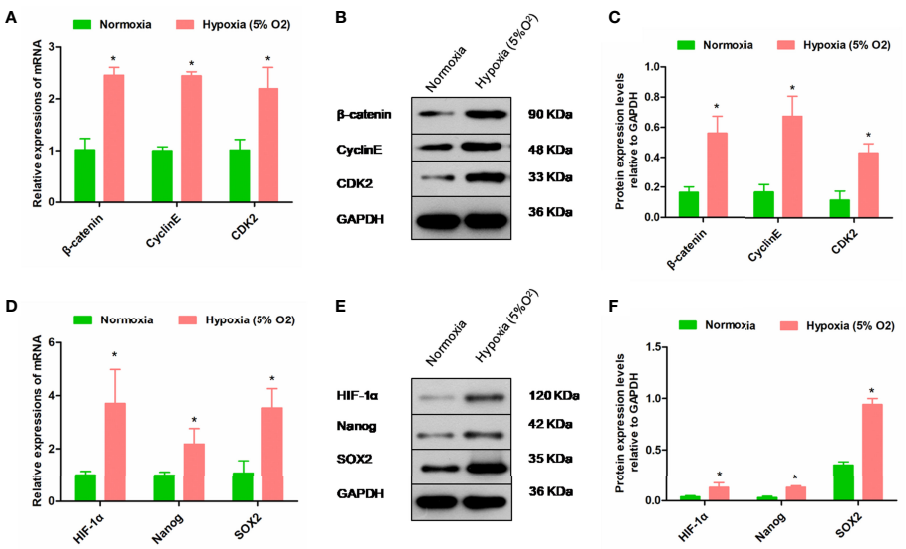

FIGURE 5 | Hypoxia regulates the expressions of cycle-related and self-renewal-related molecules. **(A–C)** mRNA and protein expression levels of *β-catenin*, *Cyclin E*, and *CDK2* in rPBMSCs treated under normoxic and hypoxic (5% O_2) conditions for 5 days. **(D–F)** mRNA and protein expression levels of *HIF-1α*, *Nanog*, and *SOX2* in rPBMSCs treated under normoxic and hypoxic (5% O_2) conditions for 24 h. All data are presented as means ± SEM. P < 0. 05; * vs control group. rPBMSCs, rat peripheral blood-derived mesenchymal stromal cells; HIF-1α, hypoxia-inducible factor 1α.

CD45, *CD34*, *CD14*, *CD19*, and *HLA II*, but highly expressed *CD73*, *CD90*, and *CD105*, indicating that the rPBMSCs had stromal cell performance, without other surface antigen markers (34, 35). Successfully isolated rPBMSCs positively expressed *CD90*, *CD73*, and *CD105*. Cell growth curve determination and cell cloning experiments revealed that 5% O_2 hypoxia can significantly promote the formation of clones and the rapid proliferation of PBMSCs. Many recent studies have

reported that an appropriate hypoxic condition can significantly stimulate the proliferation of MSCs and PBMSCs, which is consistent with the results of the present study. The recent studies confirmed hypoxia accelerated proliferation of PBMSCs, increased migration of PBMSCs, and reduced PBMSC differentiation into osteoblasts by increasing Notch1 expression (36). In our study, four oxygen concentration gradients were set up to more rigorously explore the effects of various oxygen concentrations on the proliferation and stemness of PBMSCs, as well as the role of HIF-1α pathway in the proliferation and stemness maintenance of PBMSCs.

Other studies have also reported that hypoxia promotes the proliferation of cord blood derived MSCs without changing the cellular immune phenotype (37). In this study, hypoxia significantly promoted the transition of PBMSCs from the G1 phase to the S phase. Since the S phase is an important stage of cell DNA synthesis (38, 39), under hypoxic conditions, PBMSCs pass the G1/S phase checkpoint and enter the DNA synthesis phase. Moreover, a study revealed that hypoxia can drive cells into the cell cycle and promote the expression of cyclins and related kinases to drive umbilical cord derived MSCs through cell cycle checkpoints, thereby promoting DNA synthesis (40).

HIF-1α is an extremely critical transcription factor, which is strongly induced during hypoxia and adapts to hypoxic tension (41). Studies have reported that HIF-1α causes cell cycle arrest in the G0/G1 phase through p27 expression (42); however, under different cell environments, HIF-1α activation can demonstrate varying results by affecting various aspects of cell biology (39). The present study presents that upregulating the expression of HIF-1α under 5% hypoxia can increase the proportion of rPBMSCs in the S phase. β-catenin is a typical cytoplasmic protein, as part of the classic Wnt signaling, which plays a role in cell adhesion (43). β-catenin coactivated LRH-1 on the cyclin E1 promoter and induced G1 cyclin-mediated cell proliferation, *Cyclin E* interacts with *CDK2* to control the G1/S phase transition (44). In this experiment, after hypoxic treatment of rPBMSCs, the transition of cells from the G1 phase to the S phase and the activation of *Cyclin E/CDK2* indicated that hypoxia may regulate the cell cycle position to control the self-renewal of rPBMSCs. Similar reports have suggested that HIF-1α promotes cell vitality and proliferation of MSCs (45, 46).

The expression of stemness markers was observed under hypoxic conditions. The significant role of low oxygen in altering the characteristics of various types of stromal cells was previously investigated (47). A study suggested the upregulation of stemness genes such as *OCT4* and *Nanog* of BMSCs cultured in 1% oxygen (48). Similar results were observed in the present study, where the expressions of *Nanog* and *SOX2* of rPBMSCs under 5% oxygen conditions were promoted, indicating that the stemness of rPBMSCs was enhanced by a hypoxic environment. The inhibition of senescence of MSCs suggests the increased expression of pluripotency markers (49). In this study, hypoxia-treated rPBMSCs demonstrated a higher differentiation potential, including cartilage, osteogenic, and adipogenic potentials compared with normoxia-treated cells. However, the control of hypoxia on stromal cells involves transcription factors such as HIF-1α and β-catenin. However, further research is needed to understand how HIF-1α and β-catenin regulate and interact with each other.

CONCLUSION

In summary, the stemness, proliferation, and self-renewal potential of hypoxia-treated rPBMSCs were enhanced. Therefore, conditional hypoxia (5%) culture can be used as a convenient strategy to maintain the function of rPBMSCs. The

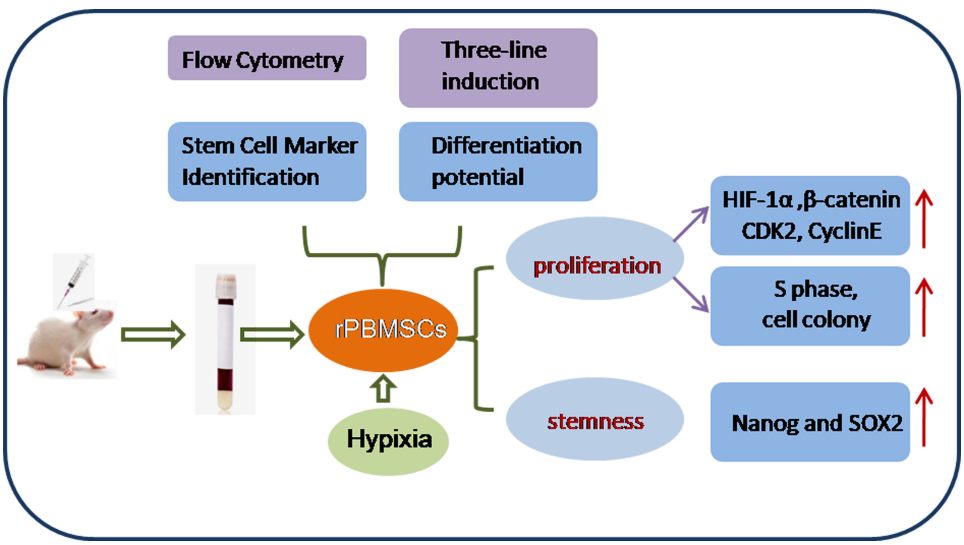

FIGURE 6 | Mechanism of hypoxia-promoted proliferation and stemness of rPBMSCs.

general process and conclusions of this study are clearly illustrated in **Figure 6**.

DATA AVAILABILITY STATEMENT

The original contributions presented in the study are included in the article/supplementary material. Further inquiries can be directed to the corresponding author.

ETHICS STATEMENT

This animal study was reviewed and approved by animal ethics committee of Guangzhou Red Cross Hospital.

AUTHOR CONTRIBUTIONS

Study design: PW; Data collection: PZ; Data analysis: CY and JW; Interpretation of data: PW; Draft manuscript: PW; Review manuscript: PW. All authors contributed to the article and approved the submitted version.

FUNDING

This work was supported by the Medical Science and Technology Research Foundation of Guangdong (A2021335, PW), Traditional Chinese Medicine Bureau of Guangdong Province (20222166, PW), and Guangdong Provincial Basic and Applied Basic Regional Joint Fund (2020A1515110009, PZ).

REFERENCES

1. Kanno K, Sakaue T, Hamaguchi M, Namiguchi K, Nanba D, Aono J. Hypoxic Culture Maintains Cell Growth of the Primary Human Valve Interstitial Cells With Stemness. *Int J Mol Sci* (2021) 29:10534. doi: 10.3390/ijms221910534
2. Abu Awwad HAM, Thiagarajan L, Kanczler JM, Amer MH, Bruce G, Lanham S, et al. Genetically-Programmed, Mesenchymal Stromal Cell-Laden & Mechanically Strong 3D Bioprinted Scaffolds for Bone Repair. *J Contr Relea* (2020) 325:335–46. doi: 10.1016/j.jconrel.2020.06.035
3. Lecourt S, Vanneaux V, Cras A, Freida D, Heraoui D, Herbi L, et al. Bone Marrow Microenvironment in an *In Vitro* Model of Gaucher Disease: Consequences of Glucocerebrosidase Deficiency. *Stem Cells Dev* (2012) 21:239–48. doi: 10.1089/scd.2011.0365
4. Granchi D, Ochoa G, Leonardi E, Devescovi V, Bagl SR, Osaba L, et al. Gene Expression Patterns Related to Osteogenic Differentiation of Bone Marrow-Derived Mesenchymal Stem Cells During *Ex Vivo* Expansion. *Tissue Eng Part C Methods* (2010) 16:511–24. doi: 10.1089/ten.tec.2009.0405
5. Takeuchi R, Katagiri W, Endo S, Kobayashi T. Exosomes From Conditioned Media of Bone Marrow-Derived Mesenchymal Stem Cells Promote Bone Regeneration by Enhancing Angiogenesis. *PloS One* (2019) 21:14:e0225472. doi: 10.1371/journal.pone.0225472
6. Zhang B, Yeo RWY, Lai RC, Sim EWK, Chin KC, Lim SK. Mesenchymal Stromal Cell Exosome-Enhanced Regulatory T-Cell Production Through an Antigen-Presenting Cell-Mediated Pathway. *Cytotherapy* (2018) 20(5):687–96. doi: 10.1016/j.jcyt.2018.02.372
7. Maria S, Samsonraj RM, Munmun F, Glas J, Silvestros M, Kotlarczyk MP, et al. Biological Effects of Melatonin on Osteoblast/Osteoclast Cocultures, Bone, and Quality of Life: Implications of a Role for MT2 Melatonin Receptors, MEK1/2, and MEK5 in Melatonin-Mediated Osteoblastogenesis. *J Pineal Res* (2018) 64(3):10.1111/jpi.12465. doi: 10.1111/jpi.12465
8. Fu WL, Xiang Z, Huang FG, Gu ZP, Yu XX, Cen SQ, et al. Coculture of Peripheral Blood-Derived Mesenchymal Stem Cells and Endothelial Progenitor Cells on Strontium-Doped Calcium Polyphosphate Scaffolds to Generate Vascularized Engineered Bone. *Tissue Eng Part A* (2015) 21:948–59. doi: 10.1089/ten.tea.2014.0267
9. Dominici M, Le Blanc K, Mueller I, Slaper-Cortenbach I, Marini F, Krause D, et al. Minimal Criteria for Defining Multipotent Mesenchymal Stromal Cells. The International Society for Cellular Therapy Position Statement. *Cytotherapy* (2006) 8(4):315–7. doi: 10.1080/14653240600855905
10. Toh WS, Lai RC, Hui JHP, Lim SK. MSC Exosome as a Cell-Free MSC Therapy for Cartilage Regeneration: Implications for Osteoarthritis Treatment. *Semin Cell Dev Biol* (2017) 67:56–64. doi: 10.1016/j.semcdb.2016.11.008
11. Cianflone E, Torella M, Biamonte F, De Angelis A, Urbanek K, Costanzo FS. Targeting Cardiac Stem Cell Senescence to Treat Cardiac Aging and Disease. *Cells* (2020) 9:1558. doi: 10.3390/cells9061558
12. Zhen G, Wen C, Jia X, Li Y, Crane JL, Mears SC, et al. Inhibition of TGF-β Signaling in Mesenchymal Stem Cells of Subchondral Bone Attenuates Osteoarthritis. *Nat Med* (2013) 19:704–12. doi: 10.1038/nm.3143
13. Ludwig TE, Levenstein ME, Jones JM, Berggren WT, Mitchen ER, Frane JL, et al. Derivation of Human Embryonic Stem Cells in Defined Conditions. *Nat Biotechnol* (2006) 24:185–7. doi: 10.1038/nbt1177
14. Foyt DA, Taheem DK, Ferreira SA, Norman MDA, Petzold J, Jell G, et al. Hypoxia Impacts Human MSC Response to Substrate Stiffness During Chondrogenic Differentiation. *Acta Biomat* (2019) 89:73–83. doi: 10.1016/j.actbio.2019.03.002
15. Theus MH, Wei L, Cui L, K Francis XH, Keogh C. *In Vitro* Hypoxic Preconditioning of Embryonic Stem Cells as a Strategy of Promoting Cell Survival and Functional Benefits After Transplantation Into the Ischemic Rat Brain. *Exp Neurol* (2008) 210:656–70. doi: 10.1016/j.expneurol.2007.12.020
16. Tsai CC, Yew TL, Yang DC, Huang WH, Hung SC. Benefits of Hypoxic Culture on Bone Marrow Multipotent Stromal Cells. *Am J Blood Res* (2012) 2:148–59.
17. Parmar K, Mauch P, Vergilio JA, Sackstein R, Down JD. Distribution of Hematopoietic Stem Cells in the Bone Marrow According to Regional Hypoxia. *Proc Natl Acad Sci USA* (2007) 104(13):5431–6. doi: 10.1073/pnas.0701152104
18. Majmundar AJ, Wong WJ, Simon MC. Hypoxiainducible Factors and the Response to Hypoxic Stress. *Mol Cell* (2010) 40(2):294–309. doi: 10.1016/j.molcel.2010.09.022
19. Semenza GL. Molecular Mechanisms Mediating Metastasis of Hypoxic Breast Cancer Cells. *Trends Mol Med* (2012) 18(9):534–43. doi: 10.1016/j.molmed.2012.08.001
20. Lavrentieva A, Majore I, Kasper C, Hass R. Effects of Hypoxic Culture Conditions on Umbilical Cordderived Human Mesenchymal Stem Cells. *Cell Commun Signal* (2010) 8(1):18. doi: 10.1186/1478-811X-8-18
21. Semenza GL. HIF-1 and Human Disease: One Highly Involved Factor. *Genes Dev* (2000) 14:1983–91. doi: 10.1101/gad.14.16.1983
22. Li H, Jia Y, Wang Y. Targeting HIF-1α Signaling Pathway for Gastric Cancer Treatment. *Pharmazie* (2019) 74:3–7. doi: 10.1691/ph.2019.8674
23. Conde E, Giménez-Moyano S, Martín-Gómez L, Rodríguez M, Ramos ME, Aguado-Fraile E, et al. HIF-1α Induction During Reperfusion Avoids Maladaptive Repair After Renal Ischemia/Reperfusion Involving Mir127-3p. *Sci Rep* (2017) 7:41099. doi: 10.1038/srep41099
24. Warbrick I, Rabkin SW. Hypoxia-Inducible Factor 1-Alpha (HIF-1α) as a Factor Mediating the Relationship Between Obesity and Heart Failure With Preserved Ejection Fraction. *Obes Rev* (2019) 20:701–12. doi: 10.1111/obr.12828
25. Sui H, Zhao J, Zhou L, Wen H, Deng W, Li C. Tanshinone IIA Inhibits β-Catenin/VEGF-Mediated Angiogenesis by Targeting TGF-β1 in Normoxic and HIF-1α in Hypoxic Microenvironments in Human Colorectal Cancer. *Cancer Lett* (2017) 403:86–97. doi: 10.1016/j.canlet.2017.05.013
26. Fang Y, Yu S, Ma Y, Sun P, Ma D, Ji C, et al. Association of Dll4/notch and HIF-1a -VEGF Signaling in the Angiogenesis of Missed Abortion. *PloS One* (2013) 8:e70667. doi: 10.1371/journal.pone.0070667

27. Mohyeldin A, Garzón-Muvdi T, Quiñones-Hinojosa A. Oxygen in Stem Cell Biology: A Critical Component of the Stem Cell Niche. *Cell Stem Cell* (2010) 6:7:150–61. doi: 10.1016/j.stem.2010.07.007
28. Fu Q, Liu Y, Liu X, Zhang Q, Chen L, Peng J, et al. Engrafted Peripheral Blood-Derived Mesenchymal Stem Cells Promote Locomotive Recovery in Adult Rats After Spinal Cord Injury. *Am J Transl Res* (2017) 9:3950–66.
29. Yusop N, Battersby P, Alraies A, Sloan AJ, Moseley R, Waddington RJ. Isolation and Characterisation of Mesenchymal Stem Cells From Rat Bone Marrow and the Endosteal Niche: A Comparative Study. *Stem Cells Int* (2018) 2018:6869128. doi: 10.1155/2018/6869128
30. Livak KJ, Schmittgen TD. Analysis of Relative Gene Expression Data Using Real-Time Quantitative PCR and the 2(-Delta Delta C(T)) Method. *Methods* (2001) 25:402–8. doi: 10.1006/meth.2001.1262
31. Calle A, Gutiérrez-Reinoso MÁ, Re M, Blanco J, de la Fuente J, Monguió-Tortajada M, et al. Bovine Peripheral Blood MSCs Chemotax Towards Inflammation and Embryo Implantation Stimuli. *J Cell Physiol* (2021) 236:1054–67. doi: 10.1002/jcp.29915
32. Yang R, Gao H, Chen L, Fang N, Chen H, Song G, et al. Effect of Peripheral Blood-Derived Mesenchymal Stem Cells on Macrophage Polarization and Th17/Treg Balance *In Vitro*. *Regener Ther* (2020) 14:275–83. doi: 10.1016/j.reth.2020.03.008
33. Otte A, Bucan V, Reimers K, Hass R. Mesenchymal Stem Cells Maintain Long-Term *In Vitro* Stemness During Explants Culture. *Tissue Eng Part C Methods* (2013) 19:937–48. doi: 10.1089/ten.tec.2013.0007
34. De Ravin SS, Reik A, Liu PQ, Li L, Wu X, Su L, et al. Targeted Gene Addition in Human CD34(+) Hematopoietic Cells for Correction of X-Linked Chronic Granulomatous Disease. *Nat Biotechnol* (2016) 34:424–9. doi: 10.1038/nbt.3513
35. Fu Q, Zhang Q, Jia LY, Fang N, Chen L, Yu LM, et al. Isolation and Characterization of Rat Mesenchymal Stem Cells Derived From Granulocyte Colony-Stimulating Factor-Mobilized Peripheral Blood. *Cells Tissue Organ* (2016) 201(6):412–22. doi: 10.1159/000445855
36. Yang M, Liu H, Wang Y, Wu G, Qiu S, Liu C, et al. Hypoxia Reduces the Osteogenic Differentiation of Peripheral Blood Mesenchymal Stem Cells by Upregulating Notch-1 Expression. *Conne Tissue Res* (2019) 60:583–96. doi: 10.1080/03008207.2019.1611792
37. Zhao D, Liu L, Chen Q, Wang F, Li Q, Zeng Q, et al. Hypoxia With Wharton's Jelly Mesenchymal Stem Cell Coculture Maintains Stemness of Umbilical Cord Blood-Derived CD34+ Cells. *Stem Cell Res Ther* (2018) 9:158. doi: 10.1186/s13287-018-0902-5
38. Williams GH, Stoeber K. The Cell Cycle and Cancer. *J Pathol* (2012) 226:352–64. doi: 10.1002/path.3022
39. Ramasamy R, Tong CK, Yip WK, Vellasamy S, Tan BC, Seow HF. Basic Fibroblast Growthfactor Modulates Cell Cycle of Human Umbilical Cord-Derived Mesenchymal Stem Cells. *Cell Prolif* (2012) 45:132–9. doi: 10.1111/j.1365-2184.2012.00808.x
40. Carmeliet P, Dor Y, Herbert JM, Fukumura D, Brusselmans K, Dewerchin M, et al. Role of HIF-1alpha in Hypoxia-Mediated Apoptosis, Cell Proliferation and Tumour Angiogenesis. *Nature* (1998) 394:485–90. doi: 10.1038/28867
41. Kumar S, Vaidya M. Hypoxia Inhibits Mesenchymal Stem Cell Proliferation Through HIF1alpha-Dependent Regulation of P27. *Mol Cell Biochem* (2016) 415:29–38. doi: 10.1007/s11010-016-2674-5
42. Palomaki S, Pietila M, Laitinen S, Pesala J, Sormunen R, Lehenkari P, et al. HIF-1alpha Is Upregulated in Human Mes-Enchymal Stem Cells. *Stem Cells* (2013) 31:1902–9. doi: 10.1002/stem.1435
43. Botrugno OA, Fayard E, Annicotte JS, Haby C, Brennan T, Wendling O, et al. Synergy Between LRH-1 and Beta-Catenin Induces G1 Cyclin-Mediated Cell Proliferation. *Mol Cell* (2004) 15:499–509. doi: 10.1016/j.molcel.2004.07.009
44. Odajima J, Wills ZP, Ndassa YM, Terunuma M, Kretschmannova K, Deeb TZ, et al. Cyclin E Constrains Cdk5 Activity to Regulate Synaptic Plasticity and Memory Formation. *Dev Cell* (2011) 21:655–68. doi: 10.1016/j.devcel.2011.08.009
45. Yu J, Liu XL, Cheng QG, Lu SS, Xu XQ, Zu QQ, et al. G-CSF and Hypoxic Conditioning Improve the Proliferation, Neural Differentiation and Migration of Canine Bone Marrow Mesenchymal Stem Cells. *Exp Ther Med* (2016) 12:1822–8. doi: 10.3892/etm.2016.3535
46. Stoeltzing O, McCarty MF, Wey JS, Fan F, Liu W, Belcheva A, et al. Role of Hypoxia-Inducible Factor 1alpha in Gastric Cancer Cell Growth, Angiogenesis, and Vessel Maturation. *J Natl Cancer Inst* (2004) 96:946–56. doi: 10.1093/jnci/djh168
47. Yamamoto Y, Fujita M, Tanaka Y, Kojima I, Kanatani Y, Ishihara M, et al. Low Oxygen Tension Enhances Proliferation and Maintains Stemness of Adipose Tissue-Derived Stromal Cells. *Biores Open Access* (2013) 2:199–205. doi: 10.1089/biores.2013.0004
48. Hung SP, Ho JH, Shih YR, Lo T, Lee OK. Hypoxia Promotes Proliferation and Osteogenic Differentiation Potentials of Human Mesenchymal Stem Cells. *J Orthop Res* (2012) 30:260–6. doi: 10.1002/jor.21517
49. Tsai CC, Su PF, Huang YF, Yew TL, Hung SC. Oct4 and Nanog Directly Regulate Dnmt1 to Maintain Self-Renewal and Undiffer- Entiated State in Mesenchymal Stem Cells. *Mol Cell* (2012) 47:169–82. doi: 10.1016/j.molcel.2012.06.020

Conflict of Interest: The authors declare that the research was conducted in the absence of any commercial or financial relationships that could be construed as a potential conflict of interest.

Publisher's Note: All claims expressed in this article are solely those of the authors and do not necessarily represent those of their affiliated organizations, or those of the publisher, the editors and the reviewers. Any product that may be evaluated in this article, or claim that may be made by its manufacturer, is not guaranteed or endorsed by the publisher.

frontiers | Frontiers in Endocrinology

CASE REPORT
published: 23 May 2022
doi: 10.3389/fendo.2022.833929

Aumolertinib Effectively Reduces Clinical Symptoms of an EGFR L858R-Mutant Non-Small Cell Lung Cancer Case Coupled With Osimertinib-Induced Cardiotoxicity: Case Report and Review

Qianqian Zhang, Haiyang Liu and Jia Yang*

Department of Respiratory and Critical Care Medicine, Henan Provincial People's Hospital, Zhengzhou, China

OPEN ACCESS

Edited by:
Ihtisham Bukhari, Fifth Affiliated Hospital of Zhengzhou University, China

Reviewed by:
Shaun Sabico, King Saud University, Saudi Arabia
Muhammad Riaz Khan, Université de Sherbrooke, Canada

***Correspondence:**
Qianqian Zhang
zxxych@163.com

Specialty section:
This article was submitted to Cancer Endocrinology, a section of the journal Frontiers in Endocrinology

Received: *12 December 2021*
Accepted: *08 April 2022*
Published: *23 May 2022*

Citation:
Zhang Q, Liu H and Yang J (2022) Aumolertinib Effectively Reduces Clinical Symptoms of an EGFR L858R-Mutant Non-Small Cell Lung Cancer Case Coupled With Osimertinib-Induced Cardiotoxicity: Case Report and Review. Front. Endocrinol. 13:833929. doi: 10.3389/fendo.2022.833929

Osimertinib, a third-generation epidermal growth factor receptor tyrosine kinase inhibitor (EGFR-TKI) first-line therapy, has shown good clinical outcomes in non-small cell lung cancer (NSCLC), but some serious adverse events such as cardiotoxicity have also been reported. Here, we present the first NSCLC case with osimertinib-induced cardiac failure. The case is successfully being treated by switching to another third-generation TKI, aumolertinib. A 62-year-old non-smoking woman was initially diagnosed with stage cT2aN2M1c IVB NSCLC with synchronous brain and bone metastasis in April 2020. Further genetic screening of the patient identified Leu858Arg (L858R) mutation in EGFR; thus, the patient was administered third-generation TKI osimertinib (80 mg/day) for 6 months. This treatment with osimertinib led to serious cardiac failure but no significant reduction in NSCLC tumor size. To cope with these conditions, another third-generation TKI, aumolertinib (110 mg/day), along with a supplement treatment plan was prescribed to the patient. Interestingly, this new treatment plan of aumolertinib significantly inhibited tumor growth in 8 months. Therefore, we conclude that the administration of second-line aumolertinib 110 mg/day has fewer adverse reactions and high efficacy against NSCLC as compared to osimertinib therapy.

Keywords: aumolertinib, L858R, osimertinib, cardiac failure, NSCLC

INTRODUCTION

Lung cancer is one of the leading causes of cancer-related death worldwide, including China (1). Lung cancer can be divided into small cell lung cancer (SCLC) and non-small cell lung cancer (NSCLC) according to cell morphology, and approximately 85% of cancers are NSCLC. It has been well established that the epidermal growth factor receptor (EGFR) is a common driver gene for NSCLC, and EGFR mutations can be detected in about 40%–60% of the East Asian population (2). In the last decades, the treatment options for NSCLC have improved dramatically and standard platinum doublet chemotherapy has been substituted by tyrosine kinase inhibitors (TKIs). More

recently, TKIs have become the standard treatment for the EGFR-mutant for NSCLC, when patients are diagnosed with pathogenic mutations. The most common cluster of mutations in *EGFR* includes deletions around the LeuArgGluAla motif (residues 746–750) of exon 19, and among all the Leu858Arg (L858R) point mutations in exon 21, each accounting for 45% of all EGFR mutations (3, 4).

The presence of these mutations in NSCLC patients showed 9–14 months of progression-free survival (PFS) from those who positively respond to the first- and second-generation TKI (5–7). Nevertheless, about 60% of the patients with the EGFR T790M mutation who initially respond positively to the EGFR inhibitors such as gefitinib, erlotinib, afatinib, and dacomitinib in NSCLC eventually develop acquired drug resistance (ADR) in 9–15 months (8, 9). Third-generation EGFR-TKIs, such as osimertinib and aumolertinib, can minimize ADR. Based on the positive results obtained from clinical trials, the Food and Drug Administration (FDA) approved osimertinib for the treatment of patients with metastatic T790M- and EGFR-positive mutation in NSCLC (7, 10). In the FLAURA clinical trial, osimertinib showed the list of adverse events (AEs), and the most reported AEs were rash or acne, diarrhea, and dry skin. Among potentially life-threatening adverse reactions, cardiac failure was reported in 12 patients (4%) in the osimertinib group. The significant characteristics of the patients in this category were ejection fraction decrease, and electrocardiogram QT prolongation was reported in 28 patients (10%). In addition, interstitial lung disease (ILD) was also reported in 11 patients (4%) from the osimertinib treatment group (10). To date, no effective and alternative therapy has been recommended to fight the side effects of the osimertinib. Here, in this short report, we present a female case diagnosed with advanced NSCLC with L858R mutation in EGFR, which has presented grade 3 cardiac failure after being treated with osimertinib for 6 months; we successfully relieved the symptoms after switching the treatment with alternative third-generation EGFR-TKI aumolertinib.

CASE PRESENTATION

A 62-year-old non-smoker Chinese woman consulted Henan Provincial People's Hospital with a complaint of mental illness in April 2020. Her family also complained chest congestion and discomfort. To diagnose the illness, the chest computed tomography (CT) scan was performed, which revealed a mass (3.9 × 2.7cm) in the left lung (**Figures 1A, F**), and a subsequent bronchoscopy revealed an NSCLC with mediastinal enlarged lymph nodes. Furthermore, the magnetic resonance imaging (MRI) scans revealed multiple metastases in the brain region in the form of nodular enhancement. In addition, chest-enhanced CT scan disclosed multiple abnormal density shadows that were considered as bone multiple metastases (data not shown).

Additionally, clinical serological laboratory testing showed elevated levels of carcinoma embryonic antigen (CEA) and neuron -specific enolase (NSE) (**Table 1**), and the immunohistochemistry analysis showed adenocarcinoma. The patient's liver and kidney were observed as normal, and the normal heart function was shown by the marker of cardiac function [N-terminal brain natriuretic peptide precursor (NT-proBNP)] with a value of 70 ng/L (normal range, <300 ng/L). According to the American Joint Committee on Cancer (AJCC) version 8.0 for the TNM staging system, the current diagnosis of the patient revealed a presence of NSCLC adenocarcinoma at the cT2aN2M1c IVB clinical stage (including brain and bone metastasis). Moreover, the next-generation sequencing analysis discovered L858R mutation in exon 21 of the EGFR gene (**Figure 2**). Following complete diagnosis, we have requested a clinical history of the patient and her family and found that her family has no history of mental disease or cancer.

The patient was asked to sign a consent form for the administration of the anti-tumor therapy. Written and verbal explanations about benefits and adverse reactions were given to the patient and attending persons. Firstly, the patient was prescribed osimertinib (80 mg po qd) and ibandronate (4 mg) for 6 months, with routine checkups. The entire treatment timeline of anti-tumor therapy is shown in a flowchart diagram (**Figure 3**). The follow-up of the first 3 months showed a stable tumor in the lung nidus (3.9 × 2.6cm) (**Figures 1B, G**). However, 6 months later, she complained of physical weakness and lower limb edema. To explore the symptoms and to dig out the causes of these complaints, chest CT, MRI, ECG, and serological analysis were performed. The results of the CT revealed no significant change in tumor size (3.9 × 2.6 cm) (**Figures 1C, H**). However, an MRI of the heart exposed pleural and pericardial effusions, and the echocardiogram (ECG) further indicated an obvious severe hypokinesis, with a left ventricular ejection fraction (LVEF) of 36% and the left ventricle was dysfunctioning (**Figure 4A**; **Tables 2** and **3**). In addition, the level of NT pro-BNP was gravely increased (6,830 ng/L) (**Figure 4B**). Considering that the patient had no history of cardiac disease and hypertension, we suspected that osimertinib may induce cardiotoxicity with CTCAE grade 3. This prompted us to discontinue osimertinib. Next, we prescribed the new treatment plan with furosemide (20 mg bid), spironolactone (20 mg bid), bisoprolol (20 mg qd), and valsartan (50 mg bid) to the patient to improve cardiac function and physical condition. Four weeks after the new treatment regimen, the LVEF improved to 52% (**Figure 4A**) including better cardiac function (**Table 3**); however, NT pro-BNP was further welled to 8,000 ng/L (**Figure 4B**). Thereafter, another third-generation EGFR-TKI aumolertinib (110 mg po qd) was administered to treat the NSCLC. The aumolertinib treatment was maintained with the cardiac failure treatment regimen for the next 4 months with routine examination. Later, tumor analysis revealed that the size of the tumor was partially decreased (2.9 × 1.6 cm) (**Figures 1D, I**). Fortunately, the cardiac function returned to normal (**Table 3**), as indicated by LVEF (57%) (**Figure 4A**) and the reduced level of NT pro-BNP (901 ng/L) (**Figure 4B**). Furthermore, the medicinal load was also reduced to furosemide (20 mg bid), spironolactone (20 mg bid), and aumolertinib (110 mg qd) for the next 4 months. Interestingly, regular follow-up showed gradual recovery in the symptoms (**Figures 1E, J**); tumor size reached stable disease (SD), the ejection fraction improved to 66% (**Figure 4A**), the pro-BNP

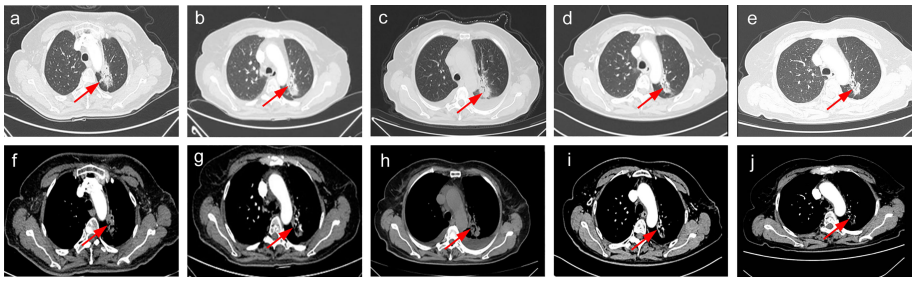

FIGURE 1 | The clinical course according to check CT scan findings. **(A, F)** Baseline CT scan at diagnosis in April 2020. **(B, G)** SD on osimertinib in July 2020. **(C, H)** SD on osimertinib in October 2020. **(D, I)** PR on aumolertinib in March 2021. **(E, J)** SD on aumolertinib in July 2021. PR, partial response. SD, stable disease.

decreased to 137 ng/L (**Figure 4B**), and the left ventricle function become normal, which showed significant improvement in the cardiac function as well as the NSCLC condition. There was a slight change in serological markers before and after switching to aumolertinib (**Table 2**), which indicated that the third-generation EGFR-TKIs performed excellently as anti-tumor medicines. The changes in electrocardiogram at cardiac failure and during recovery treatment were also monitored (**Figure 5**), which showed that RV5 was more than 2.5 mV when the patient suffered a cardiac failure, and the high voltage suggested left ventricular hypertrophy. The changes in myocardial enzymes at cardiac failure and during recovery treatment were monitored (**Table 2**), and the results showed abnormal levels of the lactic dehydrogenase (LDH) and creatine kinase of muscle and brain isozyme (CK-MB). This follow-up treatment that included alternative third-generation EGFR-TKI aumolertinib significantly soothed the condition of a patient with no further complaints of heart discomfort or liver and kidney function damage except fatigue.

DISCUSSION

Lung cancer is one of the most common malignancies and the leading cause of cancer-associated deaths worldwide (11). About 15% of Caucasian and nearly 50% of Asian advanced NSCLC patients were detected with EGFR-positive mutation, mostly in exons 18–21 (12, 13). Uncontrolled activity of the EGFR can act as an active oncogenic driver and target for precision medicine intervention in lung cancer cells (14). Several drugs such as gefitinib, erlotinib, afatinib, and dacomitinib are being used for the treatment of patients with NSCLC who have EGFR mutations. However, over the past years, the tumors have ADR to chemotherapies specifically in patients with EGFR T790M mutation in exon 20 (15–17). Among available medicines, osimertinib is an FDA-approved third-generation EGFR inhibitor. This is highly selective for NSCLC patients with EGFR mutations or first- and second-generation TKI-resistant EGFR T790M mutations. The efficacy of osimertinib can be evaluated by a significant increase in the PFS (median: 18.9 vs. 10.2 months) and overall survival (median: 38.6 vs. 31.8 months) of patients with advanced EGFR-positive or T790M-positive NSCLC patients (18). In addition, osimertinib presented a safety profile consistent with previous reports; however, QT AE prolongation was 10% and serious AE (grade ≥3) prolongation was 1% (18, 19).

Among the AEs, cardiotoxicity is continuously rising when patients are treated with osimertinib. Several cases of heart failure related to osimertinib had been reported. For instance, Watanabe et al. reported a 78-year-old woman presenting with mild exertional dyspnea 3 weeks after starting osimertinib for the treatment of EGFR T790M-positive NSCLC, and she was diagnosed with congestive heart failure caused by the osimertinib (20). Oyakawa et al. reported an 84-year-old woman without any smoking history presenting with dilated and diffusely hypocontractile left ventricle (ejection fraction 33%) with minor pericardial effusion; osimertinib was discontinued, and furosemide, enalapril, and carvedilol were initiated (21). Okutucu et al. showed that a 64-year-old woman was diagnosed with metastatic lung adenocarcinoma harboring an EGFR mutation; 2 months after osimertinib initiation, which revealed that her left ventricular systolic function was depressed, with a globally reduced ejection fraction of 24%, they concluded that the heart failure had been caused by osimertinib inhibiting human epidermal growth factor receptor 2 (HER2) (22). Reale et al. reported 5 patients treated with osimertinib who suffered from heart failure; one patient died due to further worsening of cardiac condition, another patient was suspended due to reduction of EF, one patient received reduced osimertinib dosage, and the last 2 patients continued osimertinib after heart failure treatment. Osimertinib cardiotoxicity is more

TABLE 1 | The serological examination results at cardiac failure and during recovery treatment.

Time	Serological Markers			
	CEA (ng/ml)	NSE (ng/ml)	SCC (ng/ml)	CYFRA21 (ng/ml)
2020.04	60	13.51	0.8	4.89
2020.10	5.98	7.20	0.8	3.67
2020.11	7.69	8.56	0.9	3.84
2021.03	9.94	7.08	0.6	3.52
2021.07	9.73	6.65	0.8	3.66

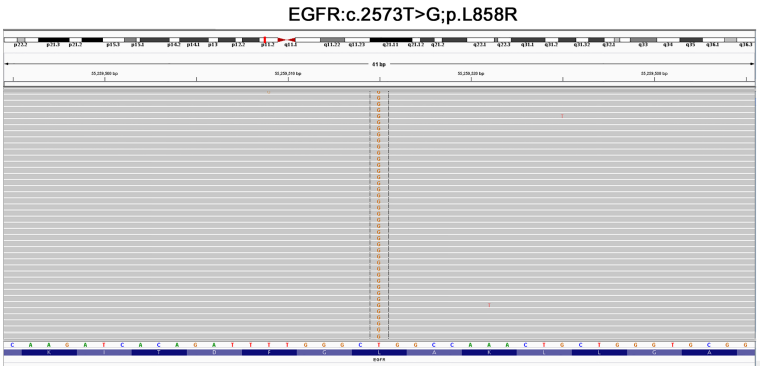

FIGURE 2 | The next-generation sequencing analysis revealed that L858R mutation in exon 21 of the EGFR gene was visualized by IGV software.

likely to be a type 2 cardiotoxicity and reversible (23). However, there is no evidence that resumption of osimertinib is harmful to patients after treating osimertinib-induced heart failure. The retrospective analyses of a pharmacovigilance database, the FDA AEs reporting system, reported a rare incidence (3.7%) regarding the occurrence of cardiotoxicity linked to EGFR-TKIs in 8,450 AEs. However, the results found that the reporting odds ratio for osimertinib compared with all other drugs was 5.4 for cardiac failure and 11.2 for QT prolongation, and compared with the 3 other EGFR TKIs, it was 2.2 for cardiac failure and 6.6 for QT prolongation (24). A systematic review and meta-analysis of randomized controlled trials (RCT) was undertaken to determine the incidence of osimertinib cardiac toxicities and showed that osimertinib notably increased the risk of cardiac toxicities with a risk ratio of 2.71 for cardiac failure and 2.62 for QT prolongation; thus, prompt monitoring and early intervention are warranted (25). Andrew et al. reported a 67-year-old woman treated with first-generation EGFR TKI erlotinib and then changed the osimertinib without resistance; 7 months after osimertinib initiation, she presented with shortness of breath and was diagnosed with heart failure and had to use erlotinib again. Osimertinib is not only highly specific for ErbB1 (EGFR), but also has demonstrated greater inhibition of wild-type ErbB2 (HER2) than that observed with erlotinib or afatinib. Whether this effect is responsible for increased cardiotoxicity requires further exploration (26). Kunimasa reported a retrospective, single-center study conducted in Japan. A total of 123 NSCLC patients with EGFR mutations were treated with osimertinib, and grade 3 or higher cardiac AEs were observed in 6 patients (4.9%). Five of those patients were women; their cardiac AEs included acute myocardial infarction (n = 1), heart failure with reduced LVEF (n = 3), and valvular heart disease (n = 2). For the patient described in case 1, LVEF recovery was delayed, and gefitinib was started 8 months after the AE; the patient in case 2 refused osimertinib re-administration and also received gefitinib. Osimertinib was re-administered to the patients described in cases 3 and 4, given the presence of the T790M mutation, whereas patients were treated with other EGFR-TKIs (cases 5 and 6). Altogether, osimertinib was discontinued in 4 of 6 patients and restarted in 2 patients; in one of those patients, osimertinib was re-administered at the reduced dose and the original dose in the other patient (27). Patel et al. reported that 3 patients suffered from cardiac failure after being initiated on osimertinib, 2 patients had basic heart disease, and LVEF decreased dramatically. Osimertinib was re-administered to only 1 patient, whereas the last 2 patients were treated with erlotinib (28). Shinomiya et al. reported a 76-year-old woman who underwent surgical resection of the left upper lobe plus lymph node dissection and used osimertinib as the second-line adjuvant therapy; 4 months after osimertinib initiation, cardiomyopathy secondary to osimertinib was diagnosed and osimertinib was discontinued (29). Ikebe et al.

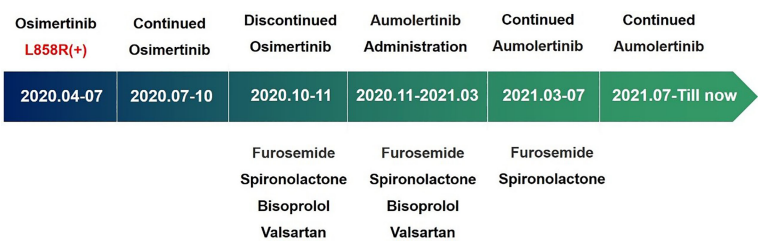

FIGURE 3 | The medicine administration with indicated time periods shown as a flowchart diagram.

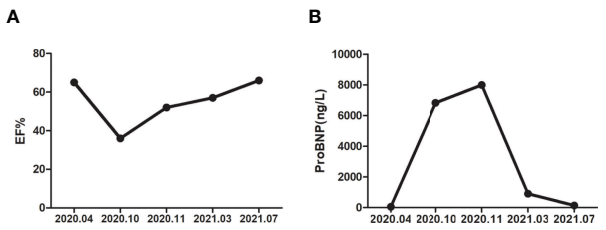

FIGURE 4 | The detection of cardiac function in different time periods. **(A)** Ejection fraction in different time periods. **(B)** Brain natriuretic peptide precursor (pro-BNP) in different time periods.

reported a rare case in which osimertinib simultaneously induced congestive heart failure and QT prolongation. The possible reason was a prior stereotactic thoracic radiotherapy; her heart was within the irradiation area, and radiation therapy could damage both cardiomyocytes and vasculature. She did not receive any other chemotherapy and died of cancer progression and cachexia at home 15 months after osimertinib discontinuation (30). In these case reports, most patients switched to other first-generation EGFR-TKIs because of osimertinib-induced cardiotoxicity, even if it was reversible.

With an increasing number of osimertinib-induced cardiotoxicity, the question arises, what could be the possible mechanism behind the cardiotoxicity triggered by osimertinib? EGFR is a receptor tyrosine kinase (RTK) in the erythroblasts leukemia viral oncogene homolog (ErbB)/human epidermal growth factor receptor (HER) family that includes HER2. HER2 is found to be important in cardiac development and the maintenance of normal cardiac structure and function under stress conditions. Moreover, treatment of cells with AZD9291 (osimertinib) inhibited phosphorylation of HER2 at moderate potency levels (31). Therefore, it is not unanticipated that cardiotoxicity has been observed with this agent.

Aumolertinib, a novel third-generation EGFR-TKI, has been used to treat NSCLC EGFR T790M-positive patients with progressive disease or recurrence as an alternative to other EGFR TKI therapies (32). Compared with osimertinib, the aumolertinib innovatively has an additional cyclopropyl group, which increases its anti-tumor activity, stability, and fat solubility. Like osimertinib, the aumolertinib also irreversibly binds with the EGFR T790M mutation sites and inhibits their function (32, 33).

TABLE 2 | The changes in myocardial enzymes at cardiac failure and during recovery treatment.

Time	Myocardial Enzymes			
	AST	LDH	CK	CKMB
2020.04	11 U/L	161 U/L	20 U/L	15 U/L
2020.10	29.5 U/L	286 U/L	30.7 U/L	37 U/L
2020.11	19.7 U/L	284 U/L	39.1 U/L	31.6 U/L
2021.03	13.8 U/L	121 U/L	29 U/L	15.7 U/L
2021.07	9.6 U/L	127 U/L	21.3 U/L	15.7 U/L

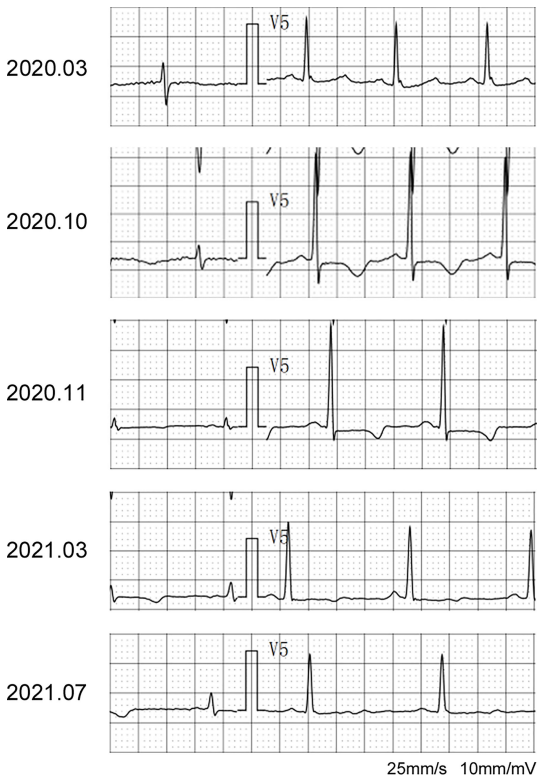

FIGURE 5 | The changes in RV5 of electrocardiogram at cardiac failure and during recovery treatment.

Promising results have been observed for aumolertinib against lung cancer EGFR mutational cells, suggesting its specificity and admirable pharmacokinetic properties in mammals (34). Aumolertinib showed great tumor-regressing efficacy in an EGFR mutant brain metastasis model (35).

In phase II clinical APOLLO trials, aumolertinib has surprisingly shown significant performance with unique anti-tumor characteristics such as the primary endpoint, the overall response rate (ORR) was 68.9%, and the secondary endpoint, the

TABLE 3 | The left ventricular echocardiography data at cardiac failure and during recovery treatment.

Time	Left Ventricular Echocardiography Data					
	LVESD (mm)	LVEDD (mm)	LVESV (ml)	LVEDV (ml)	LVPWT (mm)	EF
2020.04	38	52	61	118	8	65%
2020.10	44	55	70	130	8	36%
2020.11	45	55	72	131	8	52%
2021.03	33	48	47	110	8	57%
2021.07	26	45	31	98	8	66%

LVESD, left ventricular end systolic diameter; LVEDD, left ventricular end diastolic diameter; LVESV, left ventricular end systolic volume; LVEDV, left ventricular end diastolic volume; LVPWT, left ventricular posterior wall thickness; EF, ejection fraction.

median PFS of 12.4 months. In addition, the inhibitory effects of aumolertinib included the median duration of response (mDOR) of 15.1 months, and the disease control rate (DCR) of 93.4% (36). Additionally, the fat solubility of aumolertinib enables it to successfully cross the blood–brain barrier, thus showing adequate effectiveness in central nervous system (CNS) metastases: the CNS ORR was 60.9%, the CNS DCR was 91.3%, the median CNS PFS was 10.8 months, and the median CNS DOR was 12.5 months. It is worth mentioning here that PFS and OS of L858R and 19 deletion patients have similar benefits (36, 37). The most common treatment-related adverse reactions (TRAEs) ≥10% were blood creatine phosphokinase (CPK) increased (20.9%), rash (13.9%), aspartate aminotransferase (AST) increased (12.3%), white blood cell (WBC) count decreased (12.3%), alanine aminotransferase (ALT) increased (11.9%), and pruritus (10.7%); 15 (6.1%) patients had QT prolongation, and there was no ILD reported (36). The major AEs caused by aumolertinib include rash, diarrhea, fatigue, ALT/AST increase, and anemia, but none of the reported cases showed ILD and serious cardiotoxicity (36). Interestingly, the current patient had no history of any cardiac diseases, and the incidence of the cardiotoxicity induced by osimertinib was not obvious until aggravated after 6 months of continued treatment. Later, the treatment plan changed, which gradually improved the cardiac symptoms in 9 months.

In summary, we present an EGFR-positive NSCLC case with osimertinib-induced cardiac failure. Next, we switched the treatment plant to aumolertinib, which alienated the cardiac symptoms as well as tumorigenicity. Until now, the patient is being treated with aumolertinib for more than 9 months and maintained SD without any obvious AEs. The patient is regularly followed up to monitor the adverse reactions and improvement in treatment outcomes. Here, we report for the first time that switching from osimertinib to aumolertinib following the occurrence of osimertinib-induced cardiac failure was helpful in the gradual recovery of cardiac and NSCLC symptoms. It could be a potential therapeutic strategy for other patients with similar AEs.

DATA AVAILABILITY STATEMENT

The raw data supporting the conclusions of this article will be made available by the authors, without undue reservation.

ETHICS STATEMENT

The studies involving human participants were reviewed and approved by the Ethics Committee of the Henan Provincial Peoples' Hospital, China. The patients/participants provided their written informed consent to participate in this study.

AUTHOR CONTRIBUTIONS

QZ conceived the idea, collected data, and wrote the first draft of the manuscript. HL and JY performed data analysis, studied all clinical parameters of the patient, and reviewed and revised the manuscript. All authors contributed to the article and approved the submitted version.

ACKNOWLEDGMENTS

We are highly grateful to the doctors and paramedic staff of Henan Provincial People's Hospital for their technical support for this study, and for taking good care of this patient and other patients admitted to the hospital for regular treatments. We are highly grateful to Mr. Hangfan Liu from the Medical Oncology Scientific Group of the Central Medical Department, Jiangsu Hansoh Pharmaceutical Group Co., Ltd. for their technical support in the accomplishment of this study. We also highly acknowledge the consent of the patient and her family for being included in the current study.

REFERENCES

1. Sung H, Ferlay J, Siegel RL, Laversanne M, Soerjomataram I, Jemal A. Global Cancer Statistics 2020: GLOBOCAN Estimates of Incidence and Mortality Worldwide for 36 Cancers in 185 Countries. *CA Cancer J Clin* (2021) 71:209–49. doi: 10.3322/caac.21660
2. Liam CK, Pang YK, Poh ME. EGFR Mutations in Asian Patients With Advanced Lung Adenocarcinoma. *J Thorac Oncol* (2014) 9(9):e70–1. doi: 10.1097/JTO.0000000000000251
3. Tsao SA, Tang X, Sabloff B, Xiao L, Shigematsu H, Roth J. Clinicopathologic Characteristics of the EGFR Gene Mutation in Non-Small Cell Lung Cancer. *J Thorac Oncol* (2006) 1:231–9. doi: 10.1016/s1556-0864(15)31573-2
4. Lee SY, Kim MJ, Jin G, Yoo SS, Park JY, Choi JE. Somatic Mutations in Epidermal Growth Factor Receptor Signaling Pathway Genes in Non-Small Cell Lung Cancers. *J Thorac Oncol* (2010) 5:1734–40. doi: 10.1097/JTO.0b013e3181f0beca
5. Shepherd FA, Pereira JR, Ciuleanu T, Tan EH, Hirsh V, Thongprasert S. Erlotinib in Previously Treated Non-Small-Cell Lung Cancer. *N Engl J Med* (2005) 353:123–32. doi: 10.1056/NEJMoa050753
6. Stinchcombe TE, Socinski MA. Gefitinib in Advanced Non-Small Cell Lung Cancer: Does It Deserve a Second Chance? *Oncologist* (2008) 13:933–44. doi: 10.1634/theoncologist.2008-0019
7. Mok TS, Wu Y, Ahn M, Garassino MC, Kim HR, Ramalingam SS. Osimertinib or platinum-Pemetrexed in EGFR T790M-Positive Lung Cancer. *N Engl J Med* (2017) 376:629–40. doi: 10.1056/NEJMoa1612674
8. Yu HA, Arcila ME, Rekhtman N, Sima CS, Zakowski MF, Pao W. Analysis of Tumor Specimens at the Time of Acquired Resistance to EGFR-TKI Therapy in 155 Patients With EGFR-mutant Lung Cancers. *Clin Cancer Res* (2013) 19:2240–7. doi: 10.1158/1078-0432.CCR-12-2246
9. Wu SG, Shih JY. Management of Acquired Resistance to EGFR TKI–Targeted Therapy in Advanced Non-Small Cell Lung Cancer. *Mol Cancer* (2018) 17:38. doi: 10.1186/s12943-018-0777-1
10. Stewart EL, Tan SZ, Liu G, Tsao MS. Known and Putative Mechanisms of Resistance to EGFR Targeted Therapies in NSCLC Patients With EGFR Mutations-a Review. *Trans Lung Cancer Res* (2015) 4:67–81. doi: 10.3978/j.issn.2218-6751.2014.11.06
11. Hou DH, Li WH, Wang SC, Huang Y, Wang JW, Tang W, et al. Different Clinicopathologic and Computed Tomography Imaging Characteristics of Primary and Acquired Egfr T790M Mutations in Patients With Non-Small-Cell Lung Cancer. *Cancer Manag Res* (2021) 13:6389–401. doi: 10.2147/CMAR.S323972
12. Rosell R, Moran T, Queralt C, Porta R, Cardenal F, Camps C. Screening for Epidermal Growth Factor Receptor Mutations in Lung Cancer. *N Engl J Med* (2009) 361:958–67. doi: 10.1056/NEJMoa0904554

13. Shi YK, Au JS-K, Thongprasert S, Srinivasan S, Tsai CM, Khoa MT. A Prospective, Molecular Epidemiology Study of EGFR Mutations in Asian Patients With Advanced Non–Small-Cell Lung Cancer of Adenocarcinoma Histology (Pioneer). *J Thorac Oncol* (2014) 9:154–62. doi: 10.1097/JTO.0000000000000033
14. Rugiu ES, Melchior LC, Urbanska EM, Jakobsen JN, Stricker KD, Grauslund M. Intrinsic Resistance to EGFR-Tyrosine Kinase Inhibitors In EGFR-Mutant Non-Small Cell Lung Cancer: Differences and Similarities With Acquired Resistance. *Cancers (Basel)* (2019) 11:923. doi: 10.3390/cancers11070923
15. Mok TS, Wu Y, Thongprasert S, Yang CH, Chu DT, Saijo N. Gefitinib or Carboplatin-Paclitaxel in Pulmonary Adenocarcinoma. *N Engl J Med* (2009) 361:947–57. doi: 10.1056/NEJMoa0810699
16. Shi Y, Wang L, Han B, Li W, Yu P, Liu Y. First-Line Icotinib Versus Cisplatin/Pemetrexed Plus Pemetrexed Maintenance Therapy for Patients With Advanced EGFR Mutation-Positive Lung Adenocarcinoma (CONVINCE): A Phase 3, Open-Label, Randomized Study. *Ann Oncol* (2017) 28:2443–50. doi: 10.1093/annonc/mdx359
17. Tan CS, Gilligan D, Pacey S. Treatment Approaches for EGFR Inhibitor-Resistant Patients With Non-Small-Cell Lung Cancer. *Lancet Oncol* (2015) 16:e447–459. doi: 10.1016/S1470-2045(15)00246-6
18. Jean-Charles S, Yuichiro O, Johan V, Reungwetwattana T, Chewaskulyong B, Lee KH. Osimer-Tinib in Untreated Egfr-Mutated Advanced Non-Small-Cell Lung Cancer. *N Engl J Med* (2018) 378:113–25. doi: 10.1056/NEJMoa1713137
19. Jóri B, Stefanie Schatz S, Kaller L, Kah B, Roeper J, Ramdani HO. Comparison of Resistance Spectra After First and Second Line Osimertinib Treatment Detected by Liquid Biopsy. *Cancers (Basel)* (2021) 13:2861. doi: 10.3390/cancers13122861
20. Watanabe H, Ichihara E, Kano H, Ninomiya K, Tanimoto M, Kiura K. Congestive Heart Failure During Osimertinib Treatment for Epidermal Growth Factor Receptor (EGFR)-Mutant Non-Small Cell Lung Cancer (Nsclc). *Intern Med* (2017) 56:2195–7. doi: 10.2169/internalmedicine.8344-16
21. Oyakawa T, Nakashima K, Naito T. Cardiac Dysfunction Caused by Osimertinib. *J Thorac Oncol* (2017) 12:e159–60. doi: 10.1016/j.jtho.2017.05.016
22. Okutucu S, Sayin BY, Aksoy H, Oto A. Development of Heart Failure After Initiation of Osimertinib Treatment for Epidermal Growth Factor Receptor (EGFR)-Mutant Adenocarcinoma of the Lung. *Am J Cardiol* (2018) 121:e160–1. doi: 10.1016/j.amjcard.2018.03.348
23. Reale ML, Bianco M, Tabbò F. Osimertinib-Induced Cardiac Dysfunction in EGFR-mutated Lung Cancer: A Case Series of Five Patients. *Am J Cancer Case Rep* (2018) 6:52–60.
24. Anad K, Ensor J, Trachtenberg B, Bernicker EH. Osimertinib Induced Cardiotoxicity: A Retrospective Review of the FDA Adverse Events Reporting System (FAERS). *JACC Cardio Oncol* (2019) 1:172–9. doi: 10.1016/j.jaccao.2019.10.006
25. Thein KZ, Swarup S, Ball S, Quirch M, Vorakunthada Y, Htwe KK. Incidence of Cardiac Toxicities in Patients With Advanced Non-Small Cell Lung Cancer Treated With Osimertinib: A Combined Analysis of Two Phase III Randomized Controlled Trials. *Ann Oncol* (2018) 29 supplement 8:VIII500. doi: 10.1093/annonc/mdy292.011
26. Vallillo AP, Costa DB, Sabe MA, Asnani A. Heart Failure Associated With the Epidermal Growth Factor Receptor Inhibitor Osimertinib. *JACC Cardio Oncol* (2020) 2:119–22. doi: 10.1016/j.jaccao.2020.01.003
27. Kunimasa K, Kamada R, Oka T, Oboshi M, Kimura M, Inoue T. Cardiac Adverse Events in EGFR-Mutated Non-Small Cell Lung Cancer Treated With Osimertinib. *JACC Cardio Oncol* (2020) 2:1–10. doi: 10.1016/j.jaccao.2020.02.003
28. Patel SR, Brown SN, Kubusek JE, Mansfield AS, Duma N. Osimertinib-Induced Cardiomyopathy. *JACC Case Rep* (2020) 2:641–5. doi: 10.1016/j.jaccas.2019.12.038
29. Shinomiya S, Kaira K, Yamaguchi O, Ishikawa K, Kagamu H. Osimertinib Induced Cardiomyopathy. *Med (Baltimore)* (2020) 99:e22301. doi: 10.1097/MD.0000000000022301
30. Ikebe S, Amiya R, Minami S, Ihara S, Higuchi Y, Komuta K. Osimertinib-Induced Cardiac Failure With QT Prolongation and Torsade De Pointes in a Patient With Advanced Pulmonary Adenocarcinoma. *Int Cancer Conf J* (2021) 10:68–71. doi: 10.1007/s13691-020-00450-2
31. Cross D, Ashton SE, Ghiorghiu S, Eberlein C, Nebhan CA, Spitzler PJ. AZD9291, an Irreversible EGFR TKI, Overcomes T790M-Mediated Resistance to EGFR Inhibitors in Lung Cancer. *Cancer Discov* (2014) 4:1046–61. doi: 10.1158/2159-8290.CD-14-0337
32. Yang James C-H, Camidge DR, Yang C, Zhou J, Guo R, Chiu C. Safety, Efficacy, and Pharmacokinetics of Almonertinib (HS-10296) in Pretreated Patients With EGFR-Mutated Advanced NSCLC: A Multicenter, Open-Label, Phase 1 Trial. *J Thorac Oncol* (2020) 15:1907–18. doi: 10.1016/j.jtho.2020.09.001
33. Tanaji TT. The "Cyclopropyl Fragment" Is a Versatile Player That Frequently Appears in Preclinical/Clinical Drug Molecules. *J Med Chem* (2016) 59:8712–56. doi: 10.1021/acs.jmedchem.6b00472
34. Bao R, Gao P, Zhang F, Zhaolong Tong Z, Yu H, Xu Y. Abstract 3063: Discovery of a Third-Generation EGFR Inhibitor, Which Is Highly Selective and Potent Against Both Resistant and Activating EGFR Mutations for NSCLC Therapy. *Cancer Res* (2016) 76:3063–3. doi: 10.1158/1538-7445.AM2016-3063
35. Zhang Y, Zhang Y, Niu W, Ge X, Huang F, Pang J. Experimental Study of Almonertinib Crossing the Blood-Brain Barrier in EGFR-Mutant Nsclc Brain Metastasis and Spinal Cord Metastasis Models. *Front Pharmacol* (2021) 12:750031. doi: 10.3389/fphar.2021.750031
36. Lu S, Wang Q, Zhang G, Dong X, Yang C, Song Y. Efficacy of Aumolertinib (Hs-10296) in Patients With Advanced Egfr T790M+ Nsclc: Updated Post NMPA-Approval Results From the APOLLO Registrational Trial. *J Thorac Oncol* (2021) 17(3):411–22. doi: 10.1016/j.jtho.2021.10.024
37. Lu S, Wang Q, Zhang G, Dong X, Yang C, Song Y. 1208p Final Results of APOLLO Study: Overall Survival (OS) of Aumolertinib in Patients With Pretreated EGFR T790M-Positive Locally Advanced or Metastatic Non-Small Cell Lung Cancer (NSCLC). *Ann Oncol* (2021) 31:s962. doi: 10.1016/j.annonc.2021.08.1813

Conflict of Interest: The authors declare that the research was conducted in the absence of any commercial or financial relationships that could be construed as a potential conflict of interest.

frontiers | Frontiers in Endocrinology

REVIEW
published: 27 May 2022
doi: 10.3389/fendo.2022.897513

The Value of Multimodality PET/CT Imaging in Detecting Prostate Cancer Biochemical Recurrence

Jie Jiang[1†], Xiaoxia Tang[2†], Yongzhu Pu[1†], Yong Yang[3†], Conghui Yang[1], Fake Yang[1], Yadong Tian[1], Jindan Li[1], Hua Sun[1], Sheng Zhao[1*] and Long Chen[1*]*

[1] Department of PET/CT Center, Yunnan Cancer Hospital, The Third Affiliated Hospital of Kunming Medical University, Yunnan, China, [2] Department of Pharmacy, The Second Affiliated Hospital of Kunming Medical University, Yunnan, China, [3] Department of Urology, Yunnan Cancer Hospital, The Third Affiliated Hospital of Kunming Medical University, Yunnan, China

OPEN ACCESS

Edited by:
Ihtisham Bukhari, Fifth Affiliated Hospital of Zhengzhou University, China

Reviewed by:
Chunlei Han, Turku PET Centre, Finland
Xilin Sun, The Fourth Hospital of Harbin Medical University, China

****Correspondence:***
Long Chen
lonechen1983@hotmail.com
Hua Sun
649790827@qq.com
Sheng Zhao
8390681@qq.com

[†]These authors have contributed equally to this work

Specialty section:
This article was submitted to Cancer Endocrinology, a section of the journal Frontiers in Endocrinology

Received: *16 March 2022*
Accepted: *26 April 2022*
Published: *27 May 2022*

Citation:
Jiang J, Tang X, Pu Y, Yang Y, Yang C, Yang F, Tian Y, Li J, Sun H, Zhao S and Chen L (2022) The Value of Multimodality PET/CT Imaging in Detecting Prostate Cancer Biochemical Recurrence. Front. Endocrinol. 13:897513. doi: 10.3389/fendo.2022.897513

Prostate cancer (PCa) induced death is the predominant cause of cancer-related death among men in 48 countries. After radical treatment, biochemical recurrence has become an important factor for prognosis. The early detection and diagnosis of recurrent lesions are very helpful in guiding treatment and improving the prognosis. PET/CT is a promising method for early detection of lesions in patients with biochemical recurrence of prostate cancer. This article reviews the progress of the research on PET/CT in the PCa biochemical recurrence and aims to introduce new technologies and provide more direction for future research.

Keywords: prostate cancer, biochemical recurrence, PET/CT- Positron Emission Tomography Computed Tomography, imaging

BACKGROUND

Prostate cancer (PCa), the fifth reason of cancer-related death among male, is also the second most commonly diagnosed cancer (1). In 2020 1.4 million cases were newly diagnosed and 375,000 deaths were identified around the world (2). With the general promotion of prostate-specific antigen (PSA) screening, the improvement of biopsy technology, as well as the optimization of treatment methods, both of the incidence and mortality rates of PCa have declined or stabilized in most countries in recent years. However, the incidence of advanced PCa has increased (2, 3). Prostate cancer is a malignant tumor with extremely heterogeneous clinical behavior and has biological behaviors ranging from inertia and organ limitation to rapid invasion and easy metastasis (4). It is diagnosed mainly through digital rectal examination (DRE) and PSA testing. Once a preliminary diagnosis is made, a needle biopsy guided by a rectal ultrasound (TRUS) is performed (5). After an initial treatment *via* radical prostatectomy (RP) or local radiotherapy (RT), almost half of patients develop biochemical recurrence (BCR) and an increase in PSA. After a potential remedial treatment option, androgen deprivation therapy (ADT) is usually used for the patient. After the ADT, prostate-specific antigens begin to rise again in 2-8 years, and metastatic castration-resistant PCa can develop (6). Studies have shown that salvage RT (SRT) after early RP provides a cure for increased PSA in patients after RP (7–9), and therefore, early detection of BCR and lesion metastasis and accurate restaging guidance for the treatment of recurrent PCa is very important. Both of CT and MRI are structural imaging techniques and are of limited sensitivity and specificity for detecting a minimal

metastatic lesion, which leads to a lower diagnostic rate for common imaging techniques in asymptomatic patients (10). The molecular imaging PET/CT is believed to be superior to BCR detection.

PET/CT IMAGING AGENT FOR BCR PCA

BCR is generally defined by elevated PSA values (more than 0.2 ng/ml) in consecutively two tests after RP (11, 12). For patients receiving radiation therapy, biochemical failure is defined as the end of radiotherapy with the lowest PSA increase in the last 6 weeks being ≥ 2 ng/mL (13). Over the past decade, a variety of PET probes have achieved good results in detecting recurrent lesions and disease staging in PCa patients. PET radiotracers that are used have developed rapidly and mainly include radiolabeled choline, prostate specific membrane antigen (PSMA) ligands,^{18}F-fluciclovine, gastrin-releasing peptide receptor (GRPR), fibroblast activation protein inhibitors(FAPI) and so on (14–22) (**Table 1**).

PSMA is a highly overexpressed transmembrane glycoprotein detected in the majority of prostate cancer cells (23) and is located in the apical region of prostate cells (i.e., the prostate tube) (**Figure 1**). PSMA is expressed in peripheral epithelial cells (24), and high-grade PCa have higher PSMA expression, and PSMA expression in late and castration-resistant PCa is further increased (25). PSMA binds with high affinity to the folate hydrolase of the PC cells, allowing the PSMA to show its potential to recognize BCR sites (26), and becomes the target of PCa imaging and therapy. PSMA-PET exhibits good early detection and localization of PCa recurrence lesions and identification of BCR lymph node metastasis after RP (27, 28). (**Table 2**) And ^{68}Ga-PSMA-11 is the first FDA-approved radiotracer for PCa-specific PET/CT imaging (29, 30) (**Table 2**).

Choline radiopharmaceuticals were used for prostate cancer earlier, and often labeled with ^{11}C and ^{18}F, which can be used for the detection of recurrent lesions and the detection of early recurrence in patients with a history of BCR PCa (31, 32). ^{18}F-fluciclovine is a synthetic amino acid with good biodistribution and little urinary disturbance, is often used for restaging of BCR patients (33). Gastrin-releasing peptide receptor antagonist (RM2) binds to GRPR on PCa cells, complementary to PSMA-targeted imaging (15, 34). Fibroblast activation protein (FAP) is highly expressed in a variety of epithelial cancers, and FAP inhibitor (FAPI) PET/CT has been used for various tumor imaging. Research has confirmed the uptake of ^{68}Ga-FAPI-04 in PCa tissue was higher than that in normal prostate tissue, and FAP expression was increased after ADT, which has potential when the detection of lesions is limited after ADT (16, 21, 35).

RECURRENT LESIONS DETECTION AND LOCALIZATION

Patients with a large number of RPs have an elevated PSA, and early detection and localization of anatomical sites of recurrence are critical to guide subsequent treatment. PET/CT was believed to be better than a morphological-based standard imaging mode (CWU) (36). An analysis of prostate cancer in Asian populations showed that standard imaging was not sensitive to recurrent PCa, and none of the bone lesions detected by PET was detected by CWU (37). Choline-PET is the most widely studied method, and although it has excellent specificity (38), its sensitivity is low, especially when PSA levels are low (39). A prospective study showed a PSMA-PET/CT detection rate of 66%, which is remarkably higher than the ^{18}F-choline PET/CT detection rate of 32% (40). ^{68}Ga-PSMA PET showed an obviously higher detection rate and a higher general impact on the clinical management than ^{18}F-fluoromethylcholine (41, 42). ^{18}F-fluciclovine has excellent detection rates for low, medium and high PSA levels (43, 44), and the test results are significantly better than those obtained with ^{11}C-choline (38, 45). A meta-analysis showed that in BCR patients, the combined detection rates of ^{18}F-labeled choline, fluciclovir, and PSMA were 66%, 74%, and 83%, respectively (38). The study by Hoffmann et al. compared the detection rates of ^{18}F-PSMA and ^{68}Ga-PSMA PET, and the results showed that the detection rates of the two tracers were similar, 87.5% (112/128) and 88.9% (121/136), respectively (46). A recent study showed, ^{68}Ga-P16-093, a small molecule PSMA ligand, detected 71% of lesions in BCR patients (47) (**Table 3**).

TABLE 1 | Common PET-CT imaging agents to detect biochemical recurrence of prostate cancer.

Name	Half-life (min)	Production type	Mechanisms
^{11}C-choline	20	Cyclotron	Cell membrane synthesis
^{11}C-acetate	20	Cyclotron	Fatty acid metabolism
^{68}Ga-PSMA-11	68	Generator	PSMA binding
^{68}Ga-RM2	68	Generator	GRPR receptor binding
^{68} Ga-FAPI-04	68	Generator	FAP inhibitors
^{18}F-FDHT	107	Cyclotron	Androgen receptor binding
^{18}F-DCFPyL	107	Cyclotron	PSMA inhibitor
^{18}F-NaF	107	Cyclotron	Bone chemisorption
^{89}Zr-PSMA-DFO	4704	Generator	PSMA inhibitor

PET, positron emission tomography; ^{18}F-FDG, ^{18}F-fluoro-deoxy-glucose;
^{18}F-NaF, sodium ^{18}F-fluoride;GRPR,gastrin-releasing peptidere ceptor;
^{18}F-FDHT,^{18}F-fluorodehydrotestosterone;^{18}F-DCFPyL,^{18}F-2-(3-(1-carboxy-5-[(6-^{18}F-fluoro-pyridine-3-carbonyl)-amino]-pentyl)-ureido)-pentanedioic acid; FAP,fibroblast activation protein.

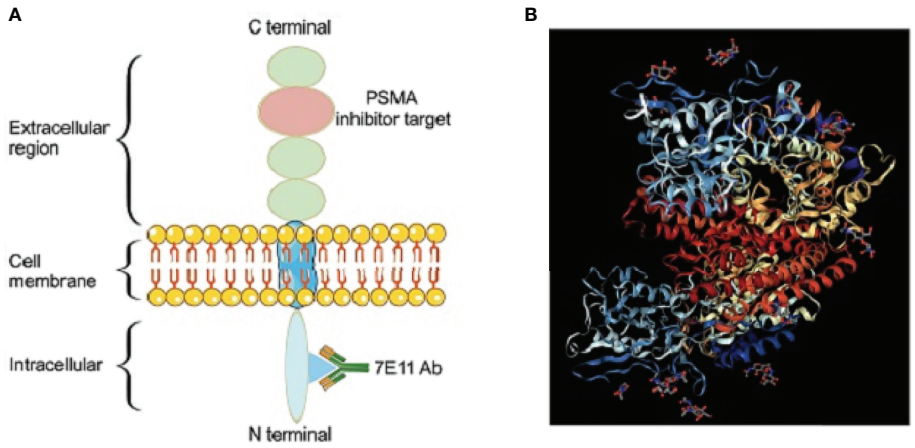

FIGURE 1 | PSMA structure diagram. **(A)** Schematic illustration of PSMA. **(B)** Cyrstal structure of PSMA.

Previous studies have shown that PSMA PET has a higher detection rate than other tracers, and some researchers have found that when PSMA expression is low or PSMA negative tumor area ≥ 50%, PSMA-PET results are negative, although PSA levels are very high (56). When PSMA expression is low, Dietlein et al. found 5 ^{89}Zr-PSMA-DFO PET-positive lesions in 14 PSMA-PET-negative patients.^{89}Zr-PSMA-DFO PET becomes a good supplement because its half-life is long enough to allow the process of ligand internalization to proceed sufficiently to make the lesions visible (22, 56, 57). Targeting gastrin-releasing peptide receptor (GRPR) is thought to complement PSMA-negative prostate cancer (PCa) patients (58), and it is helpful for the localization of recurrent lesions in ^{18}FECH PET/CT-negative patients (59).Another study showed that the detection rate of ^{18}F-FDG PET/CT in PSMA-PET negative patients was 16.7%, and patients with PSA ≥2.3 ng/mL and high Gleason score were more likely to benefit from FDG PET (60).

FACTORS AFFECTING THE DETECTION RATE

Many studies (41, 61–65) have indicated that PSMA, choline, fluciclovine PET/CT positive results possibly are significantly correlated with increased PSA levels (37). For patients with BCR, the positive rate of the PET/CT scan varies based on the clinical stage of the BCR, PSA levels as well as PSA doubling time during the scan are correlated with positive results (27, 66). A study showed that the detection rates of ^{18}F-labeled choline, fluciclovine, and PSMA were 35, 23, and 58% for a PSA level less than 0.5 ng/ml;80, 92, and 94% for a PSA level more than 2.0 ng/ml (38). The rate of increase grows with a rise in the serum PSA levels before the PET (27, 67, 68). There are studies that shown that when the PSA levels higher than 0.2 ng/ml while the PSA velocity ≥ 1 ng/ml/year, there will be a positive PSMA scan (69), and with higher PSA levels, the PSMA-PET shows better diagnostic performance (28).

It has been documented that androgen deprivation therapy experience in BCR patients is correlated with the positive rate of PSMA-PET scans (69), and there is evidence that PSMA is induced with low doses of ADT at lower PSA levels (≤0.3 ng/mL). Imaging may enhance the positive scan rate (70), but further research is needed. In addition, the time to inject the imaging agent is related to the contrast of the image. For BCR with low PSA levels, imaging 3 hours after injection is more advantageous in terms of lesion contrast (71), which may also have an effect on the positive scan rate. Scanning technology and timing also have an impact on the positive rate. Morawitz et al. (72)

TABLE 2 | The difference between PSMA and PSA.

	PSMA	PSA
Type	Integral cell-surface membrane protein	Secretory protein
Function	Several enzymatic functions	Known function-liquefaction of semen
Relationship with androgens	Upregulated with androgen deprivation	Decreased with androgen deprivation
monoclonal antibody	Ideal target for monoclonal antibody therapy	Not suitable for monoclonal antibody
Clinical Value	Neither related to clinical stage nor as diagnostic cancer marker	Useful in the clinical diagnosis and staging and an important diagnostic biomarker
Index meaning	The values may be controversial even if effective treatment	Fall to low values in response to effective treatment
Prognostic value	Elevated levels predict clinical progression or clinical resistance in more than 70% cases	Lower prognostic value

TABLE 3 | Detection rate of different imaging agents for BCR PCa.

Author	Year	Study type	Patients(n)	Imaging agents	Detection rate	Management change
De Man K (48)	2022	Prospective study	51	^{18}F-PSMA-11	82%	52%
Abghari Gerst M (49)	2022	Prospective study	2005	^{68}Ga-PSMA-11	78%	—
Ceci F (50)	2022	Retrospective study	189	^{68}Ga-PSMA-11	54.5%	31%
Mena E (51)	2021	Retrospective study	245	^{18}F-DCFPyL	79.2%	—
Zhou X (52)	2022	Retrospective study	71	^{18}F-PSMA-1007	79%	—
Christensen MT (53)	2021	Retrospective study	532	^{18}F-rhPSMA-7	80%	—
Lee H (47)	2022	Prospective study	15	^{68}Ga-P16-093	71%	41%
Filippi L (54)	2022	Retrospective study	81	^{18}F-fluciclovine	76.9%	31%
Zattoni F (55)	2021	Retrospective study	140	^{18}F-Choline	70.7%	—
Wang R (38)	2021	Meta	5324	^{18}F-choline	66%	—
			1706	^{18}F-PSMA	83%	—
			1410	^{18}F-fluciclovine	74%	—

found that ^{68}Ga-PSMA-11 PET/CT scanning in the late abdominal and pelvic stage after emptying the bladder was helpful to detect missed local recurrence lesions. Uprimny et al. (73) improved the detection rate of lesions by using furosemide before scanning.

PET IMAGING FOR BCR OF LOW PSA LEVELS

Currently, salvage RT (SRT) is one valuable treatments for patients with PSA elevation after RP. Early diagnosis of BCR at low PSA levels has a major impact on patients' follow-up treatment. EVU guidelines recommend that PSA levels greater than 0.2 ng/mL and results influence subsequent treatment decisions, imaging of biochemically recurrent PCa with PSMA-labeled PET/CT (74). A study in 2005 patients with BCR found that the detection rate of ^{68}Ga-PSMA-11 was 44.8% when the PSA was less than 0.25 ng/mL (49). A meta-analysis showed that the detection rates of ^{18}F-Choline, ^{18}F-Fluciclovine and ^{18}F-PSMA PET/CT at PSA levels less than 0.5 ng/ml were 35%, 23%, and 58%, respectively (38). PEMA-PET is superior to other imaging methods at low PSA levels, as recommended by guidelines (**Figure 2**). ^{18}F-fluciclovine PET is feasible for patients with PSA <1.0ng/ml. Filippi et al (54) found that the detection rate in 81 Italian patients was 66.7% when the PSA level was 0.2-0.57 ng/ml, and Wang et al. (75) in 46 patients with PSA level of 0.3-1.0ng/ml found the positive rate was about 33%, but it was not found positive cases in very low PSA (less than 0.3ng/ml) BCR patients. The value of ^{18}F-fluciclovine PET in detecting lesions in BCR patients with very low PSA levels remains to be explored. A recent study found that at very low PSA (≤0.1ng/ml) levels, dynamic detection of ^{11}C-choline PET was helpful in detecting early recurrence in BCR PCa patients (32). This could be a valuable new direction.

DETECTION OF METASTASES IN BCR PATIENTS

Increased serum PSA levels are sensitive to *in vitro* markers of recurrent prostate cancer; however, it is still hard to differentiate local recurrence and regional or distant metastasis. Identifying metastatic disease can impact therapeutic schedule options and contributes to prognosis assessment (27). PSMA PET/CT is most commonly used to detect LN metastases and staging in BCR patients after RP, and its performance depends on the PSA levels as well as the volume of debris from metastatic cells (28). However, in small lymph nodes, this method performs well (76). Rauscher showed that ^{68}Ga-PSMA PET detected LNM

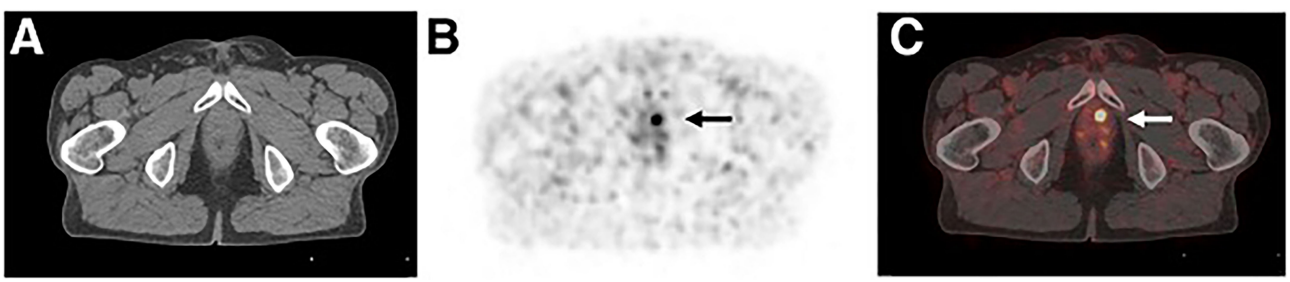

FIGURE 2 | A 78-year-old patient with biochemical recurrence (PSA of 0.54 ng/mL) after radical prostatectomy (initially pT3b N0 M0 R0 G2). ^{68}Ga-PSMA ligand PET/CT reveals focal uptake in left paramedian prostatic fossa, indicating local recurrence. The picture below shows transaxial CT **(A)**, PET **(B)**, and fused PET/CT **(C)** images respectively. Patient was referred for salvage radiation treatment. This research was originally published in JNM. Author(Schwarzenboeck SM, Rauscher I, Bluemel C, Fendler WP, Rowe SP, Pomper MG, Afshar-Oromieh A, Herrmann K, Eiber M). PSMA Ligands for PET Imaging of Prostate Cancer. J Nucl Med. 2017 Oct;58(10):1545-1552.© SNMMI.

(77.9%) in 68 histopathologically confirmed metastatic LN regions, whereas conventional imaging modality only detected 18 of 67 regions (26.9%) (77). Studies have shown that ^{18}F-rhPSMA-7 and ^{18}F-rhPSMA-7.3 PET have a detection rate of 81.3% for lymph node metastasis in BCR patients after RP, and their accuracy in evaluating lymph node metastasis is comparable to that of ^{18}F-PSMA-11 (78).PSMA-PET/CT has higher diagnostic accuracy for lymph node recurrence after RP, especially for small-volume metastases, ^{18} F-PSMA-1007 PET/CT can reliably detect malignant lymph nodes larger than 3 mm with a specificity of over 99% (79–81) (**Figure 3**).

Bone metastasis is one of the common metastasis methods of prostate cancer, and it is difficult to differentiate diagnosis by traditional imaging due to degenerative changes. Mingels et al. found in 177 BCR patients that the PPV of ^{18}F-PSMA-1007 PET to identify bone lesions was 79%, which was lower than the positive rate of the overall and LN (82). A meta-analysis showed that the highest sensitivity of NaF-PET/CT in identifying bone metastases was 0.97, followed by PSMA PET, higher than choline, MRI and bone scintigraphy (83). A recent study found that ^{18}F-NaF PET/CT detected 93.6% of bone metastases, and the interobserver agreement was very high, with stable and reproducible results (18).

PET/CT FALSE NEGATIVES AND FALSE POSITIVES

For PSMA-PET, a small fraction (<10%) of PCa expressed low PSMA, which results in little or no uptake on PSMA-PET (79, 84). In these PSMA-negative patients, PSMA-PET is ineffective (36). In addition, metal artifacts low levels of PSMA uptake and bladder overflow are also possible elements of false negatives (85).Positive images need to be differentiated from normal tissue, benign lesions, and other non-PCa malignant lesions (25, 86–88). Reports have shown that in normal tissues, high or mild ^{68} Ga-PSMA-11 uptake was observed in the renal cortex, duodenum, parotid gland, and submandibular salivary glands, spleen, lacrimal gland, and liver (89–92). In some benign tissues with high proliferation rate, just like heart valves, pleura, endometrial scars, and granulation tissue, endothelial cells also express PSMA (25, 93, 94). Abnormal accumulation of PSMA-PET were detected in lots of benign lesions, including sarcoidosis (86, 95), Paget's disease (96), healing fractures (97, 98), hemangioma (99), schwannomas (100), adenoma (101), and so on. Malignant tumors other than PCa, such as renal cell carcinoma (102, 103) and hepatocellular carcinoma (104), also have high expression. In addition, ^{18}F-fluorocholine imaging usually shows abnormal uptake in lymph nodes due to inflammatory changes (105).All of the above cause false positive results, so it is necessary to learn about the physiological uptake and normal distribution in order to reduce the false positive results in the diagnosis.

CONCLUSIONS

PSMA-PET has high accuracy in the detection of PCa BCR and the identification of metastasis, especially at low PSA levels. Its diagnostic potential is significantly better than that of choline and amino acid analogues, and this has a remarkable influence on managing patients in clinical. However, due to the expression and distribution characteristics of PSMA, it is unable to reliably recognize the PSMA-negative lesions, and other imaging methods need to be selected as supplements. According to the actual situation of patients, the combined use of complementary imaging agents to detect and locate BCR lesions is helpful for the early and effective detection and localization of recurrent lesions in BCR PCa patients, and is conducive to the selection of treatment options and the improvement of prognosis. Radiocomposites (such as ^{18}F-NOTA-GRPR-PSMA, etc.) with

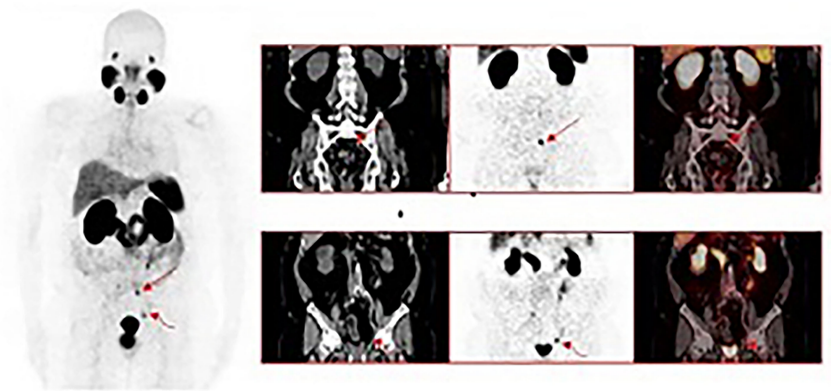

FIGURE 3 | A 63-year-old male with a history of radical prostatectomy for adenocarcinoma of the prostate, Gleason 4 + 4. ^{68}Ga-PSMA-11 PET/CT was requested for localization of disease recurrence at a serum PSA of 0.54 ng/mL. Images show intense tracer uptake in a subcentimeter left presacral node (straight arrows) and a subcentimeter left external iliac node consistent with the sites of prostate cancer recurrence. This research was originally published in JCM.Lawal IO, Lengana T, Popoola GO, Orunmuyi AT, Kgatle MM, Mokoala KMG, Sathekge MM. Pattern of Prostate Cancer Recurrence Assessed by 68Ga-PSMA-11 PET/CT in Men Treated with Primary Local Therapy. J Clin Med. 2021 Aug 29;10(17):3883.

the advantages of two or more imaging agents at the same time may become a research hotspot in the future.

AUTHOR CONTRIBUTIONS

HS conducted project management, writing review and editing. LC and SZ conducted method guidance, writing review and editing. JJ, XXT, YZP and YY conducted data collection, writing-draft preparation. CHY and FKY carried out illustration drawing and software support. YDT and JDL supervised the process. All authors contributed to manuscript revision, read, and approved the submitted version.

FUNDING

This work was supported by the National Natural Science Foundation of China (grant number 81960496), Yunnan Fundamental Research Projects (grant number 202101AT070050), the Project funded by China Postdoctoral Science Foundation (grant number 2019M653501), Scientific Research Fund of Yunnan Province Educational Department (grant number K13219357), Yunnan Provincial Science and Technology Agency/ Kunming Medical University Joint Project [grant number #2019FE001(-087)], Kunming Medical University Graduate Innovation Fund (grant number 2021S070), and the Xingdianyingcai support plan.

REFERENCES

1. Siegel RL, Miller KD, Fuchs HE, Jemal A. Cancer Statistics, 2021. *Ca-a Cancer J Clin* (2021) 71(1):7–33. doi: 10.3322/caac.21654
2. Sung H, Ferlay J, Siegel RL, Laversanne M, Soerjomataram I, Jemal A, et al. Global Cancer Statistics 2020: Globocan Estimates of Incidence and Mortality Worldwide for 36 Cancers in 185 Countries. *CA: Cancer J Clin* (2021) 71(3):209–49. doi: 10.3322/caac.21660
3. Culp MB, Soerjomataram I, Efstathiou JA, Bray F, Jemal A. Recent Global Patterns in Prostate Cancer Incidence and Mortality Rates. *Eur Urol* (2020) 77(1):38–52. doi: 10.1016/j.eururo.2019.08.005
4. Rodrigues DN, Butler LM, Estelles DL, de Bono JS. Molecular Pathology and Prostate Cancer Therapeutics: From Biology to Bedside. *J Pathol* (2014) 232 (2):178–84. doi: 10.1002/path.4272
5. Mohler JL, Antonarakis ES, Armstrong AJ, D'Amico AV, Davis BJ, Dorff T, et al. Prostate Cancer, Version 2.2019, Nccn Clinical Practice Guidelines in Oncology. *J Natl Compr Canc Netw* (2019) 17(5):479–505. doi: 10.6004/jnccn.2019.0023
6. Schwarzenboeck SM, Rauscher I, Bluemel C, Fendler WP, Rowe SP, Pomper MG, et al. Psma Ligands for Pet Imaging of Prostate Cancer. *J Nucl Med Off Publ Soc Nucl Med* (2017) 58(10):1545–52. doi: 10.2967/jnumed.117.191031
7. Pfister D, Bolla M, Briganti A, Carroll P, Cozzarini C, Joniau S, et al. Early Salvage Radiotherapy Following Radical Prostatectomy. *Eur Urol* (2014) 65 (6):1034–43. doi: 10.1016/j.eururo.2013.08.013
8. Wiegel T, Lohm G, Bottke D, Hocht S, Miller K, Siegmann A, et al. Achieving an Undetectable Psa After Radiotherapy for Biochemical Progression After Radical Prostatectomy Is an Independent Predictor of Biochemical Outcome–Results of a Retrospective Study. *Int J Radiat Oncol Biol Phys* (2009) 73(4):1009–16. doi: 10.1016/j.ijrobp.2008.06.1922
9. Soto DE, Passarelli MN, Daignault S, Sandler HM. Concurrent Androgen Deprivation Therapy During Salvage Prostate Radiotherapy Improves Treatment Outcomes in High-Risk Patients. *Int J Radiat Oncol Biol Phys* (2012) 82(3):1227–32. doi: 10.1016/j.ijrobp.2010.08.030
10. Rouviere O, Vitry T, Lyonnet D. Imaging of Prostate Cancer Local Recurrences: Why and How? *Eur Radiol* (2010) 20(5):1254–66. doi: 10.1007/s00330-009-1647-4
11. Cookson MS, Aus G, Burnett AL, Canby-Hagino ED, D'Amico AV, Dmochowski RR, et al. Variation in the Definition of Biochemical Recurrence in Patients Treated for Localized Prostate Cancer: The American Urological Association Prostate Guidelines for Localized Prostate Cancer Update Panel Report and Recommendations for a Standard in the Reporting of Surgical Outcomes. *J Urol* (2007) 177 (2):540–5. doi: 10.1016/j.juro.2006.10.097
12. Cornford P, Bellmunt J, Bolla M, Briers E, De Santis M, Gross T, et al. Eau-Estro-Siog Guidelines on Prostate Cancer. Part Ii: Treatment of Relapsing, Metastatic, and Castration-Resistant Prostate Cancer. *Eur Urol* (2017) 71 (4):630–42. doi: 10.1016/j.eururo.2016.08.002
13. Hofman MS, Murphy DG, Williams SG, Nzenza T, Herschtal A, Lourenco RA, et al. A Prospective Randomized Multicentre Study of the Impact of Gallium-68 Prostate-Specific Membrane Antigen (Psma) Pet/Ct Imaging for Staging High-Risk Prostate Cancer Prior to Curative-Intent Surgery or Radiotherapy (Propsma Study): Clinical Trial Protocol. *BJU Int* (2018) 122 (5):783–93. doi: 10.1111/bju.14374
14. Boustani AM, Pucar D, Saperstein L. Molecular Imaging of Prostate Cancer. *Br J Radiol* (2018) 91(1084):20170736. doi: 10.1259/bjr.20170736
15. Baratto L, Song H, Duan H, Hatami N, Bagshaw HP, Buyyounouski M, et al. Psma- and Grpr-Targeted Pet: Results From 50 Patients With Biochemically Recurrent Prostate Cancer. *J Nucl Med* (2021) 62(11):1545–9. doi: 10.2967/jnumed.120.259630
16. Kratochwil C, Flechsig P, Lindner T, Abderrahim L, Altmann A, Mier W, et al. (68)Ga-Fapi Pet/Ct: Tracer Uptake in 28 Different Kinds of Cancer. *J Nucl Med* (2019) 60(6):801–5. doi: 10.2967/jnumed.119.227967
17. Mohsen B, Giorgio T, Rasoul ZS, Werner L, Ali GR, Reza DK, et al. Application of C-11-Acetate Positron-Emission Tomography (Pet) Imaging in Prostate Cancer: Systematic Review and Meta-Analysis of the Literature. *BJU Int* (2013) 112(8):1062–72. doi: 10.1111/bju.12279
18. Zacho HD, Fonager RF, Nielsen JB, Haarmark C, Hendel HW, Johansen MB, et al. Observer Agreement and Accuracy of (18)F-Sodium Fluoride Pet/Ct in the Diagnosis of Bone Metastases in Prostate Cancer. *J Nucl Med* (2020) 61(3):344–9. doi: 10.2967/jnumed.119.232686
19. Beattie BJ, Smith-Jones PM, Jhanwar YS, Schöder H, Schmidtlein CR, Morris MJ, et al. Pharmacokinetic Assessment of the Uptake of 16beta-18f-Fluoro-5alpha-Dihydrotestosterone (Fdht) in Prostate Tumors as Measured by Pet. *J Nucl Med* (2010) 51(2):183–92. doi: 10.2967/jnumed.109.066159
20. Müller PJ, Dietlein M, Kobe C, Heidenreich A, Drzezga A. Oligometastatic Disease in Biochemical Recurrence of Prostate Cancer: Prevalence on Psma Pet/Ct and Consecutive Metastasis-Directed Therapy - Experience at a Tertiary Referral Center. *Nuklearmedizin* (2022). doi: 10.1055/a-1697-8111
21. Kesch C, Yirga L, Dendl K, Handke A, Darr C, Krafft U, et al. High Fibroblast-Activation-Protein Expression in Castration-Resistant Prostate Cancer Supports the Use of Fapi-Molecular Theranostics. *Eur J Nucl Med Mol Imaging* (2021) 49(1):385–9. doi: 10.1007/s00259-021-05423-y
22. Vázquez SM, Endepols H, Fischer T, Tawadros SG, Hohberg M, Zimmermanns B, et al. Translational Development of a Zr-89-Labeled Inhibitor of Prostate-Specific Membrane Antigen for Pet Imaging in Prostate Cancer. *Mol Imaging Biol* (2022) 24(1):115–25. doi: 10.1007/s11307-021-01632-x
23. Mannweiler S, Amersdorfer P, Trajanoski S, Terrett JA, King D, Mehes G. Heterogeneity of Prostate-Specific Membrane Antigen (Psma) Expression in Prostate Carcinoma With Distant Metastasis. *Pathol Oncol Res: POR* (2009) 15(2):167–72. doi: 10.1007/s12253-008-9104-2
24. DeMarzo AM, Nelson WG, Isaacs WB, Epstein JI. Pathological and Molecular Aspects of Prostate Cancer. *Lancet (London England)* (2003) 361(9361):955–64. doi: 10.1016/s0140-6736(03)12779-1
25. Bostwick DG, Pacelli A, Blute M, Roche P, Murphy GP. Prostate Specific Membrane Antigen Expression in Prostatic Intraepithelial Neoplasia and Adenocarcinoma: A Study of 184 Cases. *Cancer* (1998) 82(11):2256–61. doi: 10.1002/(sici)1097-0142(19980601)82:11<2256::aid-cncr22>3.0.co;2-s

26. Kaittanis C, Andreou C, Hieronymus H, Mao N, Foss CA, Eiber M, et al. Prostate-Specific Membrane Antigen Cleavage of Vitamin B9 Stimulates Oncogenic Signaling Through Metabotropic Glutamate Receptors. *J Exp Med* (2018) 215(1):159–75. doi: 10.1084/jem.20171052
27. Perera M, Papa N, Christidis D, Wetherell D, Hofman MS, Murphy DG, et al. Sensitivity, Specificity, and Predictors of Positive (68)Ga-Prostate-Specific Membrane Antigen Positron Emission Tomography in Advanced Prostate Cancer: A Systematic Review and Meta-Analysis. *Eur Urol* (2016) 70(6):926–37. doi: 10.1016/j.eururo.2016.06.021
28. Abufaraj M, Grubmuller B, Zeitlinger M, Kramer G, Seitz C, Haitel A, et al. Prospective Evaluation of the Performance of [(68)Ga]Ga-Psma-11 Pet/Ct (Mri) for Lymph Node Staging in Patients Undergoing Superextended Salvage Lymph Node Dissection After Radical Prostatectomy. *Eur J Nucl Med Mol Imaging* (2019) 46(10):2169–77. doi: 10.1007/s00259-019-04361-0
29. Mena E, Lindenberg LM, Choyke PL. New Targets for Pet Molecular Imaging of Prostate Cancer. *Semin Nucl Med* (2019) 49(4):326–36. doi: 10.1053/j.semnuclmed.2019.02.001
30. Fda. Approves First Psma-Targeted Pet Drug. *J Nucl Med* (2021) 62(2):11n.
31. Heidenreich A, Bastian PJ, Bellmunt J, Bolla M, Joniau S, van der Kwast T, et al. Eau Guidelines on Prostate Cancer. Part Ii: Treatment of Advanced, Relapsing, and Castration-Resistant Prostate Cancer. *Eur Urol* (2014) 65 (2):467–79. doi: 10.1016/j.eururo.2013.11.002
32. Garg I, Nathan MA, Packard AT, Kwon ED, Larson NB, Lowe V, et al. (11)C-Choline Positron Emission Tomography/Computed Tomography for Detection of Disease Relapse in Patients With History of Biochemically Recurrent Prostate Cancer and Prostate-Specific Antigen ≤0.1 Ng/Ml. *J Cancer Res Ther* (2021) 17(2):358–65. doi: 10.4103/jcrt.JCRT_373_19
33. Nappi AG, Ferrari C, Mammucci P, Rubini D, Lavelli V, Sardaro A, et al. [(18)F]Fluciclovine Pet/Ct Improves the Clinical Management of Early Recurrence Prostate Cancer Patients. *Cancers* (2022) 14(6):1461. doi: 10.3390/cancers14061461
34. Touijer KA, Michaud L, Alvarez HAV, Gopalan A, Kossatz S, Gonen M, et al. Prospective Study of the Radiolabeled Grpr Antagonist Bay86-7548 for Positron Emission Tomography/Computed Tomography Imaging of Newly Diagnosed Prostate Cancer. *Eur Urol Oncol* (2019) 2(2):166–73. doi: 10.1016/j.euo.2018.08.011
35. Gündoğan C, Güzel Y, Can C, Kaplan İ, Kömek H. Fapi-04 Uptake in Healthy Tissues of Cancer Patients in (68)Ga-Fapi-04 Pet/Ct Imaging. *Contrast Media Mol Imaging* (2021) 2021:9750080. doi: 10.1155/2021/9750080
36. Rayn KN, Elnabawi YA, Sheth N. Clinical Implications of Pet/Ct in Prostate Cancer Management. *Trans Androl Urol* (2018) 7(5):844–54. doi: 10.21037/tau.2018.08.26
37. Tan JSH, Goh CXY, Koh YS, Li Y, Tuan JKL, Chua ET, et al. (68)Gallium-Labelled Psma-Pet/Ct as a Diagnostic and Clinical Decision-Making Tool in Asian Prostate Cancer Patients Following Prostatectomy. *Cancer Biol Med* (2019) 16(1):157–66. doi: 10.20892/j.issn.2095-3941.2018.0288
38. Wang R, Shen G, Huang M, Tian R. The Diagnostic Role of (18)F-Choline, (18)F-Fluciclovine and (18)F-Psma Pet/Ct in the Detection of Prostate Cancer With Biochemical Recurrence: A Meta-Analysis. *Front Oncol* (2021) 11:684629. doi: 10.3389/fonc.2021.684629
39. Li R, Ravizzini GC, Gorin MA, Maurer T, Eiber M, Cooperberg MR, et al. The Use of Pet/Ct in Prostate Cancer. *Prostate Cancer Prostatic Dis* (2018) 21(1):4–21. doi: 10.1038/s41391-017-0007-8
40. Afshar-Oromieh A, Zechmann CM, Malcher A, Eder M, Eisenhut M, Linhart HG, et al. Comparison of Pet Imaging With a (68)Ga-Labelled Psma Ligand and (18)F-Choline-Based Pet/Ct for the Diagnosis of Recurrent Prostate Cancer. *Eur J Nucl Med Mol Imaging* (2014) 41(1):11–20. doi: 10.1007/s00259-013-2525-5
41. Morigi JJ, Stricker PD, van Leeuwen PJ, Tang R, Ho B, Nguyen Q, et al. Prospective Comparison of 18f-Fluoromethylcholine Versus 68ga-Psma Pet/Ct in Prostate Cancer Patients Who Have Rising Psa After Curative Treatment and Are Being Considered for Targeted Therapy. *J Nucl Med* (2015) 56(8):1185–90. doi: 10.2967/jnumed.115.160382
42. von Eyben FE, Picchio M, von Eyben R, Rhee H, Bauman G. (68)Ga-Labeled Prostate-Specific Membrane Antigen Ligand Positron Emission Tomography/Computed Tomography for Prostate Cancer: A Systematic Review and Meta-Analysis. *Eur Urol Focus* (2018) 4(5):686–93. doi: 10.1016/j.euf.2016.11.002
43. Bulbul JE, Grybowski D, Lovrec P, Solanki AA, Gabriel MS, Wagner RH, et al. Positivity Rate of [(18)F]Fluciclovine Pet/Ct in Patients With Suspected Prostate Cancer Recurrence at Psa Levels Below 1 Ng/Ml. *Mol Imaging Biol* (2022) 24(1):42–9. doi: 10.1007/s11307-021-01644-7
44. Garza D, Kandathil A, Xi Y, Subramaniam RM. 18f-Fluciclovine Pet/Ct Detection of Biochemical Recurrent Prostate Cancer in Patients With Psa Levels <2.00 Ng/Ml. *Nucl Med Commun* (2021) 42(8):907–13. doi: 10.1097/mnm.0000000000001412
45. Nanni C, Schiavina R, Brunocilla E, Boschi S, Borghesi M, Zanoni L, et al. 18f-Fluciclovine Pet/Ct for the Detection of Prostate Cancer Relapse: A Comparison to 11c-Choline Pet/Ct. *Clin Nucl Med* (2015) 40(8):e386–91. doi: 10.1097/rlu.0000000000000849
46. Hoffmann MA, von Eyben FE, Fischer N, Rosar F, Müller-Hübenthal J, Buchholz HG, et al. Comparison of [(18)F]Psma-1007 With [(68)Ga]Ga-Psma-11 Pet/Ct in Restaging of Prostate Cancer Patients With Psa Relapse. *Cancers* (2022) 14(6):1479. doi: 10.3390/cancers14061479
47. Lee H, Scheuermann JS, Young AJ, Doot RK, Daube-Witherspoon ME, Schubert EK, et al. Preliminary Evaluation of (68)Ga-P16-093, A Pet Radiotracer Targeting Prostate-Specific Membrane Antigen in Prostate Cancer. *Mol Imaging Biol* (2022). doi: 10.1007/s11307-022-01720-6
48. De Man K, Piron S, Van Laeken N, Delrue L, Fonteyne V, Lumen N, et al. Impact of 18F-PSMA-11 PET/CT on Management of Biochemical Recurrence and High-Risk Prostate Cancer Staging: 18F-PSMA-11 PET/CT and Impact on Prostate Cancer Management. *Mol Imaging Biol* (2022). doi: 10.1007/s11307-022-01724-2
49. Abghari-Gerst M, Armstrong WR, Nguyen K, Calais J, Czernin J, Lin D, et al. A Comprehensive Assessment of (68)Ga-Psma-11 Pet in Biochemically Recurrent Prostate Cancer: Results From a Prospective Multicenter Study on 2,005 Patients. *J Nucl Med* (2022) 63(4):567–72. doi: 10.2967/jnumed.121.262412
50. Ceci F, Rovera G, Iorio GC, Guarneri A, Chiofalo V, et al. Event-Free Survival After 68 Ga-PSMA-11 PET/CT in Recurrent Hormone-Sensitive Prostate Cancer (HSPC) Patients Eligible for Salvage Therapy. *Eur J Nucl Med Mol Imaging* (2022). doi: 10.1007/s00259-022-05741-9
51. Mena E, Rowe SP, Shih JH, Lindenberg L, Turkbey B, Fourquet A, et al. Predictors of 18F-DCFPyL-PET/CT Positivity in Patients With Biochemical Recurrence of Prostate Cancer After Local Therapy. *J Nucl Med* (2021). doi: 10.2967/jnumed.121.262347
52. Zhou X, Jiang X, Liu L, Wang X, Li C, Yao Y, et al. Evaluation of 18F-PSMA-1007 PET/CT in Prostate Cancer Patients With Biochemical Recurrence After Radical Prostatectomy. *Transl Oncol* (2022) 15(1):101292. doi: 10.1016/j.tranon.2021.101292
53. Christensen MT, Jochumsen MR, Klingenberg S, Sørensen KD, Borre M, Bouchelouche K, et al. Evaluation of Predictors of Biochemical Recurrence in Prostate Cancer Patients, as Detected by 68Ga-PSMA PET/CT. *Diagnostics (Basel)* (2022) 12(1):195. doi: 10.3390/diagnostics12010195
54. Filippi L, Bagni O, Crisafulli C, Cerio I, Brunotti G, Chiaravalloti A, et al. Detection Rate and Clinical Impact of Pet/Ct With (18)F-Facbc in Patients With Biochemical Recurrence of Prostate Cancer: A Retrospective Bicentric Study. *Biomedicines* (2022) 10(1):177. doi: 10.3390/biomedicines10010177
55. Zattoni F, Artioli P, Burei M, Chiaravalloti A, Chierichetti F, Donner D, et al. Detection Rate of 18F-Choline Positron Emission Tomography/computed Tomography in Patients With Non-Metastatic Hormone Sensitive and Castrate Resistant Prostate Cancer. *Q J Nucl Med Mol Imaging* (2021). doi: 10.23736/S1824-4785.21.03366-5
56. Ferraro DA, Rüschoff JH, Muehlematter UJ, Kranzbühler B, Müller J, Messerli M, et al. Immunohistochemical Psma Expression Patterns of Primary Prostate Cancer Tissue Are Associated With the Detection Rate of Biochemical Recurrence With (68)Ga-Psma-11-Pet. *Theranostics* (2020) 10(14):6082–94. doi: 10.7150/thno.44584
57. Dietlein F, Kobe C, Vázquez SM, Fischer T, Endepols H, Hohberg M, et al. An (89)Zr-Labeled Psma Tracer for Pet/Ct Imaging of Prostate Cancer Patients. *J Nucl Med* (2022) 63(4):573–83. doi: 10.2967/jnumed.121.262290
58. Ye S, Li H, Hu K, Li L, Zhong J, Yan Q, et al. Radiosynthesis and Biological Evaluation of 18f-Labeled Bispecific Heterodimer Targeted Dual Gastrin-Releasing Peptide Receptor and Prostate-Specific Membrane Antigen for

Prostate Cancer Imaging. *Nucl Med Commun* (2022) 43(3):323–31. doi: 10.1097/mnm.0000000000001520
59. Wieser G, Popp I, Christian Rischke H, Drendel V, Grosu AL, Bartholomä M, et al. Diagnosis of Recurrent Prostate Cancer With Pet/Ct Imaging Using the Gastrin-Releasing Peptide Receptor Antagonist (68)Ga-Rm2: Preliminary Results in Patients With Negative or Inconclusive [(18)F] Fluoroethylcholine-Pet/Ct. *Eur J Nucl Med Mol Imaging* (2017) 44 (9):1463–72. doi: 10.1007/s00259-017-3702-8
60. Chen R, Wang Y, Shi Y, Zhu Y, Xu L, Huang G, et al. Diagnostic Value of (18)F-Fdg Pet/Ct in Patients With Biochemical Recurrent Prostate Cancer and Negative (68)Ga-Psma Pet/Ct. *Eur J Nucl Med Mol Imaging* (2021) 48 (9):2970–7. doi: 10.1007/s00259-021-05221-6
61. Eiber M, Maurer T, Souvatzoglou M, Beer AJ, Ruffani A, Haller B, et al. Evaluation of Hybrid (6)(8)Ga-Psma Ligand Pet/Ct in 248 Patients With Biochemical Recurrence After Radical Prostatectomy. *J Nucl Med* (2015) 56 (5):668–74. doi: 10.2967/jnumed.115.154153
62. Afshar-Oromieh A, Avtzi E, Giesel FL, Holland-Letz T, Linhart HG, Eder M, et al. The Diagnostic Value of Pet/Ct Imaging With the (68)Ga-Labelled Psma Ligand Hbed-Cc in the Diagnosis of Recurrent Prostate Cancer. *Eur J Nucl Med Mol Imaging* (2015) 42(2):197–209. doi: 10.1007/s00259-014-2949-6
63. Hofman MS, Hicks RJ, Maurer T, Eiber M. Prostate-Specific Membrane Antigen Pet: Clinical Utility in Prostate Cancer, Normal Patterns, Pearls, and Pitfalls. *Radiographics Rev Publ Radiol Soc North Am Inc* (2018) 38(1):200–17. doi: 10.1148/rg.2018170108
64. Verburg FA, Pfister D, Heidenreich A, Vogg A, Drude NI, Voo S, et al. Extent of Disease in Recurrent Prostate Cancer Determined by [(68)Ga] Psma-Hbed-Cc Pet/Ct in Relation to Psa Levels, Psa Doubling Time and Gleason Score. *Eur J Nucl Med Mol Imaging* (2016) 43(3):397–403. doi: 10.1007/s00259-015-3240-1
65. Ceci F, Uprimny C, Nilica B, Geraldo L, Kendler D, Kroiss A, et al. (68)Ga-Psma Pet/Ct for Restaging Recurrent Prostate Cancer: Which Factors Are Associated With Pet/Ct Detection Rate? *Eur J Nucl Med Mol Imaging* (2015) 42(8):1284–94. doi: 10.1007/s00259-015-3078-6
66. Ceci F, Castellucci P, Graziani T, Farolfi A, Fonti C, Lodi F, et al. (68)Ga-Psma-11 Pet/Ct in Recurrent Prostate Cancer: Efficacy in Different Clinical Stages of Psa Failure After Radical Therapy. *Eur J Nucl Med Mol Imaging* (2019) 46(1):31–9. doi: 10.1007/s00259-018-4189-7
67. Eissa A, Elsherbiny A, Coelho RF, Rassweiler J, Davis JW, Porpiglia F, et al. The Role of 68ga-Psma Pet/Ct Scan in Biochemical Recurrence After Primary Treatment for Prostate Cancer: A Systematic Review of the Literature. *Minerva Urol Nefrol J Urol Nephrol* (2018) 70(5):462–78. doi: 10.23736/s0393-2249.18.03081-3
68. Yilmaz U, Komek H, Can C, Altindag S. The Role of [(68)Ga]Psma I&T in Biochemical Recurrence After Radical Prostatectomy: Detection Rate and the Correlation Between the Level of Psa, Gleason Score, and the Suvmax. *Ann Nucl Med* (2019) 33(8):545–53. doi: 10.1007/s12149-019-01360-x
69. Aydin AM, Haberal B, Artykov M, Bilen CY, Yazici S. Clinicopathological Predictors of Positive (68)Ga-Psma-11 Pet/Ct in Psa-Only Recurrence of Localized Prostate Cancer Following Definitive Therapy. *Ann Nucl Med* (2019) 33(5):326–32. doi: 10.1007/s12149-019-01340-1
70. Leitsmann C, Thelen P, Schmid M, Meller J, Sahlmann CO, Meller B, et al. Enhancing Psma-Uptake With Androgen Deprivation Therapy - a New Way to Detect Prostate Cancer Metastases? *Int Braz J Urol* (2019) 45(3):459–67. doi: 10.1590/s1677-5538.Ibju.2018.0305
71. Hohberg M, Kobe C, Tager P, Hammes J, Schmidt M, Dietlein F, et al. Combined Early and Late [(68)Ga]Psma-Hbed-Cc Pet Scans Improve Lesion Detectability in Biochemical Recurrence of Prostate Cancer With Low Psa Levels. *Mol Imaging Biol :MIB* (2019) 21(3):558–66. doi: 10.1007/s11307-018-1263-2
72. Morawitz J, Kirchner J, Hertelendy J, Loberg C, Schimmöller L, Dabir M, et al. Is There a Diagnostic Benefit of Late-Phase Abdomino-Pelvic Pet/Ct After Urination as Part of Whole-Body (68) Ga-Psma-11 Pet/Ct for Restaging Patients With Biochemical Recurrence of Prostate Cancer After Radical Prostatectomy? *EJNMMI Res* (2022) 12(1):12. doi: 10.1186/s13550-022-00885-z
73. Uprimny C, Bayerschmidt S, Kroiss AS, Fritz J, Nilica B, Svirydenka H, et al. Early Injection of Furosemide Increases Detection Rate of Local Recurrence in Prostate Cancer Patients With Biochemical Recurrence Referred for (68) Ga-Psma-11 Pet/Ct. *J Nucl Med* (2021) 62(11):1550–7. doi: 10.2967/jnumed.120.261866
74. Cornford P, van den Bergh RCN, Briers E, Van den Broeck T, Cumberbatch MG, De Santis M, et al. Eau-Eanm-Estro-Esur-Siog Guidelines on Prostate Cancer. Part Ii-2020 Update: Treatment of Relapsing and Metastatic Prostate Cancer. *Eur Urol* (2021) 79(2):263–82. doi: 10.1016/j.eururo.2020.09.046
75. Wang Y, Chow DZ, Ebert E, Tajmir S, Scott JA, Palmer EL. Utility of (18)F-Fluciclovine Pet/Ct for Detecting Prostate Cancer Recurrence in Patients With Low (< 1 Ng/Ml) or Very Low (< 0.3 Ng/Ml) Prostate-Specific Antigen Levels. *AJR Am J Roentgenol* (2020) 215(4):997–1001. doi: 10.2214/ajr.19.22180
76. Giesel FL, Fiedler H, Stefanova M, Sterzing F, Rius M, Kopka K, et al. Psma Pet/Ct With Glu-Urea-Lys-(Ahx)-[(6)(8)Ga(Hbed-Cc)] Versus 3d Ct Volumetric Lymph Node Assessment in Recurrent Prostate Cancer. *Eur J Nucl Med Mol Imaging* (2015) 42(12):1794–800. doi: 10.1007/s00259-015-3106-6
77. Rauscher I, Maurer T, Beer AJ, Graner FP, Haller B, Weirich G, et al. Value of 68ga-Psma Hbed-Cc Pet for the Assessment of Lymph Node Metastases in Prostate Cancer Patients With Biochemical Recurrence: Comparison With Histopathology After Salvage Lymphadenectomy. *J Nucl Med* (2016) 57(11):1713–9. doi: 10.2967/jnumed.116.173492
78. Kroenke M, Schweiger L, Horn T, Haller B, Schwamborn K, Wurzer A, et al. Validation of (18)F-Rhpsma-7 and (18)F-Rhpsma-7.3 Pet Imaging Results With Histopathology From Salvage Surgery in Patients With Biochemical Recurrence of Prostate Cancer. *J Nucl Med* (2022). doi: 10.2967/jnumed.121.263707
79. Maurer T, Gschwend JE, Rauscher I, Souvatzoglou M, Haller B, Weirich G, et al. Diagnostic Efficacy of (68)Gallium-Psma Positron Emission Tomography Compared to Conventional Imaging for Lymph Node Staging of 130 Consecutive Patients With Intermediate to High Risk Prostate Cancer. *J Urol* (2016) 195(5):1436–43. doi: 10.1016/j.juro.2015.12.025
80. Maurer T, Eiber M, Schwaiger M, Gschwend JE. Current Use of Psma-Pet in Prostate Cancer Management. *Nat Rev Urol* (2016) 13(4):226–35. doi: 10.1038/nrurol.2016.26
81. Sprute K, Kramer V, Koerber SA, Meneses M, Fernandez R, Soza-Ried C, et al. Diagnostic Accuracy of (18)F-Psma-1007 Pet/Ct Imaging for Lymph Node Staging of Prostate Carcinoma in Primary and Biochemical Recurrence. *J Nucl Med* (2021) 62(2):208–13. doi: 10.2967/jnumed.120.246363
82. Mingels C, Bohn KP, Rominger A, Afshar-Oromieh A, Alberts I. Diagnostic Accuracy of [(18)F]Psma-1007 Pet/Ct in Biochemical Recurrence of Prostate Cancer. *Eur J Nucl Med Mol Imaging* (2022) 49:2436–44. doi: 10.1007/s00259-022-05693-0
83. Zhou J, Gou Z, Wu R, Yuan Y, Yu G, Zhao Y. Comparison of Psma-Pet/Ct, Choline-Pet/Ct, Naf-Pet/Ct, Mri, and Bone Scintigraphy in the Diagnosis of Bone Metastases in Patients With Prostate Cancer: A Systematic Review and Meta-Analysis. *Skeletal Radiol* (2019) 48(12):1915–24. doi: 10.1007/s00256-019-03230-z
84. Epstein JI, Egevad L, Amin MB, Delahunt B, Srigley JR, Humphrey PA. The 2014 International Society of Urological Pathology (Isup) Consensus Conference on Gleason Grading of Prostatic Carcinoma: Definition of Grading Patterns and Proposal for a New Grading System. *Am J Surg Pathol* (2016) 40(2):244–52. doi: 10.1097/pas.0000000000000530
85. Yakar D, Noordzij W, Kwee TC. Potential Causes of False-Negative Interpretations in 68ga-Psma Pet/Ct for the Detection of Local and Recurrent Prostate Cancer: An Underexposed Issue. *Clin Nucl Med* (2019) 45(1):e32-5. doi: 10.1097/rlu.0000000000002750
86. Prasad V, Steffen IG, Diederichs G, Makowski MR, Wust P, Brenner W. Biodistribution of [(68)Ga]Psma-Hbed-Cc in Patients With Prostate Cancer: Characterization of Uptake in Normal Organs and Tumour Lesions. *Mol Imaging Biol MIB* (2016) 18(3):428–36. doi: 10.1007/s11307-016-0945-x
87. Ristau BT, O'Keefe DS, Bacich DJ. The Prostate-Specific Membrane Antigen: Lessons and Current Clinical Implications From 20 Years of Research. *Urol Oncol* (2014) 32(3):272–9. doi: 10.1016/j.urolonc.2013.09.003
88. Perry E, Talwar A, Sharma S, O'Connor D, Wong LM, Taubman K, et al. Non-Prostate Cancer Tumours: Incidence on (18)F-Dcfpyl Psma Pet/Ct and

Uptake Characteristics in 1445 Patients. *Eur J Nucl Med Mol Imaging* (2022). doi: 10.1007/s00259-022-05721-z
89. Afshar-Oromieh A, Malcher A, Eder M, Eisenhut M, Linhart HG, Hadaschik BA, et al. Pet Imaging With a [68ga]Gallium-Labelled Psma Ligand for the Diagnosis of Prostate Cancer: Biodistribution in Humans and First Evaluation of Tumour Lesions. *Eur J Nucl Med Mol Imaging* (2013) 40 (4):486–95. doi: 10.1007/s00259-012-2298-2
90. Pfob CH, Ziegler S, Graner FP, Kohner M, Schachoff S, Blechert B, et al. Biodistribution and Radiation Dosimetry of (68)Ga-Psma Hbed Cc-a Psma Specific Probe for Pet Imaging of Prostate Cancer. *Eur J Nucl Med Mol Imaging* (2016) 43(11):1962–70. doi: 10.1007/s00259-016-3424-3
91. Afshar-Oromieh A, Hetzheim H, Kubler W, Kratochwil C, Giesel FL, Hope TA, et al. Radiation Dosimetry of (68)Ga-Psma-11 (Hbed-Cc) and Preliminary Evaluation of Optimal Imaging Timing. *Eur J Nucl Med Mol Imaging* (2016) 43(9):1611–20. doi: 10.1007/s00259-016-3419-0
92. Krohn T, Verburg FA, Pufe T, Neuhuber W, Vogg A, Heinzel A, et al. [(68) Ga]Psma-Hbed Uptake Mimicking Lymph Node Metastasis in Coeliac Ganglia: An Important Pitfall in Clinical Practice. *Eur J Nucl Med Mol Imaging* (2015) 42(2):210–4. doi: 10.1007/s00259-014-2915-3
93. Kinoshita Y, Kuratsukuri K, Landas S, Imaida K, Rovito PMJr., Wang CY, et al. Expression of Prostate-Specific Membrane Antigen in Normal and Malignant Human Tissues. *World J Surg* (2006) 30(4):628–36. doi: 10.1007/s00268-005-0544-5
94. Gordon IO, Tretiakova MS, Noffsinger AE, Hart J, Reuter VE, Al-Ahmadie HA. Prostate-Specific Membrane Antigen Expression in Regeneration and Repair. *Mod Pathol Off J United States Can Acad Pathol Inc* (2008) 21 (12):1421–7. doi: 10.1038/modpathol.2008.143
95. Ardies PJ, Gykiere P, Goethals L, De Mey J, De Geeter F, Everaert H. Psma Uptake in Mediastinal Sarcoidosis. *Clin Nucl Med* (2017) 42(4):303–5. doi: 10.1097/rlu.0000000000001543
96. Froehner M, Toma M, Zophel K, Novotny V, Laniado M, Wirth MP. Psma-Pet/Ct-Positive Paget Disease in a Patient With Newly Diagnosed Prostate Cancer: Imaging and Bone Biopsy Findings. *Case Rep Urol* (2017) 2017:1654231. doi: 10.1155/2017/1654231
97. Gykiere P, Goethals L, Everaert H. Healing Sacral Fracture Masquerading as Metastatic Bone Disease on a 68ga-Psma Pet/Ct. *Clin Nucl Med* (2016) 41 (7):e346–7. doi: 10.1097/rlu.0000000000001222
98. Vamadevan S, Le K, Bui C, Mansberg R. Incidental Psma Uptake in an Undisplaced Fracture of a Vertebral Body. *Clin Nucl Med* (2017) 42(6):465–6. doi: 10.1097/rlu.0000000000001599
99. Artigas C, Otte FX, Lemort M, van Velthoven R, Flamen P. Vertebral Hemangioma Mimicking Bone Metastasis in 68ga-Psma Ligand Pet/Ct. *Clin Nucl Med* (2017) 42(5):368–70. doi: 10.1097/rlu.0000000000001631
100. Kanthan GL, Izard MA, Emmett L, Hsiao E, Schembri GP. Schwannoma Showing Avid Uptake on 68ga-Psma-Hbed-Cc Pet/Ct. *Clin Nucl Med* (2016) 41(9):703–4. doi: 10.1097/rlu.0000000000001281
101. Derlin T, Kreipe HH, Schumacher U, Soudah B. Psma Expression in Tumor Neovasculature Endothelial Cells of Follicular Thyroid Adenoma as Identified by Molecular Imaging Using 68ga-Psma Ligand Pet/Ct. *Clin Nucl Med* (2017) 42(3):e173–e4. doi: 10.1097/rlu.0000000000001487
102. Rowe SP, Gorin MA, Hammers HJ, Som Javadi M, Hawasli H, Szabo Z, et al. Imaging of Metastatic Clear Cell Renal Cell Carcinoma With Psma-Targeted (1)(8)F-Dcfpyl Pet/Ct. *Ann Nucl Med* (2015) 29(10):877–82. doi: 10.1007/s12149-015-1017-z
103. Rhee H, Blazak J, Tham CM, Ng KL, Shepherd B, Lawson M, et al. Pilot Study: Use of Gallium-68 Psma Pet for Detection of Metastatic Lesions in Patients With Renal Tumour. *EJNMMI Res* (2016) 6(1):76. doi: 10.1186/s13550-016-0231-6
104. Perez PM, Flavell RR, Kelley RK, Umetsu S, Behr SC. Heterogeneous Uptake of 18f-Fdg and 68ga-Psma-11 in Hepatocellular Carcinoma. *Clin Nucl Med* (2019) 44(3):e133–e5. doi: 10.1097/rlu.0000000000002452
105. Roland A, Drouet C, Boulahdour H, Cochet A, De Bari B. Unusual Uptakes on (18)F-Fluorocholine Positron Emission Tomography/Computed Tomography (Pet/Ct): A Retrospective Study of 368 Prostate Cancer Patients Referred for a Biochemical Recurrence or an Initial Staging. *Quant Imaging Med Surg* (2021) 11(1):172–82. doi: 10.21037/qims-19-981

Conflict of Interest: The authors declare that the research was conducted in the absence of any commercial or financial relationships that could be construed as a potential conflict of interest.

Publisher's Note: All claims expressed in this article are solely those of the authors and do not necessarily represent those of their affiliated organizations, or those of the publisher, the editors and the reviewers. Any product that may be evaluated in this article, or claim that may be made by its manufacturer, is not guaranteed or endorsed by the publisher.

frontiers | Frontiers in Endocrinology

ORIGINAL RESEARCH
published: 06 June 2022
doi: 10.3389/fendo.2022.884777

Prognostic Value of Cancer-Associated Fibroblast-Related Gene Signatures in Hepatocellular Carcinoma

*Wenge Dong, Yangyang Xie and Hai Huang**

Department of General Surgery, Hangzhou Traditional Chinese Medicine (TCM) Hospital Affiliated to Zhejiang Chinese Medical University, Hangzhou, China

OPEN ACCESS

Edited by:
Ihtisham Bukhari,
Fifth Affiliated Hospital of Zhengzhou University, China

Reviewed by:
Xin Chen,
Second Hospital of Hebei Medical University, China
Guohong Gao,
Affiliated Hospital of Weifang Medical University, China

***Correspondence:**
Hai Huang
szyyhuanghai@163.com

Specialty section:
This article was submitted to Cancer Endocrinology, a section of the journal Frontiers in Endocrinology

Received: *27 February 2022*
Accepted: *11 April 2022*
Published: *06 June 2022*

Citation:
Dong W, Xie Y and Huang H (2022) Prognostic Value of Cancer-Associated Fibroblast-Related Gene Signatures in Hepatocellular Carcinoma. Front. Endocrinol. 13:884777. doi: 10.3389/fendo.2022.884777

Hepatocellular carcinoma (HCC) is a global health challenge with an increasing incidence worldwide. Cancer-associated fibroblasts (CAFs) function critically in HCC initiation and development. However, the prognostic significance of CAF-related gene signatures in HCC remains unknown. Therefore, the specific functions of CAF-related genes in HCC were investigated to help develop potential therapeutic strategies. In this study, CAF-related genes were screened from three CAF-related gene sets. HCC data from the Gene Expression Omnibus (GEO) database was applied to verify the screened CAF-related genes. Cluster analysis was used to identify clusters based on the expression pattern of CAF-related genes and two identified clusters were found to have a significant difference in overall survival (OS) and progression free intervals (PFI). The prognosis of HCC patients was predicted using the prognostic risk score model developed based on HCC data from The Cancer Genome Atlas (TCGA) databases. High-risk group patients had a worse OS than those in low-risk group in TCGA. These results were validated in International Cancer Genome Consortium (ICGC) database. Moreover, combining the clinicopathological characteristics related to prognosis with the model, a nomogram was built for a more accurate prediction of OS of HCC patients. In addition, analyses of immune infiltration characteristics of tumor microenvironment (TME), chemosensitivity, and immunotherapy response were conducted to further evaluate the prognostic value of CAF-related genes. Patients with low-risk scores were found to have higher chemosensitivity to cisplatin, doxorubicin, and sorafenib. Individuals with high-risk scores were found with a higher expression of most immune checkpoints which indicated patients with high-risk scores may benefit more from treatment with immune checkpoint inhibitors. Furthermore, a correlation between immune infiltration characteristics of TME and patients with different risk levels was found. These findings provide a possibility for the further development of personalized treatments in HCC.

Keywords: cancer-associated fibroblasts (CAFs), hepatocellular carcinoma (HCC), chemosensitivity, immunotherapy response, tumor microenvironment

INTRODUCTION

Liver cancer has experienced an increasing incidence worldwide in recent decades (1, 2). By 2030, more than 1 million people will die from liver cancer according to World Health Organization estimate (3). As the most prevalent type of liver cancer, hepatocellular carcinoma (HCC) accounts for about 90% of all liver cancer cases. Despite new treatment methods for HCC, the cancer prognosis remains poor (4). Therefore, there is an urgent need to develop a new promising target for therapies and an effective prognostic model for patients suffering from HCC.

The malignant nature of cancer growth is controlled by paracrine communication between the tumor and surrounding stroma (5). Fibroblasts, the primary cell type inside the stroma, are known as cancer-associated fibroblasts (CAFs) and orchestrate interaction with cancer cells (6, 7) as well as exhibit various prognostic markers (8). Increasing research suggests that CAFs are essential to HCC development (9–12). Furthermore, CAFs are closely related to the tumor microenvironment (TME) of HCC and have been proven to influence HCC progression (13). Moreover, CAFs are now thought to be the primary driver of tumor growth due to complicated interactions with other cell types in the tumor microenvironment (14). Previous studies found CAFs undergo epigenetic modifications to create secreted factors, exosomes, and metabolites that regulate tumor angiogenesis, immunology, and metabolism in addition to producing extracellular matrix components that facilitate the function and formation of stroma tumor (15, 16). HCC-derived CAFs not only promote tumor cell malignancy (17–19) but also attract immune cells to allow the development of immunosuppressive phenotypes for immune escape (20, 21). Because of their putative prooncogenic functions, research on CAFs as a therapeutic target is very popular in recent years (14). However, the deeper prognostic value of CAF-related gene signatures in HCC is unknown.

This study analyzed the HCC data from TCGA database to investigate the role of CAF-related genes in HCC. Cluster analysis was used to identify clusters based on the expression pattern of CAF-related genes. Based on independent prognostic CAF-related genes, a CAF-related prognostic model was built for the prognostic prediction of HCC. To further assess the model prediction potential, the HCC data from ICGC database was utilized to verify the model. Next, risk score was combined with clinicopathological characteristics associated with prognosis to build a clinical risk model for prognostic prediction. Furthermore, for further evaluating the prognostic significance of CAF-related genes, the relationship between HCC patients with different risk scores and immune infiltration characteristics of TME, chemosensitivity, immunotherapy response, or difference in functional enrichment was investigated. To summarize, these findings suggest that CAF-related gene signatures may be exploited as possible prognostic markers in the search for novel treatments for patients suffering from HCC.

MATERIALS AND METHODS

Data Collection

From TCGA database (https://portal.gdc.cancer.gov/), the RNA sequencing data including 50 normal liver samples and 374 HCC samples were acquired. The microarray data profiles of GSE25097, including 268 HCC samples and 243 adjacent non-tumor samples, were downloaded from the GEO database (https://www.ncbi.nlm.nih.gov/geo/). Another set of RNA sequencing data, including 232 HCC samples, was acquired from ICGC database (https://icgc.org/). Besides, from the TCGA and ICGC databases, the clinical information corresponding to HCC samples (374 HCC samples from TCGA and 232 HCC samples from ICGC) was downloaded. Duplicate samples and samples with missing follow-up information were not included in this study.

Acquisition of CAF-Related Genes

From the Molecular Signature Database v7.5.1 (MSigDB), two gene sets related to CAF (MISHRA CARCINOMA ASSOCIATED FIBROBLAST UP and MISHRA CARCINOMA ASSOCIATED FIBROBLAST DN) were obtained. Another CAF gene set including 596 genes was acquired from a previous study (22). Then CAF-related genes were obtained after overlapping genes were filtered. GEO2R was utilized to screen DEGs (|log2(fold change)| >1, adjusted p-value <0.05) in GSE25097 (23). The "DESeq2" R package was utilized to screen DEGs (|log2(fold change)| >1 & adjusted p value <0.05) in TCGA (24).

Cluster Analysis

The cluster analysis was conducted using the "ComplexHeatmap" R package (25). The cluster method was Euclidean and both rows and columns were clustered. Besides, the gene expression data is standardized by row-based Z-score. The K-M curve was utilized to observe the survival difference between the two clusters. The principal component analysis (PCA) was used to verify the accuracy of cluster analysis results.

Establishment and Validation of the Prognostic Risk Score Model

First, the expression data of CAF-related genes were retrieved from the sequencing data of HCC samples in the TCGA. The clinical HCC information was then combined with those of CAF-related genes. In the next step, the DEGs in TCGA were intersected with the integrated CAF-related gene set to get CAF-related genes in TCGA, then the CAF-related genes in TCGA were verified with the DEGs in GSE25097, and finally, the verified CAF-related genes in TCGA were screened out. CAF-related genes in TCGA related to OS of HCC patients were mined by univariate Cox regression analysis ($P < 0.05$). To minimize overfitting, Least absolute shrinkage and selection operator (LASSO) logistic regression analysis (ten-fold cross-validation) was utilized to further screen key CAF-related prognostic genes. cBioPortal, a TCGA computational tool, was used to analyze the mutations and putative copy-number alterations as well as the correlation of genes in HCC samples in TCGA. Furthermore, multivariable Cox regression analyses identified

genes showing independent prognostic relevance and developed a risk score model for predicting the prognosis of TCGA patients with HCC. Each sample's risk score was computed according to risk score = Intercept (-0.38655353) + (-0.690788635)×ARHGAP11A + (0.681687351) × DLGAP5 + (0.131165649) × RFPL4B + (-0.241494247)×TOP2A + (0.626517272) × TTK.

The model was evaluated on the ICGC database to ensure its practicality. Furthermore, several test methodologies were used. Median risk scores were used as the basis for patient grouping. The K-M curve was utilized to assess survival differences. Moreover, the prognostic model's practicality was validated using receiver operating characteristic (ROC), PCA, and a heat map of survival status combined with expression difference and risk score distribution in the independent prognostic genes.

The Correlation of Risk Score With Clinicopathological Characteristics

First, according to the sample ID, corresponding clinicopathological characteristics were merged with each patients' risk score. Shapiro-Wilk was used to test for normality. Comparisons of the distributions between two groups were performed using a Wilcoxon signed-rank test. To screen clinicopathological characteristics associated with prognosis, Univariate, and multivariate COX analyses were used. Differences were considered statistically significant when they showed P value < 0.05.

Prognostic Nomogram Development

The "rms" and "survival" R packages were used to construct a prognostic nomogram. Moreover, calibration plot, DCA, and ROC curve were applied in assessing prediction capabilities of the nomogram.

Estimation of Chemotherapeutic Drug Sensitivity

To calculate IC50 of chemotherapeutic drugs for each sample, the "pRRophetic" R package was used (26). Shapiro-Wilk was used to test for normality. Spearman's rank correlation coefficient was here to evaluate the association between the two groups (risk score and IC50). Differences were considered statistically significant when they showed P-value < 0.05.

Estimation of Immunotherapy Response

The 43 immune checkpoints were acquired from previous studies (27). Comparisons of the distributions between two groups were made by Wilcoxon signed-rank test. Correlation analysis was conducted by Pearson method. Differences were considered statistically significant when they showed P-value < 0.05.

Immune Infiltration Analysis

To evaluate the relative abundance of immune cell types between high-risk and low-risk groups, CIBERSORT (28), TIMER (29), quanTIseq (30), and MCP-counter (31) was performed. Comparisons of the distributions between two groups were made by Wilcoxon signed-rank test. Correlation analysis was conducted by Pearson method. Differences were considered statistically significant when they showed P-value < 0.05.

Functional Enrichment Analysis

The enrichment score of samples from low- and high-risk score groups was calculated by Gene Set Variation Analysis (GSVA) in the "GSVA" R package (32). The minimum and maximum gene sets are set to 5 and 5,000, respectively. The gene expression profile of the two risk samples was used to evaluate the related pathways and molecular mechanisms, and the reference gene sets"c2.cp.kegg.v7.4.symbols" were downloaded from the molecular signatures database (https://www.gsea-msigdb.org/gsea/msigdb). In the low-risk and high-risk groups, differentially enriching pathways (fold change>1.5 & p value <0.05) were screened using rank sum test. Besides, to perform the GO and KEGG enrichment analysis, the "clusterProfiler" R package was employed (33).

Protein-Protein Interaction Network

In the low-risk and high-risk groups, DEGs (|log2(fold change)| >1 and adjusted p value <0.05) were screened using the "limma" R package (34). Through the STRING (https://string-db.org; version: 11.5), we obtained PPI network data (interaction score >0.9). Cytoscape (v 3.8.2) was utilized to build PPI network view and to screen out hub genes in the DEGs by degree method. To compare the distributions of the two groups, Wilcoxon signed-rank test was used. HCC patients in the TCGA were grouped into two expression groups (low and high), according to the median of hub genes' expression value. Survival differences of the two groups were shown by K-M curves. Furthermore, independent hub genes showing prognosis relevance were screened by univariate and multivariate COX regression. To investigate the association of the expressions of independent prognostic hub genes with immune infiltration fraction levels, the immune infiltration score was calculated using ssGSEA algorithm in the "GSVA"R package (32, 35).

RESULTS

Identification of CAF-Related Genes in HCC

First, 642 CAF-related genes were obtained by eliminating overlapping genes from the intersection of the three CAF-related gene sets (**Figure 1A**). From TCGA and GSE25097, 8,821 and 1,872 differentially expressed genes (DEGs) were mined by the "DESeq2" R packages and "GEO2R", respectively. In the next step, 8,821 DEGs in TCGA and 642 CAF-related genes were intersected and 127 differentially expressed CAF-related genes were identified (**Figure 1B**). Finally, 127 CAF-related genes were verified by intersecting 1,872 DEGs in GSE25097 and 55 genes were filtered (**Figure 1C**). As depicted in **Supplementary Figure 1**, the expression of the 55 genes clearly differed between normal and tumor samples. **Figure 2** illustrates the flow of this study.

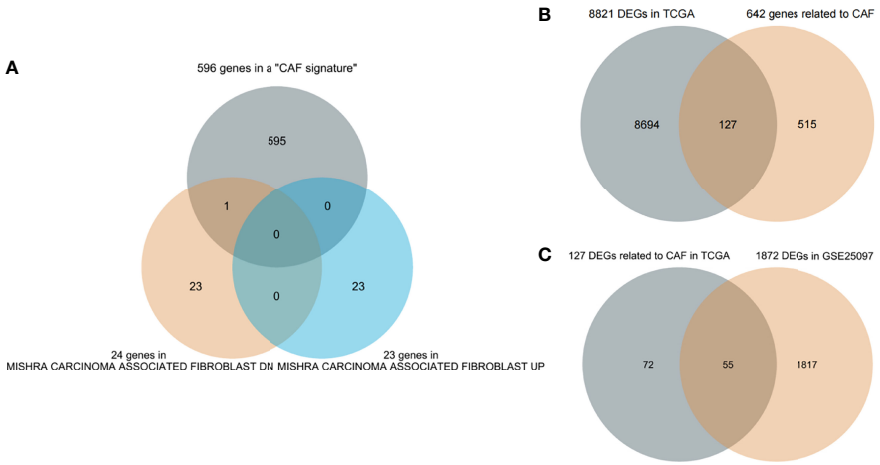

FIGURE 1 | Screening genes **(A)** Three cancer-associated fibroblast (CAF)-related gene sets intersect to filter overlapping genes. **(B)** CAF-related DEGs in The Cancer Genome Atlas (TCGA). **(C)** Further validation in GSE25097.

Cluster Analysis of CAF-Related Genes in HCC

In order to investigate the overall effect of the 55 CAF-related genes in HCC, cluster analysis was utilized to identify different clusters. As shown in the **Figure 3A**, it could be clearly observed that 369 samples were divided into two clusters (cluster 1 (n=262) and cluster 2 (n=107)) after the removal of one outlier sample. Subsequently, survival analysis was made to explore the survival difference between the two clusters. It was found that cluster 1 had a better OS and PFI than cluster 2, which was demonstrated in **Figures 3B, C**. Furthermore, PCA plot showed that the two clusters have a good resolution (**Figure 3D**), suggesting that this cluster pattern is feasible.

Development of a Prognostic Model Based On Risk Score of HCC Patients

Prognostic genes were filtered from 55 differentially expressed CAF-related genes by Univariate Cox regression analysis and 22 genes were overall survival (OS)-related (P<0.05; **Supplementary Figure 2**). According to the 22 genes, the mutation and putative

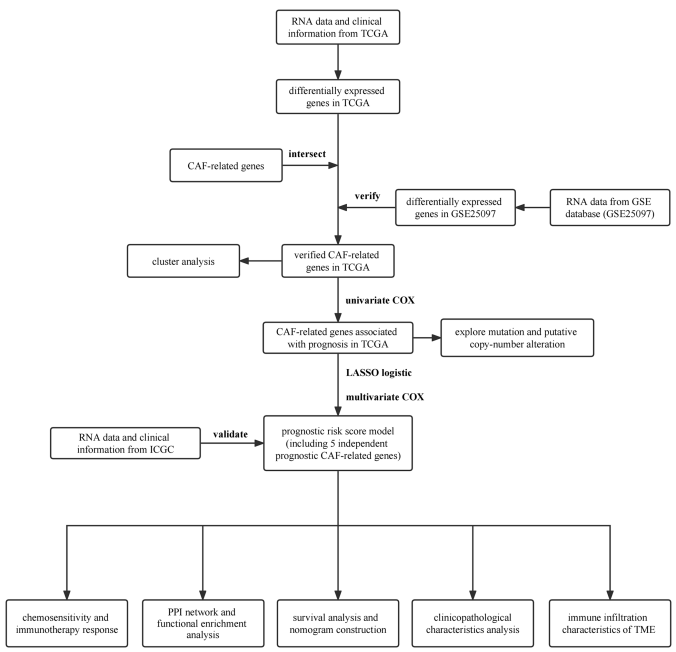

FIGURE 2 | Flow chart.

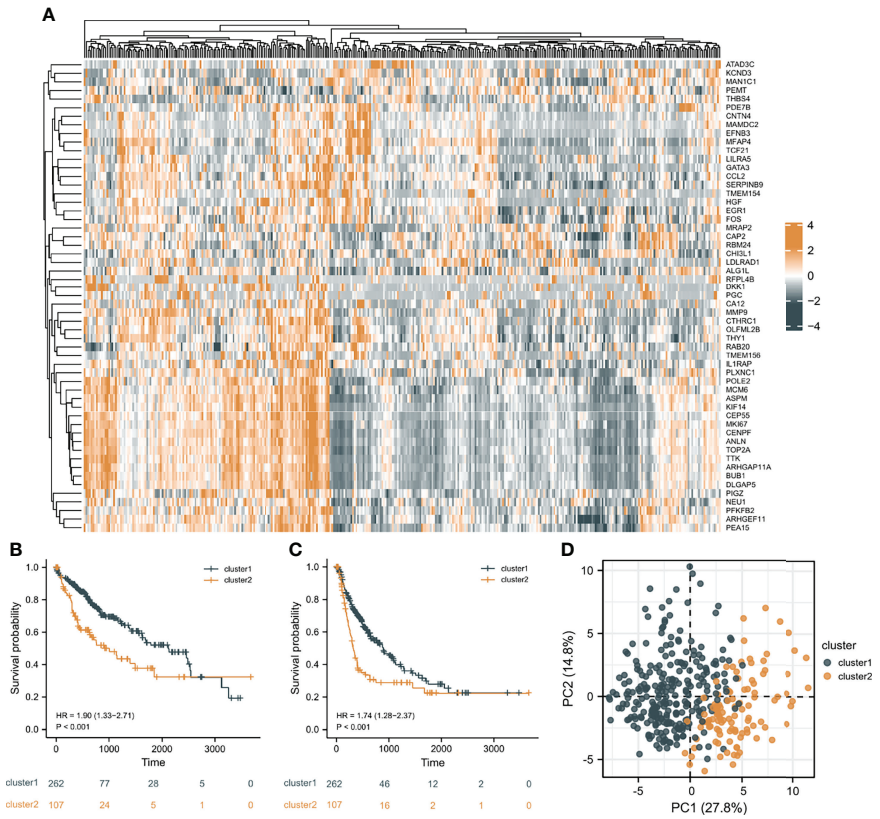

FIGURE 3 | Cluster analysis results. **(A)** The heat map of the expression differences of 55 CAF-related DEGs in the two clusters. **(B)** The overall survival (OS) difference of the two clusters. **(C)** The progression free interval (PFI) difference of the two clusters. **(D)** Principal component analysis (PCA) plot.

copy-number alterations profile of the CAF-related genes with prognostic relevance in HCC was described. Mutations and presumed copy-number changes of CAF-related genes were found in 175 of 366 HCC cases, with a frequency of 48% (**Supplementary Figure 3**). CTHRC1 had the highest mutation and putative copy-number alteration frequency than ARHGEF11. However, CEP55 exhibited few mutations and putative copy-number alterations in HCC samples. Besides, further analysis was performed to explore mutation mutual exclusivity and co-occurrence relationship. **Supplementary Figure 3** presents genes pairs with q-value <0.05 (derived from Benjamini-Hochberg FDR correction procedure) in the analysis results, which suggested that 19 pairs of genes with significant correlation only have a co-occurrence relationship, and ARHGEF11 was significantly positively correlated with most genes, including PEA15, OLFML2B, ASPM, KIF14, CENPF, and RAB20. Then, using LASSO Cox regression, 14 prognostic gene signatures were identified from the 22 CAF-related genes (**Supplementary Figure 4A, B**). **Supplementary Figure 4C** depicts the 14-gene correlation network. Finally, five genes (ARHGAP11A, DLGAP5, RFPL4B, TOP2A, TTK) with independent prognostic relevance were identified by multivariate Cox regression and were utilized to build a prognostic risk score model (**Supplementary Figure 4D**).

According to the median risk score as the cutoff value, the patients were sorted and grouped into two groups: high-risk (n = 185) and low-risk (n = 185). In TCGA, compared with the low-risk score group, the high-risk score group showed a shorter OS (P<0.001; **Figure 4A**). To the reliability of the risk score and the model, we plotted a time-dependent ROC curve, see **Figure 4B** for the areas under the curve (AUCs). Furthermore, the heat map of survival status combined with expression difference and risk score distribution in the 5 independent prognostic genes, and PCA, were utilized to differentiate individuals with distinct risk levels. As shown in **Figures 5A, B**, there is a high degree of discrimination between the high-risk and low-risk scores groups.

Verifying the Prediction Capability of the Prognostic Model

HCC samples from ICGC were categorized into low-risk and high-risk score groups to verify the prognostic risk score model, according to the median risk score. As the same results in TCGA, a shorter OS was observed in the high-risk score group (P<0.001) than in the low-risk score group in ICGC (**Figure 4C**), demonstrating that the predicting model built on risk score in TCGA had a good ability to predict OS. The AUCs were presented in **Figure 4D**. The risk model constructed based on the ICGC database was further tested using a heat map of

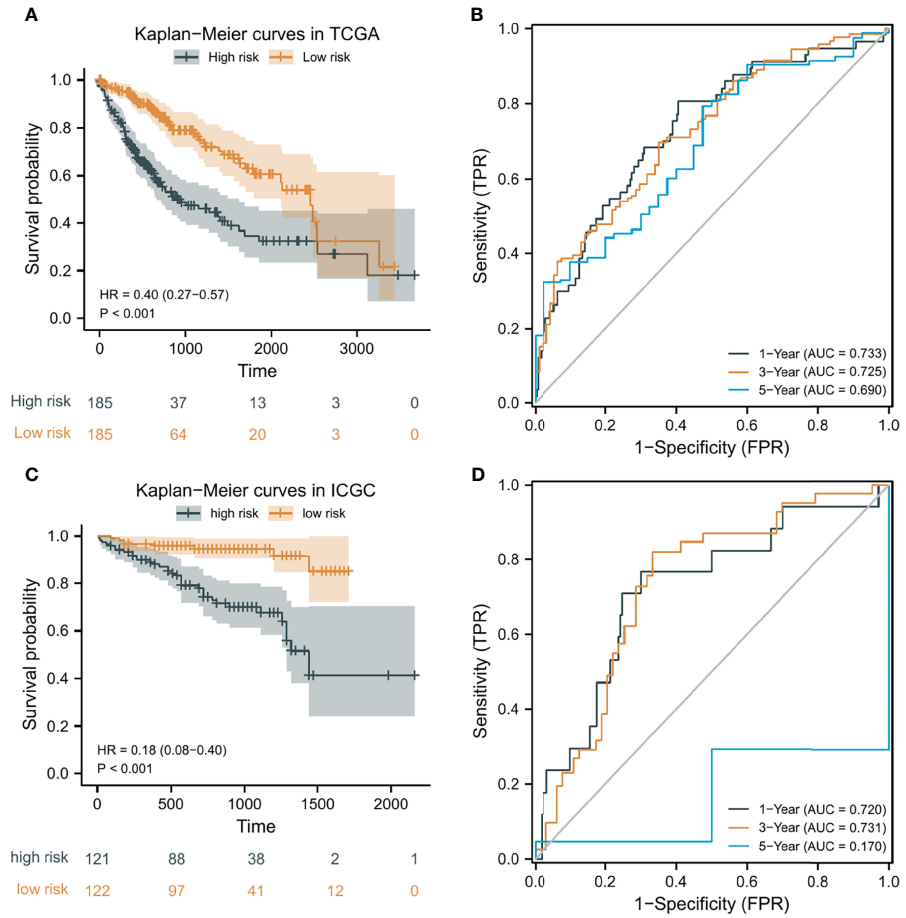

FIGURE 4 | Kaplan-Meier (K-M) curves and time-dependent receiver operating characteristic (ROC) curves of the prognostic model of HCC patients. **(A, C)** K-M curves of the prognostic model in TCGA and ICGC, respectively. **(B, D)** 1-year, 3-year, and 5-year ROC curves of the prognostic model in TCGA and ICGC, respectively.

survival status along with risk score distribution and expression difference in the 5 independent prognostic genes and PCA. As shown in **Figures 5C, D**, the prognostic model in ICGC had a strong capacity for predicting prognosis.

The Correlation of Clinicopathological Characteristics With Risk Score

The distribution of risk scores in corresponding samples was investigated in terms of age, gender, clinical stage, histological grade, and AFP level. Higher risk scores were associated with a higher pathologic stage ($P = 0.003$), histological grade ($P < 0.001$), and AFP level ($P < 0.001$) (**Supplementary Figures 5C–E**), but not with age or gender ($P > 0.05$; **Supplementary Figures 5A, B**). Univariate and multivariate Cox analysis included the following factors: age, gender, pathological stage, histological grade, AFP level, and prognostic risk score. The findings suggested that pathologic stage, gender, prognostic risk score, and age were factors related to prognosis ($P < 0.05$), and that only prognostic risk score, pathologic stage, and age were factors with independent prognosis relevance ($P < 0.05$; **Supplementary Figures 6A, B**).

Establishment of Prognostic Nomogram

The prognostic risk score was combined with age, gender, and pathologic stage to build a nomogram for OS prediction (**Figure 6A**). **Figures 6B–D** depicted the ROC curves of multiple indicators and demonstrated that the nomogram had a stronger predictive capacity than any other indicator. As illustrated in **Figures 6E–G**, the nomogram was predictive of the OS for HCC patients and demonstrated comparatively high accuracy, as shown by the calibration curves. Furthermore, decision curve analysis (DCA) revealed that the nomogram outperformed a single independent predictive parameter (**Figures 6H–J**). To summarize, the predictive potential of the prognostic nomogram was validated from several angles.

Prediction of Chemotherapeutic Drug Sensitivity

To explore potential novel therapies for HCC, the correlation between risk score and chemosensitivity was analyzed. ESMO Clinical Practice Guidelines for HCC (36) was used as a reference to get common chemotherapeutic drugs. The "pRRophetic" R package calculated half-maximal inhibitory concentration (IC50)

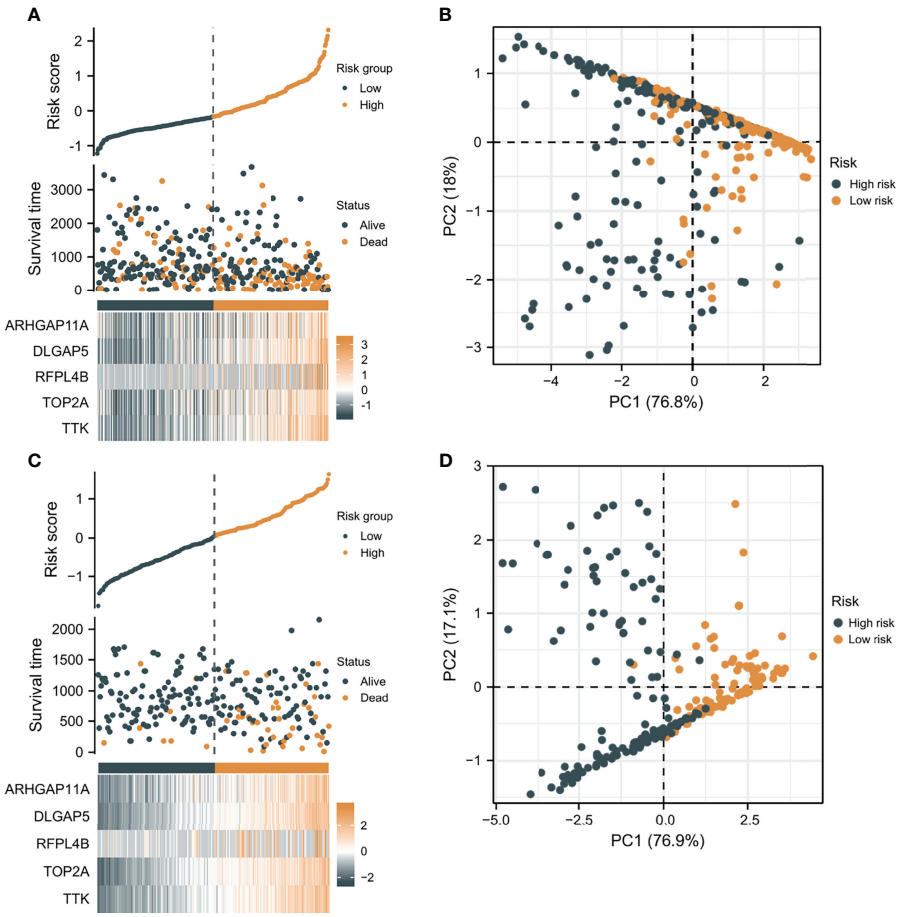

FIGURE 5 | The verification of the prognostic model's predicting power. **(A)** The heat map combined with survival status, risk score distribution, and expression difference in the 5 independent prognostic genes in TCGA. **(B)** PCA based on the 5 independent prognostic genes in TCGA. **(C)** The heat map combined with survival status, risk score distribution, and expression difference in the 5 independent prognostic genes in ICGC. **(D)** PCA of the 5 independent prognostic genes in ICGC.

for predicting the correlation of chemosensitivity between different risk score samples in TCGA. The correlation between the sensitivity to six predicable chemotherapeutic drugs and different risk scores was presented in **Figure 7**. Low-risk score samples showed higher sensitivity to cisplatin, doxorubicin, sunitinib, and sorafenib (**Figures 7B, C, E, F**); P<0.001), while high-risk score samples showed higher sensitivity to 5-Fluorouracil and Erlotinib (**Figures 7A, D**); P<0.001).

Immune Infiltration Characteristics of TME Between Low-Risk and High-Risk Groups

Since CAFs are closely associated with TME (13), an investigation was made to explore the difference in immune infiltration characteristics of TME between the two risk groups. As shown in **Figures 8A, B**, 11 of the 22 immune cells and 5 of the 13 immune-related pathways were found with a significant difference in infiltrating fraction between distinct risk levels group. Furthermore, to explore the correlation between risk score and immune infiltration score, immune analysis based on various algorithms (CIBERSORT, TIMER, quanTIseq, and MCP-counter) were performed. As shown in **Figures 8C, D**, 20 microenvironment components were positively correlated with risk scores, while 7 microenvironment components were negatively related to risk scores. B cells, CD8 T cells, and Tregs were found with a significantly positive correlation with risk scores, which were confirmed by more than one immune analysis algorithm (**Figures 8C, D**). To further explore the correlation between immune infiltration characteristics and various risk score groups, ESTIMATE was used to calculate TME scores and tumor purity. The results showed that the stromal score was found to have a significantly higher level in the low-risk group (**Supplementary Figure 7**). These findings suggested risk score based on CAFs correlated with tumor immune microenvironment.

Prediction of Immunotherapy Response

Recently, immunotherapy for hepatocellular carcinoma has been a new hot research topic, and immune checkpoint inhibitors (ICIs) are at the forefront of this revolution (37). To explore the correlation of CAF-related signatures with immunotherapy

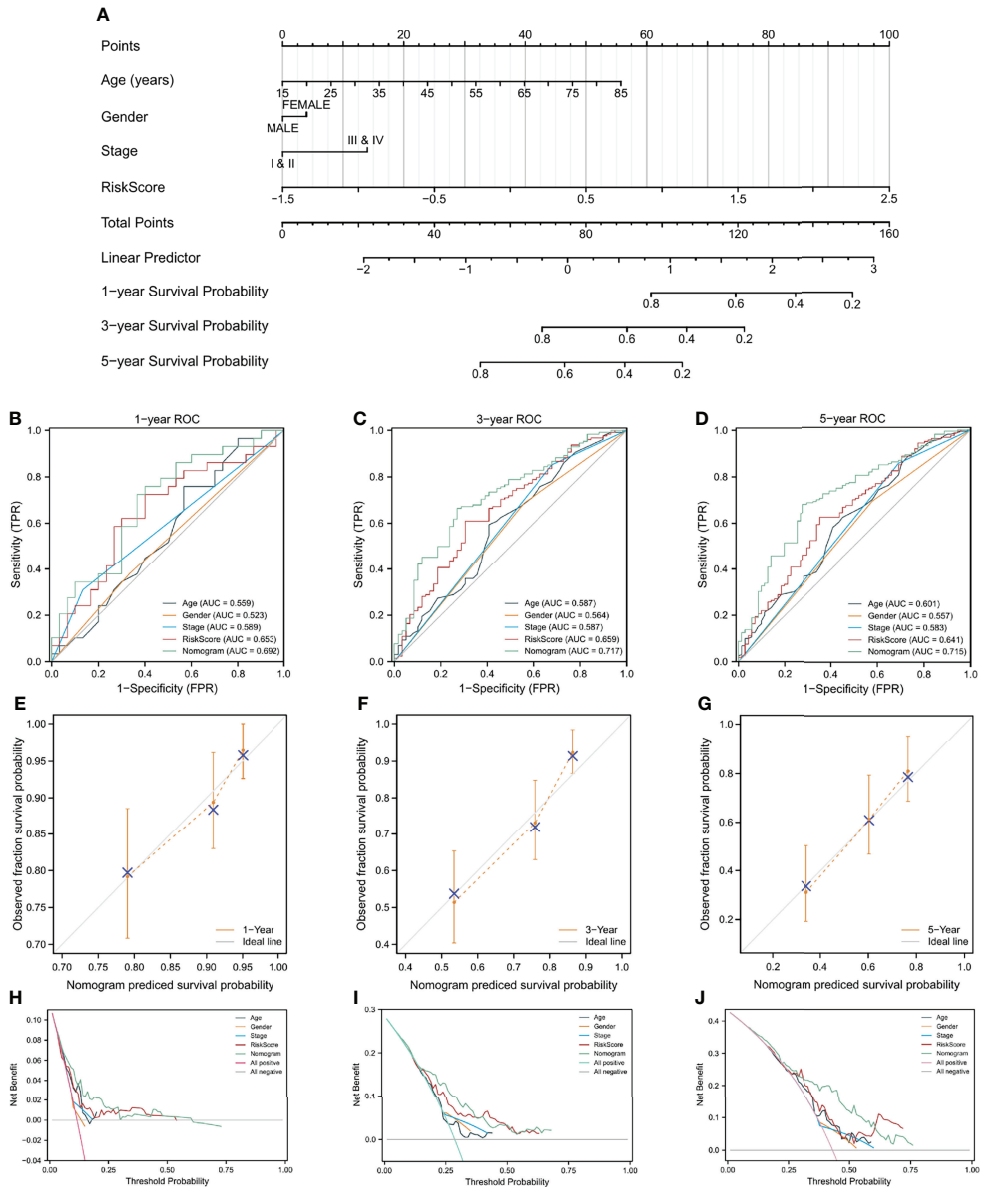

FIGURE 6 | A nomogram build on CAF-related risk score and clinicopathological characteristics related to prognosis to predict OS of HCC patients from TCGA and the verification of its accuracy. **(A)** The nomogram for predicting 1-year, 3-year, and 5-year OS of HCC patients. **(B–D)** ROC curves of the nomogram and other indicators including age, gender, stage, and risk score. **(E–G)** The calibration plots of the nomogram. **(H–J)** Decision curve analysis for evaluating the accuracy of the nomogram to predict 1-year, 3-year and 5 year OS of individuals with HCC.

response, the expression of immune checkpoints between different risk score groups was compared. As **Supplementary Figure 8A** showed, the expression of 32 of 43 immune checkpoints was found with a significant difference between low- and high-risk groups, and interestingly, all the 32 immune checkpoints were highly expressed in the high-risk group. In addition, as classical representatives of immune checkpoints, the expression of PD-1 and CTLA-4 were found to have a significantly positive correlation with risk scores (**Supplementary Figures 8B, C**). In short, these results indicated that patients with high-risk scores are more likely to benefit from treatment with ICIs.

Functional Enrichment Analysis

To investigate pathways and molecular processes between the two risk groups, gene set variation analysis (GSVA) enrichment was utilized. As demonstrated in **Supplementary Figure 9**, a wide range of molecular biological processes showed enrichment in the high-risk group, whereas the majority of metabolic pathways were enriched in the low-risk group.

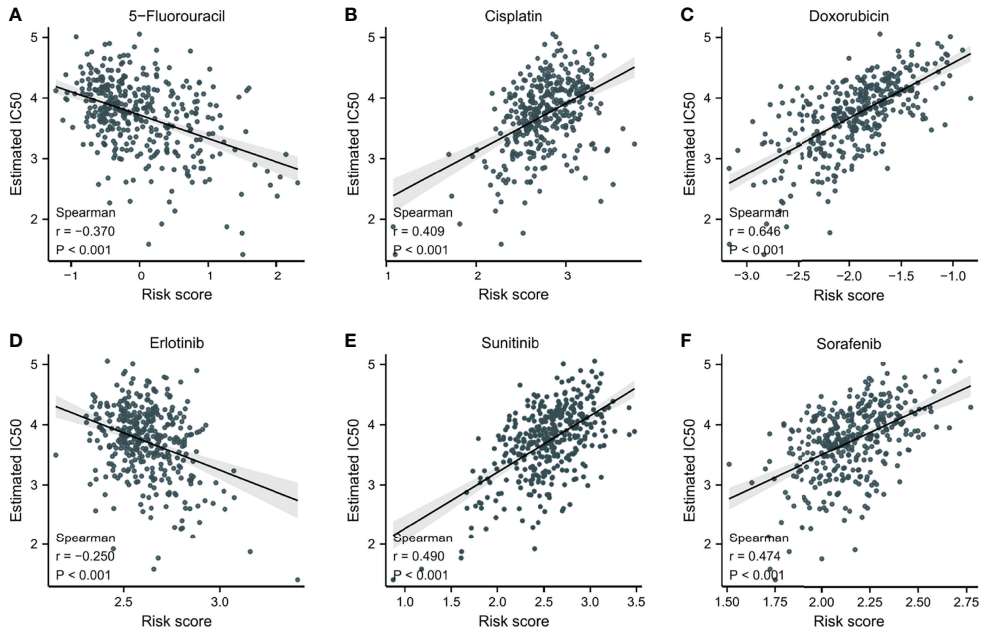

FIGURE 7 | The correlation between IC50 of different drugs and risk score in HCC patients. **(A)** 5-Fluorouracil. **(B)** Cisplatin. **(C)** Doxorubicin. **(D)** Erlotinib. **(E)** Sunitinib. **(F)** Sorafenib.

Moreover, the 5 independent prognostic genes were subjected to Gene Ontology (GO) and Kyoto Encyclopedia of Genes and Genomes (KEGG) enrichment analysis to explore possible pathways and molecular functions. **Figure 9** shows that the most highly enriched biological processes were meiotic chromosome separation, chromosome separation, sister chromatid segregation, and nuclear chromosome segregation. Additionally, KEGG enrichment analysis indicates that the 5

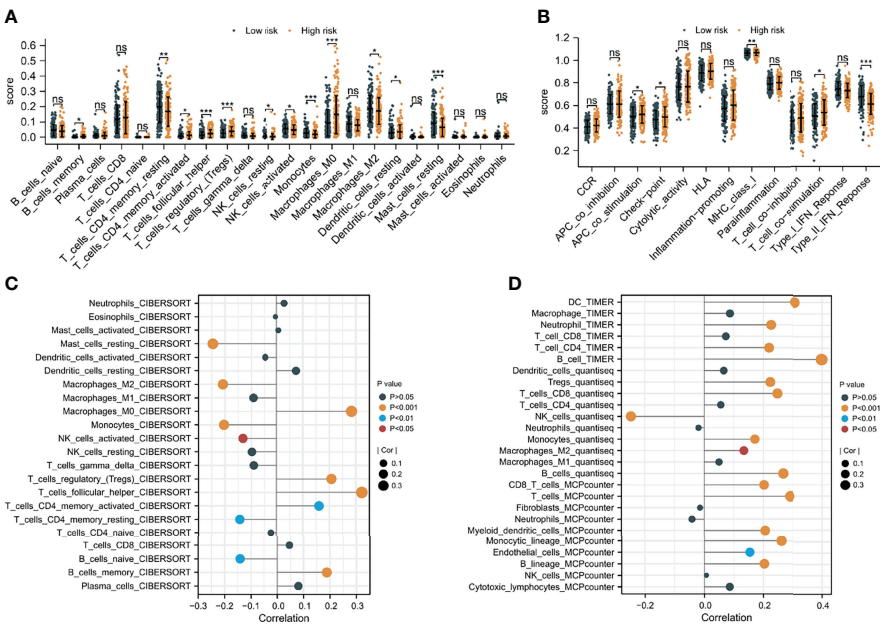

FIGURE 8 | The difference in immune infiltration characteristics of tumor microenvironment between low and high risk groups. **(A)** Immune cell infiltration analysis **(B)** immune-related pathways infiltration analysis **(C, D)** the correlation analysis of immune cells by various algorithms statistical significance is indicated by the following symbols: ns, $p \geq 0.05$; *, $p < 0.05$; **, $p < 0.01$; ***, $p < 0.001$.

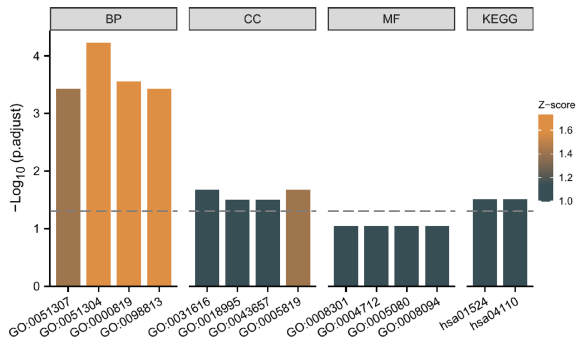

Ontology	ID	Description
BP	GO:0051307	meiotic chromosome separation
BP	GO:0051304	chromosome separation
BP	GO:0000819	sister chromatid segregation
BP	GO:0098813	nuclear chromosome segregation
CC	GO:0031616	spindle pole centrosome
CC	GO:0018995	host
CC	GO:0043657	host cell
CC	GO:0005819	spindle
MF	GO:0008301	DNA binding, bending
MF	GO:0004712	protein serine/threonine/tyrosine kinase activity
MF	GO:0005080	protein kinase C binding
MF	GO:0008094	DNA-dependent ATPase activity
KEGG	hsa01524	Platinum drug resistance
KEGG	hsa04110	Cell cycle

FIGURE 9 | Top ten representative pathways related to the 5 independent prognostic genes in GO and KEGG enrichment results.

genes might participate in pathways including platinum drug resistance and cell cycle (**Figure 9**).

Construction of PPI Network Based on DEGs Between the Low-Risk and High-Risk Groups

First, the "limma" R package screened DEGs between the low-risk and high-risk groups. STRING was utilized to develop a PPI network based on the DEGs. The PPI network was visualized using Cytoscape (**Figure 10A**), and hub genes were identified by the degree method (**Figure 10B**). CDK1, AURKB, CDC20, BUB1, KIF11, CCNB1, TOP2A, CDCA8, BUB1B, and CCNA2 were identified as the top ten hub genes. All ten genes were significantly higher-expressed in tumor samples than in normal samples. To explore the differences in survival, patients were grouped into low- and high-expression groups by the median expression of the ten genes. Except for BUB1B, the K-M curves show that the low expression group showed a longer OS (**Figure 10D** and **Supplementary Figures 10A–I**). Furthermore, biological pathways and progress related to the ten genes were identified by GO and KEGG enrichment analyses. According to the findings of KEGG enrichment analyses, ten genes were enriched in cell cycle, progesterone-mediated oocyte maturation and oocyte meiosis. In addition, the ten genes were associated with pathways such as condensed nuclear chromosome, protein serine/threonine kinase activity, mitotic cell cycle checkpoint, cyclin-dependent protein kinase activity, histone kinase activity, chromosomal region, spindle, and centromeric region, sister chromatid segregation, and nuclear division, according to the results of GO enrichment analyses (**Figure 10C**). To identify the genes with independent prognosis relevance, univariate and multivariate COX regression were used. Only CDCA8 and TOP2A were found to be independent prognostic genes (**Supplementary Figures 10J, K**). Since TOPA2 was identified as a CAF-related independent prognostic gene and its role in HCC was explored above, next only the role of CDCA8 in HCC was further investigated. As shown in **Figures 10E–G**, high CDCA8 expression is associated with a high T stage, histological stage, and pathological stage, indicating that up-regulated expression of CDCA8 is related to a highly malignant HCC. In addition, the association of CDCA8 expression level with immune cell infiltration level was studied by immune cell infiltration analysis. As shown in **Figure 10H**, patients with low CDCA8 expression have a high infiltration of cytotoxic and NK cells.

DISCUSSION

Increasing evidence has shown that CAFs are crucial players in HCC progression (15). For example, CAFs play an important role in the multicellular, stromal-dependent changes that contribute to HCC development. A previous study indicated that CAF-mediated cellular crosstalk supports HCC progression (9). The Yugawa et al. study suggested that CAFs enhance HCC development by downregulating exosomal miR-150-3p (38). Moreover, research by Chen et al. demonstrated that CAFs activate M2-polarized macrophages to promote HCC development through the plasminogen activator inhibitor-1 pathway (12). It is proven that the BAFF/NFκB axis in CAFs leads to sorafenib-resistant HCC cells (39). However, most research concentrates on the impact of a single CAF-related gene regulator in HCC and the combined effects of numerous CAF-related genes remain unclear. The investigation of the involvement of CAF-related gene signatures in HCC might aid in the understanding of CAFs in HCC development, hence, directing to an appropriate treatment strategy.

This is the first research probing into the prognostic significance of CAF-related gene signatures for HCC patients. To improve the reliability of the current results, the GEO database was used to screen CAF-related gene sets in TCGA and the potential of the prognostic model built using CAF-related genes was validated by the ICGC database. Moreover, for obtaining representative prognostic genes and increasing the applicability of the model, LASSO Cox regression and multivariate Cox regression analyses were conducted to screen core CAF-related genes with independent prognosis relevance and to construct a risk score prognostic model. Among the 5 CAF-related genes with independent prognosis relevance in TCGA, the majority of genes played roles in cancer

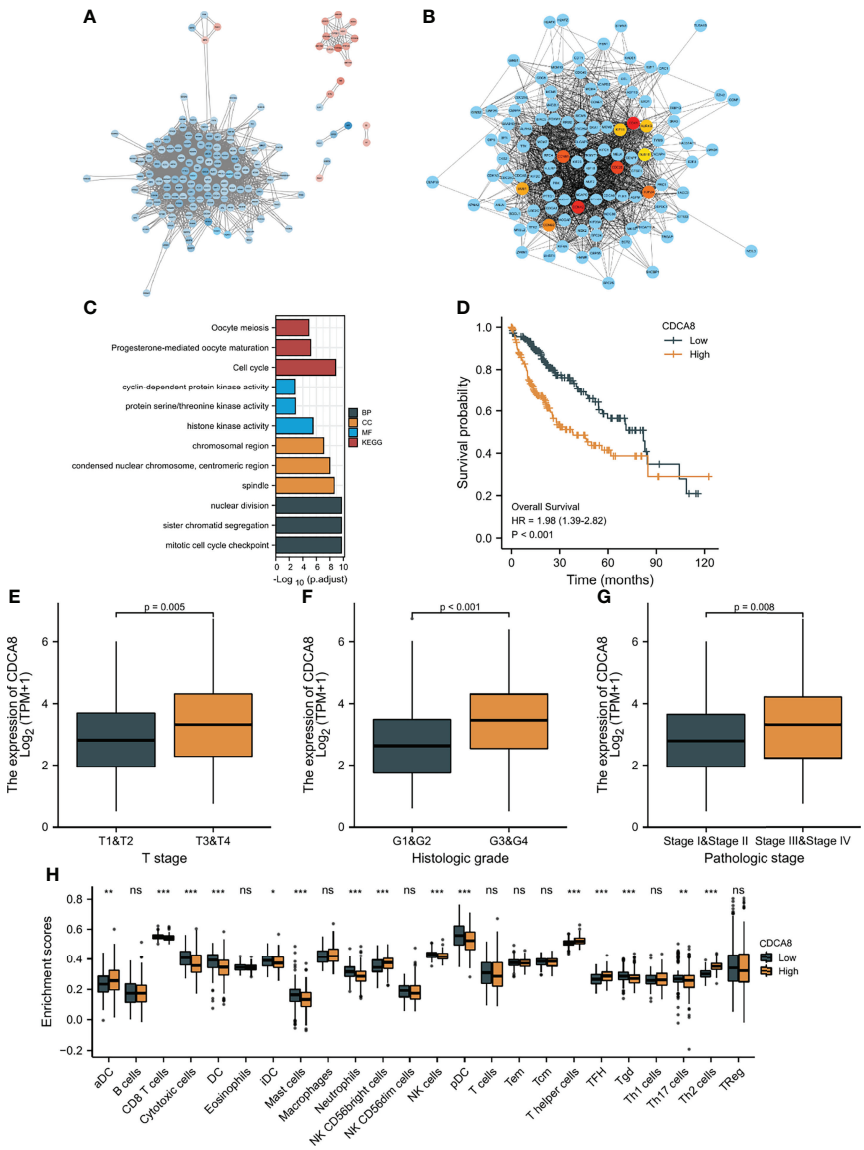

FIGURE 10 | Protein-protein interaction (PPI) analysis. **(A)** PPI network constructed using Cytoscape; Blue: high expression DEGs in high-risk group, red: high expression DEGs in low-risk group. **(B)** Top ten hub genes screen by degree method. **(C)** GO and KEGG analyses of top ten hub genes. **(D)** K-M curves of CDCA8 expression level. **(E–G)** The relationship between CDCA8 expression level and clinicopathological characteristics. **(H)** The difference in immune infiltration fraction between low and high expression groups of CDCA8 statistical significance is indicated by the following symbols: ns, $p \geq 0.05$; *, $p < 0.05$; **, $p < 0.01$; ***, $p < 0.001$.

progression. Previous research linked the overexpression of ARHGAP11A, DLGAP5, TOP2A, and TTK to the development of HCC (40–43). ARHGAP11A is a gene that encodes for a protein regulating cell cycle-dependent motility. Recently, ARHGAP11A has been shown to enhance malignant HCC development through an ARHGAP11A-Rac1B interaction (40). Moreover, the Lu et al. study demonstrated that HOXD-AS1 upregulated ARHGAP11A resulting in induced metastasis *via* competitively binding to microRNA-19a (44). However, the function of ARHGAP11A in CAFs is unknown. This study included ARHGAP11A in the CAF-related genes prognostic model to investigate the role of ARHGAP11A in CAFs.

Moreover, DLGAP5 is a microtubule-associated protein and mitotic phosphorylated substrate of Aurora-A. The Liao et al. research suggested that methylation negatively regulated DLGAP5 expression, which indicates that DLGAP5 may be a methylation biomarker in HCC (41). In a previous study (45), DNA topoisomerase 2-alpha (TOP2A) has been identified as a core gene in HCC, which was again proved by this study. TOP2A, a m6A RNA methylation-modified gene, plays an important function in controlling DNA double strand unwinding and has been therefore regarded as a therapeutic target (45). TOP2A, like DLGAP5, may also be a methylation biomarker in HCC. Monopolar spindle 1 (TTK) is a gene that encodes a dual

serine/threonine and tyrosine protein kinase and is required for chromosome alignment and the spindle assembly checkpoint (43). Prior research found that *via* the activation of the Akt/mTOR and MDM2/p53 signaling pathways, TTK stimulates migration and cell proliferation in HCC (46). In addition, some studies indicated that DLGAP5, TOP2A, and TTK were related to the prognosis of individuals with HCC (43, 47, 48). This study verified these previous conclusions again and evaluated these genes in CAFs in terms of their prognostic significance.

The prognostic risk score model developed with the 5 CAF-related genes was predictive of the OS of patients suffering from HCC. We found that the low-risk group had a longer OS than the high-risk group in the TCGA, which has been confirmed in ICGC database, suggesting that the prognostic model had a strong performance to predict the populace with poor OS in HCC. In addition, the prognostic risk score model combined with clinicopathological characteristics associated with prognosis increased the model's predictive capability and clinical applicability.

To better understand the impact of the risk score model on HCC, chemosensitivity differences among patients with two risk scores (low, high) were explored. Cisplatin and doxorubicin are widely used in the intra-arterial administration of chemotherapy in early and intermediate HCC (36). The higher sensitivity to cisplatin and doxorubicin in lower risk score patients demonstrated that the prognostic model had the ability to screen patients with relatively high sensitivity to cisplatin and doxorubicin to improve the efficacy in early and intermediate HCC. In the recent decade, sorafenib was recognized as the only available standard of care for advanced HCC (49). The chemosensitivity to sorafenib was negatively related to the risk score of HCC patients, which indicated the model could identify individuals with relatively higher sensitivity to sorafenib in advanced HCC, thus improving their prognosis.

Recently, TME is considered to be an important part of the occurrence, development, invasion and metastasis of HCC (50). A variety of immune or stromal cell types observed in HCC collaborate in the formation of an immunosuppressive TME and their presence is often associated with prognosis (51), which was also observed in this study. For instance, there was also a significant difference in stromal scores between the low-risk and high-risk groups with significantly different OS. A previous study discovered that CAFs were related to the suppression of NK cell activity in HCC (13), but the link between CAFs and other numerous immune cells in HCC is uncertain. In this research, patients scored as having a high risk showed a greater infiltration of B cells, CD8 T cells, and immunosuppressive cells such as Tregs. These findings might help with personalized immunotherapy and improvement of the treatment outcomes.

This study may have several limitations. First, the lack of in-depth mechanism research is the main limitation. Therefore, experimental research must be conducted to confirm the detailed molecular processes of the CAF-related gene signatures in the future. Secondly, further clinical research should be carried out to verify the prognostic model built on the 5 CAF-related genes. Furthermore, the study relied solely on public sources data, which may involve selection bias.

CONCLUSION

In conclusion, this study evaluated the prognostic value of CAF-related gene signatures in HCC. Based on the expression pattern of CAF-related genes, two clusters were identified and found to have a difference in OS and PFI. CAF-related prognostic risk score model can be utilized for prognostic prediction of HCC. The risk score based on CAFs can predict chemotherapy sensitivity and immunotherapy response for improving prognosis in HCC. Additionally, there was a correlation between immune infiltration characteristics of TME and patients with different risk levels, which may aid in creating a cooperative effect in CAF-targeted treatments and immunotherapy. These findings present a favorable predicting model in prognosis, potentially paving the way for individualized HCC therapy in the future.

DATA AVAILABILITY STATEMENT

Publicly available datasets were analyzed in this study. This data can be found here: GEO (https://www.ncbi.nlm.nih.gov/geo), TCGA (https://cancergenome.nih.gov), and ICGC (https://dcc.icgc.org) databases.

ETHICS STATEMENT

All data used in this study were from public databases, therefore ethical approval was not required.

AUTHOR CONTRIBUTIONS

Conception and design: WD. Collection and collation of data: WD, YX, and HH. Data analysis and interpretation: WD, YX and HH. Manuscript writing and revisions: WD, YX, and HH. Final approval of manuscript: All authors. Accountable of all aspects of work: All authors.

ACKNOWLEDGMENTS

Thanks to all researchers who provided the data for this study.

SUPPLEMENTARY MATERIAL

The Supplementary Material for this article can be found online at: https://www.frontiersin.org/articles/10.3389/fendo.2022.884777/full#supplementary-material

REFERENCES

1. Llovet JM, Zucman-Rossi J, Pikarsky E, Sangro B, Schwartz M, Sherman M, et al. Hepatocellular Carcinoma. *Nat Rev Dis Primers* (2016) 2:16018. doi: 10.1038/nrdp.2016.18
2. Villanueva A. Hepatocellular Carcinoma. *N Engl J Med* (2019) 380(15):1450–62. doi: 10.1056/NEJMra1713263
3. Karb DB, Sclair SN. Hepatocellular Carcinoma. In: SM Cohen, P Davitkov, editors. *In Liver Disease: A Clinical Casebook*. Springer International Publishing, Cham (2019). p. 141–54.
4. Njei B, Rotman Y, Ditah I, Lim JK. Emerging Trends in Hepatocellular Carcinoma Incidence and Mortality. *Hepatology* (2015) 61:191–9. doi: 10.1002/hep.27388
5. Pietras K, Ostman A. Hallmarks of Cancer: Interactions With the Tumor Stroma. *Exp Cell Res* (2010) 316(8):1324–31. doi: 10.1016/j.yexcr.2010.02.045
6. Xing F, Saidou J, Watabe K. Cancer Associated Fibroblasts (CAFs) in Tumor Microenvironment. *Front Biosci (Landmark Ed)* (2010) 15:166–79. doi: 10.2741/3613
7. Cirri P, Chiarugi P. Cancer Associated Fibroblasts: The Dark Side of the Coin. *Am J Cancer Res* (2011) 1(4):482–97.
8. Paulsson J, Micke P. Prognostic Relevance of Cancer-Associated Fibroblasts in Human Cancer. *Semin Cancer Biol* (2014) 25:61–8. doi: 10.1016/j.semcancer.2014.02.006
9. Song M, He J, Pan QZ, Yang J, Zhao J, Zhang YJ, et al. Cancer-Associated Fibroblast-Mediated Cellular Crosstalk Supports Hepatocellular Carcinoma Progression. *Hepatology* (2021) 73(5):1717–35. doi: 10.1002/hep.31792
10. Kubo N, Araki K, Kuwano H, Shirabe K. Cancer-Associated Fibroblasts in Hepatocellular Carcinoma. *World J Gastroenterol* (2016) 22(30):6841–50. doi: 10.3748/wjg.v22.i30.6841
11. Liu G, Sun J, Yang ZF, Zhou C, Zhou PY, Guan RY, et al. Cancer-Associated Fibroblast-Derived CXCL11 Modulates Hepatocellular Carcinoma Cell Migration and Tumor Metastasis Through the Circubap2/miR-4756/IFIT1/3 Axis. *Cell Death Dis* (2021) 12(3):260. doi: 10.1038/s41419-021-03545-7
12. Chen S, Morine Y, Tokuda K, Yamada S, Saito Y, Nishi M, et al. Cancer −associated Fibroblast−Induced M2−polarized Macrophages Promote Hepatocellular Carcinoma Progression *via* the Plasminogen Activator Inhibitor−1 Pathway. *Int J Oncol* (2021) 59(2):59. doi: 10.3892/ijo.2021.5239
13. Affo S, Yu LX, Schwabe RF. The Role of Cancer-Associated Fibroblasts and Fibrosis in Liver Cancer. *Annu Rev Pathol* (2017) 12:153–86. doi: 10.1146/annurev-pathol-052016-100322
14. Chen Y, McAndrews KM, Kalluri R. Clinical and Therapeutic Relevance of Cancer-Associated Fibroblasts. *Nat Rev Clin Oncol* (2021) 18(12):792–804. doi: 10.1038/s41571-021-00546-5
15. Yin Z, Dong C, Jiang K, Xu Z, Li R, Guo K, et al. Heterogeneity of Cancer-Associated Fibroblasts and Roles in the Progression, Prognosis, and Therapy of Hepatocellular Carcinoma. *J Hematol Oncol* (2019) 12(1):101. doi: 10.1186/s13045-019-0782-x
16. Hanahan D, Coussens LM. Accessories to the Crime: Functions of Cells Recruited to the Tumor Microenvironment. *Cancer Cell* (2012) 21(3):309–22. doi: 10.1016/j.ccr.2012.02.022
17. Li Y, Wang R, Xiong S, Wang X, Zhao Z, Bai S, et al. Cancer-Associated Fibroblasts Promote the Stemness of CD24+ Liver Cells *via* Paracrine Signaling. *J Mol Med (Berl)* (2019) 97(2):243–55. doi: 10.1007/s00109-018-1731-9
18. Leca J, Martinez S, Lac S, Nigri J, Secq V, Rubis M, et al. Cancer-Associated Fibroblast-Derived Annexin A6+ Extracellular Vesicles Support Pancreatic Cancer Aggressiveness. *J Clin Invest* (2016) 126(11):4140–56. doi: 10.1172/JCI87734
19. Qin X, Guo H, Wang X, Zhu X, Yan M, Wang X, et al. Exosomal miR-196a Derived From Cancer-Associated Fibroblasts Confers Cisplatin Resistance in Head and Neck Cancer Through Targeting CDKN1B and ING5. *Genome Biol* (2019) 20(1):12. doi: 10.1186/s13059-018-1604-0
20. Cheng Y, Li H, Deng Y, Tai Y, Zeng K, Zhang Y, et al. Cancer-Associated Fibroblasts Induce PDL1+ Neutrophils Through the IL6-STAT3 Pathway That Foster Immune Suppression in Hepatocellular Carcinoma. *Cell Death Dis* (2018) 9(4):422. doi: 10.1038/s41419-018-0458-4
21. Deng Y, Cheng J, Fu B, Liu W, Chen G, Zhang Q, et al. Hepatic Carcinoma-Associated Fibroblasts Enhance Immune Suppression by Facilitating the Generation of Myeloid-Derived Suppressor Cells. *Oncogene* (2017) 36(8):1090–101. doi: 10.1038/onc.2016.273
22. Herrera M, Berral-González A, López-Cade I, Galindo-Pumariño C, Bueno-Fortes S, Martín-Merino M, et al. Cancer-Associated Fibroblast-Derived Gene Signatures Determine Prognosis in Colon Cancer Patients. *Mol Cancer* (2021) 20(1):73. doi: 10.1186/s12943-021-01367-x
23. Barrett T, Wilhite SE, Ledoux P, Evangelista C, Kim IF, Tomashevsky M, et al. NCBI GEO: Archive for Functional Genomics Data Sets–Update. *Nucleic Acids Res* (2013) 41(Database issue):D991–5. doi: 10.1093/nar/gks1193
24. Love MI, Huber W, Anders S. Moderated Estimation of Fold Change and Dispersion for RNA-Seq Data With Deseq2. *Genome Biol* (2014) 15(12):550. doi: 10.1186/s13059-014-0550-8
25. Gu Z, Eils R, Schlesner M. Complex Heatmaps Reveal Patterns and Correlations in Multidimensional Genomic Data. *Bioinformatics* (2016) 32(18):2847–9. doi: 10.1093/bioinformatics/btw313
26. Geeleher P, Cox N, Huang RS. Prrophetic: An R Package for Prediction of Clinical Chemotherapeutic Response From Tumor Gene Expression Levels. *PloS One* (2014) 9(9):e107468. doi: 10.1371/journal.pone.0107468
27. Xie Y, Zhang J, Li M, Zhang Y, Li Q, Zheng Y, et al. Identification of Lactate-Related Gene Signature for Prediction of Progression and Immunotherapeutic Response in Skin Cutaneous Melanoma. *Front Oncol* (2022) 12:818868. doi: 10.3389/fonc.2022.818868
28. Newman AM, Liu CL, Green MR, Gentles AJ, Feng W, Xu Y, et al. Robust Enumeration of Cell Subsets From Tissue Expression Profiles. *Nat Methods* (2015) 12(5):453–7. doi: 10.1038/nmeth.3337
29. Li T, Fu J, Zeng Z, Cohen D, Li J, Chen Q, et al. TIMER2.0 for Analysis of Tumor-Infiltrating Immune Cells. *Nucleic Acids Res* (2020) 48(W1):W509–14. doi: 10.1093/nar/gkaa407
30. Finotello F, Mayer C, Plattner C, Laschober G, Rieder D, Hackl H, et al. Molecular and Pharmacological Modulators of the Tumor Immune Contexture Revealed by Deconvolution of RNA-Seq Data. *Genome Med* (2019) 11(1):34. doi: 10.1186/s13073-019-0638-6
31. Becht E, Giraldo NA, Lacroix L, Buttard B, Elarouci N, Petitprez F, et al. Estimating the Population Abundance of Tissue-Infiltrating Immune and Stromal Cell Populations Using Gene Expression. *Genome Biol* (2016) 17(1):218. doi: 10.1186/s13059-016-1070-5
32. Hänzelmann S, Castelo R, Guinney J. GSVA: Gene Set Variation Analysis for Microarray and RNA-Seq Data. *BMC Bioinf* (2013) 14:7. doi: 10.1186/1471-2105-14-7
33. Yu G, Wang LG, Han Y, He QY. Clusterprofiler: An R Package for Comparing Biological Themes Among Gene Clusters. *Omics: J Integr Biol* (2012) 16(5):284–7. doi: 10.1089/omi.2011.0118
34. Ritchie ME, Phipson B, Wu D, Hu Y, Law CW, Shi W, et al. Limma Powers Differential Expression Analyses for RNA-Sequencing and Microarray Studies. *Nucleic Acids Res* (2015) 43(7):e47. doi: 10.1093/nar/gkv007
35. Bindea G, Mlecnik B, Tosolini M, Kirilovsky A, Waldner M, Obenauf AC, et al. Spatiotemporal Dynamics of Intratumoral Immune Cells Reveal the Immune Landscape in Human Cancer. *Immunity* (2013) 39(4):782–95. doi: 10.1016/j.immuni.2013.10.003
36. Vogel A, Cervantes A, Chau I, Daniele B, Llovet JM, Meyer T, et al. Hepatocellular Carcinoma: ESMO Clinical Practice Guidelines for Diagnosis, Treatment and Follow-Up. *Ann Oncol* (2018) 29(Suppl 4):iv238–55. doi: 10.1093/annonc/mdy308
37. Jiang Y, Han QJ, Zhang J. Hepatocellular Carcinoma: Mechanisms of Progression and Immunotherapy. *World J Gastroenterol* (2019) 25(25):3151–67. doi: 10.3748/wjg.v25.i25.3151
38. Yugawa K, Yoshizumi T, Mano Y, Itoh S, Harada N, Ikegami T, et al. Cancer-Associated Fibroblasts Promote Hepatocellular Carcinoma Progression Through Downregulation of Exosomal miR-150-3p. *Eur J Surg Oncol* (2021) 47(2):384–93. doi: 10.1016/j.ejso.2020.08.002
39. Gao L, Morine Y, Yamada S, Saito Y, Ikemoto T, Tokuda K, et al. The BAFF/Nfκb Axis Is Crucial to Interactions Between Sorafenib-Resistant HCC Cells and Cancer-Associated Fibroblasts. *Cancer Sci* (2021) 112(9):3545–54. doi: 10.1111/cas.15041
40. Dai B, Zhang X, Shang R, Wang J, Yang X, Zhang H, et al. Blockade of ARHGAP11A Reverses Malignant Progress *via* Inactivating Rac1B in Hepatocellular Carcinoma. *Cell Commun Signal* (2018) 16(1):99. doi: 10.1186/s12964-018-0312-4

41. Liao W, Liu W, Yuan Q, Liu X, Ou Y, He S, et al. Silencing of DLGAP5 by siRNA Significantly Inhibits the Proliferation and Invasion of Hepatocellular Carcinoma Cells. *PloS One* (2013) 8(12):e80789. doi: 10.1371/journal.pone.0080789
42. Watanuki A, Ohwada S, Fukusato T, Makita F, Yamada T, Kikuchi A, et al. Prognostic Significance of DNA Topoisomerase IIalpha Expression in Human Hepatocellular Carcinoma. *Anticancer Res* (2002) 22(2B):1113–9.
43. Choi M, Min YH, Pyo J, Lee CW, Jang CY, Kim JE. TC Mps1 12, a Novel Mps1 Inhibitor, Suppresses the Growth of Hepatocellular Carcinoma Cells *via* the Accumulation of Chromosomal Instability. *Br J Pharmacol* (2017) 174 (12):1810–25. doi: 10.1111/bph.13782
44. Lu S, Zhou J, Sun Y, Li N, Miao M, Jiao B, et al. The Noncoding RNA HOXD-AS1 is a Critical Regulator of the Metastasis and Apoptosis Phenotype in Human Hepatocellular Carcinoma. *Mol Cancer* (2017) 16(1):125. doi: 10.1186/s12943-017-0676-x
45. Li Y, Qi D, Zhu B, Ye X. Analysis of M6a RNA Methylation-Related Genes in Liver Hepatocellular Carcinoma and Their Correlation With Survival. *Int J Mol Sci* (2021) 22(3):1474. doi: 10.3390/ijms22031474
46. Liu X, Liao W, Yuan Q, Ou Y, Huang J. TTK Activates Akt and Promotes Proliferation and Migration of Hepatocellular Carcinoma Cells. *Oncotarget* (2015) 6(33):34309–20. doi: 10.18632/oncotarget.5295
47. Dai Q, Liu T, Gao Y, Zhou H, Li X, Zhang W. Six Genes Involved in Prognosis of Hepatocellular Carcinoma Identified by Cox Hazard Regression. *BMC Bioinf* (2021) 22(1):167. doi: 10.1186/s12859-021-04095-7
48. Wong N, Yeo W, Wong WL, Wong NL, Chan KY, Mo FK, et al. TOP2A Overexpression in Hepatocellular Carcinoma Correlates With Early Age Onset, Shorter Patients Survival and Chemoresistance. *Int J Cancer* (2009) 124(3):644–52. doi: 10.1002/ijc.23968
49. Llovet JM, Kelley RK, Villanueva A, Singal AG, Pikarsky E, Roayaie S, et al. Hepatocellular Carcinoma. *Nat Rev Dis Primers* (2021) 7(1):7. doi: 10.1038/s41572-021-00245-6
50. Wu Q, Zhou L, Lv D, Zhu X, Tang H. Exosome-Mediated Communication in the Tumor Microenvironment Contributes to Hepatocellular Carcinoma Development and Progression. *J Hematol Oncol* (2019) 12(1):53. doi: 10.1186/s13045-019-0739-0
51. Sangro B, Sarobe P, Hervás-Stubbs S, Melero I. Advances in Immunotherapy for Hepatocellular Carcinoma. *Nat Rev Gastroenterol Hepatol* (2021) 18 (8):525–43. doi: 10.1038/s41575-021-00438-0

Conflict of Interest: The authors declare that the research was conducted in the absence of any commercial or financial relationships that could be construed as a potential conflict of interest.

Publisher's Note: All claims expressed in this article are solely those of the authors and do not necessarily represent those of their affiliated organizations, or those of the publisher, the editors and the reviewers. Any product that may be evaluated in this article, or claim that may be made by its manufacturer, is not guaranteed or endorsed by the publisher.

frontiers | Frontiers in Endocrinology

ORIGINAL RESEARCH
published: 21 June 2022
doi: 10.3389/fendo.2022.883548

Discovering a Four-Gene Prognostic Model Based on Single-Cell Data and Gene Expression Data of Pancreatic Adenocarcinoma

Weizhen Huang[1], *Jun Li*[1], *Siwei Zhou*[1], *Yi Li*[1] *and Xia Yuan*[2*]

[1] *The Second Department of Medical Oncology, Huizhou First Hospital, Huizhou, China,* [2] *Cancer Center, Huizhou First Hospital, Huizhou, China*

OPEN ACCESS

Edited by:
Ihtisham Bukhari,
Fifth Affiliated Hospital of Zhengzhou University, China

Reviewed by:
Weicai Chen,
Second Affiliated Hospital of Nanchang University, China
Min Wei,
Shanghai Jiao Tong University, China

****Correspondence:***
Xia Yuan
yuanxia71@hotmail.com

Specialty section:
This article was submitted to Cancer Endocrinology, a section of the journal Frontiers in Endocrinology

Received: *25 February 2022*
Accepted: *02 May 2022*
Published: *21 June 2022*

Citation:
Huang W, Li J, Zhou S, Li Y and Yuan X (2022) Discovering a Four-Gene Prognostic Model Based on Single-Cell Data and Gene Expression Data of Pancreatic Adenocarcinoma. Front. Endocrinol. 13:883548. doi: 10.3389/fendo.2022.883548

Background: Pancreatic cancer has a 5-year overall survival lower than 8%. Pancreatic adenocarcinoma (PAAD) is the most common type. This study attempted to explore novel molecular subtypes and a prognostic model through analyzing tumor microenvironment (TME).

Materials and Methods: Single-cell RNA sequencing (scRNA-seq) data and expression profiles from public databases were downloaded. Three PAAD samples with single-cell data and 566 samples with gene expression data were included. Seurat was used to identify cell subsets. SVA merged and removed batch effects from multichip datasets. CIBERSORT was used to evaluate the components of different cells in transcriptome, ConsensusClusterPlus was used to identify molecular subtypes, and gene set enrichment analysis was used for functional enrichment analysis. LASSO Cox was performed to construct dimensionality reduction and prognosis model.

Results: Memory B cells (MBCs) were identified to be significantly with PAAD prognosis. Two immune subtypes (IS1 and IS2) with distinct overall survival were constructed. Forty-one DEGs were identified between IS1 and IS2. Four prognostic genes (ANLN, ARNTL2, SERPINB5, and DKK1) were screened to develop a prognostic model. The model was effective in classifying samples into high-risk and low-risk groups with distinct prognosis. Three subgroups of MBCs were identified, where MBC_0 and MBC_1 were differentially distributed between IS1 and IS2, high-risk and low-risk groups.

Conclusions: MBCs were closely involved in PAAD progression, especially MBC_0 and MBC_1 subgroups. The four-gene prognostic model was predictive of overall survival and could guide immunotherapy for patients with PAAD.

Keywords: pancreatic adenocarcinoma, tumor microenvironment, memory B cells, immune subtype, prognostic model, bioinformatics analysis

INTRODUCTION

Pancreatic cancer has high death rate, and pancreatic adenocarcinoma (PAAD) is the most common pathological type. According to global cancer statistics, in 2020, 495,773 new cases of pancreatic cancer were diagnosed and 466,003 deaths occurred (1). However, the incidence varied greatly among different regions. Age-standardized rate was the highest in Europe and North America but the lowest in Africa and South Central Asia (2). Significant difference of incidence is also observed between developed countries and developing countries (3). Smoking, alcohol, obesity, and dietary factors are main risk factors contributing to the development of pancreatic cancer and its unfavorable survival (4). New diagnosed patients are common at advanced stage, resulting in a low overall survival rate of only 8% (5). Therefore, early diagnosis for pancreatic cancer is required for improving prognosis.

Tumor microenvironment (TME) plays a critical role in cancer development. The composition and distribution of different immune cells affects anti-tumor immune response and the formation of immune escape TME. Tumor-associated macrophages (TAMs), regulatory T cells (Tregs), and myeloid-derived suppressor cells (MDSCs) are major immunosuppressive cells helping tumor cells to escape immune capture. Immunosuppressive TME is involved in metastasis through activating oncogenic pathways such as angiogenesis, epithelial–mesenchymal transition (EMT), and transforming growth factor (TGF)-β signaling pathways in pancreatic cancer (6). Targeting TME is considered as a promising immunotherapy for cancer treatment. Programmed cell death protein-1 (PD-1) and cytotoxic T-lymphocyte–associated protein 4 (CTLA-4) are two important immune checkpoints that can impede anti-tumor response when combined with their receptors. The inhibitors of PD-1 and CTLA-4 could activate immune response of tumor cells in clinical trials of different cancer types, including pancreatic cancer (7). However, not all patients can benefit from immune checkpoint blockade (ICB). Further understanding of TME and molecular features in pancreatic cancer is needed to facilitate the exploration of new therapeutic drugs.

Single-cell sequencing technology facilitates a deep excavation of molecular data of TME. In this study, we introduced single-cell RNA sequencing (Single-cell RNA sequencing) data from public database and applied single-cell analysis to screen valuable information. We found that a group of immune cells, memory B cells (MBCs), was able to serve as molecular features to classify patients with PAAD into different molecular subtypes. On the basis of the markers of MBCs, we identified four prognostic genes and constructed a prognostic model that could predict overall survival for patients with PAAD. Importantly, the prognostic model was able to identify patients who may be more sensitive to ICB therapy.

MATERIALS AND METHODS

Data Source

For the workflow of this study, see **Supplementary Figure S1A**. scRNA-seq data of normal and PAAD samples were downloaded from Gene Expression Omnibus (GEO) database (https://www.ncbi.nlm.nih.gov/geo/). Expression profiles of normal and tumor samples were downloaded from GEO, The Cancer Genome Atlas (TCGA) database (https://portal.gdc.cancer.gov/), and International Cancer Genome Consortium (ICGC) database (https://dcc.icgc.org/).

Data Preprocessing

GSE165399 (8) cohort contained scRNA-seq data of one normal sample (GSM5032773) and two tumor samples (GSM5032771 and GSM5032772). Seurat R package was employed to preprocess single-cell data (9). Data were first screened under condition that each gene expressed at least in three cells and each cell expressed at least 250 genes. Then, "PercentageFeatureSet" function was conducted to calculate the percentage of mitochondria and rRNA. Finally, single cells were filtered under the standards that each cell expressed 500–6,000 genes, mitochondria percentage was less than 35% and unique molecular identifiers (UMI) of each cell was over than 1,000. Quality control of single-cell data before and after preprocessing was shown (**Supplementary Figures S1B, C, S2A**). Log-normalization was performed to normalize data of three samples. "FindVariableFeatures" function was conducted to excavate highly variable genes. Then, "FindIntegrationAnchors" was used to remove batch effects, and "IntegrateData" function was performed to combine data. Next, "ScaleData" function was used to scale data, and principle component analysis was performed to reduce data dimensionality (**Supplementary Figures S2B, C**).

For GSE21501 (10), GSE28735 (11), GSE57495 (12), GSE62452 (13), and GSE85916 cohorts, samples without survival status or survival time were excluded. To combine five cohorts, limma (14) and sva R packages were used to remove batch effects and normalize the data (named as GEO cohort) (**Supplementary Figures S2D, E**). A total of 320 PAAD samples and 16,466 genes were remained. For TCGA-PAAD and ICGC-AU cohort, samples without survival time or survival status were removed. Finally, 156 and 90 tumor samples remained in TCGA-PAAD and ICGC-AU cohort, respectively. The sample clinical characteristics of each dataset were in **Supplementary Table S1**.

Single-Cell Annotation

First, "FindNeighbors" and "FindClusters" function in Seurat R package were performed to cluster single cells under dim = 30 and resolution = 0.5. Cells were clustered into different subgroups. Markers of different immune cells were obtained from previous research (15). Single-sample gene set enrichment analysis (ssGSEA) was conducted to calculate enrichment score of immune cells and annotate subgroups. Marker genes of different cell types related to pancreatic tissue were obtained from CellMarker (http://biocc.hrbmu.edu.cn/CellMarker/) (16). The top five enriched marker genes of each subgroup were identified using "FindAllMarkers" function under logfc = 0.5 and Minpct = 0.35 ($P < 0.05$).

Gene Set Enrichment Analysis

Gene set enrichment analysis (GSEA) calculates enrichment score of genes, cells, or signatures based on expression profiles

and is widely implemented in analyzing cancer data (17). The strength of the method is to interpret biological meaning such as functional pathways and biological process based on a series of gene sets. GSEA was performed to assess the enrichment of hallmark pathways based on a gene set "h.all.v7.4.symbols.gmt" downloaded from Molecular Signatures Database (MSigDB, https://www.gsea-msigdb.org/gsea/msigdb/). SsGSEA, which is developed based on GSEA, allows a calculation of enrichment score for each sample (18). We used ssGSEA to assess the enrichment score of 10 oncogenic pathways (19).

Unsupervised Consensus Clustering

Unsupervised consensus clustering is a useful method to discover biological characteristics in cancer study. We applied ConsensusClusterPlus R package (20) to perform consensus clustering for samples in TCGA-PAAD cohort based on markers of MBCs. Expression data of markers were normalized. partitioning around medoids (PAM) algorithm was conducted, and "Canberra" was used as measurement distance. Five hundred bootstraps were conducted with each bootstrap containing 80% samples of TCGA-PAAD cohort. Cluster number k was set from 2 to 10. Cumulative distribution function (CDF) and area under CDF curve were used to confirm the optimal cluster number.

Identifying Differential Expressed Genes Between Two Subtypes

Limma R package was employed to identify differential expressed genes (DEGs) between different subtypes (21). False discovery rate (FDR < 0.05) and |log2(fold change(FC))| > 1 were set to screen DEGs (both upregulated and downregulated genes).

Constructing a Prognostic Model

TCGA-PAAD cohort served as training cohort, and GEO and ICGC-AU cohorts served as validation cohorts. Univariate Cox regression analysis in survival R package was employed to screen prognostic genes ($P < 0.05$) in TCGA-PAAD cohort. Next, least absolute shrinkage and selection operator (LASSO) Cox regression analysis in glmnet R package was performed to decrease the number of genes (22). Ten-fold cross-validation was conducted to validate the prognostic model. Receiver operating characteristic (ROC) curve analysis in timeROC R package was performed to evaluate the effectiveness of the prognostic model (23).

Tumor Immune Dysfunction and Exclusion Analysis

To predict the response to ICB, tumor immune dysfunction and exclusion (TIDE) analysis (http://tide.dfci.harvard.edu/) was introduced (24). Signatures, including T cell dysfunction, T cell exclusion, and immunosuppressive cells, were used as a basis to calculate enrichment score for high-risk and low-risk groups. TIDE analysis was effective in predicting the mechanism of immune escape within TME for various cancer types.

CIBERSORT Analysis

CIBERSORT (http://cibersort.stanford.edu/) was applied to evaluate the enrichment of 22 immune cells (25). The CIBERSORT tool could estimate the proportion of immune cells in TME based on gene expression data. In this study, we applied CIBERSORT to predict the enrichment score of different MBC subgroups.

ReactomeGSA for Analyzing Single-Cell Data

To analyze the function of MBCs, Reactome database (https://reactome.org/) and ReactomeGSA were introduced (26). ReactomeGSA tool can be linked to Reactome database and enable assessment of functional pathways on multi-omics. The top 20 differentially enriched pathways were visualized.

Statistical Analysis

All statistical analysis was performed in R software (v4.1.0). Student *t*-test was conducted between the two groups. ANOVA was conducted among three or more than three groups. Log-rank test was performed in Kaplan–Meier survival analysis. Parameters were default if there was no indication. $P < 0.05$ was considered as significant. ns, no significant, $^{*}P < 0.05$, $^{**}P < 0.01$, $^{***}P < 0.001$, and $^{****}P < 0.0001$.

RESULTS

Defining Cells in PAAD Single-Cell Data

The scRNA-seq data of three samples in GSE165399 dataset were preprocessed to screen valid data (**Supplementary Figures S1B, C, S2A**). After the screening, one gene expressed at least in three cells and one cell expressed at least 500 genes. The mitochondrial percent was lower than 35%, and UMI of each cell was more than 1,000. Then, the screening data were normalized, and three samples were combined to remove batch effects. Principle component analysis was applied to diminish dimensionality (**Supplementary Figures S2B, C**). Two-dimensional scRNA-seq data of single cells were clustered using UMAP, and 14 clusters were generated (**Figures 1A–C**). Compared to the normal sample (GSM5032773), tumor samples had an obviously different distribution of cells, suggesting that normal and tumor samples possibly had different cell types. According to the markers of 22 immune cells from a previous study (15), we annotated 14 subgroups, and finally, 12 cell types were identified (**Figure 1D**). The top five DEGs of 12 cell types were screened ($P < 0.05$, **Figure 1E**).

Identifying Cell Types Associated With PAAD Prognosis

Then, we used the screened DEGs of 12 cell types to calculate enrichment score of each sample in TCGA and GEO cohorts. Univariate Cox regression analysis revealed that four and three cell types were associated with PAAD prognosis in TCGA and

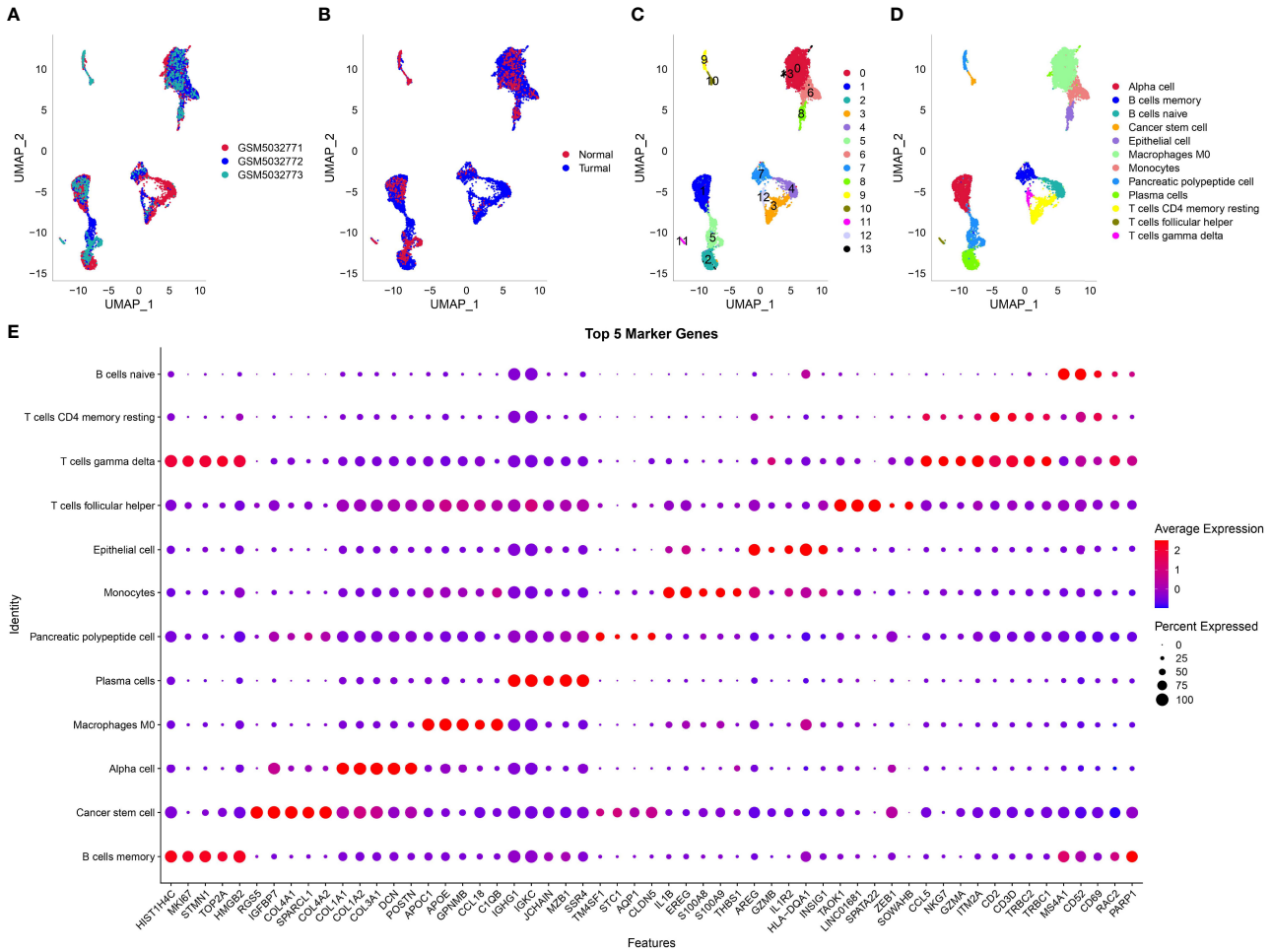

FIGURE 1 | Dimensionality reduction and subgrouping of single cells. **(A)** UMAP plot of three samples including GSM5032771, GSM5032772, and GSM5032773. **(B)** UMAP plot of normal and tumoral samples. **(C)** UMAP plot of cell subgrouping. **(D)** UMAP plot of cell type definition. **(E)** The top five enriched markers of 12 cell types. Horizontal axis indicated markers and vertical axis indicated cell types.

GEO, respectively ($P < 0.05$, **Figure 2A**). However, only MBCs were related to prognosis in both two cohorts. Survival analysis showed that the enrichment of MBCs was significantly associated with PAAD overall survival in the two cohorts ($P < 0.01$, **Figures 2B, C**). Low enrichment of MBCs had more favorable prognosis than high enrichment of MBCs.

Constructing Molecular Subtypes Based on Markers of Memory B Cells

As we identified that MBCs were an important cell groups in PAAD, we considered that the expression of their markers were associated with prognosis. Therefore, on the basis of 107 markers of MBCs, unsupervised consensus clustering was conducted to construct molecular subtypes. According to CDF curve and delta area under CDF curve (**Figures 3A, B**), cluster number k = 2 was determined to classify PAAD into two immune subtypes (IS1 and IS2, **Figure 3C**). Survival analysis showed that IS1 had better overall survival than IS2 in both two cohorts ($P < 0.01$, **Figures 3D, E**). Six types of immune subtypes were obtained from previous studies (27), namely, C1 (wound healing), C2 (inf-r dominant), C3 (inflammation), C4 (lymphocyte depletion), C5 (immunological silencing), and C6 (TGF-β dominant). Comparison of the relationship between the two molecular subtypes and these six types of immune cell infiltration showed that IS1 mainly accounted for a large proportion than C3 and C6 and that IS2 mainly enriched with C1 and C2. There were significant distribution differences between them ($p < 0.01$, **Figure 3F**). In the relation between subtypes and other clinical information, subtypes were significantly associated with survival status and grade (**Supplementary Figure S3**). Dead samples were more enriched in IS2, and grade 1 was more distributed in IS1. In addition, IS2 had obviously higher proportion of high enrichment of MBCs (**Supplementary Figure S3I**), which was consistent with previous result that high enrichment of MBCs had unfavorable prognosis.

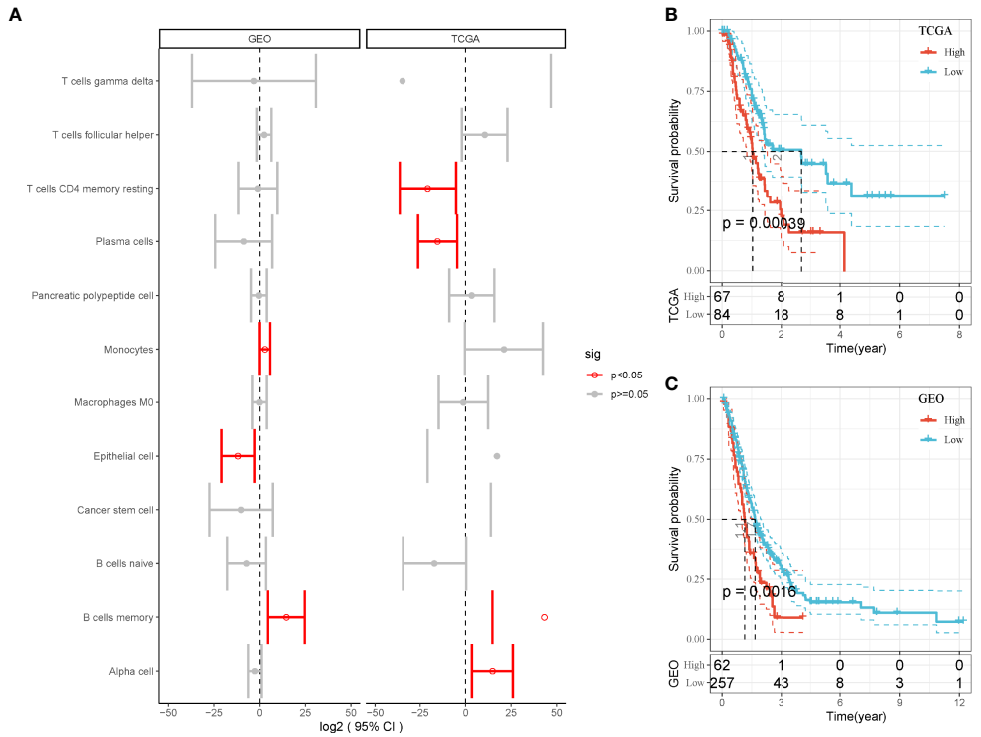

FIGURE 2 | The relation between enrichment of different cell types and PAAD prognosis. **(A)** Forest plot of different cell types in the relation to prognosis in TCGA and GEO cohorts. Red indicates $P < 0.05$. **(B, C)** Kaplan–Meier survival plots of high and low enrichment of MBCs in TCGA-PAAD **(A)** and GEO **(B)** cohorts.

Tumor-Related Pathways Were More Enriched in IS2

Next, we analyzed hallmark pathways of the two subtypes in two cohorts. In TCGA cohort, only one pathway was enriched in IS1, whereas 37 pathways were enriched in IS2. In GEO cohort, six pathways were enriched in IS1, and 18 pathways were enriched in IS2. Comparison of enriched pathways in two cohorts demonstrated that proximal tubule bicarbonate reclamation was enriched in IS1 in both two cohorts (**Figures 4A, B**). Eighteen pathways were enriched in IS2 in both cohorts, such as p53 signaling pathway, cell cycle, DNA replication, small cell lung cancer, and mismatch repair (**Figures 4C, D**). The results showed that tumor-related pathways were more activated in IS2, which may contribute to its worse prognosis.

The Relation Between DEGs and Memory B Cells

Gene expression profiles between IS1 and IS2 were compared to screen DEGs. In TCGA cohort, 100 upregulated and 237 downregulated genes were identified from IS1 (FDR < 0.05, |log2(FC)| > 1; **Figures 5A, B**). In GEO cohort, 50 upregulated and 17 downregulated genes were identified from IS1 (FDR < 0.05, |log2(FC)| > 1; **Figures 5C, D**). We found that 28 DEGs were upregulated and 13 DEGs were downregulated in IS1 in both two cohorts (**Figure 5E**). Furthermore, we assessed the correlation between the identified DEGs and MBCs. The results showed that 13 downregulated DEGs were positively correlated with the enrichment of MBCs, and 28 upregulated DEGs were negatively correlated with MBCs (**Figure 6**), suggesting that these DEGs were possibly involved in the PAAD development.

Establishing a Prognostic Model Based on DEGs

As we identified 41 DEGs associated with MBCs, a prognostic model was established based on them. Univariate Cox regression analysis was applied to these DEGs in TCGA cohort, and 16 DEGs were screened to be associated with prognosis. To further decrease the number of genes, we performed LASSO Cox regression analysis. The coefficients of DEGs close to zero showed an increasing lambda value (**Supplementary Figure S4A**). Ten-fold cross-validation calculated the confidence interval of each lambda value (**Supplementary Figure S4B**). When lambda = 0.0661, the model reached the optimal. Finally, four genes were remained, including ANLN, ARNTL2, SERPINB5, and DKK1. The four-gene prognostic model was defined as risk score = 0.294*ANLN + 0.155*ARNTL2 + 0.138*SERPINB5 + 0.058*DKK1.

Risk score was calculated for each sample in TCGA cohort. Samples were divided into high-risk and low-risk groups, according to the cut-off of z-score = 0. High-risk group had more dead samples than low-risk group (**Figure 7A**). Four genes

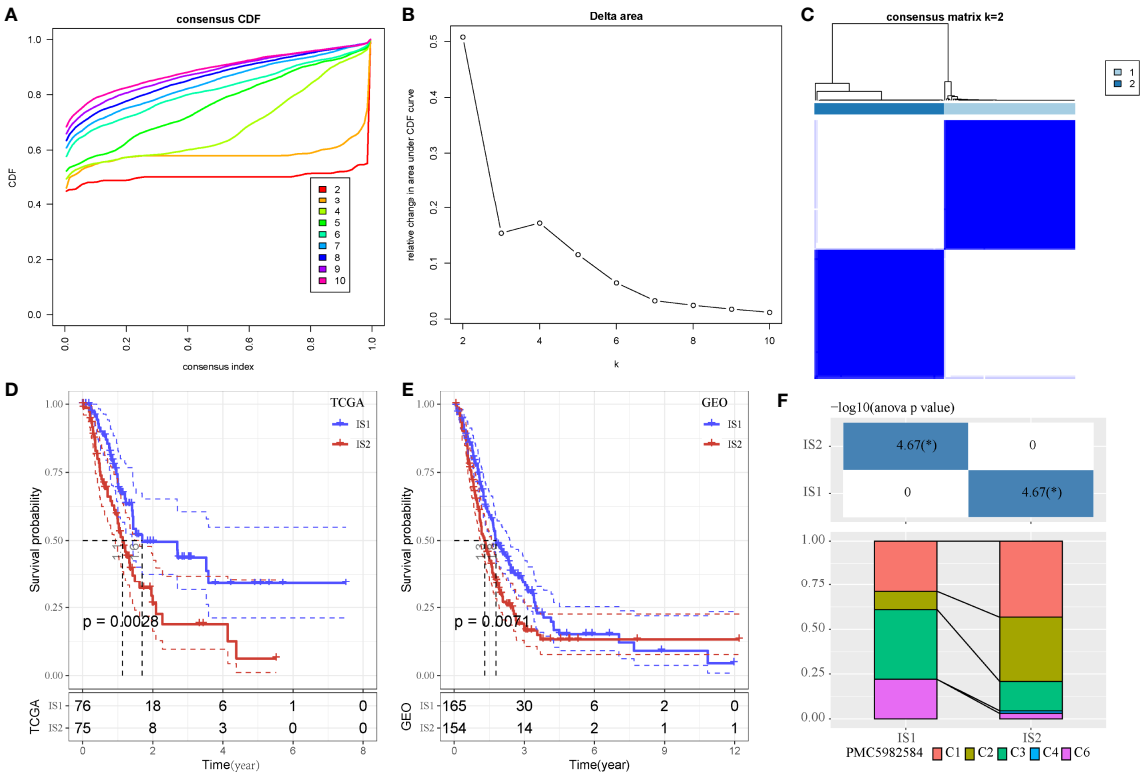

FIGURE 3 | Unsupervised consensus clustering of PAAD samples based on markers of MBCs in TCGA-PAAD cohort. **(A, B)** Consensus CDF curve and area under CDF curve when k = 2–10. **(C)** Consensus matrix when k = 2. **(D, E)** Kaplan–Meier survival plot of IS1 and IS2 groups in TCGA-PAAD and GEO cohorts. Log-rank test was conducted. CDF, cumulative distribution function. **(F)** Intersection between two molecular subtypes and the previous six immune subtypes.*$P < 0.05$.

were all high-expressed in high-risk group, compared to low-risk group. ROC analysis revealed that the prognostic model had the strongest performance in predicting 5-year overall survival (AUC = 0.74, 95% CI = 0.60–0.88; **Figure 7B**). Survival analysis showed differential overall survival of two groups (P = 0.00028, **Figure 7C**). In another two independent cohorts (GEO and ICGC), similar results were observed, and samples could be significantly classified into high-risk and low-risk groups (**Supplementary Figures S5, S6**).

Tumor Microenvironment of High-Risk and Low-Risk Groups

Then, we assessed the distribution of 22 immune cells in high-risk and low-risk groups. Macrophages and CD4 T cells contributed a large proportion in two groups (**Figure 8A**). In addition, we calculated the enrichment score of 10 oncogenic pathways, and 4 of 10 pathways were differentially enriched between the two groups ($P < 0.01$, **Figure 8B**). Cell cycle, Hippo signaling, NRF1, and WNT signaling pathways were more activated in high-risk group, indicating that these pathways were possibly involved in the PAAD development. ESTIMATE analysis revealed that low-risk group had higher immune infiltration than high-risk group (P = 0.018, **Figure 8C**), indicating that immune infiltration degree may affect the prognosis. To further understand the TME of two groups, we analyzed the expression of immune checkpoints, chemokines, and chemokine receptors. The data revealed that 26 of 47 immune checkpoints such as LAG3, CTLA4, PDCD1, and CD274 were differentially expressed between high-risk and low-risk groups ($P < 0.05$, **Figure 8D**). Twenty-one of 44 chemokines and 11 of 18 chemokine receptors were differentially expressed between the two groups ($P < 0.05$, **Figures 8E, F**). In GEO cohort, similar results were observed that high-risk group had higher immune infiltration than low-risk group (**Supplementary Figure S7**). Cell cycle and Hippo signaling pathway were also more activated in high-risk group. The above results indicated that high-risk and low-risk groups had different TME that may lead to different immune response.

Differential Immune Response to Immunotherapy of Two Groups

As high-risk and low-risk groups displayed distinct TME and expression of immune checkpoints, we speculated that they may have different response to ICB. Therefore, TIDE analysis was applied to calculate TIDE score for two groups in TCGA and GEO cohorts. In TCGA cohort, high-risk group had higher TIDE score than low-risk group, suggesting that low-risk group was more sensitive to ICB (P = 0.012, **Figure 9A**). In addition, high-

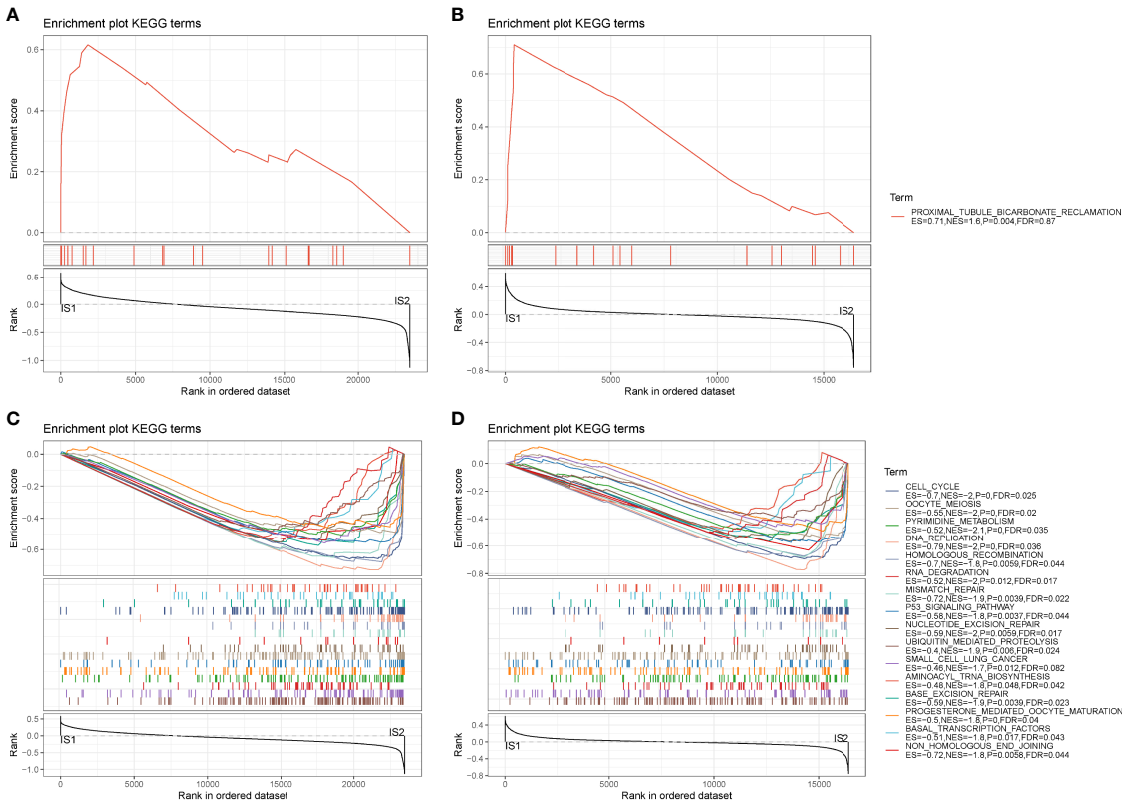

FIGURE 4 | GSEA of hallmark pathways in TCGA-PAAD and GEO cohorts. **(A, B)** Enriched pathways of IS1 in TCGA-PAAD **(A)** and GEO **(B)** cohorts. **(C, D)** Enriched pathways of IS2 in TCGA-PAAD **(C)** and GEO **(D)** cohorts.

risk group had lower score of T cell dysfunction but higher score of T cell exclusion ($P < 0.0001$, **Figures 9B, C**), indicating the different mechanism of immune escape of two groups. Moreover, MDSCs, an immunosuppressive cell type, were highly enriched in high-risk group ($P < 0.0001$, **Figure 9D**). In GEO cohort, the same results were obtained (**Figures 9E–H**), demonstrating that high-risk and low-risk groups had different immune response to immunotherapy. The prognostic model associating with MBCs was robust in predicting the response to immunotherapy. In addition, we also compared the relationship between IS1-2 and existing molecular subtypes and patients in high-risk and low-risk groups. It can be observed that patients in high-risk group mainly came from IS2, C1 and C2 immune subtypes, whereas patients in low-risk group mainly came from IS1, C3 and C6 immune subtypes (**Supplementary Figure S8A**). By mapping the four key genes into the string database, it can be observed that there was no direct interaction between them, which suggested that these genes may each perform different functions (**Supplementary Figure S8B**). Analysis on the relationship between the expression of these genes and MBCs showed that ANLN had a significant positive correlation with MBCs, and ARNTL2 and SERPINB5 had a significant negative correlation with MBCs (**Supplementary Figure S8C**).

Identifying Subgroups of MBCs Related to PAAD Prognosis

In the previous section, we found that MBCs were significantly associated with PAAD prognosis. To further evaluate the function of MBCs in PAAD development, we used unsupervised consensus clustering for 554 MBCs based on markers of MBCs. MBCs were classed into three subgroups (MBC_0, MBC_1, and MBC_2). Three subgroups expressed different markers. MBC_0 only expressed FCGR2A; MBC_1 only expressed FCGR2A, VSIR, and CXCL1; and MBC_2 only expressed CD40, CDK2, LTB, and CXCL16 (**Supplementary Figure S9A**). The three subgroups had distinct enrichment on the top 20 enriched pathways, possibly indicating different function of them (**Figure 10A**).

To understand their development and distribution, we performed monocle to reveal the cell trajectory of the three subgroups (**Figures 10B–D**). All three classes of MBCs enriched in tumor cells and slightly existed in normal cells (**Figure 10B**). State 1 located in the early pseudotime and state 3 located in the late pseudotime (**Figures 10C, D**). Of the distribution of three classes of MBCs, MBC_2 was more enriched in the early pseudotime, whereas MBC_1 majorly located in the late pseudotime (**Supplementary Figure S9B**). The expression

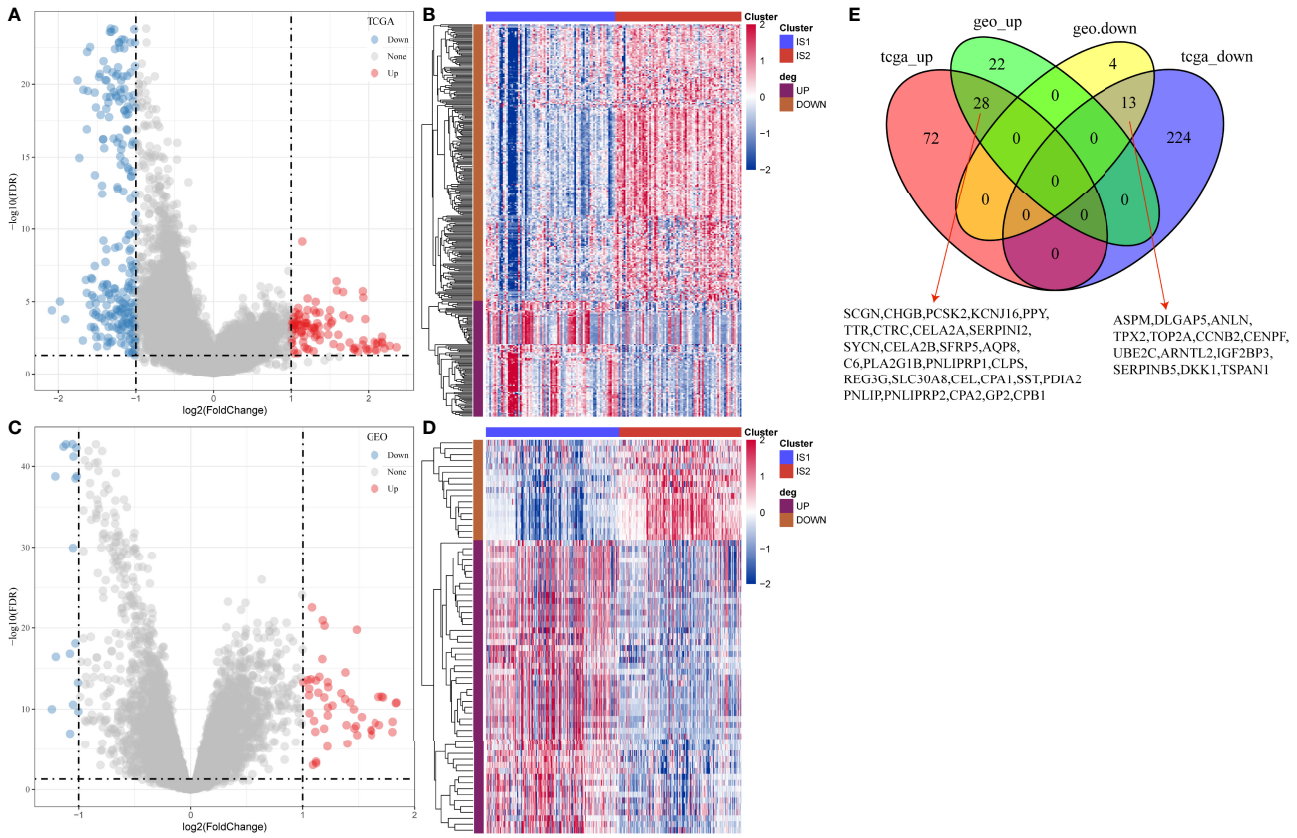

FIGURE 5 | Differential analysis between IS1 and IS2. **(A)** Volcano plot of DEGs in TCGA-PAAD cohort. **(B)** Unsupervised consensus clustering for TCGA-PAAD samples based on DEGs. **(C)** Volcano plot of DEGs in GEO cohort. **(D)** Unsupervised consensus clustering for GEO samples based on DEGs. **(E)** Venn plot of upregulated and downregulated genes in TCGA-PAAD and GEO cohorts.

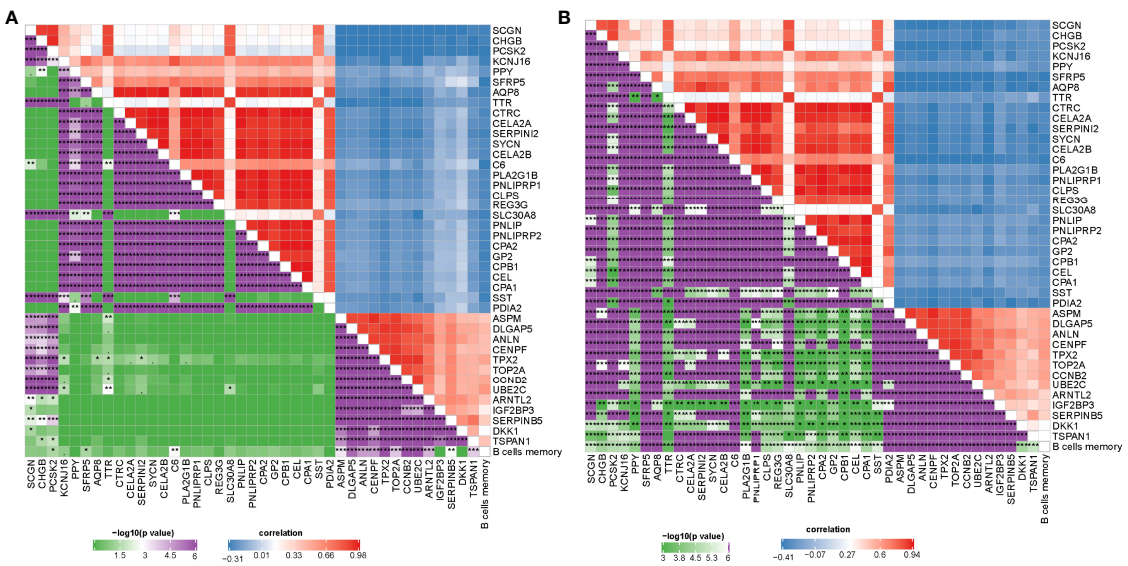

FIGURE 6 | Pearson correlation analysis between MBCs and 41 key DEGs in TCGA-PAAD **(A)** and GEO **(B)** cohorts. Blue indicates negative correlation and red indicates positive correlation. *$P < 0.05$, **$P < 0.01$, and ***$P < 0.001$.

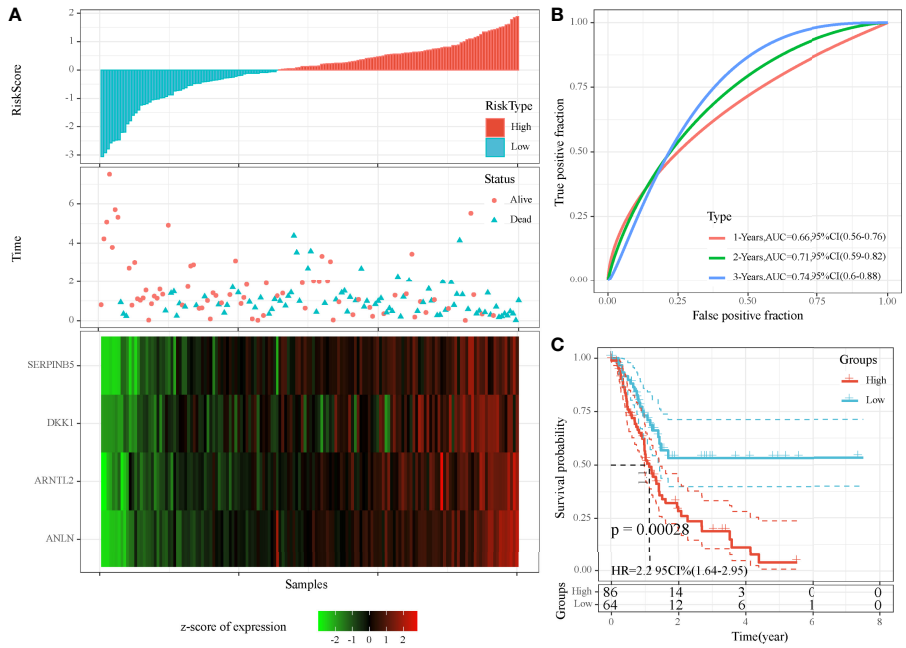

FIGURE 7 | Evaluation of the four-gene prognostic model in TCGA-PAAD cohort. **(A)** The distribution of PAAD samples and expression of prognostic genes ranking by risk score. **(B)** ROC curve of the prognostic model in predicting 1-, 3-, and 5-year overall survival. **(C)** Kaplan–Meier survival plot of high-risk and low-risk groups. Log-rank test was conducted.

trajectory of seven markers also obviously varied by pseudotime (**Supplementary Figure S9C**).

We further analyzed whether the two types of classes (IS1 and IS2, high-risk and low-risk groups) had a difference on the distribution of different MBCs using CIBERSORT. In TCGA-PAAD dataset, only MBC_0 and MBC_1 were observed. We found a significant difference of both MBC_0 and MBC_1 enrichment between IS1 and IS2 ($P < 0.0001$, **Figures 11A, B**). Specifically, IS1 had higher enrichment of MBC_0 but lower enrichment of MBC_1, suggesting that MBC_0 may be a protective factor of PAAD prognosis. The supposal was further illustrated in high-risk and low-risk groups, as low-risk group had a higher proportion of MBC_0 compared with high-risk group ($P < 0.0001$, **Figure 11C**). However, MBC_1 was highly enriched in high-risk group ($P < 0.0001$, **Figure 11D**), which was consistent with the above results.

DISCUSSION

On the basis of the analysis of single-cell data, we discovered that MBCs were significantly associated with PAAD prognosis. Therefore, we constructed two molecular subtypes based on the markers of MBCs. IS1 and IS2 showed differential overall survival and clinical features, supporting that MBCs played an important role in PAAD development. To identify functional pathways that may be involved in prognosis, we analyzed the enriched pathways in IS1 and IS2 through GSEA. Tumor-related pathways such as cell cycle, DNA replication, mismatch repair, and p53 signaling pathway were highly enriched in IS2 group, suggesting that these pathways may result in worse prognosis of IS2.

A total of 41 DEGs were found between IS1 and IS2, and they were all observed to be positively or negatively associated with the enrichment of MBCs. It could be speculated that these DEGs were possibly involved in PAAD development and MBC regulation. With this hypothesis, we screened four prognostic genes (ANLN, ARNTL2, SERPINB5, and DKK1) based on 41 DEGs and constructed a four-gene prognostic model. According to the expression of four genes, risk score was calculated for each sample. PAAD samples were divided into high-risk and low-risk groups with distinct overall survival, which demonstrated that four genes were involved in cancer progression. It was worth mentioning that the prognostic relationship of these four genes in pancancer can be assessed by SangerBox online analysis platform (http://vip.sangerbox.com). We observed that these genes not only were significantly related to prognosis in pancreatic cancer but also were associated with poor prognosis in many tumors, especially lung cancer. These genes showed significant prognostic differences in lung cancer. Moreover, ANLN, SERPINB5, and ARNTL2 were also associated with poor prognosis of RCC. DDK1 and ARNTL2 were significantly associated with poor prognosis of low-grade gliomas (**Supplementary Figures S10A–D**). Previous studies have reported that these four genes biomarkers for predicting prognosis in various cancer types. Especially, DKK1 was widely

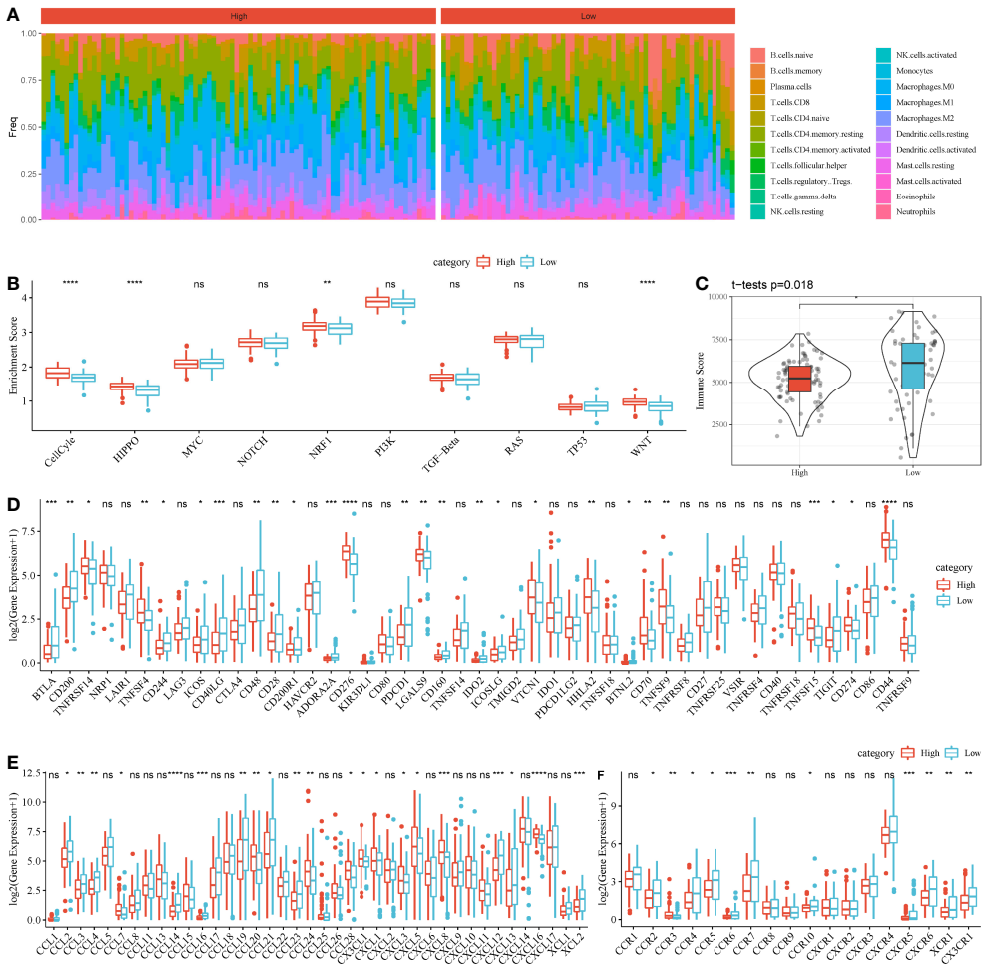

FIGURE 8 | Comparison of TME between high-risk and low-risk groups in TCGA-PAAD cohort. **(A)** A heatmap describing distribution of 22 immune cells in high-risk and low-risk groups. **(B)** Enrichment score of 10 oncogenic pathways in high-risk and low-risk groups. **(C)** Immune score of high-risk and low-risk groups. **(D–F)** Expression of immune checkpoints **(D)**, chemokines **(E)**, and chemokine receptors **(F)** in two groups. Student *t*-test was performed between two groups. ns, no significance. **P* < 0.05, ***P* < 0.01, ****P* < 0.001, and *****P* < 0.0001.

reported to participate cancer development and metastasis. In breast cancer, DKK1 stimulates the metastasis of breast-to-bone through regulating WNT signaling pathway (28). However, DKK1 inhibits lung metastasis through suppressing WNT/$Ca2^{+}$-CaMKII-NF-κB signaling, indicating a dual role of DKK1 in the metastasis of breast cancer (28). DKK1 is commonly overexpressed in many cancer types. Betella et al. proposed that DKK1 overexpression may contribute to exhaustion of effective T cells and advanced clinical stages and unfavorable prognosis in ovarian cancer (29). In our study, DKK1 was also higher-expressed in high-risk group. Moreover, a strong correlation was also found between DKK1 and MDSCs (30), where DKK1 targeted β-catenin in MDSCs in pancreatic cancer. High-risk group had a higher infiltration of MDSCs, indicating that DKK1 may have an immunomodulatory role by targeting MDSCs.

ARNTL2 was identified as a potential biomarker to predict cancer progression of colorectal cancer (31). In clear cell renal cell carcinoma, high expression of ARNTL2 is correlated with worse overall survival (32), which is consistent with our research. In addition, the group presenting high expression of ARNTL2 manifested high immune infiltration and high expression of immune checkpoints such as PD-L1 and CTLA4 (32). However, our result showed that high-risk group with high ARNTL2 expression had lower immune infiltration and lower expression of immune checkpoints, suggesting that ARNTL2 may function differentially across cancer types.

ANLN was considered to play an oncogenic role in cancer development. Zhou et al. demonstrated that knockdown of ANLN in breast cancer cell lines inhibits the proliferation of cancer cells and blocked cell cycle progression (33). Wang et al. found that ANLN expressed was significantly upregulated in

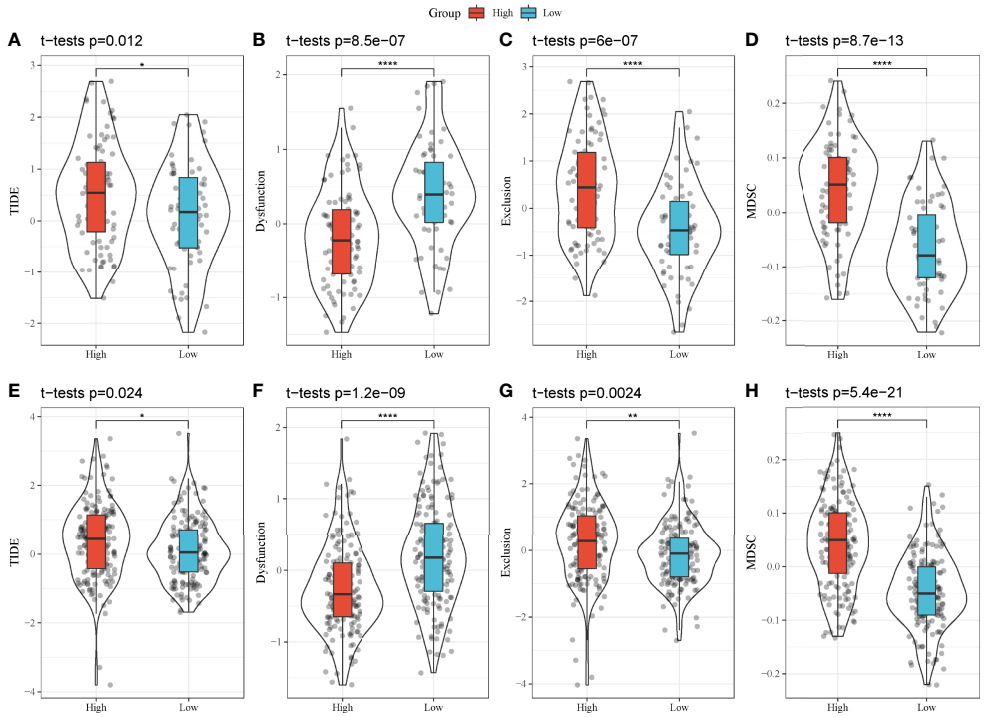

FIGURE 9 | TIDE analysis of high-risk and low-risk groups. **(A–H)** Comparison of TIDE score **(A, E)**, T cell dysfunction **(B, F)**, T cell exclusion **(C, G)** and enrichment score of MDSCs **(D, H)** between high-risk and low-risk groups in TCGA-PAAD **(A–D)** and GEO **(E–H)** cohorts. *$P < 0.05$, **$P < 0.01$, and ****$P < 0.0001$.

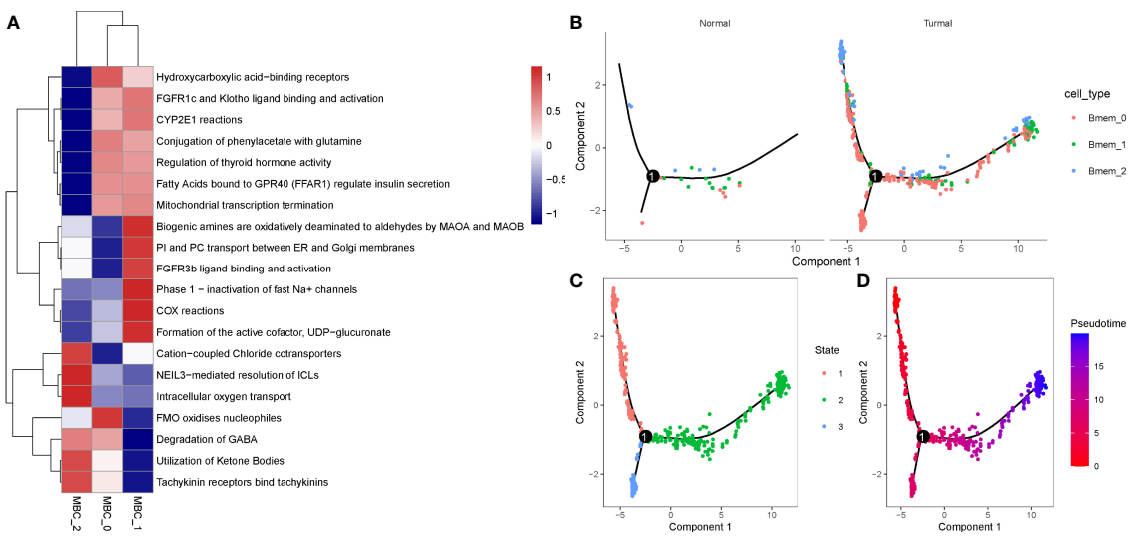

FIGURE 10 | Identification of three MBC subgroups. **(A)** The top 20 enriched pathways of three MBC subgroups. Blue indicates low enrichment and red indicates high enrichment. **(B)** The distribution of MBC_0, MBC_1, and MBC_2 in normal and tumor samples. **(C, D)** Cell trajectory of state1, state2, and state3. Red to blue indicates pseudotime from early to late.

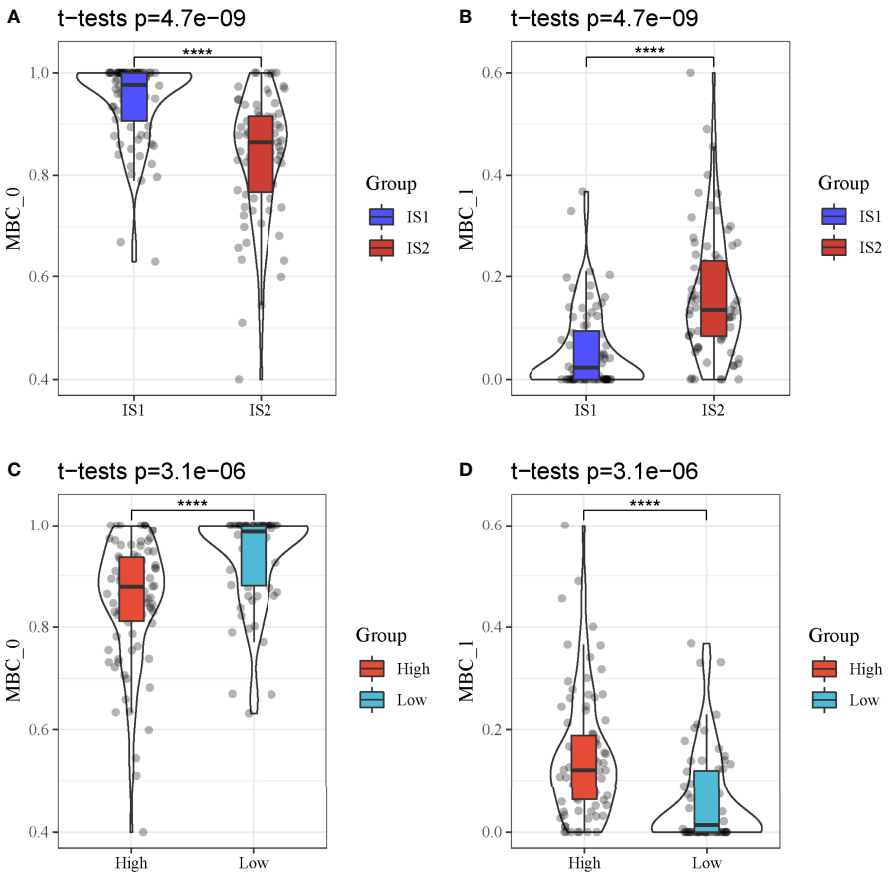

FIGURE 11 | MBC enrichment of different groups in TCGA-PAAD cohort. **(A, B)** Comparison of the enrichment of MBC_0 and MBC_1 between IS1 and IS2. **(C, D)** Comparison of the enrichment of MBC_0 and MBC_1 between high-risk and low-risk groups. ****$P < 0.0001$.

pancreatic cancer, and its downregulation greatly suppresses cell proliferation and migration (34), which illustrated the prognostic value of ANLN in pancreatic cancer.

SERPINB5 has both suppressive and promotive function on cancer progression, according to previous research. In colorectal cancer, SERPINB5 overexpression is associated with poor overall survival and progression-free survival (35). Mardin et al. illustrated that upregulated SERPINB5 expression was correlated with increased metastasis resulted from SERPINB5 methylation in pancreatic ductal adenocarcinoma (36). The above observations provided evidence that SERPINB5 can serve as a prognostic biomarker for pancreatic cancer.

Overall, these four prognostic genes identified in our research have been reported to be involved in cancer development. They all could serve as prognostic biomarkers in pancreatic cancer. Our study constructed the four-gene prognostic signature that was more accurate to predict prognosis. In addition, TIDE analysis proved that the signature has the potential to guide ICB and that patients with PAAD could benefit more from personalized therapy.

Furthermore, we identified three subgroups of MBCs that had differential molecular features. MBC_0 and MBC_1 had differential enrichment in IS1 and IS2, high-risk and low-risk groups. Although we found that higher enrichment of MBCs was associated with more favorable prognosis, it was not applicable to all MBCs. MBC_0 was identified as a group of protective cells for inhibiting cancer progression as its higher enrichment in IS1 and low-risk group. However, further assessment and experiments are needed to further analyze the role of MBCs in pancreatic cancer.

CONCLUSIONS

In conclusion, by exploring TME of pancreatic cancer using single-cell analysis, we found that MBCs were an important group of cells involved in cancer development of pancreatic cancer. The four-gene prognostic model based on markers of MBCs could predict overall survival and guide personalized therapy for pancreatic cancer patients. Importantly, we discovered two subgroups of MBCs (MBC_0 and MBC_1) with strong correlation with PAAD prognosis. Further studies are needed to explore the mechanism of MBC_0 and MBC_1 in PAAD progression.

DATA AVAILABILITY STATEMENT

The original contributions presented in the study are included in the article/**Supplementary Material**. Further inquiries can be directed to the corresponding author.

AUTHOR CONTRIBUTIONS

WH and XY conceptualized and designed the research; XY drafted the manuscript and got agreement to be accountable for all aspects of the work in ensuring that questions related to the accuracy or integrity of any part of the work are appropriately investigated and resolved; SZ and JL contributed to date acquisition; YL analyzed data; WH and XY interpreted data; XY revised the manuscript for important intellectual content. All authors contributed to the article and approved the submitted version.

SUPPLEMENTARY MATERIAL

The Supplementary Material for this article can be found online at: https://www.frontiersin.org/articles/10.3389/fendo.2022.883548/full#supplementary-material

Supplementary Figure 1. | (A) A work flow chart of this study. **(B, C)** Preprocessing of single-cell data. Quality control before **(B)** and after **(C)** preprocessing.

Supplementary Figure 2. | Horizontal axis indicates samples. **(A)** Single cell counts of raw data and clean data. **(B, C)** Principle component analysis (PCA) of single-cell data. PCA plots before **(D)** and after **(E)** data preprocessing in GSE cohorts.

Supplementary Figure 3. | The distribution of different clinical features and MBCs in IS1 and IS2.

Supplementary Figure 4. | LASSO Cox regression analysis for optimizing the prognostic model. **(A)** The coefficients of each gene with the changing lambda value. Red dotted line indicates lambda = 0.0661. **(B)** 95% confidence interval of partial likelihood deviance of different lambda values. Red dot indicates lambda = 0.0661.

Supplementary Figure 5. | Evaluation of the 4-gene prognostic model in GEO cohort. **(A)** The distribution of PAAD samples and expression of prognostic genes ranking by risk score. **(B)** ROC curve of the prognostic model in predicting 1-year, 3-year and 5-year overall survival. **(C)** Kaplan-Meier survival plot of high-risk and low-risk groups. Log-rank test was conducted.

Supplementary Figure 6. | Evaluation of the 4-gene prognostic model in ICGC-AU cohort. **(A)** The distribution of PAAD samples and expression of prognostic genes ranking by risk score. **(B)** ROC curve of the prognostic model in predicting 1-year, 3-year and 5-year overall survival. **(C)** Kaplan-Meier survival plot of high-risk and low-risk groups. Log-rank test was conducted.

Supplementary Figure 7. | Comparison of TME between high-risk and low-risk groups in GEO cohort. **(A)** A heatmap describing distribution of 22 immune cells in high-risk and low-risk groups. **(B)** Enrichment score of 10 oncogenic pathways in high-risk and low-risk groups. **(C)** Immune score of high-risk and low-risk groups. **(D–F)** Expression of immune checkpoints **(D)**, chemokines **(E)** and chemokine receptors **(F)** in two groups. Student t test was performed between two groups. ns, no significance. *P < 0.05, **P < 0.01, ***P < 0.001, ****P < 0.0001.

Supplementary Figure 8. | (A) Association between IS1-2 and existing molecular subtypes and patients in high-risk and low-risk groups. **(B)** Interaction between four key genes. **(C)** Relationship between the expression of four key genes and memory B cells.

Supplementary Figure 9. | (A) Markers of MBC_0, MBC_1 and MBC_2. **(B)** The distribution of three MBC subgroups in different pseudotime. **(C)** The distribution of seven markers in different pseudotime.

Supplementary Figure 10. | (A) Prognostic difference forest map of DDK1 in Pan cancer. **(B)** Prognostic difference forest map of ANLN in Pan cancer. **(C)** Prognostic difference forest map of SERPINB5 in Pan cancer. **(D)** Prognostic difference forest map of ARNTL2 in Pan cancer.

REFERENCES

1. Sung H, Ferlay J, Siegel RL, Laversanne M, Soerjomataram I, Jemal A, et al. Global Cancer Statistics 2020: GLOBOCAN Estimates of Incidence and Mortality Worldwide for 36 Cancers in 185 Countries. *CA: Cancer J Clin* (2021) 71(3):209–49. doi: 10.3322/caac.21660
2. Ilic M, Ilic I. Epidemiology of Pancreatic Cancer. *World J Gastroenterol* (2016) 22(44):9694–705. doi: 10.3748/wjg.v22.i44.9694
3. Wong MCS, Jiang JY, Liang M, Fang Y, Yeung MS, Sung JJY, et al. Global Temporal Patterns of Pancreatic Cancer and Association With Socioeconomic Development. *Sci Rep* (2017) 7(1):3165. doi: 10.1038/s41598-017-02997-2
4. McGuigan A, Kelly P, Turkington RC, Jones C, Coleman HG, McCain RS, et al. Pancreatic Cancer: A Review of Clinical Diagnosis, Epidemiology, Treatment and Outcomes. *World J Gastroenterol* (2018) 24(43):4846–61. doi: 10.3748/wjg.v24.i43.4846
5. Siegel RL, Miller KD, Jemal A. Cancer Statistics, 2018. *CA: Cancer J Clin* (2018) 68(1):7–30. doi: 10.3322/caac.21442
6. Ren B, Cui M, Yang G, Wang H, Feng M, You L, et al. Tumor Microenvironment Participates in Metastasis of Pancreatic Cancer. *Mol Cancer* (2018) 17(1):108. doi: 10.1186/s12943-018-0858-1
7. Morrison AH, Byrne KT, Vonderheide RH. Immunotherapy and Prevention of Pancreatic Cancer. *Trends Cancer* (2018) 4(6):418–28. doi: 10.1016/j.trecan.2018.04.001
8. Zhao X, Li H, Lyu S, Zhai J, Ji Z, Zhang Z, et al. Single-Cell Transcriptomics Reveals Heterogeneous Progression and EGFR Activation in Pancreatic Adenosquamous Carcinoma. *Int J Biol Sci* (2021) 17(10):2590–605. doi: 10.7150/ijbs.58886
9. Gribov A, Sill M, Lück S, Rücker F, Döhner K, Bullinger L, et al. SEURAT: Visual Analytics for the Integrated Analysis of Microarray Data. *BMC Med Genomics* (2010) 3:21. doi: 10.1186/1755-8794-3-21
10. Stratford JK, Yan F, Hill RA, Major MB, Graves LM, Der CJ, et al. Genetic and Pharmacological Inhibition of TTK Impairs Pancreatic Cancer Cell Line Growth by Inducing Lethal Chromosomal Instability. *PloS One* (2017) 12(4):e0174863. doi: 10.1371/journal.pone.0174863
11. Zhang G, He P, Tan H, Budhu A, Gaedcke J, Ghadimi BM, et al. Integration of Metabolomics and Transcriptomics Revealed a Fatty Acid Network Exerting Growth Inhibitory Effects in Human Pancreatic Cancer. *Clin Cancer Res* (2013) 19(18):4983–93. doi: 10.1158/1078-0432.CCR-13-0209
12. Chen DT, Davis-Yadley AH, Huang PY, Husain K, Centeno BA, Permuth-Wey J, et al. Prognostic Fifteen-Gene Signature for Early Stage Pancreatic Ductal Adenocarcinoma. *PloS One* (2015) 10(8):e0133562. doi: 10.1371/journal.pone.0133562
13. Yang S, He P, Wang J, Schetter A, Tang W, Funamizu N, et al. A Novel MIF Signaling Pathway Drives the Malignant Character of Pancreatic Cancer by Targeting Nr3c2. *Cancer Res* (2016) 76(13):3838–50. doi: 10.1158/0008-5472.CAN-15-2841
14. Law CW, Alhamdoosh M, Su S, Dong X, Tian L, Smyth GK, et al. *RNA-Seq Analysis is Easy as 1-2-3 With Limma, Glimma and edgeR. F1000Res 5*. (2016).
15. Newman AM, Liu CL, Green MR, Gentles AJ, Feng W, Xu Y, et al. Robust Enumeration of Cell Subsets From Tissue Expression Profiles. *Nat Methods* (2015) 12(5):453–7. doi: 10.1038/nmeth.3337

16. Zhang X, Lan Y, Xu J, Quan F, Zhao E, Deng C, et al. CellMarker: A Manually Curated Resource of Cell Markers in Human and Mouse. *Nucleic Acids Res* (2019) 47(D1):D721–8. doi: 10.1093/nar/gky900
17. Subramanian A, Tamayo P, Mootha VK, Mukherjee S, Ebert BL, Gillette MA, et al. Gene Set Enrichment Analysis: A Knowledge-Based Approach for Interpreting Genome-Wide Expression Profiles. *Proc Natl Acad Sci U.S.A.* (2005) 102(43):15545–50. doi: 10.1073/pnas.0506580102
18. Barbie DA, Tamayo P, Boehm JS, Kim SY, Moody SE, Dunn IF, et al. Systematic RNA Interference Reveals That Oncogenic KRAS-Driven Cancers Require TBK1. *Nature* (2009) 462(7269):108–12. doi: 10.1038/nature08460
19. Sanchez-Vega F, Mina M, Armenia J, Chatila WK, Luna A, La KC, et al. Oncogenic Signaling Pathways in The Cancer Genome Atlas. *Cell* (2018) 173 (2):321–337.e310. doi: 10.1016/j.cell.2018.03.035
20. Wilkerson MD, Hayes DN. ConsensusClusterPlus: A Class Discovery Tool With Confidence Assessments and Item Tracking. *Bioinf (Oxford England)* (2010) 26(12):1572–3. doi: 10.1093/bioinformatics/btq170
21. Ritchie ME, Phipson B, Wu D, Hu Y, Law CW, Shi W, et al. Limma Powers Differential Expression Analyses for RNA-Sequencing and Microarray Studies. *Nucleic Acids Res* (2015) 43(7):e47. doi: 10.1093/nar/gkv007
22. Friedman J, Hastie T, Tibshirani R. Regularization Paths for Generalized Linear Models *via* Coordinate Descent. *J Stat Softw* (2010) 33(1):1–22. doi: 10.18637/jss.v033.i01
23. Blanche P, Dartigues JF, Jacqmin-Gadda H. Estimating and Comparing Time-Dependent Areas Under Receiver Operating Characteristic Curves for Censored Event Times With Competing Risks. *Stat Med* (2013) 32 (30):5381–97. doi: 10.1002/sim.5958
24. Jiang P, Gu S, Pan D, Fu J, Sahu A, Hu X, et al. Signatures of T Cell Dysfunction and Exclusion Predict Cancer Immunotherapy Response. *Nat Med* (2018) 24(10):1550–8. doi: 10.1038/s41591-018-0136-1
25. Chen B, Khodadoust MS, Liu CL, Newman AM, Alizadeh AA. Profiling Tumor Infiltrating Immune Cells With CIBERSORT. *Methods Mol Biol (Clifton NJ)* (2018) 1711:243–59. doi: 10.1007/978-1-4939-7493-1_12
26. Griss J, Viteri G, Sidiropoulos K, Nguyen V, Fabregat A, Hermjakob H. ReactomeGSA - Efficient Multi-Omics Comparative Pathway Analysis. *Mol Cell Proteomics: MCP* (2020) 19(12):2115–25. doi: 10.1074/mcp.TIR120.002155
27. Thorsson V, Gibbs DL, Brown SD, Wolf D, Bortone DS, Ou Yang TH, et al. The Immune Landscape of Cancer. *Immunity* (2018) 48(4):812–830 e814. doi: 10.1016/j.immuni.2018.03.023
28. Zhuang X, Zhang H, Li X, Li X, Cong M, Peng F, et al. Differential Effects on Lung and Bone Metastasis of Breast Cancer by Wnt Signalling Inhibitor DKK1. *Nat Cell Biol* (2017) 19(10):1274–85. doi: 10.1038/ncb3613
29. Betella I, Turbitt WJ, Szul T, Wu B, Martinez A, Katre A, et al. Wnt Signaling Modulator DKK1 as an Immunotherapeutic Target in Ovarian Cancer. *Gynecol Oncol* (2020) 157(3):765–74. doi: 10.1016/j.ygyno.2020.03.010
30. D'Amico L, Mahajan S, Capietto AH, Yang Z, Zamani A, Ricci B, et al. Dickkopf-Related Protein 1 (Dkk1) Regulates the Accumulation and Function of Myeloid Derived Suppressor Cells in Cancer. *J Exp Med* (2016) 213(5):827–40. doi: 10.1084/jem.20150950
31. Mazzoccoli G, Pazienza V, Panza A, Valvano MR, Benegiamo G, Vinciguerra M, et al. ARNTL2 and SERPINE1: Potential Biomarkers for Tumor Aggressiveness in Colorectal Cancer. *J Cancer Res Clin Oncol* (2012) 138 (3):501–11. doi: 10.1007/s00432-011-1126-6
32. Wang S, Ma X, Ying Y, Sun J, Yang Z, Li J, et al. Upregulation of ARNTL2 is Associated With Poor Survival and Immune Infiltration in Clear Cell Renal Cell Carcinoma. *Cancer Cell Int* (2021) 21(1):341. doi: 10.1186/s12935-021-02046-z
33. Zhou W, Wang Z, Shen N, Pi W, Jiang W, Huang J, et al. Knockdown of ANLN by Lentivirus Inhibits Cell Growth and Migration in Human Breast Cancer. *Mol Cell Biochem* (2015) 398(1-2):11–9. doi: 10.1007/s11010-014-2200-6
34. Wang A, Dai H, Gong Y, Zhang C, Shu J, Luo Y, et al. ANLN-Induced EZH2 Upregulation Promotes Pancreatic Cancer Progression by Mediating miR-218-5p/LASP1 Signaling Axis. *J Exp Clin Cancer Res: CR* (2019) 38(1):347. doi: 10.1186/s13046-019-1340-7
35. Baek JY, Yeo HY, Chang HJ, Kim KH, Kim SY, Park JW, et al. Serpin B5 is a CEA-Interacting Biomarker for Colorectal Cancer. *Int J Cancer* (2014) 134 (7):1595–604. doi: 10.1002/ijc.28494
36. Mardin WA, Petrov KO, Enns A, Senninger N, Haier J, Mees ST. SERPINB5 and AKAP12 - Expression and Promoter Methylation of Metastasis Suppressor Genes in Pancreatic Ductal Adenocarcinoma. *BMC Cancer* (2010) 10:549. doi: 10.1186/1471-2407-10-549

Conflict of Interest: The authors declare that the research was conducted in the absence of any commercial or financial relationships that could be construed as a potential conflict of interest.

frontiers | Frontiers in Endocrinology

ORIGINAL RESEARCH
published: 08 July 2022
doi: 10.3389/fendo.2022.894754

Comprehensive Analysis of Immune-Related Metabolic Genes in Lung Adenocarcinoma

*Fangfang Li, Chun Huang, Lingxiao Qiu, Ping Li, Jiang Shi and Guojun Zhang**

Department of Respiratory Medicine, The First Affiliated Hospital of Zhengzhou University, Zhengzhou, China

Purpose: The immunotherapy of lung adenocarcinoma (LUAD) has received much attention in recent years and metabolic reprogramming is linked to immune infiltration in the tumor microenvironment. Therefore, it is indispensable to dissect the role of immune-related metabolic genes in lung adenocarcinoma.

Methods: In this study, we screened immune-related genes by Pearson correlation. The function of these genes was explored by gene ontology (GO) and KEGG (Kyoto Encyclopedia of Genes and Genomes) enrichment analysis. The differently expressed immune-related genes were analyzed by Limma. Furthermore, the LUAD patients were clustered based on immune-related genes through consensus clustering. The Unicox was used to identify survival-immune-related metabolic genes. The Least Absolute Shrinkage and Selection Operator (LASSO) regression analysis was used to optimize the gene sets. A prediction model was constructed and tested. The potential therapeutic target was selected based on two criteria, these immune-related metabolic genes that were highly expressed in tumor tissues and negatively correlated with the survival of patients in LUAD. Quantitative real-time PCR (qRT-PCR) was used for *in vitro* experimental validations.

Results: We identified 346 immune-related genes, mainly involved in arachidonic acid metabolism and peroxisome proliferator-activated receptor (PPAR) signaling. Moreover, a total of 141 immune-related genes were dysregulated between tumor and normal tissues. We clustered three subtypes of LUAD based on immune-related metabolic genes and these subtypes exhibited different survival and immune status. We found Ribonucleotide Reductase Regulatory Subunit M2 (*RRM2*) as a potential therapeutic target, which is positively correlated with the cyclin-dependent kinase family of genes.

Conclusion: We comprehensively analyzed the immune-related metabolic genes in LUAD. *RRM2* was determined as a promising metabolic checkpoint for lung adenocarcinoma.

Keywords: lung cancer, immune, metabolic, TCGA, immunotherapy

OPEN ACCESS

Edited by:
Rick Francis Thorne,
The University of Newcastle, Australia

Reviewed by:
Niaz Muhammad,
Minhaj University Lahore, Pakistan
Ranjha Khan,
University of Science and Technology of China, China

***Correspondence:**
Guojun Zhang
zgj@zzu.edu.cn

Specialty section:
This article was submitted to Cancer Endocrinology, a section of the journal Frontiers in Endocrinology

Received: *12 March 2022*
Accepted: *06 June 2022*
Published: *08 July 2022*

Citation:
Li F, Huang C, Qiu L, Li P, Shi J and Zhang G (2022) Comprehensive Analysis of Immune-Related Metabolic Genes in Lung Adenocarcinoma. Front. Endocrinol. 13:894754. doi: 10.3389/fendo.2022.894754

Abbreviations: TCGA, The Cancer Genome Atlas; KEGG, Kyoto Encyclopedia of Genes and Genomes; GO, Gene Ontology; DEGs, differentially expressed genes; LUAD, Lung adenocarcinoma; ssGSEA, single sample gene set enrichment analysis; TME, tumor microenvironment; PPI, protein-protein interaction.

INTRODUCTION

Lung cancer is one of the most common causes of cancer-related mortality. Adenocarcinoma is the most common histological type of lung cancer (1, 2). Lung adenocarcinoma (LUAD) has an unfavorable 5-year survival rate which makes only 15% (3–5). In the past few decades, surgical resection, chemotherapy, radiotherapy, and targeted molecular therapies have been carried out in clinical practices to treat LUAD. However, most LUAD patients are usually diagnosed at advanced and late stages, thus having poor prognosis. In recent years the relationship among cancer immunotherapy, tumor microenvironment, and metabolism has gotten much of attention. Hence, comprehensively understanding the role of immune-related metabolic genes involved in the occurrence and development of LUAD is crucial for the diagnositc and prognositic prospetcs.

The tumor microenvironment (TME) is the cellular environment in which the tumor develops. TME is closely related to the occurrence and development of tumors (6, 7). It included inflammatory and stromal cells that infiltrate the tumors. Lymphocytes infiltrating tumor tissues have been discovered for more than hundred years. After 1960, people began to consider the relationship between immunity and prognosis (8). It has been found that the infiltration of T cells (80%) in the majority of tumors is positively correlated with the tumor metastasis (9). Aberrant cellular metabolism is emerging as a novel therapeutic target, and the interplay between metabolic remodeling and immune regulation in cancer represents a potential area of investigations (10, 11).

Abnormal activation of oncogenic genes, such as Myc and Ras can directly regulate intracellular metabolic pathways (12). Moreover, immune cells can also change metabolic pathways and further affect cellular functions (13). The abnormal metabolism of tumors not only enables tumors to survive in an environment of hypoxia and nutrient deficiency, but the products of metabolism can inhibit immune response, promote the formation of immunosuppressive cells, and help tumors evade host immune killing (14). It has been found that in acute lymphoblastic leukemia, proliferating T and B cells exhibit abnormal metabolic stress (15, 16). Similarly, mounting evidence has confirmed that reprogramming the tumor immune microenvironment is a necessary process that drives LUAD metastasis (17). This suggests that the metabolic disorder of cancer cells may be treated by targeting some genes (18).

In this study, we identified 346 immune-related genes. Among these, 141 genes were found to be dysregulated between normal and tumor tissues. Three clusters of LUAD samples were based on immune-related metabolic genes and different clusters exhibited distinct survival and immune status. Moreover, we constructed and validated a prediction model and identified *RRM2* as a potential metabolic target which was positively correlated with the cyclin-dependent kinase (CDK) family of genes.

MATERIALS AND METHODS

Data Preprocessing

The mRNA sequencing and clinical data of 535 LUAD samples and 59 normal samples were downloaded from the TCGA data portal. The metabolism-related genes were downloaded from published work (19). The immune-related genes were downloaded from an online website (https://www.immport.org/). Low expressed genes were excluded from the study and the data was normalized to log2 (tpm+1) (average expression after normalization <0.5). Finally, 346 immune-related metabolic genes were selected by cor test using the Pearson correlation method ($P<0.05$, $|R|>0.2$).

GO and KEGG Enrichment Analysis and PPI Network Construction of Immune-Related Metabolic Genes

We divided 346 differentially expressed genes (DEGs) into up-regulated and down-regulated genes. R was used to perform GO and KEGG enrichment analysis. The "clusterProfiler", "richplot", and "ggplot2" packages were used for analysis (20, 21). The GO analysis was performed to annotate genes and classify up-regulated and down-regulated DEGs. The GO terms consisted of 3 parts: Biological Process (BP), Cellular Component (CC), and Molecular Function (MF). The KEGG database included the systematic analysis, annotation, and visualization of gene functions (22). STRING online website was used to construct a protein-protein interaction (PPI) network for the selected DEGs (23). For PPI analysis, the confidence score was set to > 0.9, and only terms with both p- and q-value of <0.05 were considered significantly enriched. Cytoscape software further analyzed the most closely connected modules and identified the top 10 central genes (24).

Identification of Dysregulated Genes Between Tumor and Normal Tissues

The "limma" package (25) in R was used to identify DEGs between Cancer and adjacent tissue samples. Merely genes with $|\log2\text{fold change}| > 1$ and $P < 0.05$ were considered as DEGs. The "pheatmap" package was used to draw heat maps, and "ggplot2" was used to draw volcano maps.

Consistent Clustering of Immune-Related Metabolic Genes

The immune-related metabolic genes were divided into different clusters by the cell consistency clustering method. We used the "ConsensusClusterPlus" package (100 iterations and 80% resampling rate, http://www.bioconductor.org/) to classify patients with LUAD into different subtypes. The heat map and dela diagram established the optimal number of clusters. The cumulative distribution function (CDF) was plotted to identify the number of best clusters. The Progress Free Survival (PFS) between various clusters was compared. The survival analysis was analyzed by the R package "survival", and the "ggplot2" package was used for plotting.

Immune Characteristics Between Clusters-Expression of Immune-Related Molecules

The expression of immune-related molecules among these clusters with the ESTIMATE algorithm was analyzed by the R "ESTIMATE" package. These immune-related genes regulate

four immune functions these included, antigen presentation, chemokine-related genes, cytokines, and immune checkpoints. "ggplot2" package was used to draw box plots.

Immune Characteristics Between Clusters-Expression of Infiltrating Immune Cells and Clinicopathological Characteristics

Four methods were used to assess the infiltration of immune cells in three clusters. These methods were single-sample gene set enrichment analysis (ssGSEA), Microenvironment Cell Populations (MCP)-counter, CIBERSORT, and Xcell (26–29). The three different immune cell infiltrating clusters were also compared and found their immune scores. We compared the pathological classification proportions between different clusters to further distinguish the differences between different clusters, including T, N, M, clinical drug treatment response, and the pathological stage.

Validation of Prognostic Prediction Based on Immune-Related Metabolic Genes Models

The expression matrix of LUAD was randomly divided into training and test sets. The training set was 70% and the test set was 30%. We used single-factor analysis on the two groups of genes. The genes with $p<0.05$ were selected. The Least Absolute Shrinkage and Selection Operator (LASSO) cox regression method was further optimized through multi-factor COX regression analysis to help us to determine the best number of genes to build a model (30, 31). Moreover, we collected 80 lung cancer samples along with complete survival information and constructed a prognostic model as a control. Finally, the gene's risk score was screened to get a good predictive ability on the patient's survival. The area under the ROC curve (AUC) was used to judge the prognostic model's predictive power. The ten-fold cross-validation based on the "glmnet" package in R was used for lasso penalty Cox regression analysis. The survival analysis was analyzed by R package "survival", while AUC was analyzed by R package "survivalROC".

Identification of Potential Metabolic Checkpoints

First we selected the immune metabolism genes that were highly expressed in the tumor site (logFC>1.5, FDR<0.05), and the immune metabolism genes in the training set that were negatively related to survival ($p \leq 0.01$). Through pan-cancer analysis (https://cistrome.shinyapps.io/timer/) and the expression level analysis of collected clinical samples, we screened out genes with higher expression abundance in tumors. The signaling pathway was determined with criterion (spearman r>2 or<-2, q value< 0.05) using online website cBioPortal (https://www.cbioportal.org/). The selected genes were used to perform GO and KEGG enrichment analyses.

Cell Culture

The different cell lines used in this study were, Human normal lung epithelial cell line (BEAS-2B) A549, NCI-H292, and Calu-3. BEAS-2B cells were purchased from Procell Life Science and Technology Co., Ltd. (Wuhan, China). A549, NCI-H292, and Calu-3 were purchased from the cell bank of the Chinese Academy of Sciences (Shanghai, China). The BEAS-2B cell line was cultured in Dulbecco's Modified Eagle's medium (DMEM; Gibco, Grand Island, NY, USA). The A549 cell line was cultured in Ham's F-12K medium (Gibco) The NCI-H292 cell line was cultured in Roswell Park Memorial Institute-1640 medium (RPMI-1640; Gibco), and the Calu-3 cell line was maintained in modified eagle medium (MEM; Gibco). All media were supplemented with 10% fetal bovine serum (FBS; Gibco) and antibiotics (100 units/ml penicillin and 100 ug/ml streptomycin; Gibco). All cells were incubated in a humidified atmosphere of 5% CO2 at 37°C.

Quantitative Real-Time PCR

Total RNA was isolated from tissues and cells using TrIzol reagent (Gibco) according to the manufacturer's instructions. The extracted RNA was reverse transcribed into complementary DNA using a reverse transcription kit (Takara, Dalian, China). Quantitative real-time PCR (qRT-PCR) was performed using the SYBR-Green PCR kit (Roche Diagnostics, Indianapolis, IN) on a Step One Plus Real-Time PCR system (Applied Biosystems, Foster City, CA). Glyceraldehyde 3-phosphate dehydrogenase (*GAPDH*) was used as an internal control. The results were analyzed using the $2^{-\Delta\Delta Ct}$ method. Primers were synthesized by Sangon Biotech (Shanghai, China). All the primer sequences were listed (**Supplementary Table 1**).

RESULTS

Identification and Function Enrichment Analysis of Immune-Related Metabolic Genes

To identify the immune-related metabolic genes, we obtained 1041 immune genes and 1613 metabolic genes. The general research design and flow of the study was shown (**Figure 1**). The correlation analysis identified 346 immune-related metabolic genes (**Figure S1**). The GO analysis consisted of three parts: BP, CC, and MF. Our results indicated that the immune-related metabolic genes were significantly enriched in the BP-associated organic acid biosynthetic process, carboxylic acid biosynthetic process, and monocarboxylic acid biosynthetic process. For the CC, the immune-related metabolic genes were mainly enriched in the Golgi, lysosomal, and vacuolar lumens. Furthermore, the MF analysis showed that the immune-related metabolic genes were significantly enriched in cofactor binding, oxidoreductase activity, acting on the CH−OH group of donors, and carboxylic acid-binding. The immune-related metabolic genes were found to be involved in Arachidonic acid metabolism, PPAR signaling pathway, and Biosynthesis of amino acids (**Figures 2A, B**). PPI network was established to further dissect the potential mechanism of these genes (**Figure 2C**). Top10 core genes were identified by Cytoscape plug-in cytoHubba: these genes included, *SDC2*, *GPC3*, *GPC1*,

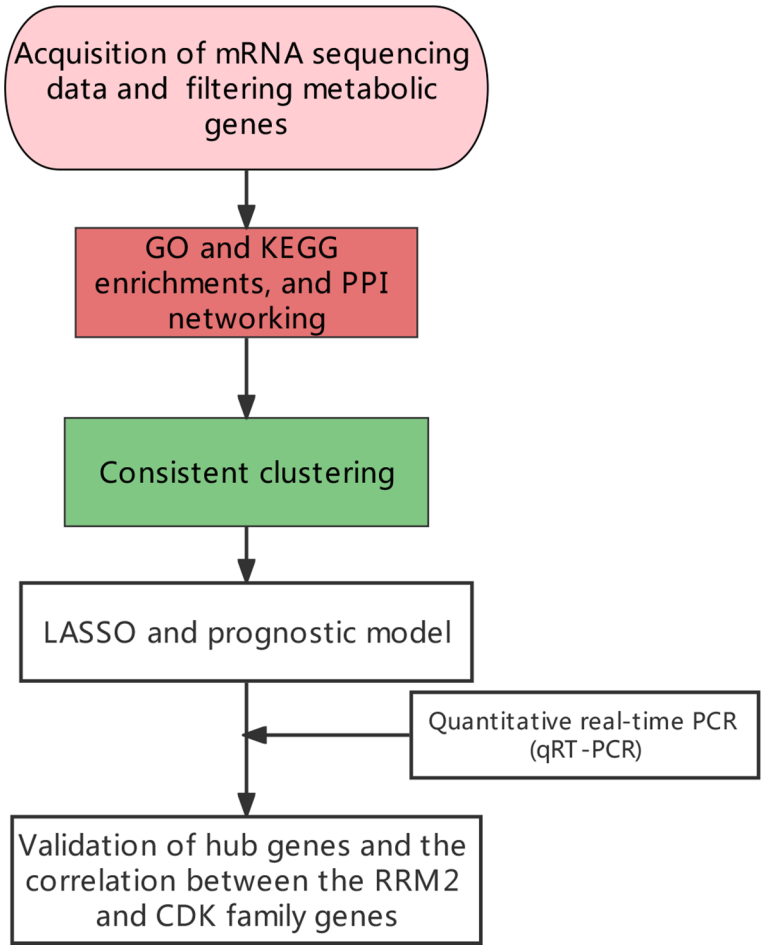

FIGURE 1 | The general research design and flow of the study.

HSPG2, *AGRN*, *GPC2*, *GPC5*, *GPC4*, *GPC6*, and *VCAN* (**Figure 2C**).

The heat map clearly distinguished the immune related metabolic genes in tumor and normal tissues (**Figure S2A**). A total of 141 DEGs were identified (|log2fold change |> 1, P< 0.05). Among these, 72 genes were up-regulated and 69 genes were down-regulated (**Figure S2B**). Then, we performed GO and KEGG enrichment analysis on 141 differential genes (**Figures S2C–F**). It was observed that DEGs were mainly involved in the fatty acid metabolic process; organic hydroxy compound metabolic process and small molecular metabolic process.

Consistent Clustering of Immune-Related Metabolic Genes

Consistent clustering of immune-related genes was performed to unwind metabolic patterns of tumor cells. Tumor samples were divided into different clusters according to the expression patterns of immune-related gens. To determine the optimal cluster number, the cumulative distribution function (CDF) was plotted and three different clusters were identified. Moreover, heat maps were drawn to compare the expression of immune-related metabolic genes among the various clusters (**Figures 3A–C**). Furthermore, the survival status of the three clusters was evaluated by comparing progression-free survival (PFS) and clinicopathological parameters. Our results showed that cluster 2 have prolonged survival in early times (**Figure 3D**). Consistent with these findings, patients in the cluster 2 have lower T, N, M, and stage as well as the status of lymph node metastasis (**Figures S3A–D**). Similarly, a comparatively more proportion of patients had a complete response to treatments in this cluster (**Figure S3E**).

Immune Characteristics of the Three Different Clusters

Furthermore, we were interested to determine immune-related genes in these clusters. We determined those immune-related genes that were involved in antigen-presentation (*B2M, HLA-A, HLA-B, HLA-C, HLA-DPA1, HLA-DQA1, TAP1, TAP2*),

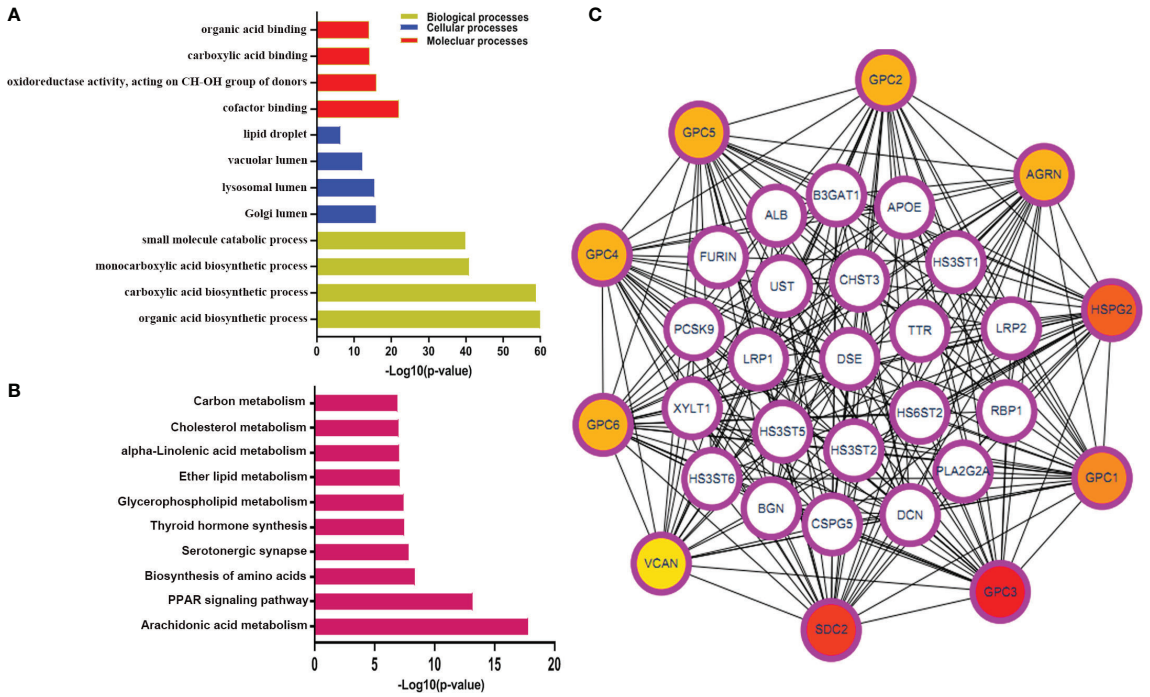

FIGURE 2 | The GO and KEGG pathway analysis for immune-related metabolic genes. **(A, B)** The GO enrichment and KEGG pathway analyses of immune-related metabolic genes; **(C)** The top 10 genes were ordered by the number of nodes. BP, biological process; CC, cellular component; MF, molecular function; KEGG, Kyoto Encyclopedia of Genes and Genomes.

chemokine-related genes (*CCL4, CCL5, CXCL10, CXCL13, CXCL9*), immune checkpoint genes (*CD226, CD274, CD276, CD40, CTLA4, HAVCR2, LAG3, PDCD1*) and genes responsible for the production of cytokines (*GZMB, GZMH, IFNG, IL2, PRF1, TNF*) expressions. We used a box plot for comparison and found that *HLA-DPA1, HLA-DQA1, HLA-B, CXCL13 and CD226* had a high expression within C2 cluster (**Figures 4A–D**).

Moreover, we determined infiltration levels of immune cells in these clusters. We used four reported methods (CIBERSORT, MCP-counter, ssGSEA, and Xcell) for this purpose. Two aspects were explored for these clusters i.e. immune effector cells (**Figures 5A–D**) and immunosuppressive cells (**Figures 5E–G**). Our analysis delineated that Cluster 1 had the least infiltration of immune effector cells and immunosuppressive cells (**Figures 5A–G**). This suggests that cluster1 might be the immunologically-cold tumors. Cluster 2 and cluster 3 were found to be enriched in the immunologically-hot tumor immune microenvironment. Both of these clusters were enriched in both immune effector and immunosuppressive cells. Activated B cells, dendritic cells (DC), and monocytes were significantly enriched in cluster 2 (**Figures 5A–G**). We compared the three different clusters and reached their immune score. The results showed that cluster 2 had higher immune and stromal scores (**Figure 5H**).

Construction of Prognostic Prediction Models of Immune-Related Metabolic Genes

Next, we were interested in whether these immune-related metabolic genes could be used to predict survival. The LUAD matrix was divided into training (70%) and test (30%) sets. We selected 80 genes having $p<0.05$ and performed Unicox analysis to compute the regression coefficient (**Figures 6A, B**). Moreover, multivariate regression was performed to calculate the formula. We identified nine genes that were used to construct a prediction model. These nine genes were, *TK1, TCN1, CAV1, ACMSD, HS3ST2, HS3ST5, AMN, ADRA2C, and ACOXL* (**Figure 6C**). Patients were categorized into high and low-risk groups in training and test sets. A survival curve was plotted according to the clinical information of two groups of patients (**Figures 6D–F**). The results showed that training and test sets with high-risk score patients had a worse Overall Survival (OS) rate than those of low score patients ($p<0.0001$) (**Figures 6D–F**). The area under the ROC curves of the predictive model for LUAD has the same performance in the first year, third year, and fifth-year (Training set: AUC at one year: 0.83, AUC at three years: 0.72, AUC at five years: 0.71; Test set: AUC at one year: 0.68, AUC at three years: 0.76, AUC at five years: 0.61) (**Figures 6E–G**). Moreover, the prediction model was validated using our clinical specimens. The validation results confirmed

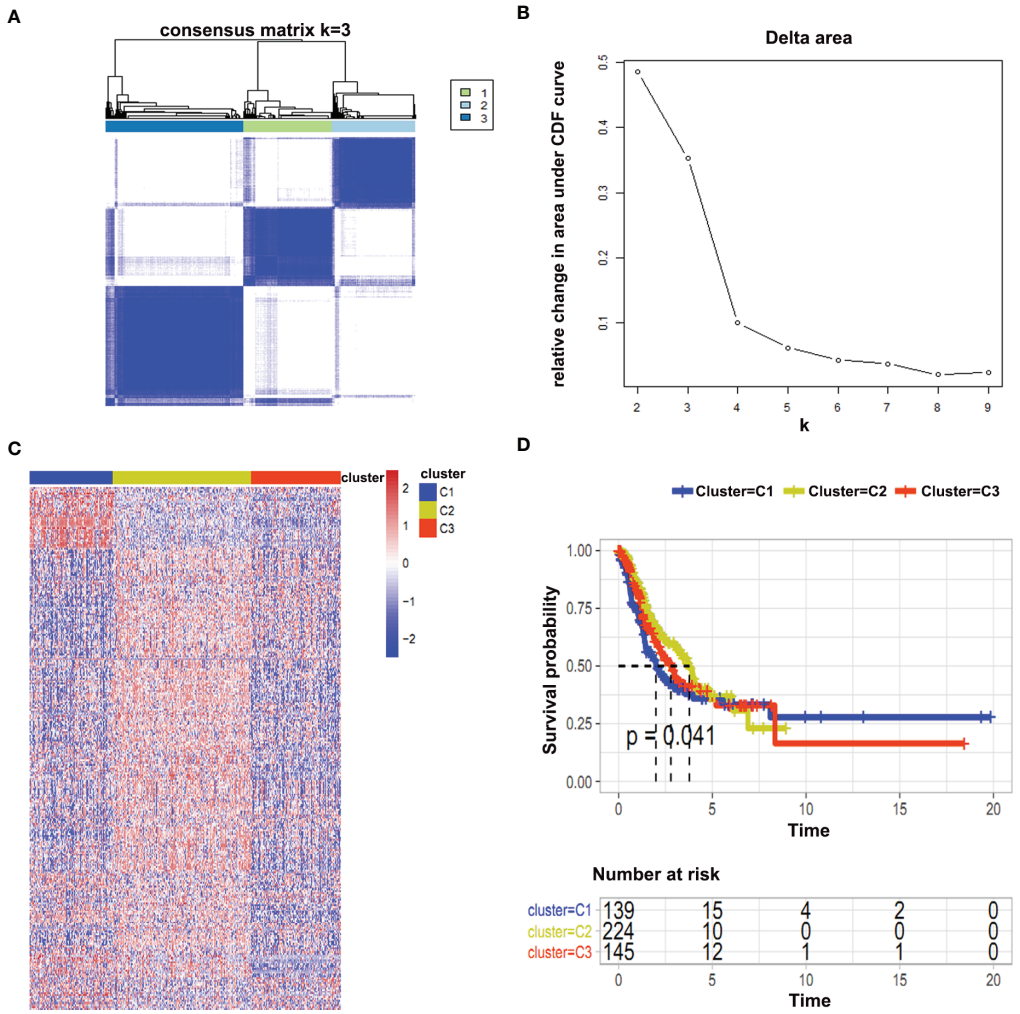

FIGURE 3 | Consistent clustering of immune-related metabolic genes. **(A, B)** Cumulative distribution function (CDF) represented an optimal number of clusters (k is 3); **(C)** Heat map represented immune-related metabolic genes in three clusters; **(D)** Survival analysis between different clusters was shown.

that the high-risk score group had a worse survival (p <0.0001) (**Figures 6H, I**). Meanwhile, our prediction model had high accuracy (AUC at one year: 0.74, AUC at three years: 0.83, AUC at four years: 0.78).

Identification of Potential Metabolic Targets

As the highly expressed genes in the tumor could be a potential factor to promote tumor growth, therefore, we selected those immune-related metabolic genes whose expression was high in the tumor site (logFC > 1.5, FDR < 0.05). Five potential targets i.e., *HMMR, PFKP, RRM2, TCN1*, and TK1 were obtained that were negatively correlated with survival rate (**Figure S4**). The expression of five hub genes in pan-carcinoma was shown (**Figure S5**). The correlation of the four genes *HMMR, PFKP, TCN1*, and *TK1* with tumor-infiltrating immune cells and the survival curve in lung cancer was shown (**Figure S6**). Furthermore, we determined the expression levels of five hub genes in our clinical specimens. We found that the expression of *RRM2* was higher in tumor tissues (**Figures 7A–E**). Similarly, the expression level of *RRM2* was significantly higher in lung cancer cell lines (A549, NCL-H292, and Calu-3) compared to normal lung epithelial cell line (BEAS-2B) (**Figure 7F**). The survival curves of *RRM2* and immune cell infiltration in lung cancer patients were determined. The overall survival of lung cancer patients showed that low *RRM2* expression had a better prognosis (p=0.000015) (**Figure 7G**), and disease-free survival also suggested that patients with low *RRM2* expression had a better prognosis (p=0.019) (**Figure 7H**). The relationship with immune cells showed that *RRM2* was associated with tumor infiltration by B cells and Neutrophils (**Figure 7I**).

To determine the function of *RRM2*, GO and KEGG analyses were performed to find correlated genes with *RRM2* (**Figure S7**). The *RRM2*-related genes were mainly enriched in catalytic

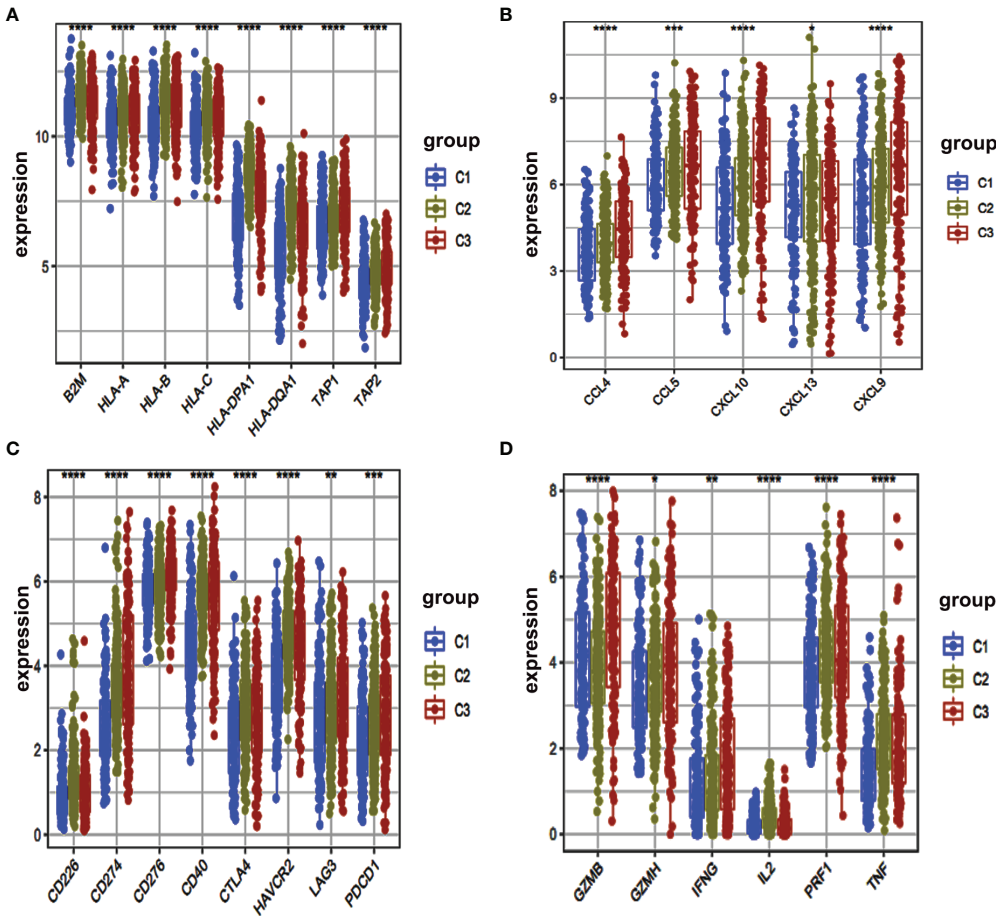

FIGURE 4 | Box plot of immune-related gene expressed among different clusters. **(A–D)** The expression levels of multiple immune genes were compared in three clusters. *, P < 0.05. **, P < 0.01. ***, P < 0.001. ****, P < 0.0001.

activities, acting on DNA as determined by GO analysis. While KEGG pathway enrichment analysis showed that *RRM2*-related genes were mainly enriched in cell cycle regulation. Moreover, the correlation between the *RRM2* gene and the CDK family of genes was analyzed. This result showed that the *RRM2* gene was highly related to the CDK family of proteins (**Figure 7J**). We also found the same results in tumor samples analyzed by qPCR, showing that this gene was associated with CDK family of proteins. Our results delineated that the expression levels of *RRM2*, *CDK2* (r=0.492, p<0.001), *CDK4* (r=0.365, p<0.01), *CDK6* (r=0.406, p<0.01) and *CDK8* (r=0.440, p<0.01) were positively correlated, which means that *RRM2* was significantly correlated with cell cycle signaling (**Figures 7K–N**).

DISCUSSION

Our study identified five potential metabolic checkpoints of LUAD and *RRM2* was chosen for further analyses. The expression of RRM2 was significantly higher in both lung cancer tissues and cell lines. In the current study, we disseminated the possible pathways regulated by *RRM2* in lung cancer. We further showed that the cell cycle could be regulated by *RRM2*.

Tumor microenvironment infiltration is closely related to immunotherapy effectiveness. The critical role of immune-related metabolic genes and immune cells in cancer is gradually being unveiled. Therefore, we were interested to find immune-related genes that play a role in immune infiltration and could produce a better immunotherapy effect. In our study, the immune-related genes were obtained from the website, https://www.immport.org/. The metabolism-related genes were downloaded from work published by Peng, X. We performed different analyses and identified ten immune-related metabolic genes. These genes were, *SDC2, GPC3, GPC1, HSPG2, AGRN, GPC2, GPC5, GPC4, GPC6, and VCAN*. These genes play important roles in the immune-related mechanisms of several cancers (colorectal (32), cervical (33), liver (34), pancreatic cancer (35), etc). Immune infiltration of tumor microenvironment in glioblastoma multiforme, breast cancer, and lung cancer play a vital role in immunotherapy and

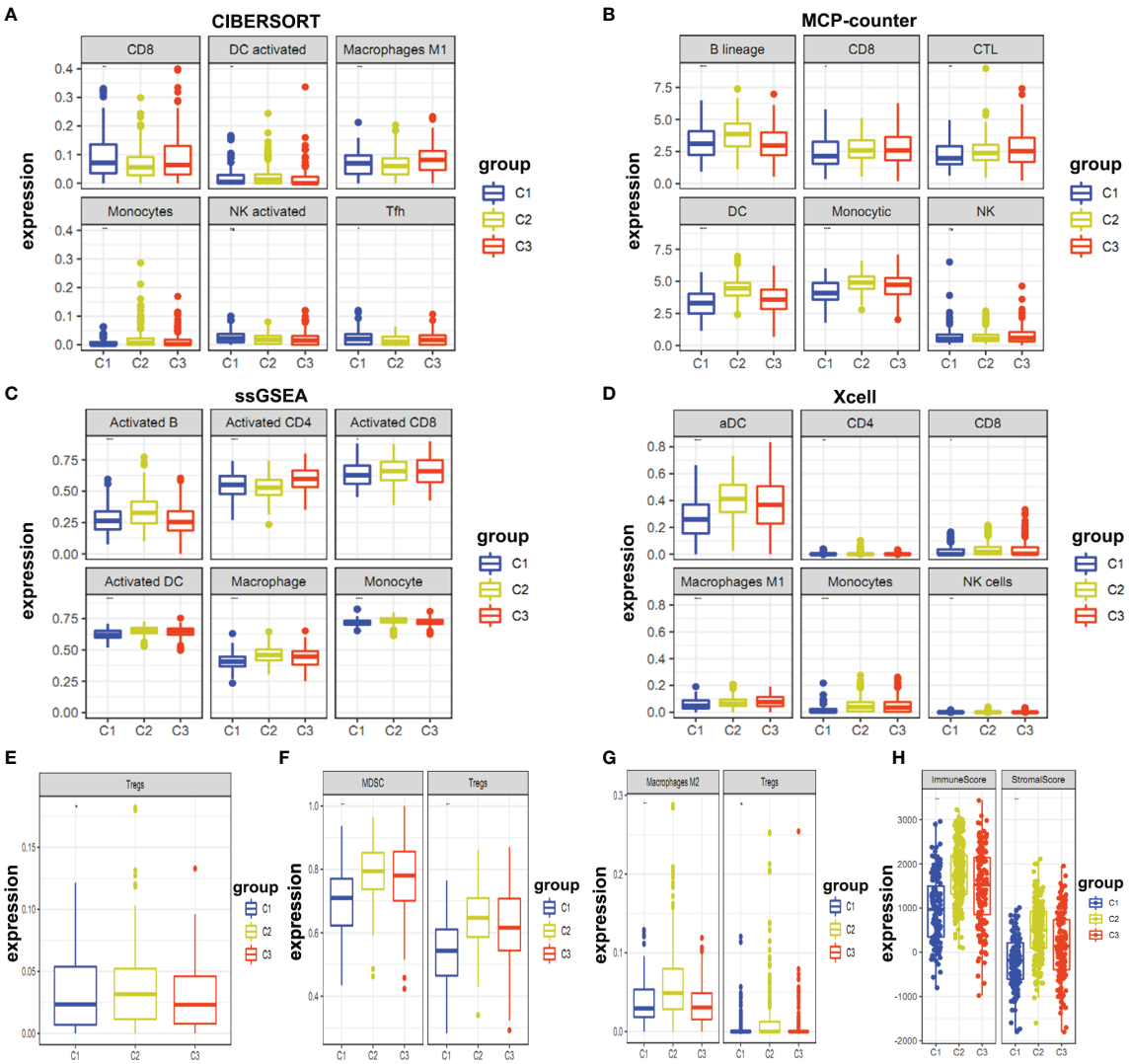

FIGURE 5 | Expression levels of immune infiltration cells. **(A–D)** Expression levels of immune effector cells between different clusters were shown; **(E–G)** Immunosuppressive cells in different clusters were shown; **(H)** Immune and stromal scores in different clusters were shown.

the increase in the degree of immune infiltration is related to better immunotherapy effect (36–39).

To explore the specific mechanisms of these immune-related metabolic genes, the samples were divided into three clusters. The levels of immune cell infiltration, immune scores, and clinicopathological information were compared. We found that among all clusters, cluster2 had prolonged survival at the early stages of the disease. *HLA-DPA1, CXCL13*, activated B cells, DC, and monocytes infiltration were highly expressed in cluster 2. *HLA-DPA1* is involved in immune responses and antigenic peptides presentation (40). Previous studies demonstrated that down-regulation of *HLA-DPA1* expression is related to the poor prognosis of tumors and may be a potential prognostic biomarker for ESCC (41–43). Therefore, higher expression of *HLA-DPA1* in cluster 2 could well represent the prolonged survival of LUAD patients. The *CXCL13/CXCR5* signal axis plays a vital role in the occurrence and development of several human cancers (44). The prognosis was found better in cluster 2 compared to cluster1 and cluster3. The pathways related to B cells play important role in tumor immunotherapy (45, 46). Similarly, monocytes also play an important role in antigen presentation in the microenvironment of tumor immune infiltration (47, 48).

Furthermore, nine genes *TK1, TCN1, CAV1, ACMSD, HS3ST2, HS3ST5, AMN, ADRA2C*, and *ACOXL* were identified for the construction of prediction model. Our findings are parallel with previous findings. *TK1, TCN1, CAV1, and HS3ST2* play indispensable roles in survival predictions and pathogenesis of various cancers (49–55).

Finally, we obtained five potential metabolic checkpoints of LUAD. These were, *HMMR, PFKP, RRM2, TCN1* and *TK1*. By

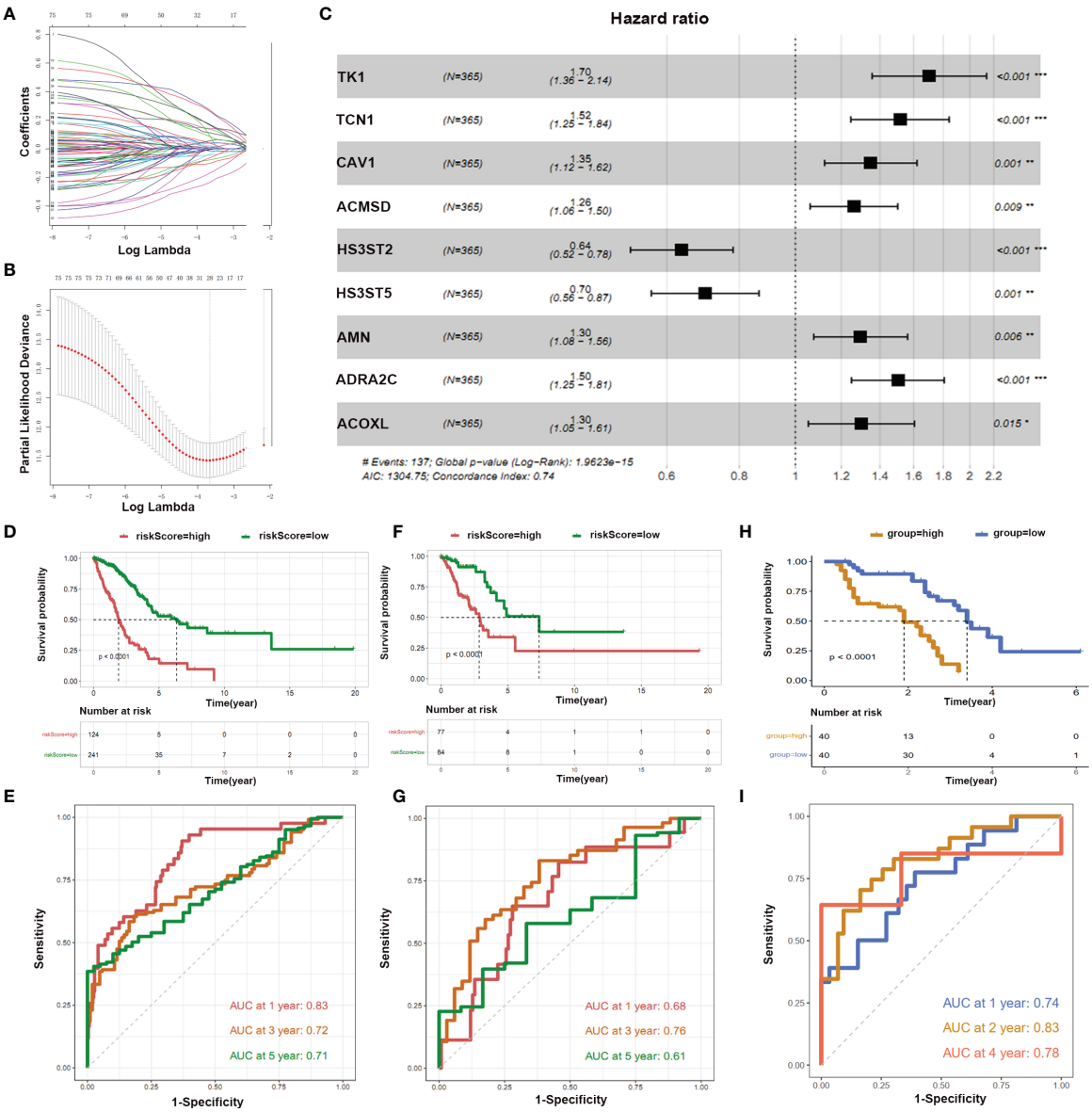

FIGURE 6 | LASSO and hub genes of prognostic model. **(A, B)** Optimal values of the penalty parameter λ; **(C)** Multivariate regression analysis of nine genes we shown; **(D, F, H)** OS in the low score group was significantly higher than in the high score group; **(E, G, I)** Time-dependent ROC curves analysis of the prediction model.

comparing their expression levels and their association with immune cells in pan-cancer and lung cancer clinical samples, we identified a critical role for *RRM2* in LUAD. *RRM2* is a rate-limiting enzyme which is involved in DNA synthesis and repair. It also plays a vital role in many critical cellular processes, such as cell proliferation, invasiveness, migration, angiogenesis, and aging (56). In breast cancer, *RRM2* overexpression in cancer cells promotes the formation and invasion of 3D colonies (57). In liver cancer (58), *RRM2* can inhibit hypertrophy by stimulating GSS to synthesize GSH. In LUAD, *RRM2* has been determined to have an independent prognostic significance. *RRM2* expression levels have significant correlations with B cells, CD4+ T cells, and neutrophil infiltration (59). We also determined that *RRM2* was highly related to the CDK family of proteins. As Cyclin-dependent kinases 4 and 6 (*CDK4/6*) are important regulators of cell cycle and inhibit the proliferation of regulatory T cells (60). Therefore, *RRM2* could also be involved in cell cycle regulation. Our findings further confirmed the relationship of *RRM2* with immunity and metabolism in LUAD. Moreover, our study provided a base and theoretical support for exploring the immunotherapy of LUAD.

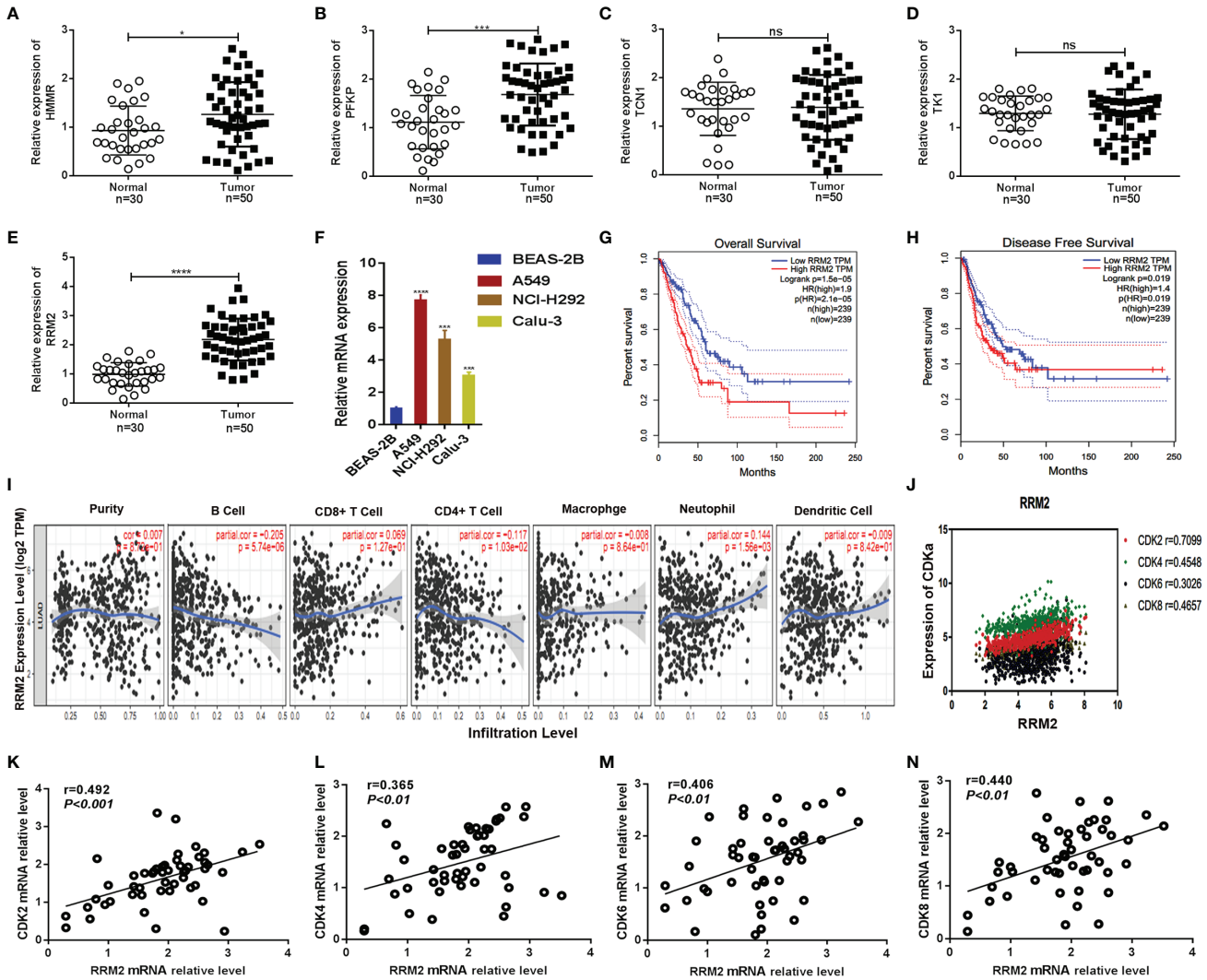

FIGURE 7 | *RRM2* was related to survival time and CDK family. **(A–E)** Expression levels of *HMMR*, *PFKP*, *TCN1*, *TK1*, and *RRM2* in non-cancerous tissues (n = 30) and LUAD tissues (n=50) were detected by qRT-PCR. *GAPDH* was used as an internal control; **(F)** *RRM2* expression levels in different cell lines were determined by qRT-PCR. *GAPDH* was used as an internal control; **(G, H)** Kaplan–Meier analysis was performed to assess the association of *RRM2* expression with overall survival and disease-free survival in LUAD patients using the TCGA databases; **(I)** Correlation of *RRM2* with immune cell infiltration in lung cancer; **(J–N)** Association of *RRM2* with the CDK2 family of proteins. *, P < 0.05. **, P < 0.01. ***, P < 0.001. ****, P < 0.0001. ns : Not Statistically Significant.

CONCLUSIONS

In this study, we first identified the vital role of immune-related metabolic genes in lung adenocarcinoma's immune and clinicopathological aspects. We clustered three subtypes of LUAD based on immune-related metabolic genes and these subtypes exhibited different survival and immune status. We identified nine genes i.e., *TK1*、*TCN1*、*CAV1*、*ACMSD*、*HS3ST2*、*HS3ST5*、*AMN*、*ADRA2C*, and *ACOXL* that were used to construct a prediction model. Finally, *RRM2* was determined as a promising metabolism checkpoint for LUAD and explored its close relationship with the CDK family of proteins. Our results are therefore, helpful for the study of immunotherapy and immune-related metabolic genes in LUAD.

DATA AVAILABILITY STATEMENT

The datasets presented in this study can be found in online repositories. The names of the repository/repositories and accession number(s) can be found in the article/**Supplementary Material**. All analyses were performed using R version 3.6.3.

ETHICS STATEMENT

The studies involving human participants were reviewed and approved by the First Affiliated Hospital of Zhengzhou University approved the study (Ethics number: 2020-KS-

HNSR188). The patients/participants provided their written informed consent to participate in this study.

AUTHOR CONTRIBUTIONS

FL: Conceptualization of the study. CH and LQ: Analyzed the data. PL: Drafted the manuscript. JS: Conducted the experiments and revised manuscript. GZ: Guided on the quality of the research. All authors read and approved the submission of the final manuscript.

ACKNOWLEDGMENTS

We thank the TCGA program for the RNA-sequence and clinical data of patients with lung adenocarcinoma.

SUPPLEMENTARY MATERIAL

The Supplementary Material for this article can be found online at: https://www.frontiersin.org/articles/10.3389/fendo.2022.894754/full#supplementary-material

REFERENCES

1. Jordan EJ, Kim HR, Arcila ME, Barron D, Chakravarty D, Gao J, et al. Prospective Comprehensive Molecular Characterization of Lung Adenocarcinomas for Efficient Patient Matching to Approved and Emerging Therapies. *Cancer Discovery* (2017) 7(6):596–609. doi: 10.1158/2159-8290.CD-16-1337
2. Siegel RL, Miller KD, Jemal A. Cancer Statistics, 2019. *CA Cancer J Clin* (2019) 69(1):7–34. doi: 10.3322/caac.21551
3. Ferlay J, Colombet M, Soerjomataram I, Mathers C, Parkin DM, Pineros M, et al. Estimating the Global Cancer Incidence and Mortality in 2018: GLOBOCAN Sources and Methods. *Int J Cancer* (2019) 144(8):1941–53. doi: 10.1002/ijc.31937
4. Cancer Genome Atlas Research N. Author Correction: Comprehensive Molecular Profiling of Lung Adenocarcinoma. *Nature* (2018) 559(7715):E12. doi: 10.1038/s41586-018-0228-6
5. Cancer Genome Atlas Research N. Comprehensive Molecular Profiling of Lung Adenocarcinoma. *Nature* (2014) 511(7511):543–50. doi: 10.1038/nature13385
6. Wood SL, Pernemalm M, Crosbie PA, Whetton AD. The Role of the Tumor-Microenvironment in Lung Cancer-Metastasis and its Relationship to Potential Therapeutic Targets. *Cancer Treat Rev* (2014) 40(4):558–66. doi: 10.1016/j.ctrv.2013.10.001
7. Quail DF, Joyce JA. Microenvironmental Regulation of Tumor Progression and Metastasis. *Nat Med* (2013) 19(11):1423–37. doi: 10.1038/nm.3394
8. Maccarty WC. Longevity in Cancer: A Study of 293 Cases. *Ann Surg* (1922) 76(1):9–12.
9. Husby G, Hoagland PM, Strickland RG, Williams RCJr. Tissue T and B Cell Infiltration of Primary and Metastatic Cancer. *J Clin Invest* (1976) 57(6):1471–82. doi: 10.1172/JCI108417
10. Buck MD, Sowell RT, Kaech SM, Pearce EL. Metabolic Instruction of Immunity. *Cell* (2017) 169(4):570–86. doi: 10.1016/j.cell.2017.04.004
11. Kesarwani P, Kant S, Prabhu A, Chinnaiyan P. The Interplay Between Metabolic Remodeling and Immune Regulation in Glioblastoma. *Neuro Oncol* (2017) 19(10):1308–15. doi: 10.1093/neuonc/nox079
12. Aird KM, Zhang R. Metabolic Alterations Accompanying Oncogene-Induced Senescence. *Mol Cell Oncol* (2014) 1(3):e963481. doi: 10.4161/23723548.2014.963481
13. Zheng Y, Delgoffe GM, Meyer CF, Chan W, Powell JD. Anergic T Cells are Metabolically Anergic. *J Immunol* (2009) 183(10):6095–101. doi: 10.4049/jimmunol.0803510
14. Biswas SK. Metabolic Reprogramming of Immune Cells in Cancer Progression. *Immunity* (2015) 43(3):435–49. doi: 10.1016/j.immuni.2015.09.001
15. Kishton RJ, Barnes CE, Nichols AG, Cohen S, Gerriets VA, Siska PJ, et al. AMPK Is Essential to Balance Glycolysis and Mitochondrial Metabolism to Control T-ALL Cell Stress and Survival. *Cell Metab* (2016) 23(4):649–62. doi: 10.1016/j.cmet.2016.03.008
16. Chan LN, Chen Z, Braas D, Lee JW, Xiao G, Geng H, et al. Metabolic Gatekeeper Function of B-Lymphoid Transcription Factors. *Nature* (2017) 542(7642):479–83. doi: 10.1038/nature21076
17. Lou Y, Diao L, Cuentas ER, Denning WL, Chen L, Fan YH, et al. Epithelial-Mesenchymal Transition Is Associated With a Distinct Tumor Microenvironment Including Elevation of Inflammatory Signals and Multiple Immune Checkpoints in Lung Adenocarcinoma. *Clin Cancer Res* (2016) 22(14):3630–42. doi: 10.1158/1078-0432.CCR-15-1434
18. Luo J, Solimini NL, Elledge SJ. Principles of Cancer Therapy: Oncogene and non-Oncogene Addiction. *Cell* (2009) 136(5):823–37. doi: 10.1016/j.cell.2009.02.024
19. Peng X, Chen Z, Farshidfar F, Xu X, Lorenzi PL, Wang Y, et al. Molecular Characterization and Clinical Relevance of Metabolic Expression Subtypes in Human Cancers. *Cell Rep* (2018) 23(1):255–69.e254. doi: 10.1016/j.celrep.2018.03.077
20. Yu G, Wang LG, Han Y, He QY. Clusterprofiler: An R Package for Comparing Biological Themes Among Gene Clusters. *OMICS* (2012) 16(5):284–7. doi: 10.1089/omi.2011.0118
21. Harris MA, Clark J, Ireland A, Lomax J, Ashburner M, Foulger R, et al. The Gene Ontology (GO) Database and Informatics Resource. *Nucleic Acids Res* (2004) 32(Database issue):D258–261. doi: 10.1093/nar/gkh036
22. Ogata H, Goto S, Sato K, Fujibuchi W, Bono H, Kanehisa M. KEGG: Kyoto Encyclopedia of Genes and Genomes. *Nucleic Acids Res* (1999) 27(1):29–34. doi: 10.1093/nar/27.1.29
23. von Mering C, Huynen M, Jaeggi D, Schmidt S, Bork P, Snel B. STRING: A Database of Predicted Functional Associations Between Proteins. *Nucleic Acids Res* (2003) 31(1):258–61. doi: 10.1093/nar/gkg034
24. Shannon P, Markiel A, Ozier O, Baliga NS, Wang JT, Ramage D, et al. Cytoscape: A Software Environment for Integrated Models of Biomolecular Interaction Networks. *Genome Res* (2003) 13(11):2498–504. doi: 10.1101/gr.1239303
25. Diboun I, Wernisch L, Orengo CA, Koltzenburg M. Microarray Analysis After RNA Amplification can Detect Pronounced Differences in Gene Expression Using Limma. *BMC Genomics* (2006) 7:252. doi: 10.1186/1471-2164-7-252
26. Newman AM, Liu CL, Green MR, Gentles AJ, Feng W, Xu Y, et al. Robust Enumeration of Cell Subsets From Tissue Expression Profiles. *Nat Methods* (2015) 12(5):453–7. doi: 10.1038/nmeth.3337
27. Barbie DA, Tamayo P, Boehm JS, Kim SY, Moody SE, Dunn IF, et al. Systematic RNA Interference Reveals That Oncogenic KRAS-Driven Cancers Require TBK1. *Nature* (2009) 462(7269):108–12. doi: 10.1038/nature08460
28. Becht E, Giraldo NA, Lacroix L, Buttard B, Elarouci N, Petitprez F, et al. Estimating the Population Abundance of Tissue-Infiltrating Immune and Stromal Cell Populations Using Gene Expression. *Genome Biol* (2016) 17(1):218. doi: 10.1186/s13059-016-1070-5
29. Aran D, Hu Z, Butte AJ. Xcell: Digitally Portraying the Tissue Cellular Heterogeneity Landscape. *Genome Biol* (2017) 18(1):220. doi: 10.1186/s13059-017-1349-1
30. Friedman J, Hastie T, Tibshirani R. Regularization Paths for Generalized Linear Models *via* Coordinate Descent. *J Stat Softw* (2010) 33(1):1–22. doi: 10.18637/jss.v033.i01
31. Sauerbrei W, Royston P, Binder H. Selection of Important Variables and Determination of Functional Form for Continuous Predictors in

Multivariable Model Building. *Stat Med* (2007) 26(30):5512–28. doi: 10.1002/sim.3148
32. Han YD, Oh TJ, Chung TH, Jang HW, Kim YN, An S, et al. Early Detection of Colorectal Cancer Based on Presence of Methylated Syndecan-2 (SDC2) in Stool DNA. *Clin Epigenet* (2019) 11(1):51. doi: 10.1186/s13148-019-0642-0
33. Hu R, Zhu Z. ELK1-Activated GPC3-AS1/GPC3 Axis Promotes the Proliferation and Migration of Cervical Cancer Cells. *J Gene Med* (2019) 21 (8):e3099. doi: 10.1002/jgm.3099
34. Fu J, Wang H. Precision Diagnosis and Treatment of Liver Cancer in China. *Cancer Lett* (2018) 412:283–8. doi: 10.1016/j.canlet.2017.10.008
35. Melo SA, Luecke LB, Kahlert C, Fernandez AF, Gammon ST, Kaye J, et al. Glypican-1 Identifies Cancer Exosomes and Detects Early Pancreatic Cancer. *Nature* (2015) 523(7559):177–82. doi: 10.1038/nature14581
36. Sokratous G, Polyzoidis S, Ashkan K. Immune Infiltration of Tumor Microenvironment Following Immunotherapy for Glioblastoma Multiforme. *Hum Vaccin Immunother* (2017) 13(11):2575–82. doi: 10.1080/21645515.2017.1303582
37. Burugu S, Asleh-Aburaya K, Nielsen TO. Immune Infiltrates in the Breast Cancer Microenvironment: Detection, Characterization and Clinical Implication. *Breast Cancer* (2017) 24(1):3–15. doi: 10.1007/s12282-016-0698-z
38. Liu X, Wu S, Yang Y, Zhao M, Zhu G, Hou Z. The Prognostic Landscape of Tumor-Infiltrating Immune Cell and Immunomodulators in Lung Cancer. *BioMed Pharmacother* (2017) 95:55–61. doi: 10.1016/j.biopha.2017.08.003
39. Chen DS, Mellman I. Oncology Meets Immunology: The Cancer-Immunity Cycle. *Immunity* (2013) 39(1):1–10. doi: 10.1016/j.immuni.2013.07.012
40. Diaz G, Amicosante M, Jaraquemada D, Butler RH, Guillen MV, Sanchez M, et al. Functional Analysis of HLA-DP Polymorphism: A Crucial Role for DPbeta Residues 9, 11, 35, 55, 56, 69 and 84-87 in T Cell Allorecognition and Peptide Binding. *Int Immunol* (2003) 15(5):565–76. doi: 10.1093/intimm/dxg057
41. Rimsza LM, Roberts RA, Miller TP, Unger JM, LeBlanc M, Braziel RM, et al. Loss of MHC Class II Gene and Protein Expression in Diffuse Large B-Cell Lymphoma Is Related to Decreased Tumor Immunosurveillance and Poor Patient Survival Regardless of Other Prognostic Factors: A Follow-Up Study From the Leukemia and Lymphoma Molecular Profiling Project. *Blood* (2004) 103(11):4251–8. doi: 10.1182/blood-2003-07-2365
42. Meissner M, Konig V, Hrgovic I, Valesky E, Kaufmann R. Human Leucocyte Antigen Class I and Class II Antigen Expression in Malignant Fibrous Histiocytoma, Fibrosarcoma and Dermatofibrosarcoma Protuberans is Significantly Downregulated. *J Eur Acad Dermatol Venereol* (2010) 24 (11):1326–32. doi: 10.1111/j.1468-3083.2010.03644.x
43. Hillman GG, Kallinteris NL, Lu X, Wang Y, Wright JL, Li Y, et al. Turning Tumor Cells *in Situ* Into T-Helper Cell-Stimulating, MHC Class II Tumor Epitope-Presenters: Immuno-Curing and Immuno-Consolidation. *Cancer Treat Rev* (2004) 30(3):281–90. doi: 10.1016/j.ctrv.2003.08.002
44. Hussain M, Adah D, Tariq M, Lu Y, Zhang J, Liu J. CXCL13/CXCR5 Signaling Axis in Cancer. *Life Sci* (2019) 227:175–86. doi: 10.1016/j.lfs.2019.04.053
45. Tokunaga R, Naseem M, Lo JH, Battaglin F, Soni S, Puccini A, et al. B Cell and B Cell-Related Pathways for Novel Cancer Treatments. *Cancer Treat Rev* (2019) 73:10–9. doi: 10.1016/j.ctrv.2018.12.001
46. Franchina DG, Grusdat M, Brenner D. B-Cell Metabolic Remodeling and Cancer. *Trends Cancer* (2018) 4(2):138–50. doi: 10.1016/j.trecan.2017.12.006
47. Riemann D, Cwikowski M, Turzer S, Giese T, Grallert M, Schutte W, et al. Blood Immune Cell Biomarkers in Lung Cancer. *Clin Exp Immunol* (2019) 195(2):179–89. doi: 10.1111/cei.13219
48. Sabado RL, Balan S, Bhardwaj N. Dendritic Cell-Based Immunotherapy. *Cell Res* (2017) 27(1):74–95. doi: 10.1038/cr.2016.157
49. Wang Y, Jiang X, Wang S, Yu H, Zhang T, Xu S, et al. Serological TK1 Predict Pre-Cancer in Routine Health Screenings of 56,178 People. *Cancer biomark* (2018) 22(2):237–47. doi: 10.3233/CBM-170846
50. Togar T, Desai S, Mishra R, Terwadkar P, Ramteke M, Ranjan M, et al. Identifying Cancer Driver Genes From Functional Genomics Screens. *Swiss Med Wkly* (2020) 150:w20195. doi: 10.4414/smw.2020.20195
51. Ketteler J, Klein D. Caveolin-1, Cancer and Therapy Resistance. *Int J Cancer* (2018) 143(9):2092–104. doi: 10.1002/ijc.31369
52. Vijaya Kumar A, Salem Gassar E, Spillmann D, Stock C, Sen YP, Zhang T, et al. HS3ST2 Modulates Breast Cancer Cell Invasiveness *via* MAP Kinase- and Tcf4 (Tcf7l2)-Dependent Regulation of Protease and Cadherin Expression. *Int J Cancer* (2014) 135(11):2579–92. doi: 10.1002/ijc.28921
53. Chen CS, Lin LW, Hsieh CC, Chen GW, Peng WH, Hsieh MT. Differential Gene Expression in Hemodialysis Patients With "Cold" Zheng. *Am J Chin Med* (2006) 34(3):377–85. doi: 10.1142/S0192415X06003916
54. Nakamura T, Satoh-Nakamura T, Nakajima A, Kawanami T, Sakai T, Fujita Y, et al. Impaired Expression of Innate Immunity-Related Genes in IgG4-Related Disease: A Possible Mechanism in the Pathogenesis of IgG4-Rd. *Mod Rheumatol* (2020) 30(3):551–7. doi: 10.1080/14397595.2019.1621475
55. Codrici E, Albulescu L, Popescu ID, Mihai S, Enciu AM, Albulescu R, et al. Caveolin-1-Knockout Mouse as a Model of Inflammatory Diseases. *J Immunol Res* (2018) 2018:2498576. doi: 10.1155/2018/2498576
56. Nordlund P, Reichard P. Ribonucleotide Reductases. *Annu Rev Biochem* (2006) 75:681–706. doi: 10.1146/annurev.biochem.75.103004.142443
57. Shah KN, Wilson EA, Malla R, Elford HL, Faridi JS. Targeting Ribonucleotide Reductase M2 and NF-kappaB Activation With Didox to Circumvent Tamoxifen Resistance in Breast Cancer. *Mol Cancer Ther* (2015) 14 (11):2411–21. doi: 10.1158/1535-7163.MCT-14-0689
58. Yang Y, Lin J, Guo S, Xue X, Wang Y, Qiu S, et al. RRM2 Protects Against Ferroptosis and is a Tumor Biomarker for Liver Cancer. *Cancer Cell Int* (2020) 20(1):587. doi: 10.1186/s12935-020-01689-8
59. Ma C, Luo H, Cao J, Gao C, Fa X, Wang G. Independent Prognostic Implications of RRM2 in Lung Adenocarcinoma. *J Cancer* (2020) 11 (23):7009–22. doi: 10.7150/jca.47895
60. Goel S, DeCristo MJ, Watt AC, BrinJones H, Sceneay J, Li BB, et al. CDK4/6 Inhibition Triggers Anti-Tumour Immunity. *Nature* (2017) 548(7668):471–5. doi: 10.1038/nature23465

Conflict of Interest: The authors declare that the research was conducted in the absence of any commercial or financial relationships that could be construed as a potential conflict of interest.

frontiers | Frontiers in Endocrinology

TYPE Original Research
PUBLISHED 26 July 2022
DOI 10.3389/fendo.2022.882431

OPEN ACCESS

EDITED BY
Ihtisham Bukhari,
Henan Provincial People's Hospital, China

REVIEWED BY
Mei-zhou Huang,
The Affiliated Hospital of Southwest Medical University, China
Jian Zhou,
Chinese Academy of Sciences (CAS), China

*CORRESPONDENCE
Le Liu
1402744723@smu.edu.cn
Ye Chen
yechen_fimmu@163.com

SPECIALTY SECTION
This article was submitted to Cancer Endocrinology, a section of the journal Frontiers in Endocrinology

RECEIVED 23 February 2022
ACCEPTED 27 June 2022
PUBLISHED 26 July 2022

CITATION
Liang L, Mai S, Mai G, Chen Y and Liu L (2022) DNA damage repair-related gene signature predicts prognosis and indicates immune cell infiltration landscape in skin cutaneous melanoma.
Front. Endocrinol. 13:882431.
doi: 10.3389/fendo.2022.882431

DNA damage repair-related gene signature predicts prognosis and indicates immune cell infiltration landscape in skin cutaneous melanoma

Liping Liang[1], Shijie Mai[2], Genghui Mai[1], Ye Chen[1,3]* and Le Liu[3]*

[1]Department of Gastroenterology, State Key Laboratory of Organ Failure Research, Guangdong Provincial Key Laboratory of Gastroenterology, Nanfang Hospital, Southern Medical University, Guangzhou, China, [2]Department of Thoracic Surgery, Nanfang Hospital, Southern Medical University, Guangzhou, China, [3]Department of Gastroenterology, Integrated Clinical Microecology Center, Shenzhen Hospital, Southern Medical University, Shenzhen, China

Background: DNA damage repair plays an important role in the onset and progression of cancers and its resistance to treatment therapy. This study aims to assess the prognostic potential of DNA damage repair markers in skin cutaneous melanoma (SKCM).

Method: In this study, we have analyzed the gene expression profiles being downloaded from TCGA, GTEx, and GEO databases. We sequentially used univariate and LASSO Cox regression analyses to screen DNA repair genes associated with prognosis. Then, we have conducted a multivariate regression analysis to construct the prognostic profile of DNA repair-related genes (DRRGs). The risk coefficient is used to calculate the risk scores and divide the patients into two cohorts. Additionally, we validated our prognosis model on an external cohort as well as evaluated the link between immune response and the DRRGs prognostic profiles. The risk signature is compared to immune cell infiltration, chemotherapy, and immune checkpoint inhibitors (ICIs) treatment.

Results: An analysis using LASSO-Cox stepwise regression established a prognostic signature consisting of twelve DRRGs with strong predictive ability. Disease-specific survival (DSS) is found to be lower among high-risk patients group as compared to low-risk patients. The signature may be employed as an independent prognostic predictor after controlling for clinicopathological factors, as demonstrated by validation on one external GSE65904 cohort. A strong correlation is also found between the risk score and the immune microenvironment, along with the infiltrating immune cells, and ICIs key molecules. The gene enrichment analysis results indicate a wide range of biological activities and pathways to be exhibited by high-risk groups. Furthermore, Cisplatin exhibited a considerable response sensitivity in low-risk groups as opposed to the high-risk incidents, while docetaxel exhibited a considerable response sensitivity in high-risk groups.

10.3389/fendo.2022.882431

Conclusions: Our findings provide a thorough investigation of DRRGs to develop an DSS-related prognostic indicator which may be useful in forecasting SKCM progression and enabling more enhanced clinical benefits from immunotherapy.

KEYWORDS

skin cutaneous melanoma, DNA damage repair, immunotherapy, prognostic factor, tumor microenvironment

Introduction

Skin cutaneous melanoma (SKCM) is identified as one of the most frequent, belligerent, and life-threatening primary malignant skin cancer usually associated with distant metastasis as well as high mortality (1). In recent years, the most common treatment modalities for SKCM are surgery, chemotherapy, and immunotherapy. Despite, great success in SKCM treatment, a 5-year overall survival (OS) rate among metastatic melanoma patients remains extremely poor which is mainly attributed to late diagnosis, rapid metastasis, and ineffective treatment response (2). Depending on the clinical characteristics of the patient, risk stratification and subsequently individualized treatment therapy based on the degree of risk may help in improved prognosis (3). Nonetheless, the existing tumor staging system is inadequate to effectively forecast the prognosis of SKCM and hence there is an unmet need to find new biomarkers which can predict the prognosis of patients with SKCM.

Abbreviations: SKCM, skin cutaneous melanoma; TCGA, the cancer genome atlas; GTEx, genotype-tissue expression; GEO, gene expression omnibus; DRRGs, DNA repair-related genes; DSS, disease-specific survival; TME, tumor microenvironment; C-index, concordance index; m5C, 5-methylcytosine; m6A, N6-methyladenosine; DDR, DNA damage repair; PARP, poly ADP-ribose polymerase; MEK5, MAP kinase-ERK kinase5; TTK, threonine tyrosine kinase; AIM1, absent in melanoma-1; MGMT, methylguanine-dna methyltransferase; LASSO, Least absolute shrinkage and selection operator; KM, Kaplan-Meier; ROC, receiver operating characteristic; AUC, area under the curve; CYT, cytolytic activity score; GSEA, gene set enrichment analysis; PCA, principal component analysis; NES, normalized enrichment score; ssGSEA, single sample gene-set enrichment analysis; TIIC, tumor-infiltrating immune cells; ICB, immune checkpoint blockade; IPS, immunophenoscore; TMB, tumor mutation burden; TILs, tumor-infiltrating lymphocytes; TIME, tumor immune microenvironment; ICIs, immune checkpoint inhibitors; TYMS, thymidylate synthase; HAX1, HCLS1-associated protein X-1; Cox17, cytochrome c oxidase assembly protein 17; LIG1, ligase 1; AK, adenylate kinase; TAMs, tumor-associated macrophages.

In recent years, the progress in the field of genomics and bioinformatics has made it possible to discover new biomarkers and drug targets. Researchers have identified many biomarkers for diagnosis, prognosis, and treatment, including noncoding RNAs (lncRNA), microRNAs (miRNAs), and messenger RNAs (mRNAs). Some immune-related markers, for example, are being utilized to assess tumor microenvironment (TME) infiltration patterns and reveal any relationship between TME and clinical properties (4). Furthermore, there are reports where prognosis has been predicted using signatures such as hypoxia, autophagy, m5C or m6A mRNA modification, and lactate metabolism (5, 6).

Researchers have thoroughly examined DNA damage repair (DDR) in the context of tumors and neoplasia where they found defective DDR can induce an accumulation of DNA damage as well as genome instability that lead to tumor occurrence. Exonuclease 5 gene germline mutations have been reported to impair DNA repair resulting in androgen-associated prostate cancer (7). Nonetheless, DNA repair may be associated with vulnerability towards anticancer treatments such as radiation therapy or poly ADP-ribose polymerase (PARP) suppressors during tumor development. In response to ionizing radiation, MAP kinase-ERK kinase 5 (MEK5) has been reported to stimulate the phosphorylation of DNA-PK (8). In breast cancer, a higher threonine tyrosine kinase (TTK) expression is linked with effective homologous recombination-mediated repair and radiation sensitivity (9). All these earlier studies have emphasized on the significance to study various functions of DNA repair genes in cancer.

In previously published reports, SKCM is considered as a belligerent tumor exhibiting significant heterogeneity and high genomic mutations which suggests that subgrouping tumors based on gene expression patterns will be ultimately key to accurately assessing melanoma progression (10, 11). As a result of such subgroupings, more targeted therapy may be devised. There have been many reports on the prognostic and biological importance of genetic changes linked to cancer such as PARP1 (12, 13), NRAS (14), absent in melanoma-1 (AIM1) (15), Methylguanine-DNA Methyltransferase (MGMT) (16) as well as KPNA2 (17) mutations in SKCM. Nevertheless, the functions

of DNA repair genes for the maintenance of genomic stability among SKCM are seldom described.

In this research, we have gathered as well as evaluated data retrieved from multiple databases like TCGA (The Cancer Genome Atlas), GTEx (The Genotype-Tissue Expression), and GEO (The Gene Expression Omnibus) to ascertain the DNA repair gene's potential for prognosis of SKCM patients. Hereby, we have constructed a forecasting model premised on the DRRGs (DNA repair-related genes) expression and assessed distinct tumor immune infiltrating landscapes linked to the gene profiles.

Materials and methods

Datasets

For this study, we have retrieved the survival information along with gene expression datasets from the combined TCGA-SKCM dataset (https://portal.gdc.cancer.gov/) which includes around 446 tumor samples for training purposes (Supplementary Table 1). SKCM patient's expression profiles with survival data are retrieved from the GEO database (http://www.ncbi.nlm.nih.gov/geo) with accession number GSE65904 for validation purposes (n = 210, Supplementary Table 2).This study also included 557 non-tumor normal samples from the GTEx dataset (https://gtexportal.org/). DDR gene data (Hallmark DNA Repair Data Set) was downloaded from MSigDB database.(http://www.gsea-msigdb.org/gsea/index.jsp). There is no need for permissions from the ethics committee as the data were obtained from TCGA, GTEx, and GEO datasets, and have been reported in this work by carefully adopting the publication criteria established by these individual databases.

Identification of DDR-related genes and development of a prognostic signature in SKCM

We have retrieved prospective DNA repair genes from the TCGA dataset which are substantially linked to the prognosis of SKCM patients using the univariate Cox regression analysis. Following that, we used LASSO (Least absolute shrinkage and selection operator) regression analysis to identify the best prognostic genes while avoiding model overfitting. As a final step, we developed a risk score algorithm using the gene expression levels weighted by regression coefficients from multivariate Cox regression analyses. Each patient's risk score is computed by using the below-mentioned algorithm:

$$Risk\ \ score = \sum_{i=1}^{n}(Coefi * xi)$$

where $Coef_i$ denotes risk coefficients, x_i stands for the expression value of DRRGs (18).

Assessment and validation of the prognostic signature

The risk score of each patient is sorted (computed as per the aforementioned algorithm) while setting the median risk score as the critical value and based on this, the training and validation cohorts are divided into high- and low-risk cohorts. To distinguish the survival times of the two patient cohorts, the Kaplan-Meier (KM) curve was used. In addition, receiver operating characteristic (ROC) curves are used to evaluate the predictive effect of the signature, where a prediction with an area under the curve (AUC) of greater than 0.60 is considered to have medium accuracy, whereas a prediction with an AUC of greater than 0.75 is considered to have high accuracy. Multivariate and univariate Cox regression analyses were undertaken to investigate if the risk score is independent of other clinical parameters such as age, gender, stage, tumor mutation burden (TMB), tumor purity, cytolytic activity score (CYT), and riskScore. Subsequently, subcohort analysis of a single gene in the DDR-related prognosis model is carried out premised on the clinical features of the patients. Additionally, using TCGA data, we examined the connection between risk scores and clinicopathological characteristics of patients with SKCM. After incorporating the recorded risk scores into the present staging method, we evaluated its usefulness in stratifying risk levels. Premised on the clinical data and risk scores of patients, the "rms" package was utilized to create a nomogram for clinical assessment. We then plotted a calibration to examine the consistency among the forecasted and the actual clinical results and computed the concordance index (C-index) for the nomogram model. The nomogram model's reliability and the prognostic value of DRRG were verified utilizing an independent dataset (GSE65904).

Gene set enrichment analysis and single sample GSEA

According to the DRRGs prognostic signature, the functional phenotype between the high- and low-risk cohorts was evaluated by gene set enrichment analysis (GSEA) software. GO gene sets (go.bp.v7.4.symbols.gmt) obtained from the Molecular Signatures Database were employed as the baseline gene set (19). The critical values used in the study included the Nominal p-value < 0.05, FDR < 0.25, and |NES| (Normalized Enrichment Score) > 1. The variation in the expression of immune-associated activities and immune cell infiltration among the patient cohorts was assessed utilizing a single sample gene-set enrichment analysis (ssGSEA).

Tumor-infiltrating immune cells (TIIC) fraction assessment

We tried to evaluate the immunological infiltration degree of about 22 immune cell types into mixed cell populations based on specific gene expression characteristics among 22 leukocyte subtypes LM22 by using the ''CIBERSORT'' method as described previously (20). The "pheatmap" program has been utilized to visualize the distribution of immune cells in the two cohorts and then the Wilcoxon rank test was applied to contrast the differences among quantities of immunological infiltrates for the low-and high-risk cohorts while p-values are determined by "vioplot" R package.

Estimation of the immunoreactivity

We have used the Wilcoxon test to evaluate the expression of PD-1, CTLA4, PD-L1, and TGFB1 among low-as well as high-risk cohorts as key hub immune response biomarkers. In order to predict response to immune checkpoint blockade (ICB) in the TCGA-SKCM dataset, we utilize the immunophenoscore (IPS) retrieved from The Cancer Immunome Atlas (TCIA) (https://tcia.at/home). Anti-CTLA-4 and anti-PD-1 antibody responses are reliably predicted by IPS. Positive correlations between IPS and ICB responses are generally seen; higher scores are associated with greater immunoreactivity (21).

Statistical analyses

The Student's *t*-test is being used to compare the differences between the two cohorts. The log-rank method is applied to compare the survival curves for disease-specific survival (DSS) rates from the KM survival analysis. The statistical analysis is carried out using GraphPad Prism (version 8.0) and R software (version 4.0.4). The p-values (<0.05) are considered statistically significant.

Results

Identification of prognosis-related DRRGs and construction of a prognostic signature

Figure 1 depicts the workflow design used in this research. We performed GSEA of SKCM and normal tissue samples. The findings demonstrated that SKCM is substantially associated with positive modulation of the DDR response (NES = 1.72, $p < 0.01$) (Figure 2A). And we have found from the TCGA-SKCM training dataset, that the univariate analysis is clearly illustrating the expression of 30 DRRGs being considerably linked to the prognosis of SKCM patients ($p < 0.05$), and among them, 14 were protective genes (hazard ratio <1), and 16 genes were associated with increased risk (hazard ratio >1) (Figure 2B). Subsequently, in order to generate a prognostic signature, the LASSO approach was used to reduce the number of candidate

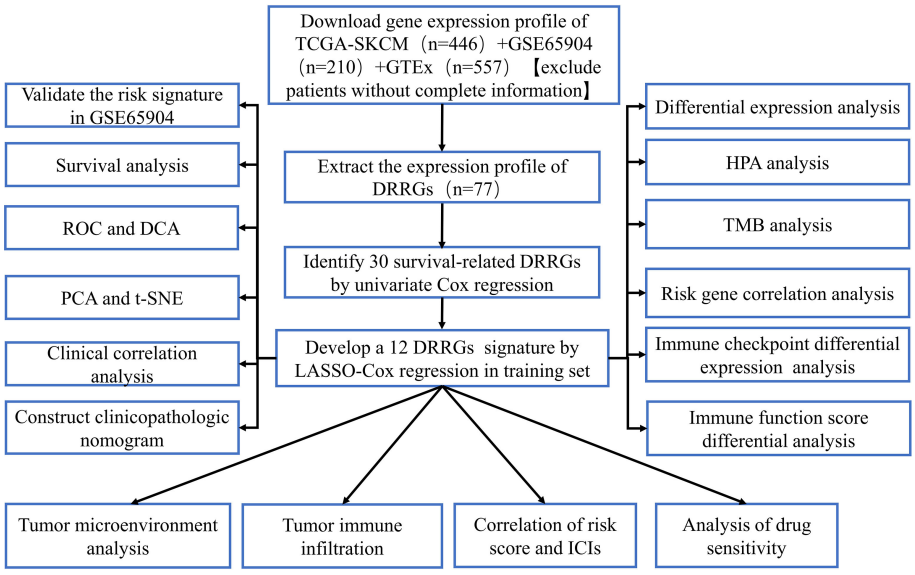

FIGURE 1
The flow diagram of this study.

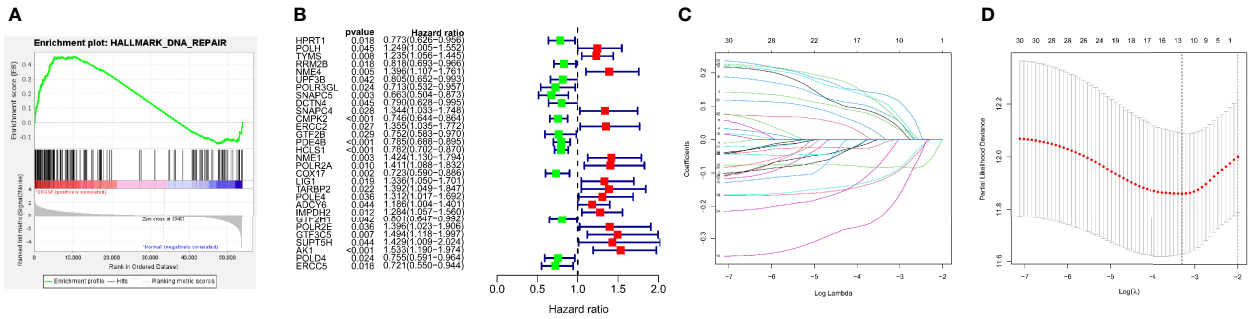

FIGURE 2
Construction of DRRGs signature. **(A)** Significant enrichment of DNA repair-related pathways in SKCM patients. NES, normalized enrichment score; **(B)** The forest plot of the univariate Cox regression depicted 30 DRRGs associated with SKCM survival; **(C)** Lasso regression for DRRGs in univariate Cox regression; **(D)** Coefficients of selected features denotes the risk coefficient is shown by lambda parameter.

genes based on the minimal penalty parameter (λ) (Figures 2C, D). In combination with Multivariate Cox regression analyses, a total of 12 DRRGs (TYMS, SNAPC5, CMPK2, PDE4B, HCLS1, NME1, POLR2A, COX17, LIG1, POLE4, GTF2H1, and AK1) were identified as predictive indicators for patients with SKCM (Supplementary Table 3). The DRRGs signature risk model was formulated as: Risk score = (0.053 * TYMS exp.) + (−0.006 * SNAPC5 exp.) + (−0.108 * CMPK2 exp.) + (-0.114 * PDE4B exp.) + (-0.084 * HCLS1 exp.) + (0.076 * NME1 exp.) + (0.107* POLR2A exp.) + (-0.215 * COX17 exp.) + (0.063 * LIG1 exp.) + (0.090 * POLE4 exp.) + (-0.048 * GTF2H1 exp.) + (0.132 * AK1 exp.).

Prognostic analysis of the 12-gene marker in TCGA-SKCM cohort

We created a prognostic signature by generating a computed risk score premised on the expression of selected 12 important prognostic genes. The specimens are categorized into high- and low-risk cohorts based on the median risk score (Figure 3A). The distribution of risk scores, a summary of the survival are shown in figure (Figures 3B, C). In addition, a heatmap displaying the expression pattern of each gene was created to illustrate the disparity between the high- and low-risk groups predicted by the prognostic model (Figures 3E, F). The risk model exhibits specificity and sensitivity in-consistent with or rather much better than other conventional prognostic variables, as illustrated by the areas under the ROC curve for risk score, age, gender, stage, TMB, ESTIMATEScore, TumorPurity, and CYT classification, which were found to be 0.714, 0.619, 0.475, 0.562, 0.393, 0.384, 0.631, and 0.337 respectively (Figure 3D). We have further utilized the human protein atlas immunohistochemistry dataset (www.proteinatlas.org) to evaluate the expression of the DRRGs visually in cancerous and non-cancerous tissue, using this we examined the protein expression of the 2 main genes in SKCM. In tumor tissues, AK1 staining was lower, while TYMS staining was higher (Figures 3G, H). Interestingly, all of genes that had protein expression staining in the tumor stromal tissue might influence tumorigenesis and prognosis of SKCM through interstitial components.

Assessment and validation of the DRRGs prognostic signature

The survival analysis is performed to assess the signature profile where the KM curve has shown a dismal prognosis for high-risk patients (Figure 4A). The ROC curve effectively revealed the performance of DRRGs prognostic signature in predicting one-, three- and five- survival rates in the TCGA-SKCM dataset as illustrated by AUC values of 0.668, 0.660, and 0.700, correspondingly (Figure 4B). The t-SNE analysis and principal component analysis (PCA) revealed that the distribution mode of the two patient cohorts are differerent (Figures 4C, D). Moreover, the results from the GSE65904 dataset are verified with a similar risk coefficient and found to agree with the findings from the TCGA-SKCM dataset where the high-risk cohort appeared to have worse results than the low-risk cohort (Figure 4E). ROC curves have shown that the AUC for one-, three-, and five-year survival rates in the GSE65904 cohort are 0.570, 0.643, and 0.603, accordingly (Figure 4F). Similarly, the t-SNE analysis and PCA plot have illustrated that specimens from 2 risk cohorts are dispersed in 2 routes (Figures 4G, H).

Construction of the nomogram to predict the survival for SKCM patients

To ascertain whether the DRRGs signature could be used as an independent predictor variable in SKCM, we have added risk scores and several clinicopathologic characteristics based on the TCGA-SKCM cohort. The results showed the

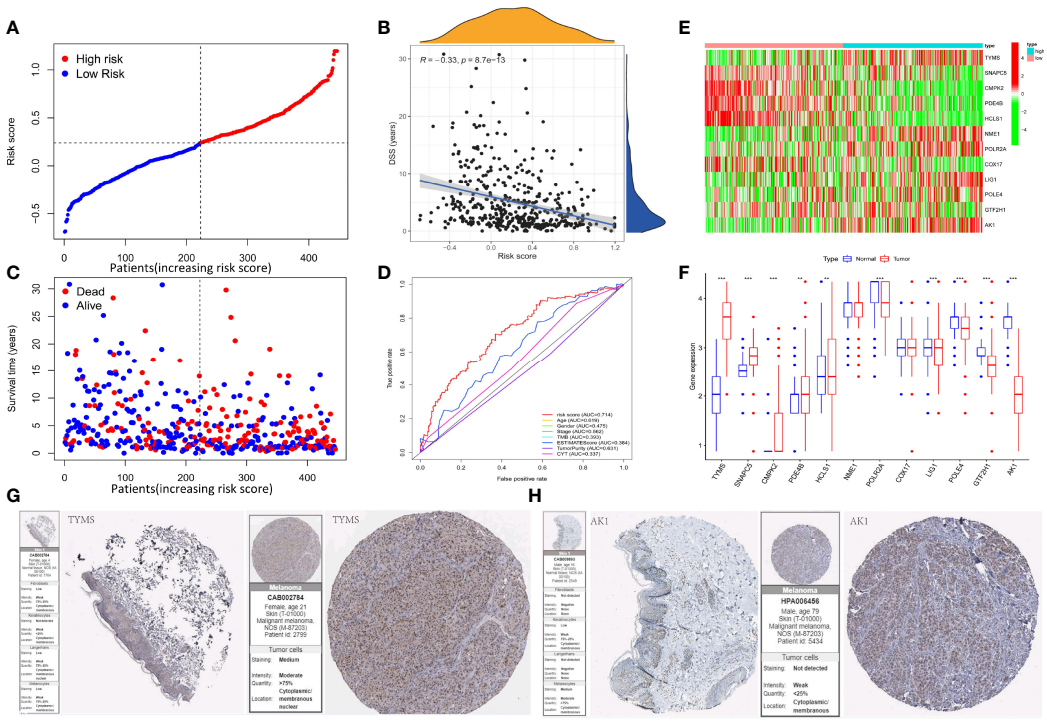

FIGURE 3
Construction of the DRRGs signature and prognostic analysis. **(A)** Risk score distribution among patients with SKCM; **(B)** Spearman correlation analysis of risk score and disease-specific survival (DSS); **(C)** Survival status of each patient with SKCM. Blue signifies low risk or alive while red signifies high risk or dead; **(D)** Heatmap of gene expression between the high and low-risk cohort; **(E)** Relative gene expression between the high and low-risk cohort; **(F)** AUC values for risk score, age, gender, stage, TMB, ESTIMATE score, tumor purity, and CYT classification; **(G)** Immunohistochemical staining images from The Human Protein Atlas of 2 key genes in SKCM.

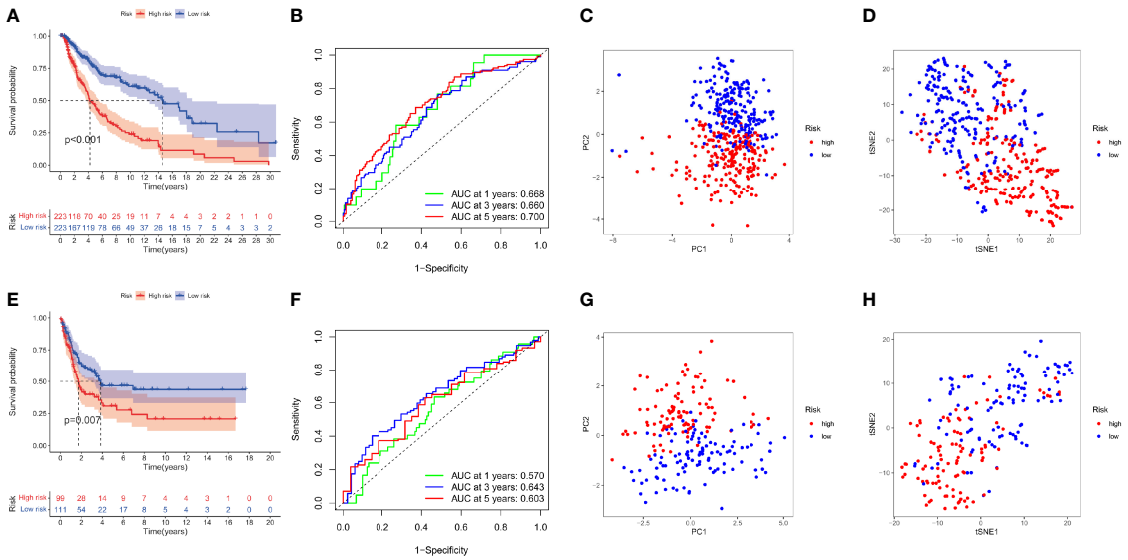

FIGURE 4
DRRGs signature based on training (TCGA-SKCM) and testing (GSE65904) cohorts. **(A)** KM plot of DSS premised on the risk scores; **(B)** ROC for DSS; **(C)**PCA plot; **(D)** t-SNE analysis in the training cohort (TCGA-SKCM); **(E)** KM plot of DSS premised on the risk scores; **(F)** ROC for DSS; **(G)** PCA plot; **(H)** t-SNE analysis in the test cohort (GSE65904).

constructed model (riskScore) remained significant through both multivariate and univariate Cox regression analyses (p<0.001, Figures 5A, B). When the combination of TMB is used, the prediction performance of the risk score is better than if they are used separately. Furthermore, it is found that the low TMB+high-risk cohort possesses a greater survival risk in the hazard than the other cohort (KM analysis, Figure 5C). Nomograms are a way to compress statistical models into a single numerical estimation of probability, such as death or recurrence. They are so widely used for cancer prognosis because they are personalized to the profile of every patient. In our study, a prognostic nomogram integrating clinical characteristics (stage, age, TMB) and the DRRGs-based signature is developed, which can predict the survival likelihood of SKCM patients (Figure 5D). The calibration curve further established the hybrid nomogram's high veracity and reliability (Figure 5E). Last but not least, we computed nomogram model scores and ROC analysis based on these scores. The outcomes showed that the model, after incorporating clinical data, appeared to increase AUC values for the TCGA dataset (one- year: 0.770, three-year: 0.754, five-year: 0.727) (Figure 5F).

Characterization of the relationship between risk score and tumor immune , microenvironment characteristics

Researchers have found a link between tumor-infiltrating lymphocytes (TILs) and the growth of cancer, resistance to drugs, and how well treatment works. We also looked at the relationship between the immune-associated score, the risk score (which we got from the R package "ESTIMATE"), the immune cell types and abundance (which we got from the CIBERSORT approach), and the expression levels of ICB-associated genes to see what role the risk score might play in the tumor immune microenvironment (TIME) characterization of SKCM. The findings of this study

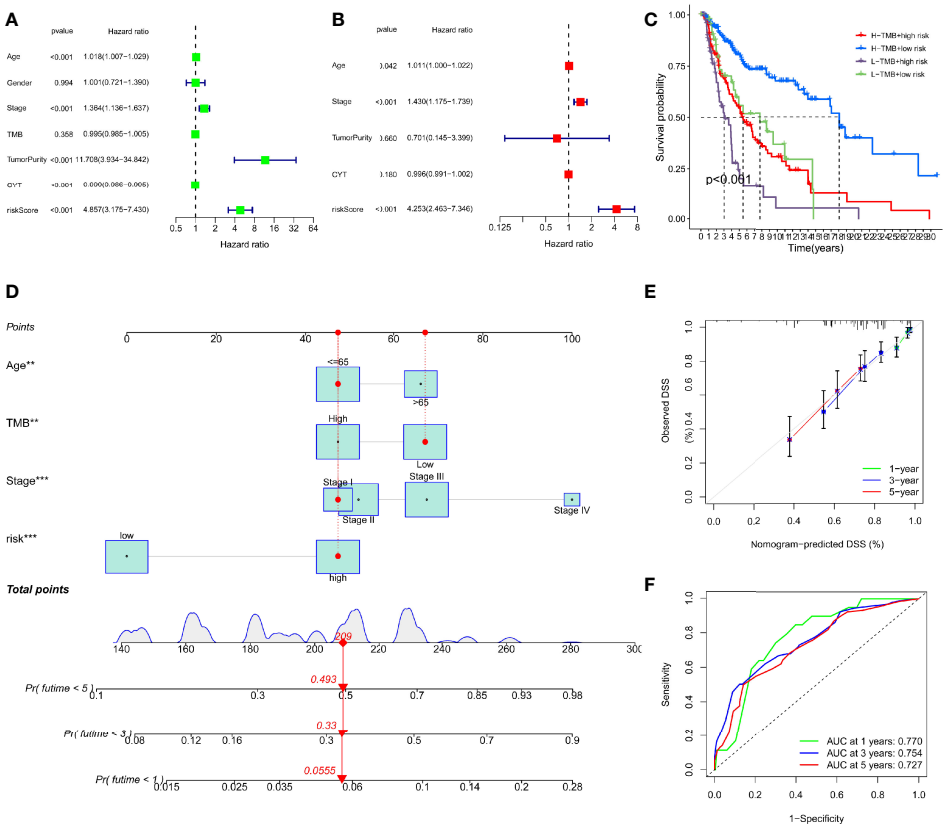

FIGURE 5
Construction of a nomogram based on the DRRGs signature. **(A)** The univariate Cox analysis illustrated that the age, stage, tumorpurity, CYT and riskScore were statistically distinct; **(B)** The multivariate cox analysis illustrated the age, stage and riskScore were 3 independent predictors of SKCM prognosis; **(C)** Survival curve for patients with distinct TMB and risks; **(D)** The nomogram integrated with the parameters (riskScore, stage, and age) amongst patients from the TCGA cohort; **(E)** Calibration curve of the nomogram at 1, 3, and 5 years; **(F)** AUC values for 1-, 3-, and 5-year survival rates premised on the nomogram.

illustrated that the low-risk cohort exhibited elevated ImmuneScore, StromalScore, and matching ESTIMATEScore as well as reduced TumorPurity than the high-risk cohort (Figures 6A–D). Additionally, we noticed a substantial correlation between the risk score and the variables ImmuneScore, StromalScore, and RNAss (Figures 6E–H). According to the GSEA, immune-associated biological processes such as CHEMOKINE_SIGNALING_PATHWAY, CYTOKINE_CYTOKINE_RECEPTOR_INTERACTION, HEMATOPOIETIC_CELL LINEAGE, INTESTINAL_IMMUNE_NETWORK_FOR_IGA_PRODUCTION, and LEISHMANIA_INFECTON are significantly enriched in the low-risk cohort (Figures 6I–L). These findings suggest that in the low-risk cohort, activating immunomodulatory processes may contribute to an improved prognosis. Also, we created a box plot to exhibit the exact proportions of 22 immune cells based on the CIBERSORT algorithm among all SKCM samples (Figure 6O). The correlation analysis of the extent of the 22 immune cells is also shown in Figure 6N. The outcomes from the Wilcoxon rank test reveal that the high-risk cohort exhibit reduced infiltration levels of macrophage M1 cells, follicular helper-T cells, CD8+ T-cells, CD4+ memory-activated T-cells, memory B-cells, and plasma cells as compared to the low-risk cohort (Figure 6O). This study also demonstrated a substantial relevance between risk scores and the expression of several immunological checkpoint-related genes where expression of all immunological checkpoint-related genes was elevated in the low-risk cohort as compared to the high-risk cohort (Figure 6P). Further, the box plots demonstrate variations for immune cell infiltration and related functions among distinct risk sub-cohorts (Figure 6Q). We hereby evaluated that the low-risk cohort possesses better cytotoxicity as well as more checkpoint signatures like HLA, CD8+T cells, NK cells, neutrophils, etc.

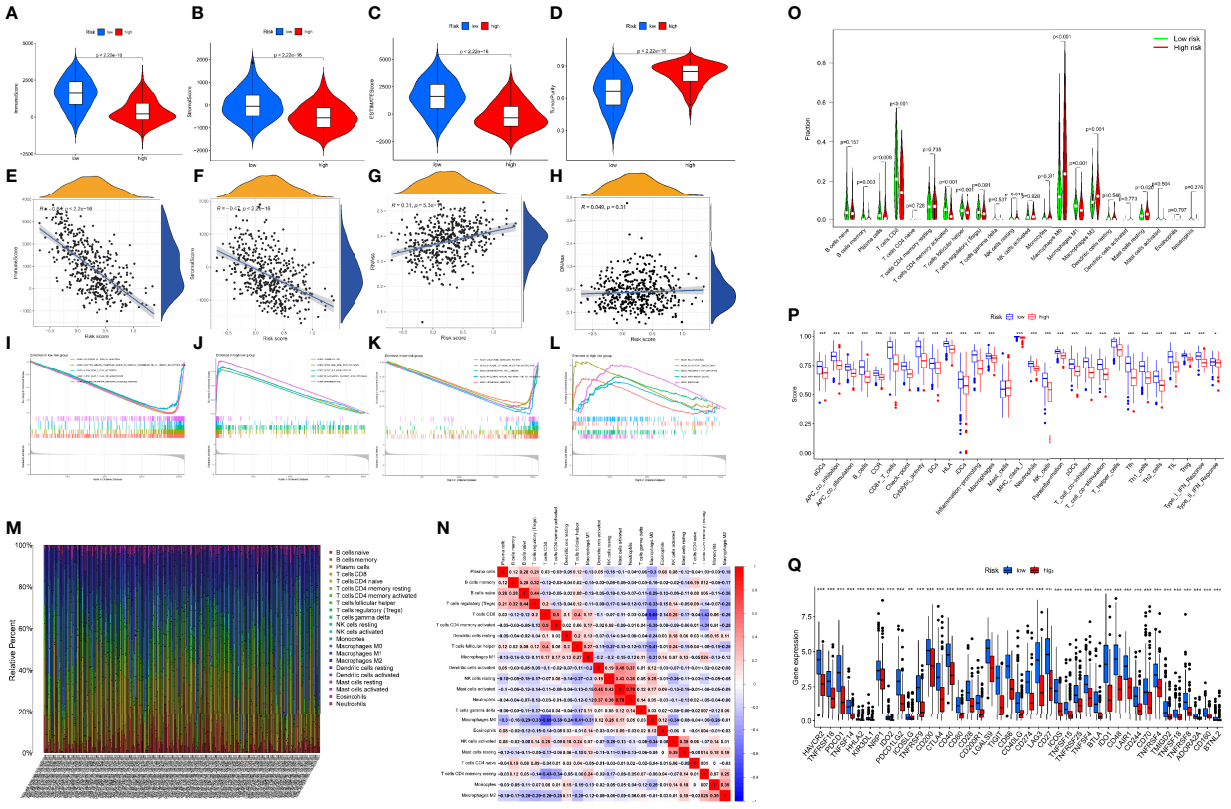

FIGURE 6
GSEA of SKCM patients premised on the DRRGs prognostic signature. **(A–D)** The expression differences of immune score, stromal score, ESTIMATE score, and tumor purity in high- vs. low-risk cohort; **(E–H)** Spearman correlation analysis of risk score with immune score, stromal score, RNAss, and DNAss; **(I–L)** GSEA outcomes illustrated substantial enrichment of immune-associated biological mechanism in the low-risk patients; **(M)** A Barplot of the 22 immune fractions designated by dissimilar colors in each SKCM sample; **(N)** Correlation heatmap of the ratio of TIICs; **(O)** Wilcoxon test of 22 immune fractions in high- vs. low-risk cohort; **(P)** Link between risk score and immune cell infiltration and related roles through the ssGSEA analysis. The score denotes the immune score, with elevated scores signifying a deeper extent of immune cell infiltration; **(Q)** ICB molecules expressed differently between high- and low-risk groups; (ns, not significant, *P < 0.05, **P < 0.01, and ***P < 0.001).

Overall, these outcomes indicate that the DRRGs-based risk characteristics may be to some extent promote a new understanding of the TIME characteristics and immune response of SKCM patients.

The DDR-related risk signature and mutation profiles

The relationship between the mutation profile and the signature was evaluated in TCGA-SKCM patients with available somatic mutation data. The top ten mutated genes in SKCM patients were: TTN, MUC16, DNAH5, BRAF, PCLO, LRP1B, ADGRV1, ANK3, CSMD1, and CSMD2. The most frequently mutated genes in the low-risk and high-risk groups are presented in Figures 7A, B. Surprisingly, TMB and the result was statistically significant (p = 0.032; Figures 7C, D). In addition, we proposed to investigate the function of gene mutation in risk scores and examined the fraction of mutation genes in both low- and high-risk groups in accordance with the results of somatic mutation data. While TTN mutation was similar in the two different risk groups, we found that MUC16 and DNAH5 mutations were substantially connected with a risk score (Figures 7E–J). The fact that there is a correlation between the amount of TMB and the risk score in SKCM, when taken together, suggests that TMB may play an important part in predicting the outcomes of patients.

Response of high- and low-risk patients to immunotherapy, targeted therapy, and chemotherapy

We attempted to examine the effects of DRRGs-based signature on TIME of SKCM for which around 4 hub immune checkpoint inhibitors (ICIs)-associated genes (i.e. PDCD1, CD274, CTLA-4, TGFB1) are singled out for additional research. Here an assessment of the connections between risk score and immunological checkpoint gene expression could yield novel therapeutic concepts. The expression patterns of inhibitory receptors (PDCD1, CD274, CTLA4, and TGFB1) are considerably elevated in the low-risk cohort in comparison to the high-risk cohort (Figures 8A–H). It is found that there may be a connection between TIIC alterations and the survival time of SKCM patients based on differences between the two cohorts. IPS is a reliable predictor of anti-CTLA-4 and anti-PD-1 antibody responses. Immunophenoscore (IPS) accurately predicts anti-CTLA-4 and anti-PD-1 antibody responses. IPS are typically connected positively with the ICB response. We studied the association between IPS and our DRRGs risk model in TCGA-SKCM, and the results indicate that there was no significant variation in immunophenoscore between risk groups in IPS_CTLA4_neg_PD1_neg (Figures 8I). In the low-risk group, IPS-PD1, IPS-CTLA4, and IPS-PD1-CTLA4 blocker scores were higher, indicating greater immunotherapeutic benefits (Figures 8J–L). The fact that chemotherapy is also a common treatment method for SKCM prompted us to assess the

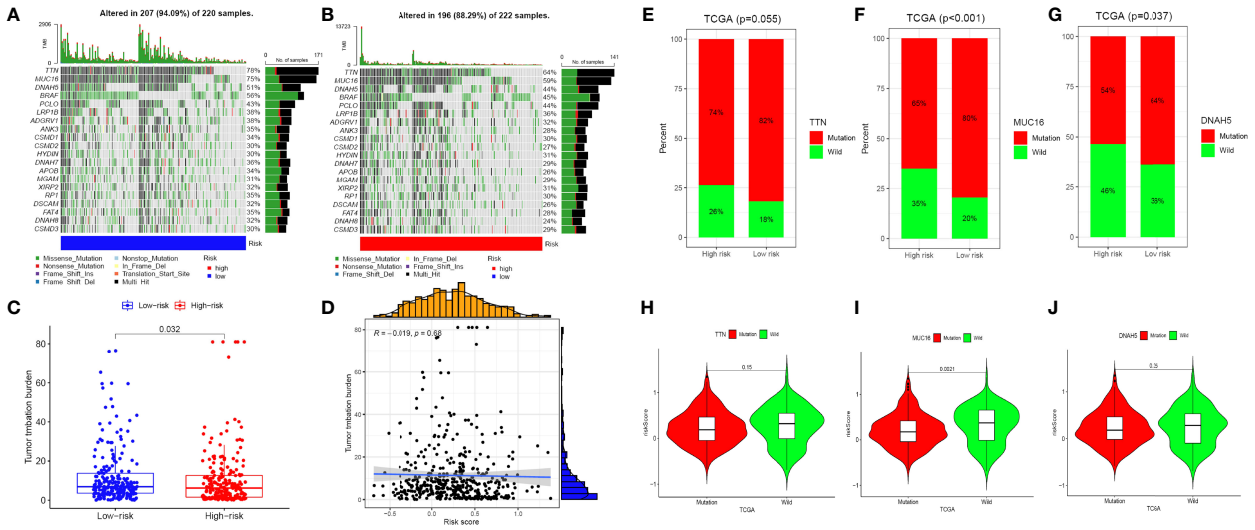

FIGURE 7
The mutation profile and TMB among low-risk and high-risk groups. **(A, B)** Mutation profile of low-risk and high-risk groups. **(C, D)** The relationship between the immune-related risk signature and TMB. **(E–G)** The proportion of mutation of TTN, MUC16 and DNAH5 in both low-/high-risk groups form the TCGA-SKCM dataset. **(H–J)** Comparison of the risk score between mutation and wild groups.(ns, not significant, *P < 0.05, **P < 0.01, and ***P < 0.001).

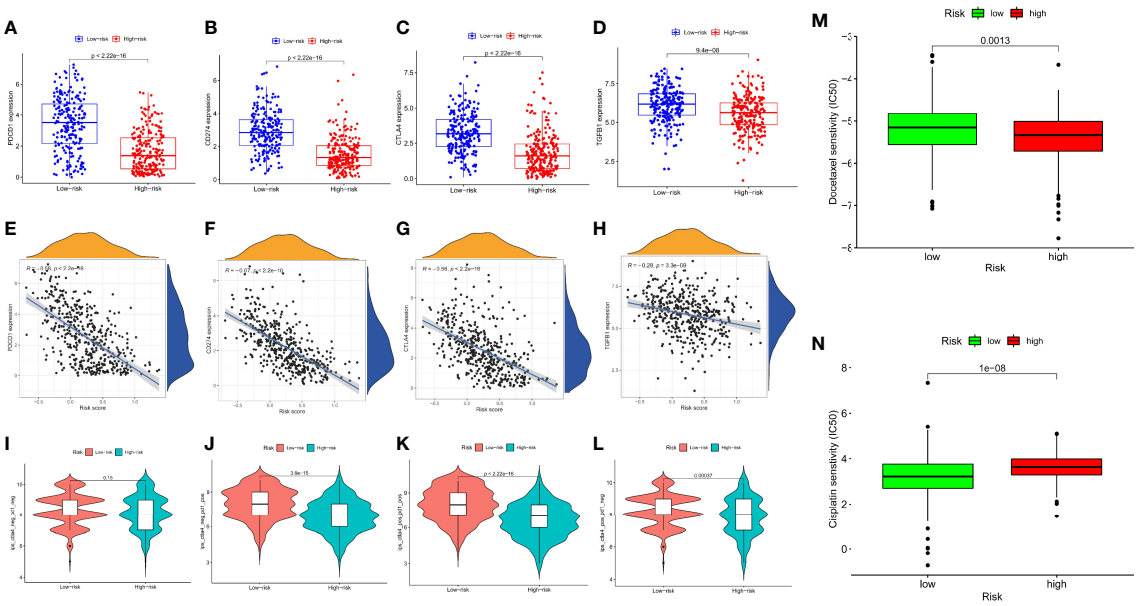

FIGURE 8
Relationship Between the Prognosis-Associated Immune Signature and Drug Response in SKCM. The differential expression of **(A)** PDCD1, **(B)** CD274, **(C)** CTLA4, **(D)** TGFB1 in the two subgroups, correspondingly; Spearman correlation analysis of risk score and **(E)** PDCD1, **(F)** CD274, **(G)** CTLA4, **(H)** TGFB1; **(I)** IPS score distribution plot; **(J)** IPS-PD1 blocker score distribution plot; **(K)** IPS-CTLA4/PD1 blocker score distribution plot; **(L)** IPS-CTLA4 blocker score distribution plot; **(M)** Boxplot comparing patient response to docetaxel chemotherapy; **(N)** Boxplot comparing patient response to cisplatin chemotherapy. (ns, not significant, *P < 0.05, **P < 0.01, and ***P < 0.001).

sensitivity of known anticancer clinical drugs (cisplatin and docetaxel) through the "pRRophetic" R package premised on the assessment of the tumor genes expression level. After calculating the sample's IC_{50}, we found that docetaxel exhibits a considerably higher response sensitivity in high-risk incidents than in low-risk incidents, contrary cisplatin shows higher response sensitivity in low-risk incidents (Figures 8M, N).

Discussion

Due to its high rate of metastasis, invasiveness, and yearly increasing prevalence, SKCM has been reported as the leading cause of skin cancer death worldwide. There are several complicated multistep mechanisms responsible for the onset, progression, and metastasis of SKCM, yet its pathogenesis remains unknown, and there are no effective prognostic indicators for the disease. Therefore, understanding the underlying molecular mechanisms and identifying novel biomarkers is helpful for the prognostic prediction, risk stratification, and therapeutic target of SKCM. The current investigation was designed as a pilot study to find possible biomarkers associated with prognosis and also to test novel research ideas for the future. As a means of guiding individual therapy, prediction models have been investigated for many years. According to reports, models based on tumor gene expression could predict how patients would respond to gemcitabine and fluorouracil (22). Using genetic characteristics, Zhao et al. classified triple-negative breast tumors into different subgroups and evaluated the clinical effect of subtyping-based targeted treatment (23). It is uncommon for SKCM patients to receive individualized treatment based on molecular subtyping.

Research has shown that DNA damage response pathways are critical for correcting and repairing DNA damage, which can prevent cell aging, apoptosis, and carcinogenesis in the long run, as well as ensure activities of daily living (24). Specific DDR pathways include Specifically, DDR is made up of 8 pathways which include: variable DNA synthesis, Fanconi's anemia, checkpoint factor, non-homologous end ligation, mismatch repair, homologous recombination repair, nucleotide excision repair, and base excision repair (25). Together, these mechanisms could repair DNA damage properly and promptly, maintain genomic integrity, and avoid gene distortion. Recent research has revealed that increased DNA damage and decreased cancer cell DNA repair capacity result in cancer cell genome distortion and that differentiating these cells from normal cells could enhance cancer therapy efficacy (26). DDR genes are cancer-driving and play an important role in clinical and translational medicine, and as a result, they can provide additional treatment options for cancer patients (27). SKCM has been connected to the DDR-related pathway, and the

expression of particular DNA repair components has been found to be associated with the prognosis of the patient (28).

Numerous prognostic models premised on immunology, glycolysis, and autophagy genes have been developed, and their predictive usefulness in various kinds of cancer has been examined. Nevertheless, the prognostic value of DNA damage genes in cancer is still debatable. The present study examined the effects of DNA repair genes on SKCM development and patient outcome. Thirty DRRGs were identified using univariate Cox regression analysis, and the best 12 were identified using LASSO-Cox regression analysis (TYMS, SNAPC5, CMPK2, PDE4B, HCLS1, NME1, POLR2A, COX17, LIG1, POLE4, GTF2H1, and AK1). Following the completion of the calculation of risk scores using the risk coefficients, the patients were divided into two distinct groups. According to the examination of the survival data, high-risk patients as per the score appeared to have a dismal prognosis. Additionally, multivariate and univariate Cox regression studies illustrated that the tumor stage and signature were 2 independent prognostic variables. Moreover, the DRRGs prognostic signature was validated by utilizing the independent data set GSE65904.

5-FU has been reported to be an antimetabolite drug that causes cytotoxicity primarily by inhibiting thymidylate synthase (TYMS) resulting in dTMP depletion, compromising DNA synthesis. Patients diagnosed with CRC who were given chemotherapy based on 5-FU to address their condition, have been shown to have higher TYMS expression and lower survival when the insertion (ins) allele or the triple tandem repeat (3R variant) is present (29). Despite the lack of documentation of SNAPC5's involvement in cancers, the results of this research suggest that further investigation will be needed. There is also evidence that CMPK2 and PDE4B, which are immune checkpoint proteins in cancers, inhibit cell proliferation and induce apoptosis (30, 31). HAX1 is implicated in apoptosis, cell migration, and calcium homeostasis. HAX1 protein partners were identified and their significance in oxidative stress and aggregation was studied (32). NME1/NM23-H1 nucleoside diphosphate kinase is a well-recognized metastasis inhibitor, with NME1 downregulation influencing in situ-to-invasive shift in the process of breast cancer development (33). POLR2A *de novo* germline variant has recently been linked to neurodevelopmental disease. POLR2A-associated developmental disorders are most likely a spectrum of linked, multi-systemic developmental diseases caused by different processes that converge at a single locus (34). The human cytochrome C oxidase assembly protein 17 (Cox17) has been recognized as an essential copper chaperone that facilitates the transfer of copper ions to the mitochondrion. *In vitro* investigations led by Zhao et al. have recently revealed that the Cox17 protein is involved in cisplatin transport to mitochondria and leads to cisplatin's overall cytotoxicity (35). DNA ligase 1, also known as LIG1, has been singled out as a potentially fruitful therapeutic modification target for ovarian cancer (36). POLE3 supports epigenetic integrity and H3-H4 chaperone activity at the replication fork. WI/SNF gene mutations cause all cancers. GTF2H1 levels affect SWI/SNF-deficient cells' sensitivity to cisplatin and UV damage (37). As a result, GTF2H1 may be an important prognostic indicator of platinum drug susceptibility in SWI/SNF-deficient cancer cells. Adenylate kinase (AK), which interconverts two adenine nucleotides into stoichiometric quantities of ATP and AMP, performs a crucial function in buffering adenine nucleotides across the tail to sustain flagellar movements. Martin Frejno et al. reported that AK1 inhibits cytarabine and that elevated levels of AK1 correlate with poor survival rates for patients with acute myeloid leukemia treated with Cytarabine (38). Research in this study found that AK1 was closely related to SKCM prognosis. Despite this, the exact mechanism of action is yet to be determined in SKCM. Hence, more research is needed into the role of AK1 in SKCM pathophysiology.

DNA damage repair is linked to immune cell activation in several types of cancer. Chatzinikolaou et al. found a direct connection between DNA damage and innate immune signaling (39). Researchers have discovered that inhibiting PARP and CHK1 increases the number of TILs (40). Moreover, Sato's group discovered that genotoxic stress, including PARP suppression or irradiation, might upmodulate PD-L1 expression *via* the ATM-ATR/CHK1 pathway (41). According to Jiao et al. (42), PD-L1 may be upregulated by PARP suppressors, resulting in immunological suppression. Based on their study, Garsed et al. identified mutations in the DDR pathways as the cause of immune cell activation and infiltration (43). There has also been evidence that DNA repair mutations and immunological regulation genes contribute to bladder cancer (44). Furthermore, evidence has shown that DDR gene mutations that induce loss of function are common in metastatic SKCM, which could have an impact on immunotherapy efficacy (45). As a result, we conducted this bioinformatics research to investigate the possible link between DDR and immunological escape. According to GSEA functional enrichment analysis, the low-risk cohort was enriched in pathways associated with DDR and immunological modulation, suggesting immunomodulation was associated with a better prognosis. In this research, immune evasion genes were discovered to be overexpressed in SKCM patients who were at a reduced risk. We hypothesized that low-risk patients could derive benefits from immunotherapy because antibodies against immunological escape genes have been shown to enhance the responses of tumor-related T cells to tumor-related antigens, and upregulation of PD-L1 on tumor cells or immune cells has been linked to improved anti-PD1/PD-L1 immunotherapy effectiveness. The study of TIICs, which are recognized for stimulating tumor growth and development, is also a significant method for researching the TME of SKCM. As a result of CIBERSORT analysis, lymphocytes and monocytes were found to be elevated in SKCM samples rather than granulocytes. Subsequently, we evaluated the association between the infiltration of TIICs and risk score and discovered that the extent of immune cell infiltration in the high-risk cohort decreased significantly, as did immune-related functions such as modulation of checkpoints, T cell co-inhibition, and

inflammation. These results imply that persons at high risk may develop systemic immunosuppression, which may affect their prognosis.

By suppressing anti-tumor immune cell function, the TME supports tumor growth. The immunosuppressive TME is formed by cancer cells, organ-specific niches, and immune cells with immunoregulatory roles. MDSCs, M2 macrophages, and Foxp3+ Treg cells contribute to the immunosuppressive TME. In our results, the level of M2 macrophage infiltration is positively correlated with the risk score. It has been discovered that M2 macrophages, also known as tumor-associated macrophages (TAMs), serve as immunosuppressive cells in TME. It has been hypothesized that the infiltration of M2 macrophages occurred at an increased level in the low-risk SKCM samples. The M2 macrophages have been shown to express PD-L1, and produce immune-suppressive enzymes, chemokines, and cytokines, thus aiding SKCM tumor angiogenesis and metastasis (46). The level of M1 macrophage, CD8+T cell, infiltrations, on the other hand, is negatively connected with the risk score. It's worth mentioning that the link between higher riskscores and more infiltrative immune cells needs to be investigated further. The proportions of immune cells in TME changed the aggressive phenotypes induced by deregulation of DRRGs, showing that these genes are involved in the process of activation of the immune system response. DNA repair genes were linked to immunological and metastatic signals, as well as SKCM development and onset. Future SKCM research will require extensive TIICs analysis and large-scale sample research. We anticipated that high-risk patients' cancers may be more responsive to chemotherapy (such as docetaxel) using the GDSC dataset. To improve survival, high-risk patients may take the corresponding chemotherapy after surgery. In the future, it might be necessary to conduct clinical chemotherapeutic trials.

It is important to highlight that our research has certain limitations as well. To begin with, the data utilized only consisted of a few participants, which might lead to selection bias. Second, in the corresponding publicly accessible GTEx and TCGA datasets, the proportion of healthy samples and SKCM samples was substantially distinct, potentially distorting the findings. Therefore, more tumor specimens should be examined in the future. Finally, since this is bioinformatics research premised on public datasets, experimental and clinical investigations are needed to confirm these results.

Conclusions

Our research discovered a 12-DRRG signature that might be used to forecast prognosis in SKCM patients. As a result of the present research, we propose that risk scores generated by our model could be used to enhance the current clinical staging system and predict clinical outcomes more accurately. However, more research needs to be conducted to verify our findings.

Data availability statement

The datasets presented in this study can be found in online repositories. The names of the repository/repositories and accession number(s) can be found in the article/supplementary material.

Author contributions

The work was created by LL and LPL. The data analysis was carried out by LL, SM, and GM. The draft was written by LPL and LL. The manuscript was amended and proofread by YC and LL. The manuscript was reviewed by all authors, who approved the final version before submission.

Funding

This work was supported by grants from the National Natural Science Foundation of China (Grant No. 81900470) and the Basic and Applied Basic Research Foundation of Guangdong Province (2021A1515110216).

Acknowledgments

We appreciate the free use provided by TCGA and GEO.

Conflict of interest

The authors declare that the research was conducted in the absence of any commercial or financial relationships that could be construed as a potential conflict of interest.

Publisher's note

Supplementary material

The Supplementary Material for this article can be found online at: https://www.frontiersin.org/articles/10.3389/fendo.2022.882431/full#supplementary-material.

References

1. Leonardi GC, Falzone L, Salemi R, Zanghi A, Spandidos DA, Mccubrey JA, et al. Cutaneous melanoma: From pathogenesis to therapy (Review). *Int J Oncol* (2018) 52:1071–80. doi: 10.3892/ijo.2018.4287

2. Lee KA, Nathan P. Cutaneous melanoma - a review of systemic therapies. *Acta Derm Venereol* (2020) 100:v141. doi: 10.2340/00015555-3496

3. Li X, Cai Y. Risk stratification of cutaneous melanoma reveals carcinogen metabolism enrichment and immune inhibition in high-risk patients. *Aging (Albany NY)* (2020) 12:16457–75. doi: 10.18632/aging.103734

4. Petitprez F, Meylan M, de Reynies A, Sautes-Fridman C, Fridman WH. The tumor microenvironment in the response to immune checkpoint blockade therapies. *Front Immunol* (2020) 11:784. doi: 10.3389/fimmu.2020.00784

5. Chen XY, Zhang J, Zhu JS. The role of m(6)A RNA methylation in human cancer. *Mol Canc* (2019) 18:103. doi: 10.1186/s12943-019-1033-z

6. Jing X, Yang F, Shao C, Wei K, Xie M, Shen H, et al. Role of hypoxia in cancer therapy by regulating the tumor microenvironment. *Mol Canc* (2019) 18:157. doi: 10.1186/s12943-019-1089-9

7. Ali S, Zhang Y, Zhou M, Li H, Jin W, Zheng L, et al. Functional deficiency of DNA repair gene EXO5 results in androgen-induced genomic instability and prostate tumorigenesis. *Oncogene* (2020) 39:1246–59. doi: 10.1038/s41388-019-1061-6

8. Broustas CG, Duval AJ, Chaudhary KR, Friedman RA, Virk RK, Lieberman HB. Targeting MEK5 impairs nonhomologous end-joining repair and sensitizes prostate cancer to DNA damaging agents. *Oncogene* (2020) 39:2467–77. doi: 10.1038/s41388-020-1163-1

9. Chandler BC, Moubadder L, Ritter CL, Liu M, Cameron M, Wilder-Romans K, et al. TTK inhibition radiosensitizes basal-like breast cancer through impaired homologous recombination. *J Clin Invest* (2020) 130:958–73. doi: 10.1172/JCI130435

10. Farquhar N, Thornton S, Coupland SE, Coulson JM, Sacco JJ, Krishna Y, et al. Patterns of BAP1 protein expression provide insights into prognostic significance and the biology of uveal melanoma. *J Pathol Clin Res* (2018) 4:26–38. doi: 10.1002/cjp2.86

11. Abbas O, Miller DD, Bhawan J. Cutaneous malignant melanoma: Update on diagnostic and prognostic biomarkers. *Am J Dermatopathol* (2014) 36:363–79. doi: 10.1097/DAD.0b013e31828a2ec5

12. Kupczyk P, Simiczyjew A, Marczuk J, Dratkiewicz E, Beberok A, Rok J, et al. PARP1 as a marker of an aggressive clinical phenotype in cutaneous melanoma-a clinical and an *in vitro* study. *Cells-Basel* (2021) 10:286. doi: 10.3390/cells10020286

13. Zhang X, Wang Y, Gari A, Qu C, Chen J. Pan-cancer analysis of PARP1 alterations as biomarkers in the prediction of immunotherapeutic effects and the association of its expression levels and immunotherapy signatures. *Front Immunol* (2021) 12:721030. doi: 10.3389/fimmu.2021.721030

14. Yin C, Zhu B, Zhang T, Liu T, Chen S, Liu Y, et al. Pharmacological targeting of STK19 inhibits oncogenic NRAS-driven melanomagenesis. *Cell* (2019) 176:1113–27. doi: 10.1016/j.cell.2019.01.002

15. Hoshimoto S, Kuo CT, Chong KK, Takeshima TL, Takei Y, Li MW, et al. AIM1 and LINE-1 epigenetic aberrations in tumor and serum relate to melanoma progression and disease outcome. *J Invest Dermatol* (2012) 132:1689–97. doi: 10.1038/jid.2012.36

16. Tuominen R, Jewell R, van den Oord JJ, Wolter P, Stierner U, Lindholm C, et al. MGMT promoter methylation is associated with temozolomide response and prolonged progression-free survival in disseminated cutaneous melanoma. *Int J Canc* (2015) 136:2844–53. doi: 10.1002/ijc.29332

17. Yang F, Li S, Cheng Y, Li J, Han X. Karyopherin alpha 2 promotes proliferation, migration and invasion through activating NF-kappaB/p65 signaling pathways in melanoma cells. *Life Sci* (2020) 252:117611. doi: 10.1016/j.lfs.2020.117611

18. Huang Z, Lan T, Wang J, Chen Z, Zhang X. Identification and validation of seven RNA binding protein genes as a prognostic signature in oral cavity squamous cell carcinoma. *Bioengineered* (2021) 12:7248–62. doi: 10.1080/21655979.2021.1974328

19. Subramanian A, Tamayo P, Mootha VK, Mukherjee S, Ebert BL, Gillette MA, et al. Gene set enrichment analysis: A knowledge-based approach for interpreting genome-wide expression profiles. *Proc Natl Acad Sci U S A* (2005) 102:15545–50. doi: 10.1073/pnas.0506580102

20. Ait SS, Chraa D, El AK, Sahraoui S, Olive D, Badou A. Prognostic gene expression signature in patients with distinct glioma grades. *Front Immunol* (2021) 12:685213. doi: 10.3389/fimmu.2021.685213

21. Charoentong P, Finotello F, Angelova M, Mayer C, Efremova M, Rieder D, et al. Pan-cancer immunogenomic analyses reveal genotype-immunophenotype relationships and predictors of response to checkpoint blockade. *Cell Rep* (2017) 18:248–62. doi: 10.1016/j.celrep.2016.12.019

22. Clayton EA, Pujol TA, McDonald JF, Qiu P. Leveraging TCGA gene expression data to build predictive models for cancer drug response. *BMC Bioinf* (2020) 21:364. doi: 10.1186/s12859-020-03690-4

23. Zhao S, Liu XY, Jin X, Ma D, Xiao Y, Shao ZM, et al. Molecular portraits and trastuzumab responsiveness of estrogen receptor-positive, progesterone receptor-positive, and HER2-positive breast cancer. *Theranostics* (2019) 9:4935–45. doi: 10.7150/thno.35730

24. Matt S, Hofmann TG. The DNA damage-induced cell death response: A roadmap to kill cancer cells. *Cell Mol Life Sci* (2016) 73:2829–50. doi: 10.1007/s00018-016-2130-4

25. Ciccia A, Elledge SJ. The DNA damage response: Making it safe to play with knives. *Mol Cell* (2010) 40:179–204. doi: 10.1016/j.molcel.2010.09.019

26. Malfatti MC, Antoniali G, Codrich M, Burra S, Mangiapane G, Dalla E, et al. New perspectives in cancer biology from a study of canonical and non-canonical functions of base excision repair proteins with a focus on early steps. *Mutagenesis* (2020) 35:129–49. doi: 10.1093/mutage/gez051

27. Pilie PG, Tang C, Mills GB, Yap TA. State-of-the-art strategies for targeting the DNA damage response in cancer. *Nat Rev Clin Oncol* (2019) 16:81–104. doi: 10.1038/s41571-018-0114-z

28. Khan AQ, Travers JB, Kemp MG. Roles of UVA radiation and DNA damage responses in melanoma pathogenesis. *Environ Mol Mutagen* (2018) 59:438–60. doi: 10.1002/em.22176

29. Dong SQ, Wang TM, Zhang JB, He YQ, Xue WQ, Wu ZY, et al. Polymorphisms in TYMS for prediction of capecitabine-induced hand-foot syndrome in chinese patients with colorectal cancer. *Cancer Res Treat* (2021) 53:724–32. doi: 10.4143/crt.2020.457

30. Kashiwagi E, Shiota M, Yokomizo A, Itsumi M, Inokuchi J, Uchiumi T, et al. Downregulation of phosphodiesterase 4B (PDE4B) activates protein kinase a and contributes to the progression of prostate cancer. *Prostate* (2012) 72:741–51. doi: 10.1002/pros.21478

31. Choy CT, Wong CH, Chan SL. Embedding of genes using cancer gene expression data: Biological relevance and potential application on biomarker discovery. *Front Genet* (2018) 9:682. doi: 10.3389/fgene.2018.00682

32. Wakula M, Balcerak A, Rubel T, Chmielarczyk M, Konopinski R, Lyczek F, et al. The interactome of multifunctional HAX1 protein suggests its role in the regulation of energy metabolism, de-aggregation, cytoskeleton organization and RNA-processing. *Biosci Rep* (2020) 40. BSR20203094.doi: 10.1042/BSR20203094

33. Lodillinsky C, Fuhrmann L, Irondelle M, Pylypenko O, Li XY, Bonsang-Kitzis H, et al. Metastasis-suppressor NME1 controls the invasive switch of breast cancer by regulating MT1-MMP surface clearance. *Oncogene* (2021) 40:4019–32. doi: 10.1038/s41388-021-01826-1

34. Hansen AW, Arora P, Khayat MM, Smith LJ, Lewis AM, Rossetti LZ, et al. Germline mutation in POLR2A: A heterogeneous, multi-systemic developmental disorder characterized by transcriptional dysregulation. *HGG Adv* (2021) 2: 100014. doi: 10.1016/j.xhgg.2020.100014

35. Zhao L, Cheng Q, Wang Z, Xi Z, Xu D, Liu Y. Cisplatin binds to human copper chaperone Cox17: The mechanistic implication of drug delivery to mitochondria. *Chem Commun (Camb)* (2014) 50:2667–9. doi: 10.1039/c3cc48847k

36. Ali R, Alabdullah M, Algethami M, Alblihy A, Miligy I, Shoqafi A, et al. Ligase 1 is a predictor of platinum resistance and its blockade is synthetically lethal in XRCC1 deficient epithelial ovarian cancers. *Theranostics* (2021) 11:8350–61. doi: 10.7150/thno.51456

37. Ribeiro-Silva C, Aydin OZ, Mesquita-Ribeiro R, Slyskova J, Helfricht A, Marteijn JA, et al. DNA Damage sensitivity of SWI/SNF-deficient cells depends on TFIIH subunit p62/GTF2H1. *Nat Commun* (2018) 9:4067. doi: 10.1038/s41467-018-06402-y

38. Frejno M, Meng C, Ruprecht B, Oellerich T, Scheich S, Kleigrewe K, et al. Proteome activity landscapes of tumor cell lines determine drug responses. *Nat Commun* (2020) 11:3639. doi: 10.1038/s41467-020-17336-9

39. Chatzinikolaou G, Karakasilioti I, Garinis GA. DNA Damage and innate immunity: Links and trade-offs. *Trends Immunol* (2014) 35:429–35. doi: 10.1016/j.it.2014.06.003

40. Sen T, Rodriguez BL, Chen L, Corte C, Morikawa N, Fujimoto J, et al. Targeting DNA damage response promotes antitumor immunity through STING-mediated t-cell activation in small cell lung cancer. *Cancer Discovery* (2019) 9:646–61. doi: 10.1158/2159-8290.CD-18-1020

41. Sato H, Niimi A, Yasuhara T, Permata T, Hagiwara Y, Isono M, et al. DNA Double-strand break repair pathway regulates PD-L1 expression in cancer cells. *Nat Commun* (2017) 8:1751. doi: 10.1038/s41467-017-01883-9

42. Jiao S, Xia W, Yamaguchi H, Wei Y, Chen MK, Hsu JM, et al. PARP inhibitor upregulates PD-L1 expression and enhances cancer-associated

immunosuppression. *Clin Cancer Res* (2017) 23:3711–20. doi: 10.1158/1078-0432.CCR-16-3215

43. Garsed DW, Alsop K, Fereday S, Emmanuel C, Kennedy CJ, Etemadmoghadam D, et al. Homologous recombination DNA repair pathway disruption and retinoblastoma protein loss are associated with exceptional survival in high-grade serous ovarian cancer. *Clin Cancer Res* (2018) 24:569–80. doi: 10.1158/1078-0432.CCR-17-1621

44. Desai NB, Bagrodia A. The challenge of matching assays to biology in DNA damage response biomarkers for response to radiotherapy in bladder cancer. *Transl Androl Urol* (2019) 8:S514–6. doi: 10.21037/tau.2019.07.05

45. Eddy K, Shah R, Chen S. Decoding melanoma development and progression: Identification of therapeutic vulnerabilities. *Front Oncol* (2020) 10:626129. doi: 10.3389/fonc.2020.626129

46. Yang CC, Chang MT, Chang CK, Shyur LF. Phytogalactolipid dLGG inhibits mouse melanoma brain metastasis through regulating oxylipin activity and re-programming macrophage polarity in the tumor microenvironment. *Cancers (Basel)* (2021) 13:4120. doi: 10.3390/cancers13164120

frontiers | Frontiers in Endocrinology

TYPE Review
PUBLISHED 22 August 2022
DOI 10.3389/fendo.2022.929572

OPEN ACCESS

EDITED BY
Yang Mi,
Henan Key Laboratory for Helicobacter pylori &Microbiota and Gastrointestinal Cancer, China

REVIEWED BY
Miguel Luiz Batista Júnior,
Boston Medical Center, United States
Lianjun Zhang,
Suzhou Institute of Systems Medicine (ISM), China
Colt Egelston,
City of Hope National Medical Center, United States

*CORRESPONDENCE
Jose S. Lopez-Gonzalez
slopezgonzalez@yahoo.com

†These authors share first authorship

SPECIALTY SECTION
This article was submitted to Cancer Endocrinology, a section of the journal Frontiers in Endocrinology

RECEIVED 27 April 2022
ACCEPTED 01 August 2022
PUBLISHED 22 August 2022

CITATION
Aguilar-Cazares D, Chavez-Dominguez R, Marroquin-Muciño M, Perez-Medina M, Benito-Lopez JJ, Camarena A, Rumbo-Nava U and Lopez-Gonzalez JS (2022) The systemic-level repercussions of cancer-associated inflammation mediators produced in the tumor microenvironment. *Front. Endocrinol.* 13:929572. doi: 10.3389/fendo.2022.929572

The systemic-level repercussions of cancer-associated inflammation mediators produced in the tumor microenvironment

Dolores Aguilar-Cazares[1†], Rodolfo Chavez-Dominguez[1,2†], Mario Marroquin-Muciño[1,3†], Mario Perez-Medina[1,3], Jesus J. Benito-Lopez[1,2], Angel Camarena[4], Uriel Rumbo-Nava[5] and Jose S. Lopez-Gonzalez[1*]

[1]Laboratorio de Investigacion en Cancer Pulmonar, Departamento de Enfermedades Cronico-Degenerativas, Instituto Nacional de Enfermedades Respiratorias "Ismael Cosio Villegas", Mexico City, Mexico, [2]Posgrado en Ciencias Biologicas, Universidad Nacional Autonoma de Mexico, Mexico City, Mexico, [3]Laboratorio de Quimioterapia Experimental, Departamento de Bioquimica, Escuela Nacional de Ciencias Biologicas, Instituto Politecnico Nacional, Mexico City, Mexico, [4]Laboratorio de Human Leukocyte Antigen (HLA), Instituto Nacional de Enfermedades Respiratorias "Ismael Cosio Villegas", Mexico City, Mexico, [5]Clinica de Neumo-Oncologia, Instituto Nacional de Enfermedades Respiratorias "Ismael Cosio Villegas", Mexico City, Mexico

The tumor microenvironment is a dynamic, complex, and redundant network of interactions between tumor, immune, and stromal cells. In this intricate environment, cells communicate through membrane–membrane, ligand–receptor, exosome, soluble factors, and transporter interactions that govern cell fate. These interactions activate the diverse and superfluous signaling pathways involved in tumor promotion and progression and induce subtle changes in the functional activity of infiltrating immune cells.

The immune response participates as a selective pressure in tumor development. In the early stages of tumor development, the immune response exerts anti-tumor activity, whereas during the advanced stages, the tumor establishes mechanisms to evade the immune response, eliciting a chronic inflammation process that shows a pro-tumor effect.

The deregulated inflammatory state, in addition to acting locally, also triggers systemic inflammation that has repercussions in various organs and tissues that are distant from the tumor site, causing the emergence of various symptoms designated as paraneoplastic syndromes, which compromise the response to treatment, quality of life, and survival of cancer patients. Considering the tumor–host relationship as an integral and dynamic biological system, the chronic inflammation generated by the tumor is a communication mechanism among tissues and organs that is primarily orchestrated through different signals, such as cytokines, chemokines, growth factors, and exosomes, to provide the tumor with energetic components that allow it to continue proliferating. In this review, we aim to provide a succinct overview of the involvement of cancer-related inflammation at the local and systemic level

throughout tumor development and the emergence of some paraneoplastic syndromes and their main clinical manifestations. In addition, the involvement of these signals throughout tumor development will be discussed based on the physiological/biological activities of innate and adaptive immune cells. These cellular interactions require a metabolic reprogramming program for the full activation of the various cells; thus, these requirements and the by-products released into the microenvironment will be considered. In addition, the systemic impact of cancer-related proinflammatory cytokines on the liver—as a critical organ that produces the leading inflammatory markers described to date—will be summarized. Finally, the contribution of cancer-related inflammation to the development of two paraneoplastic syndromes, myelopoiesis and cachexia, will be discussed.

KEYWORDS

cancer, tumor microenvironment, inflammatory mediators, cytokines, systemic inflammation, paraneoplastic syndromes, systemic immune-inflammatory markers

Introduction

In 2020, GLOBOCAN estimated the global cancer statistics as 19.3 million new cases and 10 million deaths yearly (1). The increasing incidence and mortality rates reflect the growth and aging of the population and the increase in risk factors associated with socioeconomic development. Great efforts have been made to detect cancer early; however, most cases are detected at advanced stages.

Inflammation is a well-conserved process in which a distinct subset of cells from the innate and adaptive immune response is recruited to eliminate harmful agents in the host. This process is essential for the host's defense against pathogens and is accompanied by tissue repair and wound healing to regulate tissue homeostasis. However, when dysregulated, inflammation contributes to the emergence and development of cancer. Tumor-associated inflammation is a well-recognized tumor-enabling characteristic that promotes or sustains the acquisition of some characteristics termed the hallmarks of cancer (2, 3). During tumor development, tumor-associated inflammation shapes the anti-tumor immune response towards a more permissive and pro-tumoral state (3). In this regard, the relationship between the tumor and the immune response is well known; according to immunoediting theory, at the early stages of tumor development, the immune system exerts anti-tumor activity through immunosurveillance (4). In this setting, as the tumor evolves, so does its microenvironment and the immune response, favoring the establishment of a pro-tumoral immune response. Several reports have indicated that the shift from anti-tumor immunity towards a pro-tumoral response is supported by a myriad of factors released from the tumor, immune, and stromal cells into the tumor microenvironment, which act to establish a persistent tumor-associated inflammatory state (5).

Nonetheless, the tumor-associated inflammatory state not only has repercussions in its immediate local microenvironment, but the release of various components into the bloodstream that promote or sustain inflammatory activity at the systemic level primes a cancer-induced systemic inflammatory response (6). At the plasma level, high concentrations of these proinflammatory factors can affect different organs or systems, such as the endocrine, nervous, dermatological, and hematological systems, among others, resulting in the alteration of the expression of some molecules or set of circulating cells, which are currently used as markers of systemic inflammation associated with cancer (5). In addition to the known cytokines, chemokines, and growth factors, it is now recognized that exosomes are one of the main factors capable of reaching different organs or systems, leading to the development of additional comorbidities called paraneoplastic syndromes (6). Among these paraneoplastic syndromes, neuropathy, hypercalcemia, dermatomyositis, cachexia, and dysregulated hematopoiesis cause detrimental effects on the patient's quality of life and are sometimes manifested before cancer detection (7). In some instances, the clinical manifestation of paraneoplastic syndromes contributes to the promotion of tumor growth-promoting capabilities, leading to decreased overall survival (8, 9).

The study of cancer initially focused on the tumor's genetic alterations and biological activity. Recently, the role of the bidirectional interactions between the tumor and its microenvironment as an integral and evolving biological system has been considered. Although human tumors are composed of heterogeneous cell populations, employing tumor

cell lines and animal models has allowed us to deepen our understanding of the participation of the microenvironment throughout tumor development.

This review highlights the intricate signaling mediated by the different components released in the tumor microenvironment and their contribution at the systemic level. First, we will describe the interaction between the tumor and the immune cells and its evolution during tumor development. The local production of immune-stimulating factors by the stroma and immune inhibitory mediators induced or produced by the tumor will also be considered. At the systemic level, the effect of the main proinflammatory cytokines reaching their target organs and their impact on the production of inflammation markers will be addressed. Finally, the clinical manifestations associated with the development of inflammatory cytokines-induced paraneoplastic syndromes will be examined.

Tumor microenvironment

According to the multistep carcinogenesis model, a tumor is shaped by a group of heterogeneous cells harboring genomic and epigenomic alterations. Transformed cells carrying driver mutations and epigenetic alterations activate aberrant signaling pathways that hinder the apoptotic process and promote uncontrolled cell proliferation. The growth of these transformed cells leads to changes in tissue architecture, which induces stress in the cells of the surrounding stroma, causing an increase in the production of soluble inflammatory mediators and growth factors and exosome release. These factors maintain a chronic inflammatory microenvironment that enables tumorigenesis (10). As the tumor grows, heterogeneous cell populations are generated due to the high and stochastic proliferation rate. Some of these new populations in the tumor mass acquire immune evasion mechanisms or produce soluble factors that modify immune cell phenotypes to support pro-tumor activity (11).

It has been recognized that the tumor microenvironment (TME) participates in cancer development and promotes the acquisition of some hallmarks of cancer (2). The composition of TME is heterogeneous; it is mainly composed of—but not limited to—cells such as endothelial cells, cancer-associated fibroblasts, pericytes, cancer stem cells, and immune-inflammatory cells, in addition to diverse extracellular matrix components (2).

In this context, the TME is a complex, redundant, and dynamic network that is constantly evolving throughout tumor development and progression. In this network, tumor, immune, and non-immune cells establish membrane–membrane and ligand–receptor interactions as well as communicate through the paracrine, juxtacrine, and internal secretion of various substances, such as proteins, different types of RNA, lipids, and biological mediators, which are delivered through the production of exosomes (12–14). Exosomes are vesicles between 40 and 160 nm in diameter. Exosomes arise from an early endosome in a process mediated by the endosomal sorting complex required for transport (ESCRT) (15). These mature endosomes are also known as multivesicular bodies (MVBs). MVBs can fuse with lysosomes for the degradation of their contents or can fuse with the plasma membrane, releasing their vesicles into the extracellular space (16). Exosomes can contain proteins, RNA, DNA, lipids, and carbohydrates. Initially considered as waste products of cells, exosomes are now known to play an essential role in cell communication (17). Most reports indicate that exosomes play paramount roles in tumor cell invasion, metastasis, and angiogenesis. In addition, exosomes are involved in modulating the TME, altering cellular metabolism, and promoting or inhibiting the immune response (18).

All of these interactions and molecule transfers activate diverse signaling pathways that affect gene expression, support the metabolic demands of different cell types, and induce the synthesis of various proteins that act as critical biomolecules to induce the participation of the immune response against genotoxic insults, incipient tumor formation, and tumor development (19, 20). During the early stage of tumor development, a nascent transformed cell develops in close interaction with the resident immune cells, among which the incipient transformed cell proliferates to form a small group of cells that lead to the distortion of the local tissue morphology. In this regard, and as part of the innate immune response, natural killer (NK) cells and resident macrophages eliminate susceptible tumor cells by releasing cytotoxic molecules that insert themselves into the tumor cell membrane, altering its permeability and causing cell death (21). Throughout this process, the dying cells expose molecules on their membrane or release intracellular molecules that acquire a new function, acting as alarmins or damage-associated molecular patterns (DAMPs) that promote the recruitment of other populations of immune cells, such as those involved in the adaptive immune response.

At this point, some reports have indicated that the exosomes released by tumor cells express class I and II MHC molecules and can prime and activate the immune response. As tumor cells develop and persistent growth occurs, the activation of the immune response continues and chronic inflammation is promoted, which initially stimulates an anti-tumor immune response (see below). However, it is known that chronic inflammation allows for the acquisition of new mutations and increased genome instability. Chronic inflammation causes the cellular composition of the tumor to become heterogeneous, resulting in a progressive change in the activities of the immune and stromal cells to promote a microenvironment that favors progression, invasion, and metastasis (22–24).

10.3389/fendo.2022.929572

Participation of the immune response in cancer

The relationship between chronic inflammation and cancer development is well known and is considered a hallmark of cancer (2). Virchow's observations led him to propose that chronic inflammation provoked by the presence of an immune infiltrate was associated with the development of cancer (25). Afterward, Dvorak reported similar features between inflammation and cancer, such as proliferation, cell survival, angiogenesis, and migration (26).

The immune system is composed of an intricate network of cells, including NK cells, which are part of the innate lymphoid cells (ILCs) (27) and NKT cells, along with macrophages and dendritic cells (DCs), which are cells of the phagocytic mononuclear system that are involved in antigen presentation. As part of the adaptive immune response includes T lymphocytes, such as CD4+ T and CD8+ T cells, and B lymphocytes (28). The detailed study of tumor-infiltrating immune cells in biopsied material obtained from cancer patients has indicated that immune cells interact with tumor cells through the production of diverse factors, such as cytokines, chemokines, the by-products of cell metabolism, growth factors, and the components of exosomes, which participate during the tumor development stages (29). It has been suggested that immune cells and the soluble factors they secrete induce a particular microenvironment that, in the early stages of tumor development, supports anti-tumor activities; nevertheless, the microenvironment evolves, and in the advanced stages of the tumor, the immune cells are modulated to promote tumor growth (29).

According to emerging knowledge on the biological role and physiological importance of the different cells that compose the immune system, it has been proposed that NK cells patrol the human body to recognize normal self-cells, a process carried out by two types of receptors. Thus, NK cell activation is tightly regulated by an intricate balance between activation and inhibition signals (30, 31). In a normal cell, the peptides derived from self-proteins are loaded onto class I MHC molecules and are recognized by NK cells through the killer cell immunoglobulin-like receptor (KIR). In contrast, the recognition of self-cell ligands, such as the stress-induced proteins MICA, MICB, and ULBP-1, is mediated by the natural cytotoxic receptor (NCR) (32, 33). In tumor cells, tumoral peptides are associated with class I molecules, impeding recognition by KIR receptors and triggering effector activity. For full activation, NK cells depend on glycolysis and oxidative phosphorylation (OXPHOS), which are modulated by mTORC1 (34, 35). NK cells fight tumors by releasing cytolytic molecules, such as perforin, granzymes, and granulysin, causing the death of sensitive tumor cells. Some authors have also shown that NK cells can release exosomes containing these cytolytic molecules that reduce or eliminate malignant cells in both tumor-bearing animal models and human tumor cell lines of distinct origins (36–38).

In addition, activated NK cells release several soluble mediators, such as tumor necrosis factor-alpha (TNF-α); interferon-gamma (IFN-γ); interleukin (IL)-10; chemokines, including CCL3, CCL4, CCL5, XCL1, etc.; and growth factors, such as granulocyte macrophage colony-stimulating factor (GM-CSF), etc. (39). IFN-γ is known to be essential for immune cell activation; in NK cells, it increases cell activity and cytolytic potential (40, 41). From this point of view, NK cell overactivity increases the proportion of dying tumor cells and releases more DAMPs are released, which act as "find me" signals, and tumor antigens. These tumor-released compounds promote the arrival of inflammatory and immune cells, initiating an acute inflammatory process (42, 43). In this setting, tissue-resident macrophages, dendritic cells (DCs), and recruited monocyte-derived DCs comprise the mononuclear phagocytic system (44, 45), playing a critical role in homeostasis, tissue repair, the immune response, and cancer (46). In local tissues, resident and immature DCs (iDCs) exhibit elevated phagocytic activity mediated by the expression of a variety of pattern recognition receptors (PRRs) (47), which recognize the DAMPs and tumor antigens released from dead and dying tumor cells. Then, the iDCs trigger a rigorous metabolic process to meet the cell's energy demands, including increased aerobic glycolysis, decreased OXPHOS with a concomitant increase in nitric oxide (NO) production, and increased fatty acid (FA) metabolism (48, 49). ROS production regulates the acidification of the lysosomal compartment for the degradation of phagocytosed antigens to peptides, while FA metabolism supplies the components for cell membranes. During these events, the endoplasmic reticulum and Golgi apparatus are expanded for protein synthesis, which assists in the upregulation of class II MHC molecules and antigen cross-presentation by class I MHC molecules; the expression of the costimulatory molecules CD80, CD86, and CD40; the expression of receptors for chemokines; and cytokine secretion, including interleukin (IL)-1, TNF-α, IL-6, IL-8, IL-12, IL-15, IL-18, etc. All of these activities induce the progressive maturation of DCs to become professional antigen-presenting cells (APCs). Then, the APCs travel to the lymph node through the lymphatic vessels, a process in which glucose metabolism plays a critical role (50, 51).

In the lymph node, DCs (mDCs) act as potent APCs that stimulate the proliferation and maturation of naïve antigen-specific CD4+ T cell clones and, by antigen cross-presentation, the activation of naïve antigen-specific CD8+ T cells. In addition to direct cell–cell interactions, some studies have indicated that exosomes released by APCs can also induce T-cell activation. It has been demonstrated that they express peptides associated with class I and II MHC and costimulatory molecules. In addition, they can also activate T and NK cells through the NKG2D–NKG2D ligand interaction (52–58).

Soon after the initial T-lymphocyte priming, T cells upregulate aerobic glycolysis, increasing glucose transporters and enzymes to meet their energetic demands; glutaminolysis and increased amino acid uptake favor OXPHOS for ROS and NO synthesis. In addition to mitochondrial biogenesis, lipogenesis by the endoplasmic

reticulum and Golgi apparatus are required. Following this PI3K-AKT-mTORC1-dependent metabolic reprogramming, effector CD4+ T cells secrete several cytokines, such as IL-2, IFN-γ, etc., that induce the activation of specific transcriptional programs for the stimulation of antigen-specific CD8+ T cells and the overactivation of NK cells (59–61). The CD8+ T cells then release various cytokines, such as IFN-γ, IL-2, and TNF-α, and synthesize cytolytic molecules to become effector cytotoxic T lymphocytes (CTLs) (60, 62). After T-cell expansion, effector CD4+ T cells and CTLs migrate through the bloodstream and infiltrate the tumor, becoming critical cells for tumor destruction (63). A recent report from Rezaei R et al. using a CT-26-induced BALB/c mouse model of colorectal cancer indicated that when incorporated into tumor-derived exosomes, miR-124-3p, which acts as a post-transcriptional regulator of gene expression, stimulates a potent antitumor immune response, diminishing T regulatory (Treg) cells, reducing tumor mass, and increasing the overall survival rate (64). This miRNA is downregulated in colon cancer compared to non-malignant tissue, and *in vitro* studies have indicated that in Treg cells, PD-L1 expression is inhibited by cytokines such as TGF- β and IL-10 (65). All of this information suggests the possible involvement of exosomes released by tumor cells in the induction of a potent anti-tumor immune response. The cytokines released by T cells create a positive feedback loop that perpetuates the inflammatory process, as the array of pro-inflammatory cytokines leads to the overstimulation of innate immune cells. In addition, the overstimulated NK cells upregulate the activity of tissue-resident macrophages and the recruited neutrophils at the tumor site. These phagocytic cells carry out the respiratory burst to further produce pro-inflammatory cytokines and release ROS and NOS, promoting the M1 and N1 cell phenotypes, respectively. The induced anti-tumor activity leads to the additional destruction of tumor cells (66). Exosomes released by these metabolically activated cells mimic the tumoricidal activity of M1 and N1 cells (67–69).

A chronic inflammatory process is induced when this cellular circuit is maintained to eliminate tumor cells which mutations generate immunogenic changes in the synthetized tumor proteins. Reports have indicated that the chronic inflammatory process causes the release of transferrin-bound iron, which accumulates in the extracellular space. It is known that tumor cells take up this element, which promotes the production of DNA-damaging ROS. Increased DNA damage may lead to cell death in some vulnerable tumor cells in a process known as cell death mediated by ferroptosis (70). Conversely, these and other mutation-causing factors could promote genomic instability and epigenetic changes in other cells within the tumor cell population, which could lead to the maintenance of cell viability and enhance tumor proliferation, induce resistance to apoptosis, and, concomitantly, increase tumor heterogeneity (71).

Thus, the tumor comprises new tumor cell clones, increasing phenotypic heterogeneity, and the tumor mass itself. Oncogenic changes promote the activation of various signaling pathways in the heterogeneous tumor population, increasing the release of exosomes with different molecules or soluble factors that reinforce the inflammatory phase of chronic inflammation. For example, driver mutations in genes, such as *MYC, K-RAS*, or *RET* activate signaling pathways that promote the synthesis and release of proinflammatory cytokines, such as IL-8, IL-1, and CXC chemokines (72–74).

Depending on the tumor type, stage of tumor progression, genetic background, clinicopathological characteristics of the patient, etc., the distribution and density of non-malignant cells infiltrating the tumor vary greatly. Tumor and non-malignant cells produce several cytokines, growth and differentiation factors, chemokines, lipids, and nucleic acids that are released or loaded into exosomes, generating a wide array of molecules that promote cancer. Various research groups have published excellent reviews describing the signaling pathways involving cytokines, growth factors, and exosome components that may play a role in cancer (14, 18, 54, 75–77).

In the more advanced stages of cancer development, the surrounding tumor, stromal, and immune cells show a high rate of proliferation that requires high metabolic activity, resulting in the release of various by-products. In addition to the factors released by the various cells that make up the tumor, these metabolic by-products create a complex and changing microenvironment, which gradually promotes cancer cell survival and tumor mass growth. High metabolic activity is indispensable due to the chronic inflammatory process induced by the tumor. The increased energy and biosynthetic requirements mediated by increased glucose uptake and aerobic glycolysis favor the tumor's proliferation, differentiation, and growth and affect the stromal cells. During this metabolic reprogramming, tumor cells produce—or induce the immune and stromal cells to produce—several cytokines that stimulate tumor growth while inhibiting or blocking the effector activity of immune cells. Some of the cytokines produced include IL-10, IL-6, IL-4, High Mobility Group-Box 1 (HMGB1) protein, etc., while several growth factors are generated as well, such as Epithelial Growth Factor (EGF), vascular endothelial growth factor (VEGF)-A, transforming growth factor-β (TGF-β), platelet-derived growth factor subunit A (PDGF-A), angiopoietin-like 4 (ANGPTL4), etc.; information about these factors is summarized in Table 1. In addition, some chemokines and their receptors play an important role in the TME and are expressed by tumor, immune, and stromal cells. Due to their anti- and pro-tumor effects, α-chemokines, i.e., CXC chemokines that contain a CXC motif at their N-terminus, have attracted attention. Some reports have indicated that CXCR3 and its corresponding ligands, CXCL14 and CXCL16, recruit primary immune cells with immune regulatory functions and pro-tumor activities, such as tumor-associated macrophages (TAMs) and neutrophils (TANs), myeloid-derived suppressor cells (MDSCs), and Treg cells (120–122). Chemerin was initially described as a chemotactic factor for NK cells, macrophages, and myeloid and plasmacytoid DCs (123–125), favoring tumor infiltration by

10.3389/fendo.2022.929572

TABLE 1 Cytokines and Growth Factors associated with cancer-related inflammation.

Cytokine	Primary Target Cell	Biological activity in cancer	Ref.
IFN-γ	Macrophages, NK, and T-cells	Up-regulates expression of MHC-I and-II molecules and antigen presentation. Inhibits proliferation of tumor cells and induces necroptotic cell death.	(78–80)
IL-1	NK, T-, M1 macrophages, and tumor cells	Promotes systemic and local inflammation. Facilitates angiogenesis through activation of endothelium and metastasis. Participates in mobilization of HSPCs in bone marrow to yield MDSCs.	(81, 82)
IL-2	T-CD4/CD8 and NK cells	Drives the activation of tumor-infiltrating CD8+ T cells.	(83)
IL-4	Th2 cells, basophils, eosinophils, and macrophages	Decreases the activity of TAM and CD8+ T cells. Induce the expression of Th2 cytokines modulating the antitumor immune response. Induce a regulatory phenotype on NK cells by modulating DCs. Stimulates the growth of tumor cells and cell death resistance.	(84–88)
IL-6	Monocytes, macrophages, endothelial cells, B- and T-cells, and tumor cells	Regulation of acute phase response, activation of T helper cells. Promotes the growth of tumor cells and favors their survival. Implicated in angiogenesis.	(89–91)
IL-8	Neutrophils, endothelial cells, and pericytes	Attraction of MDSCs into the tumor. Activation of angiogenesis. Regulation of stem cell properties.	(92, 93)
IL-10	T-, B-, dendritic cells (DCs), Th2 lymphocytes, Tregs, and macrophages	Inhibits the expression of MHC class I and II molecules and antigen presentation in APCs and tumor cells. Contribute to immunosuppression by hindering the effector activity NK, Th1, and CD8+ T cells. Negatively correlates with tumor-infiltrating CD8+ IFN-γ+.	(94–97)
IL-12	NK, APCs, and T-cells	Promotes proliferation and cytotoxic effect of NK cells. Enhance the anti-tumor activity of M1 and Th1 cells.	(98)
IL-17	Mucosal tissues, fibroblast, epithelial, endothelial, Th17, NK cells, and monocytes	Contributes in tumor growth, metastasis and cancer-related inflammation.	(99, 100)
IL-18	Th1, NK, DCs, macrophages, keratinocytes, and B cells	Pro-inflammatory cytokine. Cooperates with IL-12 inducing IFN-γ production from T helper and NK cells, leading to NK cell activation; up-regulates antigen presentation and exhibits antiviral and antitumoral functions. Suppress tumor growth by downregulating VEGF production within tumor.	(101, 102)
TNF-α	Neutrophils, macrophages, monocytes, and endothelial cells	Increase tumor cell growth, angiogenesis, and metastasis. Participates in promoting cancer-associated inflammation.	(103)
TGF-β	MDSCs, Tregs, and tumor cells	Increase the expression of PD-1 on intra-tumoral CD8+ T cells resulting in their dysfunction and exhaustion. Inversely correlates with the frequency of CD8+ T cells in the tumor niche. Suppress the cytotoxic activity of NK cells. Promotes the activation of the EMT program.	(104–107)
GM-CSF	Lymphocytes, macrophages, fibroblast, endothelial cells, and tumor cells	Promotes DCs differentiation, in response to cytokine or inflammatory stimuli, activates the effector functions of myeloid cells at the resolution of inflammation to promote wound healing and tissue repair.	(108)
G-CSF	Fibroblast, stromal cells, monocytes, macrophages, and endothelial cells	Stimulates extramedullary hematopoiesis in the liver. Causes the differentiation of HPSCs into myeloid precursors in bone marrow. Recruits DCs and activates Tregs and secretion of Th2 cytokines.	(109, 110)
PDGF	Platelets, macrophages, osteoblasts, fibroblasts, and tumor cells	Chemoattractant of fibroblasts. Stimulates angiogenesis and activation of EMT.	(111–113)
VEGF	Smooth muscle cells, keratynocytes, platelets, endothelial cells, neutrophils, macrophages, and tumor cells	In endothelial cells induces a mitogenic effect and resistance to cell death. Promotes apoptosis of CTLs through Fas-FasL in tumor vasculature. Hampers the maturation of DCs.	(114–116)
EGF	Epithelial cells, fibroblast, platelets, endothelial cells, glands, and tumor cells	Over-expression correlates with TGF- β, tumor growth, metastasis, and resistance to anti-tumor agents	(117–119)

leukocytes and the regulation of cell metabolism. Current reports indicate that different cell types produce chemerin, including fibroblasts, epithelial cells residing in the tumor niche, and cells from distant organs, such as hepatocytes and adipocytes (126–128). Although most tumors downregulate the expression of chemerin, the potential pro- and anti-tumor activities of this molecule have been reported in the TME and have been suggested as a prognosis marker (129). More information on this topic is beyond the scope of this review; however, further information can be obtained from previous studies (130, 131).

In the TME, the high proliferation rate of tumor cells induces hypoxia, leading to hypoxia-induced acidosis caused by the release of lactate (132). During this metabolic reprogramming in liver cancer, the lncRNA HULC modulates the activity of crucial glycolytic enzymes through phosphorylation (133). In addition, LINC00261 promotes aerobic glycolysis in pancreatic cancer by activating the miR-222-3p/HIPK2/ERK axis (134). The participation of exosomes during hypoxia is an emerging research area. In one study, the long-intergenic non-coding RNA regulator of reprogramming (LINC-RoR) contained in the exosomes released by hepatocellular cancer cells under hypoxic conditions was shown to lead to increased HIF-α expression and the poorer survival of patients (135). In addition, in colorectal cancer,

LINC00152 has been shown to be released in exosomes under hypoxic conditions, participating in the pathogenesis and progression of this cancer (136, 137). The production and secretion of lactate by tumor and infiltrating immune cells induce a gradual reconversion of immune cells from anti-tumor to pro-tumor activity to promote tumor immune evasion and support the migration and invasion of tumor cells (138, 139).

Tumor cells increase their iron uptake to supply their bioenergetic demand. Iron metabolism impacts DNA synthesis, cell cycle progression, and morphogenesis in physiological processes during normal cell life. This metabolic program also participates in invasion, metastasis, and EMT (140). However, as mentioned previously, increased cytoplasmic iron levels could induce a type of cell death known as ferroptosis (141). Cells undergoing ferroptosis release DAMPs associated with cell death, such as HMGB1, ATP, etc. (142). In the TME, extracellular ATP released by dead or dying cancer cells is hydrolyzed by several families of ectonucleotidases (143), mainly CD39 and CD73, which are expressed by immune and endothelial cells (144, 145). These enzymes are responsible for the conversion of extracellular ATP to adenosine. Adenosine accumulation in hypoxic cancer tissue is sensed by A2AR and A2BR receptors on immune cells that hamper the anti-tumor immune response. It is known that A2AR blocks the immune cells secretion of IFN- γ and IL-2. At the same time, A2BR prevents antigen presentation by mDCs and induces the polarization of M1 to M2 macrophages and the stimulation of MDSCs (146, 147).

Additionally, metabolic reprogramming activates signaling pathways that lead to aberrant gene expression due to epigenetic changes that alter tumor and stromal cells. These metabolic changes produce cells that also display the pro-tumor properties, such as cancer-associated fibroblasts (CAFs), induced by the TGF- β and EGF secreted by the tumor (148). In addition, they produce several chemokines; TGF- β ; IL6; some growth factors such as hepatocyte growth factor, insulin-like growth factor, etc.; and release exosomes. Furthermore, this environment favors the recruitment of MDSCs (149), TAMs (150), mesenchymal stem cells (MSCs) (151), and Tregs (152, 153). The role of exosomes in promoting the participation of these subsets of immune cells displaying pro-tumoral activity is discussed in the following reviews (154, 155).

In the TME, the accumulation of cytokines, chemokines, soluble factors, and a mixture of biomolecules in exosomes compromises the immune response during the advanced stages of cancer (156–158). Soluble factors with immunosuppressant activity, such as IL-10, TGF-b, IL-4, IL-6, etc., impair the function of NK cells (159, 160) and CTLs (161, 162) by inhibiting their effector activity and downregulating the expression of transcripts coding for cytolytic molecules. This cytokine environment induces the differentiation of CD4+ T to Treg cells (163–165) and maintains a stage of dedifferentiation in MDSCs by enhancing the expression of TGF-β and IL-10. In addition, tumor-resident MDSCs produce cyclo-oxygenase 2 (COX-2), arginase 1 (ARG1), inducible NO synthase (iNOS), IL-10, and indoleamine 2,3-dioxygenase (IDO), which accentuate the suppressor milieu (166). In hypoxia, pyruvate is reduced to lactate, which decreases the local pH. Moreover, IL-4 or IL-13 stimulates the polarization of the macrophages from the M1 to M2 phenotype to support tumor progression and angiogenesis (167) (Figure 1).

The systemic effect of tumor microenvironment-derived cytokines

Studies performed with cancer patients and animal models have studied several local and systemic cytokines. In cancer patients, diverse cytokines and soluble factors showing pro- and anti-inflammatory activities may be detected as free circulating or exosome membrane-bound molecules (168). Reports have indicated that the cytokines IL-1, TNF-α, IL-6, G-CSF, and GM-CSF mainly act at the systemic level, affecting the function of some organs (169). Our group quantified eight cytokines at the systemic level in smoking patients with lung adenocarcinoma and found a significant increase in IL-2, IL-4, IL-6, and IL-10 compared to their levels in healthy smoking subjects. Among these cytokines, the concentration of IL-6 was the highest in the peripheral blood of cancer patients, showing an increase of approximately sevenfold. To explain the increased systemic levels of IL-6, several reports from distinct groups, including ours, have pointed out that tumor cells from different types of cancers produce this cytokine (170, 171). Currently, the roles of these cytokines in cancer have gained considerable attention. In particular, those cytokines acting at the systemic level have been associated with the development of some clinical signs or symptoms of paraneoplastic syndromes.

TNF-α

As discussed in the previous section, the tumor and its stroma release cytokines that act on various systems and organs. TNF-α is a pro-inflammatory cytokine with diverse functions that participates in homeostatic and distinct pathological conditions. The biological activity of TNF-α is exerted *via* binding with its cognate receptors: TNF-α receptor 1 (TNFR1) and 2 (TNFR2). TNFR1 is ubiquitously expressed in cells and is activated by the transmembrane or the soluble form of TNF-α. To the contrary, the expression of TNFR2 is limited to specific cells, such as immune and endothelial cells and cells of the central nervous system, and its activation mainly depends on the transmembrane form of the ligand (172). The role of these receptors in homeostasis has been described. The activation of TNFR1 mainly promotes

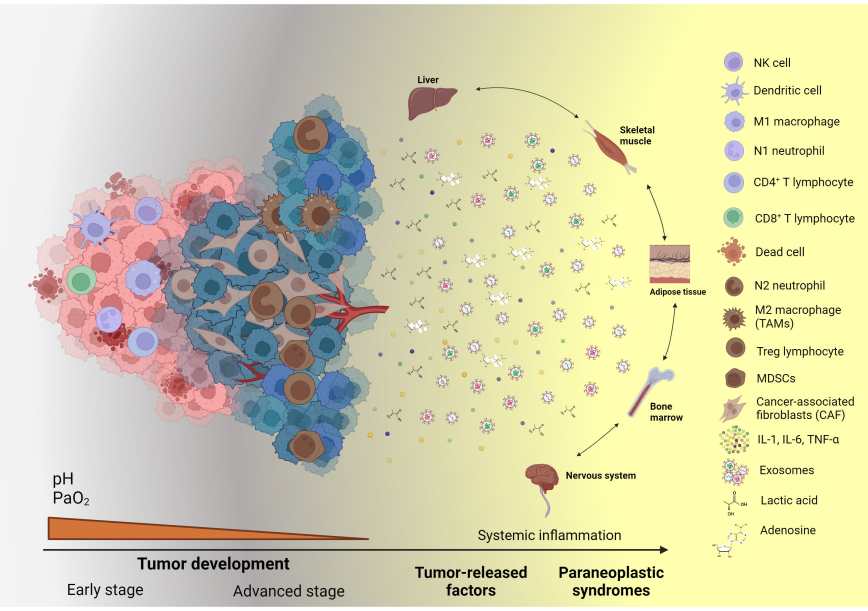

FIGURE 1
Systemic effects and paraneoplastic syndromes caused by cancer-associated inflammation. During the advanced stages of tumor development, tumor and stromal cells release an array of soluble factors, such as cytokines, chemokines, growth factors, metabolic by-products, exosomes, and ncRNAs, which sustain the local inflammatory state. Moreover, these soluble factors, when released into the bloodstream, reach distinct organs, systems, and tissues, causing alterations in their function and the production of diverse molecules and subsets of cells, which can be employed as biomarkers to assess cancer-related systemic inflammation. Created with BioRender.com.

inflammation, the induction of cell death *via* apoptosis or necroptosis, and tissue degeneration.

Conversely, the activation of TNFR2 is associated with cell survival and the wound healing process (172). Once TNF-α is produced and released into the bloodstream, this cytokine can reach the adipose tissue, where it modifies the adipocytes glucose and lipid metabolism. In this regard, TNF-α decreases glucose uptake by inhibiting the signaling pathways triggered by insulin and, as a result, downregulates the mRNA and protein expression of GLUT-4 (173, 174). Simultaneously, TNF-α activates lipolysis *via* the inhibition of the peroxisome proliferator-activated receptor (PPAR)- γ and CCAAT enhancer-binding protein, causing an increase in the expression of neutral lipases (175). These observations might explain the increased levels of serum lipids detected in cancer; however, more studies are required to demonstrate the role of TNF-α during the dyslipidemia observed in cancer (176).

Studies in cancer patients have demonstrated that cancer-associated systemic inflammation is associated with a sense of pain or hyperalgesia from an unknown source. In peripheral nerves, TNF-α is linked with this phenomenon. In this setting, the interaction of TNF-α with TNFR1 causes the activation of the p38/MAPK signaling pathway, which culminates in the activation of Na+ and K+ ionic channels in peripheral nerves, leading to pain generation (177, 178).

In addition, the findings from a recent study indicated that in hepatocellular carcinoma, TNF-α released in exosomes promoted osteoclast differentiation. During this phenomenon, the TNF-α stored in the exosomes produced by hepatocellular Huh-7 cells caused the expression of osteoclast-associated differentiation markers when added to murine macrophage/monocyte cell lines through the activation of the NF-κB/cathepsin K/triiodothyronine receptor auxiliary protein axis. These findings explain the tendency of hepatocellular cancer cells to generate bone metastases (179).

Interleukin-1

IL-1 is a pleiotropic cytokine that is involved in various inflammatory processes. IL-1 belongs to the Ig-like receptor superfamily, which is characterized by the presence of the Toll/interleukin-1 receptor (TIR) domain. The TIR domain is essential for the biological activity of IL-1 (180, 181). The ligands of the IL-1 family are IL-1, IL-18, IL-33, and IL-36. These agonists bind to three receptors: IL-1α and IL-1β perform cell activation when bound to IL-1R1; IL-18 is a ligand of IL-18Ra; IL-33 binds to ST2 (IL-1R4); and IL-36α, β, and γ are agonists of IL-1Rp2 (IL-1R6). The primary function of this family of ligands and receptors is to participate in inflammatory processes (182, 183).

IL-1α and IL-1β are encoded by different genes and have minimal homology. IL-1α is synthesized as pro-IL-1α, which

can be proteolytically cleaved by calpain, granzyme B, elastase, and chymase. When the mature form of IL-1α is released, it acts as an "alarmin," activating the innate immune response against noxious stimuli (184). IL-1β is a critical player in the inflammasome. The activation of the inflammasome in innate immune response cells, such as monocytes and neutrophils, occurs when pathogen-associated molecular patterns (PAMPs) and DAMPs bind to Toll-like (TLRs) and NOD-like (NLRs) receptors. The assembly of the inflammasome causes the cleavage of pro-caspase 1, and caspase 1 is released, which then cleaves pro-IL-1β and pro-IL-18. IL-1α and IL-1β establish chronic inflammation in the process of carcinogenesis (185). In IL-1/IL-1R1 knockout murine models, it was observed that IL-1 was a critical factor in the inflammatory process associated with 3-methylcholanthrene carcinogenesis (186). Both IL-1α and IL-1β participate in the systemic inflammation associated with cancer. Tumor and stromal cells in the tumor microenvironment produce and release IL-1.

Recent reports have indicated that cancer-derived exosomes from prostate and lung cancer as well as glioblastoma cell lines stimulate the production and release of IL-1β in immune and non-immune cells (187–189). In this setting, cancer-derived exosomes may trigger distinct intracellular signaling pathways in receptor cells, culminating in NF-κB activation and the subsequent expression of the *IL-1β* gene or the activation of inflammasomes through NLRP3 for the cleavage of pro-IL-1β into its active form (190, 191). In support of this, Linton et al. reported that exosomes derived from pancreatic ductal adenocarcinoma (PDAC) cell lines caused the polarization of M0 into immunosuppressive pro-tumoral M2 macrophages, which increased the production and release of IL-1β (327). In this regard, PDAC-derived exosomes were shown to contain increased levels of arachidonic acid, leading to its subsequent metabolism into free fatty acids, which activate inflammasomes through NLRP3 (193). Several reports have indicated that IL-1 in circulation affects several organs and may contribute to establishing paraneoplastic syndromes, such as cachexia (see below) (194–197).

IL-6

Low blood levels of IL-6 ranging between 1 and 5 pg/mL have been reported under normal conditions (198). In addition, soluble forms of the receptors IL-6R and gp130 have been detected. After local production by tumor cells in the inflammatory niche, IL-6 is released into the bloodstream and eventually reaches the liver, where it has several biological effects on hepatocytes. In one study, an increase in the production of acute phase proteins (APPs), such as C-reactive protein (CRP), serum amyloid A (SAA), fibrinogen, haptoglobin, and α1-antichymotrypsin, and an opposing decrease in albumin, fibronectin, and transferrin were detected. In addition, IL-6 regulates the transporters of iron and zinc associated with anemia that are detected in chronic inflammation (199). IL-6 also promotes megakaryocyte maturation in the bone marrow, increasing the serum platelet count (200).

The varied effects induced by IL-6 are detected mainly in chronic inflammatory diseases. In addition, this cytokine exerts various biological actions on the distinct types of immune cells, maintaining a deregulated and persistent positive feedback loop. IL-6 has evident pleiotropic effects in hematopoiesis, inflammation, the immune response, and cancer.

Parameters to assess systemic immune-inflammatory markers

The liver is a primordial organ that eliminates waste and toxic compounds, mainly found in dietary products, or harmful particles from pathogens. In addition, it provides nutrients and produces mediators that alert immune cells to induce an inflammatory response that eliminates harmful agents and induces the restoration of tissue homeostasis. The products of pathogens (PAMPs) or those derived from the host's damaged cells (DAMPs) induce the release of acute phase proteins from the liver (201, 202). Kupffer cells and macrophages produce proinflammatory cytokines, such as IL-6, IL-1β, and TNF-α, to generate a series of products associated with the inflammatory response (203, 204). These cytokines activate resident cells, such as hepatocytes, endothelial cells, hepatic stellate cells, and diverse immune cells, from the hepatic arteries and portal vein in the liver. In addition, the liver releases diverse enzymes that inactivate harmful drugs and produces serum proteins, such as albumin and coagulation factors (205) (Figure 1).

Local inflammation appears to be reflected at the systemic level, and this is supported by several studies (6, 206, 207). Routine hematological parameters have been used in recent years as indicators of systemic inflammation. Among these simple parameters, the proportions of circulating inflammatory cells, including the white blood cell (WBC) count, lymphocyte count, neutrophil count, platelet count (PLTs), mean platelet volume (MPV), and levels of hemoglobin (Hb) and serum CRP, have been screened (208, 209). Analyte-based scores or ratios of some of these parameters have been reported to assess systemic inflammation, and their correlation with the prognosis of numerous pathologies, including cancer, has been described.

The Glasgow prognostic score/modified Glasgow prognostic score (GPS/mGPS) is an inflammatory indicator (210, 211). The GPS/mGPS reflects the systematic inflammatory response and nutritional status. Recent studies have shown that the GPS/mGPS is a novel inflammatory index that can predict outcomes in various cancers (212–214). However, the molecular mechanisms underlying the relationship between the GPS/mGPS and poor prognostic outcomes are still unclear. A plausible explanation is that an elevated GPS/mGPS may

reflect an individual's immune and nutritional status. The GPS/mGPS comprises albumin and CRP; both are acute-phase proteins synthesized in the liver. The CRP level is regulated by several pro-inflammatory cytokines, such as IL-1, TNF-α, TGF-β, IFN-γ, and IL-6 (215). Studies have shown that IL-6 correlates with OS and SOC in CRC, and its effect could explain the promotion of tumorigenesis and metastasis (216, 217).

Additionally, CRP is associated with the activity of infiltrated immune cells, including DCs, T cells, and NK cells (218, 219). Many studies have shown that CRP is an independent biomarker for predicting prognostic outcomes in various cancers (220, 221). The serum albumin level is used to evaluate liver function and nutritional status. Hypoalbuminemia is a common feature of the systemic inflammatory response, cancer recurrence, and metastasis. In addition, it has been shown to be positively correlated with the OS and CSS of patients with various cancers, including CRC and ovarian cancer (222, 223).

Albumin

Albumin is a low-molecular-weight protein of 66 kDa consisting of a single polypeptide chain with 585 amino acid residues that is fully synthesized in the liver, which produces approximately 15 g daily. Albumin maintains a plasma concentration of 35–45 g/L and is the most abundant protein in plasma, contributing to the maintenance of oncotic pressure and the permeability of the microvasculature. In addition, it has been implicated in important metabolic functions as it transports several endogenous ligands, such as free FAs, bilirubin, and ion metals, as well as some exogenous ligands (224, 225). Albumin expression is mainly regulated at the transcriptional level. Decreased albumin synthesis leads to hypoalbuminemia, which contributes to the development of edema by the transudation of fluids into extravascular spaces. TNF-α is a key cytokine involved in the inhibition of albumin synthesis, although other cytokines, such as IL-1β and IL-6, may contribute as well.

The serum albumin level is a marker of nutritional status, and a level less than 35 g/L is considered to indicate hypoalbuminemia. Albumin acts as an anti-inflammatory molecule; its increase is associated with blocking the migration of neutrophils through the endothelium by decreasing the expression of VCAM-1 in a TNF-α-dependent manner (226). Regardless of the disease, decreased serum albumin has been proposed as a risk factor and predictor for morbidity and mortality.

Platelets

Platelets, or thrombocytes, are nonnucleated and discoidal fragments derived from precursor megakaryocytes during megakaryopoiesis. Platelets maintain normal hemostasis and participate in several biological processes, such as the control of blood vessels and their interactions with endothelial cells. They also form a platelet plug with various extracellular matrix components, which inhibits vascular leakage. In addition, they are vital in acute and chronic inflammation due to their release of cytokines and chemokines that attract leukocytes and favor immune cells to reach the damaged tissue for wound healing. Furthermore, they are critical participants in the pathophysiology of several diseases, including cancer (227–229). Platelet characteristics have been found to be significantly associated with the clinical outcomes of several pathologies. Two of these features are the number of circulating platelets, designated as the platelet count, and the mean platelet volume (MPV).

The complete blood count includes the platelet count and the MPV. The platelet count quantifies the number of platelets in the blood; there are usually between 150,000 and 450,000 platelets in each microliter. Platelet parameters are used in the diagnosis of a patient's general condition and have a prognostic value in some pathologies. A platelet count is related to pathologies associated with a chronic condition (229). MPV is a measure of platelet size that results from a higher production by megakaryocytes; hence, it indicates if there are more young platelets circulating in the bloodstream. The MPV ranges between 7.5 and 12.0 fl (229). The value is inversely related to the platelet count, hemostasis maintenance, and the preservation of a constant platelet mass. MPV is a marker of platelet activity, and it has been related to prothrombotic and proinflammatory diseases (230).

Under inflammatory conditions, the increase in IL-6 causes an increase in the ploidy of megakaryocytic nuclei and an increase in the cytoplasmic volume, leading to the generation of a large number of platelets. These platelets migrate to the site of inflammation, where they undergo activation and are depleted, triggering a decrease in the MPV of the patient's blood during the development of the inflammatory process (229).

Fibrinogen

Fibrinogen is produced in the liver during general acute-phase inflammatory provocation. Inflammatory cytokines induce fibrinogen synthesis by hepatocytes and Kupffer cells. Several reports have indicated that IL-6 is a key cytokine that promotes fibrinogen production due to the presence of several IL-6 response elements in the fibrinogen genes. In addition, IL-6 regulates fibrinogen transcripts *via* the MEK-ERK signaling pathway (231, 232).

In association with other molecules, fibrinogen participates in coagulation, fibrinolysis, and cellular and matrix interactions that support cell migration, inflammation, and wound healing. An increased risk of cardiovascular disease has been associated with elevated fibrinogen levels (233). Cancer patients present with malfunctions in the coagulation process, and this molecule

has been associated with cancer development. Fibrinogen binds to growth factors, such as fibroblast growth factor-2 (FGF-2, bFGF) and (VEGF, to enhance tumor growth and increase the migration, invasion, and metastasis of tumor cells, as well as angiogenesis—processes which are considered to be hallmarks of cancer. The fibrinogen/albumin (F/A) ratio is considered a promising inflammation-based marker. A high FAR was shown to be associated with clinical–pathological features and survival in some cancers (234). However, multicentral clinical trials are needed to analyze the clinical impact of this relationship on medical oncology.

The evidence presented thus far provides an explanation for the usage of these hematological parameters and their diverse relationships to analyze the systemic inflammatory state. These ratios are associated with prognosis and survival in inflammatory diseases, including cancer (235). Owing to the extensive information indicating the prognostic value of these ratios, we only refer to those works in which these indices were assessed in the most frequent types of cancer. The reported ratios are indicated in Table 2.

Paraneoplastic syndromes

Understanding the local inflammation associated with cancer allows for a better understanding of the interaction between tumor cells, immune cells, stromal cells, and the soluble factors released by this system. The release of proinflammatory factors from tumor or stromal cells—in the form of soluble factors or those contained in exosomes—into the bloodstream alters the production of APPs, metabolites, and cells, which impacts organs and systems, causing the appearance of symptoms unrelated to the tumor itself, called paraneoplastic syndromes (6). Approximately 8% of cancer patients present one or more paraneoplastic syndromes. Paraneoplastic syndromes are classified as neurologic, rheumatologic, dermatologic, or hematologic, depending on the type of tumor (264, 265). The manifestation of paraneoplastic syndromes has detrimental effects on patient's quality of life and outcome. In addition, some paraneoplastic syndromes may exhibit tumor-promoting capabilities (7). In this section, we will discuss the development of myelopoiesis and cachexia.

Stimulation of myelopoiesis in cancer-related inflammation

One of the main targets of pro-inflammatory mediators in the bone marrow is a process known as hematopoiesis, whereby hematopoietic stem and progenitor cells (HSPCs) differentiate into mature blood cells. Under physiological conditions, denominated as steady-state hematopoiesis, local and external signals promote the retention of HSPCs in the bone marrow. For this purpose, the bone marrow stroma cells, including endothelial, vascular, and osteolineage cells and macrophages, participate in a well-orchestrated network to control the proliferation and differentiation of HSPCs (266). However, during acute systemic infection or inflammation, factors released from pathogens and damaged cells, as well as proinflammatory cytokines (IL-6, IL-1β, and TNF-α), impact HSPCs and stromal cells, causing the rapid mobilization and differentiation of HSPCs into myeloid cells, a process known as emergency myelopoiesis (267, 268).

TABLE 2 Available systemic inflammation indices predicting prognosis and outcome in cancer patients.

Index	Calculation	Ref.
Glasgow prognostic score (GPS)	CRP ≤ 10 mg/L and albumin ≥35 g/L Score 0 CRP ≤ 10 mg/L and albumin <35 g/L Score 1 CRP>10 mg/L and albumin ≥35 g/L Score 1 CRP>10 mg/L and albumin <35 g/L Score 2	(236–238)
Modified Glasgow prognostic score (mGPS)	CRP ≤ 10 mg/L and albumin ≥35 g/L Score 0 CRP ≤ 10 mg/L and albumin <35g/L Score 0 CRP>10 mg/L and albumin ≥35 g/L Score 1 CRP>10 mg/L and albumin <35 g/L Score 2	(238–241)
C-reactive protein-to-albumin (CAR)	$\frac{CRP}{Albumin}$	(242–244)
Neutrophil-to-lymphocyte ratio (NLR)	$\frac{Neutrophil\ \ count}{Lymphocyte\ \ count}$	(245–248)
Derived neutrophil-to-lymphocyte ratio (dNLR)	$\frac{Neutrophil\ \ count}{White\ \ cell\ \ count - neutrophil\ \ count}$	(249–252)
Monocyte-to-lymphocyte ratio (MLR)	$\frac{Monocyte\ \ count}{Lymphocyte\ \ count}$	(248, 253–255)
Platelet-to-lymphocyte ratio (PLR)	$\frac{Platelet\ \ count}{Lymphocyte\ \ count}$	(256–258)
Systemic immune-inflammation index (SII)	*Neutrophil * PLR*	(259–262)
Aggregate index of systemic inflammation (AISI)	*Neutrophil * platelet * MLR*	(263)

CRP, C-reactive protein.

In cancer, it has been demonstrated that tumors take advantage of emergency myelopoiesis to rapidly expand pools of myeloid-derived cells showing immune suppressive and tumor-promoting activities (266). These cells are known as MDSCs and can be classified as granulocytic (CD11b+CD14-CD15+) or monocytic (CD11b+CD14+CD15-) depending on the myeloid progenitor from which they were derived (269).

As mentioned above, the plasma concentration of proinflammatory cytokines, such as IL-1β, TNF-α, and IL-6, increases in several types of cancer due to the sustained inflammatory environment caused by the tumor and its stroma. These cytokines, along with other bioactive soluble factors, such as GM-CSF and G-CSF, travel freely in circulation or are stored in exosomes reaching the bone marrow, causing the proliferation, mobilization, and skewed differentiation of HSPCs towards myeloid cells (270). Reports on G-CSF have indicated that as the G-CSF level in the bone marrow decreases, the expression of maintenance molecules for HPSCs, such as CXCL12, osteopontin, Kit-1, angiopoietin, and vascular cell adhesion molecule 1 (271) increases, thus promoting their proliferation. In the bone marrow, IL-6 binds to IL-6R—which is mainly expressed on hematopoietic multipotent progenitors but not in short- or long-term repopulating HPSCs—suppressing the differentiation of lymphoid cells and stimulating myeloid differentiation (272). Marigo et al. demonstrated in mice that GM-CSF, G-CSF, and IL-6 in the bone marrow caused the activation of the master regulator of emergency granulopoiesis, the C/EBPβ transcription factor, which is responsible for the differentiation of HSPCs into MDSCs and their immunosuppressive activity (273). Initial studies in humans by Wu et al. showed that increased frequencies of HSPCs and granulocytic progenitors in different cancer types were found in cancer patient's blood compared to those of healthy donors (274). The increase in these cell populations was negatively correlated with several clinical parameters, including the time to progression and the stage of the disease, suggesting that activated bone marrow myelopoiesis is a phenomenon that promotes tumor progression.

However, these proinflammatory cytokines are not only responsible for the expansion and differentiation of HSPCs in the bone marrow. In a mouse model of breast and lung cancer, Sayed et al. found that hematopoiesis was biased towards myelopoiesis due to the action of TNF-α released from infiltrating CD4+ T cells (275). During this process, TNF-α caused a skewed differentiation of HSPCs towards MDSCs, with a concomitant decrease in erythroid and lymphoid precursors (275). In this scenario, TNF-α acted on HSPCs and MDSCs through TNFR-2, upregulating the expression of the caspase-8 inhibitor c-FLIP and promoting their survival (276). In these works, it has been demonstrated that tumor-promoting inflammation has profound systemic effects during the advanced stages of cancer, causing biased hematopoiesis toward the production of immunosuppressive myeloid cells and sustaining tumor progression. In addition, the results from these studies have helped to explain the altered percentages of hematological inflammatory parameters detected in cancer patients by the effect of these pro-inflammatory cytokines and growth factors in the bone marrow.

In recent years, owing to the use of NGS approaches and elegant *in vivo* models, it has been shown that hematopoiesis is altered and biased towards myelopoiesis in the early stages of tumor development (277). Surprisingly, pro-inflammatory cytokines play a significant role during this process by activating hematopoiesis in the bone marrow to direct the production of myeloid progenitors and micro-RNAs (miRNAs) delivered from the tumor. The TME plays a critical role in controlling this process. Some of these tumor-associated miRNAs, such as miR-23b-3p, miR-27a-3p, and miR-671-5p, in bone marrow downregulate the expression of genes involved in B-cell receptor signaling and antigen processing. With this work, it is tempting to speculate that other subsets of non-coding RNA, in addition to miRNAs, are released from the tumor or its stroma to activate myelopoiesis in the bone marrow. However, studies to demonstrate this proposal are required.

In addition to proinflammatory cytokines and non-coding regulatory RNA, myelopoiesis is controlled directly or indirectly by the metabolites released from the tumor as part of the metabolic reprogramming of cancer cells (2, 278). For example, the direct control of myelopoiesis by metabolites involves the participation of oxysterols and desmosterol in the differentiation and expansion of MDSCs. These cholesterol metabolites bind to retinoic acid-related orphan receptors expressed in the cell precursors of MDSCs (278). They have been detected in distinct pathologies, such as obesity, metabolic disorder, diabetes, and cancer (279). Recent evidence from Vladimirov et al. demonstrated that colorectal cancer patients had significantly increased values of cholesterol serum precursors compared to healthy donors, suggesting that cholesterol metabolism is altered in cancer (280). This evidence allows us to speculate that such patients might present altered myelopoiesis and thus increased numbers of MDSCs and other immunoregulatory cell populations; however, intensive research using *in vitro* and *in vivo* models in distinct types of cancer is needed to confirm this hypothesis. The activation of aerobic glycolysis indirectly affects cancer metabolic reprogramming in myelopoiesis. In a triple-negative breast cancer mouse model, Li et al. demonstrated that aerobic glycolysis stimulated the release of G-CSF and GM-CSF *via* C/EBP-β and liver-enriched activator protein. This glycolytic-dependent production of G-CSF and GM-CSF was correlated with increased MDSCs and low T lymphocyte counts in breast cancer patients (281). Although these results are pioneering, more studies are necessary to uncover the complete impact of altered metabolism on myelopoiesis in cancer.

Recent studies have demonstrated that hematopoiesis can occur outside the bone marrow under distinct inflammatory

conditions, a phenomenon known as extramedullary hematopoiesis (269). In cancer, extramedullary hematopoiesis is mainly found in the liver and spleen, where HPSCs or myeloid progenitors arrive (282). In this setting, the accumulation of immunosuppressive cells, such as MDSCs, Tregs, and erythroid progenitor cells, in the spleen was found in a mouse model of breast cancer. Several reports have demonstrated that splenectomy in animals bearing tumors is associated with a decrease in the number of peripheral MDSCs cells and cytokines related to HPSCs mobilization (9, 283). In this scenario, a survival benefit was achieved due to decreased tumor growth following the splenectomy, suggesting that extramedullary hematopoiesis has a critical role in sustaining tumor growth and progression. However, in humans, a concomitant splenectomy following colon, liver, gastric, and pancreatic cancer has not shown any beneficial effects on patient's overall survival (284). Nevertheless, owing to technical and experimental barriers, little is known about this process in humans; thus, most of the studies in this field are performed using animal models. For this reason, further research exploring the implications of extramedullary hematopoiesis in solid human tumors is required.

In solid tumors, the shift in anti-tumoral immunity towards a pro-tumoral response not only depends on the reshaping of the local tumor microenvironment by cytokines, chemokines, metabolic by-products, exosomes, or other released factors. The development of populations showing immune regulatory functions occurs in distinct and distant organs away from the primary lesion due to the systemic release of the factors mentioned above. In this setting, a considerable increase in the production of MDSCs in the bone marrow and secondary lymphoid organs and their subsequent migration to the tumor support the development of some cancer hallmarks by providing growth and angiogenic factors, cytokines, chemokines, and extracellular matrix remodeling enzymes (285) (Figure 1). In addition, these MDSCs strengthen the immunosuppressive tumor microenvironment by releasing immunomodulatory cytokines, metabolites, and other soluble factors and by expressing immune checkpoints on their surface, thus causing the recruitment of M2 macrophages, N2 neutrophils, and Tregs (286).

Cachexia in cancer-related inflammation

Advanced tumors release a spectrum of factors that induce systemic inflammation, which is reflected in paraneoplastic syndromes, such as cachexia. Cancer cachexia is a multifactorial syndrome characterized by progressive sarcopenia that may be accompanied by a loss in adipose tissue. This pathology involves a harmful protein and energy balance and an abnormal metabolism due to anorexia. Cachexia cannot be reversed entirely with nutritional support, resulting in a detriment to the quality of life of cancer patients (287). In addition, cachexia is responsible for 20–30% of deaths in patients with advanced cancer. Tumors in which cachexia may develop include pancreatic, gastric, colon, lung, Hodgkin's and non-Hodgkin's lymphoma, breast, sarcoma, and leukemia (288).

The cellular mechanisms that induce cachexia are not yet fully understood; thus far, it is known to be a syndrome that involves several organs and is orchestrated at the systemic level by inflammatory factors released by the tumor and its microenvironment. Although systemic inflammation is not considered in the current classification as a parameter for diagnosing cancer cachexia, several authors have considered the measurement of inflammatory markers, such as CRP and IL-6, at the blood level (289). Biswas and Acharyya (290) mentioned that factors secreted directly by the tumor and non-tumor cells of the neoplastic microenvironment can mediate cachexia and other syndromes. These factors can directly interact with various tissues, such as muscle, liver, brain, and adipose tissue, and can induce metabolic reprogramming, leading to a negative metabolic energy state at the systemic level.

As mentioned above, as tumors continue to proliferate, the lack of oxygen and nutrients induces hypoxia. Hypoxia generates critical changes, for example, the metabolic turnover of tumor cells for energy. A hypoxic microenvironment releases several factors, including VEGF (291), which induces angiogenesis and recruits inflammatory cells, such as macrophages. In addition to the above components of the tumor microenvironment, the release of DAMPs by dead cells increases inflammation and generates extra-tumoral cytokines. Another important metabolite in cancer that contributes to tumor development and results from metabolic turnover is lactate (292, 293). The hypermetabolism of tumor cells leads them to consume large amounts of glucose and excrete lactic acid, which has pleiotropic activity, is involved in energy metabolism, has an immunosuppressive function, and promotes angiogenesis (294).

Lactate in the liver is converted to glucose in a process called gluconeogenesis. The glucose generated can be utilized by both the tumor cells and the host organism, increasing blood glucose. This hyperglycemia leads to insulin resistance, which is related to muscle wasting. The relationship between the tumor and liver *via* lactate is called the Cori cycle and is considered as a futile cycle in cancer cachexia (292). Insulin resistance in patients with cachexia, as well as in murine models, has been associated with muscle wasting and is induced by TNF-α (295). Noguchi et al. found a high correlation between TNF-α expression in muscle tissue obtained from the intestine of cancer patients and insulin resistance and muscle wasting. After tumor resection, the patients showed complete improvement in insulin resistance (296). More recent studies using a murine model of C-26 colon adenocarcinoma cell cachexia showed that insulin resistance occurred before weight loss. In the quadriceps muscle of these

mice, the expression of four muscle atrophy-promoting genes, Atrogin-1, and MuRF-1, ubiquitin ligases E3 and Bnip3, was increased (297). Systemic inflammation is also associated with skeletal muscle wasting during cancer cachexia. The ubiquitin-proteasome pathway is activated during cachexia and is responsible for the degradation of most skeletal muscle proteins. Type IIB muscle fibers in an ApcMin/+ mouse model, which produced colon polyps, were shown to be highly susceptible to IL-6-mediated muscle wasting, as it induced the overexpression of the Atrogin-1 gene (298). In mouse bladder and colorectal cancer models, increased TNF-α, IL-6, and IL-1 in circulation and decreased muscle mass were associated with high Atrogin-1 and MurRF1 expression (299).

Among the factors that tumors can release are exosomes, which may contain molecules that promote muscle wasting. In a mouse model of cachexia, a group of researchers found that cachexigenic tumors released Hsp70/90 heat shock proteins into extracellular vesicles; furthermore, they participated in muscle wasting through TLR4 activation (300). Similarly, miR-181a-3p found in exosomes from a conditioned medium of oral squamous cell carcinoma induced endoplasmic reticulum stress and skeletal muscle wasting (301). Another study showed that HMGB1 protein, a DAMP contained in the exosomes of CT26 mouse colon cancer cells, induced the expression of the Atrogin1 and MuRF1 genes, leading to muscle wasting through the activation of TLR4/NF-κB axis (302). Another factor in exosomes that promotes muscle wasting is growth differentiation factor 15 (GDF-15), identified in the exosomes of CT26 colon cancer cells. GDF-15 can interact with C2C12 myotube cells, regulate Bcl-2/caspase, and induce cell apoptosis, favoring muscle atrophy in cancer cachexia (303).

The insulin resistance and systemic inflammatory cytokines in cancer cachexia patients also impact adipose tissue (304). In adults, adipose tissue is composed primarily of white adipocytes (WAT), although brown adipocyte fat deposits (BAT) exist in specific anatomic locations, such as the perivascular viscera and periviscus. BAT can also be found in supraclavicular, axillary, and inguinal subcutaneous fat and the intestinal walls (305). The difference between WAT and BAT is that the latter contain many mitochondria expressing uncoupling protein-1 (UCP-1). This molecule "uncouples" an electron in the process of ATP synthesis *via* OXPHOS across the inner membrane of the mitochondrion, which generates heat (306). Virtually all fat ingested in food is stored as WAT. In states of excessive exercise or prolonged fasting, triglycerides in WAT are degraded by three lipases: adipose triglyceride lipase (ATGL), hormone-sensitive lipase (HSL), and monoacylglycerol lipase (MGL). The regulation of lipases is highly influenced by several hormones, such as insulin, catecholamines, and growth hormone (307, 308).

In cancer cachexia, various cytokines, such as TNF-α and IL-6, promote the lipolysis of triglycerides in WAT (309). Shaw and Wolfe found increased lipolysis associated with increased blood fatty acids in patients with cachexia (310), indicating that lipid metabolism is dysregulated in cachexia states. In a muscle stem cell model, as well as in models of cachexia induced by human kidney neoplasia in mice, researchers observed that the process of muscle atrophy was preceded by an increase in FA β-oxidation as well as inflammatory factors, such as IL-1 β, IL-6, IL-8, and TNF-α. In this work, blocking FA β -oxidation using a carnitine-palmitoyltransferase-1 inhibitor also blocked muscle wasting (311). Another mechanism of adipose tissue degradation is the browning of WAT. For a long time, it was believed that the function of WAT was lipid storage, while BAT was involved in heat dissipation and the regulation of temperature (312). It is now known that WAT can be converted to BAT *via* specific mechanisms, such as hypothermia. The browning of WAT has been associated with cachexia.

Petruzzelli et al., using several genetically engineered mouse models, observed that the browning of WAT was an event that preceded muscle wasting. They also showed that IL-6 and catecholamines increased UCP-1 expression in the WAT of these cachexic mice (312). Recently, a study in cancer patients with and without cachexia showed an association between tumor-derived factors and inflammatory changes in the adipose tissue of the cachectic patients (313), suggesting that factors released by the tumor and its microenvironment modify adipose tissue metabolism. Exosomes have been found to play an important role in adipose tissue wasting.

Exosomes derived from cell lines and the plasma of gastric cancer patients contain ciRS-133, which induces the browning of WAT (314). Exosomes derived from lung adenocarcinoma cell lines containing TGF- β were shown to inhibit adipogenesis in primary adipocyte cultures from healthy subjects (315). The miR155 in gastric cancer exosomes was shown to promote the browning of adipose tissue through the transcription factor CCAAT/enhancer-binding protein β, which upregulates UCP1 (316).

Finally, circulating inflammatory cytokines produced by the tumor microenvironment affect the central nervous system, amplifying and orchestrating the symptoms of cancer-associated cachexia and causing anorexia, fatigue, and the wasting of muscle and fat tissue. In particular, a loss of appetite has been associated with hypothalamus inflammation. The nucleus of the hypothalamus regulates energy homeostasis (290, 317, 318). Increased cytokine expression in the brain alters the neurochemistry of the hypothalamus nucleus, where cytokines activate pro-opiomelanocortin (POMC) and cocaine- and amphetamine-regulated transcript (CART) neurons, which mediate satiety and reduce food intake. The activation of these neurons induces serotonin release, suppressing appetite. In addition, cytokines are likely to inhibit neuropeptide Y (NPY) and agouti-related peptide (AgRP) neurons, which mediate appetite

and energy intake. These changes in the neurochemistry of the hypothalamus result in a "resistance" to signals that inform the brain of energy deficits in the periphery. As mentioned above, adipose tissue wasting leads to the circulation of free FA, which generates a satiety signal in the hypothalamus, contributing to anorexia (290, 317, 318). On the other hand, some reports have indicated that the stimulation of the hypothalamic–pituitary–adrenal axis with IL-1 induces the release of glucocorticoids that act on skeletal muscle and accelerate protein degradation (317, 319, 320).

Cancer patients present two types of damage: that produced locally by the tumor, which can be direct damage to the organ where it is located, and immunopathological damage that occurs when the tumor and the tumor microenvironment release compounds that cause metabolic derangement and systemic inflammation, such as in cachexia. IL-1, IL-6, and TNF-α play an essential role at the systemic level as inducers of cancer cachexia (321). In the 1970s, although there was not yet a methodology with sufficient sensitivity to measure these cytokines in cancer patients and obtain consistent results, treatment with anti-TNF- and IL-6 antibodies was proven to be effective in reducing cachexia in mouse tumor models (322).

Jafri et al. proposed a cachexia index to estimate the degree of cachexia in patients with advanced non-small-cell lung carcinoma (NSCLC) and to identify which patients might respond to cancer cachexia treatment (323). This index considers albumin; the skeletal muscle index, which results from comparing abdominal and paraspinal muscle scans between the time of diagnosis and one month later; and the NLR (323). In another paper, a sarcopenia index was defined as the muscle area at the third vertebra/height^2, and values of ≤ 55 cm^2/m^2 for men and ≤ 39 cm^2/m^2 for women indicated sarcopenia. This index was correlated with CRP and the neutrophil/lymphocyte ratio in patients with small-cell lung carcinoma. Sarcopenia was found to have a linear relationship with CRP (324). Finally, Barrer et al. found that the neutrophil/lymphocyte ratio was associated with weight loss in patients with colon, lung, and prostate cancer cachexia (325).

The cachexia syndrome is characterized by the metabolic dysregulation of carbohydrates, lipids, and proteins in various organs and the sympathetic activation of the nervous system. All this leads to a poor quality of life for patients, and their diminished physical condition may not be suitable for treatment. The incidence of the anorexia–cachexia syndrome is high in cancer patients, affecting the evolution of the underlying disease at the clinical level. Unfortunately, its clinical management is complex in cancer patients. Consequently, cancer patients severely compromised nutritional status and weight loss remain standard features. It is essential to recognize and treat this syndrome early, together with antitumor therapy, to prolong survival and positively influence the quality of life of cancer patients.

Concluding remarks and perspectives

During the uncontrolled growth of tumors, several inflammatory factors, including—but not limited to—cytokines, chemokines, growth factors, metabolites, and ncRNAs, are produced and released by both tumor and stromal cells. The continuous release of these factors causes impacts at the local level; their delivery into the bloodstream reaches other systems or organs, such as the liver, nervous system, bone marrow, adipose tissue, skeletal muscle, etc. In this setting, the continuous presence of these factors, in particular IL-6, IL-1, TNF-α, G-CSF, and GM-CSF, promotes cancer-associated systemic inflammation. Due to their pleiotropic activity, these molecules impact distinct subsets of cells, such as endothelial, epithelial, mesenchymal, neurologic, and hematologic cells, amplifying the inflammatory state and the clinical manifestations of the aberrant function of organs and systems, known as paraneoplastic syndromes. Paraneoplastic syndromes have detrimental effects on the patient's quality of life and can sometimes cause their demise.

In addition, paraneoplastic syndromes can be exacerbated during the administration of cytotoxic antitumor therapies focused on eliminating tumor cells. Because advanced-stage tumors deregulate communication between the immune, endocrine, and neurological systems, a deeper we believe that, in addition to using antitumor agents, knowledge of the regulation of neuro–endocrine–immune intercommunication during cancer-associated inflammation will to could favor the development of upcoming therapies that will impact patient survival and quality of life. In support of this proposal, recent reports have demonstrated that nonsteroidal anti-inflammatory drugs may be used in cancer to reduce systemic inflammation (326). However, in clinically advanced tumors, cancer-associated systemic inflammation is dysregulated at another level; thus, these anti-inflammatory drugs would have no effect. Furthermore, the use of steroid drugs, such as glucocorticoids, could suppress the antitumor immune response, as they block the function of CD8+ effector T and NK cells (327). To address this issue, models that capture the complexity of tumor–host organ interactions will help clarify the picture and offer new therapeutic alternatives to improve patient outcomes.

Author contributions

Conceptualization and design of the entire manuscript and draft: DA-C, RC-D, MM-M, and JL-G. JL-G, DA-C, and MM-M wrote the microenvironment section. JL-G, RC-D, and AC wrote the participation of the immune response in cancer section. DA-C, RC-D, JB-L, and MP-M wrote the systemic tumor microenvironment-derived cytokines section. JL-G, UR-N, and

MM-M wrote the parameters to assess systemic immune-inflammatory markers section. DA-C, RC-D, and AC wrote the paraneoplastic syndromes section. Figure 1 was designed by RC-D, DA-C, and JB-L. Tables 1, 2 was designed by JL-G, RC-D and MM-M. All authors contributed to the article and approved the submitted version.

Funding

This manuscript was partially funded by Consejo Nacional de Ciencia y Tecnologia (CONACYT) (grant number: 284775).

Acknowledgments

The authors acknowledge Instituto Nacional de Enfermedades Respiratorias Ismael Cosio Villegas. RC-D, JB-L, MM-M, and MP-M are students from the Posgrado en Ciencias Biologicas Universidad Nacional Autonoma de Mexico, Mexico and Posgrado en Ciencias en Biomedicina y Biotecnologia Molecular, Instituto Politecnico Nacional, Mexico, Mexico, respectively. All are recipients of a fellowship from CONACYT (RC-D 631047) (JJB-L 1085486) (MM-M 718959) (MP-M 740805).

Conflict of interest

The authors declare that the research was conducted in the absence of any commercial or financial relationships that could be construed as a potential conflict of interest.

Publisher's note

References

1. Sung H, Ferlay J, Siegel RL, Laversanne M, Soerjomataram I, Jemal A, et al. Global cancer statistics 2020: GLOBOCAN estimates of incidence and mortality worldwide for 36 cancers in 185 countries. *CA Cancer J Clin* (2021) 71:209–49. doi: 10.3322/caac.21660

2. Hanahan D, Weinberg RA. Hallmarks of cancer: The next generation. *Cell* (2011) 144:646–74. doi: 10.1016/j.cell.2011.02.013

3. Greten FR, Grivennikov SI. Inflammation and cancer: Triggers, mechanisms, and consequences. *Immunity* (2019) 51:27–41. doi: 10.1016/j.immuni.2019.06.025

4. Dunn GP, Old LJ, Schreiber RD. The three Es of cancer immunoediting. *Annu Rev Immunol* (2004) 22:329–60. doi: 10.1146/annurev.immunol.22.012703.104803

5. Gajewski TF, Schreiber H, Fu Y-X. Innate and adaptive immune cells in the tumor microenvironment. *Nat Immunol* (2013) 14:1014–22. doi: 10.1038/ni.2703

6. Dolan RD, Lim J, McSorley ST, Horgan PG, McMillan DC. The role of the systemic inflammatory response in predicting outcomes in patients with operable cancer: Systematic review and meta-analysis. *Sci Rep* (2017) 7:16717. doi: 10.1038/s41598-017-16955-5

7. Pelosof LC, Gerber DE. Paraneoplastic syndromes: An approach to diagnosis and treatment. *Mayo Clin Proc* (2010) 85:838–54. doi: 10.4065/mcp.2010.0099

8. Oh SY, Jun HJ, Park SJ, Park IK, Lim GJ, Yu Y, et al. A randomized phase II study to assess the effectiveness of fluid therapy or intensive nutritional support on survival in patients with advanced cancer who cannot be nourished *via* enteral route. *J Palliat Med* (2014) 17:1266–70. doi: 10.1089/jpm.2014.0082

9. Wu C, Ning H, Liu M, Lin J, Luo S, Zhu W, et al. Spleen mediates a distinct hematopoietic progenitor response supporting tumor-promoting myelopoiesis. *J Clin Invest* (2018) 128:3425–38. doi: 10.1172/JCI97973

10. Almagro J, Messal HA, Elosegui-Artola A, van Rheenen J, Behrens A. Tissue architecture in tumor initiation and progression. *Trends Cancer* (2022) 8:494–505. doi: 10.1016/j.trecan.2022.02.007

11. Beatty GL, Gladney WL. Immune escape mechanisms as a guide for cancer immunotherapy. *Clin Cancer Res* (2015) 21:687–92. doi: 10.1158/1078-0432.CCR-14-1860

12. Song W, Li D, Tao L, Luo Q, Chen L. Solute carrier transporters: the metabolic gatekeepers of immune cells. *Acta Pharm Sin B* (2020) 10:61–78. doi: 10.1016/j.apsb.2019.12.006

13. Wang S, Wang J, Wei W, Ma G. Exosomes: The indispensable messenger in tumor pathogenesis and the rising star in antitumor applications. *Adv Biosyst* (2019) 3:1900008. doi: 10.1002/adbi.201900008

14. Kalluri R, LeBleu VS. The biology, function , and biomedical applications of exosomes. *Science* (2020) 367:eaau6977. doi: 10.1126/science.aau6977

15. Ruivo CF, Adem B, Silva M, Melo SA. The biology of cancer exosomes: Insights and new perspectives. *Cancer Res* (2017) 77:6480–8. doi: 10.1158/0008-5472.CAN-17-0994

16. Pegtel DM, Gould SJ. Exosomes. *Annu Rev Biochem* (2019) 88:487–514. doi: 10.1146/annurev-biochem-013118-111902

17. Beach A, Zhang H-G, Ratajczak MZ, Kakar SS. Exosomes: An overview of biogenesis, composition and role in ovarian cancer. *J Ovarian Res* (2014) 7:14. doi: 10.1186/1757-2215-7-14

18. Boussadia Z, Zanetti C, Parolini I. Role of microenvironmental acidity and tumor exosomes in cancer immunomodulation. *Transl Cancer Res* (2020) 9:5775–86. doi: 10.21037/tcr.2020.03.69

19. Qu X, Tang Y, Hua S. Immunological approaches towards cancer and inflammation: A cross talk. *Front Immunol* (2018) 9:563. doi: 10.3389/fimmu.2018.00563

20. Bebelman MP, Smit MJ, Pegtel DM, Baglio SR. Biogenesis and function of extracellular vesicles in cancer. *Pharmacol Ther* (2018) 188:1–11. doi: 10.1016/j.pharmthera.2018.02.013

21. Paul S, Kulkarni N, Shilpi, Lal G. Intratumoral natural killer cells show reduced effector and cytolytic properties and control the differentiation of effector Th1 cells. *OncoImmunology* (2016) 5:e1235106. doi: 10.1080/2162402X.2016.1235106

22. Ronca R, Van Ginderachter JA, Turtoi A. Paracrine interactions of cancer-associated fibroblasts, macrophages and endothelial cells: tumor allies and foes. *Curr Opin Oncol* (2018) 30:45–53. doi: 10.1097/CCO.0000000000000420

23. Obacz J, Pastorekova S, Vojtesek B, Hrstka R. Cross-talk between HIF and p53 as mediators of molecular responses to physiological and genotoxic stresses. *Mol Cancer* (2013) 12:93. doi: 10.1186/1476-4598-12-93

24. Abhange K, Makler A, Wen Y, Ramnauth N, Mao W, Asghar W, et al. Small extracellular vesicles in cancer. *Bioact Mat* (2021) 6:3705–43. doi: 10.1016/j.bioactmat.2021.03.015

25. Virchow R. As based upon physiological and pathological histology. *Nutr Rev* (2009) 47:23–5. doi: 10.1111/j.1753-4887.1989.tb02747.x

26. Dvorak HF. Tumors: wounds that do not heal. similarities between tumor stroma generation and wound healing. *N Engl J Med* (1986) 315:1650–9. doi: 10.1056/nejm198612253152606

27. Daniotti JL, Lardone RD, Vilcaes AA. Dysregulated expression of glycolipids in tumor cells: From negative modulator of anti-tumor immunity to promising targets for developing therapeutic agents. *Front Oncol* (2016) 5:300. doi: 10.3389/fonc.2015.00300

28. de Visser KE, Eichten A, Coussens LM. Paradoxical roles of the immune system during cancer development. *Nat Rev Cancer* (2006) 6:24–37. doi: 10.1038/nrc1782

29. Chimal-Ramírez GK, Espinoza-Sánchez NA, Fuentes-Pananá EM. Protumor activities of the immune response: Insights in the mechanisms of immunological shift, oncotraining, and oncopromotion. *J Oncol* (2013) 2013:1–16. doi: 10.1155/2013/835956

30. Diefenbach A, Raulet DH. Innate immune recognition by stimulatory immunoreceptors. *Curr Opin Immunol* (2003) 15:37–44. doi: 10.1016/S0952-7915(02)00007-9

31. Sivori S, Della Chiesa M, Carlomagno S, Quatrini L, Munari E, Vacca P, et al. Inhibitory receptors and checkpoints in human NK cells, implications for the immunotherapy of cancer. *Front Immunol* (2020) 11:2156. doi: 10.3389/fimmu.2020.02156

32. Malmberg KJ, Carlsten M, Björklund A, Sohlberg E, Bryceson YT, Ljunggren HG. Natural killer cell-mediated immunosurveillance of human cancer. *Semin Immunol* (2017) 31:20–9. doi: 10.1016/j.smim.2017.08.002

33. Dulberger CL, McMurtrey CP, Hölzemer A, Neu KE, Liu V, Steinbach AM, et al. Human leukocyte antigen F presents peptides and regulates immunity through interactions with NK cell receptors. *Immunity* (2017) 46:1018–29.e7. doi: 10.1016/j.immuni.2017.06.002

34. Isaacson B, Mandelboim O. Sweet killers: NK cells need glycolysis to kill tumors. *Cell Metab* (2018) 28:183–4. doi: 10.1016/j.cmet.2018.07.008

35. Donnelly RP, Loftus RM, Keating SE, Liou KT, Biron CA, Gardiner CM, et al. mTORC1-dependent metabolic reprogramming is a prerequisite for NK cell effector function. *J Immunol* (2014) 193:4477–84. doi: 10.4049/jimmunol.1401558

36. Zhu L, Gangadaran P, Kalimuthu S, Oh JM, Baek SH, Jeong SY, et al. Novel alternatives to extracellular vesicle-based immunotherapy – exosome mimetics derived from natural killer cells. *Artif Cells Nanomed Biotechnol* (2018) 46:S166–79. doi: 10.1080/21691401.2018.1489824

37. Lugini L, Cecchetti S, Huber V, Luciani F, Macchia G, Spadaro F, et al. Immune surveillance properties of human NK cell-derived exosomes. *J Immunol* (2012) 189:2833–42. doi: 10.4049/jimmunol.1101988

38. Cochran AM, Kornbluth J. Extracellular vesicles from the human natural killer cell line NK3.3 have broad and potent anti-tumor activity. *Front Cell Dev Biol* (2021) 9:698639. doi: 10.3389/fcell.2021.698639

39. Fauriat C, Long EO, Ljunggren H-G, Bryceson YT. Regulation of human NK-cell cytokine and chemokine production by target cell recognition. *Blood* (2010) 115:2167–76. doi: 10.1182/blood-2009-08-238469

40. Jorgovanovic D, Song M, Wang L, Zhang Y. Roles of IFN-γ in tumor progression and regression: A review. *biomark Res* (2020) 8:49. doi: 10.1186/s40364-020-00228-x

41. Aquino-López A, Senyukov VV, Vlasic Z, Kleinerman ES, Lee DA. Interferon gamma induces changes in natural killer (NK) cell ligand expression and alters NK cell-mediated lysis of pediatric cancer cell lines. *Front Immunol* (2017) 8:391. doi: 10.3389/fimmu.2017.00391

42. Chavez-Dominguez R, Perez-Medina M, Aguilar-Cazares D, Galicia-Velasco M, Meneses-Flores M, Islas-Vazquez L, et al. Old and new players of inflammation and their relationship with cancer development. *Front Oncol* (2021) 11:722999. doi: 10.3389/fonc.2021.722999

43. Hernandez C, Huebener P, Schwabe RF. Damage-associated molecular patterns in cancer: A double-edged sword. *Oncogene* (2016) 35:5931–41. doi: 10.1038/onc.2016.104

44. Haniffa M, Bigley V, Collin M. Human mononuclear phagocyte system reunited. *Semin Cell Dev Biol* (2015) 41:59–69. doi: 10.1016/j.semcdb.2015.05.004

45. Gardner A, de Mingo Pulido Á, Ruffell B. Dendritic cells and their role in immunotherapy. *Front Immunol* (2020) 11:924. doi: 10.3389/fimmu.2020.00924

46. Hoeffel G, Chen J, Lavin Y, Low D, Almeida FF, See P, et al. C-myb+ erythro-myeloid progenitor-derived fetal monocytes give rise to adult tissue-resident macrophages. *Immunity* (2015) 42:665–78. doi: 10.1016/j.immuni.2015.03.011

47. André F, Schartz NEC, Chaput N, Flament C, Raposo G, Amigorena S, et al. Tumor-derived exosomes: A new source of tumor rejection antigens. *Vaccine* (2002) 20:A28–31. doi: 10.1016/S0264-410X(02)00384-5

48. Everts B, Amiel E, Huang SC-C, Smith AM, Chang C-H, Lam WY, et al. TLR-driven early glycolytic reprogramming *via* the kinases TBK1-IKKε supports the anabolic demands of dendritic cell activation. *Nat Immunol* (2014) 15:323–32. doi: 10.1038/ni.2833

49. Krawczyk CM, Holowka T, Sun J, Blagih J, Amiel E, DeBerardinis RJ, et al. Toll-like receptor–induced changes in glycolytic metabolism regulate dendritic cell activation. *Blood* (2010) 115:4742–9. doi: 10.1182/blood-2009-10-249540

50. Jantsch J, Chakravortty D, Turza N, Prechtel AT, Buchholz B, Gerlach RG, et al. Hypoxia and hypoxia-inducible factor-1α modulate lipopolysaccharide-induced dendritic cell activation and function. *J Immunol* (2008) 180:4697–705. doi: 10.4049/jimmunol.180.7.4697

51. Sinclair C, Bommakanti G, Gardinassi L, Loebbermann J, Johnson MJ, Hakimpour P, et al. mTOR regulates metabolic adaptation of APCs in the lung and controls the outcome of allergic inflammation. *Science* (2017) 357:1014–21. doi: 10.1126/science.aaj2155

52. Hao S, Bai O, Li F, Yuan J, Laferte S, Xiang J. Mature dendritic cells pulsed with exosomes stimulate efficient cytotoxic T-lymphocyte responses and antitumour immunity. *Immunology* (2007) 90–120. doi: 10.1111/j.1365-2567.2006.02483.x

53. Wang Y, Xiang Y, Xin VW, Wang X-W, Peng X-C, Liu X-Q, et al. Dendritic cell biology and its role in tumor immunotherapy. *J Hematol OncolJ Hematol Oncol* (2020) 13:107. doi: 10.1186/s13045-020-00939-6

54. Record M, Subra C, Silvente-Poirot S, Poirot M. Exosomes as intercellular signalosomes and pharmacological effectors. *Biochem Pharmacol* (2011) 81:1171–82. doi: 10.1016/j.bcp.2011.02.011

55. Lindenbergh MFS, Stoorvogel W. Antigen presentation by extracellular vesicles from professional antigen-presenting cells. *Annu Rev Immunol* (2018) 36:435–59. doi: 10.1146/annurev-immunol-041015-055700

56. Théry C, Duban L, Segura E, Véron P, Lantz O, Amigorena S. Indirect activation of naïve CD4+ T cells by dendritic cell–derived exosomes. *Nat Immunol* (2002) 3:1156–62. doi: 10.1038/ni854

57. Du Z, Huang Z, Chen X, Jiang G, Peng Y, Feng W, et al. Modified dendritic cell-derived exosomes activate both NK cells and T cells through the NKG2D/NKG2D-l pathway to kill CML cells with or without T315I mutation. *Exp Hematol Oncol* (2022) 11:36. doi: 10.1186/s40164-022-00289-8

58. Théry C, Ostrowski M, Segura E. Membrane vesicles as conveyors of immune responses. *Nat Rev Immunol* (2009) 9:581–93. doi: 10.1038/nri2567

59. Greyer M, Whitney PG, Stock AT, Davey GM, Tebartz C, Bachem A, et al. T Cell help amplifies innate signals in CD8 + DCs for optimal CD8 + T cell priming. *Cell Rep* (2016) 14:586–97. doi: 10.1016/j.celrep.2015.12.058

60. Pipkin ME, Sacks JA, Cruz-Guilloty F, Lichtenheld MG, Bevan MJ, Rao A. Interleukin-2 and inflammation induce distinct transcriptional programs that promote the differentiation of effector cytolytic T cells. *Immunity* (2010) 32:79–90. doi: 10.1016/j.immuni.2009.11.012

61. Zhang H, Zhu Z, Modrak S, Little A. Tissue-resident memory CD4 $^{+}$ T cells play a dominant role in the initiation of antitumor immunity. *J Immunol* (2022) 208:2837–46. doi: 10.4049/jimmunol.2100852

62. Nicolet BP, Guislain A, van Alphen FPJ, Gomez-Eerland R, Schumacher TNM, van den Biggelaar M, et al. CD29 identifies IFN-γ–producing human CD8 $^{+}$ T cells with an increased cytotoxic potential. *Proc Natl Acad Sci* (2020) 117:6686–96. doi: 10.1073/pnas.1913940117

63. Borst J, Ahrends T, Bąbała N, Melief CJM, Kastenmüller W. CD4+ T cell help in cancer immunology and immunotherapy. *Nat Rev Immunol* (2018) 18:635–47. doi: 10.1038/s41577-018-0044-0

64. Rezaei R, Baghaei K, Hashemi SM, Zali MR, Ghanbarian H, Amani D. Tumor-derived exosomes enriched by miRNA-124 promote anti-tumor immune response in CT-26 tumor-bearing mice. *Front Med* (2021) 8:619939. doi: 10.3389/fmed.2021.619939

65. Roshani Asl E, Rasmi Y, Baradaran B. MicroRNA-124-3p suppresses PD-L1 expression and inhibits tumorigenesis of colorectal cancer cells *via* modulating STAT3 signaling. *J Cell Physiol* (2021) 236:7071–87. doi: 10.1002/jcp.30378

66. Rogers T, DeBerardinis RJ. Metabolic plasticity of neutrophils: Relevance to pathogen responses and cancer. *Trends Cancer* (2021) 7:700–13. doi: 10.1016/j.trecan.2021.04.007

67. Yang D, Yang L, Cai J, Li H, Xing Z, Hou Y. Phosphoinositide 3-kinase/Akt and its related signaling pathways in the regulation of tumor-associated macrophages polarization. *Mol Cell Biochem* (2022). doi: 10.1007/s11010-022-04461-w

68. Pu Y, Ji Q. Tumor-associated macrophages regulate PD-1/PD-L1 immunosuppression. *Front Immunol* (2022) 13:874589. doi: 10.3389/fimmu.2022.874589

69. Li Z, Suo B, Long G, Gao Y, Song J, Zhang M, et al. Exosomal miRNA-16-5p derived from M1 macrophages enhances T cell-dependent immune response by

regulating PD-L1 in gastric cancer. *Front Cell Dev Biol* (2020) 8:572689. doi: 10.3389/fcell.2020.572689

70. Bebber CM, Müller F, Prieto Clemente L, Weber J, von Karstedt S. Ferroptosis in cancer cell biology. *Cancers* (2020) 12:164. doi: 10.3390/cancers12010164

71. Kundu J, Surh Y. Inflammation: Gearing the journey to cancer. *Mutat Res Mutat Res* (2008) 659:15–30. doi: 10.1016/j.mrrev.2008.03.002

72. Borrello MG, Alberti L, Fischer A, Degl'innocenti D, Ferrario C, Gariboldi M, et al. Induction of a proinflammatory program in normal human thyrocytes by the RET/PTC1 oncogene. *Proc Natl Acad Sci U A* (2005) 102:14825–30. doi: 10.1073/pnas.0503039102

73. Shchors K, Shchors E, Rostker F, Lawlor ER, Brown-Swigart L, Evan GI. The myc-dependent angiogenic switch in tumors is mediated by interleukin 1beta. *Genes Dev* (2006) 20:2527–38. doi: 10.1101/gad.1455706

74. Hamarsheh S, Osswald L, Saller BS, Unger S, De Feo D, Vinnakota JM, et al. Oncogenic KrasG12D causes myeloproliferation *via* NLRP3 inflammasome activation. *Nat Commun* (2020) 11:1659. doi: 10.1038/s41467-020-15497-1

75. Corrado C, Raimondo S, Chiesi A, Ciccia F, De Leo G, Alessandro R. Exosomes as intercellular signaling organelles involved in health and disease: Basic science and clinical applications. *Int J Mol Sci* (2013) 14:5338–66. doi: 10.3390/ijms14035338

76. Othman N, Jamal R, Abu N. Cancer-derived exosomes as effectors of key inflammation-related players. *Front Immunol* (2019) 10:2103. doi: 10.3389/fimmu.2019.02103

77. Shen M, Ren X. New insights into the biological impacts of immune cell-derived exosomes within the tumor environment. *Cancer Lett* (2018) 431:115–22. doi: 10.1016/j.canlet.2018.05.040

78. Martini M, Testi MG, Pasetto M, Picchio MC, Innamorati G, Mazzocco M, et al. IFN-γ-mediated upmodulation of MHC class I expression activates tumor-specific immune response in a mouse model of prostate cancer. *Vaccine* (2010) 28:3548–57. doi: 10.1016/j.vaccine.2010.03.007

79. Thapa RJ, Basagoudanavar SH, Nogusa S, Irrinki K, Mallilankaraman K, Slifker MJ, et al. NF-κB protects cells from gamma interferon-induced RIP1-dependent necroptosis. *Mol Cell Biol* (2011) 31:2934–46. doi: 10.1128/MCB.05445-11

80. Song M, Ping Y, Zhang K, Yang L, Li F, Zhang C, et al. Low-dose IFNγ induces tumor cell stemness in tumor microenvironment of non–small cell lung cancer. *Cancer Res* (2019) 79:3737–48. doi: 10.1158/0008-5472.CAN-19-0596

81. Carmi Y, Voronov E, Dotan S, Lahat N, Rahat MA, Fogel M, et al. The role of macrophage-derived IL-1 in induction and maintenance of angiogenesis. *J Immunol* (2009) 183:4705–14. doi: 10.4049/jimmunol.0901511

82. Carmi Y, Rinott G, Dotan S, Elkabets M, Rider P, Voronov E, et al. Microenvironment-derived IL-1 and IL-17 interact in the control of lung metastasis. *J Immunol* (2011) 186:3462–71. doi: 10.4049/jimmunol.1002901

83. Sun Z, Ren Z, Yang K, Liu Z, Cao S, Deng S, et al. A next-generation tumor-targeting IL-2 preferentially promotes tumor-infiltrating CD8+ T-cell response and effective tumor control. *Nat Commun* (2019) 10:3874. doi: 10.1038/s41467-019-11782-w

84. Nappo G, Handle F, Santer FR, McNeill RV, Seed RI, Collins AT, et al. The immunosuppressive cytokine interleukin-4 increases the clonogenic potential of prostate stem-like cells by activation of STAT6 signalling. *Oncogenesis* (2017) 6:e342–2. doi: 10.1038/oncsis.2017.23

85. Li Z, Jiang J, Wang Z, Zhang J, Xiao M, Wang C, et al. Endogenous interleukin-4 promotes tumor development by increasing tumor cell resistance to apoptosis. *Cancer Res* (2008) 68:8687–94. doi: 10.1158/0008-5472.CAN-08-0449

86. Gocheva V, Wang H-W, Gadea BB, Shree T, Hunter KE, Garfall AL, et al. IL-4 induces cathepsin protease activity in tumor-associated macrophages to promote cancer growth and invasion. *Genes Dev* (2010) 24:241–55. doi: 10.1101/gad.1874010

87. Apte SH, Groves P, Olver S, Baz A, Doolan DL, Kelso A, et al. IFN-γ inhibits IL-4–induced type 2 cytokine expression by CD8 T cells *In vivo* and modulates the anti-tumor response. *J Immunol* (2010) 185:998–1004. doi: 10.4049/jimmunol.0903372

88. Agaugué S, Marcenaro E, Ferranti B, Moretta L, Moretta A. Human natural killer cells exposed to IL-2, IL-12, IL-18, or IL-4 differently modulate priming of naive T cells by monocyte-derived dendritic cells. *Blood* (2008) 112:1776–83. doi: 10.1182/blood-2008-02-135871

89. De Simone V, Franzè E, Ronchetti G, Colantoni A, Fantini MC, Di Fusco D, et al. Th17-type cytokines, IL-6 and TNF-α synergistically activate STAT3 and NF-kB to promote colorectal cancer cell growth. *Oncogene* (2015) 34:3493–503. doi: 10.1038/onc.2014.286

90. Lin M-T, Juan C-Y, Chang K-J, Chen W-J, Kuo M-L. IL-6 inhibits apoptosis and retains oxidative DNA lesions in human gastric cancer AGS cells through up-regulation of anti-apoptotic gene mcl-1. *Carcinogenesis* (2001) 22:1947–53. doi: 10.1093/carcin/22.12.1947

91. Huang Y-H, Yang H-Y, Huang S-W, Ou G, Hsu Y-F, Hsu M-J. Interleukin-6 induces vascular endothelial growth factor-c expression *via* src-FAK-STAT3 signaling in lymphatic endothelial cells. *PloS One* (2016) 11:e0158839. doi: 10.1371/journal.pone.0158839

92. Alfaro C, Sanmamed MF, Rodríguez-Ruiz ME, Teijeira Á, Oñate C, González Á, et al. Interleukin-8 in cancer pathogenesis, treatment and follow-up. *Cancer Treat Rev* (2017) 60:24–31. doi: 10.1016/j.ctrv.2017.08.004

93. Ginestier C, Liu S, Diebel ME, Korkaya H, Luo M, Brown M, et al. CXCR1 blockade selectively targets human breast cancer stem cells *in vitro* and in xenografts. *J Clin Invest* (2010) 120:485–97. doi: 10.1172/JCI39397

94. Sato T, Terai M, Tamura Y, Alexeev V, Mastrangelo MJ, Selvan SR. Interleukin 10 in the tumor microenvironment: A target for anticancer immunotherapy. *Immunol Res* (2011) 51:170–82. doi: 10.1007/s12026-011-8262-6

95. Wang X, Wong K, Ouyang W, Rutz S. Targeting IL-10 family cytokines for the treatment of human diseases. *Cold Spring Harb Perspect Biol* (2019) 11:a028548. doi: 10.1101/cshperspect.a028548

96. Hamidullah, Changkija B, Konwar R. Role of interleukin-10 in breast cancer. *Breast Cancer Res Treat* (2012) 133:11–21. doi: 10.1007/s10549-011-1855-x

97. Li L, Ma Y, Xu Y. Follicular regulatory T cells infiltrated the ovarian carcinoma and resulted in CD8 T cell dysfunction dependent on IL-10 pathway. *Int Immunopharmacol* (2019) 68:81–7. doi: 10.1016/j.intimp.2018.12.051

98. Mirlekar B, Pylayeva-Gupta Y. IL-12 family cytokines in cancer and immunotherapy. *Cancers* (2021) 13:167. doi: 10.3390/cancers13020167

99. Schmidt-Weber CB, Akdis M, Akdis CA. TH17 cells in the big picture of immunology. *J Allergy Clin Immunol* (2007) 120:247–54. doi: 10.1016/j.jaci.2007.06.039

100. Moseley TA, Haudenschild DR, Rose L, Reddi AH. Interleukin-17 family and IL-17 receptors. *Cytokine Growth Factor Rev* (2003) 14:155–74. doi: 10.1016/S1359-6101(03)00002-9

101. Arend WP, Palmer G, Gabay C. IL-1, IL-18, and IL-33 families of cytokines. *Immunol Rev* (2008) 223:20–38. doi: 10.1111/j.1600-065X.2008.00624.x

102. Xing Y, Tian Y, Kurosawa T, Matsui S, Touma M, Wu Q, et al. Inhibition of blood vessel formation in tumors by IL-18-polarized M1 macrophages. *Genes Cells* (2016) 21:287–95. doi: 10.1111/gtc.12329

103. Wang X, Lin Y. Tumor necrosis factor and cancer, buddies or foes? *Acta Pharmacol Sin* (2008) 29:1275–88. doi: 10.1111/j.1745-7254.2008.00889.x

104. Chen X, Wang L, Li P, Song M, Qin G, Gao Q, et al. Dual TGF-β and PD-1 blockade synergistically enhances MAGE-A3-specific CD8 $^{+}$ T cell response in esophageal squamous cell carcinoma. *Int J Cancer* (2018) 143:2561–74. doi: 10.1002/ijc.31730

105. Shen Y, Teng Y, Lv Y, Zhao Y, Qiu Y, Chen W, et al. PD-1 does not mark tumor-infiltrating CD8+ T cell dysfunction in human gastric cancer. *J Immunother Cancer* (2020) 8:e000422. doi: 10.1136/jitc-2019-000422

106. Yu H, Yang J, Jiao S, Wang J, Li Y. TGF-β1 precursor and CD8 are potential prognostic and predictive markers in operated breast cancer. *J Huazhong Univ Sci Technolog Med Sci* (2014) 34:51–8. doi: 10.1007/s11596-014-1231-2

107. Fujii R, Jochems C, Tritsch SR, Wong HC, Schlom J, Hodge JW. An IL-15 superagonist/IL-15Rα fusion complex protects and rescues NK cell-cytotoxic function from TGF-β1-mediated immunosuppression. *Cancer Immunol Immunother* (2018) 67:675–89. doi: 10.1007/s00262-018-2121-4

108. Kumar A, Taghi Khani A, Sanchez Ortiz A, Swaminathan S. GM-CSF: A double-edged sword in cancer immunotherapy. *Front Immunol* (2022) 13:901277. doi: 10.3389/fimmu.2022.901277

109. Rahmati M, Petitbarat M, Dubanchet S, Bensussan A, Chaouat G, Ledee N. Granulocyte-colony stimulating factor related pathways tested on an endometrial *ex-vivo* model. *PloS One* (2014) 9:e102286. doi: 10.1371/journal.pone.0102286

110. He K, Liu X, Hoffman RD, Shi R, Lv G, Gao J. G-CSF / GM-CSF -induced hematopoietic dysregulation in the progression of solid tumors. *FEBS Open Bio* (2022) 12:1268–85. doi: 10.1002/2211-5463.13445

111. Dong J, Grunstein J, Tejada M, Peale F, Frantz G, Liang W-C, et al. VEGF-null cells require PDGFR α signaling-mediated stromal fibroblast recruitment for tumorigenesis. *EMBO J* (2004) 23:2800–10. doi: 10.1038/sj.emboj.7600289

112. Kong D, Banerjee S, Ahmad A, Li Y, Wang Z, Sethi S, et al. Epithelial to mesenchymal transition is mechanistically linked with stem cell signatures in prostate cancer cells. *PloS One* (2010) 5:e12445. doi: 10.1371/journal.pone.0012445

113. Grismaldo A, Sobrevia L, Morales L. Role of platelet-derived growth factor c on endothelial dysfunction in cardiovascular diseases. *Biochim Biophys Acta BBA - Gen Subj* (2022) 1866:130188. doi: 10.1016/j.bbagen.2022.130188

114. Geindreau M, Bruchard M, Vegran F. Role of cytokines and chemokines in angiogenesis in a tumor context. *Cancers* (2022) 14:2446. doi: 10.3390/cancers14102446

115. Motz GT, Santoro SP, Wang L-P, Garrabrant T, Lastra RR, Hagemann IS, et al. Tumor endothelium FasL establishes a selective immune barrier promoting tolerance in tumors. *Nat Med* (2014) 20:607–15. doi: 10.1038/nm.3541

116. Bai W, Zhang W, Hu B. Vascular endothelial growth factor suppresses dendritic cells function of human prostate cancer. *OncoTargets Ther* (2018) 11:1267–74. doi: 10.2147/OTT.S161302

117. Singh B, Carpenter G, Coffey RJ. EGF receptor ligands: recent advances. *F1000Research* (2016) 5:2270. doi: 10.12688/f1000research.9025.1

118. Sasaki T, Hiroki K, Yamashita Y. The role of epidermal growth factor receptor in cancer metastasis and microenvironment. *BioMed Res Int* (2013) 2013:1–8. doi: 10.1155/2013/546318

119. Ferreira AS, Lopacinski A, Batista M, Hiraiwa PM, Guimarães BG, Zanchin NIT. A toolkit for recombinant production of seven human EGF family growth factors in active conformation. *Sci Rep* (2022) 12:5034. doi: 10.1038/s41598-022-09060-9

120. Do HTT, Lee CH, Cho J. Chemokines and their receptors: Multifaceted roles in cancer progression and potential value as cancer prognostic markers. *Cancers* (2020) 12:287. doi: 10.3390/cancers12020287

121. Krawczyk KM, Nilsson H, Allaoui R, Lindgren D, Arvidsson M, Leandersson K, et al. Papillary renal cell carcinoma-derived chemerin, IL-8, and CXCL16 promote monocyte recruitment and differentiation into foam-cell macrophages. *Lab Invest* (2017) 97:1296–305. doi: 10.1038/labinvest.2017.78

122. Redjimi N, Raffin C, Raimbaud I, Pignon P, Matsuzaki J, Odunsi K, et al. CXCR3 $^{+}$ T regulatory cells selectively accumulate in human ovarian carcinomas to limit type I immunity. *Cancer Res* (2012) 72:4351–60. doi: 10.1158/0008-5472.CAN-12-0579

123. Wittamer V, Franssen J-D, Vulcano M, Mirjolet J-F, Le Poul E, Migeotte I, et al. Specific recruitment of antigen-presenting cells by chemerin, a novel processed ligand from human inflammatory fluids. *J Exp Med* (2003) 198:977–85. doi: 10.1084/jem.20030382

124. Samson M, Edinger AL, Stordeur P, Rucker J, Verhasselt V, Sharron M, et al. ChemR23, a putative chemoattractant receptor, is expressed in monocyte-derived dendritic cells and macrophages and is a coreceptor for SIV and some primary HIV-1 strains. *Eur J Immunol* (1998) 28:1689–700. doi: 10.1002/(SICI)1521-4141(199805)28:05<1689::AID-IMMU1689>3.0.CO;2-I

125. Parolini S, Santoro A, Marcenaro E, Luini W, Massardi L, Facchetti F, et al. The role of chemerin in the colocalization of NK and dendritic cell subsets into inflamed tissues. *Blood* (2007) 109:3625–32. doi: 10.1182/blood-2006-08-038844

126. Eisinger K, Bauer S, Schäffler A, Walter R, Neumann E, Buechler C, et al. Chemerin induces CCL2 and TLR4 in synovial fibroblasts of patients with rheumatoid arthritis and osteoarthritis. *Exp Mol Pathol* (2012) 92:90–6. doi: 10.1016/j.yexmp.2011.10.006

127. Goralski KB, Jackson AE, McKeown BT, Sinal CJ. More than an adipokine: The complex roles of chemerin signaling in cancer. *Int J Mol Sci* (2019) 20:4778. doi: 10.3390/ijms20194778

128. Banas M, Zabieglo K, Kasetty G, Kapinska-Mrowiecka M, Borowczyk J, Drukala J, et al. Correction: Chemerin is an antimicrobial agent in human epidermis. *PloS One* (2013) 1–8. doi: 10.1371/annotation/4dfd522c-f0fd-40db-aadc-44cbef367a40

129. Dubois-Vedrenne I, Al Delbany D, De Henau O, Robert V, Vernimmen M, Langa F, et al. The antitumoral effects of chemerin are independent from leukocyte recruitment and mediated by inhibition of neoangiogenesis. *Oncotarget* (2021) 12:1903–19. doi: 10.18632/oncotarget.28056

130. Bhat AA, Nisar S, Singh M, Ashraf B, Masoodi T, Prasad CP, et al. Cytokine- and chemokine-induced inflammatory colorectal tumor microenvironment: Emerging avenue for targeted therapy. *Cancer Commun* (2022) 1–27. doi: 10.1002/cac2.12295

131. Gowhari Shabgah A, Jadidi-Niaragh F, Ebrahimzadeh F, Mohammadi H, Askari E, Pahlavani N, et al. A comprehensive review of chemokine CXC17 (VCC1) in cancer, infection, and inflammation. *Cell Biol Int* (2022) 1–14. doi: 10.1002/cbin.11846

132. Helmlinger G, Sckell A, Dellian M, Forbes NS, Jain RK. Acid production in glycolysis-impaired tumors provides new insights into tumor metabolism. *Clin Cancer Res Off J Am Assoc Cancer Res* (2002) 8:1284–91.

133. Wang C, Li Y, Yan S, Wang H, Shao X, Xiao M, et al. Interactome analysis reveals that lncRNA HULC promotes aerobic glycolysis through LDHA and PKM2. *Nat Commun* (2020) 11:3162. doi: 10.1038/s41467-020-16966-3

134. Zhai S, Xu Z, Xie J, Zhang J, Wang X, Peng C, et al. Epigenetic silencing of LncRNA LINC00261 promotes c-myc-mediated aerobic glycolysis by regulating miR-222-3p/HIPK2/ERK axis and sequestering IGF2BP1. *Oncogene* (2021) 40:277–91. doi: 10.1038/s41388-020-01525-3

135. Takahashi K, Yan IK, Haga H, Patel T. Modulation of hypoxia-signaling pathways by extracellular long non-coding RNA regulator of reprogramming. *J Cell Sci* (2014) (7):1585–94. doi: 10.1242/jcs.141069

136. Nishizawa Y, Konno M, Asai A, Koseki J, Kawamoto K, Miyoshi N, et al. Hypoxia stimulates the cytoplasmic localization of oncogenic long noncoding RNA LINC00152 in colorectal cancer. *Int J Oncol* (2017) (52):453–60. doi: 10.3892/ijo.2017.4218

137. Ng CT, Azwar S, Yip WK, Zahari Sham SY, Faisal Jabar M, Sahak NH, et al. Isolation and identification of long non-coding RNAs in exosomes derived from the serum of colorectal carcinoma patients. *Biology* (2021) 10:918. doi: 10.3390/biology10090918

138. Mendler AN, Hu B, Prinz PU, Kreutz M, Gottfried E, Noessner E. Tumor lactic acidosis suppresses CTL function by inhibition of p38 and JNK/c-jun activation. *Int J Cancer* (2012) 131:633–40. doi: 10.1002/ijc.26410

139. Raychaudhuri D, Bhattacharya R, Sinha BP, Liu CSC, Ghosh AR, Rahaman O, et al. Lactate induces pro-tumor reprogramming in intratumoral plasmacytoid dendritic cells. *Front Immunol* (2019) 10:1878. doi: 10.3389/fimmu.2019.01878

140. Brown RAM, Richardson KL, Kabir TD, Trinder D, Ganss R, Leedman PJ. Altered iron metabolism and impact in cancer biology, metastasis, and immunology. *Front Oncol* (2020) 10:476. doi: 10.3389/fonc.2020.00476

141. Galluzzi L, Vitale I, Aaronson SA, Abrams JM, Adam D, Agostinis P, et al. Molecular mechanisms of cell death: recommendations of the nomenclature committee on cell death 2018. *Cell Death Diff* (2018) 25:486–541. doi: 10.1038/s41418-017-0012-4

142. Efimova I, Catanzaro E, van der Meeren L, Turubanova VD, Hammad H, Mishchenko TA, et al. Vaccination with early ferroptotic cancer cells induces efficient antitumor immunity. *J Immunother Cancer* (2020) 8:e001369. doi: 10.1136/jitc-2020-001369

143. Yegutkin GG. Enzymes involved in metabolism of extracellular nucleotides and nucleosides: Functional implications and measurement of activities. *Crit Rev Biochem Mol Biol* (2014) 49:473–97. doi: 10.3109/10409238.2014.953627

144. Resta R, Yamashita Y, Thompson LF. Ecto-enzyme and signaling functions of lymphocyte CD 7 3. *Immunol Rev* (1998) 161:95–109. doi: 10.1111/j.1600-065X.1998.tb01574.x

145. Allard B, Longhi MS, Robson SC, Stagg J. The ectonucleotidases CD39 and CD73: Novel checkpoint inhibitor targets. *Immunol Rev* (2017) 276:121–44. doi: 10.1111/imr.12528

146. Raskovalova T, Lokshin A, Huang X, Jackson EK, Gorelik E. Adenosine-mediated inhibition of cytotoxic activity and cytokine production by IL-2/NKp46-Activated NK cells: Involvement of protein kinase a isozyme I (PKA I). *Immunol Res* (2006) 36:91–100. doi: 10.1385/IR:36:1:91

147. Csóka B, Selmeczy Z, Koscsó B, Németh ZH, Pacher P, Murray PJ, et al. Adenosine promotes alternative macrophage activation *via* A2A and A2B receptors. *FASEB J* (2012) 26:376–86. doi: 10.1096/fj.11-190934

148. Augsten M, Hägglöf C, Olsson E, Stolz C, Tsagozis P, Levchenko T, et al. CXCL14 is an autocrine growth factor for fibroblasts and acts as a multi-modal stimulator of prostate tumor growth. *Proc Natl Acad Sci* (2009) 106:3414–9. doi: 10.1073/pnas.0813144106

149. Shi H, Han X, Sun Y, Shang C, Wei M, Ba X, et al. Chemokine (C-X-C motif) ligand 1 and CXCL 2 produced by tumor promote the generation of monocytic myeloid-derived suppressor cells. *Cancer Sci* (2018) 109:3826–39. doi: 10.1111/cas.13809

150. Unver N, Esendagli G, Yilmaz G, Guc D. CXCL7-induced macrophage infiltration in lung tumor is independent of CXCR2 expression. *Cytokine* (2015) 75:330–7. doi: 10.1016/j.cyto.2015.07.018

151. Kasashima H, Yashiro M, Nakamae H, Kitayama K, Masuda G, Kinoshita H, et al. CXCL1–chemokine (C-X-C motif) receptor 2 signaling stimulates the recruitment of bone marrow–derived mesenchymal cells into diffuse-type gastric cancer stroma. *Am J Pathol* (2016) 186:3028–39. doi: 10.1016/j.ajpath.2016.07.024

152. Deng S, Deng Q, Zhang Y, Ye H, Yu X, Zhang Y, et al. Non-platelet-derived CXCL4 differentially regulates cytotoxic and regulatory T cells through CXCR3 to suppress the immune response to colon cancer. *Cancer Lett* (2019) 443:1–12. doi: 10.1016/j.canlet.2018.11.017

153. Yan M, Jene N, Byrne D, Millar EK, O'Toole SA, McNeil CM, et al. Recruitment of regulatory T cells is correlated with hypoxia-induced CXCR4 expression, and is associated with poor prognosis in basal-like breast cancers. *Breast Cancer Res* (2011) 13:R47. doi: 10.1186/bcr2869

154. Shao C, Yang F, Miao S, Liu W, Wang C, Shu Y, et al. Role of hypoxia-induced exosomes in tumor biology. *Mol Cancer* (2018) 17:120. doi: 10.1186/s12943-018-0869-y

155. Chalmin F, Ladoire S, Mignot G, Vincent J, Bruchard M, Remy-Martin J-P, et al. Membrane-associated Hsp72 from tumor-derived exosomes mediates STAT3-dependent immunosuppressive function of mouse and human myeloid-derived suppressor cells. *J Clin Invest* (2010) (2):457–71. doi: 10.1172/JCI40483

156. Jafari R, Rahbarghazi R, Ahmadi M, Hassanpour M, Rezaie J. Hypoxic exosomes orchestrate tumorigenesis: molecular mechanisms and therapeutic implications. *J Transl Med* (2020) 18:474. doi: 10.1186/s12967-020-02662-9

157. Zhang Q, Zhong C, Shen J, Chen S, Jia Y, Duan S. Emerging role of LINC00461 in cancer. *BioMed Pharmacother* (2022) 152:113239. doi: 10.1016/j.biopha.2022.113239

158. Fabbri M, Paone A, Calore F, Galli R, Gaudio E, Santhanam R, et al. MicroRNAs bind to toll-like receptors to induce prometastatic inflammatory response. *Proc Natl Acad Sci* (2012) 109:E2110–6. doi: 10.1073/pnas.1209414109

159. Balsamo M, Manzini C, Pietra G, Raggi F, Blengio F, Mingari MC, et al. Hypoxia downregulates the expression of activating receptors involved in NK-cell-mediated target cell killing without affecting ADCC: Innate immunity. *Eur J Immunol* (2013) 43:2756–64. doi: 10.1002/eji.201343448

160. Xu Y, Zeng H, Jin K, Liu Z, Zhu Y, Xu L, et al. Immunosuppressive tumor-associated macrophages expressing interlukin-10 conferred poor prognosis and therapeutic vulnerability in patients with muscle-invasive bladder cancer. *J Immunother Cancer* (2022) 10:e003416. doi: 10.1136/jitc-2021-003416

161. Chang L-Y, Lin Y-C, Mahalingam J, Huang C-T, Chen T-W, Kang C-W, et al. Tumor-derived chemokine CCL5 enhances TGF-β–mediated killing of CD8 $^+$ T cells in colon cancer by T-regulatory cells. *Cancer Res* (2012) 72:1092–102. doi: 10.1158/0008-5472.CAN-11-2493

162. Chen M-L, Pittet MJ, Gorelik L, Flavell RA, Weissleder R, von Boehmer H, et al. Regulatory T cells suppress tumor-specific CD8 T cell cytotoxicity through TGF-β signals *in vivo*. *Proc Natl Acad Sci* (2005) 102:419–24. doi: 10.1073/pnas.0408197102

163. Donkor MK, Sarkar A, Li MO. Tgf-β1 produced by activated CD4 $^+$ T cells antagonizes T cell surveillance of tumor development. *OncoImmunology* (2012) 1:162–71. doi: 10.4161/onci.1.2.18481

164. Barilla RM, Diskin B, Caso RC, Lee KB, Mohan N, Buttar C, et al. Specialized dendritic cells induce tumor-promoting IL-10+IL-17+ FoxP3neg regulatory CD4+ T cells in pancreatic carcinoma. *Nat Commun* (2019) 10:1424. doi: 10.1038/s41467-019-09416-2

165. Ye S-B, Zhang H, Cai T-T, Liu Y-N, Ni J-J, He J, et al. Exosomal miR-24-3p impedes T-cell function by targeting *FGF11* and serves as a potential prognostic biomarker for nasopharyngeal carcinoma: Role of exosomal miR-24 in immune regulation of nasopharyngeal carcinoma. *J Pathol* (2016) 240:329–40. doi: 10.1002/path.4781

166. Li Y, Patel SP, Roszik J, Qin Y. Hypoxia-driven immunosuppressive metabolites in the tumor microenvironment: New approaches for combinational immunotherapy. *Front Immunol* (2018) 9:1591. doi: 10.3389/fimmu.2018.01591

167. Sawa-Wejksza K, Dudek A, Lemieszek M, Kaławaj K, Kandefer-Szerszeń M. Colon cancer–derived conditioned medium induces differentiation of THP-1 monocytes into a mixed population of M1/M2 cells. *Tumor Biol* (2018) 40:101042831879788. doi: 10.1177/1010428318797880

168. Walsh SA, Davis TA. Key early proinflammatory signaling molecules encapsulated within circulating exosomes following traumatic injury. *J Inflammation* (2022) 19:6. doi: 10.1186/s12950-022-00303-0

169. Zamarron BF, Chen W. Dual roles of immune cells and their factors in cancer development and progression. *Int J Biol Sci* (2011) 7:651–8. doi: 10.7150/ijbs.7.651

170. Islas-Vazquez L, Aguilar-Cazares D, Galicia-Velasco M, Rumbo-Nava U, Meneses-Flores M, Luna-Rivero C, et al. IL-6, NLR, and SII markers and their relation with alterations in CD8+ T-lymphocyte subpopulations in patients treated for lung adenocarcinoma. *Biology* (2020) 9:376. doi: 10.3390/biology9110376

171. Iliopoulos D, Hirsch HA, Wang G, Struhl K. Inducible formation of breast cancer stem cells and their dynamic equilibrium with non-stem cancer cells *via* IL6 secretion. *Proc Natl Acad Sci* (2011) 108:1397–402. doi: 10.1073/pnas.1018898108

172. Kalliolias GD, Ivashkiv LB. TNF biology, pathogenic mechanisms and emerging therapeutic strategies. *Nat Rev Rheumatol* (2016) 12:49–62. doi: 10.1038/nrrheum.2015.169

173. Stephens JM, Pekala PH. Transcriptional repression of the GLUT4 and C/EBP genes in 3T3-L1 adipocytes by tumor necrosis factor-alpha. *J Biol Chem* (1991) 266:21839–45. doi: 10.1016/S0021-9258(18)54714-1

174. Palacios-Ortega S, Varela-Guruceaga M, Algarabel M, Milagro FI, Martínez JA, de Miguel C. Effect of TNF-alpha on caveolin-1 expression and insulin signaling during adipocyte differentiation and in mature adipocytes. *Cell Physiol Biochem* (2015) 36:1499–516. doi: 10.1159/000430314

175. Xing H, Northrop JP, Grove JR, Kilpatrick KE, Su J-L, Ringold GM. TNFα-mediated inhibition and reversal of adipocyte differentiation is accompanied by suppressed expression of PPARγ without effects on pref-1 expression*. *Endocrinology* (1997) 138:2776–83. doi: 10.1210/endo.138.7.5242

176. Zhang L, Han L, He J, Lv J, Pan R, Lv T. A high serum-free fatty acid level is associated with cancer. *J Cancer Res Clin Oncol* (2020) 146:705–10. doi: 10.1007/s00432-019-03095-8

177. Watkins LR, Goehler LE, Relton J, Brewer MT, Maier SF. Mechanisms of tumor necrosis factor-α (TNF-α) hyperalgesia. *Brain Res* (1995) 692:244–50. doi: 10.1016/0006-8993(95)00715-3

178. Czeschik JC, Hagenacker T, Schäfers M, Büsselberg D. TNF-α differentially modulates ion channels of nociceptive neurons. *Neurosci Lett* (2008) 434:293–8. doi: 10.1016/j.neulet.2008.01.070

179. Li C, Palanisamy K, Li X, Yu S, Wang I, Li C, et al. Exosomal tumor necrosis factor-α from hepatocellular cancer cells (Huh-7) promote osteoclast differentiation. *J Cell Biochem* (2021) 122:1749–60. doi: 10.1002/jcb.30127

180. Fields JK, Günther S, Sundberg EJ. Structural basis of IL-1 family cytokine signaling. *Front Immunol* (2019) 10:1412. doi: 10.3389/fimmu.2019.01412

181. Gelfo V, Romaniello D, Mazzeschi M, Sgarzi M, Grilli G, Morselli A, et al. Roles of IL-1 in cancer: From tumor progression to resistance to targeted therapies. *Int J Mol Sci* (2020) 21:6009. doi: 10.3390/ijms21176009

182. Zhang W, Borcherding N, Kolb R. "IL-1 signaling in tumor microenvironment.,". In: A Birbrair, editor. *Tumor microenvironment. advances in experimental medicine and biology*. Cham: Springer International Publishing (2020). p. 1–23. doi: 10.1007/978-3-030-38315-2_1

183. Malik A, Kanneganti T-D. Function and regulation of IL-1α in inflammatory diseases and cancer. *Immunol Rev* (2018) 281:124–37. doi: 10.1111/imr.12615

184. Afonina IS, Müller C, Martin SJ, Beyaert R. Proteolytic processing of interleukin-1 family cytokines: Variations on a common theme. *Immunity* (2015) 42:991–1004. doi: 10.1016/j.immuni.2015.06.003

185. Santoni G, Cardinali C, Morelli M, Santoni M, Nabissi M, Amantini C. Danger- and pathogen-associated molecular patterns recognition by pattern-recognition receptors and ion channels of the transient receptor potential family triggers the inflammasome activation in immune cells and sensory neurons. *J Neuroinflamm* (2015) 12:21. doi: 10.1186/s12974-015-0239-2

186. Huang F-Y, Chan AO-O, Rashid A, Wong DK-H, Seto W-K, Cho C-H, et al. Interleukin-1β increases the risk of gastric cancer through induction of aberrant DNA methylation in a mouse model. *Oncol Lett* (2016) 11:2919–24. doi: 10.3892/ol.2016.4296

187. Mezzasoma L, Costanzi E, Scarpelli P, Talesa VN, Bellezza I. Extracellular vesicles from human advanced-stage prostate cancer cells modify the inflammatory response of microenvironment-residing cells. *Cancers* (2019) 11:1276. doi: 10.3390/cancers11091276

188. Chen J, Sun W, Zhang H, Ma J, Xu P, Yu Y, et al. Macrophages reprogrammed by lung cancer microparticles promote tumor development *via* release of IL-1β. *Cell Mol Immunol* (2020) 17:1233–44. doi: 10.1038/s41423-019-0313-2

189. Arienti C, Pignatta S, Zanoni M, Zamagni A, Cortesi M, Sarnelli A, et al. High-pressure oxygen rewires glucose metabolism of patient-derived glioblastoma cells and fuels inflammasome response. *Cancer Lett* (2021) 506:152–66. doi: 10.1016/j.canlet.2021.02.019

190. Wu L, Zhang X, Zhang B, Shi H, Yuan X, Sun Y, et al. Exosomes derived from gastric cancer cells activate NF-κB pathway in macrophages to promote cancer progression. *Tumor Biol* (2016) 37:12169–80. doi: 10.1007/s13277-016-5071-5

191. Liang M, Chen X, Wang L, Qin L, Wang H, Sun Z, et al. Cancer-derived exosomal TRIM59 regulates macrophage NLRP3 inflammasome activation to promote lung cancer progression. *J Exp Clin Cancer Res* (2020) 39:176. doi: 10.1186/s13046-020-01688-7

192. Linton SS, Abraham T, Liao J, Clawson GA, Butler PJ, Fox T, et al. Tumor-promoting effects of pancreatic cancer cell exosomes on THP-1-derived macrophages. *PloS One* (2018) 13:e0206759. doi: 10.1371/journal.pone.0206759

193. Wen H, Gris D, Lei Y, Jha S, Zhang L, Huang MT-H, et al. Fatty acid–induced NLRP3-ASC inflammasome activation interferes with insulin signaling. *Nat Immunol* (2011) 12:408–15. doi: 10.1038/ni.2022

194. Laird BJ, McMillan D, Skipworth RJE, Fallon MT, Paval DR, McNeish I, et al. The emerging role of interleukin 1β (IL-1β) in cancer cachexia. *Inflammation* (2021) 44:1223–8. doi: 10.1007/s10753-021-01429-8

195. Song X, Voronov E, Dvorkin T, Fima E, Cagnano E, Benharroch D, et al. Differential effects of IL-1α and IL-1β on tumorigenicity patterns and invasiveness. *J Immunol* (2003) 171:6448–56. doi: 10.4049/jimmunol.171.12.6448

196. Fonsatti E, Altomonte M, Coral S, Cattarossi I, Nicotra M, Gasparollo A, et al. Tumour-derived interleukin 1α (IL-1α) up-regulates the release of soluble intercellular adhesion molecule-1 (sICAM-1) by endothelial cells. *Br J Cancer* (1997) 76:1255–61. doi: 10.1038/bjc.1997.545

197. Mishra D, Banerjee D. "Metabolic interactions between tumor and stromal cells in the tumor microenvironment. In: D Banerjee and RK Tiwari, editors. *Tumor microenvironment: Cellular, metabolic and immunologic interactions. advances in experimental medicine and biology*. Cham: Springer International Publishing (2021). p. 101–21. doi: 10.1007/978-3-030-83282-7_5

198. Rose-John S. IL-6 trans-signaling *via* the soluble IL-6 receptor: Importance for the pro-inflammatory activities of IL-6. *Int J Biol Sci* (2012) 8:1237–47. doi: 10.7150/ijbs.4989

199. Bode JG, Albrecht U, Häussinger D, Heinrich PC, Schaper F. Hepatic acute phase proteins – regulation by IL-6- and IL-1-type cytokines involving STAT3 and its crosstalk with NF-κB-dependent signaling. *Eur J Cell Biol* (2012) 91:496–505. doi: 10.1016/j.ejcb.2011.09.008

200. Ishibashi T, Kimura H, Uchida T, Kariyone S, Friese P, Burstein SA. Human interleukin 6 is a direct promoter of maturation of megakaryocytes *in vitro*. *Proc Natl Acad Sci* (1989) 86:5953–7. doi: 10.1073/pnas.86.15.5953

201. Gauldie J, Richards C, Harnish D, Lansdorp P, Baumann H. Interferon beta 2/B-cell stimulatory factor type 2 shares identity with monocyte-derived hepatocyte-stimulating factor and regulates the major acute phase protein response in liver cells. *Proc Natl Acad Sci* (1987) 84:7251–5. doi: 10.1073/pnas.84.20.7251

202. Liu C, Chu D, Kalantar-Zadeh K, George J, Young HA, Liu G. Cytokines: From clinical significance to quantification. *Adv Sci* (2021) 8:2004433. doi: 10.1002/advs.202004433

203. Geiger T, Andus T, Klapproth J, Hirano T, Kishimoto T, Heinrich PC. Induction of rat acute-phase proteins by interleukin 6 *in vivo*. *Eur J Immunol* (1988) 18:717–21. doi: 10.1002/eji.1830180510

204. Andus T, Geiger T, Hirano T, Kishimoto T, Heinrich PC. Action of recombinant human interleukin 6, interleukin 1β and tumor necrosis factor α on the mRNA induction of acute-phase proteins. *Eur J Immunol* (1988) 18:739–46. doi: 10.1002/eji.1830180513

205. Duvigneau JC, Luís A, Gorman AM, Samali A, Kaltenecker D, Moriggl R, et al. Crosstalk between inflammatory mediators and endoplasmic reticulum stress in liver diseases. *Cytokine* (2019) 124:154577. doi: 10.1016/j.cyto.2018.10.018

206. Germolec DR, Shipkowski KA, Frawley RP, Evans E. Markers of inflammation. *Methods Mol Biol* (2018) 1803:57–79. doi: 10.1007/978-1-4939-8549-4_5

207. Rumba R, Cipkina S, Cukure F, Vanags A. Systemic and local inflammation in colorectal cancer. *Acta Med Litu* (2019) 25:185–96. doi: 10.6001/actamedica.v25i4.3929

208. Proctor MJ, McMillan DC, Morrison DS, Fletcher CD, Horgan PG, Clarke SJ. A derived neutrophil to lymphocyte ratio predicts survival in patients with cancer. *Br J Cancer* (2012) 107:695–9. doi: 10.1038/bjc.2012.292

209. Schiefer S, Wirsik NM, Kalkum E, Seide SE, Nienhüser H, Müller B, et al. Systematic review of prognostic role of blood cell ratios in patients with gastric cancer undergoing surgery. *Diagnostics* (2022) 12:593. doi: 10.3390/diagnostics12030593

210. Laird BJA, Fallon M, Hjermstad MJ, Tuck S, Kaasa S, Klepstad P, et al. Quality of life in patients with advanced cancer: Differential association with performance status and systemic inflammatory response. *J Clin Oncol* (2016) 34:2769–75. doi: 10.1200/JCO.2015.65.7742

211. McMillan DC. The systemic inflammation-based Glasgow prognostic score: A decade of experience in patients with cancer. *Cancer Treat Rev* (2013) 39:534–40. doi: 10.1016/j.ctrv.2012.08.003

212. Yamamura K, Sugimoto H, Kanda M, Yamada S, Nomoto S, Nakayama G, et al. Comparison of inflammation-based prognostic scores as predictors of tumor recurrence in patients with hepatocellular carcinoma after curative resection. *J Hepato-Biliary-Pancreat Sci* (2014) 21:682–8. doi: 10.1002/jhbp.114

213. Kurahara H, Maemura K, Mataki Y, Sakoda M, Iino S, Hiwatashi K, et al. Prognostication by inflammation-based score in patients with locally advanced pancreatic cancer treated with chemoradiotherapy. *Pancreatology* (2015) 15:688–93. doi: 10.1016/j.pan.2015.09.015

214. Crumley ABC, McMillan DC, McKernan M, McDonald AC, Stuart RC. Evaluation of an inflammation-based prognostic score in patients with inoperable gastro-oesophageal cancer. *Br J Cancer* (2006) 94:637–41. doi: 10.1038/sj.bjc.6602998

215. Morris-Stiff G, Gomez D, Prasad KR. C-reactive protein in liver cancer surgery. *Eur J Surg Oncol EJSO* (2008) 34:727–9. doi: 10.1016/j.ejso.2008.01.016

216. Mauer J, Denson JL, Brüning JC. Versatile functions for IL-6 in metabolism and cancer. *Trends Immunol* (2015) 36:92–101. doi: 10.1016/j.it.2014.12.008

217. Lasry A, Zinger A, Ben-Neriah Y. Inflammatory networks underlying colorectal cancer. *Nat Immunol* (2016) 17:230–40. doi: 10.1038/ni.3384

218. Inatsu A, Kinoshita M, Nakashima H, Shimizu J, Saitoh D, Tamai S, et al. Novel mechanism of c-reactive protein for enhancing mouse liver innate immunity. *Hepatology* (2009) 49:2044–54. doi: 10.1002/hep.22888

219. Van Vré EA, Bult H, Hoymans VY, Van Tendeloo VFI, Vrints CJ, Bosmans JM. Human c-reactive protein activates monocyte-derived dendritic cells and induces dendritic cell-mediated T-cell activation. *Arterioscler Thromb Vasc Biol* (2008) 28:511–8. doi: 10.1161/ATVBAHA.107.157016

220. Rasmussen LJH, Schultz M, Gaardsting A, Ladelund S, Garred P, Iversen K, et al. Inflammatory biomarkers and cancer: CRP and suPAR as markers of incident cancer in patients with serious nonspecific symptoms and signs of cancer: Biomarkers in the DOC. *Int J Cancer* (2017) 141:191–9. doi: 10.1002/ijc.30732

221. Pletnikoff PP, Laukkanen JA, Tuomainen T-P, Kauhanen J, Rauramaa R, Ronkainen K, et al. Cardiorespiratory fitness, C-reactive protein and lung cancer risk: A prospective population-based cohort study. *Eur J Cancer* (2015) 51:1365–70. doi: 10.1016/j.ejca.2015.04.020

222. Komrokji RS, Corrales-Yepez M, Kharfan-Dabaja MA, Al Ali NH, Padron E, Rollison DE, et al. Hypoalbuminemia is an independent prognostic factor for overall survival in myelodysplastic syndromes. *Am J Hematol* (2012) 87:1006–9. doi: 10.1002/ajh.23303

223. Ataseven B, du Bois A, Reinthaller A, Traut A, Heitz F, Aust S, et al. Pre-operative serum albumin is associated with post-operative complication rate and overall survival in patients with epithelial ovarian cancer undergoing cytoreductive surgery. *Gynecol Oncol* (2015) 138:560–5. doi: 10.1016/j.ygyno.2015.07.005

224. Tabata F, Wada Y, Kawakami S, Miyaji K. Serum albumin redox states: More than oxidative stress biomarker. *Antioxidants* (2021) 10:503. doi: 10.3390/antiox10040503

225. Chojkier M. Inhibition of albumin synthesis in chronic diseases: Molecular mechanisms. *J Clin Gastroenterol* (2005) 39:S143–6. doi: 10.1097/01.mcg.0000155514.17715.39

226. Zhang W. Albumin selectively inhibits TNFα-induced expression of vascular cell adhesion molecule-1 in human aortic endothelial cells. *Cardiovasc Res* (2002) 55:820–9. doi: 10.1016/S0008-6363(02)00492-3

227. Tijssen MR, Ghevaert C. Transcription factors in late megakaryopoiesis and related platelet disorders. *J Thromb Haemost* (2013) 11:593–604. doi: 10.1111/jth.12131

228. Shameer K, Denny JC, Ding K, Jouni H, Crosslin DR, de Andrade M, et al. A genome- and phenome-wide association study to identify genetic variants influencing platelet count and volume and their pleiotropic effects. *Hum Genet* (2014) 133:95–109. doi: 10.1007/s00439-013-1355-7

229. Korniluk A, Koper-Lenkiewicz OM, Kamińska J, Kemona H, Dymicka-Piekarska V. Mean platelet volume (MPV): New perspectives for an old marker in the course and prognosis of inflammatory conditions. *Mediators Inflammation* (2019) 2019:1–14. doi: 10.1155/2019/9213074

230. Shen X-B, Wang Y, Shan B-J, Lin L, Hao L, Liu Y, et al. Prognostic significance of platelet-To-Lymphocyte ratio (PLR) and mean platelet volume (MPV) during etoposide-based first-line treatment in small cell lung cancer patients. *Cancer Manag Res* (2019) 11:8965–75. doi: 10.2147/CMAR.S215361

231. Rein-Smith CM, Anderson NW, Farrell DH. Differential regulation of fibrinogen γ chain splice isoforms by interleukin-6. *Thromb Res* (2013) 131:89–93. doi: 10.1016/j.thromres.2012.09.017

232. Duan HO, Simpson-Haidaris PJ. Functional analysis of interleukin 6 response elements (IL-6REs) on the human γ-fibrinogen promoter. *J Biol Chem* (2003) 278:41270–81. doi: 10.1074/jbc.M304210200

233. Fuller GM, Zhang Z. Transcriptional control mechanism of fibrinogen gene expression. *Ann N Y Acad Sci* (2006) 936:469–79. doi: 10.1111/j.1749-6632.2001.tb03534.x

234. Zhang Y, Xiao G. Prognostic significance of the ratio of fibrinogen and albumin in human malignancies: A meta-analysis. *Cancer Manag Res* (2019) 11:3381–93. doi: 10.2147/CMAR.S198419

235. Kubota K, Ito R, Narita N, Tanaka Y, Furudate K, Akiyama N, et al. Utility of prognostic nutritional index and systemic immune-inflammation index in oral cancer treatment. *BMC Cancer* (2022) 22:368. doi: 10.1186/s12885-022-09439-x

236. Nozoe T, Matono R, Ijichi H, Ohga T, Ezaki T. Glasgow Prognostic score (GPS) can be a useful indicator to determine prognosis of patients with colorectal carcinoma. *Int Surg* (2014) 99:512–7. doi: 10.9738/INTSURG-D-13-00118.1

237. Aurello P, Tierno SM, Berardi G, Tomassini F, Magistri P, D'Angelo F, et al. Value of preoperative inflammation-based prognostic scores in predicting overall survival and disease-free survival in patients with gastric cancer. *Ann Surg Oncol* (2014) 21:1998–2004. doi: 10.1245/s10434-014-3533-9

238. Hoshimoto S, Hishinuma S, Shirakawa H, Tomikawa M, Ozawa I, Ogata Y. Validation and clinical usefulness of pre- and postoperative systemic inflammatory parameters as prognostic markers in patients with potentially resectable pancreatic cancer. *Pancreatology* (2020) 20:239–46. doi: 10.1016/j.pan.2019.12.004

239. Hu X, Wang Y, Yang W-X, Dou W-C, Shao Y-X, Li X. Modified Glasgow prognostic score as a prognostic factor for renal cell carcinomas: A systematic review and meta-analysis. *Cancer Manag Res* (2019) 11:6163–73. doi: 10.2147/CMAR.S208839

240. Proctor MJ, Morrison DS, Talwar D, Balmer SM, O'Reilly DSJ, Foulis AK, et al. An inflammation-based prognostic score (mGPS) predicts cancer survival independent of tumour site: A Glasgow inflammation outcome study. *Br J Cancer* (2011) 104:726–34. doi: 10.1038/sj.bjc.6606087

241. Fan H, Shao Z-Y, Xiao Y-Y, Xie Z-H, Chen W, Xie H, et al. Comparison of the Glasgow prognostic score (GPS) and the modified Glasgow prognostic score

(mGPS) in evaluating the prognosis of patients with operable and inoperable non-small cell lung cancer. *J Cancer Res Clin Oncol* (2016) 142:1285–97. doi: 10.1007/s00432-015-2113-0

242. Sun F, Peng H-X, Gao Q-F, Li S-Q, Zhang J, Chen Q-G, et al. Preoperative circulating FPR and CCF score are promising biomarkers for predicting clinical outcome of stage II–III colorectal cancer patients. *Cancer Manag Res* (2018) 10:2151–61. doi: 10.2147/CMAR.S167398

243. Martin D, Rödel F, Balermpas P, Winkelmann R, Fokas E, Rödel C. C-reactive protein-to-Albumin ratio as prognostic marker for anal squamous cell carcinoma treated with chemoradiotherapy. *Front Oncol* (2019) 9:1200. doi: 10.3389/fonc.2019.01200

244. Zhou Q, Li X. C-reactive protein to albumin ratio in colorectal cancer: A meta-analysis of prognostic value. *Dose-Response* (2019) 17:155932581988981. doi: 10.1177/1559325819889814

245. Xiao Y, Xie Z, Shao Z, Chen W, Xie H, Qin G, et al. Neutrophil and lymphocyte counts at diagnosis are associated with overall survival of pancreatic cancer: A retrospective cohort study. *Med (Baltimore)* (2016) 95:e5024. doi: 10.1097/MD.0000000000005024

246. Chen L, Wang X, Shu J, Xu S, Wu Q, Yu Y. Diagnostic value of serum D-dimer, CA 125, and neutrophil-to-lymphocyte ratio in differentiating ovarian cancer and endometriosis. *Int J Gynecol Obstet* (2019) 147:212–8. doi: 10.1002/ijgo.12949

247. Wang J, Zhang F, Jiang F, Hu L, Chen J, Wang Y. Distribution and reference interval establishment of neutral-to-lymphocyte ratio (NLR), lymphocyte-to-monocyte ratio (LMR), and platelet-to-lymphocyte ratio (PLR) in Chinese healthy adults. *J Clin Lab Anal* (2021) 35:e23935. doi: 10.1002/jcla.23935

248. Cho U, Park HS, Im SY, Yoo CY, Jung JH, Suh YJ, et al. Prognostic value of systemic inflammatory markers and development of a nomogram in breast cancer. *PloS One* (2018) 13:e0200936. doi: 10.1371/journal.pone.0200936

249. Song S, Li C, Li S, Gao H, Lan X, Xue Y. Derived neutrophil to lymphocyte ratio and monocyte to lymphocyte ratio may be better biomarkers for predicting overall survival of patients with advanced gastric cancer. *OncoTargets Ther* (2017) 10:3145–54. doi: 10.2147/OTT.S138039

250. Troppan K, Deutsch A, Gerger A, Stojakovic T, Beham-Schmid C, Wenzl K, et al. The derived neutrophil to lymphocyte ratio is an independent prognostic factor in patients with diffuse large B-cell lymphoma. *Br J Cancer* (2014) 110:369–74. doi: 10.1038/bjc.2013.763

251. Yang T, Hao L, Yang X, Luo C, Wang G, Lin Cai C, et al. Prognostic value of derived neutrophil-to-lymphocyte ratio (dNLR) in patients with non-small cell lung cancer receiving immune checkpoint inhibitors: a meta-analysis. *BMJ Open* (2021) 11:e049123. doi: 10.1136/bmjopen-2021-049123

252. Grenader T, Nash S, Adams R, Kaplan R, Fisher D, Maughan T, et al. Derived neutrophil lymphocyte ratio is predictive of survival from intermittent therapy in advanced colorectal cancer: a *post hoc* analysis of the MRC COIN study. *Br J Cancer* (2016) 114:612–5. doi: 10.1038/bjc.2016.23

253. Xu Z, Zhang J, Zhong Y, Mai Y, Huang D, Wei W, et al. Predictive value of the monocyte-to-lymphocyte ratio in the diagnosis of prostate cancer. *Med (Baltimore)* (2021) 100:e27244. doi: 10.1097/MD.0000000000027244

254. Jakubowska K, Koda M, Grudzińska M, Kańczuga-Koda L, Famulski W. Monocyte-to-lymphocyte ratio as a prognostic factor in peripheral whole blood samples of colorectal cancer patients. *World J Gastroenterol* (2020) 26:4639–55. doi: 10.3748/wjg.v26.i31.4639

255. Huszno J, Kołosza Z, Mrochem-Kwarciak J, Zajusz A. Prognostic value of the neutrophil-lymphocyte, platelet-lymphocyte, and monocyte-lymphocyte ratios in Male breast cancer patients. *Oncology* (2020) 98:487–92. doi: 10.1159/000505627

256. Luo H, He L, Zhang G, Yu J, Chen Y, Yin H, et al. Normal reference intervals of neutrophil-To-Lymphocyte ratio, platelet-To-Lymphocyte ratio, lymphocyte-To-Monocyte ratio, and systemic immune inflammation index in healthy adults: a Large multi-center study from Western China. *Clin Lab* (2019) 65. doi: 10.7754/Clin.Lab.2018.180715

257. Chen J-H, Zhai E-T, Yuan Y-J, Wu K-M, Xu J-B, Peng J-J, et al. Systemic immune-inflammation index for predicting prognosis of colorectal cancer. *World J Gastroenterol* (2017) 23:6261. doi: 10.3748/wjg.v23.i34.6261

258. Deng M, Ma X, Liang X, Zhu C, Wang M. Are pretreatment neutrophil-lymphocyte ratio and platelet-lymphocyte ratio useful in predicting the outcomes of patients with small-cell lung cancer? *Oncotarget* (2017) 8:37200–7. doi: 10.18632/oncotarget.16553

259. Eraslan E, Adas YG, Yildiz F, Gulesen AI, Karacin C, Arslan UY. Systemic immune-inflammation index (SII) predicts pathological complete response to neoadjuvant chemoradiotherapy in locally advanced rectal cancer. *J Coll Phys Surg Pak* (2021) 31:399–404. doi: 10.29271/jcpsp.2021.04.399

260. Guo W, Cai S, Zhang F, Shao F, Zhang G, Zhou Y, et al. Systemic immune-inflammation index (SII) is useful to predict survival outcomes in patients with surgically resected non-small cell lung cancer. *Thorac Cancer* (2019) 10:761–8. doi: 10.1111/1759-7714.12995

261. Atasever Akkas E, Yucel B. Prognostic value of systemic ımmune ınflammation ındex in patients with laryngeal cancer. *Eur Arch Otorhinolaryngol* (2021) 278:1945–55. doi: 10.1007/s00405-021-06798-2

262. Rice SJ, Belani CP. Diversity and heterogeneity of immune states in non-small cell lung cancer and small cell lung cancer. *PloS One* (2021) 16:e0260988. doi: 10.1371/journal.pone.0260988

263. Zinellu A, Collu C, Nasser M, Paliogiannis P, Mellino S, Zinellu E, et al. The aggregate index of systemic inflammation (AISI): A novel prognostic biomarker in idiopathic pulmonary fibrosis. *J Clin Med* (2021) 10:4134. doi: 10.3390/jcm10184134

264. Zuffa M, Kubancok J, Rusnák I, Mensatoris K, Horváth A. Early paraneoplastic syndrome in medical oncology: clinicopathological analysis of 1694 patients treated over 20 years. *Neoplasma* (1984) 31:231–6.

265. Sardiña González C, Martínez Vivero C, López Castro J. Paraneoplastic syndromes review: The great forgotten ones. *Crit Rev Oncol Hematol* (2022) 174:103676. doi: 10.1016/j.critrevonc.2022.103676

266. Mitroulis I, Kalafati L, Bornhäuser M, Hajishengallis G, Chavakis T. Regulation of the bone marrow niche by inflammation. *Front Immunol* (2020) 11:1540. doi: 10.3389/fimmu.2020.01540

267. Chiba Y, Mizoguchi I, Hasegawa H, Ohashi M, Orii N, Nagai T, et al. Regulation of myelopoiesis by proinflammatory cytokines in infectious diseases. *Cell Mol Life Sci* (2018) 75:1363–76. doi: 10.1007/s00018-017-2724-5

268. Helbling PM, Piñeiro-Yáñez E, Gerosa R, Boettcher S, Al-Shahrour F, Manz MG, et al. Global transcriptomic profiling of the bone marrow stromal microenvironment during postnatal development, aging, and inflammation. *Cell Rep* (2019) 29:3313–3330.e4. doi: 10.1016/j.celrep.2019.11.004

269. Wildes TJ, DiVita Dean B, Flores CT. Myelopoiesis during solid cancers and strategies for immunotherapy. *Cells* (2021) 10:968. doi: 10.3390/cells10050968

270. Yu S, Liu C, Su K, Wang J, Liu Y, Zhang L, et al. Tumor exosomes inhibit differentiation of bone marrow dendritic cells. *J Immunol* (2007) 178:6867–75. doi: 10.4049/jimmunol.178.11.6867

271. Méndez-Ferrer S, Michurina TV, Ferraro F, Mazloom AR, MacArthur BD, Lira SA, et al. Mesenchymal and haematopoietic stem cells form a unique bone marrow niche. *Nature* (2010) 466:829–34. doi: 10.1038/nature09262

272. Reynaud D, Pietras E, Barry-Holson K, Mir A, Binnewies M, Jeanne M, et al. IL-6 controls leukemic multipotent progenitor cell fate and contributes to chronic myelogenous leukemia development. *Cancer Cell* (2011) 20:661–73. doi: 10.1016/j.ccr.2011.10.012

273. Marigo I, Bosio E, Solito S, Mesa C, Fernandez A, Dolcetti L, et al. Tumor-induced tolerance and immune suppression depend on the C/EBPβ transcription factor. *Immunity* (2010) 32:790–802. doi: 10.1016/j.immuni.2010.05.010

274. Wu W-C, Sun H-W, Chen H-T, Liang J, Yu X-J, Wu C, et al. Circulating hematopoietic stem and progenitor cells are myeloid-biased in cancer patients. *Proc Natl Acad Sci* (2014) 111:4221–6. doi: 10.1073/pnas.1320753111

275. Al Sayed MF, Amrein MA, Bührer ED, Huguenin A-L, Radpour R, Riether C, et al. T-cell–secreted TNFα induces emergency myelopoiesis and myeloid-derived suppressor cell differentiation in cancer. *Cancer Res* (2019) 79:346–59. doi: 10.1158/0008-5472.CAN-17-3026

276. Zhao X, Rong L, Zhao X, Li X, Liu X, Deng J, et al. TNF signaling drives myeloid-derived suppressor cell accumulation. *J Clin Invest* (2012) 122:4094–104. doi: 10.1172/JCI64115

277. Chiodoni C, Cancila V, Renzi TA, Perrone M, Tomirotti AM, Sangaletti S, et al. Transcriptional profiles and stromal changes reveal bone marrow adaptation to early breast cancer in association with deregulated circulating microRNAs. *Cancer Res* (2019). doi: 10.1158/0008-5472.CAN-19-1425

278. Strauss L, Guarneri V, Gennari A, Sica A. Implications of metabolism-driven myeloid dysfunctions in cancer therapy. *Cell Mol Immunol* (2021) 18:829–41. doi: 10.1038/s41423-020-00556-w

279. Yamauchi Y, Rogers MA. Sterol metabolism and transport in atherosclerosis and cancer. *Front Endocrinol* (2018) 9:509. doi: 10.3389/fendo.2018.00509

280. Vladimirov S, Gojkovic T, Zeljkovic A, Jelic-Ivanovic Z, Zeljkovic D, Antonic T, et al. Can non-cholesterol sterols indicate the presence of specific dysregulation of cholesterol metabolism in patients with colorectal cancer? *Biochem Pharmacol* (2022) 196:114595. doi: 10.1016/j.bcp.2021.114595

281. Li W, Tanikawa T, Kryczek I, Xia H, Li G, Wu K, et al. Aerobic glycolysis controls myeloid-derived suppressor cells and tumor immunity *via* a specific CEBPB isoform in triple-negative breast cancer. *Cell Metab* (2018) 28:87–103.e6. doi: 10.1016/j.cmet.2018.04.022

282. Bao Y, Liu Z, Guo M, Li B, Sun X, Wang L. Extramedullary hematopoiesis secondary to malignant solid tumors: a case report and literature review. *Cancer Manag Res* (2018) 10:1461–70. doi: 10.2147/CMAR.S161746

283. Levy L, Mishalian I, Bayuch R, Zolotarov L, Michaeli J, Fridlender ZG. Splenectomy inhibits non-small cell lung cancer growth by modulating anti-tumor

adaptive and innate immune response. *OncoImmunology* (2015) 4:e998469. doi: 10.1080/2162402X.2014.998469

284. Cadili A, de Gara C. Complications of splenectomy. *Am J Med* (2008) 121:371–5. doi: 10.1016/j.amjmed.2008.02.014

285. Veglia F, Sanseviero E, Gabrilovich DI. Myeloid-derived suppressor cells in the era of increasing myeloid cell diversity. *Nat Rev Immunol* (2021) 21:485–98. doi: 10.1038/s41577-020-00490-y

286. Yang Y, Li C, Liu T, Dai X, Bazhin AV. Myeloid-derived suppressor cells in tumors: From mechanisms to antigen specificity and microenvironmental regulation. *Front Immunol* (2020) 11:1371. doi: 10.3389/fimmu.2020.01371

287. Fearon K, Strasser F, Anker SD, Bosaeus I, Bruera E, Fainsinger RL, et al. Definition and classification of cancer cachexia: an international consensus. *Lancet Oncol* (2011) 12:489–95. doi: 10.1016/S1470-2045(10)70218-7

288. Ni J, Zhang L. Cancer cachexia: Definition, staging, and emerging treatments. *Cancer Manag Res* (2020) 12:5597–605. doi: 10.2147/CMAR.S261585

289. Evans WJ, Morley JE, Argilés J, Bales C, Baracos V, Guttridge D, et al. Cachexia: A new definition. *Clin Nutr* (2008) 27:793–9. doi: 10.1016/j.clnu.2008.06.013

290. Biswas AK, Acharyya S. Cancer-associated cachexia: A systemic consequence of cancer progression. *Annu Rev Cancer Biol* (2020) 4:391–411. doi: 10.1146/annurev-cancerbio-030419-033642

291. Aguilar-Cazares D, Chavez-Dominguez R, Carlos-Reyes A, Lopez-Camarillo C, Hernadez de la Cruz ON, Lopez-Gonzalez JS. Contribution of angiogenesis to inflammation and cancer. *Front Oncol* (2019) 9:1399. doi: 10.3389/fonc.2019.01399

292. Ippolito L, Morandi A, Giannoni E, Chiarugi P. Lactate: A metabolic driver in the tumour landscape. *Trends Biochem Sci* (2019) 44:153–66. doi: 10.1016/j.tibs.2018.10.011

293. Ferguson BS, Rogatzki MJ, Goodwin ML, Kane DA, Rightmire Z, Gladden LB. Lactate metabolism: historical context, prior misinterpretations, and current understanding. *Eur J Appl Physiol* (2018) 118:691–728. doi: 10.1007/s00421-017-3795-6

294. Choi SYC, Collins CC, Gout PW, Wang Y. Cancer-generated lactic acid: a regulatory, immunosuppressive metabolite? *J Pathol* (2013) 230:350–5. doi: 10.1002/path.4218

295. Rohm M, Zeigerer A, Machado J, Herzig S. Energy metabolism in cachexia. *EMBO Rep* (2019) 20:e47258. doi: 10.15252/embr.201847258

296. Noguchi Y, Yoshikawa T, Marat D, Doi C, Makino T, Fukuzawa K, et al. Insulin resistance in cancer patients is associated with enhanced tumor necrosis factor-α expression in skeletal muscle. *Biochem Biophys Res Commun* (1998) 253:887–92. doi: 10.1006/bbrc.1998.9794

297. Asp ML, Tian M, Wendel AA, Belury MA. Evidence for the contribution of insulin resistance to the development of cachexia in tumor-bearing mice. *Int J Cancer* (2010) 126:756–63. doi: 10.1002/ijc.24784

298. Baltgalvis KA, Berger FG, Peña MMO, Davis JM, White JP, Carson JA. Muscle wasting and interleukin-6-induced atrogin-I expression in the cachectic apc min/+ mouse. *Pflüg Arch - Eur J Physiol* (2009) 457:989–1001. doi: 10.1007/s00424-008-0574-6

299. Chen M-C, Hsu W-L, Hwang P-A, Chen Y-L, Chou T-C. Combined administration of fucoidan ameliorates tumor and chemotherapy-induced skeletal muscle atrophy in bladder cancer-bearing mice. *Oncotarget* (2016) 7:51608–18. doi: 10.18632/oncotarget.9958

300. Zhang G, Liu Z, Ding H, Zhou Y, Doan HA, Sin KWT, et al. Tumor induces muscle wasting in mice through releasing extracellular Hsp70 and Hsp90. *Nat Commun* (2017) 8:589. doi: 10.1038/s41467-017-00726-x

301. Qiu L, Chen W, Wu C, Yuan Y, Li Y. Exosomes of oral squamous cell carcinoma cells containing miR-181a-3p induce muscle cell atrophy and apoptosis by transmissible endoplasmic reticulum stress signaling. *Biochem Biophys Res Commun* (2020) 533:831–7. doi: 10.1016/j.bbrc.2020.09.066

302. Li L, Liu H, Tao W, Wen S, Fu X, Yu S. Pharmacological inhibition of HMGB1 prevents muscle wasting. *Front Pharmacol* (2021) 12:731386. doi: 10.3389/fphar.2021.731386

303. Zhang W, Sun W, Gu X, Miao C, Feng L, Shen Q, et al. GDF-15 in tumor-derived exosomes promotes muscle atrophy *via* bcl-2/caspase-3 pathway. *Cell Death Discovery* (2022) 8:162. doi: 10.1038/s41420-022-00972-z

304. Masi T, Patel BM. Altered glucose metabolism and insulin resistance in cancer-induced cachexia: a sweet poison. *Pharmacol Rep* (2021) 73:17–30. doi: 10.1007/s43440-020-00179-y

305. Sacks H, Symonds ME. Anatomical locations of human brown adipose tissue. *Diabetes* (2013) 62:1783–90. doi: 10.2337/db12-1430

306. Weber BZC, Arabaci DH, Kir S. Metabolic reprogramming in adipose tissue during cancer cachexia. *Front Oncol* (2022) 12:848394. doi: 10.3389/fonc.2022.848394

307. Bolsoni-Lopes A, Alonso-Vale MIC. Lipolysis and lipases in white adipose tissue – an update. *Arch Endocrinol Metab* (2015) 59:335–42. doi: 10.1590/2359-3997000000067

308. Dalal S. Lipid metabolism in cancer cachexia. *Ann Palliat Med* (2019) 8:13–23. doi: 10.21037/apm.2018.10.01

309. Das SK, Hoefler G. The role of triglyceride lipases in cancer associated cachexia. *Trends Mol Med* (2013) 19:292–301. doi: 10.1016/j.molmed.2013.02.006

310. Shaw JHF, Wolfe RR. Fatty acid and glycerol kinetics in septic patients and in patients with gastrointestinal cancer: The response to glucose infusion and parenteral feeding. *Ann Surg* (1987) 205:368–76. doi: 10.1097/00000658-198704000-00005

311. Fukawa T, Yan-Jiang BC, Min-Wen JC, Jun-Hao ET, Huang D, Qian C-N, et al. Excessive fatty acid oxidation induces muscle atrophy in cancer cachexia. *Nat Med* (2016) 22:666–71. doi: 10.1038/nm.4093

312. Petruzzelli M, Schweiger M, Schreiber R, Campos-Olivas R, Tsoli M, Allen J, et al. A switch from white to brown fat increases energy expenditure in cancer-associated cachexia. *Cell Metab* (2014) 20:433–47. doi: 10.1016/j.cmet.2014.06.011

313. de Matos-Neto EM, Lima JDCC, de Pereira WO, Figuerêdo RG, Riccardi DM dos R, Radloff K, et al. Systemic inflammation in cachexia – is tumor cytokine expression profile the culprit? *Front Immunol* (2015) 6:629. doi: 10.3389/fimmu.2015.00629

314. Zhang H, Zhu L, Bai M, Liu Y, Zhan Y, Deng T, et al. Exosomal circRNA derived from gastric tumor promotes white adipose browning by targeting the miR-133/PRDM16 pathway. *Int J Cancer* (2019) 144:2501–15. doi: 10.1002/ijc.31977

315. Wang S, Li X, Xu M, Wang J, Zhao RC. Reduced adipogenesis after lung tumor exosomes priming in human mesenchymal stem cells *via* TGFβ signaling pathway. *Mol Cell Biochem* (2017) 435:59–66. doi: 10.1007/s11010-017-3056-3

316. Liu Y, Wang M, Deng T, Liu R, Ning T, Bai M, et al. Exosomal miR-155 from gastric cancer induces cancer-associated cachexia by suppressing adipogenesis and promoting brown adipose differentiation *via* C/EPBβ. *Cancer Biol Med* (2022) 19. doi: 10.20892/j.issn.2095-3941.2021.0220

317. Argilés JM, Stemmler B, López-Soriano FJ, Busquets S. Inter-tissue communication in cancer cachexia. *Nat Rev Endocrinol* (2019) 15:9–20. doi: 10.1038/s41574-018-0123-0

318. Olson B, Diba P, Korzun T, Marks DL. Neural mechanisms of cancer cachexia. *Cancers* (2021) 13:3990. doi: 10.3390/cancers13163990

319. Gwosdow AR, Kumar MS, Bode HH. Interleukin 1 stimulation of the hypothalamic-pituitary-adrenal axis. *Am J Physiol-Endocrinol Metab* (1990) 258:E65–70. doi: 10.1152/ajpendo.1990.258.1.E65

320. Gądek-Michalska A, Bugajski J. Interleukin-1 (IL-1) in stress-induced activation of limbic-hypothalamic-pituitary adrenal axis. *Pharmacol Rep* (2010) 62:969–82. doi: 10.1016/S1734-1140(10)70359-5

321. Maccio A, Sanna E, Neri M, Oppi S, Madeddu C. Cachexia as evidence of the mechanisms of resistance and tolerance during the evolution of cancer disease. *Int J Mol Sci* (2021) 22:2890. doi: 10.3390/ijms22062890

322. Noguchi Y, Yoshikawa T, Matsumoto A, Svaninger G, Gelin J. Are cytokines possible mediators of cancer cachexia? *Surg Today* (1996) 26:467–75. doi: 10.1007/BF00311551

323. Jafri SHR, Previgliano C, Khandelwal K, Shi R. Cachexia index in advanced non-Small-Cell lung cancer patients. *Clin Med Insights Oncol* (2015) 9. doi: 10.4137/CMO.S30891

324. Kim EY, Kim YS, Seo J-Y, Park I, Ahn HK, Jeong YM, et al. The relationship between sarcopenia and systemic inflammatory response for cancer cachexia in small cell lung cancer. *PloS One* (2016) 11:e0161125. doi: 10.1371/journal.pone.0161125

325. Barker T, Fulde G, Moulton B, Nadauld LD, Rhodes T. An elevated neutrophil-to-lymphocyte ratio associates with weight loss and cachexia in cancer. *Sci Rep* (2020) 10:7535. doi: 10.1038/s41598-020-64282-z

326. Zappavigna S, Cossu AM, Grimaldi A, Bocchetti M, Ferraro GA, Nicoletti GF, et al. Anti-inflammatory drugs as anticancer agents. *Int J Mol Sci* (2020) 21:2605. doi: 10.3390/ijms21072605

327. Chiossone L, Vitale C, Cottalasso F, Moretti S, Azzarone B, Moretta L, et al. Molecular analysis of the methylprednisolone-mediated inhibition of NK-cell function: evidence for different susceptibility of IL-2– versus IL-15–activated NK cells. *Blood* (2007) 109:3767–75. doi: 10.1182/blood-2006-07-037846

frontiers | Frontiers in Endocrinology

TYPE Review
PUBLISHED 25 August 2022
DOI 10.3389/fendo.2022.918869

OPEN ACCESS

EDITED BY
Yang Mi,
Henan Key Laboratory for Helicobacter pylori & Microbiota and Gastrointestinal Cancer, China

REVIEWED BY
Yanfeng Wang,
Xiangya Hospital, Central South University, China
Xing Huang,
Zhejiang University, China
Xiaoyan Zhou,
Nanchang University, China

*CORRESPONDENCE
Yu Zujiang
johnyuem@zzu.edu.cn

†These authors have contributed equally to this work

SPECIALTY SECTION
This article was submitted to Cancer Endocrinology, a section of the journal Frontiers in Endocrinology

RECEIVED 12 April 2022
ACCEPTED 05 August 2022
PUBLISHED 25 August 2022

CITATION
Guizhen Z, Guanchang J, Liwen L, Huifen W, Zhigang R, Ranran S and Zujiang Y (2022) The tumor microenvironment of hepatocellular carcinoma and its targeting strategy by CAR-T cell immunotherapy. *Front. Endocrinol.* 13:918869. doi: 10.3389/fendo.2022.918869

The tumor microenvironment of hepatocellular carcinoma and its targeting strategy by CAR-T cell immunotherapy

Zhang Guizhen[1,2,3†], Ji Guanchang[4†], Liu Liwen[1,2,3], Wang Huifen[1,2,3], Ren Zhigang[1], Sun Ranran[1] and Yu Zujiang[1,2*]

[1]Department of Infectious Diseases, The First Affiliated Hospital of Zhengzhou University, Zhengzhou, China, [2]Presion Medicine Cencter Gene Hospital of Henan Province, Zhengzhou, China, [3]Academy of Medical Sciences, Zhengzhou University, Zhengzhou, China, [4]Department of Urology People's Hospital of Puyang, Puyang, China

Hepatocellular carcinoma (HCC) is the major subtype of liver cancer, which ranks sixth in cancer incidence and third in mortality. Although great strides have been made in novel therapy for HCC, such as immunotherapy, the prognosis remains less than satisfactory. Increasing evidence demonstrates that the tumor immune microenvironment (TME) exerts a significant role in the evolution of HCC and has a non-negligible impact on the efficacy of HCC treatment. In the past two decades, the success in hematological malignancies made by chimeric antigen receptor-modified T (CAR-T) cell therapy leveraging it holds great promise for cancer treatment. However, in the face of a hostile TME in solid tumors like HCC, the efficacy of CAR-T cells will be greatly compromised. Here, we provide an overview of TME features in HCC, discuss recent advances and challenges of CAR-T immunotherapy in HCC.

KEYWORDS

hepatocellular carcinoma, tumor microenvironment, immunotherapy, adoptive cell therapy, chimeric antigen receptor

Introduction

Primary liver cancer, represents the sixth most commonly diagnosed cancer and the third leading cause of cancer-related mortality currently according the Global Cancer Statistics 2020, with approximately 906,000 new cases and 830,000 deaths (1). In the vast majority of cases, HCC frequently develops from cirrhosis, caused by viral (hepatitis B or C virus) and non-viral (alcoholic or non-alcoholic fatty liver disease) risk factors (2). Frustratingly, HCC is an insidious tumor often diagnosed in advanced stage. For the patients with advanced stages, the treatments of choice are usually palliative. Despite aggressive treatment regimes, including surgery, combined radio and chemotherapy,

HCC patients will still experience tumor recurrence and metastasis with the death rates increasing by 2–3% per year (3, 4). Therefore, identification new factors underlying therapy resistance and novel therapeutic strategies for HCC are urgently needed.

Among patients with HCC who are diagnosed as the same TNM stage and experience similar clinical management, clinical outcomes are different, indicating that HCC is highly heterogeneous. Additionally, the complexity of heterogeneity is not only reflected in different patients, but also reflected in the disease progression and treatment courses of the individual patient (5). Recent accumulating evidence has revealed that this extraordinarily heterogeneity is closely related to TME of HCC, and contributes to the inconsistent outcome of anti-cancer therapy. Consequently, TME received considerable attention in recent years, and targeting TME is increasingly recognized as a new battlefield for HCC therapy, especially immunotherapy including vaccines, antibodies, immune checkpoint inhibitors, and adoptive cell therapy (ACT), such as CAR-T cells (6–8). CAR-T cell therapy, as the most encouraged immunotherapy, has made great strides in hematological malignancies. Meanwhile, intensive endeavors to target HCC by CAR-T has demonstrated promising efficacy with manageable toxicity and safety. The present review aims to provide a comprehensive picture of TME in HCC, discuss efforts to develop treatments by CAR-T.

Overview of TME in HCC

The tumor microenvironment is an intricate system, which comprises cellular and non-cellular components (Figure 1). The major cellular components include tumor cells, activated hepatic stellate cells, myeloid-derived suppressor cells (MDSCs), cancer-associated fibroblasts (CAFs), tumor-associated macrophages (TAMs), tumor-associated neutrophils (TANs), immune and endothelial cells (9, 10). Produced by these cells, the tumor stroma includes extracellular matrix (ECM) proteins, proteolytic enzymes, cytokines and growth factors (7). Crosstalk between cancer cells and TME has been identified to have a profound effect on cancer progression through prompting cell proliferation, survival and the ability of migration and evasion. Thus, a better understanding of the adverse TME would facilitate to develop novel therapeutic approaches for treatment of HCC in future.

Hepatic stellate cells (HSCs)

HSCs are the most principal cell players responsible for collagen synthesis in the liver and have a quiescent and an activated state, the latter being transformed from the former upon liver injury (11). Activated HSCs (a-HSCs) can produce the extensive accumulation of ECM in chronically damaged livers, leading to the development of hepatic fibrosis (12).

Although some researchers advocate that HSCs act as a tumor suppressor in HCC, the mainstream view is that HSCs in TME may facilitate tumor growth, involving tumor angiogenesis, invasion and metastasis (13). It was reported that a-HSCs strongly affect the malignant phenotype of HCC *via* paracrine feedback mechanisms through activating NF-κB and extracellular regulated protein kinases (ERK), two major signaling pathways in hepatocarcinogenesis (14). Another research demonstrated that HSCs can be activated under acidic condition depending on the phosphorylation of ERK1/2 and secrete osteopontin to promote

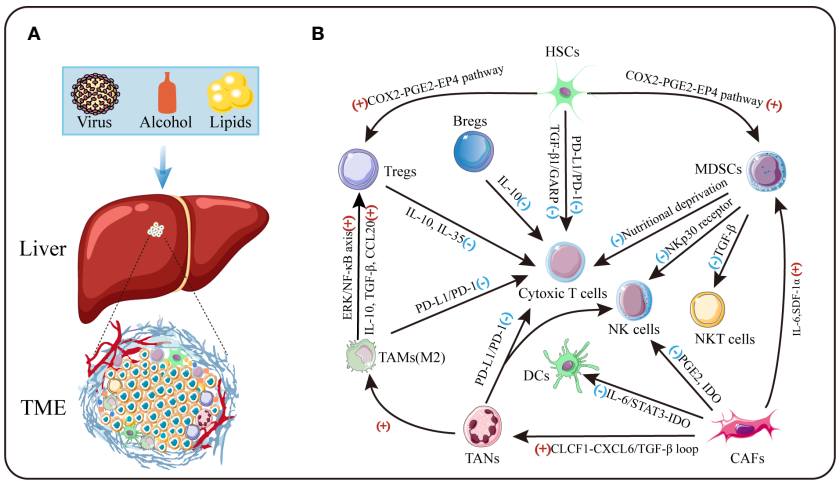

FIGURE 1
The tumor microenvironment of HCC. **(A)** TME is the cellular milieu in which the HCC cells grow. **(B)** Crosstalk among diverse suppressive immune cells in TME. IDO:indoleamine 2,3-dioxgenase.

HCC metastasis (15). Also, IL-6/STAT3 pathway has proven important, by which HSCs increased cancer cell viability and migration ability in HCC (16). Furthermore, Franziska and colleagues have identified that proteinase-activated receptor 2 expressed by HSCs can promote secretion and migration of pro-mitotic and pro-angiogenic factors to accelerate HCC growth (17). HSCs' function in angiogenesis was also verified in Lin's research (18). As elucidated by Yuta et al, in the HCC microenvironment, an increase of HSCs may be involved in tumor progression by producing GDF15 in an autophagy-dependent manner (19). In addition, mechanistic studies indicated that a-HSCs can accelerate HCC progression through miR-1246-RORα-Wnt/β-catenin axis (20). Furthermore, HSCs can indirectly affect HCC by cross talking with immune cells and impairing immune surveillance. A-HSCs have been elucidated to aggravate HCC by interacting with monocytes and macrophages, shifting them from an inflammatory to an immunosuppressive phenotype (21, 22). Li et al. provided the evidence that HSCs inhibit T cells proliferation and IFN-γ production through active TGF-β1 from a cell-surface-bound latent TGF-β1/GARP complex (23). It could also act in an autocrine fashion for HSCs to indirectly induce T cells apoptosis through upregulating expression of programmed death-ligand 1 (PD-L1) (24). Notably, HSCs can also induce regulatory T cells (Tregs) and MDSCs probably through activating COX2-PGE2-EP4 pathway provide an immunosuppressive milieu for HCC (25, 26). Clinically, it's well evidenced that HSCs are associated with recurrence and poor survival of patients with HCC (21, 27). Collectively, previous studies unraveled the significant role of HSCs in HCC progression and presented possibilities for HSCs as therapeutic targets.

Myeloid-derived suppressor cells (MDSCs)

MDSCs, characterized by a pathological state of activation, represent a heterogeneous population of immature myeloid cells, and exert inhibitory function in antitumor immunity in patients (28, 29). Studies investigated that CXCL1/CXCR2 and CCL26/CX3CR1 axis are two important pathways that induce the homing of MDSCs to the HCC microenvironment, thereby promoting immune escape and tumor growth (30, 31). Additionally, HIF-1α exerts a critical role by recruiting MDSCs into the hypoxia region of HCC foci *via* mediating ENTPD2 over-expression in HCC cells (32).

As a powerful inhibitory immune modulator, infiltrated MDSCs exert versatile immunosuppressive effects in HCC by inhibiting effector T cells, reducing natural killer (NK) cells cytotoxicity, expanding immune checkpoint signaling through diverse mechanisms. Researchers have reported that MDSCs suppressed autologous T cell proliferation and activation by depleting energy resources (e.g. arginine and cysteine) (33). Interestingly, Baumann et al. identified that T cells can be stunned by MDSCs *via* cell-cell transfer of the metabolite methylglyoxal (34). Infiltration into tumor sites is a prerequisite for immune cells to exert anti-tumor effects. Unfortunately, it was reported that MDSCs are significantly associated with reduced tumor infiltrating lymphocytes (TILs) in HCC (35). Additionally, MDSCs can reduce cytotoxicity and cytokine release of NK cells via the NKp30 receptor (36). Mechanistic studies indicated NKT cells are also one of the targets of MDSCs to exert immunosuppressive effects by selectively suppressing the secretion of IFN-γ deriving from NKT cells (37). As such, MDSCs can allow tumor cells to evade immune surveillance by interacting with other immune cells. Evidence has shown that MDSCs promote tumor growth and are associated with diminished efficacy of immunotherapy (38, 39).

Cancer-associated fibroblasts (CAFs)

CAFs are defined as the fibroblastic type of cells in a tumor mass, which are thought to interplay tightly with cancer cells (40). As an abundant and active cell type within the TME, CAFs are mainly activated from resident fibroblasts, stellate cells, mesenchymal stem cells or mesothelial cells, but evidence from a lineage-tracing analysis is still lacking (40, 41).

Although there is no denial that CAFs may exert a tumor-suppressing function, recent emerging data has convincingly indicated the tumor-promoting effects of CAFs. In tumors, CAFs function as remodeling machine to aid the creation of a desmoplastic TME and the signaling center to participate in the crosstalk with tumor and non-tumor cells (41). Firstly, CAFs could facilitate HCC cells epithelial-to-mesenchymal transition (EMT) through the transglutaminase 2-dependent IL-6/IL6R/STAT3 pathway, and promote HCC metastasis by activating HIF1α/ZEB1 axis (42–44). Secondly, a great deal of findings reported that CAFs could accelerate tumor growth by producing epidermal growth factor (EGF), fibroblast growth factor (FGF), hepatocyte growth factor (HGF), cytokines and chemokines (45–47). An *in vitro* experiment demonstrated that CAFs activated by TIMP-1 markedly inhibited HCC apoptosis by upregulating BCL-2/BAX ratio *via* SDF-1/CXCR4 axis (48). Also, Mano et al. provided important evidence that endogenous and exogenous BMP4 play a key role in the transformation of fibroblasts to CAFs which subsequently produce large amounts of cytokines to enhance invasiveness of HCC cells (49). Notably, CAFs-mediated cellular crosstalk is another important mechanism by which they promote tumor progression. Very recently, a study revealed that CAFs-derived CLCF1 could increase the secretion of CXCL6 and TGF-β in HCC cells, which subsequently enhance stemness of cancer cells and promote TANs infiltration and polarization in autocrine and paracrine manners, respectively. Interestingly, CXCL6 and

TGF-β in turn activate CAFs to express more CLCF1, thus forming a positive feedback loop that promotes tumor progression (50). Moreover, it's well evidenced that IL-6 and SDF-1α derived from CAFs can induce MDSCs generation, which subsequently impairs T-cell proliferation and alter the phenotype and function of T cells, which create favorable conditions for HCC progression (51). Crosstalk between CAFs and other cells such as NK and dendritic cells was also reported (52, 53).

Tumor-associated macrophages (TAMs)

TAMs are termed as macrophages within the tumor stroma and play pro-tumoral or sometimes anti-tumoral roles due to the ability to acquire M1 (classic) or M2 (alternative) phenotype-depending on signals from the tumor stroma (54). The classically activated macrophages or M1-type which exert their cytotoxic function through their T cell-stimulating activity, can be induced by Th1 cytokine such as INF-γ and through Toll-like receptor 4 engagement. Unfortunately, TAMs are also polarized towards an M2 phenotype with decreased antigen-presenting ability by Th2 cytokines IL-4/IL-13, functioning immunosuppressor in the TME (54, 55).

An immunogenic analysis showed that macrophages are prone to polarize to the M2 phenotype in HCC. Patients with high presence of M2 macrophages tend to have a more aggressive phenotype (56). A great deal number of studies confirmed and extended this observation. Bartneck's study demonstrated that immunosuppressive TAMs are abundant in the center of HCC and that $CCR2^+$ TAMs accumulate at the highly vascularized border of tumor; *In vivo* experiments showed that inflammatory and angiogenic pathways are activated in $CCR2^+$ TAMs (57). Consistently, TAMs accumulation had significant prognosis value in HCC patients (56). Mechanistically, TAMs can produce cytokines such as VEGF, EGF, platelet-derived growth factor (PDGF) to promote tumor angiogenesis, and matrix metalloproteinases secreted by TAMs can remodel TME to facilitate tumor metastasis (58). In addition, TAMs can also induce Treg cells infiltration into tumor tissue *via* producing cytokines and chemokines, such as IL-10, TGF-β and CCL20 (59, 60). As elucidated by Wu and colleagues, $TREM\text{-}1^+$ TAMs promote the recruitment of $CCR6^+Foxp3^+$ Tregs through the ERK/NF-κB axis, which endows HCC with anti-PD-L1 therapy resistance (61). Kupffer cells, which are liver-resident macrophages,can inhibit $CD8^+$ T cytotoxicity by PD-L1/PD-1 interaction and thus inhibit $CD8^+$ T-dependent immune response (62). Hence, the role of TAMs in HCC deserves much attention and TAMs may be a promising target in the treatment of HCC. It has been verified that macrophages mediate sorafenib resistance in HCC and TAMs depletion can improve the therapeutical efficacy of sorafenib (63, 64).

Tumor-associated neutrophils (TANs)

Neutrophils, derived from the bone marrow, are the first subset of immune cells to be recruited to lesions responding against infectious and inflammatory insults (65). In TME, neutrophils infiltrating into lesions can exhibit N1 (anti-tumoral) or N2 (pro-tumoral) phenotype-depending on the presence of TGF-β (66, 67).

As one of the most abundant components in HCC, Neutrophils have been recognized to play pivotal roles in regulating cancer development. It was verified that increased intra-tumoral neutrophils are correlated strongly with decreased recurrence free survival (RFS)/overall survival (OS) and can act as an independent prognostic factor in HCC patients (68). These results were reinforced in other studies (69–71). Zheng's and his coworkers provided evidence that neutrophils can be induced by IL-17 to migrate to tumor stroma through epithelial cell-derived CXC chemokines; Besides, high infiltration of TANs is positively associated with angiogenesis at tumor-invading border of HCC (72). They further identified that TANs also perform autophagy *via* the synergy of ERK1/2, p38 and NF-κB signaling axis and subsequently facilitate tumor progression by enhancing the secretion of OSM and MMP9, suggesting a regulatory loop between tumor cells and neutrophils (73). A positive feedback loop was also verified and exerts an essential function in the generation of stem-like cells in HCC (74). In addition, as the major source of c-Met ligand HGF, the accumulated neutrophils can actively promote the metastasis of HCC through the HGF/c-Met pathway. Of note, high infiltration of neutrophils in HCC determined malignant cell c-Met-associated clinical outcome of patients (75). A series of studies have shown that TANs also interact with other immune cells to exert their tumor-promoting function. The research conducted by He and colleagues has unraveled that infiltrating neutrophils express a higher frequency of PD-L1 in the presence of GM-CSF and TNF-α in TME; In turn, the $PD\text{-}L1^+$ neutrophils effectively impaired anti-tumor immunity *via* suppressing the proliferation and activation of T cells through the PD-L1/PD-1 signaling axis (76). Another study came to a similar conclusion (77). These TANs could also drive HCC progression and sorafenib resistance by recruiting macrophages, Treg cells and NK cells (69, 78).

Lymphocytes

Regulatory T cells (Tregs), defined as $CD4^+$ and $CD8^+$ T cells with immunosuppressive function, are known for their critical role in suppressing inflammation, and thus can antagonize the anti-tumor effect of immune responses (79). Studies have shown that Tregs are the main type of tumor-infiltrating T cells in HCC, which can significantly prejudice $CD8^+$ T cells proliferation, activation and suppress cytolytic molecule release and production of $CD8^+$ T cells

like granzymes, perforin (80). It was also evidenced that Tregs promote HCC invasion *via* TGF-β1-induced EMT (81). Tregs mediate sorafenib resistance, and blocking Tregs with inhibitors can overcome sorafenib resistance and increase tumor sensitivity to immunotherapy (82).

Recently, a research demonstrated that HCC tissue has a significantly higher TIM-1$^+$ regulatory B cells (Bregs) infiltration than the adjacent benign tissue. These Bregs show a CD5^{high}CD24$^-$CD27$^{-/+}$CD38$^{+/-}$ phenotype, secrete much immunosuppressive cytokine IL-10 and suppress CD8$^+$ T cells strongly. In addition, the infiltration of Bregs is correlated with advanced disease stage, predicted early recurrence and decreased survival of patients with HCC (83). It was verified that CD40/CD154 signaling axis may be one of the pathways by which Bregs promote HCC progression (84).

Th17 cells are CD4$^+$ lymphocytes producing IL-17. Wang's work demonstrated that Th17 synchronically increases with Tregs and Bregs in the peripheral circulation and in tumor tissues in HCC patients. Also, further studies indicated that the production and proliferation of Th17 are promoted by tumor cells in TME mainly through cell-contact independent mechanisms (85). Furthermore, clinical studies showed that increased Th17 cells in tumor stroma are correlated with poor survival and higher postoperative recurrence, suggesting that Th17 cells may facilitate the development of HCC (86).

Tumor-associated endothelial cells (TAECs)

Endothelial cells are essential components in the process of tissue vascularization. It has been verified that migration of endothelial cells to tumor sites promotes the formation of the tumor neo-vasculature. TAECs express angiogenic surface receptors, such as VEGFR, EGFR and CXCL12, which conduct signaling through the interaction with their corresponding ligands to regulate endothelial cell survival, proliferation, mobilization, and invasion (87, 88). Compared with those in normal tissues, TAECs have accelerated cell cycle, increased ability of migration, and overexpressed CD105 and TGF-β1. TGF-β1 promotes the recruitment of CD105$^+$ endothelial cells, thereby contributing to angiogenesis of tumor (89). CD105$^+$ endothelial cells could make HCC resistant to chemotherapeutic drugs and angiogenesis inhibitors by increasing angiogenic activity of tumors (90).

Extracellular matrix

ECM, consisted of proteoglycans, glycoproteins and hyaluronan, is one of the major components of tumors that exert various crucial functions, including structural support, modulation of the microenvironment, and mediating intercellular communication (91). As one of the major components of TME, dysregulation of the ECM is a distinctive feature in cancer (91, 92).

Heparin sulfate, chondroitin sulfate, and keratan sulfate are the major components of proteoglycans in ECM, providing binding receptors for growth factors, cytokines, chemokines and are involved in many physiological and pathological processes (91). For example, Heparin sulfate proteoglycan (HSPG) acts as a co-receptor for binding of FGF-2 to its cognate FGF receptors, thus forming a ternary complex critical for cell proliferation and angiogenesis (93, 94). Glypican 3 (GPC3), an oncofetal HSPG anchored to the cell membrane, exhibits elevated expression in tumor cells and tumor vascular cells in HCC, and its expression correlates with a poor prognosis (95). Mechanistically, the oncogenic role of GPC3 is exerted through Wnt/β-Catenin pathway (96). SULF1 and SULF2 are two heparin-degrading endosulfatase enzymes that regulate heparin-dependent signaling in cells by altering the sulfation of HSPGs. Decreased expression of SULF1 was verified in the majority of HCC cell lines and approximately 30% of HCCs, but almost all HCC cell lines and 60% of HCC samples demonstrate elevated expression of SULF2 (97). Besides, upregulation of SULF2 predict a significant poor prognosis and higher postoperative recurrence rates (98, 99). Mechanistically, Lai et al. found that overexpression of SULF2 could enhance GPC3 expression and exert the oncogenic role by GPC3-dependent Wnt activation (99).

Collagens are the most abundant ECM proteins to support mechanical structure. Aberrant expression of collagen probably acts as a barrier for tumor metastasis, but may also promote tumor metastasis as a foothold for its movement (100). It was verified that COL1A1 is highly expressed in HCC tumor tissues compared with benign tissues and confers a survival advantage to liver cancer cells and enhances their oncogenicity (101).

Laminin, together with collagen, constitutes a component of the basement membrane. Laminin is involved in various biological activities, including cell adhesion, growth, differentiation, migration and angiogenesis (100). Laminin-5, which is not detected in normal liver, but overexpressed in HCC tissues, correlating with more proliferative and metastatic phenotypes. Together with TGF-β, Laminin-5 promotes EMT by upregulating Snail and downregulating E-cadherin in HCC (102). Also, Laminin B1 stimulates integrin-dependent focal adhesion kinase/Src proto-oncogene non-receptor tyrosine kinase signaling and supports tumor progression at the invasive front of HCC through the PDGFRα-laminin B1-keratin 19 cascade (103).

Taken together, these data provide solid evidence supporting the important role of the TME in the development of HCC and reveal the complex interaction among the components in the TME, also explain why traditional therapy fail in the treatment of HCC, and thus the development of novel therapeutic modalities is urgently needed.

Chimeric antigen receptor T cell immunotherapy

A recently-developed adoptive cell therapy is to generate tumor-specific CAR-T cells. The typical CAR is composed of an extracellular single-chain variable fragment (scFv) for recognizing antigens, a hinge region to provide flexibility, a transmembrane region and intracellular signaling domain (104). Due to the requirements of functional improvement, the intracellular signaling domain can be modified, and according to this, CAR can be divided into five generations (Figure 2). The first generation CARs only have a single signal domain CD3ζ chain for T-cell activation; The second and third generation CARs are characterized by the addition of one or two costimulatory domains, respectively; Most commonly derived from CD28 or 4-1BB, costimulatory domains endow CAR-T cells improved proliferation and persistence, enhanced cytokine secretion and increased anti-tumor cytotoxicity; The fourth generation CAR-T incorporates a costimulatory domain and inducible cytokine cassette and is termed "T cells redirected for universal cytokine-mediated killing" (TRUCK) to release the proinflammatory cytokines to activate innate immune response against the tumor and resist inhibitory components in TME, such as Tregs and MDSCs (104, 105). Recently, the fifth generation CARs, encoding a truncated cytoplasmic domain from IL-2Rβ and a STAT3-binding tyrosine-X-X-glutamine motif, together with CD3ζ and CD28 domains, were also developed. These novel CARs can activate the JAK-STAT signaling pathways in an antigen-dependent manner, which confers CAR-T cells superior persistence and antitumor effect (106).

Compared with the traditional T cell receptor-T cells, CAR-T can specifically recognize a wide array of antigens in a non-major histocompatibility complex (MHC) restricted manner, and solve the immune escape caused by the downregulation of MHC molecules (107). Furthermore, additional genes could be introduced to modify intracellular signaling domains enabling T cells resistant to immune suppression. CAR-T therapy has shown remarkable success for hematological malignancies and received its approval by the U.S. Food and Drug Administration as gene therapy which paves the way for further extension of this approach to solid malignancies including HCC (108, 109). In present, significant progresses have been made in the preclinical models and clinical trials utilizing CAR-T cells in HCC. Next, this review discusses several CAR-T targeting different antigens currently being evaluated in HCC. The latest clinical trials on CAR-T therapy for HCC is summarized in Table 1.

GPC3

Gao and his coworkers firstly reported the experience on CAR-T cells for the treatment of HCC. They constructed the first (αGPC3-Z CAR-T) and third generation CAR (αGPC3-28BBZ CAR-T) targeting GPC3. Results indicated that both generations of CAR-T specifically lysed HCC cell lines *in vitro*. αGPC3-28BBZ CAR -T cells could inhibit the growth of tumor in immunodeficient mice. It is of note that the third generation CAR-T cells secreted more IL-2 and IFN-γ, which has a positive correlation with the level of GPC3 expression on HCC cells (110). Another group reached the similar conclusion that the second and third generation CAR-T had a superior performance than the first generation construct *in vivo* (111). They found that T cells signaling *via* CD28 had higher cytotoxicity than those *via* 4-1BB *in vitro*; However, CAR-T cells containing the 4-1BB costimulatory domain had better proliferative activity *in vitro* and *in vivo*, indicating that the choice of costimulatory domain might affect the behavior of CAR-T cells. In two phase I trials, 13

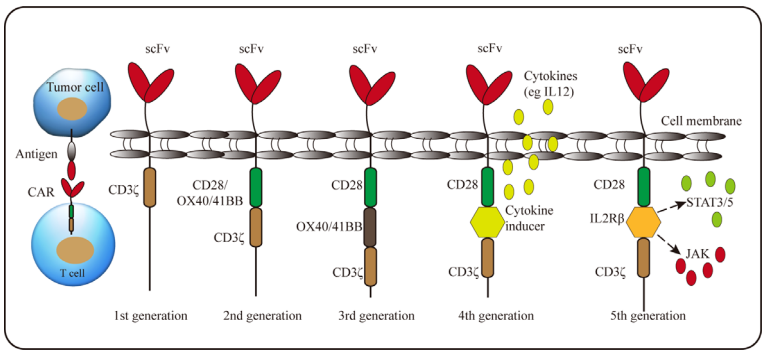

FIGURE 2
Schematic representation of the CAR structure. A CAR consists of single-chain variable fragment with a hinge, transmembrane domain, and CD3ζ (1st generation). 2nd generation and 3rd generation CARs contain one or two costimulatory molecules, respectively. Whereas the signal domain of the 4th generation CAR includes an inducible cytokine cassette. The 5th generation CAR encodes a truncated cytoplasmic domain of IL-2 receptor β with a binding site for the STAT3 to activate JAK-STAT pathway.

TABLE 1 Clinical trials in HCC using CAR-T.

NCT Number	Phase	Antigen	CAR-T Type	Status	Sample Size (n)	Conditions	Outcome Measures
NCT05123209	I	GPC3	2nd generation Autologous	Recruiting	12	LC	1 AEs 2 ORR, DOR, PFS and OS 3 Plasma α-AFP cells infusion 4 Persistence of CAR-T
NCT02932956	I	GPC3	N/A	Recruiting	10	LC	1 DLT 2 CR or PR 3 Median T cell persistence
NCT04093648	I	GPC3	2nd generation Autologous	Withdrawn	N/A	HCC	1 DLT 2 Response rate
NCT05003895	I	GPC3	N/A	Recruiting	38	HCC	1 Safety and feasibility 2 OS 3 Best overall response rate
NCT04951141	I	GPC3	N/A	Recruiting	10	HCC	1 AEs 2 ORR 3 OS
NCT04377932	I	GPC3	N/A Autologous	Recruiting	24	Basket including LC	1 DLT 2 Median CAR-T cell persistence 3 Best response as either CR or PR
NCT04715191	I	GPC3	N/A Autologous	Not yet recruiting	24	Basket including LC	1 DLT 2 Median CAR-T cell persistence 3 Best response as either CR or PR
NCT05103631	I	GPC3	N/A Autologous	Recruiting	27	LC	1 DLT 2 Median CAR-T cell persistence 3 Best response as either CR or PR
NCT02959151	I/II	GPC3	N/A Autologous /Donated	Unknown	20	Basket including HCC	1 AEs 2 Tumor response 3 Detection of CAR-T in the circulation
NCT03198546	I	GPC3	3rd/4th generation Autologous	Recruiting	30	HCC	1 DLT 2 Median CAR-T cell persistence 3 Best response as either CR or PR
NCT04506983	I	GPC3	2nd generation Autologous	Suspended	12	HCC	1 AEs 2 ORR 3 Proliferation ratio of CAR-T cells
NCT04121273	I	GPC3	2nd generation Autologous	Recruiting	20	HCC	1 DLT 2 Evaluation of tumor size 3 Peripheral tumor marker 4 Number of peripheral CAR-T cell
NCT03884751	I	GPC3	2nd generation Autologous	Completed	9	Advanced HCC	1 DLT, MTD and AEs 2 CAR-T expansion and persistence 3 PFS, ORR, OS, DOR, DCR and DOC
NCT02715362	I/II	GPC3	2nd generation Autologous	Unknown	30	HCC	1 AEs 2 Tumor response 3 Detection of CAR-T in blood 4 Serum cytokine levels
NCT02395250	I	GPC3	2nd generation Autologous	Completed	13	HCC	AEs
NCT02905188	I	GPC3	2nd generation Autologous	Active, not recruiting	9	HCC	1 DLT 2 Best response as either CR or PR 3 Median CAR-T cell persistence
NCT03980288	I	GPC3	4th generation Autologous	Completed	6	Advanced HCC	1 DLT, MTD and AEs 2 CAR-T expansion 3 ORR, DCR, DOC, DOR, PFS and OS
NCT03130712	I/II	GPC3	2nd generation Autologous	Unknown	10	Basket including HCC	1 AEs 2 Tumor response 3 Serum cytokine levels
NCT05155189	I	GPC3	2nd generation Autologous	Recruiting	20	HCC	1 AEs and limiting toxicities 2 Tumor response 3 Serum cytokine levels
NCT03146234	N/A	GPC3	N/A Autologous	Completed	7	HCC	1 Safety and tolerance 2 Engraftment 3 ORR, PFS and OS 4 Time of tumor progression
NCT05070156	I	GPC3	N/A Autologous	Recruiting	3	Advanced HCC	1 AEs, cellular kinetics 2 PFS, OS, ORR, DCR, DOR and DOC 3 Serum free GPC3, cytokines, CRP and lymphocyte subsets
NCT03084380	I/II	GPC3	2nd generation Autologous	Unknown	20	HCC	1 AEs 2 Overall complete remission rate 3 Duration of CAR-T in circulation

(Continued)

TABLE 1 Continued

NCT Number	Phase	Antigen	CAR-T Type	Status	Sample Size (n)	Conditions	Outcome Measures
NCT05344664	I	GPC3	N/A	Not yet recruiting	12	HCC	AEs
NCT02729493	II	EpCAM	N/A Autologous	Unknown	25	LC	DCR
NCT03013712	I/II	EpCAM	3rd generation Autologous	Unknown	60	Basket including HCC	1 Toxicity profile 2 Persistence of CAR-T 3 Anti-tumor efficacy
NCT03672305	I	c-Met/ PD-L1	N/A Autologous	Unknown	50	HCC	1 The efficacy of CAR-T in the treatment of HCC 2 AEs 3 The amplification and persistence of CAR-T
NCT05028933	I	EpCAM	N/A Autologous	Recruiting	48	Basket including HCC	1 DLT, MTD and AEs 2 ORR, DCR, DOR, PFS, OS 3 Level of tumor cells in peripheral blood
NCT04348643	I/II	CEA	N/A	Recruiting	40	Basket including LC	1 AEs 2 Persistence of CAR-T 3 ORR, DOR, PFS and OS 4 Levels of CEA, IL-6 and CRP in Serum
NCT03993743	I	CD147	3rd generation Autologous	Recruiting	34	Advanced HCC	1 DLT, MTD and AEs 2 Activity of CAR-T cell 3 CAR-T detection in extrahepatic sites
NCT02541370	I/II	CD133	N/A Autologous	Completed	20	Basket including LC	1 Occurrence of study related AEs 2 Anti-tumor responses to CAR-T
NCT03349255	I	AFP	2nd generation Autologous	Terminated	3	Basket including HCC	1 DLT 2 Response rate 3 CAR-T cell engraftment
NCT04550663	I	NKG2D	N/A Autologous	Not yet recruiting	10	Basket including HCC	1 MTD and AEs 2 Monitoring 3 ORR, PFS and OS

N/A, not available; AEs, adverse events; DLT, dose limiting toxicity; MTD, maximum tolerated dose; ORR, objective remission rate; CR, complete remission; PR, partial remission; PFS, progression-free survival; OS, overall survival; DOR, duration of response; DCR, disease control rate; DOC, duration of disease control. For more information, please visit the website: https://clinicaltrials.gov/.

patients with advanced HCC received autologous GPC3 CAR-T treatment to assess the safety. Most patients experienced manageable side effects, including pyrexia, decreased lymphocyte count, and grade 1/2 cytokine release syndrome (CRS). Grade 5 CRS occurred in only one patient and none of the patients experienced grade 3/4 neurotoxicity. The OS rates at 3 years, 1 year and 6 months were 10.5%, 42.0% and 50.3%, respectively. Additionally, two partial responses (PR) were confirmed. One patient with sustained stable disease (SD) was alive after 44.2 months (112).

In order to further improve the therapeutic efficacy, Pang et al. developed CAR-T cells which express IL-7 to induce proliferation and CCL19 to enhance migration of CAR-T cells. Results showed that incorporation of IL-7 and CCL19 into CAR-T cells remarkably promoted the antitumor ability. Surprisingly, these CAR-T cells eliminated the tumor completely 30 days after intratumor injection in a patient with advanced $GPC3^+$ HCC in a phase I clinical trial (NCT03198546) (113). Similarly, another group verified that pretreatment the tumor by a recombinant adeno-associated virus carrying the CCL19 gene (AAV-CCL19) could increase the infiltration of GPC3 CAR-T to tumor tissue and significantly prolonged the survival time of mice (114). Besides, the impact of serum GPC3(sGPC3) on CAR-T treatment is also noteworthy. sGPC3 was reported to be associated with poor prognosis in postoperative patients with HCC (115). sGPC3 can competitively bind to CARs with membrane GPC3, but fail to activate CAR-T cells effectively, thus resulting in an inhibitory effect on CAR-T cells in HCC (116). Combination chemotherapy or immune checkpoint inhibitors may provide more possibilities for GPC3 CAR-T in the treatment of HCC.

CD133

Expressed by cancer stem cells, CD133 is a pentaspan transmembrane glycoprotein. CD133 has attracted considerable attention as a potential cancer therapeutic target. Wang et al. constructed CD133-specific CAR-T cells (CD133 CAR-T) and found that CD133 CAR-T displayed distinctive lysis activity and secreted high level of cytokines targeting $CD133^+$ cells and remarkably suppressed tumor growth *in vivo*. Surprisingly, high level of CAR gene copy was detectable in tumor tissue (117). Given these surprising results, they conducted a clinical trial (NCT02541370) to evaluate the antitumor effect of CD133 CAR-T cells in patients with advanced HCC. 21 patients were included and received CD133 CAR-T cells across phases I and II. Hyperbilirubinemia as the most common high-grade adverse event, this trial showed feasibility and controllable toxicities.

The median OS and progression free survival (PFS) were 12 months and 6.8 months, respectively. Of 21 evaluable patients, 1 had a PR, 14 had SD for 2 to 16.3 months, and 6 progressed after T-cell infusion (118).

c-Met

c-Met is a tyrosine kinase receptor encoded by MET proto-oncogene and can binds to HGF with high affinity (119). As previously described, c-Met exerts an important role in metastasis of HCC through c-Met/HGF signaling pathway. c-Met-targeting CAR-T cells have demonstrated anti-tumor efficacy in c-Met positive several malignancies such as renal carcinoma, gastric cancer and breast cancer (120–122). Huang and coworkers constructed the second and third generation of c-Met CAR-T and evaluated their anti-tumor abilities *in vitro* and *in vivo*. They confirmed that c-Met CAR-T cells could specifically lyse HCC cells with the third generation CAR-T cells displaying more potent anti-tumor capability *in vivo* (123). Additionally, to weaken the influence of HCC-suppressive tumor microenvironment on CAR-T, scientists tried to design a dual CAR directing c-Met and PD-L1. In comparison with c-Met CAR-T cells or PD-L1 CAR-T cells, this dual CAR-T showed increased anti-tumor ability against c-Met$^+$ PD-L1$^+$ HCC cells. Moreover, improved survival persistence was observed in these dual CAR-T cells (124).

Alpha-fetoprotein (AFP)

AFP is a 70-KDa glycoprotein which is a well-established biomarker for HCC (125). In most HCC patients, AFP is detected at elevated levels and is associated with HCC progression and drug resistance (125, 126). Demonstrated by Liu et al., intratumoral administration of AFP CAR-T cells efficiently inhibited both HepG2 and AFP_{158}-expressing tumors *in vivo*. Moreover, intravenous injection of AFP CAR-T cells suppressed tumor growth rapidly and profoundly in tumor-bearing mice. AFP CAR-T cells also showed potent antitumor activity in an established intraperitoneal HCC xenograft model (127).

CD147

CD147, a transmembrane glycoprotein belonging to the immunoglobulin superfamily, is upregulated in kinds of malignancies, such as non-small cell lung cancer, breast cancer, and HCC (128, 129). Its involvement in the regulation of the TME and cancer progression, suggesting its potential as a promising target in cancers (129, 130). In Zhang's research, a novel CAR-T cell system targeting CD147 induced by Doxycycline (Dox) was developed. The supply of Dox can be terminated immediately once severe adverse events occur, in which case the expression of CD147 CAR on T-cells will return to the baseline within 24-48 hours to minimize potential toxicities of CAR-T cells (131). Similarly, researchers also developed logic-gated (log) GPC3-synNotch-inducible CD147 CAR to minimize any on-target/off-tumor toxicity. LogCD147-CAR selectively lyses dual antigen (GPC3$^+$CD147$^+$), but not single antigen (GPC3$^-$CD147$^+$) positive cells and severe toxicity was not occurred in a human CD147 transgenic mouse model (132). Currently, a phase I clinical trial (NCT03993743) is ongoing to assess the clinical response of CD147 CAR-T in patients with advanced HCC.

NK group 2 member D (NKG2D)

NKG2D, a type II transmembrane glycoprotein, is expressed on all NK cells, CD8$^+$ T cells, some autoreactive CD4$^+$ T cells and subsets of γδ T cells (133). Generally, NKG2D ligands (NKG2DL) are not detected on normal cells but exhibit elevated expression on tumor cells, suggesting potential targets for immunotherapy (134). In Sun's study, the second generation human NKG2D CAR-T cells efficiently eliminated the NKG2DLs-expressing HCC cell *in vitro*, whereas they less efficiently killed NKG2DL-silenced or -negative cells; The subcutaneous xenograft model further illuminated that T cells expressing the NKG2D CAR effectively suppress tumor growth. Interestingly, NKG2D CAR-T cells derived from patients with HCC demonstrated anti-tumor ability and specifically eradicated NKG2DL-high HCC cells (134).

Other promising targets

At present, various other potential targets for HCC are under investigated. MUC1 is a transmembrane glycoprotein, whose aberrant overexpression is identified on the surface of diverse human malignancies (135). Immunohistochemical analysis demonstrated that MUC1 was strong positive in 70.8% of liver cancer, while absent in normal liver tissues. Functionally, MUC1 participates in the migration and invasion by interacting with the HGF/c-Met and JNK/TGF-β signaling pathway and strongly correlates with metastasis and poor prognosis of HCC (136–138). Of note, MUC1 CAR-T exhibited antitumor potential against breast cancer (139, 140). At present, a basket trial of MUC1 CAR-T is underway in several malignancies including HCC (NCT02587689)

The melanoma antigen gene (MAGE) protein family consists of type I and II proteins (141). Normally, numerous MAGE proteins are only expressed in reproduction-related tissues, but aberrant expressions are observed in various tumors including HCC (141, 142). MAGE-1 and MAGE-3 mRNA expression is identified in 68% of HCC cases, but MAGE expression was no detected in the non-tumor samples (143). Wei's search showed that overexpression

of MAGE-A9 contributes to stemness and malignancy of HCC (144). To date, MAGE CAR-T cells for the treatment of lung cancer is underway in a phase I/II clinical trial (NCT03356808). Little information is available for MAGE CAR-T in HCC.

Epithelial cell adhesion molecule (EpCAM) is a transmembrane glycoprotein (145). Immunohistochemistry analysis revealed that EpCAM is broadly expressed by HCC and normal adjacent tissues; However, its expression is upregulated in tumor tissues and associated with poor prognosis in HCC patients (146). Functionally, EpCAM can maintain the capacity for malignant proliferation, invasion and metastasis (147–149). Several clinical trials to evaluate the EpCAM CAR-T cells for the treatment of advanced HCC are carrying out (NCT05028933, NCT03013712, NCT02729493).

As a foetal glycoprotein, carcinoembryonic antigen (CEA), is not usually expressed in significant quantity after birth but can be overexpressed on the cell surface of various cancers, such as colorectal, gastric, pancreatic, ovarian and lung cancer (150, 151). Under physiological conditions, the expression of CEA is restricted to the apical surface of epithelial cells towards the lumen to avoid recognition by immune cells (151). This unique expression pattern makes CEA an attractive target for immunotherapy. Currently, clinical trials using CEA CAR-T are mainly for the treatment of liver metastasis. A phase I/II basket trial to evaluate the efficacy and safety of CEA-targeted CAR-T cells is recruiting patients with relapse/refractory CEA^+ tumors including liver cancer (NCT04348643).

Tumor endothelial marker 1 (TEM1) is the prototypical member of a family of genes expressed in the stroma of tumors, cancer cells and pericytes (152). In HCC, TEM1 is mainly expressed in CAFs and its expression inversely correlates with patient prognosis (153). TEM1 also contributes to the vascular adhesion, migration and invasion of tumor cells (105, 153). Julie et al. successfully constructed a second generation CAR-T to specifically target $TEM1^+$ cells, confirming TEM1 as an attractive target for cancer immunotherapy (154).

New York esophageal squamous cell carcinoma (NY-ESO-1), a promising cancer testes antigen, is expressed by 43.9% of cases of HCC (155, 156). Very recently, NY-ESO-1 CAR-T cells constructed by Liu et al. suppressed tumor growth and prolonged the OS of mice in breast cancer and melanoma model (157).

Challenges and strategies for CAR-T towards TME

To date, the research of CAR-T therapy for HCC is in full swing around the world. Given its exceptional success in hematological malignancies, it may be very promising as a new approach for HCC treatment in future. But before that, there are still a series of difficulties remains to be overcome. In addition to tumor antigen heterogeneity and serious adverse events, the TME plays a non-negligible role in compromising the efficacy of CAR-T in HCC (Figure 3), and scientists are making much efforts to solve these problems (Figure 4).

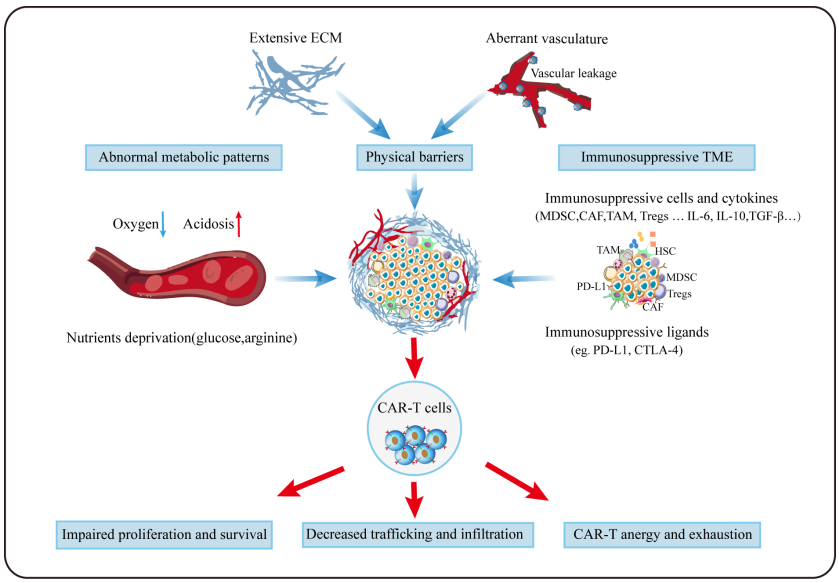

FIGURE 3
Challenges for CAR-T cells in TME. Aberrant vasculature and extensive ECM forms the special physical barriers making it difficult for CAR-T to efficiently traffic and infiltrate towards tumor tissues. Due to aberrant vasculature and the enhanced metabolism of tumor, CAR-T cells grow in a hypoxic, acidic and nutrition-deprivation milieu. Besides, immunosuppressive cellular and noncellular components can deactivate T cells *via* diverse mechanisms.

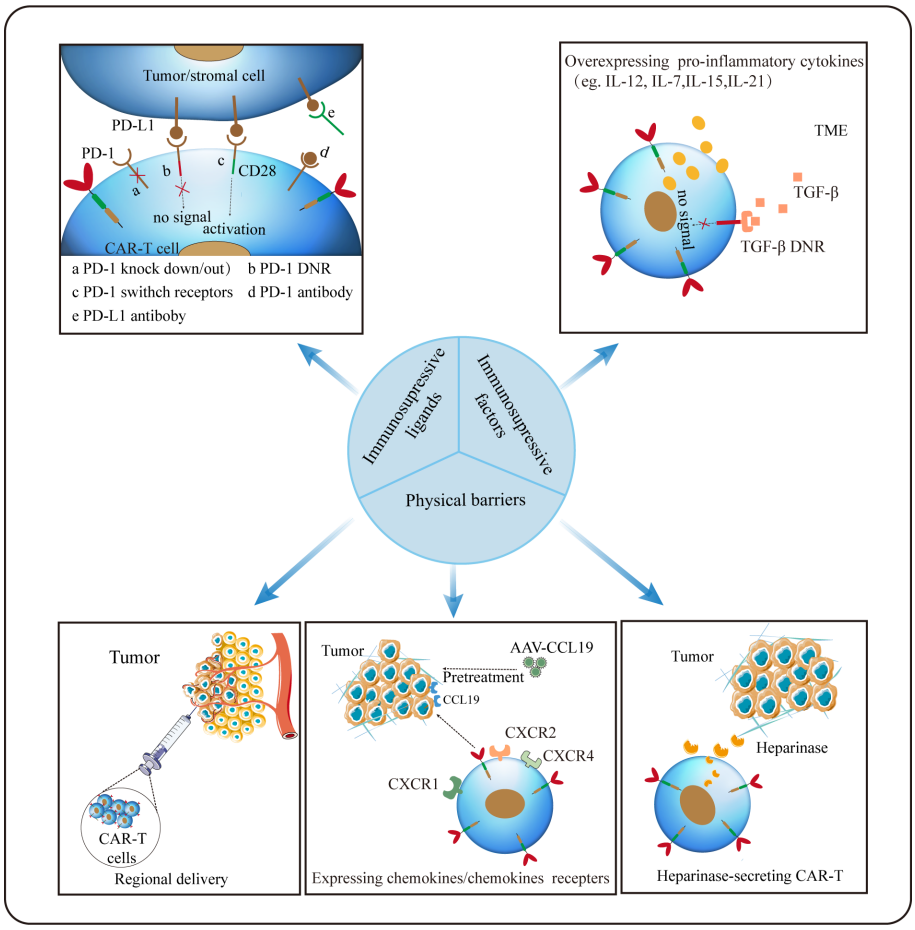

FIGURE 4
Strategies for CAR-T cells to overcome hostile TME. Regional delivery allows CAR-T cells to reach the tumor site directly. Inducing secretion of enzymes by CAR-T (eg. heparanase) to degrade ECM and optimizing CAR-T to express chemokines/chemokines receptors appears to remarkably improve CAR-T trafficking and infiltration. Disrupting the PD-1 expression on CAR-T cells or silencing/reversing the PD-1/PD-L1 axis can augment CAR-dependent antitumor activity. And modifying CAR-T to secrete pro-inflammatory factors may be an effective strategy against the inhibitory tumor microenvironment.

Trafficking towards and infiltration into tumor tissue is a prerequisite for CAR-T cells to exert the anti-tumor function. Different from hematological malignancies, where CAR-T can directly target malignant cells, regarding to solid tumors, CAR-T need to traffic to the tumor lesions to bind to their target, which is often greatly limited by the hostile TME. On the one hand, special physical barriers such as abundant and aberrant neovascularization, wide gap of vessel walls, extensive vascular leakage and ECM make it difficult for CAR-T to efficiently go home to tumor tissues (158, 159). Obviously, HCC that develops from liver fibrosis and cirrhosis are highly fibrotic, which hamper CAR-T to traffic and infiltrate into tumor sites physically. On the other hand, solid malignancies often secret chemokines such as CXCL1, CXCL2 and CXCL5 to impede the migration and penetration of T cells (160, 161). Theoretically, regional delivery of CAR-T can compensate for poor trafficking while reducing systemic toxicity linked with intravenous administration (162). Notably, regional delivery of CAR-T cells to treat malignant pleural diseases has proven feasible, safe and demonstrated antitumor activity in a phase I trial (163). It was reported that inducing secretion of enzymes by CAR-T cells (eg. heparanase) to degrade ECM have resulted in improved infiltration (164). As aforementioned, the addition of CCL19 in CAR-T treatment improved CAR-T cells infiltration and survival in mice (114). Besides, optimizing CAR-T cells to express the corresponding receptors of chemokines derived from tumors appears to remarkably improve CAR-T cell trafficking. In HCC, CXCR2-expressing CAR-T cells significantly accelerate trafficking and accumulation in tumor, and exhibit improved anti-tumor efficacy (165). Overexpression of other chemokines receptors

such as CXCR1 and CXCR4 also provide the advantage of penetration for therapeutic T cells (166, 167).

Unfortunately, even after migration into the tumor lesions successfully, it is still harsh for CAR-T cells to survive in a hostile milieu with various immunosuppressive factors (168). Firstly, TME is characterized by hypoxia, acidosis and nutrients deprivation resulting from the enhanced glycolytic metabolism of tumor cells (105). Secondly, as previously mentioned, immunosuppressive cellular components such as MDSCs, CAFs, TAMs and Tregs can deactivate T cells *via* diverse mechanisms including the production of tumor facilitating cytokines and growth factors. Thirdly, immune checkpoints like PD-1 and CTLA-4 in TME can act as suppressors to compromise antitumor immunity (168). Thus, combination checkpoint blockade with CAR-T cells is considered as the next immunotherapy modality. To date, much efforts to overcome these problems has been made. Christopher et al. constructed PSMA CAR-T cells which express a dominant-negative receptor (DNR) to block TGF-β signaling, and results showed that these T cells exhibit increased proliferation, cytokine release, decreased exhaustion and long-term persistence *in vivo* (169). Disrupting the PD-1 expression on CAR-T cells to evade PD-1/PD-L1 pathway has proven to augment CAR-dependent antitumor activity (170, 171). Given its improved efficacy in mesothelioma, combination checkpoints antibody with CAR-T after lymphodepletion may provide more possibilities for tumor immunotherapy (163). In addition, other investigations focusing on the pro-inflammatory cytokines instead of inhibitory signals have been carried out (172, 173). It was reported that inducible expression of IL-12 in CAR-T could boost antitumor activity in HCC (172).

Conclusion

HCC is a highly heterogeneous malignant tumor. Its carcinogenesis and progression are the consequence of the interaction of multiple factors and mechanisms. The tumor microenvironment is an intricate network that plays a pivotal role in the evolution of HCC. Enhancing our knowledge of mechanisms of carcinogenesis and development in HCC will greatly benefit the exploration of novel therapeutic modalities. The success of CAR-T therapy in hematological malignancies demonstrates the potential of immunity and also bring the light of HCC immunotherapy, but more efforts are needed to improve its antitumor efficacy and safety before its widespread clinical application. Moreover, the role of TME in the treatment of HCC with CAR-T cells cannot be ignored. We are optimistic about that with the further in-depth study of cancer molecular biology and immunology, the treatment of HCC will finally usher in the dawn.

Author contributions

YZ, SR, and RZ contributed to conception and design of the study. ZG and JG wrote the first draft of the manuscript. LL and WH wrote sections of the manuscript. All authors contributed to manuscript revision, read, and approved the submitted version

Funding

This work was supported by National Natural Science Foundation of China (No. 82070643 and U1904164).

Acknowledgments

We are grateful to National Natural Science Foundation of China for its support.

Conflict of interest

The authors declare that the research was conducted in the absence of any commercial or financial relationships that could be construed as a potential conflict of interest.

Publisher's note

References

1. Sung HA-O, Ferlay J, Siegel RA-O, Laversanne M, Soerjomataram I, Jemal A, et al. Global cancer statistics 2020: Globocan estimates of incidence and mortality worldwide for 36 cancers in 185 countries. *CA Cancer J Clin* (2021) 71:209–49. doi: 10.3322/caac.21660

2. Llovet JM, Kelley RK, Villanueva A, Singal AG, Pikarsky E, Roayaie S, et al. Hepatocellular carcinoma. *Nat Rev Dis Primers* (2021) 7:7. doi: 10.1038/s41572-021-00245-6

3. Wang W, Wei C. Advances in the early diagnosis of hepatocellular carcinoma. *Genes Dis* (2020) 7:308–19. doi: 10.1016/j.gendis.2020.01.014

4. Yang JD, Heimbach JK. New advances in the diagnosis and management of hepatocellular carcinoma. *BMJ* (2020) 371:m3544. doi: 10.1136/bmj.m3544

5. Losic B, Craig AJ, Villacorta-Martin C, Martins-Filho SN, Akers N, Chen X, et al. Intratumoral heterogeneity and clonal evolution in liver cancer. *Nat Commun* (2020) 11:291. doi: 10.1038/s41467-019-14050-z

6. Amicone L, Marchetti A. Microenvironment and tumor cells: Two targets for new molecular therapies of hepatocellular carcinoma. *Transl Gastroenterol Hepatol* (2018) 3:24. doi: 10.21037/tgh.2018.04.05

7. Fu Y, Liu S, Zeng S, Shen H. From bench to bed: The tumor immune microenvironment and current immunotherapeutic strategies for hepatocellular carcinoma. *J Exp Clin Cancer Res* (2019) 38:396. doi: 10.1186/s13046-019-1396-4

8. Lurje I, Werner W, Mohr R, Roderburg C, Tacke F, Hammerich L. *In situ* vaccination as a strategy to modulate the immune microenvironment of hepatocellular carcinoma. *Front Immunol* (2021) 12:650486. doi: 10.3389/fimmu.2021.650486

9. Lu C, Rong D, Zhang B, Zheng W, Wang X, Chen Z, et al. Current perspectives on the immunosuppressive tumor microenvironment in hepatocellular carcinoma: Challenges and opportunities. *Mol Cancer* (2019) 18:130. doi: 10.1186/s12943-019-1047-6

10. Satilmis B, Sahin TT, Cicek E, Akbulut S, Yilmaz S. Hepatocellular carcinoma tumor microenvironment and its implications in terms of anti-tumor immunity: Future perspectives for new therapeutics. *J Gastrointest Cancer* (2021) 52:1198–205. doi: 10.1007/s12029-021-00725-8

11. Tsuchida T, Friedman SL. Mechanisms of hepatic stellate cell activation. *Nat Rev Gastroenterol Hepatol* (2017) 14:397–411. doi: 10.1038/nrgastro.2017.38

12. Yan Y, Zeng J, Xing L, Li C. Extra- and intra-cellular mechanisms of hepatic stellate cell activation. *Biomedicines* (2021) 9: 1014. doi: 10.3390/biomedicines9081014

13. Mogler C, Konig C, Wieland M, Runge A, Besemfelder E, Komljenovic D, et al. Hepatic stellate cells limit hepatocellular carcinoma progression through the orphan receptor endosialin. *EMBO Mol Med* (2017) 9:741–9. doi: 10.15252/emmm.201607222

14. Amann T, Bataille F, Spruss T, Muhlbauer M, Gabele E, Scholmerich J, et al. Activated hepatic stellate cells promote tumorigenicity of hepatocellular carcinoma. *Cancer Sci* (2009) 100:646–53. doi: 10.1111/j.1349-7006.2009.01087.x

15. Song J, Ge Z, Yang X, Luo Q, Wang C, You H, et al. Hepatic stellate cells activated by acidic tumor microenvironment promote the metastasis of hepatocellular carcinoma *Via* osteopontin. *Cancer Lett* (2015) 356:713–20. doi: 10.1016/j.canlet.2014.10.021

16. Iwahashi S, Shimada M, Morine Y, Imura S, Ikemoto T, Saito Y, et al. The effect of hepatic stellate cells on hepatocellular carcinoma progression. *J Clin Oncol* (2019) 37:265–. doi: 10.1200/JCO.2019.37.4_suppl.265

17. Mussbach F, Ungefroren H, Gunther B, Katenkamp K, Henklein P, Westermann M, et al. Proteinase-activated receptor 2 (PAR2) in hepatic stellate cells - evidence for a role in hepatocellular carcinoma growth *in vivo*. *Mol Cancer* (2016) 15:54. doi: 10.1186/s12943-016-0538-y

18. Lin N, Meng L, Lin J, Chen S, Zhang P, Chen Q, et al. Activated hepatic stellate cells promote angiogenesis in hepatocellular carcinoma by secreting angiopoietin-1. *J Cell Biochem* (2020) 121:1441–51. doi: 10.1002/jcb.29380

19. Myojin Y, Hikita H, Sugiyama M, Sasaki Y, Fukumoto K, Sakane S, et al. Hepatic stellate cells in hepatocellular carcinoma promote tumor growth *Via* growth differentiation factor 15 production. *Gastroenterology* (2021) 160:1741–54.e16. doi: 10.1053/j.gastro.2020.12.015

20. Huang JL, Fu YP, Gan W, Liu G, Zhou PY, Zhou C, et al. Hepatic stellate cells promote the progression of hepatocellular carcinoma through microrna-1246-Roralpha-Wnt/Beta-Catenin axis. *Cancer Lett* (2020) 476:140–51. doi: 10.1016/j.canlet.2020.02.012

21. Ji J, Eggert T, Budhu A, Forgues M, Takai A, Dang H, et al. Hepatic stellate cell and monocyte interaction contributes to poor prognosis in hepatocellular carcinoma. *Hepatology* (2015) 62:481–95. doi: 10.1002/hep.27822

22. Matsuda M, Seki E. Hepatic stellate cell-macrophage crosstalk in liver fibrosis and carcinogenesis. *Semin Liver Dis* (2020) 40:307–20. doi: 10.1055/s-0040-1708876

23. Li Y, Kim BG, Qian S, Letterio JJ, Fung JJ, Lu L, et al. Hepatic stellate cells inhibit T cells through active TGF-Beta1 from a cell surface-bound latent TGF-Beta1/GARP complex. *J Immunol* (2015) 195:2648–56. doi: 10.4049/jimmunol.1500139

24. Charles R, Chou HS, Wang L, Fung JJ, Lu L, Qian S. Human hepatic stellate cells inhibit T-cell response through B7-H1 pathway. *Transplantation* (2013) 96:17–24. doi: 10.1097/TP.0b013e318294caae

25. Zhao W, Zhang L, Xu Y, Zhang Z, Ren G, Tang K, et al. Hepatic stellate cells promote tumor progression by enhancement of immunosuppressive cells in an orthotopic liver tumor mouse model. *Lab Invest* (2014) 94:182–91. doi: 10.1038/labinvest.2013.139

26. Xu Y, Zhao W, Xu J, Li J, Hong Z, Yin Z, et al. Activated hepatic stellate cells promote liver cancer by induction of myeloid-derived suppressor cells through cyclooxygenase-2. *Oncotarget* (2016) 7:8866–78. doi: 10.18632/oncotarget.6839

27. Zhang DY, Goossens N, Guo J, Tsai MC, Chou HI, Altunkaynak C, et al. A hepatic stellate cell gene expression signature associated with outcomes in hepatitis c cirrhosis and hepatocellular carcinoma after curative resection. *Gut* (2016) 65:1754–64. doi: 10.1136/gutjnl-2015-309655

28. Ma T, Renz BW, Ilmer M, Koch D, Yang Y, Werner J, et al. Myeloid-derived suppressor cells in solid tumors. *Cells* (2022) 11: 310. doi: 10.3390/cells11020310

29. Tcyganov E, Mastio J, Chen E, Gabrilovich DI. Plasticity of myeloid-derived suppressor cells in cancer. *Curr Opin Immunol* (2018) 51:76–82. doi: 10.1016/j.coi.2018.03.009

30. Li YM, Liu ZY, Wang JC, Yu JM, Li ZC, Yang HJ, et al. Receptor-interacting protein kinase 3 deficiency recruits myeloid-derived suppressor cells to hepatocellular carcinoma through the chemokine (C-X-C motif) ligand 1-chemokine (C-X-C motif) receptor 2 axis. *Hepatology* (2019) 70:1564–81. doi: 10.1002/hep.30676

31. Chiu DK, Xu IM, Lai RK, Tse AP, Wei LL, Koh HY, et al. Hypoxia induces myeloid-derived suppressor cell recruitment to hepatocellular carcinoma through chemokine (C-c motif) ligand 26. *Hepatology* (2016) 64:797–813. doi: 10.1002/hep.28655

32. Chiu DK, Tse AP, Xu IM, Di Cui J, Lai RK, Li LL, et al. Hypoxia inducible factor HIF-1 promotes myeloid-derived suppressor cells accumulation through ENTPD2/CD39L1 in hepatocellular carcinoma. *Nat Commun* (2017) 8:517. doi: 10.1038/s41467-017-00530-7

33. Srivastava MK, Sinha P, Clements VK, Rodriguez P, Ostrand-Rosenberg S. Myeloid-derived suppressor cells inhibit T-cell activation by depleting cystine and cysteine. *Cancer Res* (2010) 70:68–77. doi: 10.1158/0008-5472.CAN-09-2587

34. Baumann T, Dunkel A, Schmid C, Schmitt S, Hiltensperger M, Lohr K, et al. Regulatory myeloid cells paralyze T cells through cell-cell transfer of the metabolite methylglyoxal. *Nat Immunol* (2020) 21:555–66. doi: 10.1038/s41590-020-0666-9

35. Liu M, Zhou J, Liu X, Feng Y, Yang W, Wu F, et al. Targeting monocyte-intrinsic enhancer reprogramming improves immunotherapy efficacy in hepatocellular carcinoma. *Gut* (2020) 69:365–79. doi: 10.1136/gutjnl-2018-317257

36. Hoechst B, Voigtlaender T, Ormandy L, Gamrekelashvili J, Zhao F, Wedemeyer H, et al. Myeloid derived suppressor cells inhibit natural killer cells in patients with hepatocellular carcinoma *Via* the Nkp30 receptor. *Hepatology* (2009) 50:799–807. doi: 10.1002/hep.23054

37. Zhang H, Li Z, Wang L, Tian G, Tian J, Yang Z, et al. Critical role of myeloid-derived suppressor cells in tumor-induced liver immune suppression through inhibition of NKT cell function. *Front Immunol* (2017) 8:129. doi: 10.3389/fimmu.2017.00129

38. Burga RA, Thorn M, Point GR, Guha P, Nguyen CT, Licata LA, et al. Liver myeloid-derived suppressor cells expand in response to liver metastases in mice and inhibit the anti-tumor efficacy of anti-cea CAR-T. *Cancer Immunol Immunother* (2015) 64:817–29. doi: 10.1007/s00262-015-1692-6

39. Deng X, Li X, Guo X, Lu Y, Xie Y, Huang X, et al. Myeloid-derived suppressor cells promote tumor growth and sorafenib resistance by inducing Fgf1 upregulation and fibrosis. *Neoplasia* (2022) 28:100788. doi: 10.1016/j.neo.2022.100788

40. Ganguly D, Chandra R, Karalis J, Teke M, Aguilera T, Maddipati R, et al. Cancer-associated fibroblasts: Versatile players in the tumor microenvironment. *Cancers (Basel)* (2020) 12: 2652. doi: 10.3390/cancers12092652

41. Liu T, Zhou L, Li D, Andl T, Zhang Y. Cancer-associated fibroblasts build and secure the tumor microenvironment. *Front Cell Dev Biol* (2019) 7:60. doi: 10.3389/fcell.2019.00060

42. Jia C, Wang G, Wang T, Fu B, Zhang Y, Huang L, et al. Cancer-associated fibroblasts induce epithelial-mesenchymal transition *Via* the transglutaminase 2-dependent IL-6/Il6r/STAT3 axis in hepatocellular carcinoma. *Int J Biol Sci* (2020) 16:2542–58. doi: 10.7150/ijbs.45446

43. Bhowmick NA, Neilson EG, Moses HL. Stromal fibroblasts in cancer initiation and progression. *Nature* (2004) 432:332–7. doi: 10.1038/nature03096

44. Xu H, Zhao J, Li J, Zhu Z, Cui Z, Liu R, et al. Cancer associated fibroblast-derived Ccl5 promotes hepatocellular carcinoma metastasis through activating Hif1alpha/Zeb1 axis. *Cell Death Dis* (2022) 13:478. doi: 10.1038/s41419-022-04935-1

45. Lin ZY, Chuang YH, Chuang WL. Cancer-associated fibroblasts up-regulate Ccl2, Ccl26, Il6 and Loxl2 genes related to promotion of cancer progression in hepatocellular carcinoma cells. *BioMed Pharmacother.* (2012) 66:525–9. doi: 10.1016/j.biopha.2012.02.001

46. Liu F, Zhang W, Yang F, Feng T, Zhou M, Yu Y, et al. Interleukin-6-Stimulated progranulin expression contributes to the malignancy of hepatocellular carcinoma cells by activating mtor signaling. *Sci Rep* (2016) 6:21260. doi: 10.1038/srep21260

47. Affo S, Yu LX, Schwabe RF. The role of cancer-associated fibroblasts and fibrosis in liver cancer. *Annu Rev Pathol* (2017) 12:153–86. doi: 10.1146/annurev-pathol-052016-100322

48. Song T, Dou C, Jia Y, Tu K, Zheng X. Timp-1 activated carcinoma-associated fibroblasts inhibit tumor apoptosis by activating SDF1/CXCR4 signaling in hepatocellular carcinoma. *Oncotarget* (2015) 6:12061–79. doi: 10.18632/oncotarget.3616

49. Mano Y, Yoshio S, Shoji H, Tomonari S, Aoki Y, Aoyanagi N, et al. Bone morphogenetic protein 4 provides cancer-supportive phenotypes to liver fibroblasts in patients with hepatocellular carcinoma. *J Gastroenterol* (2019) 54:1007–18. doi: 10.1007/s00535-019-01579-5

50. Song M, He J, Pan QZ, Yang J, Zhao J, Zhang YJ, et al. Cancer-associated fibroblast-mediated cellular crosstalk supports hepatocellular carcinoma progression. *Hepatology* (2021) 73:1717–35. doi: 10.1002/hep.31792

51. Deng Y, Cheng J, Fu B, Liu W, Chen G, Zhang Q, et al. Hepatic carcinoma-associated fibroblasts enhance immune suppression by facilitating the generation of myeloid-derived suppressor cells. *Oncogene* (2017) 36:1090–101. doi: 10.1038/onc.2016.273

52. Li T, Yang Y, Hua X, Wang G, Liu W, Jia C, et al. Hepatocellular carcinoma-associated fibroblasts trigger NK cell dysfunction *Via* PGE2 and IDO. *Cancer Lett* (2012) 318:154–61. doi: 10.1016/j.canlet.2011.12.020

53. Cheng JT, Deng YN, Yi HM, Wang GY, Fu BS, Chen WJ, et al. Hepatic carcinoma-associated fibroblasts induce IDO-producing regulatory dendritic cells through IL-6-Mediated STAT3 activation. *Oncogenesis* (2016) 5:e198. doi: 10.1038/oncsis.2016.7

54. Cassetta L, Pollard JW. Tumor-associated macrophages. *Curr Biol* (2020) 30:R246–R8. doi: 10.1016/j.cub.2020.01.031

55. Pan Y, Yu Y, Wang X, Zhang T. Tumor-associated macrophages in tumor immunity. *Front Immunol* (2020) 11:583084. doi: 10.3389/fimmu.2020.583084

56. Dong P, Ma L, Liu L, Zhao G, Zhang S, Dong L, et al. CD86(+)/CD206(+), diametrically polarized tumor-associated macrophages, predict hepatocellular carcinoma patient prognosis. *Int J Mol Sci* (2016) 17:320. doi: 10.3390/ijms17030320

57. Bartneck M, Schrammen PL, Mockel D, Govaere O, Liepelt A, Krenkel O, et al. The CCR2(+) macrophage subset promotes pathogenic angiogenesis for tumor vascularization in fibrotic livers. *Cell Mol Gastroenterol Hepatol* (2019) 7:371–90. doi: 10.1016/j.jcmgh.2018.10.007

58. Fu LQ, Du WL, Cai MH, Yao JY, Zhao YY, Mou XZ. The roles of tumor-associated macrophages in tumor angiogenesis and metastasis. *Cell Immunol* (2020) 353:104119. doi: 10.1016/j.cellimm.2020.104119

59. Zhou J, Ding T, Pan W, Zhu LY, Li L, Zheng L. Increased intratumoral regulatory T cells are related to intratumoral macrophages and poor prognosis in hepatocellular carcinoma patients. *Int J Cancer* (2009) 125:1640–8. doi: 10.1002/ijc.24556

60. Sung PS. Crosstalk between tumor-associated macrophages and neighboring cells in hepatocellular carcinoma. *Clin Mol Hepatol* (2021) 28: 333–350. doi: 10.3350/cmh.2021.0308

61. Wu Q, Zhou W, Yin S, Zhou Y, Chen T, Qian J, et al. Blocking triggering receptor expressed on myeloid cells-1-Positive tumor-associated macrophages induced by hypoxia reverses immunosuppression and anti-programmed cell death ligand 1 resistance in liver cancer. *Hepatology* (2019) 70:198–214. doi: 10.1002/hep.30593

62. Wu K, Kryczek I, Chen L, Zou W, Welling TH. Kupffer cell suppression of Cd8+ T cells in human hepatocellular carcinoma is mediated by B7-H1/Programmed death-1 interactions. *Cancer Res* (2009) 69:8067–75. doi: 10.1158/0008-5472.CAN-09-0901

63. Zhang W, Zhu XD, Sun HC, Xiong YQ, Zhuang PY, Xu HX, et al. Depletion of tumor-associated macrophages enhances the effect of sorafenib in metastatic liver cancer models by antimetastatic and antiangiogenic effects. *Clin Cancer Res* (2010) 16:3420–30. doi: 10.1158/1078-0432.CCR-09-2904

64. Dong N, Shi X, Wang S, Gao Y, Kuang Z, Xie Q, et al. M2 macrophages mediate sorafenib resistance by secreting HGF in a feed-forward manner in hepatocellular carcinoma. *Br J Cancer* (2019) 121:22–33. doi: 10.1038/s41416-019-0482-x

65. Arvanitakis K, Mitroulis I, Germanidis G. Tumor-associated neutrophils in hepatocellular carcinoma pathogenesis, prognosis, and therapy. *Cancers (Basel)* (2021) 13: 2899. doi: 10.3390/cancers13122899

66. Kalafati L, Mitroulis I, Verginis P, Chavakis T, Kourtzelis I. Neutrophils as orchestrators in tumor development and metastasis formation. *Front Oncol* (2020) 10:581457. doi: 10.3389/fonc.2020.581457

67. Fridlender ZG, Sun J, Kim S, Kapoor V, Cheng G, Ling L, et al. Polarization of tumor-associated neutrophil phenotype by TGF-beta: "N1" versus "N2" tan. *Cancer Cell* (2009) 16:183–94. doi: 10.1016/j.ccr.2009.06.017

68. Li YW, Qiu SJ, Fan J, Zhou J, Gao Q, Xiao YS, et al. Intratumoral neutrophils: A poor prognostic factor for hepatocellular carcinoma following resection. *J Hepatol* (2011) 54:497–505. doi: 10.1016/j.jhep.2010.07.044

69. Zhou SL, Zhou ZJ, Hu ZQ, Huang XW, Wang Z, Chen EB, et al. Tumor-associated neutrophils recruit macrophages and T-regulatory cells to promote progression of hepatocellular carcinoma and resistance to sorafenib. *Gastroenterology* (2016) 150:1646–58.e17. doi: 10.1053/j.gastro.2016.02.040

70. Kim CG, Kim C, Yoon SE, Kim KH, Choi SJ, Kang B, et al. Hyperprogressive disease during PD-1 blockade in patients with advanced hepatocellular carcinoma. *J Hepatol* (2021) 74:350–9. doi: 10.1016/j.jhep.2020.08.010

71. Li L, Xu L, Yan J, Zhen ZJ, Ji Y, Liu CQ, et al. CXCR2-CXCL1 axis is correlated with neutrophil infiltration and predicts a poor prognosis in hepatocellular carcinoma. *J Exp Clin Cancer Res* (2015) 34:129. doi: 10.1186/s13046-015-0247-1

72. Kuang DM, Zhao Q, Wu Y, Peng C, Wang J, Xu Z, et al. Peritumoral neutrophils link inflammatory response to disease progression by fostering angiogenesis in hepatocellular carcinoma. *J Hepatol* (2011) 54:948–55. doi: 10.1016/j.jhep.2010.08.041

73. Li XF, Chen DP, Ouyang FZ, Chen MM, Wu Y, Kuang DM, et al. Increased autophagy sustains the survival and pro-tumourigenic effects of neutrophils in human hepatocellular carcinoma. *J Hepatol* (2015) 62:131–9. doi: 10.1016/j.jhep.2014.08.023

74. Zhou SL, Yin D, Hu ZQ, Luo CB, Zhou ZJ, Xin HY, et al. A positive feedback loop between cancer stem-like cells and tumor-associated neutrophils controls hepatocellular carcinoma progression. *Hepatology* (2019) 70:1214–30. doi: 10.1002/hep.30630

75. He M, Peng A, Huang XZ, Shi DC, Wang JC, Zhao Q, et al. Peritumoral stromal neutrophils are essential for c-Met-Elicited metastasis in human hepatocellular carcinoma. *Oncoimmunology* (2016) 5:e1219828. doi: 10.1080/2162402X.2016.1219828

76. He G, Zhang H, Zhou J, Wang B, Chen Y, Kong Y, et al. Peritumoural neutrophils negatively regulate adaptive immunity *Via* the PD-L1/PD-1 signalling pathway in hepatocellular carcinoma. *J Exp Clin Cancer Res* (2015) 34:141. doi: 10.1186/s13046-015-0256-0

77. Cheng Y, Li H, Deng Y, Tai Y, Zeng K, Zhang Y, et al. Cancer-associated fibroblasts induce $PDL1^+$ neutrophils through the IL6-STAT3 pathway that foster immune suppression in hepatocellular carcinoma. *Cell Death Dis* (2018) 9:422. doi: 10.1038/s41419-018-0458-4

78. Sun R, Xiong Y, Liu H, Gao C, Su L, Weng J, et al. Tumor-associated neutrophils suppress antitumor immunity of NK cells through the PD-L1/PD-1 axis. *Transl Oncol* (2020) 13:100825. doi: 10.1016/j.tranon.2020.100825

79. Stockis J, Roychoudhuri R, Halim TYF. Regulation of regulatory T cells in cancer. *Immunology* (2019) 157:219–31. doi: 10.1111/imm.13064

80. Han Y, Yang Y, Chen Z, Jiang Z, Gu Y, Liu Y, et al. Human hepatocellular carcinoma-infiltrating CD4(+)CD69(+)Foxp3(-) regulatory T cell suppresses T cell response *Via* membrane-bound TGF-Beta1. *J Mol Med (Berl)* (2014) 92:539–50. doi: 10.1007/s00109-014-1143-4

81. Shi C, Chen Y, Chen Y, Yang Y, Bing W, Qi J. $CD4^{(+)}$ $Cd25^{(+)}$ regulatory T cells promote hepatocellular carcinoma invasion *Via* TGF-Beta1-Induced epithelial-mesenchymal transition. *Onco Targets Ther* (2019) 12:279–89. doi: 10.2147/OTT.S172417

82. Gao Y, You M, Fu J, Tian M, Zhong X, Du C, et al. Intratumoral stem-like $CCR4^+$ regulatory T cells orchestrate the immunosuppressive microenvironment in HCC associated with hepatitis b. *J Hepatol* (2022) 76:148–59. doi: 10.1016/j.jhep.2021.08.029

83. Ye L, Zhang Q, Cheng Y, Chen X, Wang G, Shi M, et al. Tumor-derived exosomal Hmgb1 fosters hepatocellular carcinoma immune evasion by promoting $Tim\text{-}1^{(+)}$ regulatory b cell expansion. *J Immunother Cancer* (2018) 6:145. doi: 10.1186/s40425-018-0451-6

84. Shao Y, Lo CM, Ling CC, Liu XB, Ng KT, Chu AC, et al. Regulatory b cells accelerate hepatocellular carcinoma progression *Via* CD40/CD154 signaling pathway. *Cancer Lett* (2014) 355:264–72. doi: 10.1016/j.canlet.2014.09.026

85. Wang W, Wang Z, Qin Y, Tang G, Cai G, Liu Y, et al. Th17, synchronically increased with tregs and bregs , promoted by tumour cells *Via* cell-contact in primary hepatic carcinoma. *Clin Exp Immunol* (2018) 192:181–92. doi: 10.1111/cei.13094

86. Zhang JP, Yan J, Xu J, Pang XH, Chen MS, Li L, et al. Increased intratumoral IL-17-Producing cells correlate with poor survival in hepatocellular carcinoma patients. *J Hepatol* (2009) 50:980–9. doi: 10.1016/j.jhep.2008.12.033

87. Tsai CN, Yu SC, Lee CW, Pang JS, Wu CH, Lin SE, et al. SOX4 activates CXCL12 in hepatocellular carcinoma cells to modulate endothelial cell migration and angiogenesis *in vivo*. *Oncogene* (2020) 39:4695–710. doi: 10.1038/s41388-020-1319-z

88. Dai W, Wang Y, Yang T, Wang J, Wu W, Gu J. Downregulation of exosomal CLEC3B in hepatocellular carcinoma promotes metastasis and angiogenesis *Via* ampk and VEGFSignals. *Cell Commun Signal* (2019) 17:113. doi: 10.1186/s12964-019-0423-6

89. Benetti A, Berenzi A, Gambarotti M, Garrafa E, Gelati M, Dessy E, et al. Transforming growth factor-Beta1 and Cd105 promote the migration of hepatocellular carcinoma-derived endothelium. *Cancer Res* (2008) 68:8626–34. doi: 10.1158/0008-5472.CAN-08-1218

90. Xiong YQ, Sun HC, Zhang W, Zhu XD, Zhuang PY, Zhang JB, et al. Human hepatocellular carcinoma tumor-derived endothelial cells manifest increased angiogenesis capability and drug resistance compared with normal endothelial cells. *Clin Cancer Res* (2009) 15:4838–46. doi: 10.1158/1078-0432.CCR-08-2780

91. Huang J, Zhang L, Wan D, Zhou L, Zheng S, Lin S, et al. Extracellular matrix and its therapeutic potential for cancer treatment. *Signal Transduct Target Ther* (2021) 6:153. doi: 10.1038/s41392-021-00544-0

92. Popova NV, Jucker M. The functional role of extracellular matrix proteins in cancer. *Cancers (Basel)* (2022) 14: 238. doi: 10.3390/cancers14010238

93. Garcia J, Patel N, Basehore S, Clyne AM. Fibroblast growth factor-2 binding to heparan sulfate proteoglycans varies with shear stress in flow-adapted cells. *Ann BioMed Eng.* (2019) 47:1078–93. doi: 10.1007/s10439-019-02202-7

94. Dong ZR, Sun D, Yang YF, Zhou W, Wu R, Wang XW, et al. TMPRSS4 drives angiogenesis in hepatocellular carcinoma by promoting hb-EGF expression and proteolytic cleavage. *Hepatology* (2020) 72:923–39. doi: 10.1002/hep.31076

95. Liu H, Yang C, Lu W, Zeng Y. Prognostic significance of glypican-3 expression in hepatocellular carcinoma: A meta-analysis. *Med (Baltimore)* (2018) 97:e9702. doi: 10.1097/MD.0000000000009702

96. Hu P, Ke C, Guo X, Ren P, Tong Y, Luo S, et al. Both glypican-3/Wnt/Beta-Catenin signaling pathway and autophagy contributed to the inhibitory effect of curcumin on hepatocellular carcinoma. *Dig Liver Dis* (2019) 51:120–6. doi: 10.1016/j.dld.2018.06.012

97. Lai JP, Thompson JR, Sandhu DS, Roberts LR. Heparin-degrading sulfatases in hepatocellular carcinoma: Roles in pathogenesis and therapy targets. *Future Oncol* (2008) 4:803–14. doi: 10.2217/14796694.4.6.803

98. Lai JP, Sandhu DS, Yu C, Han T, Moser CD, Jackson KK, et al. Sulfatase 2 up-regulates glypican 3, promotes fibroblast growth factor signaling, and decreases survival in hepatocellular carcinoma. *Hepatology* (2008) 47:1211–22. doi: 10.1002/hep.22202

99. Lai JP, Oseini AM, Moser CD, Yu C, Elsawa SF, Hu C, et al. The oncogenic effect of sulfatase 2 in human hepatocellular carcinoma is mediated in part by glypican 3-dependent wnt activation. *Hepatology* (2010) 52:1680–9. doi: 10.1002/hep.23848

100. Wu SD, Ma YS, Fang Y, Liu LL, Fu D, Shen XZ. Role of the microenvironment in hepatocellular carcinoma development and progression. *Cancer Treat Rev* (2012) 38:218–25. doi: 10.1016/j.ctrv.2011.06.010

101. Ma HP, Chang HL, Bamodu OA, Yadav VK, Huang TY, Wu ATH, et al. Collagen 1a1 (Col1a1) is a reliable biomarker and putative therapeutic target for hepatocellular carcinogenesis and metastasis. *Cancers (Basel)* (2019) 11: 786. doi: 10.3390/cancers11060786

102. Giannelli G, Bergamini C, Fransvea E, Sgarra C, Antonaci S. Laminin-5 with transforming growth factor-Beta1 induces epithelial to mesenchymal transition in hepatocellular carcinoma. *Gastroenterology* (2005) 129:1375–83. doi: 10.1053/j.gastro.2005.09.055

103. Govaere O, Petz M, Wouters J, Vandewynckel YP, Scott EJ, Topal B, et al. The PDGFRalpha-laminin B1-keratin 19 cascade drives tumor progression at the invasive front of human hepatocellular carcinoma. *Oncogene* (2017) 36:6605–16. doi: 10.1038/onc.2017.260

104. Hong M, Clubb JD, Chen YY. Engineering CAR-T cells for next-generation cancer therapy. *Cancer Cell* (2020) 38:473–88. doi: 10.1016/j.ccell.2020.07.005

105. Dal Bo M, De Mattia E, Baboci L, Mezzalira S, Cecchin E, Assaraf YG, et al. New insights into the pharmacological, immunological, and CAR-T-Cell approaches in the treatment of hepatocellular carcinoma. *Drug Resist Update* (2020) 51:100702. doi: 10.1016/j.drup.2020.100702

106. Kagoya Y, Tanaka S, Guo T, Anczurowski M, Wang CH, Saso K, et al. A novel chimeric antigen receptor containing a JAK-STAT signaling domain mediates superior antitumor effects. *Nat Med* (2018) 24:352–9. doi: 10.1038/nm.4478

107. June CH, O'Connor RS, Kawalekar OU, Ghassemi S, Milone MC. CAR T cell immunotherapy for human cancer. *Science* (2018) 359:1361–5. doi: 10.1126/science.aar6711

108. Bouchkouj N, Kasamon YL, de Claro RA, George B, Lin X, Lee S, et al. FDA Approval summary: Axicabtagene ciloleucel for relapsed or refractory Large b-cell lymphoma. *Clin Cancer Res* (2019) 25:1702–8. doi: 10.1158/1078-0432.CCR-18-2743

109. O'Leary MC, Lu X, Huang Y, Lin X, Mahmood I, Przepiorka D, et al. FDA Approval summary: Tisagenlecleucel for treatment of patients with relapsed or refractory b-cell precursor acute lymphoblastic leukemia. *Clin Cancer Res* (2019) 25:1142–6. doi: 10.1158/1078-0432.CCR-18-2035

110. Gao H, Li K, Tu H, Pan X, Jiang H, Shi B, et al. Development of T cells redirected to glypican-3 for the treatment of hepatocellular carcinoma. *Clin Cancer Res* (2014) 20:6418–28. doi: 10.1158/1078-0432.CCR-14-1170

111. Li W, Guo L, Rathi P, Marinova E, Gao X, Wu MF, et al. Redirecting T cells to glypican-3 with 4-1BB zeta chimeric antigen receptors results in Th1 polarization and potent antitumor activity. *Hum Gene Ther* (2017) 28:437–48. doi: 10.1089/hum.2016.025

112. Shi D, Shi Y, Kaseb AO, Qi X, Zhang Y, Chi J, et al. Chimeric antigen receptor-Glypican-3 T-cell therapy for advanced hepatocellular carcinoma: Results of phase I trials. *Clin Cancer Res* (2020) 26:3979–89. doi: 10.1158/1078-0432.CCR-19-3259

113. Pang N, Shi J, Qin L, Chen A, Tang Y, Yang H, et al. IL-7 and CCL19-secreting CAR-T cell therapy for tumors with positive glypican-3 or mesothelin. *J Hematol Oncol* (2021) 14:118. doi: 10.1186/s13045-021-01128-9

114. Meng M, Wu YC. Combination of AAV-CCL19 and GPC3 CAR-T cells in the treatment of hepatocellular carcinoma. *J Immunol Res* (2021) 2021:1782728. doi: 10.1155/2021/1782728

115. Haruyama Y, Yorita K, Yamaguchi T, Kitajima S, Amano J, Ohtomo T, et al. High preoperative levels of serum glypican-3 containing n-terminal subunit are associated with poor prognosis in patients with hepatocellular carcinoma after partial hepatectomy. *Int J Cancer* (2015) 137:1643–51. doi: 10.1002/ijc.29518

116. Sun L, Gao F, Gao Z, Ao L, Li N, Ma S, et al. Shed antigen-induced blocking effect on CAR-T cells targeting glypican-3 in hepatocellular carcinoma. *J Immunother Cancer* (2021) 9:e001875. doi: 10.1136/jitc-2020-001875

117. Wang Y, Chen M, Wu Z, Tong C, Dai H, Guo Y, et al. CD133-directed CAR T cells for advanced metastasis malignancies: A phase I trial. *Oncoimmunology* (2018) 7:e1440169. doi: 10.1080/2162402X.2018.1440169

118. Dai H, Tong C, Shi D, Chen M, Guo Y, Chen D, et al. Efficacy and biomarker analysis of CD133-directed CAR T cells in advanced hepatocellular carcinoma: A single-arm, open-label, phase ii trial. *Oncoimmunology* (2020) 9:1846926. doi: 10.1080/2162402X.2020.1846926

119. Bouattour M, Raymond E, Qin S, Cheng AL, Stammberger U, Locatelli G, et al. Recent developments of c-met as a therapeutic target in hepatocellular carcinoma. *Hepatology* (2018) 67:1132–49. doi: 10.1002/hep.29496

120. Kang CH, Kim Y, Lee DY, Choi SU, Lee HK, Park CH. C-Met-Specific chimeric antigen receptor T cells demonstrate anti-tumor effect in c-met positive gastric cancer. *Cancers (Basel)* (2021) 13:5738. doi: 10.3390/cancers13225738

121. Mori JI, Adachi K, Sakoda Y, Sasaki T, Goto S, Matsumoto H, et al. Anti-tumor efficacy of human anti-C-Met CAR-T cells against papillary renal cell carcinoma in an orthotopic model. *Cancer Sci* (2021) 112:1417–28. doi: 10.1111/cas.14835

122. Tchou J, Zhao Y, Levine BL, Zhang PJ, Davis MM, Melenhorst JJ, et al. Safety and efficacy of intratumoral injections of chimeric antigen receptor (CAR) T cells in metastatic breast cancer. *Cancer Immunol Res* (2017) 5:1152–61. doi: 10.1158/2326-6066.CIR-17-0189

123. Huang X, Guo J, Li T, Jia L, Tang X, Zhu J, et al. C-Met-Targeted chimeric antigen receptor T cells inhibit hepatocellular carcinoma cells *in vitro* and *in vivo*. *J BioMed Res* (2021) 36:10–21. doi: 10.7555/JBR.35.20200207

124. Jiang W, Li T, Guo J, Wang J, Jia L, Shi X, et al. Bispecific c-Met/PD-L1 CAR-T cells have enhanced therapeutic effects on hepatocellular carcinoma. *Front Oncol* (2021) 11:546586. doi: 10.3389/fonc.2021.546586

125. Xue J, Cao Z, Cheng Y, Wang J, Liu Y, Yang R, et al. Acetylation of alpha-fetoprotein promotes hepatocellular carcinoma progression. *Cancer Lett* (2020) 471:12–26. doi: 10.1016/j.canlet.2019.11.043

126. Li W, Liu K, Chen Y, Zhu M, Li M. Role of alpha-fetoprotein in hepatocellular carcinoma drug resistance. *Curr Med Chem* (2021) 28:1126–42. doi: 10.2174/0929867327999200729151247

127. Liu H, Xu Y, Xiang J, Long L, Green S, Yang Z, et al. Targeting alpha-fetoprotein (Afp)-mhc complex with CAR T-cell therapy for liver cancer. *Clin Cancer Res* (2017) 23:478–88. doi: 10.1158/1078-0432.CCR-16-1203

128. Lian C, Guo Y, Zhang J, Chen X, Peng C. Targeting CD147 is a novel strategy for antitumor therapy. *Curr Pharm Des* (2017) 23:4410–21. doi: 10.2174/1381612823666170710144759

129. Landras A, Reger de Moura C, Jouenne F, Lebbe C, Menashi S, Mourah S. CD147 is a promising target of tumor progression and a prognostic biomarker. *Cancers (Basel)* (2019) 11: 1803. doi: 10.3390/cancers11111803

130. Sun J, Hemler ME. Regulation of MMP-1 and MMP-2 production through CD147/Extracellular matrix metalloproteinase inducer interactions. *Cancer Res* (2001) 61:2276–81. doi: 10.1046/j.1523-5394.2001.009002104.x

131. Zhang RY, Wei D, Liu ZK, Yong YL, Wei W, Zhang ZY, et al. Doxycycline inducible chimeric antigen receptor T cells targeting CD147 for hepatocellular carcinoma therapy. *Front Cell Dev Biol* (2019) 7:233. doi: 10.3389/fcell.2019.00233

132. Tseng HC, Xiong W, Badeti S, Yang Y, Ma M, Liu T, et al. Efficacy of anti-CD147 chimeric antigen receptors targeting hepatocellular carcinoma. *Nat Commun* (2020) 11:4810. doi: 10.1038/s41467-020-18444-2

133. Zhang J, Basher F, Wu JD. NKG2D ligands in tumor immunity: Two sides of a coin. *Front Immunol* (2015) 6:97. doi: 10.3389/fimmu.2015.00097

134. Sun B, Yang D, Dai H, Liu X, Jia R, Cui X, et al. Eradication of hepatocellular carcinoma by NKG2D-based CAR-T cells. *Cancer Immunol Res* (2019) 7:1813–23. doi: 10.1158/2326-6066.CIR-19-0026

135. Chen W, Zhang Z, Zhang S, Zhu P, Ko JK, Yung KK. UC1: Structure, function, and clinic application in epithelial cancers. *M Int J Mol Sci* (2021) 22: 6567. doi: 10.3390/ijms22126567

136. Bozkaya G, Korhan P, Cokakli M, Erdal E, Sagol O, Karademir S, et al. Cooperative interaction of MUC1 with the HGF/C-met pathway during hepatocarcinogenesis. *Mol Cancer* (2012) 11:64. doi: 10.1186/1476-4598-11-64

137. Li Q, Liu G, Shao D, Wang J, Yuan H, Chen T, et al. Mucin1 mediates autocrine transforming growth factor beta signaling through activating the c-jun n-terminal Kinase/Activator protein 1 pathway in human hepatocellular carcinoma cells. *Int J Biochem Cell Biol* (2015) 59:116–25. doi: 10.1016/j.biocel.2014.11.012

138. Yuan SF, Li KZ, Wang L, Dou KF, Yan Z, Han W, et al. Expression of MUC1 and its significance in hepatocellular and cholangiocarcinoma tissue. *World J Gastroenterol* (2005) 11:4661–6. doi: 10.3748/wjg.v11.i30.4661

139. Nalawade SA, Shafer P, Bajgain P, McKenna MK, Ali A, Kelly L, et al. Selectively targeting myeloid-derived suppressor cells through trail receptor 2 to enhance the efficacy of CAR T cell therapy for treatment of breast cancer. *J Immunother Cancer* (2021) 9: e003237. doi: 10.1136/jitc-2021-003237

140. Zhou R, Yazdanifar M, Roy LD, Whilding LM, Gavrill A, Maher J, et al. CAR T cells targeting the tumor MUC1 glycoprotein reduce triple-negative breast cancer growth. *Front Immunol* (2019) 10:1149. doi: 10.3389/fimmu.2019.01149

141. Li S, Shi X, Li J, Zhou X. Pathogenicity of the MAGE family. *Oncol Lett* (2021) 22:844. doi: 10.3892/ol.2021.13105

142. Kerkar SP, Wang ZF, Lasota J, Park T, Patel K, Groh E, et al. MAGE-a is more highly expressed than NY-ESO-1 in a systematic immunohistochemical analysis of 3668 cases. *J Immunother*. (2016) 39:181–7. doi: 10.1097/CJI.0000000000000119

143. Tahara K, Mori M, Sadanaga N, Sakamoto Y, Kitano S, Makuuchi M. Expression of the MAGE gene family in human hepatocellular carcinoma. *Cancer* (1999) 85:1234–40. doi: 10.1002/(SICI)1097-0142(19990315)85:6<1234::AID-CNCR4>3.0.CO;2-7

144. Wei Y, Wang Y, Gong J, Rao L, Wu Z, Nie T, et al. High expression of MAGE-A9 contributes to stemness and malignancy of human hepatocellular carcinoma. *Int J Oncol* (2018) 52:219–30. doi: 10.3892/ijo.2017.4198

145. Patriarca C, Macchi RM, Marschner AK, Mellstedt H. Epithelial cell adhesion molecule expression (CD326) in cancer: A short review. *Cancer Treat Rev* (2012) 38:68–75. doi: 10.1016/j.ctrv.2011.04.002

146. Ko CJ, Li CJ, Wu MY, Chu PY. Overexpression of epithelial cell adhesion molecule as a predictor of poor outcome in patients with hepatocellular carcinoma. *Exp Ther Med* (2018) 16:4810–6. doi: 10.3892/etm.2018.6794

147. Park DJ, Sung PS, Kim JH, Lee GW, Jang JW, Jung ES, et al. EpCAM-high liver cancer stem cells resist natural killer cell-mediated cytotoxicity by upregulating Ceacam1. *J Immunother Cancer* (2020) 8:e000301. doi: 10.1136/jitc-2019-000301

148. Maetzel D, Denzel S, Mack B, Canis M, Went P, Benk M, et al. Nuclear signalling by tumor-associated antigen EpCAM. *Nat Cell Biol* (2009) 11:162–71. doi: 10.1038/ncb1824

149. Wang MH, Sun R, Zhou XM, Zhang MY, Lu JB, Yang Y, et al. Epithelial cell adhesion molecule overexpression regulates epithelial-mesenchymal transition, stemness and metastasis of nasopharyngeal carcinoma cells *Via* the PTEN/Akt/mTOR pathway. *Cell Death Dis* (2018) 9:2. doi: 10.1038/s41419-017-0013-8

150. Hall C, Clarke L, Pal A, Buchwald P, Eglinton T, Wakeman C, et al. A review of the role of carcinoembryonic antigen in clinical practice. *Ann Coloproctol.* (2019) 35:294–305. doi: 10.3393/ac.2019.11.13

151. Wang L, Ma N, Okamoto S, Amaishi Y, Sato E, Seo N, et al. Efficient tumor regression by adoptively transferred CEA-specific CAR-T cells associated with symptoms of mild cytokine release syndrome. *Oncoimmunology* (2016) 5: e1211218. doi: 10.1080/2162402X.2016.1211218

152. Nanda A, Karim B, Peng Z, Liu G, Qiu W, Gan C, et al. Tumor endothelial marker 1 (Tem1) functions in the growth and progression of abdominal tumors. *Proc Natl Acad Sci U.S.A.* (2006) 103:3351–6. doi: 10.1073/pnas.0511306103

153. Yang F, Wei Y, Han D, Li Y, Shi S, Jiao D, et al. Interaction with CD68 and regulation of GAS6 expression by endosialin in fibroblasts drives recruitment and polarization of macrophages in hepatocellular carcinoma. *Cancer Res* (2020) 80:3892–905. doi: 10.1158/0008-5472.CAN-19-2691

154. Fierle JK, Brioschi M, de Tiani M, Wetterwald L, Atsaves V, Abram-Saliba J, et al. Soluble trivalent engagers redirect cytolytic T cell activity toward tumor endothelial marker 1. *Cell Rep Med* (2021) 2:100362. doi: 10.1016/j.xcrm.2021.100362

155. Wang H, Chen D, Wang R, Quan W, Xia D, Mei J, et al. NY-ESO-1 expression in solid tumors predicts prognosis: A systematic review and meta-analysis. *Med (Baltimore)* (2019) 98:e17990. doi: 10.1097/MD.0000000000017990

156. Nakamura S, Nouso K, Noguchi Y, Higashi T, Ono T, Jungbluth A, et al. Expression and immunogenicity of NY-ESO-1 in hepatocellular carcinoma. *J Gastroenterol Hepatol* (2006) 21:1281–5. doi: 10.1111/j.1440-1746.2006.04271.x

157. Liu X, Xu Y, Xiong W, Yin B, Huang Y, Chu J, et al. Development of a TCR-like antibody and chimeric antigen receptor against NY-ESO-1/HLA-A2 for cancer immunotherapy. *J Immunother Cancer* (2022) 10: e0004035. doi: 10.1136/jitc-2021-004035

158. Zhang GZ, Li TF, Han SY. Mesothelin-targeted CAR-T cells for adoptive cell therapy of solid tumors. *Arch Med Sci* (2021) 17:1213–20. doi: 10.5114/aoms.2019.84888

159. Katayama Y, Uchino J, Chihara Y, Tamiya N, Kaneko Y, Yamada T, et al. Tumor neovascularization and developments in therapeutics. *Cancers (Basel)* (2019) 11: 316. doi: 10.3390/cancers11030316

160. Kershaw MH, Wang G, Westwood JA, Pachynski RK, Tiffany HL, Marincola FM, et al. Redirecting migration of T cells to chemokine secreted from tumors by genetic modification with CXCR2. *Hum Gene Ther* (2002) 13:1971–80. doi: 10.1089/10430340260355374

161. Korbecki J, Kojder K, Kapczuk P, Kupnicka P, Gawronska-Szklarz B, Gutowska I, et al. The effect of hypoxia on the expression of CXC chemokines and CXC chemokine receptors-a review of literature. *Int J Mol Sci* (2021) 22: 843. doi: 10.3390/ijms22020843

162. Sridhar P, Petrocca F. Regional delivery of chimeric antigen receptor (CAR) T-cells for cancer therapy. *Cancers (Basel)* (2017) 9: 92. doi: 10.3390/cancers9070092

163. Adusumilli PS, Zauderer MG, Riviere I, Solomon SB, Rusch VW, O'Cearbhaill RE, et al. A phase I trial of regional mesothelin-targeted CAR T-cell therapy in patients with malignant pleural disease, in combination with the anti-PD-1 agent pembrolizumab. *Cancer Discovery* (2021) 11:2748–63. doi: 10.1158/2159-8290.CD-21-0407

164. Caruana I, Savoldo B, Hoyos V, Weber G, Liu H, Kim ES, et al. Heparanase promotes tumor infiltration and antitumor activity of CAR-redirected T lymphocytes. *Nat Med* (2015) 21:524–9. doi: 10.1038/nm.3833

165. Liu G, Rui W, Zheng H, Huang D, Yu F, Zhang Y, et al. CXCR2-modified CAR-T cells have enhanced trafficking ability that improves treatment of hepatocellular carcinoma. *Eur J Immunol* (2020) 50:712–24. doi: 10.1002/eji.201948457

166. Jin L, Tao H, Karachi A, Long Y, Hou AY, Na M, et al. CXCR1- or CXCR2-modified CAR T cells Co-opt IL-8 for maximal antitumor efficacy in solid tumors. *Nat Commun* (2019) 10:4016. doi: 10.1038/s41467-019-11869-4

167. Khan AB, Carpenter B, Santos ESP, Pospori C, Khorshed R, Griffin J, et al. Redirection to the bone marrow improves T cell persistence and antitumor functions. *J Clin Invest.* (2018) 128:2010–24. doi: 10.1172/JCI97454

168. Oura K, Morishita A, Tani J, Masaki T. Tumor immune microenvironment and immunosuppressive therapy in hepatocellular carcinoma: A review. *Int J Mol Sci* (2021) 22: 5801. doi: 10.3390/ijms22115801

169. Kloss CC, Lee J, Zhang A, Chen F, Melenhorst JJ, Lacey SF, et al. Dominant-negative TGF-beta receptor enhances PSMA-targeted human CAR T cell proliferation and augments prostate cancer eradication. *Mol Ther* (2018) 26:1855–66. doi: 10.1016/j.ymthe.2018.05.003

170. Ren J, Liu X, Fang C, Jiang S, June CH, Zhao Y. Multiplex genome editing to generate universal CAR T cells resistant to PD1 inhibition. *Clin Cancer Res* (2017) 23:2255–66. doi: 10.1158/1078-0432.CCR-16-1300

171. Guo X, Jiang H, Shi B, Zhou M, Zhang H, Shi Z, et al. Disruption of PD-1 enhanced the anti-tumor activity of chimeric antigen receptor T cells against hepatocellular carcinoma. *Front Pharmacol* (2018) 9:1118. doi: 10.3389/fphar.2018.01118

172. Liu Y, Di S, Shi B, Zhang H, Wang Y, Wu X, et al. Armored inducible expression of IL-12 enhances antitumor activity of glypican-3-Targeted chimeric antigen receptor-engineered T cells in hepatocellular carcinoma. *J Immunol* (2019) 203:198–207. doi: 10.4049/jimmunol.1800033

173. Batra SA, Rathi P, Guo L, Courtney AN, Fleurence J, Balzeau J, et al. Glypican-3-Specific CAR T cells coexpressing IL15 and IL21 have superior expansion and antitumor activity against hepatocellular carcinoma. *Cancer Immunol Res* (2020) 8:309–20. doi: 10.1158/2326-6066

Frontiers in Endocrinology

Explores the endocrine system to find new therapies for key health issues The second most-cited endocrinology and metabolism journal, which advances our understanding of the endocrine system. It uncovers new therapies for prevalent health issues such as obesity, diabetes, reproduction, and aging.

Discover the latest Research Topics

See more →

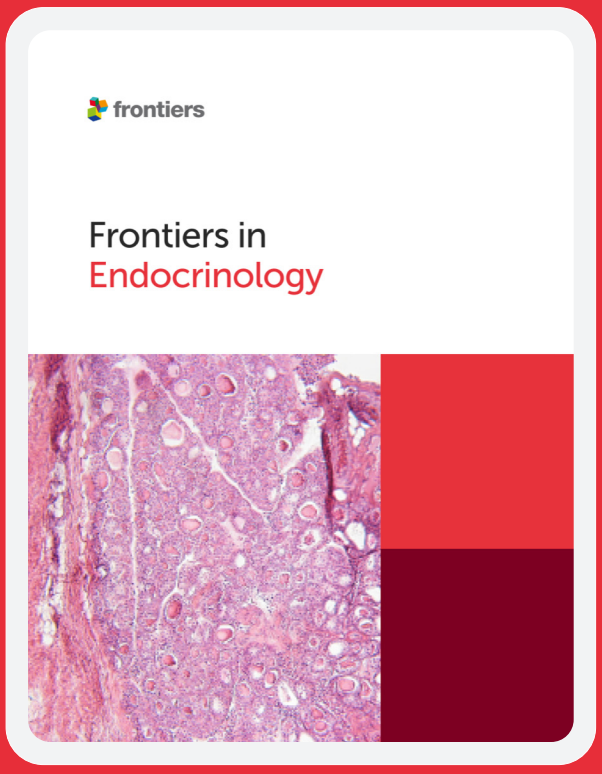

Frontiers

Avenue du Tribunal-Fédéral 34
1005 Lausanne, Switzerland
frontiersin.org

Contact us

+41 (0)21 510 17 00
frontiersin.org/about/contact